

DISS. ETH NO. 23108

**BIOTRANSFORMATION OF AMINE-CONTAINING
MICROPOLLUTANTS IN ACTIVATED SLUDGE:
pH-DEPENDENCY AND BIOTRANSFORMATION
REACTIONS**

A thesis submitted to attain the degree of
DOCTOR OF SCIENCES of ETH ZURICH
(Dr. sc. ETH Zurich)

presented by

REBEKKA KAROLINA GULDE

Dipl.-Chem., Karlsruher Institut für Technologie
born on 18.08.1984
citizen of Germany

accepted on the recommendation of

Prof. Dr. Kristopher McNeill, examiner

PD Dr. Kathrin Fenner, co-examiner

Prof. Dr. Damian E. Helbling, co-examiner

Prof. Dr. Christopher P. Higgins, co-examiner

2015

Dank

Mein grösster Dank gilt meiner Betreuerin Kathrin Fenner. Sie hat mir die Möglichkeit gegeben meine Dissertation zu einem sehr spannenden und umweltrelevanten Thema durchzuführen. Das Themengebiet der Umweltchemie war für mich als Diplomandin mit Hintergrund in der Theoretischen Chemie neu und ich bin sehr dankbar für diese Möglichkeit und ihr Vertrauen. Viele gemeinsame Diskussionen haben nicht nur zu dieser erfolgreichen Arbeit geführt, sondern auch, dass ich, wie ich finde, die Fähigkeiten gelernt habe, die man einem Doktor zuspricht. Besonders geschätzt habe ich zudem, dass Kathrin mir zum einen die Freiheit gegeben hat selbst herauszufinden wie und was die nächsten Schritte sind, mich zum anderen aber sehr intensiv betreut hat z. B. beim Schreiben der wissenschaftlichen Texte.

A huge thank you goes to Damian Helbling. While he was still at Eawag, Damian taught me nearly everything about the experimental work. His door was always open and during many discussions with him (including late nights over beer), I learned a lot about the different aspects of science. Furthermore, I am very thankful for his exhaustive feedback to our manuscripts from overseas. They were crucial for the development of a consistent storyline. Finally, thank you for coming over the great ocean to my exam.

I would also like to thank my Doktorvater Kris McNeill and my external co-examiner Chris Higgins for being members of my committee.

Des Weiteren möchte ich all denen Danken, die ausserdem direkt zu der vorliegenden Arbeit beigetragen haben: Andreas Scheidegger für seine Unterstützung bzgl. der statistischen Auswertung mit Bayessischer Inferenz; Ulf Meier für die Entwicklung der non-target Methode mit Sieve und der Aufklärung einiger Strukturen; Emma Schymanski für viele wertvolle Diskussionen über Strukturaufklärung, die gemeinsame

Entwicklung der Levels, die vieles vereinfachen, die Durchsicht aller 101 (!) Strukturdeutungen, und die Aufnahme der Daten in MassBank; Hans-Peter Kohler für die sehr intensive Diskussion der Biotransformationsreaktionen; Samuel Derrer für die Synthese einiger TP-standards; Daniel Rentsch für das Messen und Interpretieren der NMR-Daten; und Adriano Joss sowie Jennifer Schollee für wertvolle Diskussionen über die vorliegende Arbeit.

Während meines Doktorats durfte ich vier Semesterarbeiten und zwei Masterarbeiten (mit)betreuen, die nicht nur zum wissenschaftlichen Verständnis beigetragen haben, sondern durch die ich auch viel über das Betreuen an sich lernen konnte. Mein herzlicher Dank geht an Pascal Wallimann, Rebekka Schwaninger/Teichler, Johanna Otto und Ulf Meier. Im Speziellen möchte ich Ulf für seine Treue über drei Arbeiten hinweg danken.

Ein ganz besonderer Dank geht an Jennifer Schollee. Durch die vielen Diskussionen mit Jen über diverse Aspekte unserer Arbeiten, des ganzen Themengebiets sowie der Wissenschaft an sich hatte ich das Gefühl die Wissenschaft tatsächlich zu leben. Ausserdem möchte ich Dir für die Korrektur meiner englischen Texte danken.

Ich bin sehr dankbar, dass ich diese Arbeit innerhalb des sehr unterstützenden und angenehmen Umfelds der Uchem Abteilung bzw. der ganzen Eawag durchführen konnte. Viele verschiedene Personen haben mich innerhalb meiner Arbeit unterstützt, zu einer hervorragenden Atmosphäre beigetragen, haben mir lustige Stunden im Büro oder Labor verschafft oder sind über die Arbeit hinaus Freunde geworden, die ich an Abenden, Wochenenden und in den Ferien nicht mehr missen möchte. Ein herzliches Dankeschön geht an Alfi, Andrea, Anne, Aurea, Birgit, Christa, Christian, Christoph, Devon, Diogo, Fred, Heinz, Irene, Jana, Jelena, Jen, Jonas, Jürgen, Juliane, Kov, Laura, Luba, Marc, Martin Loos, Marita, Matze, Michele, Michi, Nico, Nicole, Philipp, Richi, RoKi, Sabine, Sarah, Supergötti, Stefan, Stephie, Thomas, Tobi, Yuije und viele mehr!

Ausserdem gibt's noch ein Leben neben der Arbeit. Deshalb möchte ich meiner Familie danken, die mich bei allen meinen Vorhaben immer unterstützt hat. Ein grosses Danke dafür an: Mama, Papa, Andrea, Benny, Micha, Flori, Christine, Manu, Susi, Marlene, Kilian, Johanna, Louis und Tamino. Ganz besonders dankbar bin ich Tamino dafür, dass Du bei uns warst! Wegen Dir habe ich kaum eine schlaflose Nacht wegen dieser

Doktorarbeit verbracht. Du hast mir gezeigt was wirklich wichtig ist.

Den Lindy Hop Tänzern möchte ich für den fröhlichen Ausgleich danken, allen voran Sue, Roli, David und Mirjam. Auch der regelmässige Yogaunterricht hat sehr zum Ausgleich beigetragen. Bedanken möchte ich mich zudem bei all denen, die mir beim Umbau meiner Bude geholfen haben sowie allen anderen, die ich zu meinen Freunden zählen darf. Zum Schluss möchte ich noch Tobi danken. Du hast Dir viele langweilige Details meiner Arbeit angehört, mich trotzdem lecker bekocht und mir viele schöne Stunden der Ablenkung bereitet.

Table of contents

Summary	vii
Zusammenfassung	xi
1 Introduction	1
1.1 Behavior of micropollutants during wastewater treatment	2
1.1.1 Removal efficiencies and influencing factors during activated sludge treatment	3
1.1.2 Transformation reactions during activated sludge treatment . .	5
1.2 Pertinent structural features	6
1.2.1 Why focus on one specific functional group?	6
1.2.2 The amine functional group	7
1.3 Goals	8
1.4 Methodological approach	9
1.4.1 Compound selection	9
1.4.2 Laboratory-based batch experiments	9
1.4.3 Chemical analysis based on liquid-chromatography high-resolution tandem mass spectrometry	10
2 pH-dependent biotransformation of ionizable organic micropollutants in activated sludge	13
2.1 Introduction	14
2.2 Materials and methods	18
2.2.1 Micropollutant selection	18
2.2.2 Biotransformation test system	18
2.2.3 Analytical method	21
2.2.4 Estimation of kinetic parameters	22
2.3 Results and discussion	23
2.3.1 Operating conditions in pH-controlled batch experiments	23
2.3.2 Concentration time series and kinetic parameter estimation . .	24

Table of contents

2.3.3	Interpretation of pH-dependence of biotransformation rate constants	28
2.3.4	Interpretation of sorption coefficients	31
2.3.5	Environmental relevance	32
3	Systematic exploration of biotransformation reactions of amine-containing micropollutants in activated sludge	35
3.1	Introduction	36
3.2	Materials and methods	39
3.2.1	Micropollutant selection	39
3.2.2	Biotransformation test system	39
3.2.3	Analytical method	40
3.2.4	Transformation product identification by suspect and non-target screening	40
3.2.5	Structure elucidation	41
3.2.6	Assignment of biotransformation reactions	41
3.3	Results and discussion	43
3.3.1	Biotransformation reactions	48
3.3.1.1	N-oxidation	48
3.3.1.2	α -C-hydroxylation and subsequent N-dealkylation, oxidation to amides, or dehydration to iminium species	49
3.3.1.3	N-acylation of secondary and primary amines	51
3.3.1.4	Further biotransformation reactions	54
3.3.1.5	Metabolic logic	56
3.3.2	Implications for pathway prediction	57
3.3.3	Environmental relevance	59
4	Conclusions and outlook	61
4.1	pH-dependent biotransformation	62
4.2	Biotransformation reactions	63
4.3	Outlook	66
4.4	Proposal for a research project	67
	Appendix A: supporting information to Chapter 2	69
	Appendix B: supporting information to Chapter 3	89
	Appendix C: list of abbreviations	301
	Literature	305
	Curriculum vitae	319

Summary

A variety of organic micropollutants (MPs) enter wastewater treatment plants (WWTPs). Conventional activated sludge (CAS) treatment is one of the most important treatment steps to reduce the MP load to receiving water bodies. However, the removal of MPs during wastewater treatment is often not complete, and can lead to the formation of stable transformation products (TPs). Evidence is increasing that the receiving aquatic ecosystems are negatively affected by anthropogenic chemicals. To reduce the risk originating from the mixture of countless MPs and their TPs which are discharged from WWTPs, wastewater treatment can either be adjusted to yield a better removal of MPs, or prevalent MPs that have a high risk potential (either themselves or through TPs) can be restricted or banned by authorities. Both approaches rely on a better understanding of what influences the removal of MPs and which TPs are formed during activated sludge treatment. Several studies that tried to investigate these processes for a limited set of structurally diverse MPs have shown that studying MPs with a confined set of structural features is a necessary complement to obtain a more fundamental understanding and, hence, more predictive power. The amine functional group is highly abundant in wastewater-relevant MPs and most of the amine-containing MPs are polar organical compounds. The pH-dependent speciation of these compounds is an important aspect also relevant for many other functional groups in polar organic MPs. For these compounds, the most relevant removal process during CAS treatment is biotransformation, whereas sorption is known to be of minor importance.

Therefore, the following research questions were addressed within this thesis: How does pH influence biotransformation and what kind of biotransformation reactions occur for amine-containing MPs during activated sludge treatment?

To study the influence of pH, biotransformation experiments as well as sorption and abiotic control experiments were conducted for 15 amine-containing MPs with cationic-neutral speciation, one control MP with neutral-anionic speciation, and two neutral MPs. The experiments were performed in bioreactors seeded with a single activated sludge microbial community, which were then adjusted to pH 6, 7, and 8. Samples were analyzed by liquid-chromatography high-resolution tandem mass spectrometry (LC-HR-MS/MS) to yield concentration time series. From these, biotransformation rate constants corrected for sorption and abiotic processes, as well as sorption coefficients, were estimated with Bayesian inference. We found that biotransformation is pH-dependent and correlates with the neutral fraction of the ionizable MPs, which agrees with the assumption that uptake of the neutral species into the cells is favored. However, quantitatively, the data suggested a slight attenuation relative to the simple speciation model. Therefore, additional mechanisms where the ionic species also plays a role were discussed. Furthermore, sorption was found to be of minor importance for the investigated polar organic MPs and no notable pH-dependency was observed. From this, we concluded that pH-dependent biotransformation is more likely than pH-dependent sorption to cause variability in the removal of polar, ionizable MPs during activated sludge treatment.

The exploration of initial biotransformation reactions of amine-containing MPs was achieved by conducting experiments with 19 MPs that contained 25 structurally diverse primary, secondary, and tertiary amine moieties in activated sludge-seeded bioreactors. Samples taken as a time series were analyzed with an LC-HR-MS/MS instrument. By means of suspect and non-target screening, 144 TP candidates were identified. The structure of 101 of these were elucidated and associated with initial biotransformation reactions, which were interpreted relative to existing knowledge about mammalian metabolism. We found that biotransformation mostly led to the parallel formation of several TPs with N-oxidation, N-dealkylation, N-acetylation, and N-succinylation reactions being the major reaction paths. Especially the oxidative reactions were in line with what is known from mammalian metabolism of amines, including dependencies on electronic and steric features. The data further suggest that rarely reported TPs, namely N-succinylated, N-malonylated, and N-fumarylated TPs might be formed during activated sludge treatment. Pathway prediction systems play a crucial role in

facilitating the identification of TPs in the aquatic environment by generating a list of predicted TPs from all of the relevant biotransformation reactions for suspect screening purposes.

Therefore, we generalized our findings on initial biotransformation reactions to make suggestions on how to improve the prediction of TPs of amine-containing xenobiotics, especially with the Eawag-PPS, which is the former University of Minnesota Pathway Prediction System (UM-PPS). We suggest that all amine biotransformation reactions that were judged as important, namely N-oxidation, N-dealkylation, N-acetylation, and N-succinylation are implemented. Additionally, we assigned likelihood levels to these reactions to express the difference in metabolic relevance of predicted biotransformations.

Overall, our results provide a mechanistic understanding of how the effects of pH influence biotransformation of polar, ionizable MPs as well as a comprehensive picture about initial biotransformation reactions and resulting TPs of amine-containing MPs during activated sludge treatment. Thus, this thesis contributes to the overall understanding of how operational parameters influence the removal of MPs and what transformation reactions occur during wastewater treatment. Such knowledge is crucial to properly explore potential approaches to mitigate the risk caused by the presence of MPs and their TPs in the aquatic environment.

Summary

Zusammenfassung

Zahlreiche organische Mikroschadstoffe (Micropollutants, MPs) von verschiedenster Art und Herkunft gelangen in Kläranlagen. Dort ist das konventionelle Belebtschlammverfahren eine der wichtigsten Behandlungsstufen, um die Belastung des aufnehmenden Gewässers mit MPs zu verringern. Die Abwasserreinigung kann jedoch oft keine komplette Entfernung von MPs bewirken und sogar zur Bildung von stabilen Transformationsprodukten (TPs) führen. Immer mehr Anzeichen deuten darauf hin, dass die aufnehmenden Gewässer durch diese anthropogenen Chemikalien negativ beeinflusst werden. Um das von der Mischung aus unzähligen MPs und TPs ausgehende Risiko zu verringern, können entweder die Verfahren der Abwasserreinigung erweitert werden, um damit die Entfernung der MPs zu verbessern, oder MPs, die selbst oder durch ihre TPs ein hohes Potential haben aquatischen Ökosystemen zu schaden, können von Behörden eingeschränkt oder verboten werden. Für beide Herangehensweisen ist ein besseres Verständnis dessen nötig, was die Entfernung von MPs beeinflusst und welche TPs bei der Abwasserreinigung entstehen. Die Ergebnisse mehrerer Studien, die versucht haben diese Prozesse für strukturell vielfältige MPs zu untersuchen, zeigen, dass es vorteilhaft sein könnte, MPs mit einer eingeschränkten Menge an strukturellen Merkmalen zu untersuchen, um die Vorgänge grundlegend zu verstehen und somit Vorhersagen zu ermöglichen. Die funktionelle Gruppe der Amine ist in abwasserrelevanten MPs sehr oft zu finden. Ihre pH-abhängige Speziierung ist ein wichtiges Merkmal, das auch für viele andere funktionelle Gruppen in polaren organischen MPs relevant ist. Die meisten aminhaltigen MPs sind polare organische Chemikalien. Für diese ist Biotransformation der wichtigste zur Entfernung führende Prozess während des Belebtschlammverfahrens. Sorption hingegen ist für polare Substanzen von geringer Bedeutung.

Deshalb wurden in dieser Doktorarbeit die folgenden Forschungsfragen gestellt:

Wie beeinflusst der pH den Bioabbau aminhaltiger MPs? Und welche Transformationsreaktionen finden während des Belebtschlammverfahrens statt?

Um den Einfluss des pHs zu untersuchen, wurden Biotransformationsexperimente sowie Sorptionskontroll- und abiotische Kontrollexperimente mit 15 aminhaltigen MPs mit kationisch-neutraler Speziierung, einer Kontrollsubstanz mit neutraler-anionischer Speziierung und zwei neutralen Substanzen durchgeführt. In den Experimenten wurden Bioreaktoren mit einer einzigen mikrobiellen Klärschlammgemeinschaft befüllt und der pH auf 6, 7 und 8 eingestellt. Die Proben wurden mit Flüssigchromatographie-hochauflösender-Massenspektrometrie (liquid-chromatography high-resolution tandem mass spectrometry, LC-HR-MS/MS) analysiert, um Konzentrationszeitreihen zu erhalten. Aus diesen wurden mittels Bayesscher Inferenz Abbaugeschwindigkeitskonstanten bestimmt, die um Sorptions- und abiotische Prozesse korrigiert wurden, sowie Sorptionskoeffizienten ermittelt. Wir fanden heraus, dass Biotransformation pH-abhängig ist und mit dem neutralen Anteil der ionisierbaren MPs korreliert. Dies stimmt mit der Annahme überein, dass die Aufnahme der neutralen Spezies in die Zelle bevorzugt wird. Eine quantitative Betrachtung hingegen deutet darauf hin, dass der Effekt in den Daten im Vergleich zu diesem einfachen Speziierungsmodell leicht abgeschwächt ist. Deshalb wurden weitere Mechanismen diskutiert, in denen die ionische Spezies auch eine Rolle spielt.

Des Weiteren stellte sich heraus, dass Sorption für die untersuchten polaren, organischen MPs von geringer Bedeutung und zudem keine nennenswerte pH-Abhängigkeit der Sorption beobachtet wurde. Zusammenfassend lässt sich daraus schliessen, dass pH-abhängige Biotransformation eher zu Schwankungen in der Entfernung von polaren, ionisierbaren MPs während der biologischen Reinigungsstufe führt als pH-abhängige Sorption.

Transformationsreaktionen von aminhaltigen MPs wurden in Experimenten mit Klärschlamm befüllten Bioreaktoren untersucht. Hierbei wurden 19 MPs verwendet, die insgesamt 25 strukturell diverse primäre, sekundäre und tertiäre Amingruppen enthielten. Proben wurden als Zeitreihe entnommen und mittels LC-HR-MS/MS gemessen. Unter Anwendung von Suspect- und Non-target-Screening Methoden wurden 144 TPs identifiziert. Die Struktur von 101 dieser TPs wurde aufgeklärt und Transformations-

reaktionen zugeordnet. Diese Transformationsreaktionen wurden im Vergleich zum bekannten Säugetiermetabolismus von Aminen interpretiert. Festzustellen war, dass durch Biotransformation meist verschiedene TPs gleichzeitig gebildet wurden, wobei N-oxidation, N-dealkylierung, N-acylierung und N-succinylierung die wichtigsten Reaktionspfade waren. Vor allem die oxidativen Reaktionen verliefen ähnlich wie im Säugetiermetabolismus wobei auch elektronische und sterische Einflüsse erkennbar wurden. Die Daten deuten darauf hin, dass bisher wenig beschriebene TPs wie N-succinylierte, N-malonylierte und N-fumarylierte TPs während des Belebtschlammverfahrens gebildet werden können. Abbauvorhersagesysteme spielen eine zentrale Rolle bei der Identifikation von TPs in der aquatischen Umwelt, da durch sie Listen mit vorhergesagten TPs für Suspect-Screening Methoden erstellt werden können. Um Vorschläge für eine verbesserte Vorhersage für aminhaltigen MPs zu machen, haben wir unsere Resultate über Transformationsreaktionen generalisiert. Im Speziellen haben wir uns auf das Abbauvorhersagesystem Eawag-PPS konzentriert, welches das ehemalige UM-PPS (University of Minnesota Pathway Prediction System) ist. Wir schlagen vor, alle als wichtig eingestuften Aminbiotransformationsreaktionen zu implementieren, nämlich N-oxidation, N-dealkylierung, N-acetylierung und N-succinylierung. Zusätzlich haben wir diesen Reaktionen Wahrscheinlichkeitslevel zugeschrieben, um die unterschiedliche metabolische Relevanz der vorhergesagten Reaktionen zum Ausdruck zu bringen.

Insgesamt liefert unsere Arbeit ein mechanistisches Verständnis dessen, wie der pH die Biotransformation von polaren, ionisierbaren MPs beeinflusst und bietet ein umfangreiches Bild über Transformationsreaktionen und entstehende TPs von aminhaltigen MPs während des Belebtschlammverfahrens. Damit trägt diese Arbeit zu einem verbesserten Verständnis der Einflüsse von betrieblichen Parametern auf die Entfernung von MPs und der ablaufenden Transformationsreaktionen während der Abwasserreinigung bei. Ein solches Wissen ist essentiell, um mögliche Handlungsansätze zur Minderung des von MPs und deren TPs ausgehenden Risikos in der aquatischen Umwelt sachgerecht zu untersuchen.

Chapter 1

Introduction

A variety of MPs such as pharmaceuticals, personal care products, and biocides enter WWTPs. There, a substantial amount of the MP load is removed. However, some MPs are persistent or only partly removed and thus released into the aquatic environment with the effluent of WWTPs.¹ Additionally, the removal of MPs during wastewater treatment does often not lead to full mineralization but rather to the formation of TPs. These TPs can be found along with untransformed MPs in the effluent of WWTPs and in the receiving water bodies.^{2,3} Evidence is increasing that the receiving water bodies are negatively affected by the mixture of anthropogenic chemicals.^{4–7} In principle, there are two possibilities to reduce the risk originating from the mixture of countless MPs and their TPs in the effluents of WWTPs. On the one hand, wastewater treatment can be adjusted or upgraded to yield better or even close to complete removal of MPs.⁸ On the other hand, the environmental risk of MPs can be evaluated and those that have a high potential to cause harm to aquatic ecosystems and are highly prevalent after wastewater treatment, could be restricted or even completely banned by authorities. In doing so, TPs that are formed during wastewater treatment should also be considered.⁹ Both approaches to mitigate harmful effects of wastewater-borne MPs on aquatic ecosystems critically rely on a better understanding of what influences the removal of MPs and what kind of TPs are formed during wastewater treatment.

1.1 Behavior of micropollutants during wastewater treatment

WWTPs were originally introduced and upgraded to remove solids, easily and moderately biodegradable organic matter, nutrients, and pathogens via physical, chemical, and biological processes.¹⁰ The additional need to also remove organic MPs emerged in the last decades.¹¹ Even though the WWTPs were not designed to remove MPs, they are partially successful in doing so. Most relevant for removal is thereby the activated sludge treatment, which is present in any conventional WWTP.^{1,12} However, due to the insufficient removal of some MPs and the formation of TPs, different optimization strategies are explored, such as advanced treatment processes like ozonation and activated carbon adsorption. However, besides being still in development, these treatments are costly and require maintenance on a high technological level, which hinders their

broad implementation. Therefore, it is important to understand the removal processes of MP within conventional activated sludge treatment, both to address the resulting environmental exposure and hence risk, as well as to explore possibilities to improve their removal.

1.1.1 Removal efficiencies and influencing factors during activated sludge treatment

Removal efficiencies of structurally diverse MPs vary strongly within the same conventional activated sludge (CAS) system,^{13,14} which indicates that the structural features of MPs have a strong influence on their removal. Relevant removal processes during activated sludge treatment are biotransformation, sorption to excess sludge, and volatilization. The latter two are physical processes and their importance for the removal of different MPs can be predicted by the physico-chemical properties that are determined by the structure of the MPs. Sorption to sludge is important for hydrophobic MPs and can be predicted with reasonable accuracy by the solid-water distribution coefficient (K_d).^{15–17} Volatilization is important for volatile compounds and can be characterized by the Henry's law constant (K_H).¹⁸ Biotransformation, on the contrary, is important for non-volatile, polar organic MPs, which are the majority of MPs entering WWTPs.¹⁹ Biotransformation is a more complex process and is governed by the ability of the activated sludge microbial community to take up and biotransform the individual MPs.

In an attempt to correlate biotransformability of MPs with the presence of specific structural features, Tadkaew *et al.* (2011) examined 24 polar, structurally diverse MPs.¹⁷ They divided functional groups into either electron donating or electron withdrawing to analyze the effect the groups had on biotransformation. One of their conclusions was that electron withdrawing groups such as amides are poorly biotransformed. This contrasts a more systematic investigation on 30 amide-containing compounds by Helbling *et al.* (2010),²⁰ where it was found that sterically less hindered primary and secondary amides are hydrolyzed rather readily while the biotransformation of sterically hindered and tertiary amides was relatively slow. Since the amides contained in the substance set of Tadkaew *et al.* were all tertiary amides, the observations are actually in accordance with the ones of Helbling *et al.* However, the generalized con-

clusion of Tadkaew *et al.* that all amides are biotransformed slowly was not correct. The presumable misinterpretations of Tadkaew *et al.* are caused by the attempt to interpret the influence of too many structural features on the biotransformability of the corresponding MPs at once, without a detailed understanding of the occurring processes.

Another attempt to connect the presence of structural features with the biotransformability of the corresponding MPs is made in the BIOWIN tool. This is a computer-based quantitative structure biodegradability relationship (QSBR) program that estimates the biodegradability of MPs based on activities that are related to substructures and physico-chemical properties.^{21–23} While results of biotransformation experiments with 19 priority substances agreed with predictions of this program,¹³ inconsistencies between predicted and experimentally determined biodegradability were found within a study investigating the removal of 18 pharmaceuticals and personal care products.²⁴ The latter finding does not necessarily come as a surprise, since variations in removal of individual compounds over different CAS systems were found to be large,^{1,14} highlighting that not only the MP structures dictate compound-specific removal efficiencies, but that also other factors, such as operational parameters, play an important role. Such factors can influence the efficiencies of biotransformation in two ways, namely (i) by influencing the biotransformation capability of the microbial community (*e.g.*, longer solid retention time is reported to facilitate the buildup of more slowly growing bacteria, such as nitrifying bacteria, which are reported to have a positive effect on the removal of MPs such as ibuprofen, naproxen, trimethoprim, erythromycin, galaxolide, tonalide, ethinylestradiol, bisphenol A, nonylphenol, bezafibrate, fluoxetine, citalopram, triclosan);^{1,25–29} and (ii) by changing the characteristics of the MPs (*e.g.*, pH influences the degree of speciation of ionizable MPs). Thus, operational parameters might influence biotransformation efficiencies to varying extents by one or both mechanisms mentioned.

The majority of studies that investigated the influence of operational parameters on removal efficiencies were conducted with a small number of structurally diverse MPs in a rather empiric way. The outcomes of those studies rarely lead to results that can be generalized. For example, certain redox conditions, such as aerobic and anaerobic conditions, were found to be beneficial for the removal of some MPs, but unfavorable for others.^{1,26,30–35}

In conclusion, operational parameters can have a strong influence on the removability of MPs. However, to assess their influence, a mechanistic understanding is required to assess how these parameters in combination with the structural features of MPs affect the removal.

One important operational parameter is pH, for which the influence on the characteristic of MPs is obvious. In activated sludge compartments of different WWTPs the pH can vary by nearly two pH units; across 10 Swiss WWTPs it was reported that the pH ranged from 6.2 to 8.1.¹⁴ Such a difference has a direct effect on the degree of speciation for ionizable MPs. Thus, the degree of speciation of MPs with a pK_a value in the range of 5-9 (like compounds containing amine or carboxylic acid moieties) will vary strongly in different CAS systems.

1.1.2 Transformation reactions during activated sludge treatment

A variety of TPs from known MPs can be found in the effluent of WWTPs as well as in receiving water bodies.^{2,3} Since TPs have the potential to be as or more toxic than their parent MPs,^{3,36} they need to be considered when evaluating the two presented possibilities to reduce the risk originating from anthropogenic compounds. To do so, it is beneficial to know about major occurring transformation reactions rather than relying on being able to comprehensively analyze emerging TPs. This is due to the following reasons: First, it is challenging to detect and analyze TPs without *a priori* knowledge (often referred to as *non-target screening*) due to their presence at low concentrations in complex environmental matrices. Therefore the method of choice for the identification of TPs is *suspect screening*, wherein LC-HR-MS/MS data are screened for the exact masses of expected candidate TPs. To generate a list of such suspect TPs, knowledge about likely transformation reactions is important. This information can be catalogued and made easily accessible through pathway prediction systems.^{2,37} Second, another benefit of having information about likely transformation reactions is that it can also readily be integrated into risk assessment of new MPs before they are being released. This is especially true when this information is easily accessible and well organized as provided by pathway prediction systems.³⁸ And finally, when exploring different treatment options to achieve a better removal of anthropogenic compounds,

it is important to consider not only the unaltered MPs but also the TPs that might be formed. As slight changes in treatment conditions can lead to the formation of different TPs,³⁹ it is important to know what transformation reactions occur under the different treatment conditions and ideally to also understand how changes within the treatment processes influence the most likely occurring transformation reactions.

Up to now, the majority of information about microbial transformation reactions has been obtained under conditions that are not necessarily representative of activated sludge treatment, namely in pure culture studies where the compound of interest is the sole or major carbon and energy source. These data might be useful to indicate what kind of transformation reactions can possibly occur within the mixed microbial community, but they need to be further tested under relevant conditions. Some information is available on transformation reactions in activated sludge from studies exploring the fate of selected MPs (assembled in²). However, these data are not yet sufficient to yield a comprehensive understanding of what transformation reactions are likely to occur at the different structural moieties present in MPs.

1.2 Pertinent structural features

1.2.1 Why focus on one specific functional group?

As discussed in the previous section, the various structural features that are commonly present in polar organic MPs are one reason why gaining a better understanding of how operational parameters influence the removal of MPs and what kind of transformation reactions are most likely to occur is difficult. Therefore, reducing the number of variables, *i.e.*, by focusing on a confined set of structural features, is a helpful strategy when studying biotransformation of MPs. Focusing on MPs with one specific, pertinent functional group will improve the understanding of biotransformation reactions at this moiety and will potentially also foster a more fundamental understanding of what conditions are influencing removal of MPs containing this functional group. If this is done step by step for different common functional groups, a comprehensive picture of MP biotransformation can emerge.

1.2.2 The amine functional group

Organic MPs are made up of a carbon backbone that might consist of different saturated and unsaturated aliphatic and aromatic parts, and usually one or several heteroatom-containing functional groups such as alcohols, phenols, ethers, carbonyls, carboxylic acids, esters, amines, amides, urea derivatives, thioethers, phosphates, haloalkanes and other more complex systems.

Amongst the various functional groups present in wastewater-relevant MPs, compounds bearing an amine functional group are particularly abundant. According to Manallack (2009), about 32.7% of pharmaceuticals, which are a dominant substance class in wastewater influents,⁴⁰ hold at least one amine functional group.⁴¹ According to Verlicchi *et al.* (2012), 32 out of 48 pharmaceuticals discharged in highest amounts through secondary effluents, and 28 out of 51 pharmaceuticals assessed to show highest risk are amines.⁴² Similarly, our own analysis of functional groups present in 461 wastewater-relevant contaminants showed that amine functional groups are present in around 20% of all compounds and are amongst the most frequently found heteroatom-containing functional groups, besides haloalkanes, ethers, and amides (Helbling, personal communication).

Amines are derivatives of ammonia, where one to three hydrogen atoms are replaced by alkyl or aryl groups. Depending on the number of alkyl or aryl substituents, they are called primary, secondary, or tertiary amines when holding one, two, or three substituents, respectively. The lone pair of the nitrogen atom leads to several characteristic features of amines. Amine moieties undergo nucleophilic addition or substitution reactions, are rather polar, act as hydrogen bond acceptors and, in the case of primary and secondary amines, also hydrogen bond donors, and are able to bind protons yielding cationic species with typical pK_a values of the protonated species of 5-10. Therefore, amine-containing MPs are ionizable with a cationic-neutral speciation within the typical pH range of most environmental compartments and in particular the activated sludge compartment. Speciation in the environmentally relevant pH range has been shown to lead to pH-dependence of the environmental fate, but also the toxicity of ionizable compounds.^{43–46}

Furthermore, amines are ubiquitous in biological systems. For example, they are released through the breakdown of amino acids, they are components of neurotrans-

mitters and the primary amine moiety of lysine is important for the three-dimensional structure of proteins. Thus, reactions involving the amine functional group are very common in living cells. Therefore, it is likely that organisms possess enzyme systems that transform natural amine functional groups, which potentially might also act on amine functional groups of MPs. Such reactions are elaborately reported for mammalian systems^{47–52} and were also observed for microbial systems.⁵³ However, a systematic study on how this functional group is biotransformed by a mixed microbial community in activated sludge is missing.

1.3 Goals

The overall goal of this thesis is to contribute to a better understanding of factors influencing the removal of MPs and the transformation reactions that occur during wastewater treatment. To do so, we focused on (i) conventional activated sludge treatment because it is worldwide one of the most used treatment processes and hence an important barrier for organic MPs released into wastewater; (ii) MPs containing one specific functional group because the reduced number of structural features improves our ability to mechanistically interpret and generalize our observations; and (iii) pH as an operational parameter since it influences the degree of speciation of ionizable MPs. In particular, we investigated biotransformation of amine-containing MPs since the amine moiety is highly abundant in wastewater-relevant MPs and its pH-dependent speciation is representative for many other functional groups. Specifically, the following two research question were addressed in this thesis:

How does pH influence biotransformation of amine-containing MPs during activated sludge treatment (Chapter 2)?

What biotransformation reactions occur for amine-containing MPs during activated sludge treatment (Chapter 3)?

Chapter 2 describes how biotransformation and sorption of 15 amine-containing MPs with cationic-neutral speciation, two neutral MPs, and one MP with neutral-anionic speciation are affected at three different pH levels, namely pH 6, 7, and 8.

Chapter 3 describes the investigation of initial microbial transformation reactions of 19

parent compounds that contain 25 structurally diverse tertiary, secondary, and primary amine moieties.

1.4 Methodological approach

1.4.1 Compound selection

For this thesis, compounds were selected that, on the one hand, contain structurally diverse primary, secondary, and tertiary amine functional groups, and, on the other hand, were environmentally relevant, *i.e.*, by being pharmaceuticals, pesticides, and other wastewater-relevant chemicals. Some of the selected MPs also have other heteroatom-containing functional groups, such as alcohols, halogen substituents, ethers, and amides. However, care has been taken to select compounds that contained no other functional groups that were suspected to react more readily than the amine functional groups themselves.

For testing the influence of pH on MP removal (Chapter 2), the MPs with cationic-neutral speciation were selected to hold aliphatic amine moieties with pK_a values ranging from 7 to 10. Additionally, control MPs were included in the study that were either neutral or exhibited neutral-anionic speciation in the relevant pH range.

For exploring biotransformation reactions (Chapter 3), aliphatic and aromatic amines were selected with varying structural features around the amine moieties.

1.4.2 Laboratory-based batch experiments

Laboratory-based experiments were conducted, where batch reactors were seeded with activated sludge collected from a full-scale WWTP. This enabled investigations under relevant conditions with the following additional benefits: (i) sorption and abiotic control experiments could be conducted in parallel, so the different processes contributing to observed removal could be distinguished; (ii) treatment conditions, such as pH and temperature, could be controlled, and hence the influence of these parameters could be investigated; (iii) test MPs could be added in slightly elevated concentrations so samples could be measured without the need for an enrichment step prior to analysis while maintaining quasi-realistic concentrations; (iv) biotransformation kinetics could be determined since samples could be collected at defined time intervals and spiked

and unspiked reactions could be compared.

However, the drawback of this method is that ultimately the results observed still need to be verified in full-scale WWTPs. Unfortunately, this verification was out of scope of this thesis.

1.4.3 Chemical analysis based on liquid-chromatography high-resolution tandem mass spectrometry

Samples were analyzed by LC-HR-MS/MS since it allows for the efficient detection of a multiplicity of compounds in parallel and at low concentrations, with the additional benefit of obtaining evidence for structural interpretation.^{2,37,54} However, due to the simultaneous presence of environmental matrices, it is not trivial to identify signals that are related to MPs or their TPs among the large numbers of matrix-related signals. Therefore, additional information is required to enable identification of signals that are related to anthropogenic chemicals. There are three main approaches to identify those signals depending on the additional information available, namely *target screening*, *suspect screening*, and *non-target screening*.^{55,56} Within the *target screening* approach, known compounds for which a reference standards is available are covered. For these compounds the measured signals can be confirmed by comparison to the measured signals of the reference standards. Compounds included in a target screening can also be quantified by estimating the amount through comparison of the area of the signal to calibration standards with known concentrations. Within the *suspect screening* approach, peaks at the exact masses of expected compounds are screened for in the mass spectrum. At the moment, this is the method of choice for the identification of TPs in the environment. To do so, a list of suspected TPs is usually obtained from literature research or by using computational prediction tools.^{2,37} Within the *non-target screening* approach, additional information to identify signals being possibly related to TPs can be obtained for example by using statistical tools to identify parent-TP pairs in influent and effluent samples of WWTPs;⁵⁷ or by screening for emerging signals within a time series of samples taken from biotransformation experiments.⁵⁸

However, the identification of possible TP-related signals within the suspect or non-target screening approaches does not yet provide reliable information if a TP was truly found and which structure it has. Therefore, additional LC-HR-MS/MS-based evidence

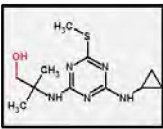
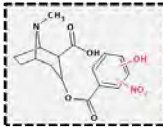
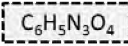
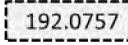
Example	Identification confidence	Minimum data requirements
	Level 1: Confirmed structure by reference standard	MS, MS ² , RT, Reference Std.
	Level 2: Probable structure a) by library spectrum match b) by diagnostic evidence	MS, MS ² , Library MS ² MS, MS ² , Exp. data
	Level 3: Tentative candidate(s) structure, substituent, class	MS, MS ² , Exp. data
	Level 4: Unequivocal molecular formula	MS isotope/adduct
	Level 5: Exact mass of interest	MS

Figure 1.1: Identification confidence levels as proposed by Schymanski *et al.*⁵⁹

that can be used for structural interpretation is helpful. However, the structural evidence and hence also the degree of confidence in the structural assignment of different TPs varies. To transparently communicate the confidence of structural assignment, a level system was proposed by Schymanski *et al.* (2014).⁵⁹ The different levels range from simply an *exact mass* (Level 5) through to *confirmed structure* (Level 1). They are explained together with the required structural data in Figure 1.1. Examples of TP structure elucidation from the work presented in this thesis were essential for developing the level system, and the level system is systematically applied to communicate the confidence in structural assignment throughout Chapter 3 of this thesis.

Chapter 2

pH-dependent biotransformation of ionizable organic micropollutants in activated sludge

Rebekka Gulde, Damian E. Helbling, Andreas Scheidegger, and Kathrin Fenner. pH-dependent biotransformation of ionizable organic micropollutants in activated sludge. *Environ. Sci. Technol.*, 48(23):13760-13768, 2014.

This paper was awarded as “Second runner-up for Best Paper in the Category Environmental Science” by the journal *Environmental Science and Technology* in 2014.

Abstract

Removal of MPs during activated sludge treatment can mainly be attributed to biotransformation and sorption to sludge flocs, whereby the latter process is known to be minor for polar organic micropollutants. In this work, we investigated the influence of pH on the biotransformation of MPs with cationic-neutral speciation in an activated sludge microbial community. We performed batch biotransformation, sorption control, and abiotic control experiments for 15 MPs with cationic-neutral speciation, one control MP with neutral-anionic speciation, and two neutral MPs at pHs 6, 7, and 8. Biotransformation rate constants corrected for sorption and abiotic processes were estimated from measured concentration time series with Bayesian inference. We found that biotransformation is pH-dependent and correlates qualitatively with the neutral fraction of the ionizable MPs. However, a simple speciation model based on the assumption that only the neutral species is efficiently taken up and biotransformed by the cells tends to overpredict the effect of speciation. Therefore, additional mechanisms such as uptake of the ionic species and other more complex attenuation mechanism are discussed. Finally, we observed that the sorption coefficients derived from our control experiments were small and showed no notable pH-dependence. From this we conclude that pH-dependent removal of polar, ionizable organic MPs in activated sludge systems is less likely an effect of pH-dependent sorption but rather of pH-dependent biotransformation. The latter has the potential to cause marked differences in the removal of polar, ionizable MPs at different operational pHs during activated sludge treatment.

2.1 Introduction

A variety of organic MPs are conveyed by sanitary sewers or by surface runoff and storm water sewers to WWTPs where they are partially removed during activated sludge treatment.^{12,60} The extent of removal within a WWTP is known to vary among different MPs due to different chemical properties, as well as for single MPs between different WWTPs.^{10,12} The latter case is attributed to differences in operational parameters of the WWTPs such as total suspended solids concentration (TSS), solids and hydraulic retention times, dissolved oxygen, temperature, and pH.⁶¹ However, so far no single operational parameter has been identified that can explain differences

in removal efficiency for a range of MPs between different WWTPs.¹⁴ Rather, there might be varying degrees of influence of the operational parameters on the removal efficiency of different MPs. Because a complex mixture of only partially removed MPs in WWTP effluents can negatively affect water quality,⁶² it is of interest to understand how operational parameters influence MP removal.

The pH of activated sludge systems in WWTPs is one such operational parameter and can vary by nearly two pH units; across 10 Swiss WWTPs, the pH of activated sludge samples ranged from 6.2 to 8.1.¹⁴ At the same time, many MPs entering the WWTPs contain ionizable functional groups with pK_a values within that pH range. For instance, around 40% of pharmaceuticals, which are a dominant substance class in wastewater influents,⁴⁰ contain at least one functional group with pK_a values in the range of 5-10 and cationic-neutral speciation,⁴¹ and about 10% contain at least one functional group with neutral-anionic speciation in the same pK_a range. Thus, the degree of speciation of such ionizable MPs will vary across activated sludge systems with different operational pHs.

Previous studies have shown that the removal efficiency for MPs with ionizable functional groups is pH-dependent.⁶³⁻⁶⁵ Removal during activated sludge treatment can mainly be attributed to biotransformation and sorption to activated sludge. Because chemical speciation can influence sorption as well as biotransformation, both processes could potentially lead to pH-dependent removal.

pH-dependent sorption of organic MPs to activated sludge was studied previously for MPs with neutral-anionic speciation.^{63,64} For these MPs, a decrease in sorption affinity was observed at higher pH levels where the fraction of anionic species is increased. The surface of activated sludge flocs is predominantly negatively charged.⁶⁶ As a result, it is assumed that the sorption affinity is weakened at higher pH levels by the increased solubility of the charged species in water and the increased electrostatic repulsion between the negatively charged MPs and the activated sludge flocs. pH-dependent sorption of MPs with cationic-neutral speciation is considerably less well understood. In this case, it is more difficult to formulate expectations on how sorption affinities change with pH, due to several contributing factors. First, the negative charge of the sludge flocs is expected to decrease with decreasing pH,⁶⁶ while the fraction of positively charged compounds increases with decreasing pH for MPs with cationic-neutral speciation. Hence, the extent of electrostatic interaction of the cations with

the negatively charged flocs could already result in different pH-trends depending on the particular speciation behavior of the sludge and the MP in question. Second, positively charged compounds exhibit not only an increased electrostatic interaction with the predominantly negatively charged flocs, but are also more water-soluble than the corresponding neutral species, which are opposing trends. Third, other factors like the ionic strength and the ionic composition of the bulk medium are known to affect the sorption affinity of the cationic species as well.^{67,68} Therefore, it is not surprising that some studies observed no systematic trend of the sorption behavior of MPs with cationic-neutral speciation with pH,^{69,70} whereas other studies did.⁷¹ Finally, although the sorption affinity of ionizable MPs may vary in the pH range of 6-8, the majority of MPs entering the WWTPs are rather polar¹⁹ with sorption coefficients (K_d) typically < 300 L/kg.⁷² It has therefore been suggested that sorption is not a significant process for the removal of polar organic MPs in WWTPs.¹⁵ Consequently, we do not expect sorption to cause a significant pH-dependence in overall removal.

Rather, several possible effects of pH-induced chemical speciation on MP biotransformation seem plausible. If the enzymes responsible for biotransformation are extra-cellular, chemical speciation could influence the interaction affinity between MPs and enzymes because enzymes often have high affinities for only one species of a given substrate. For example, ammonia monooxygenase can utilize NH_3 as a substrate but not NH_4^+ , which is thought to explain the known pH-dependence of nitrification.^{73,74} In the case of MP removal through oxidative transformation, the majority of enzymes are expected to be intracellular because of their dependence on enzymatic co-factors and their coupling to the electron transfer chain. Thus, in the more likely case of intracellular biotransformation, chemical speciation might directly affect uptake efficiency since charged species are less likely to permeate cell membranes.⁷⁵ This mechanism is also commonly used to explain observations of pH-dependent toxicity of ionizable compounds, for which it was shown that toxicity typically increases under pH conditions where the majority of the compound is present as neutral species.⁴⁵

All three studies⁶³⁻⁶⁵ that examine pH-dependent removal of ionizable MPs in WWTPs so far investigated MPs with neutral-anionic speciation. In those studies, a clear pH-dependence was observed, with increasing removal efficiencies at lower pHs where the neutral fraction of the MPs is higher. Although in the three studies additional experiments were conducted to account for sorption, it remained difficult to clearly

disentangle the effects of pH-dependent biotransformation and sorption. All three studies concluded that the observed higher sorption affinities of the neutral species led to increased removal efficiencies. But only Tadkaew *et al.* (2010) explicitly considered sorption to sludge and subsequent withdrawal of excess sludge as the mechanism behind the observed pH-dependent removal. In contrast, Urase and Kikuta (2005) as well as Kimura *et al.* (2010) interpreted sorption as a necessary first step in the biotransformation process. Thus, they seemed to suggest that close proximity to the cells and subsequently, enhanced uptake into the cells explains the observed pH-dependence.

The difficulty in investigating the underlying mechanism of pH-dependent removal of MPs with neutral-anionic speciation is that the pH-dependence of sorption and the pH-dependence of permeation through the cell membrane are aligned; namely, both processes show increasing efficiencies at lower pH levels. In this study, we focused on MPs with cationic-neutral speciation instead for two reasons. First, to our knowledge, the effect of varying pH on the removal of these MPs has not been explored so far. Second, the expected different effects of pH on sorption and biotransformation of compounds with cationic-neutral speciation might help to distinguish the contribution of these two processes on pH-dependent removal of ionizable MPs in general. The goal of our research was to gain a more mechanistic understanding of the effect of varying pH on the biotransformation of ionizable, polar MPs. Specifically, we hypothesize that the biotransformation of MPs with cationic-neutral speciation correlates with their degree of speciation due to increased uptake efficiency of the neutral species, resulting in an increased biotransformation efficiency at higher pH levels. To test this hypothesis, we first performed biotransformation experiments, as well as sorption and abiotic control experiments, for 15 MPs with cationic-neutral speciation, two neutral MPs, and one MP with neutral-anionic speciation in a single activated sludge microbial community adjusted to three different pH levels. The latter three compounds were included to confirm that chemical speciation rather than a direct effect of pH on sludge viability and structure was the major reason for any observed pH-dependence. We then quantified the pH-dependence of the biotransformation rate constants corrected for abiotic and sorption processes for all 18 MPs, and finally discuss the results in light of the potential underlying mechanisms.

2.2 Materials and methods

2.2.1 Micropollutant selection

We selected 18 environmentally relevant MPs including 15 that undergo cationic-neutral speciation, one that undergoes neutral-anionic speciation, and two MPs that remain predominately neutral in the pH range investigated. Chemical structures as well as pK_a values are presented in Table 2.1. All MPs with cationic-neutral speciation contain an amine functional group. The pK_a of seven of these MPs was in the usual range for aliphatic amines between 9.1 and 10.0 (atenolol, mexiletine, pheniramine, primaquine, pyrilamine, propranolol, and venlafaxine). The other eight amines were selected to exhibit a lower pK_a in the range between 6.9 and 8.4 (1-(3-chlorophenyl)piperazine, deprenyl, lidocaine, mianserin, nicotine, orphenadrine, pargyline, and pramoxine). The MP with neutral-anionic speciation is trinexapac-ethyl. The two neutral MPs, azoxystrobin and isoproturon, were selected to control for direct effects of pH changes on the viability, structure, and sorption capacity of the activated sludge. MPs were purchased from Dr. Ehrenstorfer GmbH (Augsburg, Germany), Sigma-Aldrich Chemie GmbH (Buchs, Switzerland), Lipomed AG (Arlesheim, Switzerland), and Toronto Research Chemicals (Toronto, Canada).

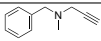
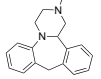
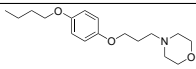
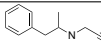
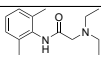
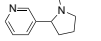
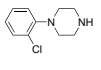
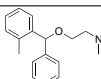
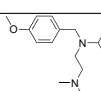
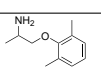
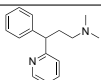
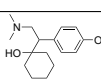
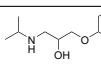
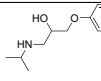
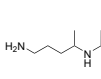
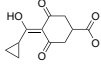
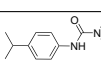
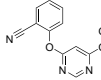
2.2.2 Biotransformation test system

The experimental set-up for the biotransformation batch experiments was adopted from Helbling *et al.* (2010a).⁵⁸ pH adjustment was done as described in Wick *et al.* (2009).²⁸ The combined experimental set-up used in this study is given in the following. Activated sludge (2.5 L) was sampled from the nitrification basin of a half municipal and half industrial WWTP (ARA Neugut, Dübendorf, Switzerland) and was diluted with tap water (1 L), resulting in a TSS of approximately 2 g_{SS}/L (g_{SS}: gram suspended solids). This sludge was used for three different experiments, namely the biotransformation experiments (BEs), the sorption control experiments (SEs), and the abiotic control experiments (AEs). Each experiment was conducted at three pH levels in triplicate.

For the BEs, reactors (100 mL amber Schott bottles) were filled with 50 mL activated sludge and stirred at 130 rpm on a multiple stir plate. Air or air/CO₂ (Carbagas,

Table 2.1: Compound ID, Compound Name, Structure, pK_a Values with Reference

* Charge state of ionic species.

	ID	Name	Structure	pK_a
cationic*	PAR	Pargyline		6.9 ⁷⁶
	MIA	Mianserin		6.9 ⁷⁷
	PRA	Pramoxine		7.1 ⁷⁷
	DEP	Deprenyl		7.5 ⁷⁸
	LID	Lidocaine		8.0 ⁷⁸
	NIC	Nicotine		8.2 ⁷⁸
	CHLO	1-(3-chlorophenyl) piperazine		8.4 ⁷⁹
	ORP	Orphenadrine		8.4 ⁸⁰
	PYR	Pyrilamine		9.1 ⁷⁸
	MEX	Mexiletine		9.1 ⁸¹
	PHE	Pheniramine		9.3 ⁷⁶
	VEN	Venlafaxine		9.4 ⁸⁰
	PRO	Propranolol		9.6 ⁷⁸
	ATE	Atenolol		9.6 ⁷⁸
	PRI	Primaquine		10.0 ⁸¹
anionic*	TRI	Trinexapac-ethyl		4.8 ⁸²
neutral	ISO	Isoproturon		
	AZO	Azoxystrobin		

Gümligen, Switzerland) mixtures were distributed via lines that were connected with a Luerlock to a syringe tip (diameter: 0.6 mm, length: 8 mm, Carl Roth AG). The syringe tip was inserted into one of two holes in the cap of the batch reactors and adjusted to near the bottom of the reactors. Stirring and bubbling air through the medium ensured continuous mixing and aeration. CO₂(g) was mixed at different ratios with pressurized air using rotameters (Aalborg, Orangeburg, USA). The mixing ratios were adjusted manually to establish approximate pH values of 6 and 7 in the respective reactors. Bubbling of air without additional CO₂ was used in the remaining reactors to establish a pH value of approximately 8. BEs were started earliest one hour after pH adjustment and within six hours of activated sludge sampling. Then, 100 µL of a MP mix solution (50 mg/L each in methanol:ethanol:DMSO 16:3:1) were spiked into each batch reactor, resulting in final concentrations of 100 µg/L for each MP. Kern *et al.* (2010)⁸³ showed that biotransformation kinetics derived from similar batch experiments, in which the MP concentration was also roughly three orders of magnitude higher than in actual sewage, were appropriate to predict measured mass flows in actual WWTPs. Furthermore, we assume that by treating all reactors in the same way the comparison of kinetic parameters amongst pH values was still valid, even if the addition of the organic carbon of the solvent or other batch reactor adjustments might have caused a shift of the microbial community and/or the introduction of the MPs as a mixture instead of single MPs might have altered individual rate constants. Triplicate time zero samples were taken within five minutes after spiking. Subsequent samples were withdrawn at approximately 2h, 4h, 8h, 1d (in triplicate), 1.5d, 2d, 3d, and 4d after the start of the experiment. At each time point, samples (approx. 1.5 mL) were withdrawn from the reactor with a 10 mL glass syringe, transferred to a centrifuge tube (1.7 mL Safeseal Microcentrifuge Tubes, Sorenson Bioscience, Inc.), and centrifuged for 10 minutes at approximately 13000 g (14000 rpm, ALC, micro centrifuge 4214). The supernatants (0.5 mL) were transferred into 2 mL amber vials and stored between 1 hour and 10 days at 4°C in the dark until analysis. One unspiked reactor at each pH level was used for preparing matrix-matched, pH-specific external calibration rows by adding 50 µL standard solutions (mixture of MPs at various concentrations in methanol) to 950 µL samples. Additionally, compensation of evaporated water was done and operational parameters, including pH, temperature, TSS, and oxygen uptake rates, were measured. Details on the methods and the results

are given in Chapter A.1 in Appendix A.

The SEs and AEs were processed in the same way as the BEs except for the following: For the SEs, reactors (100 mL amber Schott bottles) filled with 50 mL activated sludge were autoclaved twice (24 hours apart) at 121°C and 103 kPa for 20 minutes. Triplicate samples of each SE reactor were taken once, approximately two hours after the start of the experiment. For the AEs, reactors (100 mL amber Schott bottles) were filled with 50 mL activated sludge filtrate (sterile filter: 0.2 µm, Sartorius Stedium, Göttingen, Germany) and autoclaved in the same way. Samples were taken at 0h (in triplicate), 4h, 1d, 2d, and 3d after start. Additional reactors were used to prepare matrix-matched, pH-specific external calibration rows for the SEs and AEs at each pH level.

2.2.3 Analytical method

For chemical analysis, reversed-phase liquid chromatography coupled to a high-resolution quadrupole orbitrap mass spectrometer (Qexactive, Thermo Scientific) was used. We adopted an analytical method from Kern *et al.* (2009)⁸⁴ and adjusted it. Details are reported in Chapter A.2 in Appendix A. Briefly, sample separation was achieved by running a gradient of nanopure water (Barnstead Nanopure, Thermo Scientific) and methanol (HPLC-grade, Fisher Scientific), both augmented with 0.1% formic acid (98-100%, Merck), over a C18 Atlantis-T3 column (particle size 3 µm, 3.0x150 mm, Waters). Detection was done by full scan acquisition (resolution of 70000 and scan range of 50-750 m/z) followed by three data-dependent MS/MS scans (resolution of 17500) in electrospray ionization positive-negative switch mode. A matrix blank and a matrix-matched, pH-specific external calibration row over a range from 5 to 100 µg/L with six calibration points were measured prior to the sample series of the corresponding experiments. The lowest calibration point of 5 µg/L was treated as the limit of quantification (LOQ). The triplicate time zero samples of each reactor were used to calculate the method precision with respect to sampling and analysis. The relative recoveries were determined from the time zero samples of the AE reactors.

2.2.4 Estimation of kinetic parameters

In order to compare biotransformation rate constants for a given MP between different pH levels, the observed transformation rate constants were corrected for sorption and abiotic processes with help of the control experiments. To do so, a model describing the contribution of all three processes to the observed decrease of the aqueous concentration of individual MPs was adopted from Helbling *et al.* (2010b).²⁰

$$C_{\text{aq}}(t) = C_{\text{aq}}(0) \exp[-f_{\text{aq}}(k_{\text{bio}}TSS + k_a)t] \quad (2.1)$$

where $C_{\text{aq}}(0)$ is the initial aqueous concentration, k_{bio} the suspended solids concentration-normalized biotransformation rate constant of the dissolved compound fraction f_{aq} , and k_a the abiotic transformation rate constant. For the sake of a simplicity, equation 2.1 is expressed with the dissolved compound fraction f_{aq} instead of the sorption coefficient K_d of the original equation. The two parameters can be related to each other by considering the total suspended solids concentration TSS

$$K_d = \frac{1 - f_{\text{aq}}}{f_{\text{aq}}TSS} \quad (2.2)$$

with the fraction f_{aq} defined as

$$f_{\text{aq}} = \frac{C_{\text{aq}}}{C_t} \quad (2.3)$$

where C_t is the total concentration of the compound.

Because various sources of uncertainty had to be taken into account while estimating the kinetic parameters, a Bayesian model allowing for a combination of information in the data with prior knowledge about the parameters was constructed. Equation 2.1 was applied to model the concentrations measured in the BEs and AEs according to equations 2.4 and 2.5.

$$C_{\text{aq}}^{p,e,r}(t) = C_{\text{aq}}^{p,e,r}(0) \exp[-\alpha^{p,e}t] + \epsilon^{p,e,r,t} \quad (2.4)$$

with

$$\alpha^{p,e} = \begin{cases} k_a^p & \text{if } e = \text{AE} \\ f_{\text{aq}}^p (k_{\text{bio}}^p TSS^p + k_a^p) & \text{if } e = \text{BE} \end{cases} \quad (2.5)$$

where the index $e \in \{\text{BE}, \text{AE}\}$ distinguishes biotransformation and abiotic control experiments, $p \in 6, 7, 8$ distinguishes the three pH-levels, and $r \in 1, 2, 3$ the three replicates. For every pH-level, values for k_{bio}^p , k_a^p , f_{aq}^p , and TSS^p were inferred across all replicates, while the initial concentration $C_{\text{aq}}^{p,e,r}(0)$ was inferred separately for every single experiment to account for varying spike levels. For further details see Chapter A.4 in Appendix A.

The model was implemented in JAGS⁸⁵ version 3.4.0. JAGS provides Markov chain Monte Carlo samples from the posterior distribution of the parameters. Five chains of 35000 samples were generated of which the first 5000 were removed as “burn-in”, and thereafter every 10th sample saved for analysis. Each chain was visually inspected to check for convergence. Median as well as 5% and 95% percentile values were calculated for k_{bio} , K_d , and k_a from sample values for each MP and each pH level. The resulting 90% intervals represent parametric, conceptual, and measurement errors. In order to estimate the quality of the fit, root-mean-square error (RMSE) values were calculated for each MP at each pH level.

2.3 Results and discussion

2.3.1 Operating conditions in pH-controlled batch experiments

The average pH values for the three pH levels 6, 7, and 8 measured in triplicate BE reactors over time were 6.3 ± 0.3 , 7.1 ± 0.2 , and 8.1 ± 0.2 , respectively. For further analysis, these effective pH values were used, labeled as pH6, pH7, and pH8 (see Chapter A.1 for more details). The oxygen uptake rates measured on the first day of the experiments at pH6, pH7, and pH8, were -20.8 ± 0.6 mg/(L h), -44.8 ± 1.0 mg/(L h), and -40.8 ± 1.1 mg/(L h), respectively. The value at pH6 was approximately half of the values measured at pH7 and pH8. This indicates that the low pH may have directly

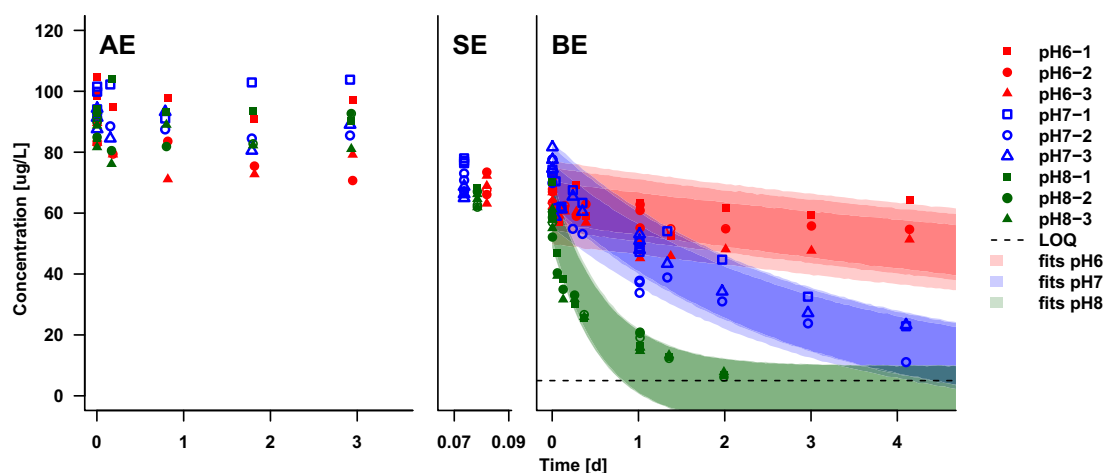


Figure 2.1: Concentration time series of the abiotic control experiments (AEs), the sorption control experiments (SEs), and the biotransformation experiments (BEs) for propranolol. Each experiment was conducted at pH6 (red symbols), pH7 (blue symbols), and pH8 (green symbols) in triplicate (squares, circles, or triangles). The dashed line at 5 µg/L indicates the limit of quantification (LOQ) below which all measurements were censored. The shaded areas show the 90% credibility intervals of the model fit to the biotransformation data. The intervals represent parametric, conceptual, and measurement errors and are shown for each replicate.

affected the activity of at least some members of the microbial community. A strong reduction in activity below 6.7 is, for instance, well-described for nitrifying bacteria.⁸⁶ Therefore, in the following analysis, while the experimental data were analyzed for all pH levels, it needs to be kept in mind that k_{bio} values at pH6 might be biased towards low values. This point will be revisited when examining the pH-dependence of the k_{bio} values of the neutral control MPs.

2.3.2 Concentration time series and kinetic parameter estimation

The concentration time series from the AEs, SEs, and BEs at the three different pH levels, as shown in Figure 2.1 for propranolol and for all test compounds in Figure A.3-A.8 in Appendix A, show good precision and agreement between replicates (for details on the method precisions and relative recoveries see Chapter A.2.1 and A.2.2, respectively, in Appendix A). The AE data for propranolol show hardly any disappear-

ance over time, indicating little abiotic transformation. The same was true for all other MPs, except for pargyline and deprenyl (Figures A.3 and A.4 in Appendix A). As is the case for propranolol in Figure 2.1, the concentrations in the SE were in good agreement with the initial concentrations in the BE for most test compounds. This indicates that autoclaving the sludge did not notably change its sorption capacity for the test chemicals. Furthermore, no noticeable differences in the SE concentrations at different pH levels is visible, indicating pH-independence of sorption. As for propranolol, the BE concentration time series of most MPs are clearly different at the three pH levels indicating a pH-dependence of biotransformation efficiency. This was more quantitatively evaluated by kinetic parameter estimation.

Modeling the concentration data by Bayesian inference was successful for all MPs. The quality of the fits can be assessed based on the 90% intervals indicated as shaded areas in the BE graphs (see Figure 2.1 and Figures A.3-A.8 in Appendix A), and by the average deviation of the predicted concentration values from the measured ones, which is discussed in Chapter A.4.1 in Appendix A. The kinetic parameter estimation yielded median, 5%, and 95% percentile values for k_{bio} and K_d , which are illustrated for all MPs in Figure 2.2 and 2.3, respectively, and are listed in Tables A.8 and A.9 in Appendix A. k_a values are given in Table A.10 in Appendix A.

As can be seen from Figure 2.2, k_{bio} values increased with increasing pH for cationic-neutral MPs, except for mianserin and nicotine, and decreased with increasing pH for the neutral-anionic compound trinexapac-ethyl. For a more precise assessment, we defined the effect of pH as significant if the probability for an increase in k_{bio} between adjacent values for cationic-neutral MPs or a decrease in k_{bio} between adjacent values for anionic-neutral MPs was greater than 97%. For neutral MPs both possibilities were tested to assess significance. In Figure 2.2, significant differences in k_{bio} between adjacent pH levels are marked with asterisks. In total, the effect of pH was significant for 23 out of 32 k_{bio} possible cases. By comparing the pH trend of the k_{bio} values with the trend of the neutral fraction (f_n), a qualitative correlation of the rate constants with the neutral fraction is clearly apparent. This finding is corroborated by the results for the two neutral MPs, for which the effect of pH on the k_{bio} values was not significant for three out of four pH changes. The only significant change was observed for azoxystrobin at pH6. This is in line with the observed reduced oxygen uptake rate at pH6, indicating a potential bias towards low k_{bio} due to a reduced microbial activity at pH6, which

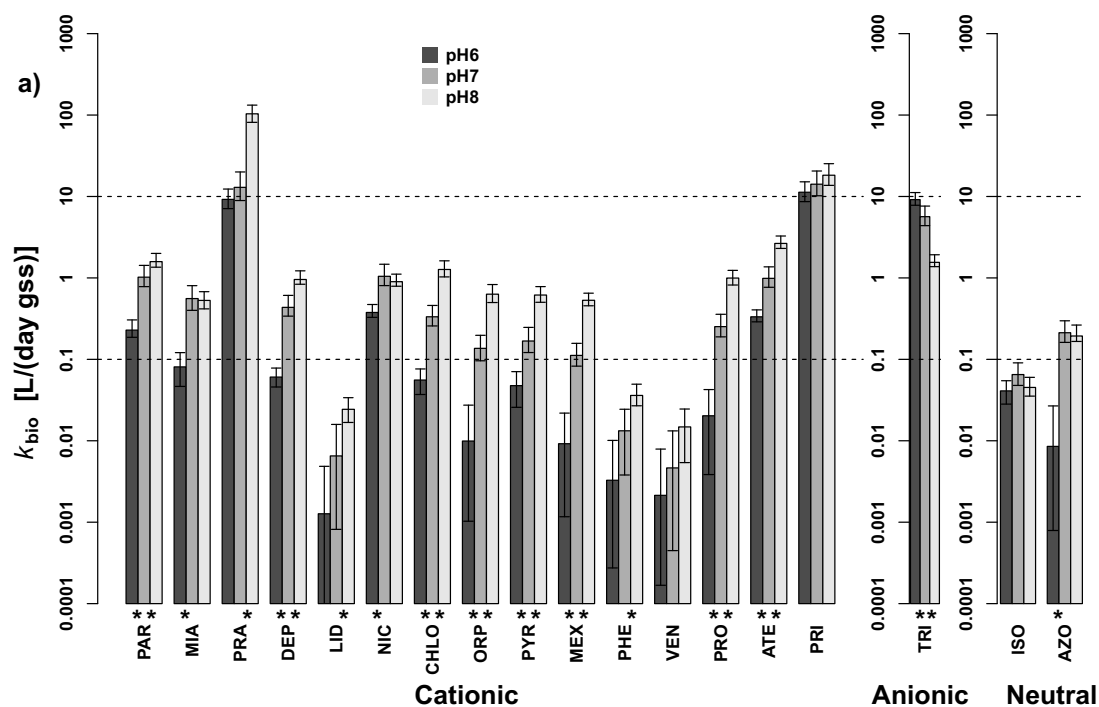


Figure 2.2: Comparison of biotransformation rate constants (k_{bio}) at pH6, pH7, and pH8. Cationic-neutral micropollutants (MPs) are ordered in order of increasing pK_a , followed by the neutral-anionic and the two neutral MPs. The error bars represent the 90% credibility intervals. The asterisks indicate a significant change of k_{bio} values between adjacent pH-levels (see main text for definition). The dashed lines represent a classification scheme proposed in⁸⁷, wherein $k_{bio} > 10$ L/(g_{SS} days) convert to significant removal (>90%), $k_{bio} < 0.1$ L/(g_{SS} days) convert to no removal (<20%), and k_{bio} values in-between convert to moderate removal of MPs in conventional wastewater treatment plants (WWTPs).

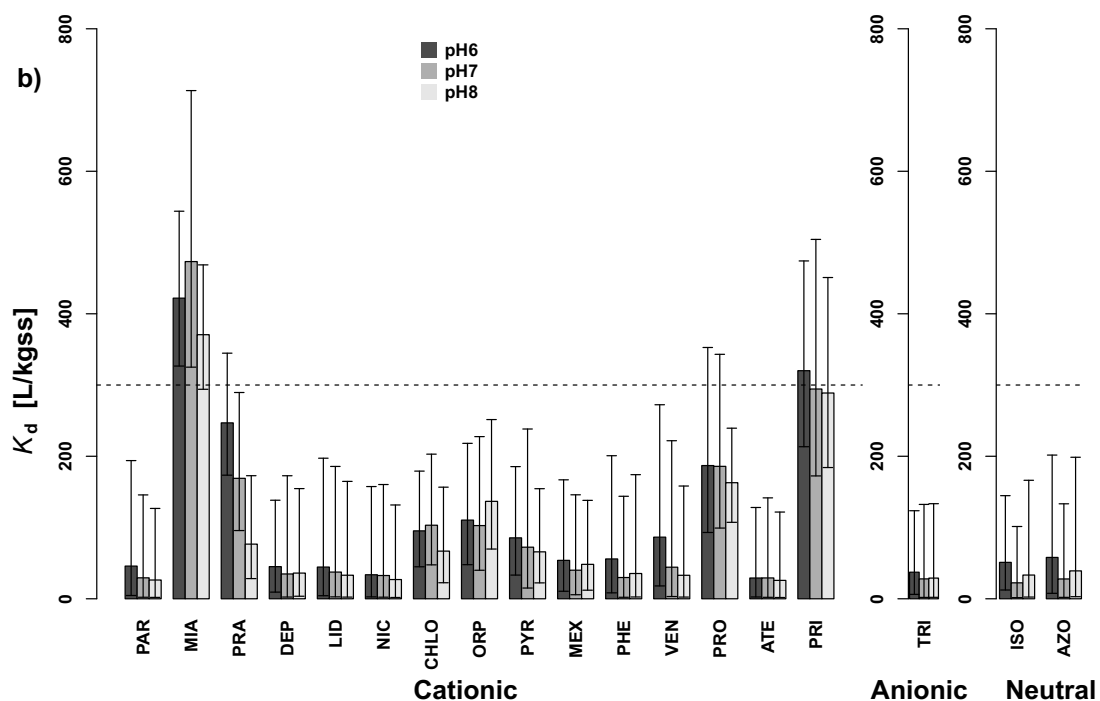


Figure 2.3: Comparison of sorption coefficients (K_d) at pH6, pH7, and pH8. Cationic-neutral micropollutants (MPs) are ordered in order of increasing pK_a , followed by the neutral-anionic and the two neutral MPs. The error bars represent the 90% credibility intervals. The dashed line represents a limit proposed in¹⁵, wherein for K_d below 300 L/kg_{SS} no removal through sorption to sludge and subsequent sludge withdrawal is expected in conventional WWTPs.

might affect certain biotransformation pathways such as the one of azoxystrobin. Due to this uncertainty at pH6, the following quantitative interpretation of the observed pH-dependence was restricted to pH7 and pH8, which is also the more relevant range for pH values commonly present in activated sludge systems at WWTPs.

2.3.3 Interpretation of pH-dependence of biotransformation rate constants

The simplest explanation for the qualitative correlation of k_{bio} with the neutral fraction of the ionizable MPs is that charged compounds are inhibited from permeating through the cell membranes and therefore the uptake into the cell is dominated by the uncharged species. This leads to a change in uptake efficiency as a function of pH and hence an apparent pH-dependence of the observed k_{bio} values. Thus, we analyzed the data under the following simple assumptions: i) pH- and pK_a -dependent speciation in the bulk aqueous phase is established instantaneously after addition of the test compounds; ii) only the neutral species permeates the cell membranes; iii) permeation equilibration is fast compared to biotransformation in the cell, which is the rate-determining step; and iv) the enzymatic transformation within the cell is independent of the external pH. Hence, the resulting k_{bio} values measured in the bulk aqueous phase are a function of the neutral fraction in the bulk phase, f_n , and the internal biotransformation rate constant, k_{int} as described in equation 2.6 for MPs with cationic-neutral speciation (an analogous calculation was done for the neutral-anionic MP).

$$k_{\text{bio}}(\text{pH}) = k_{\text{int}} f_n = \frac{k_{\text{int}}}{(1 + 10^{pK_a - \text{pH}})} \quad (2.6)$$

To compare this simple speciation model against our measured data, we examined the ratios of k_{bio} values measured at pH7 and pH8 since they are independent of the actual internal biotransformation rate constant (equation 2.7).

$$\text{ratio} = \frac{k_{\text{bio}}(\text{pH8})}{k_{\text{bio}}(\text{pH7})} = \frac{(1 + 10^{pK_a - \text{pH7}})}{(1 + 10^{pK_a - \text{pH8}})} \quad (2.7)$$

Figure 2.4 shows the comparison of predicted and experimentally determined ratios. The error bars represent the 90% credibility intervals, which were calculated for the predicted ratios by Monte Carlo Simulation, *i.e.*, by evaluating equation 2.7 15,000

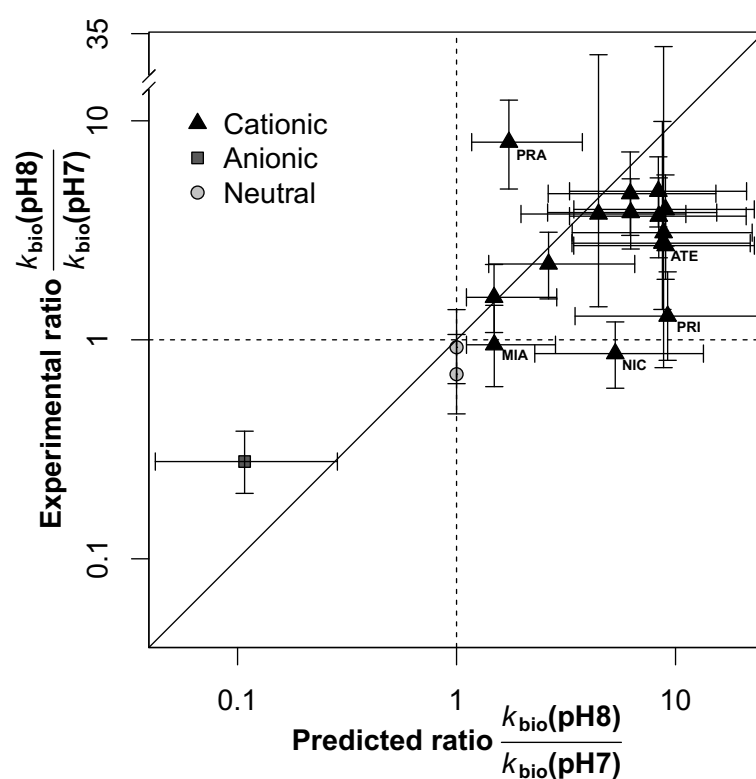


Figure 2.4: Ratios between the biotransformation rate constants (k_{bio}) at pH8 and at pH7 as determined experimentally and predicted for all micropollutants (MPs). The predictions were based on the assumption that only the neutral fraction in the bulk aqueous phase permeates through cell membranes and is therefore biotransformed. The dashed lines separate MPs with k_{bio} values that are decreasing (ratios < 1) and increasing (ratios > 1) from pH7 to pH8. The 1:1-line indicates a perfect match between the predicted and experimental ratios. The error bars represent the 90% credibility intervals of the ratios. The credibility intervals of the five labeled MPs (PRA, MIA, NIC, PRI, ATE) do not overlap with the 1:1-line.

times with randomly sampled values for pK_a and pH. For pK_a , a normal distribution around its literature value with a standard deviation of 0.3 was assumed, and the pH distribution was modeled as a normal distribution with mean and standard deviation as determined experimentally. Because the effective pH values between pH7 and pH8 differ by exactly one unit, the predicted ratios (shown on the x-axis of Figure 2.4) can only vary from 1 to 10 for the cationic-neutral MPs, from 0.1 to 1 for the neutral-anionic MP, and are expected to be 1 for the neutral MPs.

As can be seen from Figure 2.4, the 90% credibility intervals of 13 out of 18 compounds overlap with the 1:1-line, indicating considerable agreement between the experimental and predicted ratios of k_{bio} between pH7 and pH8. The five MPs that do not overlap with the 1:1-line are mianserin, pramoxine, nicotine, atenolol, and primaquine. Pramoxine is the only cationic-neutral MP where the ratio of k_{bio} between pH7 and pH8 is considerably underpredicted by the simple speciation model. Pramoxine possesses a comparably small pK_a value of 7.1 and is therefore already partially neutral at pH7. Thus, a rather small increase in k_{bio} from pH7 to pH8 was expected. However, the measured increase was one of the largest and no obvious explanation was found for this observation. For all other MPs with cationic-neutral speciation, the experimentally determined ratio tend towards lower values than the simple speciation model predicts. This is most evident for the remaining four outliers. The opposite trend is observed for the neutral-anionic MP trinexepac-ethyl, which shows a higher experimental ratio compared to the predicted ratios. This means that the simple model is overpredicting the effect of speciation. In other words, the predicted increase in the MPs' degree of speciation in the bulk aqueous phase was more than the observed pH-dependence of the rate constants. Furthermore, when analyzing the relative difference between the predicted and observed ratio of k_{bio} at pH7 and pH8 as a function of pK_a (see Figure A.9 in Appendix A), we observe increasing relative differences with increasing pK_a . This suggests that, most likely, the contribution of the ionic species to the observed k_{bio} values is underestimated by the simple speciation model. A similar attenuation of the observed effect compared to the degree of speciation has also been observed in other studies investigating the uptake of ionizable compounds into cells.^{43,44,88}

Thus, the simple speciation model seems to neglect some relevant mechanisms. We acknowledge that some of the assumptions in our speciation model are rather simplistic and the mechanisms are known to be more complex. Specifically, with respect to

assumption ii), charged compounds are also known to permeate cell membranes, but to a lesser extent than the neutral species.⁷⁵ As to assumption iii), it is discussed that prior to diffusion through the membrane molecules have to diffuse through an unstirred water layer; this step may be part of the rate-determining step and may be similarly fast for neutral and charged species.⁴³ Regarding assumption iv), the transformation within the cell might not be fully independent of the external pH.⁸⁹ While all of these mechanisms can attenuate the effect of a MP's degree of speciation on its biotransformation, our data are currently not sufficient to determine which of these processes occur and how much they contribute.

2.3.4 Interpretation of sorption coefficients

Although the SEs were designed as controls to correct the k_{bio} values for sorption, we also used them to investigate the potential contribution of sorption to pH-dependent removal of ionizable, polar MPs at the scale of conventional WWTPs. Therefore, we examined the estimated K_d values as shown in Figure 2.3 and listed in Table A.9 in Appendix A. As can be seen in Figure 2.3, the 90% credibility intervals between the different pH levels overlap for all MPs and the median values typically differ by less than a factor of 2. Two conclusions can be drawn based on this observation. First, the lack of pH-dependent sorption affinities for the seven MPs that have a $\text{p}K_a > 9$ and are therefore nearly completely ($>90\%$) positively charged at all pH levels indicates that the possible increased protonation of the sludge organic matter at lower pH does not have a relevant influence on the sorption behavior of cationic amines. Second, the lack of pH-dependent sorption affinities for the five MPs that have a $\text{p}K_a \leq 8$ and hence experience substantial changes in speciation over the three pH levels indicates that the sorption affinity of the charged species does not differ considerably from that of their corresponding neutral species. A similar observation was also made by Droge and Goss, who examined the effect of pH on the sorption affinities of compounds with cationic-neutral speciation to natural organic matter at different electrolyte compositions.⁶⁷ They observed close to pH-independent sorption affinities if the ionic strength (150 mM) and especially the concentration of divalent inorganic cations (50 mM CaCl_2) was high. Ionic strength was lower in our experiments at about 15 mM with a concentration of divalent inorganic cations of about 3.5 mM. However,

since the type of solid organic matter and the test compounds were also different in our experiment, it remains difficult to argue whether the ionic composition can rationalize the observed lack of pH-dependence.

Generally, we observed low sorption coefficients for our test compounds. The K_d values for 16 out of 18 investigated MPs were below 300 L/kg, which is considered the lower limit for sorption to be a relevant removal process at the scale of conventional WWTPs.¹⁵ However, these values need to be treated with caution since our experiments were carried out with MP concentrations that were roughly three orders of magnitude higher than those typically found in WWTPs. Therefore, our K_d values are expected to be lower than those observed under more realistic conditions. In conclusion, while our more hydrophobic test compounds could experience some removal due to sorption to sludge and subsequent withdrawal of excess sludge at the WWTP, our data suggest that such a removal by sorption would not show a notable pH-dependence.

2.3.5 Environmental relevance

Regarding the removal of ionizable organic MPs in the activated sludge system of a full-scale WWTP, our results highlight some important aspects. First, measured sorption coefficients were typically small indicating that any pH-dependent removal of polar, ionizable organic MPs during activated sludge treatment is more likely an effect of pH-dependent biotransformation than of pH-dependent sorption. This stands in contrast to previous suggestions that variations in sorption to sludge explain pH-dependent removal of MPs with neutral-anionic speciation.^{63–65} Second, biotransformation rate constants did qualitatively correlate with the neutral fraction of the analyzed MPs, but the pH-dependence was not as strong as predicted with a simple speciation model, which assumes that only the neutral species permeate through cell membranes and are therefore biotransformed. Thus, our understanding of the process is not yet sufficient to suggest re-calculating rates observed at one pH value to other pH values. Nevertheless, it can be expected that the qualitative trend of pH-dependent biotransformation of ionizable MPs is reflected in their removal efficiencies. Thus, a one-unit pH increase could promote MPs with cationic-neutral speciation from showing no removal to showing moderate removal (see the classification limits proposed by Joss *et al.* (2006) in Figure 2.2⁸⁷). Since close to 50% of pharmaceuticals contain ionizable

functional groups in the relevant pK_a range, the observed variability in the removal of pharmaceuticals and other ionizable MPs during activated sludge treatment could be partially caused by pH-dependent biotransformation. Therefore, pH-dependent biotransformation should be considered along with other possible factors such as other operating parameters of WWTPs or sludge community composition when interpreting variability in the removal of ionizable organic MPs across different WWTPs.

Acknowledgment

We thank the operators and staff of the WWTP ARA Neugut for providing activated sludge samples. Additionally, we thank Dr. Adriano Joss for fruitful discussions. Funding for this project was provided by the Swiss National Science Foundation (project 200021_134677).

Chapter 3

Systematic exploration of biotransformation reactions of amine-containing micropollutants in activated sludge

Rebekka Gulde, Ulf Meier, Emma L. Schymanski, Hans-Peter E. Kohler, Damian E. Helbling, Samuel Derrer, Daniel Rentsch, and Kathrin Fenner. Systematic exploration of biotransformation reactions of amine-containing micropollutants in activated sludge. *Environ. Sci. and Technol.* 2016.

Abstract

The main removal process for polar organic MPs during activated sludge treatment is biotransformation, which often leads to the formation of stable TPs. As the analysis of TPs is challenging, the use of pathway prediction systems can help by generating a list of suspected TPs. To complete and refine pathway prediction, comprehensive biotransformation studies for compounds exhibiting pertinent functional groups under environmentally relevant conditions are needed. As many polar organic MPs present in wastewater contain one or several amine functional groups, we systematically explored amine biotransformation by conducting experiments with 19 compounds that contained 25 structurally diverse primary, secondary, and tertiary amine moieties. Identification of 144 TP candidates and structure elucidation of 101 of these resulted in a comprehensive view on initial amine biotransformation reactions. The reactions with the highest relevance were N-oxidation, N-dealkylation, N-acetylation, and N-succinylation. While many of the observed reactions were similar to those known for the mammalian metabolism of amine-containing xenobiotics, some N-acylation reactions were not previously described. In general, different reactions at the amine functional group occurred in parallel. Finally, recommendations on how these findings can be implemented to improve microbial pathway prediction of amine-containing MPs are given.

3.1 Introduction

Organic MPs such as the active ingredients of pharmaceuticals, personal care products, and pesticides are conveyed by sanitary sewers or by surface runoff and storm sewers to WWTPs. There, the main removal process for polar organic MPs is microbial biotransformation in the activated sludge compartment.^{12,15} However, most MPs are not fully mineralized, but rather biotransformed to TPs, which are then released with the WWTP effluents into the aquatic environment.^{3,90,91} It has been shown that some TPs have the potential to be as or even more toxic than their parent MPs, and thus contribute to the toxicological effects of anthropogenic chemicals on aquatic ecosystems.^{36,39,54,92,93} To comprehensively assess the risk of MPs, it is therefore desirable to also determine the occurrence and prevalence of their TPs in environmental water bodies. However, due to their presence at low concentrations in complex environ-

mental matrices, the detection and identification of unknown TPs or MPs in general is challenging. Recently, screening for expected compounds in a so-called suspect screening approach has been successfully applied in different environmental matrices, e.g., wastewater effluents, lake sediments, and surface waters.^{2,56,94–96}

In order to generate a list of expected TPs for suspect screening, pathway prediction systems are helpful.^{37,84} Currently freely available systems for the prediction of microbial biotransformation reactions for given parent MPs include PathPred,⁹⁷ CRAFT,⁹⁸ the OECD toolbox,⁹⁹ and the EAWAG-PPS. The EAWAG-PPS derives from the former University of Minnesota pathway prediction system (UM-PPS),^{100,101} and is now hosted by Eawag, the Swiss Federal Institute of Aquatic Science and Technology.¹⁰² The predictions of these tools are mainly based on a set of generalized biotransformation rules extracted from literature-reported, microbially mediated metabolic pathways and enzyme-catalyzed reactions. Biotransformation rules recognize functional groups present in the query compound structure and predict transformation reactions at these functional groups.¹⁰⁰ Currently, rule-based pathway prediction systems are generally sensitive, but of rather poor selectivity when validated with observed TPs from environmental simulation or monitoring studies. This means that the systems predict most of the observed TPs, but also many others. Therefore, the number of false positives increases rapidly, resulting in combinatorial explosion when the rules are applied iteratively to predict consecutive steps of biotransformation reactions.¹⁰³ There are two potential reasons. First, the biotransformation rules corresponding to the different functional groups are based on too little microbial biotransformation data and are not refined to account for specific structural factors around the functional group. Second, the majority of available microbial pathways are not specified on environmental conditions but are rather based on pure culture studies or ready biodegradability assays, where the compound of interest serves as sole or major carbon source. Thus, the derived biotransformation rules might include reactions that are unlikely to occur under environmentally relevant conditions, where the MPs that are present in trace concentrations are most likely turned over co-metabolically by mixed microbial communities.¹⁰⁴

Comprehensive biotransformation studies conducted under environmentally relevant conditions for a set of structurally diverse compounds could help overcoming these limitations. A systematic set of initial transformation reactions observed for a given

pertinent functional group can be used to improve prediction by refining the specificity of existing biotransformation rules, both in terms of structural features that affect the likelihood of certain types of reactions and by learning about previously not implemented reactions that occur under relevant conditions. Such endeavors have recently become much more accessible through the development of efficient workflows using LC-HR-MS/MS to screen for suspect and non-target TPs formed in biotransformation studies.^{20,58}

Primary, secondary, and tertiary amine functional groups are highly abundant in wastewater-relevant MPs, such as the active ingredients of pharmaceuticals.⁴¹ From the extensive exploration of the mammalian metabolism of xenobiotics, three main reactions that involve the amine functional groups are known, namely (i) N-oxidation, leading to the formation of N-oxides for tertiary amines, and to the formation of hydroxylamines for secondary and primary amines; (ii) α -C-hydroxylation, leading to unstable hemiaminals that are either spontaneously cleaved to a carbonyl and an amine product by a so-called N-dealkylation reaction, oxidized to amides, or dehydrated to iminium species; and (iii) conjugation reactions such as N-acetylations for secondary and primary amines. The corresponding data were assembled by Testa *et al.*^{47–51} who elaborated on the corresponding enzymatic systems, mechanistic details, and structural and electronic features that influence the different types of reactions. All three main reactions have been observed in microbial systems.⁵³ These and additional data on other functional groups suggest that microbial transformation reactions of MPs are similar to those observed in the mammalian metabolism of xenobiotics, even though individual major products for certain MPs might differ.^{53,83,92,105} Overall, it can be hypothesized that the microbial metabolism of amine-containing MPs will be similar to that of mammalian systems.

The objective of our research was to elucidate biotransformation pathways of a set of structurally diverse amine-containing compounds in an environmentally relevant microbial system to obtain a consistent set of initial microbial transformation reactions involving the amine functional group. The observed reactions should then be rationalized by comparison to mammalian systems and generalized to suggest biotransformation rules for improved prediction of microbial biotransformation of amine-containing MPs. To do so, we performed systematic biotransformation experiments in activated sludge-seeded bioreactors under environmentally relevant conditions with 19 parent

compounds that contain altogether 25 different primary, secondary, and tertiary amine moieties. First generation TP candidates were identified by LC-HR-MS/MS-based approaches, and the corresponding TP structures were elucidated where possible, with confidence levels assigned as proposed by Schymanski *et al.* (2014).⁵⁹ Reactions were assigned to observed parent-TP pairs and compared with the known mammalian biotransformation reactions of amines. Finally, generalized rules for biotransformation reactions were extracted for tertiary, secondary, and primary amines.

3.2 Materials and methods

The following is a concise presentation of materials and methods; full details are given in the Appendix B.

3.2.1 Micropollutant selection

Environmentally relevant compounds (e.g., pharmaceuticals, pesticides, and other wastewater-derived chemicals) were selected to cover a variety of primary, secondary, and tertiary amine functional groups, and as few as possible other functional groups that were expected to be readily biotransformed. The final set of 19 test compounds contained 25 amine moieties, including 13 tertiary, eight secondary, and four primary ones. All names and chemical structures are given in Table 3.1. Additionally, five N-oxide TPs (of PHE, VEN, LID, DEP, and PAR) were also included in the biotransformation experiments.

3.2.2 Biotransformation test system

The experimental setup for the biotransformation batch experiments was adopted from Helbling *et al.* (2010).⁵⁸ Activated sludge (3 L) was sampled from the nitrification basin of a half municipal and half industrial WWTP (ARA Neugut, Dübendorf, Switzerland). Reactors (100 mL amber Schott bottles) were filled with 50 mL activated sludge and spiked with 60 µL compound solution (100 mg/L in methanol:water 1:9) to a final concentration of 120 µg/L for each individual compound. The 19 amine-containing compounds were split into two groups, which were spiked separately in two reactors. Additionally, each parent compound was spiked in individual reactors. One reactor was

spiked with a mixture containing the five N-oxide TPs. Samples (1.5 mL) were taken at approximately 0 h, 2 h, 4 h, 8 h, 1 d, 1.5 d, 2 d, 3 d, and 4 d after the start of the experiment and centrifuged. The supernatants (0.5 mL) were stored at 4 °C in the dark until analysis for a maximal duration of 10 d. Additional sorption and abiotic control experiments were conducted to test for abiotic processes.

3.2.3 Analytical method

For chemical analysis, reversed-phase liquid chromatography coupled to a high-resolution quadrupole Orbitrap mass spectrometer (Q Exactive, Thermo Scientific) was used. The analytical method from Gulde *et al.* (2014)¹⁰⁶ was adjusted as follows: Three data-dependent MS² scans were conducted after each full-scan in positive or positive-negative ionization switch mode. The dynamic exclusion was set to 7 s for acquisition in positive mode and to 3 s for acquisition in positive-negative switch mode. Data-dependent MS² were triggered on all selected parent compounds and a list of candidate TP masses, which was assembled from previously found TPs in similar unpublished experiments, EAWAG-PPS predictions,¹⁰² metaprint2D predictions,¹⁰⁷ and by manually applying a range of plausible atomic modifications. For all identified TP peaks, additional MS² measurements were conducted later with a Q Exactive or Q Exactive Plus instrument (Thermo Scientific). In individual runs for each TP, six targeted MS² scans were triggered after each full-scan in positive ionization-mode with normalized collision energies of 15, 30, 45, 60, 75, 90 (dimensionless).

3.2.4 Transformation product identification by suspect and non-target screening

For TP identification, the underlying principles from Helbling *et al.* (2010)⁵⁸ were applied using Compound Discoverer 1.0 (Thermo Scientific) for suspect and non-target screening and Sieve 2.2 (Thermo Scientific) for non-target screening. While we screened for a list of plausible TP candidates with the suspect screening approach, we used the non-target screening approach to discover additional TP candidate peaks. For both approaches, likely TP candidate peaks had to fulfill the following criteria in order to be selected for further analysis: (i) intensity above a set threshold; (ii) reasonable peak shape; (iii) presence in both treated reactors and absence or significantly

lower amounts in control reactors; (iv) TP-like time series pattern, *i.e.*, increase or increase and decrease over the time of the experiment; and (v) a reasonable chemical formula derived from the exact mass and the isotopic pattern (Details are given in Chapter B.1.4 in Appendix B). Identified TP candidate peaks were then integrated manually using Xcalibur 2.2 (Thermo Scientific) to yield time series of TP peak areas. Because the overall goal of this study was to explore and interpret the initial biotransformation reactions of amine-containing compounds, we focused our analysis on first generation TPs. Therefore, TPs were omitted from further analysis that were clearly higher generation products according to their time series patterns or initial structural evidence. TPs formed by multiple, sequential reactions would only be kept for further analysis if they pointed towards a specific initial reaction for which no first generation TP was observed.

3.2.5 Structure elucidation

Structure elucidation was conducted either with the Compound Discoverer 1.0 software or manually based on the interpretation of: (i) the exact masses and the isotopic patterns of the positive and, if available, negative MS spectra to propose chemical formulas; and (ii) the MS² fragments and neutral losses of the positive and, if available, negative MS² spectra to propose structural features. Afterwards, the interpretations were combined and further supported by the use of the MassFrontier 7.0 software (Thermo Scientific) to propose plausible TP structures. Apart from the confirmation of some TP structures through purchased or synthesized reference standards, the outcome and confidence of the structural interpretation could vary significantly due to the availability of varying structural evidence. To transparently communicate the confidence in our structural interpretation, we assigned confidence levels as proposed by Schymanski *et al.* (2014),⁵⁹ which ranged from Level 5 – *exact mass*, over Level 4 – *unequivocal molecular formula*, Level 3 – *tentative candidates*, and Level 2 – *probable structure*, to Level 1 – *confirmed structure*.

3.2.6 Assignment of biotransformation reactions

In order to interpret the results in terms of biotransformation reactions, it was necessary to assign reactions to observed parent-TP pairs. However, the certainty with which

a biotransformation reaction can be attributed depends on the confidence in the TP structure and whether or not the formation of the respective TP from the corresponding parent compound can unambiguously be attributed to a plausible reaction. We therefore classified the attributed reactions as *certain*, *likely*, *possible*, and *unknown*.

To assess the importance of different reactions in terms of how much of the parent compounds was biotransformed via a specific reaction, we considered the frequency with which a given reaction was observed and the amount of the respective TPs formed. This analysis was carried out separately for tertiary, secondary and primary amines. To assess the *relative frequency* of a reaction, we counted all first-generation TPs that were certain or likely to be formed through that specific reaction and related them to the number of TPs that could potentially have been formed via the same reaction. To assess the amounts of TPs formed, we determined the detected maximal peak area of each TP and related it to degree of biotransformation of the parent compound at that same time point (*i.e.*, the change in the peak area of the biotransformed parent compound between time zero and the time point of maximal peak area of the TP) to yield a so-called *maximal relative amount*. This procedure might be fairly uncertain due to the fact that TPs and parent compounds might have different ionization efficiencies. However, since the comparison of ionization efficiencies of 15 parent-TP pairs that were transformed by N-dealkylation and N-oxidation showed that the average difference in ionization efficiency was 1.5 (maximal: 3.1; Details are given in Chapter B.10 in Appendix B), it was considered sufficient to yield a rough estimate of the relative amount of TPs formed. To evaluate the overall importance of a given type of reaction, we summed the *maximal relative amounts* of all first-generation TPs that were *certain* or *likely* to be formed through the reaction of interest and divided it by the number of TPs that could have been formed through this reaction, resulting in a so-called *mean maximal relative amount*. It should be noted that the actual maximal relative amount of a TP can be much higher than the observed TP areas suggest since the TP might itself be further transformed to some extent. Therefore, we additionally characterized the time series patterns as *rising*, *rising and steady*, or *rising and falling* to qualitatively assess the stability of the TPs. However, we cannot fully exclude the occurrence of transformation reactions whose resulting TPs are so readily further transformed that we are not able to observe them.

3.3 Results and discussion

In total, 144 TPs were identified for the 19 investigated parent amines. Of these, 43 were omitted since they were likely higher generation TPs. For these, information on exact mass, retention time, and proposed elemental formula are given in Table B.10 in Appendix B. The structures of the remaining 101 TPs were elucidated and confidence levels were assigned. As a result, the structural confidence could be considered *confirmed* (Level 1) for 21 TPs, *probable* (Level 2b) for nine TPs, *tentative* (Level 3) for 68 TPs, whereas for three TPs only an *unequivocal molecular formula* (Level 4) could be assigned. The evidence for structure elucidation is given in Chapter B.4 in Appendix B and is electronically available in the MassBank database.¹⁰⁸

The biotransformation reactions that were assigned to the observed parent-TP pairs for reactions involving the amine functional group are listed in Table 3.1 together with their corresponding certainty, structural confidence level, *maximal relative amount*, degree of biotransformation of the parent compound at the time point where TP was maximal, and characterization of time series patterns. The same is given in Chapter B.8 in Appendix B for the remaining observed reactions that did not involve an amine moiety. Related further information can be found in Chapter B.6 in Appendix B, which contains maps of the biotransformation pathways for each parent compound, area time series of the parent compounds and their TPs, and the observed concentration time series for the parent compound in the abiotic control, the sorption control, and the biotransformation reactors.

For 18 parent amines (all except CLE), multiple biotransformation reactions were observed in parallel. No TPs were found for CLE, despite the presence of a secondary and primary amine and a decrease in parent concentration within the range of the other parent amines. For the remaining 18 parent compounds, between one and nine reactions that possibly involve the amine functional group were observed to occur in parallel. Besides those, additional reactions that did not involve the amine functional group were observed. This is in contrast to previous observations for amides, where for primary and secondary amides mostly only one type of reaction, namely hydrolysis, and only for tertiary amides multiple reactions were observed.²⁰

The two principal initial oxidative reactions at the amine functional group that are known from mammalian metabolism of xenobiotics were also observed for the acti-

vated sludge system, namely (i) N-oxidation, and (ii) α -C-hydroxylation followed by N-dealkylation, oxidation to amide, or dehydration to iminium species. Additionally, several N-acylation reactions, namely N-formylation, N-acetylation, N-propionylation, N-malonylation, N-succinylation and presumably desaturation to N-fumarylated products were observed, of which only N-acetylation is known from the mammalian metabolism of xenobiotics. These reactions will be discussed in detail in the following sections. A schematic illustration of all reactions involving the amine functional group is given in Chapter B.3 in Appendix B.

Additional observed reactions that did not involve the amine functional groups were O-demethylation, hydroxylation at groups other than the amine-N or the α -C, desaturation, oxidation of a hydroxylated product to a carbonyl or carboxylic acid product, dehydration of an aliphatic alcohol to an alkene, and combinations of several reactions including decarboxylation and β -oxidation. For some TPs, no plausible reactions leading to their formation could be assigned.

Table 3.1: Products and biotransformation reactions involving amine functional groups

Structure	Reaction	A*	B*	C*	Structure	Reaction	A*	B*	C*
	Pheniramine (PHE)					Pargyline (PAR)			
	N-oxidation	C ^p	6.0 (73)	r		N-oxidation	C ^p	76.6 (100)	rf
	N-demethylation	C ^p	8.4 (73)	r		N-demethylation	C ²	4.4 (66)	rf
	α-C-oxidation to formamide or N-formylation	P ^s	0.6 (73)	r		α-C-oxidation to amide or N-demethylation followed by N-formylation	P ^s	6.8 (96)	rf
						N-demethylation followed by either N-hydroxylation, reaction at the terminal alkyne, or α-C-hydroxylation to hemiaminal	P ³	0.5 (85)	rf
	Venlafaxine (VEN)					Chlorocyclizine (CLC)			
	N-oxidation	C ^p	5.1 (64)	r		N-demethylation	C ^p	0.2 (97)	r
	N-demethylation	C ^p	3.0 (64)	r					
	Lidocaine (LID)					Pyrilamine (PYR)			
	N-oxidation	C ^p	19.1 (47)	r		N-oxidation	L ³	16.2 (96)	rs
	N-deethylation	C ^p	12.3 (77)	r		N-demethylation	C ²	1.8 (96)	r
	N-dealkylation (deamination) followed by reduction of the aldehyde product to an alcohol	L ³	0.3 (75)	rs		N-debenzylation	C ²	0.5 (96)	rs
	Spiroxamine (SPI)					N-dealkylation (deamination) followed by oxidation of aldehyde product to a carboxylic acid	L ³	0.6 (96)	rs
	N-deethylation	C ²	0.3 (91)	rf		α-C-oxidation to amide or N-demethylation followed by N-formylation	P ^s	0.3 (93)	rf
	N-depropylation	C ²	0.3 (91)	rf					
	Deprenyl (DEP)					N,N-dimethyl-p-chloroaniline (DCA)			
	N-oxidation	C ^p	69.4 (99)	rf		N-oxidation, α-C-hydroxylation to hemiaminal, or hydroxylation	P ³	1.9 (98)	f
	α-C-hydroxylation to a hemiaminal or reaction at the terminal alkyne	P ³	0.5 (98)	rf		N-demethylation	C ^p	20.9 (86)	f
	N-demethylation	C ^p	5.6 (77)	rf		α-C-oxidation to formamide or N-demethylation followed by N-formylation	P ²	11.8 (98)	rf
	N-depropargylation	C ^p	13.7 (100)	r		1-[(4-chlorophenyl)phenylmethyl]piperazine (CPP)			
	α-C-oxidation to amide or N-demethylation followed by N-formylation	P ³	0.6 (90)	rf		N-acetylation	L ³	0.9 (99)	rs
	N-depropargylation followed by N-formylation	L ³	0.1 (100)	rs					
	N-demethylation followed by N-acetylation	L ³	0.2 (99)	rf					

* **A:** certainty of assigned reaction as *certain* (C), *likely* (L), and *possible* (P). Superscripts indicate structural confidence levels, whereby ^p and ^s represent TP structures with Level 1 that were confirmed by purchased or synthesized reference standards, respectively; **B:** maximal relative amount in % and, in brackets, degree of biotransformation of the parent compound at the time point where the TP is maximal, in %; and **C:** characterization of time series pattern as rising (r), rising and steady (rs), and rising and falling (rf)

Table 3.1: continued

Structure	Reaction	A*	B*	C*
	N-succinylation	L ³	10.3 (97)	rs
	Ortho-chlorophenylpiperazine (OCP)			
	N-hydroxylation or α-C-hydroxylation to hemiaminal	P ³	0.5 (75)	rf
	N-dealkylation of 3° and 2° amine, followed by oxidation of aldehyde product to carboxylic acid	L ³	1.1 (93)	rs
	either α-C-oxidation to lactam or N-hydroxylation followed by oxidation to nitrene	P ³	0.4 (95)	rf
	α-C-oxidation to lactam	L ³	0.5 (93)	rs
	N-formylation	L ³	2.5 (75)	rf
	N-acetylation	L ³	5.5 (85)	rf
	N-malonylation	L ³	1.0 (95)	r
	N-succinylation	C ^p	3.1 (91)	rf
	N-fumarylation or N-succinylation followed by desaturation	P ³	2.4 (95)	r
	N-demethylpheniramine (NPE)			
	N-dealkylation (deamination)	L ³	0.5 (33)	rs
	N-dealkylation (deamination) followed by oxidation of aldehyde product to carboxylic acid	L ³	0.8 (14)	rf
	α-C-oxidation	L ³	0.6 (39)	rs
	α-C-oxidation to formamide or combination of N-formylation and N-demethylation or vice versa	P ³	1.8 (40)	r
	N-formylation	C ^s	3.3 (40)	rs
	N-acetylation	L ³	1.3 (33)	r
	N-acetylation followed by N-demethylation or vice versa	P ³	0.9 (40)	r
	N-demethylvenlafaxine (NVE)			
	N-dealkylation (deamination) followed by oxidation of the aldehyde product to carboxylic acid and dehydration to alkene	L ³	0.6 (32)	rs
	either hydroxylation followed by oxidation to a carbonyl, hydroxylation in combination with desaturation, α-C-oxidation to amide, combination of N-demethylation and N-formylation, or N-hydroxylation followed by oxidation to nitrene	P ³	1.0 (32)	r
	either α-C-oxidation to amide or N-hydroxylation and subsequent reaction to nitrene or combination of N-demethylation and N-formylation	P ³	0.3 (32)	r
	combination of N-demethylation and N-acetylation and dehydration to alkene	L ³	0.5 (32)	r
	Fluoxetine (FLU)			
	N-acetylation or combination of N-demethylation and N-propionylation	P ³	0.1 (32)	r
	N-succinylation	L ³	0.2 (96)	rf
	Feniramine (FEN)			
	N-deethylation	C ^p	2.4 (84)	r
	combination of N-deethylation and N-hydroxylation	L ³	0.7 (84)	rs
	either hydroxylation followed by oxidation to carbonyl, combination of hydroxylation and desaturation, or N-hydroxylation followed by oxidation to nitrene	P ³	2.2 (84)	r
	α-C-oxidation to acetamide or combination of N-deethylation and N-acetylation	P ³	0.3 (84)	rs

* **A**: certainty of assigned reaction as *certain* (C), *likely* (L), and *possible* (P). Superscripts indicate structural confidence levels, whereby ^p and ^s represent TP structures with Level 1 that were confirmed by purchased or synthesized reference standards, respectively; **B**: maximal relative amount in % and, in brackets, degree of biotransformation of the parent compound at the time point where the TP is maximal, in %; and **C**: characterization of time series pattern as rising (r), rising and steady (rs), and rising and falling (rf)

Table 3.1: continued

Structure	Reaction	A*	B*	C*
	Clenisopentrol (CLE)			
	Primaquine (PRI)			
	N-dealkylation of 2° amine	C ²	5.5 (100)	rf
	N-dealkylation (deamination) of 1° amine and successive oxidation of aldehyde product to carboxylic acid	L ³	64.7 (99)	rf
	N-formylation of 2° amine in addition to N-dealkylation (deamination) of 1° amine followed by oxidation to carboxylic acid,	L ³	0.2 (99)	rf
	N-acetylation of 1° amine	L ³	4.0 (99)	rf
	desaturation or oxidation of 2° amine to imine in addition to N-dealkylation (deamination) of 1° amine followed by oxidation to carboxylic acid,	P ³	5.3 (100)	rf
	Mexiletine (MEX)			
	desaturation or oxidation of primary amine to imine	P ³	0.7 (85)	r
	N-formylation	L ³	0.5 (81)	rf
	N-demethylfluoxetine (NFL)			
	N-acetylation	L ³	2.4 (100)	rf
	N-propionylation	P ³	2.2 (100)	rf
	N-succinylation	L ³	1.9 (96)	rf

* **A**: certainty of assigned reaction as *certain* (C), *likely* (L), and *possible* (P). Superscripts indicate structural confidence levels, whereby ³ and ⁵ represent TP structures with Level 1 that were confirmed by purchased or synthesized reference standards, respectively; **B**: maximal relative amount in % and, in brackets, degree of biotransformation of the parent compound at the time point where the TP is maximal, in %; and **C**: characterization of time series pattern as rising (r), rising and steady (rs), and rising and falling (rf)

3.3.1 Biotransformation reactions

3.3.1.1 N-oxidation

N-oxidation reactions involve the direct introduction of an oxygen atom on the nitrogen of the amine functional group, resulting in N-oxide products for tertiary amines and hydroxylamine products for secondary and primary amines. This reaction is known from microbial⁵³ and mammalian metabolism of amines. For the mammalian metabolism of xenobiotics the following findings have been reported:^{47,49,52} N-oxidation reactions occur for a broad range of amines, such as aliphatic amines, azaheterocycles, pyridine derivatives, and aniline derivatives. Whereas tertiary amines are preferably oxidized by flavin-containing monooxygenases (FMOs), primary amines tend to be transformed by cytochrome P450 (CYPs) enzymes. For secondary amines, both enzyme systems are reported to be active. Furthermore, for compounds with two tertiary amine moieties, the N-oxidation reaction is reported to occur preferably at the more basic amine moiety. In addition, N-hydroxylated products are known to be further transformed to products such as nitrones (for secondary amines) and nitroso, nitro, and oxime products (for primary amines). Both N-oxides and hydroxylamines can be reduced and backtransformed to the original parent amine.

As can be seen in Table 3.1, six (PHE, VEN, LID, DEP, PAR, PYR) out of 13 tertiary amines were *likely* or *certainly* transformed to N-oxides, and one more amine (DCA) was *possibly* transformed by that same reaction. We thus observed the N-oxidation reaction to occur for a broad range of aliphatic tertiary amines with variable N-substituents and possibly also for aromatic tertiary amines. We additionally found evidence of regioselectivity towards the more basic amine moiety (PHE, PYR). Noteworthy, the *maximal relative amounts* of four N-oxide TPs (LID, DEP, PAR, PYR) were rather high at over 15%, especially for the two methylpropargyl amines DEP and PAR with values of 69.4% and 76.6%, respectively. This indicates that amines substituted with a propargyl moiety might be particularly amenable to the N-oxidation reaction. Overall, N-oxidation reactions were abundant for tertiary amines and thus constitute a major microbial biotransformation pathway for these compounds.

To test if N-oxidized products can be reduced back to tertiary amines, we spiked an additional biotransformation reactor with a mixture of five N-oxide standards (PENO of PHE, VENO of VEN, LINO of LID, DENO of DEP, PANO of PAR). Indeed, we observed

the formation of the respective amines for PENO, VENO, and LINO, which clearly indicates that the backtransformation of N-oxide TPs to tertiary amines is possible. The corresponding time series are shown in Chapter B.7 in Appendix B. Interestingly, no clear formation of the parent amines was observed for the N-oxides of DEP and PAR. This suggests that the lack of backtransformation of the methylpropargyl N-oxides could explain their high occurrence in the parent amine reactors. We additionally observed the formation of the N-dealkylated products for all N-oxides, which were formed in a similar or even higher amount (NPE, NVE) than when formed from the respective tertiary amines. It remains unclear whether the formation of the N-dealkylated product is caused by a direct reaction from the N-oxide to the N-dealkylated product, or whether it is formed in two steps, namely the reduction of the N-oxide to the amine followed by the N-dealkylation of the amine. Similar processes were observed for the N-oxide of N,N-dimethylaniline in mammalian systems.⁵² A hydroxylamine product was *likely* observed for FEN and *possibly* for PAR and OCP. Additionally, four nitrone products (OCP, 2xNVE, FEN) were identified as *possible*. The confidence of the corresponding structural assignment is low due to a number of other possible structures that would also match the available structural evidence.

3.3.1.2 α -C-hydroxylation and subsequent N-dealkylation, oxidation to amides, or dehydration to iminium species

From both mammalian and microbial metabolism of xenobiotics, the hydroxylation of C-atoms in α -position to N-atoms of amine functional groups is known to be catalyzed by cytochrome P450 (CYPs) enzymes.^{47,49,53} This reaction, which requires at least one hydrogen atom at the α -carbon, results in hemiaminal intermediates, which are usually unstable. For most compounds, these hemiaminals are spontaneously cleaved yielding amine and carbonyl products. This reaction is called N-dealkylation. However, two less common alternative reactions of hemiaminal intermediates have also been reported.^{47,49,52} On the one hand, oxidation of the hemiaminal intermediates to amides, which requires two hydrogen atoms at the α -carbon, is possible, especially for cyclic amines. On the other hand, dehydration of the hemiaminal intermediate may lead to the formation of an iminium species. The N-dealkylation reaction cleaves the substrate into two products and since it is more likely to detect the product that bears the major structural unit, the reaction is sometimes also named deamination

if the carbonyl product bears the major structural unit. In mammalian systems, N-dealkylation reactions occur for a variety of amines such as aliphatic, aromatic, and cyclic amines. The readiness of the reaction decreases from tertiary over secondary to primary amines. Sterically less hindered N-substituents (methyl and ethyl) are more readily cleaved than longer and α -branched N-substituents. For the carbonyl product it is known that further biotransformation reactions are likely to occur, such as the oxidation to a carboxylic acid moiety in case of aldehydes or the reduction to an alcohol moiety.^{47,49,52}

Four hemiaminals were *possibly* observed (DEP, PAR, DCA, OCP). However, also other structures such as N-oxides, hydroxylamines, or hydroxylated TPs match the structural evidence. Since hemiaminals are usually unstable and a certain stability is only known for less basic amines, it is possible that only some of the less basic aliphatic amines DEP and PAR and the aniline-derivative DCA actually formed hemiaminals.

For 11 of the 13 tertiary amine moieties (the exceptions being the inner amines of the piperazine moieties of CLC, CPP), one or two products of N-dealkylation were identified. N-demethylation occurred for all seven tertiary methylamines (PHE, VEN, DEP, PAR, CLC, PYR, DCA). Other N-substituents for which dealkylation was observed were ethyl (LID, SPI), propyl (SPI), propargyl (DEP), and p-methoxybenzyl (PYR). We additionally found oxidative ring opening (OCP) and cleavage of diethylamine and demethylamine in the case of LID and PYR, respectively, to yield an alcohol (LID) or carboxylic acid product (PYR) as the major structural unit. The *maximal relative amounts* for four of these TPs were higher than 5%, with a distinctly high value for the N-demethylated product of DCA of 20.9%. For the eight secondary amines, *certain* or *likely* N-dealkylation was observed five times with cleavage of the following N-substituents: piperazine ring (OCP), major structural unit (NPE, NVE), ethyl (FEN), and an α -branched ω -amino alkyl chain (PRI). Additionally, *possible* demethylation was observed for three compounds (NPE, NVE, FLU). For the three primary amines, only one deamination product was observed (PRI). However, this TP was formed with an outstandingly high *maximal relative amount* of 64.7%.

Overall, our observations regarding the N-dealkylation reactions concurred with findings from mammalian systems with respect to the frequent occurrence of N-dealkylation for a range of tertiary, secondary, and primary alkyl, alkyl-aryl, and cyclic amines. Again, in agreement with mammalian systems, we also observed the sterically less hindered

substituents to be more readily cleaved than more sterically hindered moieties.^{47,49,52} The further oxidation of hemiaminal intermediates to amide products was *likely* observed for the two aliphatic amines OCP and NPE, where the α -carbon of the N-substituent bearing the major structural unit was oxidized. Besides that, eight formamide or acetamide products were observed (PHE, DEP, PAR, PYR, DCA, NPE, NVE, FEN) that could *possibly* be formed through α -C-oxidation. However, since these products have been observed for methyl- and ethylamines, they could also have been formed through N-demethylation and subsequent N-formylation, or N-deethylation followed by N-acetylation, respectively, as described in the next section. The fact that only two amide TPs were observed where the α -C-oxidation occurred at the longer N-substituents suggests that either α -C-oxidation occurs more readily for methyl and ethyl substituents or their formation is mediated via the two-step reaction path. Findings from mammalian systems indicate that for α -C-oxidation reactions to compete with spontaneous cleavage of the hemiaminal a certain stability of the hemiaminal intermediates is required. This is given for less basic amines such as aniline-derivatives, or for cyclic amines exhibiting a ring-chain tautomerism, but less likely for the methyl- and ethylamines for which we observed amide formation. Therefore, and due to several arguments discussed in the following section, it is likely that the observed formamides and acetamides are mostly formed via sequential N-dealkylation and N-acylation. Overall, the formation of amides through α -C-oxidation reactions seems to be a minor pathway compared to N-dealkylation. The third alternative reaction of hemiaminals, *i.e.*, the formation of iminium species, was *possibly* observed twice (PRI, MEX). However, other structures would also match the available structural evidence.

3.3.1.3 N-acylation of secondary and primary amines

For the mammalian metabolism of xenobiotics, N-acetylation reactions are mainly known for primary aryl amines and are catalyzed by N-acetyltransferase enzymes that use acetyl-coenzyme A as an acetyl donor.⁵¹ This reaction was also observed to occur for an even broader substrate spectrum, including aliphatic amines, in microbial systems.^{109–111} Other N-acylation reactions such as N-formylation, N-propionylation, N-malonylation, and N-succinylation were not yet known for the metabolism of xenobiotics in mammalian systems but were observed in other contexts such as the modification of lysine residues of proteins.¹¹² Similarly, N-acetylation and N-succinylation of

lysine residues were also reported for bacteria.¹¹³

For 9 of the 12 primary and secondary amines (the exceptions being both amine moieties of CLE and the secondary amine of PRI), an N-acetylation reaction was *likely* (CPP, OCP, NPE, NVE, PRI, MEX, NFL) or *possibly* (FLU, FEN) observed. Additionally, the N-demethylated product of the tertiary amine of DEP underwent N-acetylation. The N-acetylated product of MEX was formed in a remarkably high *maximal relative amount* of 54.8%. This, in addition to the frequent occurrence of the N-acetylation reaction for primary and secondary amines, indicates the importance of this reaction. Formamide products, indicating the occurrence of an N-formylation reaction, were observed 12 times. Five of these TPs (DEP, OCP, NPE, PRI, MEX) were formed *certainly* or *likely* via N-formylation. For the remaining seven TPs (PHE, DEP, PAR, PYR, DCA, NPE, NVE), two reaction paths are *possible*, as mentioned in the previous section, namely N-demethylation followed by N-formylation or an α -C-oxidation of a methylamine to a formamide product. Beyond the arguments supporting the two-step reaction pathway already mentioned in the previous section, we further observed the following: for five of the seven TPs in question, the intermediate N-demethylation product was formed; the other N-formylated TPs demonstrate that N-formylation of secondary and primary amines is a common reaction; and two TPs of DEP are *likely* formed by a combination of N-dealkylation and N-acylation. We further inspected the time series pattern of the N-dealkylated and formamide products for evidence of a sequential reaction (*i.e.*, transient patterns for the dealkylated products and an initial slow increase of the N-acylation products). No consistent pattern that pointed towards one of the two reaction paths was found. Overall, we nevertheless conclude that formamide products of methylamine parents were more likely formed via combination of N-demethylation and N-formylation.

Further, we identified TPs that pointed towards *possible* (FLU, NFL) or *likely* (MEX) N-propionylation reactions, one *likely* N-malonylation reaction (OCP), and *certain* or *likely* N-succinylation reactions for four out of eight secondary amines (CPP, OCP, NPE, FLU) and two out of four primary amines (MEX, NFL). The N-succinylated TP of OCP was confirmed by a reference standard, which considerably increased our confidence in the structural assignments of all N-succinylated products. The two products of CPP and NPE were formed in *maximal relative amounts* of 10.3% and 9.2%, respectively. These amounts and the occurrence of the N-succinylation reaction for half

of the secondary and primary amines indicates the importance of this reaction, which, to the best of our knowledge, has only been observed as microbial biotransformation reaction of a xenobiotic once before.¹¹⁴

We also observed three N-fumarylated products (OCP, NPE, MEX), with the TP of MEX confirmed by a reference standard. These products can be formed either through direct N-fumarylation or by desaturation of the N-succinylated product. The latter reaction path is supported by the following: for all N-fumarylated TPs also an N-succinylation TP was observed; the time series patterns of the N-fumarylated product in comparison to those of the N-succinylated products point towards a sequential reaction path (see Chapter B.6 in the Appendix B); and the desaturation of succinate to fumarate is a common process in the metabolism of cells. Therefore, it is more likely that the N-fumarylated products were formed through a desaturation of the N-succinylated amines.

It should also be noted that the N-acylation products with short chains could be formed from an N-acylation reaction with a longer substituent that is subsequently cleaved, rather than by direct N-acylation. However, the frequency of detection, the time series patterns, and the similarity to reactions observed in mammalian systems suggests that especially the N-acetylation, N-formylation, and N-succinylation TPs were formed directly.

Overall, N-acetylation and N-succinylation and to a lesser extent N-formylation reactions were highly relevant for secondary and primary amines. N-propionylated, N-malonylated and N-fumarylated products were also observed. Except for N-acetylation, these N-acylation reactions represent the greatest difference between what we observed for microbial biotransformation relative to what is known from mammalian systems, in which the latter type of transformation has not been reported for xenobiotics so far. However, the biochemical reactions themselves are known from other contexts for both microbial as well as mammalian systems. The respective N-acyltransferase enzymes are likely to transform the amines co-metabolically.

It should further be noted that the products of N-acylation reactions of primary and secondary amines are secondary and tertiary amides. It is known from both mammalian⁵⁰ and microbial metabolism²⁰ that especially the former ones can be readily hydrolysed to form a carboxylic acid and an amine product. This means that especially primary amines that undergo N-acylation reactions to form secondary amides are likely

Table 3.2: Relative importance of reactions involving amine functional groups

	tertiary amines			secondary amines			primary amines		
	frequency		mean maximal relative amount [%]	frequency		mean maximal relative amount [%]	frequency		mean maximal relative amount [%]
	abs.	rel. [%]		abs.	rel. [%]		abs.	rel. [%]	
N-oxidation	6 / 13	46.2	14.8	0 / 8	0.0	-	0 / 4	0.0	-
N-dealkylation [°]	12 / 27	44.4	2.6	3 / 13	23.1	0.6	0 / 3	0.0	-
- N-demethylation	7 / 7	100.0	6.3	0 / 3	0.0	-	0 / 3	0.0	-
- N-deethylation	2 / 2	100.0	6.3	1 / 1	100.0	2.4	0 / 3	0.0	-
- N-dealkylation of longer substituents #	3 / 18	16.7	0.8	2 / 9	22.2	0.7	0 / 3	0.0	-
α-C-oxidation to amide *	0 / 16	0.0	-	2 / 7	28.6	0.16	0 / 1	0.0	-
N-formylation	0 / 0	-	-	2 / 8	25.0	0.7	1 / 4	25.0	0.1
N-acetylation	0 / 0	-	-	3 / 8	37.5	1	3 / 4	75.0	15.3
N-propionylation	0 / 0	-	-	0 / 8	0.0	-	1 / 4	25.0	0.5
N-malonylation	0 / 0	-	-	1 / 8	12.5	0.1	0 / 4	0.0	-
N-succinylation	0 / 0	-	-	4 / 8	50.0	2.9	2 / 4	50.0	0.6

[°] the following three specific N-dealkylation reactions are a subset of this general one. # including direct deamination products, i.e., carbonyl products, but not further transformed products such as carboxylic acids or alcohols. * not including the formation of formamides / acetamides from methylamines / ethylamines. Frequency is given as absolute (abs.) or relative (rel.) value. Reactions that were judged important (see text) are highlighted in bold.

to be back-transformed through hydrolysis.

3.3.1.4 Further biotransformation reactions

Additionally to reactions at the amine functional group, we found the following transformation reactions (Table 3.1 or Chapter B.8 in Appendix B): O-demethylation (VEN, PYR, NVE), which was observed for three of four methylarylamines; desaturation (LID, PRI, MEX); dehydration of an aliphatic alcohol to an alkene (2x NVE); and hydroxylation (2x VEN, LID, 2x SPI, DEP, PAR, CLC, DCA, NVE). Additionally, the following reactions likely occurred after hydroxylation: TPs with an atomic modification of -2H +O that could have been formed through a combination of either hydroxylation and subsequent oxidation to a carbonyl product or hydroxylation and independent desaturation (2x VEN, SPI, 2x NVE, FEN); hydroxylation followed by oxidation to a carboxylic acid product (LID); and TPs for which a combination of several of the discussed reactions as well as decarboxylation reactions or β-oxidations are possible (VEN, 2x SPI, PRI). With this, we possibly found for 12 of 19 test compounds additional biotransformation reactions in parallel to transformations involving the amine functional groups. Furthermore, although seven TPs were successfully assigned for SPI and PRI, for six TPs of the two parent amines it was not possible to assign any reaction since the structural evidence was insufficient to propose a meaningful structure.

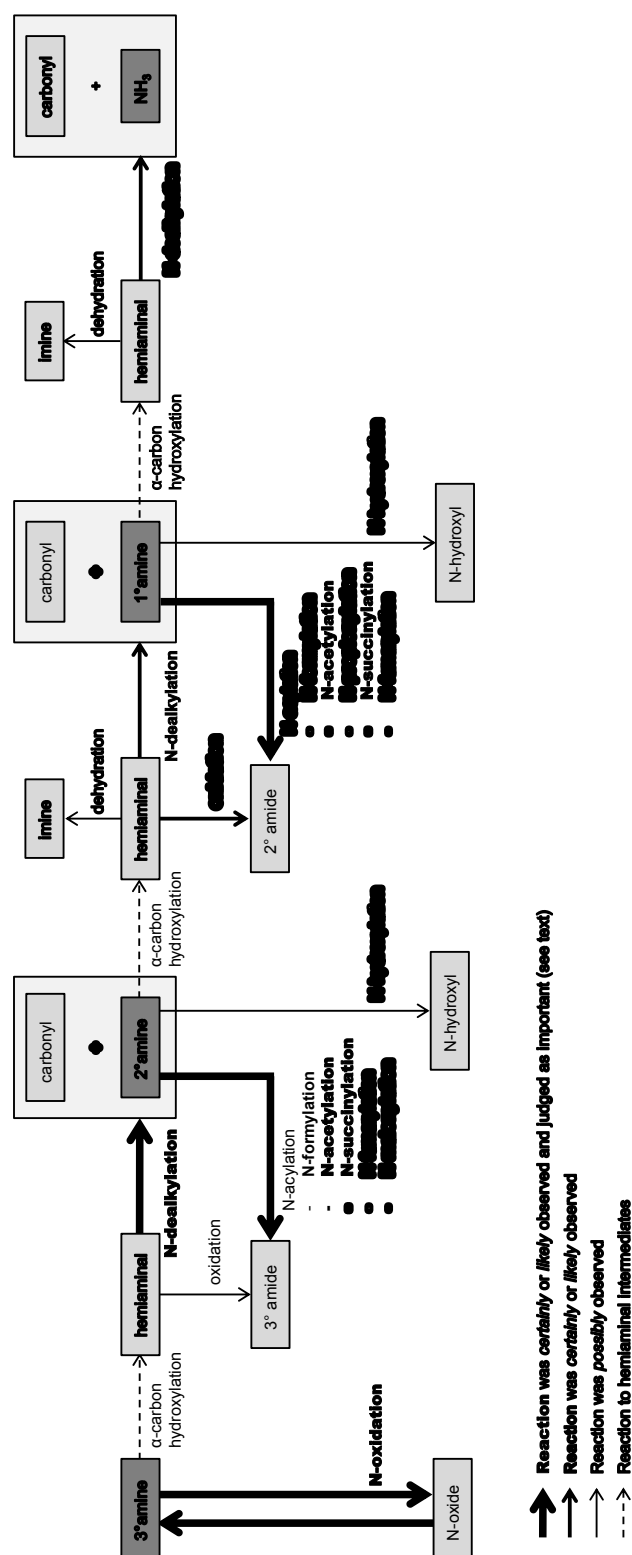


Figure 3.1: Overview of all observed reactions involving tertiary, secondary, and primary amine functional groups.

3.3.1.5 Metabolic logic

Overall, we found that biotransformation reactions of amine-containing xenobiotics were indeed fairly similar in mammalian and microbial systems. This was certainly true for all transformations that were initiated by oxidative reactions. Additionally, these reactions also showed dependencies, where observable, on electronic and steric features that were consistent with those known from mammalian systems. However, we also observed a number of N-acylation reactions that have not been previously described for the metabolism of xenobiotics in mammalian systems, and which are most likely co-metabolically catalyzed by N-acyltransferases expressed for the regulation of proteins.

Figure 3.1 illustrates all observed reactions for the tertiary, secondary, and primary amine moieties. Observed reactions that did not concern the amine functional group are not displayed. To assess and compare the importance of the different reactions in terms of how much of the amines were biotransformed through each type of reaction, the following values were calculated based on all first-generation products that were formed *certainly* or *likely* through each type of reaction: the *relative frequency*, i.e., the number of observed products relative to the number of theoretically possible products, and the *mean maximal relative amounts* of all TPs formed, taking into account again the number of theoretically possible products. The values are given in Table 3.2. Reactions with either a *relative frequency* >30% or a *mean maximal relative amount* >1% were judged as important compared to the spectrum of possible reactions and are illustrated in bold in Table 3.2 and with a thick arrow in Figure 3.1.

As can be seen in Figure 3.1 and Table 3.2, tertiary amines were predominantly biotransformed through N-oxidation and N-dealkylation reactions. N-acetylation and N-succinylation reactions were most important for secondary and primary amines. A proper evaluation of N-oxidation of primary and secondary amines to form hydroxylamines and subsequent nitron products was impeded by the fact that structural assignment remained ambiguous. For all types of amines studied, diverse other, mainly oxidative reactions that did not involve the amine functional group were observed to proceed in parallel.

3.3.2 Implications for pathway prediction

With respect to improving tools for pathway prediction, particularly the Eawag-PPS system, this study results in a number of suggestions concerning the rules for biotransformation of amine functional groups. While the N-dealkylation reaction is already implemented in the Eawag-PPS system and is triggered without any further specification for all types of amines, the other amine reactions that we observed have so far not been implemented. While some of these reactions are specific for certain types of amines, *i.e.*, tertiary, secondary, or primary amines, the different biotransformation reactions at the amine functional group were generally observed to occur in parallel. No structural features could be identified that would promote certain reactions to occur more readily than others. Therefore, rather than reducing combinatorial explosion, the implementation of new rules will lead to an increase of predicted products for amine-containing compounds.

One rather crude, but, in the light of still limited data, tangible way to guide interpretation of the outcomes of pathway prediction towards the more important products is to assign likelihoods to reactions. In the Eawag-PPS, one of five levels of aerobic likelihood (*very likely*, *likely*, *neutral*, *unlikely*, and *very unlikely*) is assigned to each biotransformation rule to express expert knowledge about the likelihood of the reaction occurring under aerobic conditions.^{101,115} These likelihood levels could be used to express the differences in metabolic relevance of the observed amine biotransformation reactions. When doing so, the likelihoods for reactions at the amine functional group should be consistent with the likelihoods of reaction occurring at other functional groups.

The fact that reactions involving the amine functional group were observed to occur in parallel with O-demethylation reactions of aromatic ethers and miscellaneous C-hydroxylation reactions, which are both implemented as *neutral* in the Eawag-PPS, suggests that they should also be implemented as *neutral*. This is further supported by the hydrolysis reaction for primary and secondary amides being implemented as *likely*, which is known to be preferred over (i) reactions at the amine functional group for atenolol¹⁴, and (ii) oxidative N-dealkylation reactions from data collected for amides.²⁰ Therefore, we suggest the implementation of reactions involving the amine functional group with a likelihood of *neutral*. In order to prevent overrepresentation of less likely

reactions, we suggest the implementation of only those reactions that were judged to be important. For the Eawag-PPS this would result in the implementation of the following new rules: reversible N-oxidation for tertiary amines, and N-acylation reactions such as N-acetylation and N-succinylation for secondary and primary amines. Further, the already implemented N-dealkylation rule (bt0063), which is triggered for all N-substituents of an amine moiety and predicts the corresponding N-dealkylated and deaminated products, should be reassigned from *likely* to *neutral*. The latter rule could be further refined based on the observation that N-dealkylation was found to be less prevalent for secondary and primary amines and for the cleavage of sterically hindered substituents of tertiary amines. This could be represented by implementing the N-dealkylation rule with a variable aerobic likelihood,^{100,101} so that N-dealkylation reactions of tertiary amines are assigned as *neutral* for methyl and ethyl, whereas N-dealkylation of secondary and primary amines and tertiary amines that involve bond cleavage of larger substituents are assigned as *unlikely*. Updating of rules in Eawag-PPS as suggested, would not only increase the sensitivity of the prediction for amine-containing compounds, but would also gear predictions towards more specifically predicting microbial biotransformation under environmentally relevant conditions.

While implementation of fixed likelihood levels is the currently most tangible way of guiding interpretation of predicted pathways, more refined ways of learning from our data are currently being developed. Recently, Eawag-PPS has been redesigned and reimplemented into a new system called enviPath.¹¹⁶ The new system was specifically designed to facilitate entry of micropollutant biotransformation data, *i.e.*, biotransformation reactions and half-lives, and storage of meta-data, *e.g.*, on environmental conditions. It also supports learning more sophisticated relative reasoning models on the data. We plan to add the data reported in this study into the enviPath system and also would like to encourage others to enter own data on biotransformation of micropollutants in activated sludge communities. Ultimately, the collection of these data should enable training pathway prediction engines that are more specific to activated sludge systems.

3.3.3 Environmental relevance

The finding that microbial and mammalian transformation reactions were fairly similar suggests that predicted as well as experimental transformation data from the mammalian metabolism of pharmaceuticals can be used for suspect screening approaches targeted at TPs in the environment. Additionally, the well explored reactions of the mammalian system can support the interpretation of biotransformation reactions in less explored microbial systems as it was done in the present study.

Additionally, if we assume that our findings in activated sludge-seeded bioreactors can be extrapolated to full-scale WWTPs, we can expect that amine-containing compounds, which do not contain any other functional groups that are biotransformed more readily, undergo several reactions in parallel. Other studies exploring more structurally complex amine-containing MPs than we did also reported the products of transformation at the amine functional group to be found alongside products formed through reactions at other functional groups.^{7 7 7} Since we found that very few of the resulting TPs were formed in major amounts, it is reasonable to assume that a complex mixture of the parent MPs and a number of low-level TPs will be present after activated sludge treatment unless the compound contains some other readily transformed functional group. Hence, the potential resulting (eco-)toxicological effects depend on the relative toxicity of the remaining parent compounds and the individual TPs. In cases where the amine moiety is involved in inducing a toxic effect of the parent compound, biotransformation at this site might result in less toxic TPs. This was shown for the N-acetylated TP of the herbicide glyphosate¹⁰⁹ as well as for the N-oxidized TPs of the antibiotics clarithromycin¹¹⁷ and danofloxacin¹¹⁸. However, since we know that N-oxide TPs as well as N-acylated TPs can be back-transformed to the parent amines - also reported for MPs holding other functional groups^{119,120} - their toxic effect could be regained in the environment. Therefore, it is important to also consider the individual TPs and their potential reactions when assessing the risk of MPs.

Acknowledgements

We thank Jennifer Schollee for fruitful discussions. Additionally, we thank the operators and staff of the WWTP ARA Neugut for providing activated sludge samples. Fund-

ing for this project was provided by the Swiss National Science Foundation (project 200021_134677) and the NMR hardware was partially granted by the Swiss National Science Foundation (SNFS, grant No. 150638).

Chapter 4

Conclusions and outlook

The work presented in this PhD thesis contributes to an improved understanding of how operational parameters influence the removal of MPs and what transformation reactions occur during wastewater treatment. Such an understanding is necessary to explore potential approaches to mitigate the harm caused by the presence of MPs and their TPs in the aquatic environment, either by improving the removal of MPs or by restricting or even banning MPs that prove to be of high risk. In particular, our results provide important information about the effect of pH on biotransformation as well as on initial biotransformation reactions and resulting TPs of amine-containing micropollutants during activated sludge treatment.

4.1 pH-dependent biotransformation

In Chapter 2, biotransformation experiments as well as sorption and abiotic control experiments are described for 15 amine-containing compounds with cationic-neutral speciation, two neutral MPs, and one MP with neutral-anionic speciation with a single activated sludge microbial community adjusted to pH 6, 7, and 8. Samples analyzed by LC-HR-MS/MS techniques yielded concentration time series, which were evaluated by means of Bayesian inference to test pH-dependency.

With this set-up, we achieved a thorough understanding of how the degree of speciation of polar, ionizable MPs influences the different processes contributing to their removal. Biotransformation was found to be pH-dependent and to associate with the neutral fraction of the ionizable MPs, which agrees with the assumption that uptake of the neutral species into the cells is favored. However, quantitatively, the data suggested a slight attenuation relative to the simple speciation model, suggesting additional mechanisms where the ionic species might also play a role. Since the presented data were not sufficient to provide more details about these additional mechanisms, investigating them remains as a subject for further research.

Sorption was found to be of minor importance for the investigated polar organics. However, the data from the sorption control experiments suggested that neither a pH-induced potential change of protonation of the sludge organic matter nor the degree of speciation of the ionizable MPs influenced the sorption affinities. This was somewhat surprising since other studies that observed pH-dependent removal for MPs with neutral-anionic speciation considered sorption to be the process inducing the observed

pH-dependency.^{63–65} However, in these studies, the differentiation between biotransformation and sorption was not completely clear. Our results however clearly show that pH-dependent biotransformation is an important process that can lead to pH-dependent removal. Still, our sorption experiments were designed as controls and, thus, the corresponding results were not ideal to investigate the influence of varying pH on sorption affinities. To do so, further sorption experiments at lower and multiple MP concentrations would be necessary.

Overall, we concluded that pH-dependent biotransformation is more likely than pH-dependent sorption to cause variability in the removal of polar, ionizable MPs during activated sludge treatment. However, these results should not be interpreted as suggesting pH adjustment of CAS treatment to facilitate better biotransformation of ionizable MPs, for two reasons. First, while a higher pH favors the removal of ionizable MPs with cationic-neutral speciation, a lower pH is beneficial for the removal of ionizable MPs with neutral-anionic speciation. Due to these opposing trends it is not advisable to shift the pH away from neutral. Second, varying pH does not only influence the speciation of ionizable MPs, but also the composition of the microbial community. While this work gives valuable information on the former, the longer-term influence of pH on the composition of the microbial communities and the related shifts in their biotransformation capacity still needs to be investigated. However, the outcome of this study can already be used to rationalize variability in the removal of polar, ionizable MPs when CAS systems are operated at different pH levels.

4.2 Biotransformation reactions

In Chapter 3, biotransformation experiments were conducted with 19 MPs that contained altogether 25 different tertiary, secondary, and primary amine functional groups in activated sludge-seeded bioreactors. Samples taken as a time-series after start of the experiment were analyzed with LC-HR-MS/MS, and first-generation TPs were identified by suspect and non-target screening approaches. Corresponding TP structures were elucidated and confidence levels assigned. Observed parent-TP pairs were interpreted to obtain a comprehensive picture of initial biotransformation reactions. These were interpreted by comparing to the well explored mammalian metabolism of amine-containing xenobiotics and the relative importance of the different initial bio-

transformation reactions was assessed by the frequency with which they were observed and the amount of TPs formed.

Several different reactions involving the amine functional groups were observed, most of which occurred in parallel. The most important reactions were N-oxidation and N-dealkylation, which were observed for all types of amines, and N-acetylation and N-succinylation for secondary and primary amines. Especially the oxidative reactions were fairly similar to what is reported from mammalian metabolism, also in terms of how steric and electronic features of the amine functional group influenced the likelihood of the reactions. Except for N-acetylation, the observed N-acylation reactions were not previously known from mammalian metabolism of xenobiotics, and have also rarely been reported for microbial metabolism. However, the corresponding TPs are most likely formed co-metabolically by N-acyltransferases expressed for the regulation of proteins.

Overall, our study yielded valuable information on what biotransformation reactions are likely to occur for amine-containing MPs during activated sludge treatment and what TPs can be expected. At least initially, the identification of TPs in environmental matrices is usually done by suspect screening. For this purpose, the list of expected TP candidates is often generated using pathway prediction systems. We therefore attempted to generalize the findings in order to improve the prediction of TPs of amine-containing xenobiotics, especially within the Eawag-PPS, which is curated by our group. We suggest that all amine biotransformation reactions that were judged as important, namely N-oxidation, N-dealkylation, N-acetylation, and N-succinylation be implemented. With this, pathway prediction of amine-containing MPs will not only be more sensitive, but also be more specific to relevant conditions such as the activated sludge compartment.

It would be essential to investigate if the observed reactions from this work also occur during full-scale CAS treatment. With the implementation of all relevant amine biotransformation rules into the Eawag-PPS as suggested in our study, these TPs will be predicted in the future and will promote the screening for these TPs in the frame of upcoming studies. This will support investigation of their relevance in full-scale systems. To truly confirm the presence of TPs of amine-containing MPs in environmental samples, we not only need to look for the right suspect TP structures, but also need analytical methods to enable their analysis. In an attempt to analyze N-

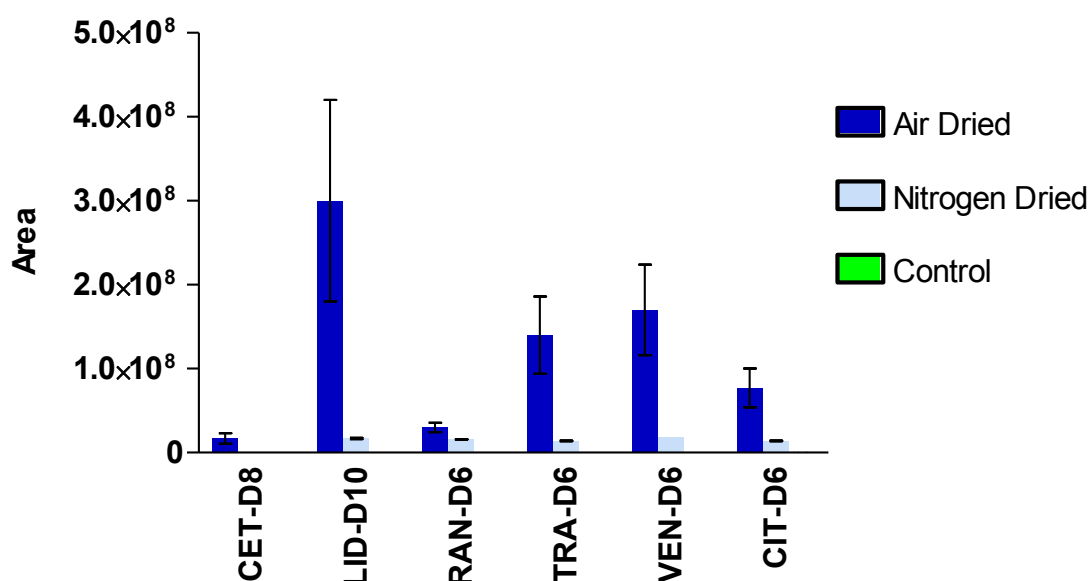


Figure 4.1: Area of N-oxides which were formed from the six isotope labeled MPs cetrizine (CET), lidocaine (LID), ranitidine (RAN), tramadol (TRA), venlafaxine (VEN), and citalopram (CIT) after drying the cartridge of solid phase extraction with air and nitrogen and a control without extraction step.

oxide TPs, which were found to be on average the most important TPs of tertiary amine-containing MPs, we tested several enrichment procedures.¹²¹ As can be seen in Figure 4.1, we observed that N-oxide TPs were formed accidentally during solid phase extraction when the loaded cartridges were dried with air. This artifact could mostly be avoided by drying the cartridge under a nitrogen stream. This work shows that special attention is needed during method development to ensure that structurally related compounds, such as MPs and their corresponding TPs, are not accidentally transformed into each other during sample work-up.

With respect to the environmental relevance, our data suggest that during activated sludge treatment biotransformation of amine-containing compounds most likely yields a mixture of remaining parent amine and a number of low-level TPs, provided that these compounds do not contain other functional groups which are more easily transformed. Further research is needed to determine if such mixtures are of more or less toxicological

concern than the parent amines alone. Particular attention needs to be paid to the fact that TPs have the potential to be transformed back to the original MP. This was observed within this study with N-oxide TPs and has also been demonstrated for N-acetylated products like N-acetyl-sulfamethoxazole¹²² and others.^{119,120}

Additionally, we observed the following interesting but so far unexplained phenomenon. The concentration time series of the parent amines decreased for a certain time interval but at later time points leveled off. This phenomenon was also observed for amine-containing MPs in biotransformation experiments with very different settings, e.g., pure culture studies or sequencing batch reactors. In the sequencing batch reactor experiments, biotransformation of other MPs was also investigated. However, this trend was only observed for amine-containing MPs (personal communication Yuije Men and Stefan Achermann). In contrast, Blair *et al.* (2015) have recently reported that the same phenomenon was observed for other MPs such as acetaminophen, caffeine, and metformin in biotransformation batch experiments.¹²³ To be confident about interpreting the decrease in concentration time series as biotransformation, it is crucial to understand what processes cause this phenomenon. Further research to study this phenomenon is currently being conducted within our research group.

4.3 Outlook

It would be beneficial to complement this work by studying how other operational parameters influence the biotransformation of amine-containing MPs, to understand variabilities in removal and ultimately to improve the removal during activated sludge treatment. To do so, it might be helpful to determine which microorganisms biotransform amine-containing compounds, how the abundance of these microorganisms in the mixed microbial community is effected by varying operational parameters, and if this influences the biotransformation reactions.

Finally, by extending such investigations to MPs containing all kinds of different structural features, a general understanding can be reached on what influences biotransformation and which biotransformation reactions and resulting TPs occur. Such follow-up studies are and will be conducted within the *PROduCTS* project in our research group. With a broader understanding we get closer to being able to reduce the risk originating from anthropogenic chemicals.

4.4 Proposal for a research project

It is essential to know which stable TPs are released with the effluent of WWTPs and thus might occur in the aquatic environment. However, the preferred suspect-screening approach for the identification of TPs is dependent on knowledge about relevant transformation reactions. Since not all transformation reactions are known or can be known, a variety of TPs might be present that go completely unnoticed. Therefore, a complementary approach to identify these TPs would be helpful, but their identification in environmental samples without additional knowledge remains challenging. Based on the experience of this PhD thesis, I would propose a follow-up project that aims to efficiently identify relevant TPs by taking full advantage of the benefits of laboratory biotransformation experiments but still focuses on TPs that are present in environmental samples.

By conducting this thesis, I experienced that structure elucidation is the most time-consuming step, while the identification of unknown TP candidates within time-series samples by non-target screening is straightforward. This is especially true because the necessary data analysis workflows have now been developed within this PhD thesis and are readily available. Therefore, I propose to conduct biotransformation experiments in activated-sludge seeded bioreactors with around 200 wastewater-relevant MPs that are available in the environmental chemistry department at Eawag.

These MPs would be divided into several mixtures which are then spiked into individual reactors. The mixtures are prepared in such a way that a subsequent attribution of identified TP candidates to corresponding parents is possible. TP candidates would be identified as described in Chapter 3 by taking time-series of samples, analyzing them with LC-HR-MS/MS, and applying suspect and non-target screening approaches. The identified TP candidates would be prioritized before the time-consuming structure elucidation step by comparing if the corresponding signals were also present in real samples of WWTP effluents. The structure of the TP candidates that are most prevalent in different WWTP effluents would be elucidated as described in Chapter 3. The limits are that only those TPs that are well ionizable and can be enriched by the applied enrichment procedure will be identified. However, this approach would provide a comprehensive view on exposure-relevant TPs formed from 200 wastewater-relevant MPs during wastewater treatment.

Appendix A:

Supporting information to Chapter 2

A.1 Biotransformation test system

A.1.1 Compensation for evaporation of water

For compensation of evaporated water the mass of each reactor was measured after and before sampling at time points that were more than 12 hours apart. If the mass loss between sampling time points was >0.3 g, nanopure water (Barnstead Nanopure, Thermo Scientific) was added to the respective reactor for compensation.

A.1.2 pH values in reactors

The pH in the BE, SE, and AE reactors was measured shortly before or after sampling (HQ30d Flexi Meter, Hach Lange, Vesenaz, Switzerland). pH time series for the three pH-levels are given in Figure A.1. One of the triplicate pH6-SE reactors was excluded from further analysis because the effective pH was too high (7.5). The excluded data are not shown, resulting in a reduced pH6-SE data set. The effective pH for each experiment was estimated by averaging the values measured in triplicate reactors over time (see Table A.1). The average pH of the control reactors (SE and AE) differed by maximally 0.35 units from the respective BE reactors. These differences are in the range of the pH variations among triplicate BE reactors, indicating good agreement between the pH of the control and the biotransformation reactors.

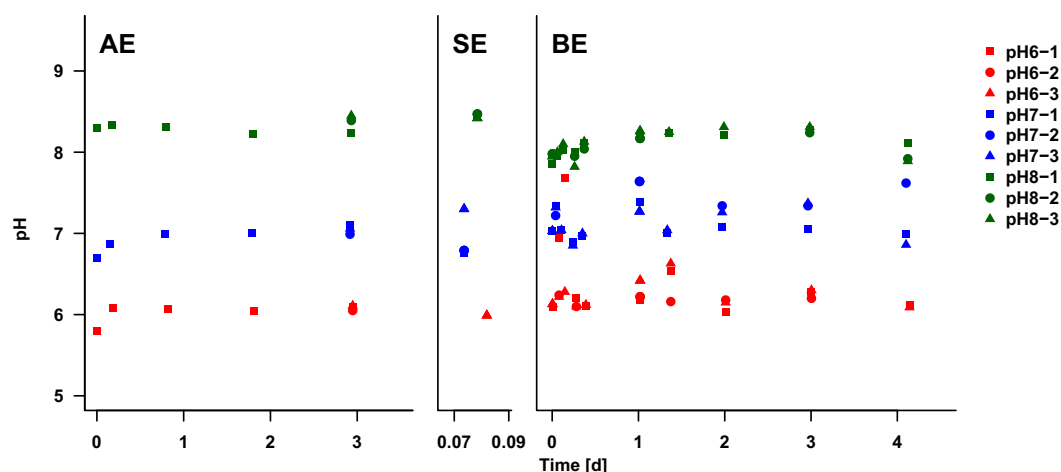


Figure A.1: pH time series

Table A.1: Effective pH

	pH		
	BE	SE	AE
pH6	6.3±0.3	6.00±0.01	6.0±0.1
pH7	7.1±0.2	7.0±0.3	7.0±0.1
pH8	8.1±0.2	8.45±0.03	8.3±0.1

Data are given as mean and standard deviation.

A.1.3 Temperature values in reactors

The temperature in the BE reactors was measured shortly before or after sampling (HQ30d Flexi Meter, Hach Lange, Vesenz, Switzerland). Temperature time series are given in Figure A.2. The effective temperature at each pH level was estimated by averaging the values measured in triplicate reactors over time (see Table A.2). The temperature of the pH7 reactors was consistently about 2°C higher than the temperature in the pH6 and pH8 reactors. This temperature difference was most likely caused by different positions of the reactors in the laboratory. However, a commonly used temperature-correction factor (Q_{10}) for activated sludge systems indicates that a temperature increase of 2°C can cause an increase in biotransformation rate constants by no more than a factor of 1.2.¹²⁴

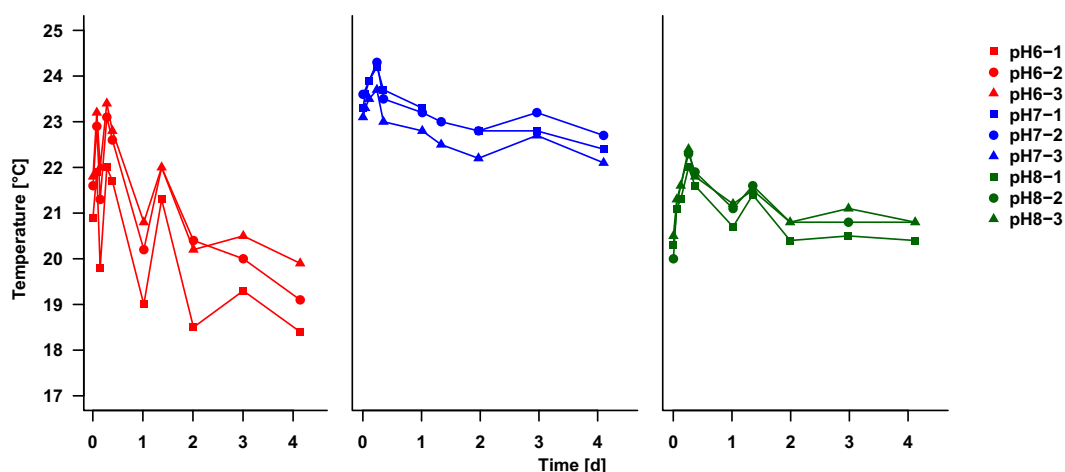
**Figure A.2:** Temperature time series

Table A.2: Temperature (T)

	T [°C]
pH6	21.1±1.4
pH7	23.2±0.6
pH8	21.2±0.6

Data are given as mean and standard deviation.

A.1.4 Total suspended solids concentration

The total suspended solids concentration (TSS) was measured in triplicates at the first and last day of the experiment per standard method 2540B (see Table A.3).¹²⁵

Table A.3: Total Suspended Solids Concentration (TSS)

	TSS [g/L] day 0	TSS [g/L] day 4
pH6	2.0±0.1	2.1±0.2
pH7	1.9±0.3	2.5±0.1
pH8	2.3±0.1	2.3±0.1

Data are given as mean and standard deviation.

A.1.5 Oxygen uptake rate

The oxygen uptake rate (OUR) was measured by filling an 25 mL-Erlenmeyer with a magnetic stir bar completely with sludge. The sludge was fiercely stirred for approximately one minute to ensure for high dissolved oxygen levels. Afterwards, an O₂ probe (HQ30d Flexi Meter, Hach Lange, Vesenaz, Switzerland) was inserted and the vial was sealed with Parafilm so that no headspace remained. The O₂ concentration was metered at least 10 times over a period of 3-10 mins. The OUR was determined as the slope of the O₂ decline with time (see Table A.4).

Table A.4: Oxygen Uptake Rate (OUR)

	OUR [mg/(L h)]
	day 0
pH6	-20.8±0.6
pH7	-44.8±1.0
pH8	-40.8±1.1

Data are given as mean and standard deviation.

A.2 Analytical method

For chemical analysis, reversed-phase liquid chromatography coupled to a high-resolution quadrupole orbitrap mass spectrometer (Qexactive, Thermo Scientific) was used. In detail, 20 μ L samples were injected onto a guard cartridge (particle size 3 μ m, 3.9x20 mm, Waters) connected to a C18 Atlantis-T3 column (particle size 3 μ m, 3.0x150 mm, Waters) at 30°C. For separation, a mobile phase consisting of nanopure water (Barnstead Nanopure, Thermo Scientific) and methanol (HPLC-grade, Fisher Scientific) both augmented with 0.1% formic acid (98-100%, Merck) at a flow rate of 300 μ L/min was used. The mobile phase gradient went within 15 min from an initial ratio of 95:5 water:methanol to 5:95. There it was kept for 6 min, before it was set back to a ratio of 95:5 water:methanol for a column conditioning of 5 min. Detection with the mass spectrometer was done in positive-negative ionization switch mode. Electrospray ionization was triggered at a capillary temperature of 350°C and a spray voltage of 4 kV and 3 kV for positive and negative ionization, respectively. A mass calibration and mass accuracy check was carried out prior to the measurement with an in-house amino acid solution, which enhanced calibration for small masses. Mass accuracy was always better than 1.5 ppm. The analytes were measured in full-scan mode at a resolution of 70000 and a scan range of 50-750 m/z. Three data-dependent MS/MS were triggered after each full-scan with a resolution of 17500 on the target masses. A matrix blank and a matrix-matched, pH-specific external calibration row over a range from 5 to 100 μ g/L with six calibration points were measured prior to the sample series of the corresponding experiments. Post-acquisition processing and quantification was

done with the Xcalibur 2.2 software (Thermo Scientific). All analytes were processed in positive mode. The calibration rows were in the linear range for all analytes and experiments. All analytes were quantified within a mass window of 10 ppm, except for primaquine and propranolol, for which a mass window of 15 ppm was necessary. The reason for that was a mass shift that can be observed for analytes with similar masses. The lowest calibration point that included spiked analytes was 5 µg/L. Therefore, this concentration was treated as the limit of quantification (LOQ).

A.2.1 Method precision

The triplicate time zero samples of each reactor were used to calculate the method precision by calculating the relative standard deviation. The method precision accounts for sampling uncertainties as well as for analytical uncertainties. The method precision was <10 µg/L for all MPs except for pramoxine and primaquine (see Table A.5). For these MPs, higher deviations were only observed in the BE reactors, which are, most likely, caused by their rapid biotransformation. In these cases, the significant concentration change within the approximately 12 minutes needed for sampling resulted in higher uncertainties.

Table A.5: Method precision

Method precision [%]									
Biotransformation experiments				Sorption experiments				Abiotic experiments	
pH6	pH7	pH8	pH6*	pH7	pH8	pH6	pH7	pH8	
PAR	7 / 10 / 3	2 / 4 / 5	6 / 3 / 1	NA / 4 / 9	2 / 4 / 1	3 / 4 / 7	4 / 4 / 6	3 / 2 / 4	3 / 4 / 3
MIA	3 / 5 / 3	2 / 4 / 3	8 / 3 / 2	NA / 3 / 6	2 / 4 / 3	1 / 6 / 4	3 / 4 / 5	3 / 1 / 5	1 / 6 / 5
PRA	4 / 15 / 12	10 / 13 / 16	25 / 6 / 12	NA / 3 / 6	1 / 6 / 3	2 / 6 / 5	2 / 7 / 4	5 / 3 / 3	3 / 5 / 7
DEP	2 / 5 / 3	2 / 9 / 7	4 / 3 / 3	NA / 5 / 4	3 / 3 / 3	2 / 7 / 6	1 / 6 / 3	3 / 2 / 4	4 / 6 / 7
LID	2 / 4 / 4	2 / 8 / 6	3 / 2 / 3	NA / 4 / 7	3 / 3 / 4	2 / 6 / 6	1 / 5 / 4	4 / 2 / 5	4 / 6 / 5
NIC	2 / 8 / 1	1 / 7 / 6	4 / 2 / 2	NA / 4 / 6	2 / 1 / 4	1 / 5 / 7	1 / 3 / 3	3 / 2 / 4	2 / 4 / 4
CHLO	2 / 4 / 3	2 / 5 / 4	6 / 2 / 1	NA / 3 / 4	1 / 3 / 1	1 / 6 / 4	2 / 4 / 3	3 / 2 / 4	1 / 3 / 4
ORP	1 / 4 / 2	2 / 7 / 8	4 / 3 / 3	NA / 6 / 6	3 / 4 / 4	2 / 6 / 4	1 / 5 / 5	3 / 1 / 2	2 / 4 / 8
PYR	3 / 7 / 7	1 / 5 / 5	4 / 3 / 1	NA / 1 / 6	4 / 3 / 2	2 / 4 / 3	1 / 5 / 6	3 / 3 / 8	3 / 4 / 6
MEX	4 / 5 / 2	2 / 5 / 6	6 / 3 / 2	NA / 3 / 7	3 / 3 / 1	0 / 5 / 6	0 / 6 / 3	3 / 1 / 6	3 / 4 / 3
PHE	0 / 5 / 4	1 / 7 / 5	5 / 5 / 1	NA / 3 / 7	2 / 2 / 3	1 / 5 / 7	1 / 4 / 4	3 / 3 / 5	2 / 5 / 5
VEN	2 / 3 / 4	4 / 7 / 5	7 / 4 / 1	NA / 4 / 7	1 / 4 / 0	2 / 5 / 6	3 / 6 / 6	4 / 2 / 4	3 / 5 / 6
PRO	3 / 4 / 4	1 / 6 / 5	10 / 6 / 5	NA / 6 / 7	1 / 4 / 3	1 / 4 / 3	3 / 6 / 4	4 / 1 / 4	6 / 4 / 7
ATE	4 / 3 / 2	1 / 5 / 3	6 / 1 / 3	NA / 2 / 6	2 / 6 / 1	2 / 4 / 5	2 / 2 / 5	4 / 3 / 5	1 / 3 / 4
PRI	11 / 12 / 4	3 / 7 / 7	13 / 8 / 2	NA / 1 / 4	6 / 2 / 3	0 / 4 / 3	1 / 8 / 9	8 / 8 / 5	3 / 4 / 6
TRI	2 / 6 / 1	1 / 6 / 2	8 / 2 / 1	NA / 3 / 6	1 / 6 / 1	2 / 4 / 7	1 / 4 / 5	3 / 1 / 4	1 / 5 / 6
ISO	3 / 3 / 5	3 / 7 / 3	8 / 5 / 1	NA / 3 / 6	2 / 4 / 3	2 / 6 / 6	1 / 4 / 6	2 / 1 / 3	2 / 6 / 6
AZO	3 / 6 / 5	3 / 7 / 5	7 / 3 / 1	NA / 5 / 7	1 / 6 / 2	1 / 6 / 7	1 / 6 / 7	2 / 1 / 3	1 / 8 / 8

The method precision was calculated as relative standard deviation. The three values for each individual experiment correspond to values measured in triplicate reactor. *One of the triplicate pH6-SE reactors was excluded from analysis because the effective pH was too high (7.5), resulting in a reduced pH6-SE data set.

A.2.2 Relative recovery

The relative recoveries were determined from the time zero samples of the abiotic control reactors by calculating the mean value and dividing it by the theoretical spiked amount of 100 µg/L (see Table A.6).

Table A.6: Relative Recoveries

	Relative recoveries [%]		
	Abiotic experiments		
	pH6	pH7	pH8
PAR	99 / 91 / 92	99 / 98 / 92	92 / 86 / 91
MIA	93 / 87 / 86	91 / 90 / 85	80 / 76 / 81
PRA	96 / 91 / 88	91 / 87 / 83	82 / 76 / 80
DEP	98 / 93 / 91	95 / 96 / 92	94 / 87 / 90
LID	99 / 91 / 90	99 / 96 / 93	96 / 88 / 90
NIC	95 / 88 / 85	92 / 94 / 88	91 / 85 / 90
CHLO	99 / 91 / 89	99 / 98 / 96	96 / 87 / 96
ORP	95 / 90 / 87	95 / 92 / 90	90 / 83 / 90
PYR	96 / 89 / 86	97 / 94 / 92	96 / 88 / 94
MEX	98 / 92 / 89	97 / 95 / 92	101 / 91 / 98
PHE	102 / 92 / 91	97 / 94 / 91	97 / 87 / 94
VEN	101 / 93 / 91	97 / 95 / 88	95 / 87 / 93
PRO	101 / 89 / 86	98 / 92 / 91	91 / 89 / 88
ATE	99 / 95 / 91	101 / 102 / 95	94 / 89 / 95
PRI	87 / 86 / 88	90 / 93 / 89	82 / 81 / 88
TRI	101 / 96 / 96	97 / 95 / 91	94 / 90 / 94
ISO	98 / 93 / 92	93 / 95 / 92	91 / 86 / 93
AZO	89 / 86 / 83	90 / 88 / 87	84 / 78 / 83

The three values for each individual experiment correspond to values measured in triplicate reactor.

A.3 Concentration time series

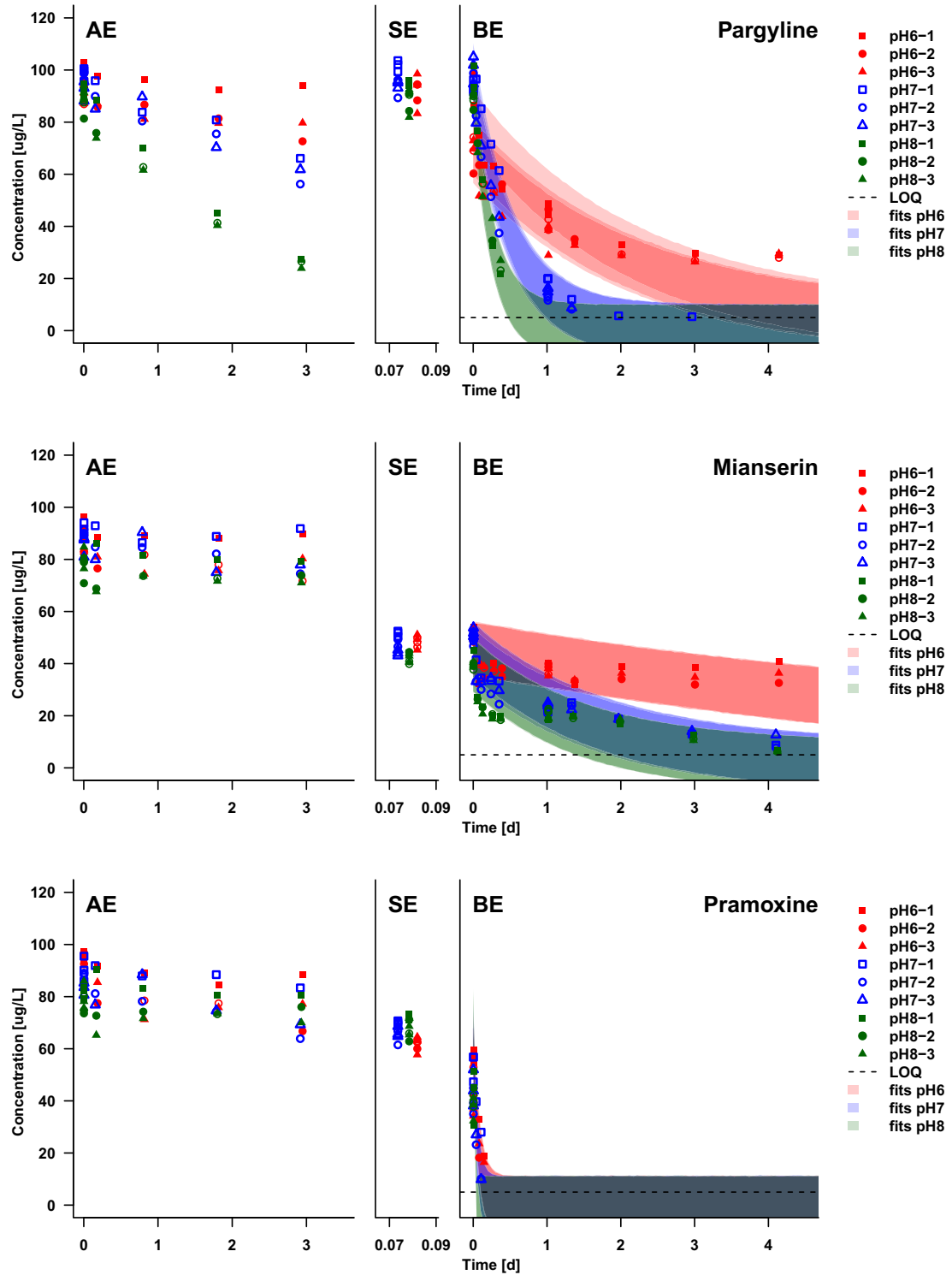


Figure A.3: Concentration time series of pargyline, mianserin, and pramoxine

Appendix A

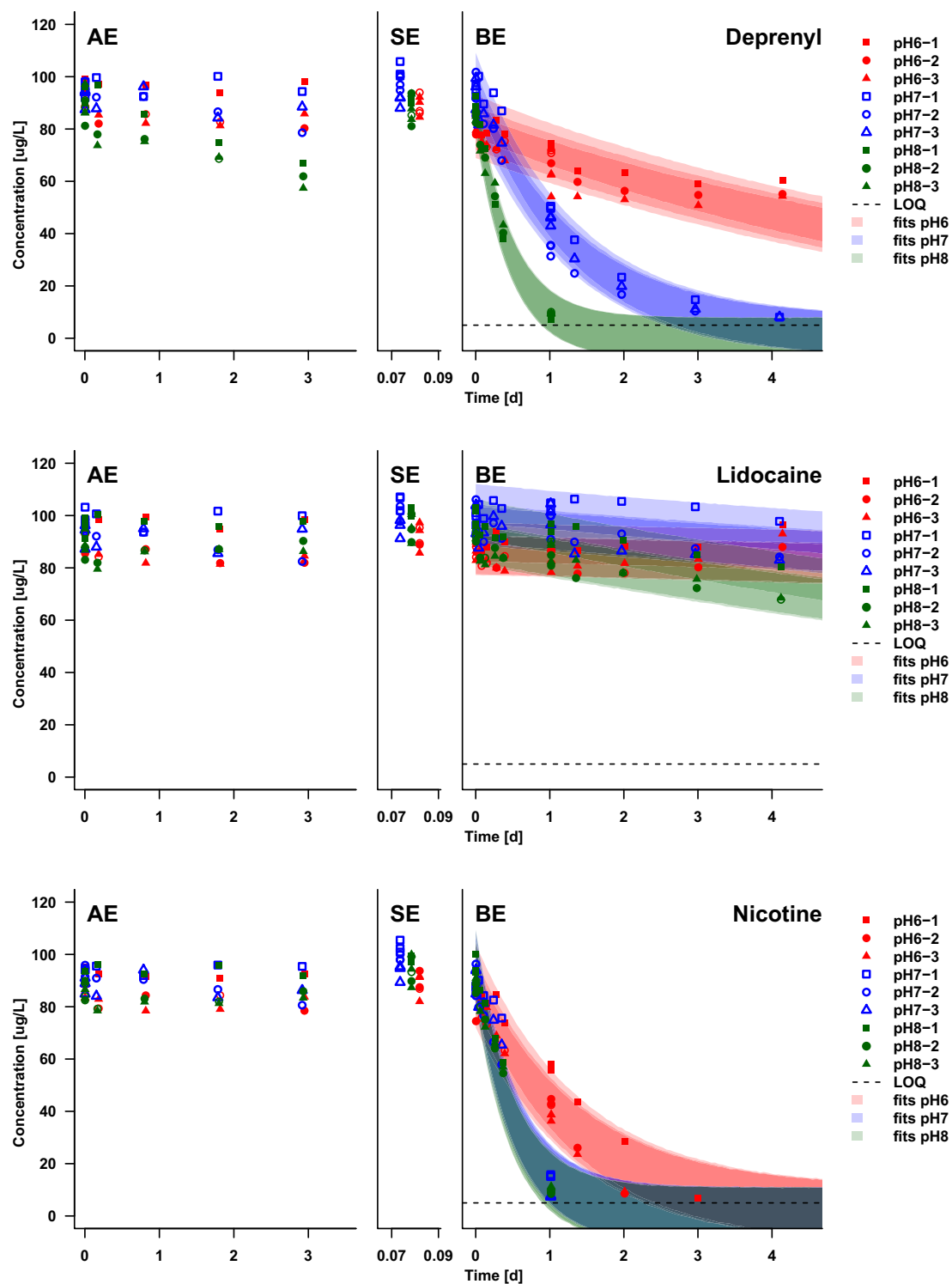


Figure A.4: Concentration time series of deprenyl, lidocaine, and nicotine

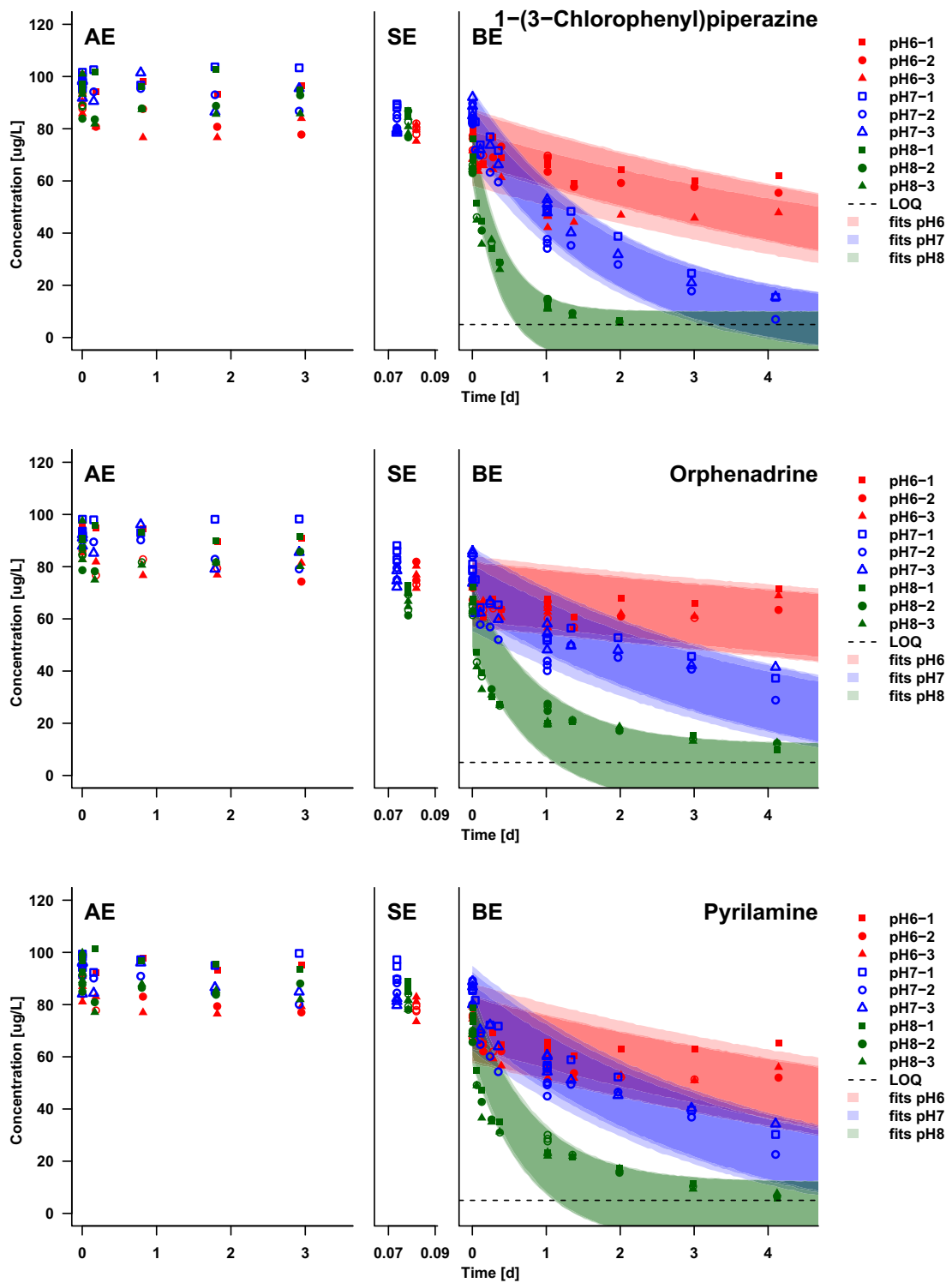


Figure A.5: Concentration time series of 1-(3-chlorophenyl)piperazine, orphenadrine, and pyrilamine

Appendix A

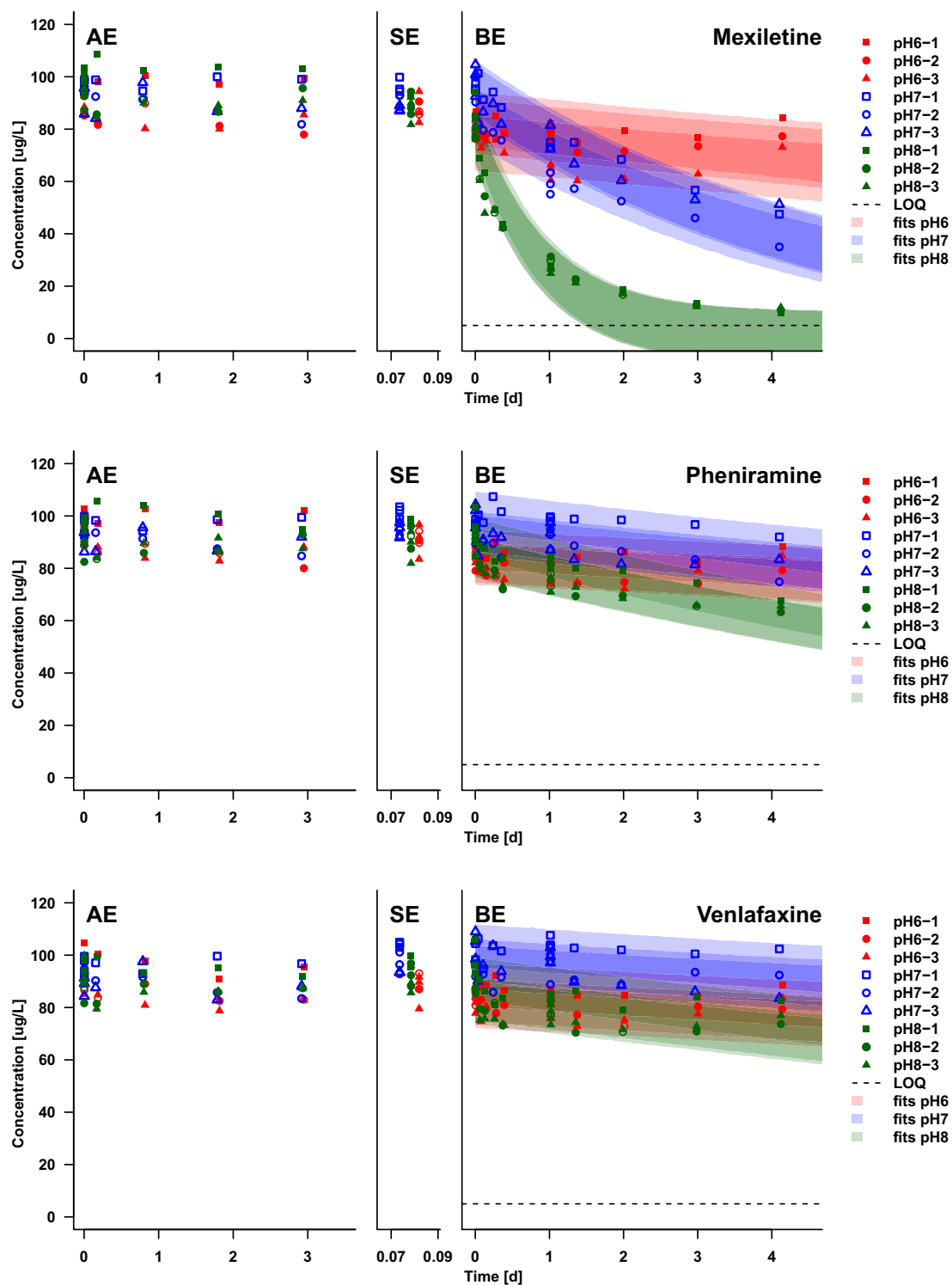


Figure A.6: Concentration time series of mexiletine, pheniramine, and venlafaxine

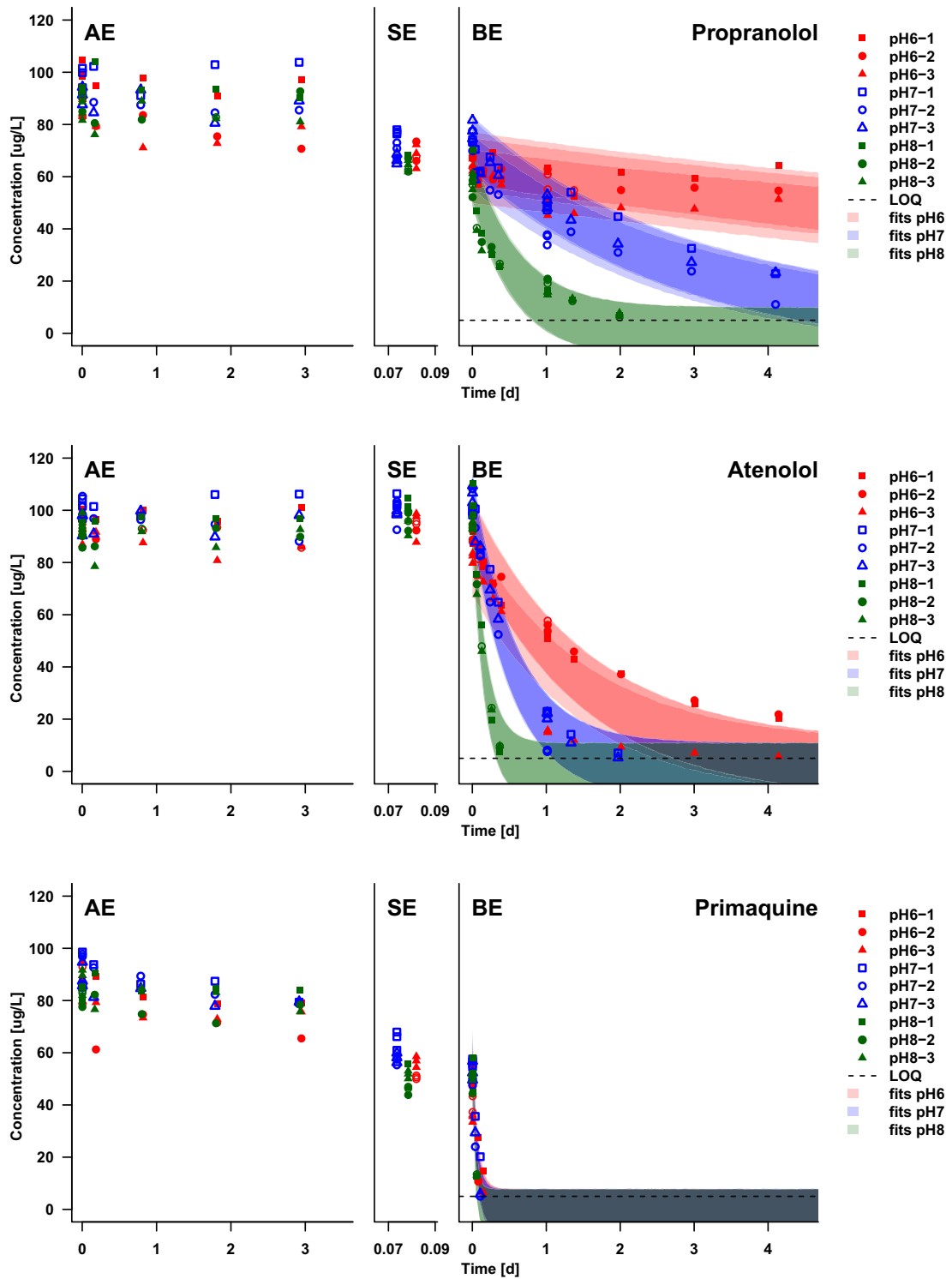


Figure A.7: Concentration time series of propranolol, atenolol, and primaquine

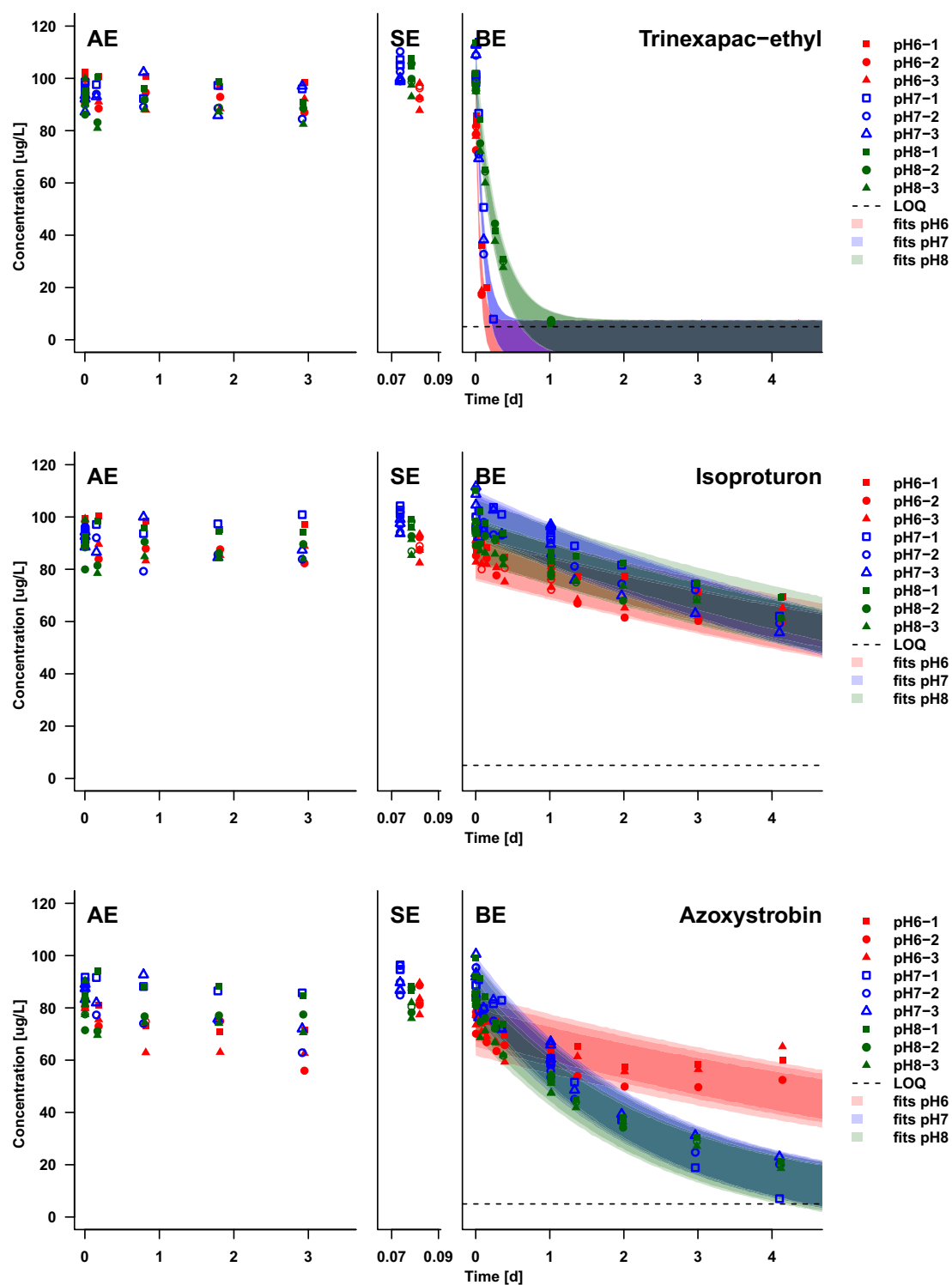


Figure A.8: Concentration time series of trinexapac-ethyl, isoproturon, and azoxystrobin

A.4 Estimation of kinetic parameters

For the error terms $\epsilon^{p,e,r,t}$, a normal distribution was assumed with the same (inferred) standard deviation σ for all measurements. Concentrations below the LOQ (5 μL) were treated as left-censored observations. Because not all parameters were identifiable from the BE and AE measurements alone, data from the SE as well as TSS measurements were used to define informative prior distributions for the parameters f_{aq}^p , $C_{\text{aq}}^{p,e,r}(0)$, and TSS^p . For f_{aq}^p a beta distribution was used as prior because it can only range from 0 to 1. The mode of the prior was estimated as $\bar{C}_{\text{aq}}^{\text{SE}}(2\text{h})/\bar{C}_{\text{aq}}^{\text{AE}}(0\text{h})$, where $\bar{C}_{\text{aq}}^{\text{AE}}(0\text{h})$ and $\bar{C}_{\text{aq}}^{\text{SE}}(2\text{h})$ are the means of the aqueous concentrations of the respective triplicate experiments, and the standard deviation of the prior was derived by error propagation. Normal distributions were used as priors for the initial concentrations. Mean and standard deviation of these were calculated from measured SE data, when modelling BE data, or were set to 100 and 20, respectively, when modelling AE data. Similarly, for TSS^p a normal distribution was used with mean and standard deviation derived from triplicate TSS measurements at pH-level p .

A.4.1 Root-mean-square errors

The quality of the fits to the data can be assessed by the root-mean-square error (RMSE), which gives the average deviation of the predicted concentration values from the measured ones. RMSE values for all MPs at each pH level are given in Table A.7. They were generally below 11.4 $\mu\text{g/L}$, which is in the same range as the method precision.

Table A.7: Root mean square errors (RMSEs)

	RMSE [$\mu\text{g/L}$]		
	pH6	pH7	pH8
PAR	8.9	5.5	3.5
MIA	5.9	5.9	7.4
PRA	10.0	11.4	5.8
DEP	5.3	5.2	3.0
LID	3.9	5.0	3.8
NIC	6.1	9.1	5.7
CHLO	6.8	5.3	7.2
ORP	5.3	7.7	9.9
PYR	6.6	6.7	10.0
MEX	5.0	6.0	8.1
PHE	3.9	4.6	4.9
VEN	3.4	5.2	5.5
PRO	4.9	5.8	7.5
ATE	10.1	5.0	3.3
PRI	5.5	4.0	3.4
TRI	6.0	6.2	3.6
ISO	5.5	4.9	3.6
AZO	4.0	5.3	4.3

A.4.2 Estimated biotransformation rate constants

Table A.8: Biotransformation rate constants (k_{bio})

	k_{bio} [L/(gss days)]		
	pH6	pH7	pH8
PAR	0.23 [0.19 ,0.30]	1.0 [0.78 ,1.4]	1.6 [1.4 ,2.0]
MIA	0.081 [0.047 ,0.12]	0.56 [0.40 ,0.80]	0.53 [0.42 ,0.68]
PRA	9.2 [7.1 ,12]	13. [8.9 ,20]	100. [81. ,130]
DEP	0.061 [0.046 ,0.078]	0.43 [0.34 ,0.61]	0.96 [0.84 ,1.2]
LID	0.0013 [0.000091 ,0.0049]	0.0065 [0.00082 ,0.016]	0.024 [0.017 ,0.034]
NIC	0.38 [0.33 ,0.47]	1.0 [0.81 ,1.5]	0.90 [0.79 ,1.1]
CHLO	0.056 [0.037 ,0.076]	0.33 [0.26 ,0.46]	1.3 [1.0 ,1.6]
ORP	0.0099 [0.0010 ,0.027]	0.14 [0.096 ,0.20]	0.63 [0.50 ,0.83]
PYR	0.048 [0.026 ,0.071]	0.17 [0.12 ,0.25]	0.62 [0.50 ,0.78]
MEX	0.0092 [0.0012 ,0.022]	0.11 [0.083 ,0.16]	0.53 [0.45 ,0.65]
PHE	0.0033 [0.00027 ,0.010]	0.013 [0.0038 ,0.024]	0.036 [0.027 ,0.050]
VEN	0.0021 [0.00017 ,0.0079]	0.0046 [0.00045 ,0.013]	0.015 [0.0054 ,0.025]
PRO	0.020 [0.0038 ,0.043]	0.25 [0.19 ,0.36]	1.0 [0.82 ,1.2]
ATE	0.33 [0.29 ,0.41]	0.99 [0.77 ,1.4]	2.7 [2.3 ,3.3]
PRI	11 [8.6 ,15]	14 [10 ,21]	18 [14 ,25]
TRI	9.2 [7.8 ,11]	5.7 [4.4 ,7.6]	1.6 [1.4 ,1.9]
ISO	0.041 [0.028 ,0.055]	0.065 [0.048 ,0.091]	0.045 [0.035 ,0.060]
AZO	0.0085 [0.00079 ,0.027]	0.21 [0.16 ,0.30]	0.19 [0.17 ,0.26]

Data are given as median and 90% credibility interval.

A.4.3 Estimated sorption coefficients

Table A.9: Sorption coefficients (K_d)

	K_d [L/g _{ss}]		
	pH6	pH7	pH8
PAR	0.046 [0.0046 ,0.19]	0.029 [0.0021 ,0.15]	0.026 [0.0020 ,0.13]
MIA	0.42 [0.33 ,0.54]	0.47 [0.33 ,0.71]	0.37 [0.29 ,0.47]
PRA	0.25 [0.17 ,0.34]	0.17 [0.096 ,0.29]	0.077 [0.028 ,0.17]
DEP	0.045 [0.0093 ,0.14]	0.035 [0.0025 ,0.17]	0.036 [0.0035 ,0.15]
LID	0.045 [0.0043 ,0.20]	0.037 [0.0027 ,0.19]	0.033 [0.0023 ,0.16]
NIC	0.034 [0.0027 ,0.16]	0.033 [0.0022 ,0.16]	0.027 [0.0018 ,0.13]
CHLO	0.095 [0.045 ,0.18]	0.10 [0.048 ,0.20]	0.067 [0.023 ,0.16]
ORP	0.11 [0.048 ,0.22]	0.10 [0.040 ,0.23]	0.14 [0.070 ,0.25]
PYR	0.086 [0.033 ,0.19]	0.072 [0.015 ,0.24]	0.066 [0.022 ,0.15]
MEX	0.054 [0.011 ,0.17]	0.040 [0.0057 ,0.15]	0.048 [0.012 ,0.14]
PHE	0.056 [0.0083 ,0.20]	0.030 [0.0021 ,0.14]	0.035 [0.0025 ,0.17]
VEN	0.086 [0.018 ,0.27]	0.044 [0.0031 ,0.22]	0.033 [0.0024 ,0.16]
PRO	0.19 [0.093 ,0.35]	0.19 [0.099 ,0.34]	0.16 [0.11 ,0.24]
ATE	0.029 [0.0025 ,0.13]	0.029 [0.0020 ,0.14]	0.026 [0.0018 ,0.12]
PRI	0.32 [0.21 ,0.47]	0.29 [0.17 ,0.50]	0.29 [0.18 ,0.45]
TRI	0.037 [0.0061 ,0.12]	0.028 [0.0019 ,0.13]	0.029 [0.0020 ,0.13]
ISO	0.051 [0.012 ,0.14]	0.022 [0.0016 ,0.10]	0.033 [0.0024 ,0.17]
AZO	0.058 [0.0076 ,0.20]	0.028 [0.0020 ,0.13]	0.039 [0.0029 ,0.20]

Data are given as median and 90% credibility interval.

A.4.4 Estimated abiotic transformation rate constants

Table A.10: Abiotic transformation rate constants (k_a)

	k_a [1/day]		
	pH6	pH7	pH8
PAR	0.048 [0.025 ,0.073]	0.15 [0.12 ,0.18]	0.42 [0.37 ,0.48]
MIA	0.034 [0.011 ,0.060]	0.033 [0.010 ,0.058]	0.023 [0.0037 ,0.049]
PRA	0.061 [0.033 ,0.090]	0.060 [0.031 ,0.091]	0.023 [0.0033 ,0.052]
DEP	0.024 [0.0068 ,0.042]	0.027 [0.0094 ,0.045]	0.13 [0.10 ,0.15]
LID	0.0048 [0.00047 ,0.013]	0.013 [0.0024 ,0.025]	0.0061 [0.00057 ,0.019]
NIC	0.021 [0.0030 ,0.046]	0.019 [0.0027 ,0.044]	0.014 [0.0014 ,0.036]
CHLO	0.029 [0.0077 ,0.054]	0.014 [0.0016 ,0.034]	0.012 [0.0012 ,0.031]
ORP	0.030 [0.0076 ,0.054]	0.024 [0.0038 ,0.051]	0.016 [0.0017 ,0.042]
PYR	0.028 [0.0049 ,0.057]	0.024 [0.0039 ,0.051]	0.020 [0.0026 ,0.047]
MEX	0.019 [0.0034 ,0.037]	0.020 [0.0032 ,0.043]	0.010 [0.0010 ,0.029]
PHE	0.012 [0.0024 ,0.024]	0.012 [0.0016 ,0.026]	0.0078 [0.00080 ,0.021]
VEN	0.017 [0.0049 ,0.031]	0.011 [0.0017 ,0.023]	0.012 [0.0015 ,0.028]
PRO	0.041 [0.018 ,0.064]	0.013 [0.0015 ,0.033]	0.013 [0.0013 ,0.033]
ATE	0.020 [0.0028 ,0.043]	0.012 [0.0013 ,0.033]	0.0088 [0.00078 ,0.027]
PRI	0.059 [0.038 ,0.081]	0.049 [0.030 ,0.069]	0.022 [0.0050 ,0.042]
TRI	0.018 [0.0038 ,0.034]	0.013 [0.0020 ,0.029]	0.015 [0.0025 ,0.031]
ISO	0.020 [0.0049 ,0.038]	0.014 [0.0021 ,0.031]	0.0077 [0.00074 ,0.022]
AZO	0.099 [0.076 ,0.12]	0.058 [0.036 ,0.082]	0.017 [0.0023 ,0.038]

Data are given as median and 90% credibility interval.

A.5 Interpretation of pH-dependence of biotransformation rate constants

Figure A.9 shows the relative differences between the experimentally determined (r_{exp}) and the predicted ratio (r_{pred}) of k_{bio} at pH7 and pH8 against the $\text{p}K_{\text{a}}$ of the cationic-neutral MPs. The error bars represent the 90% credibility interval. The 5% interval of lidocaine and venlafaxine are outside of the range of the graph. The numbers above the arrows represent the out of range values. As discussed in the main manuscript, pramoxine is an outlier. Its median value and the 90% credibility interval are -3.49 and [-7.48, -0.89], respectively. Therefore, it is not shown in Figure A.9.

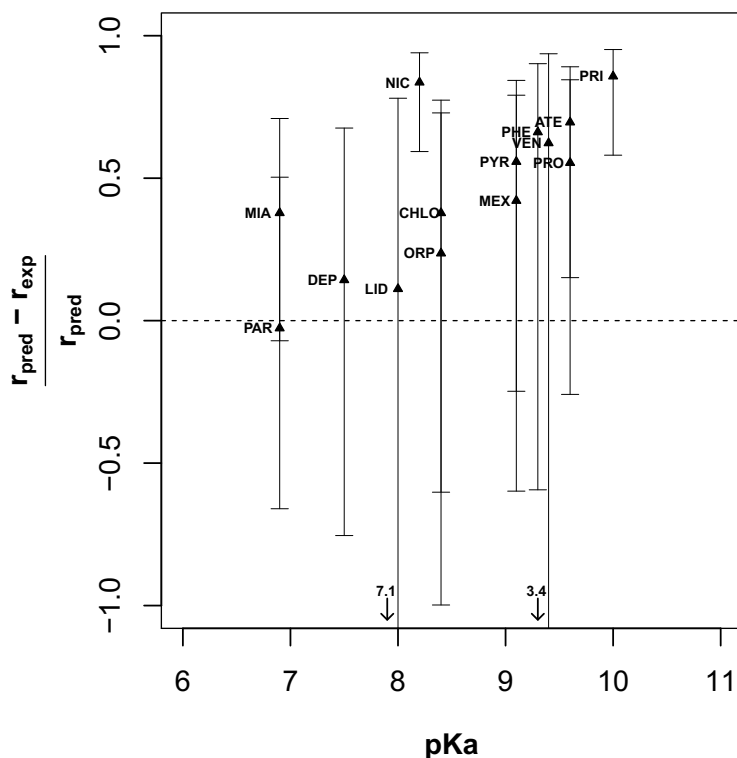


Figure A.9: Relative differences between the experimentally determined (r_{exp}) and the predicted ratio (r_{pred}) of k_{bio} at pH7 and pH8 against the $\text{p}K_{\text{a}}$ of the cationic-neutral MPs.

Appendix B:

Supporting information to Chapter 3

B.1 Materials and methods

B.1.1 Micropollutant selection

The 19 selected micropollutants (MPs) contained 25 amine moieties, including 13 tertiary, eight secondary, and four primary amines. One tertiary amine only was present in pheniramine (PHE), venlafaxine (VEN), lidocaine (LID), spiroxamine (SPI), deprenyl (DEP), pargyline (PAR), N,N-dimethyl-p-chloroaniline (DCA). Two tertiary amine moieties were present in chlorcyclizine (CLC) and pyrilamine (PYR). One tertiary and one secondary amine moiety were present in 1[(4-chlorophenyl)phenylmethyl]piperazine (CPP) and ortho-chlorophenylpiperazine (OCP). Only one secondary amine moiety was present in N-demethylpheniramine (NPE), N-demethylvenlafaxine (NVE), fluoxetine (FLU), and feniramine (FEN). One secondary and one primary amine were present in clenisopenterole (CLE) and primaquine (PRI). Only one primary amine was present in mexiletine (MEX) and N-demethylfluoxetine (NFL). To compare the biotransformation of tertiary and secondary or secondary and primary amines with the same structural backbone, three tertiary amines (venlafaxine, pheniramine, and chlorcyclizine) and one secondary amine (fluoxetine) were complemented with the respective secondary/primary amines that had the same backbone but differed by one methyl group at the amine functional group. The chemical structures are presented in Table 1 in the main text. Additionally, five N-oxide TPs were selected, namely lidocaine N-oxide (LINO), pheniramine N-oxide (PENOX), pargyline N-oxide (PANOX), deprenyl N-oxide (DENOX), and venlafaxine N-oxide (VENOX). The following seven deuterated amines were used as internal standards for quantification of the parent compounds as given in Table B.1: lidocaine-d10, venlafaxine-d6, fluoxetine-d5, N-demethylvenlafaxine-d3, N,N-didemethylvenlafaxine-d6, N,O-didemethylvenlafaxine-d3, and O-demethylvenlafaxine-d6. Standards were purchased from LGC Standards GmbH (Wesel, Germany), Toronto Research Chemicals (Toronto, Canada), Sigma-Aldrich Chemie GmbH (Buchs, Switzerland), Capot Chemical Co. (Hangzhou, China), and SRC Alinda (Moscow, Russia).

B.1.2 Biotransformation test system

The experimental set-up for the biotransformation batch experiments was adopted from Helbling *et al.* (2010).⁵⁸ Briefly, activated sludge (3 L) was sampled from the nitrification basin of a half municipal and half industrial WWTP (3th of November 2014, ARA Neugut, Dübendorf, Switzerland, details are given in Table B.2). The total suspended solids concentration (TSS), measured in triplicates per standard method 2540B,¹²⁵ was 3.4 ± 0.1 g SS /L (g SS : gram suspended solids). This sludge was used for three different experiments, namely the biotransformation experiments (BEs), the sorption control experiments (SEs), and the abiotic control experiments (AEs).

For the BEs, reactors (100 mL amber Schott bottles) were filled with 50 mL activated sludge and shaken at 160 rpm on a circulating shaker table. Shaking ensured continuous mixing and aeration. The pH of the reactors was 8.0 ± 0.2 . The BEs were started within four hours after activated sludge sampling by spiking 60 μ L compound solution (100 mg/L in methanol:water 1:9) into the reactors, resulting in final concentrations of about 120 μ g/L for each MP. The 19 selected amine-containing compounds were spiked individually in one reactor each, hereafter called “single spiked reactors”. Additionally, three reactors were spiked with three different compound mix solutions. Mix A contained the compounds MEX, PRI, FLU, NVE, CPP, DEP, LID, DCA, and PHE, mix B contained NFL, OCP, CLE, FEN, NPE, CLC, PAR, PYR, SPI, and VEN, and mix N contained the five N-oxide compounds LINO, PENO, PANO, DENO, and VENO, as shown in Table B.1. As a result, each parent compound was spiked into two reactors, the respective single spiked reactor and the respective mixed spiked reactor. Both “treated” reactors were used to screen for forming transformation products (TPs). However, the single spiked reactor was necessary to determine which TP belonged to which parent compound. Reactors where the respective parent compound were not spiked could be used as “control” reactors. Triplicate time zero samples were taken within 16 minutes of spiking. Subsequent samples were withdrawn at approximately 2h, 4h, 8h, 1d, 1.5d, 2d, 3d, and 4d after the start of the experiment. At each time point, samples (approx. 1.5 mL) were withdrawn from the reactor with a 10 mL glass syringe, transferred to a centrifuge tube (1.7 mL Safeseal Microcentrifuge Tubes, Sorenson Bioscience, Inc.), and centrifuged for 10 minutes at approximately 13000 g (14000 rpm, ALC, micro centrifuge 4214). The supernatants (0.5 mL)

were transferred into 1.5 mL amber vials and 20 μ L of the internal standard mix solution (1 mg/L in methanol) were added to each vial. Vials were stored between 1 and 10 days at 4°C in the dark until analysis. For compensation of evaporated water, the mass of each reactor was measured before and after sampling at time points that were more than 12 hours apart. If the mass loss between sampling time points was >0.2 g, nanopure water (Barnstead Nanopure, Thermo Scientific) was added to the respective reactor. During the course of the experiment no additional nutrients were added. One additional unspiked reactor was used for preparing matrix-matched, external calibration rows by adding 50 μ L standard solutions (mixture of MPs at various concentrations in methanol) to 950 μ L samples. For the SEs and AEs, triplicate reactors were processed in the same way as the BEs except for the following: For the SEs, reactors (100 mL amber Schott bottles) filled with 50 mL activated sludge were autoclaved twice (24 hours apart) at 121°C and 103 kPa for 20 minutes. Then, 60 μ L of a MP mix solution containing all compounds from mixture A, B, and N (100 mg/L of each MP in methanol) were spiked. Triplicate samples of each SE reactor were taken once, approximately two hours after the start of the experiment. For the AEs, reactors (100 mL amber Schott bottles) were filled with 50 mL activated sludge filtrate (sterile filter: 0.2 μ m, Sartorius Stedium, Göttingen, Germany) and autoclaved in the same way. Then, 60 μ L of the same MP mix solution as for the SE were spiked. Samples were taken at 0h (in triplicate), 1d, 2d, and 3d after start. Additional reactors were used to prepare matrix-matched, external calibration rows for the SEs and AEs.

Table B.1: ID, name, and mixture for all test compounds, and internal standards for their quantification

ID	Name	Mixture	Internal Standard
MEX	Mexiletine	A	Fluoxetine-d5
PRI	Primaquine	A	Venlafaxine-d6
FLU	Fluoxetine	A	Fluoxetine-d5
NVE	N-desmethyl venlafaxine	A	N-desmethyl venlafaxine-d3
CPP	1[(4-chlorophenyl)phenylmethyl]piperazine	A	Fluoxetine-d5
DEP	Deprenyl	A	Lidocaine-d10
LID	Lidocaine	A	Lidocaine-d10
DCA	N,N-dimethyl-p-chloroaniline	A	Venlafaxine-d6
PHE	Pheniramine	A	Lidocaine-d10
NFL	Norfluoxetine	B	Fluoxetine-d5
OCP	o-chlorophenylpiperazine	B	Venlafaxine-d6
CLE	Clenisopentrol	B	Fluoxetine-d5
FEN	Fenfluramine	B	Venlafaxine-d6
NPE	N-desmethyl pheniramine	B	Lidocaine-d10
CLC	Chlorcyclizine	B	Venlafaxine-d6
PAR	Pargyline	B	Lidocaine-d10
PYR	Pyrilamine	B	Venlafaxine-d6
SPI	Spiroxamine	B	Venlafaxine-d6
VEN	Venlafaxine	B	Venlafaxine-d6
LINO	Lidocaine N-oxide	N	Venlafaxine-d6
PENO	Pheniramine N-oxide	N	O-desmethyl venlafaxine-d6
PANO	Pargyline N-oxide	N	Lidocaine-d10
DENO	Deprenyl N-oxide	N	Venlafaxine-d6
VENO	Venlafaxine N-oxide	N	Venlafaxine-d6

Table B.2: Details on sampled wastewater treatment plant (ARA Neugut, Dübendorf, Switzerland)

Population equivalent	100'000 (40'000 inhabitants, 10'000 commuters, 50'000 industry)
Primary treatment step	Mechanical treatment: grit, sand and oil trap, primary clarifier
Secondary treatment step	Conventional activated sludge system with nitrification / denitrification and biological phosphorous elimination steps
Advanced treatment step	Since March 2014, Switzerland's first full-scale ozonation treatment
Final step	Sand filtration
Sewage flow	80 - 350 L/s (under dry weather conditions)
Sludge age	25 days
Hydraulic retention time	20 hours (under dry weather conditions)

B.1.3 Analytical method

For chemical analysis, reversed-phase liquid chromatography coupled to a high-resolution quadrupole Orbitrap mass spectrometer (Qexactive, Thermo Scientific) was used. The method used previously was modified for this experiment.¹⁰⁶ In detail, 20 μL samples were injected onto a guard cartridge (particle size 3 μm , 3.9x20 mm, Waters) connected to a C18 Atlantis-T3 column (particle size 3 μm , 3.0x150 mm, Waters) at 30°C. For separation, a mobile phase consisting of nanopure water (Barnstead Nanopure, Thermo Scientific) and methanol (HPLC-grade, Fisher Scientific) both augmented with 0.1% formic acid (98-100%, Merck) was used at a flow rate of 300 $\mu\text{L}/\text{min}$. The mobile phase gradient went within 15 min from an initial ratio of 95:5 water:methanol to 5:95. There it was kept for 6 min, before it was set back to a ratio of 95:5 water:methanol for a column conditioning of 5 min. Detection with the mass spectrometer was done in positive or positive-negative ionization switch mode depending on the sample type as given in Table B.3. Electrospray ionization was triggered at a capillary temperature of 350°C and a spray voltage of 4 kV and 3 kV for positive and negative ionization, respectively. The sheath gas flow rate was adjusted to 40, the auxiliary gas flow rate to 15, and the sweep gas flow rate to 0. Mass calibration and mass accuracy checks were carried out prior to the measurement with an in-house amino acid solution, which enhanced calibration for small masses. Thereby, mass accuracy in the full-scan was always better than 1.0 ppm. Full-scan acquisition was conducted at a resolution of 70'000 at m/z 200 and a scan range of m/z 50-750 with an injection time of 50 ms and an AGC target value of 5×10^5 . Three data-dependent MS/MS scans were conducted after each full-scan with a resolution of 17'500 at m/z 200, an injection time of 100 ms, an AGC target value of 2×10^5 , and an isolation width of 1.0 Da. The dynamic exclusion was set to 7 sec or 3 sec depending on the sample type as given in Table B.3. The data-dependent MS/MS were triggered after each full-scan on the $[\text{M}+\text{H}]^+$ and if negative ionization mode acquisition was conducted on the $[\text{M}-\text{H}]^-$ masses of a list of candidates, depending on the sample type as given in Table B.3. The collision energy with which the MS/MS scans were triggered were calculated as $(-0.41) \times \text{exact mass} + 160$ for masses below m/z 350 and were set to 15 for masses above 350 m/z . The different candidate lists used were:

1. standards: the selected MPs;

2. previously found TPs refers to TPs that were found in similar pre-experiments, which were not published;
3. EAWAG-PPS predictions refers to TPs that were predicted by the EAWAG-PPS^{100–102} in October 2014 with the following settings: relative reasoning off, predictions of all aerobic likelihoods included, and predictions until the second generation;
4. metaprint2D predictions refers to TPs that were predicted by the pathway prediction system MetaPrint2D-React^{107,126,127} in October 2014 with the default settings and the selected model ALL. TPs were only included if they were generated by reactions involving the amine functional groups;
5. manually generated extended suspect list refers to TPs that were generated manually by applying atomic modifications similar to the ones given in Table B.6, B.7, and B.5 to the parent compounds.

Table B.3: LC-HR-MS/MS-settings for the different sample types

Sample types	Ionization mode	Dynamic exclusion	Lists of candidates for which data-dependent-MS ² scans were triggered
AE, SE, BE-mix-N	positive	7 s	standards and previously found TPs
BE-mix-A, BE-mix-B	positive	7 s	standards, previously found TPs, EAWAG-PPS predictions, and metaprint2D predictions
BE-single spiked	positive-negative switch	3 s	standards, previously found TPs, EAWAG-PPS predictions, metaprint2D predictions, and manually generated extended suspect list

For the BE samples, a matrix blank and a matrix-matched, external calibration row over a range from 0.5 to 125 µg/L with ten calibration points were measured prior to

and after the sample series. The lowest calibration point of 0.5 µg/L was treated as the limit of quantification (LOQ) for the BE samples. For the AE and SE samples, the calibration rows consisted of seven calibration points ranging from 5 to 125 µg/L and were measured prior to the sample series. Quantification was done with the Xcalibur 2.2 software (Thermo Scientific). All analytes were processed in positive mode within a mass window of 10 ppm. The internal standards that were used for the respective compounds are given in Table B.1. The calibration rows were in the linear range for all analytes.

B.1.3.1 Additional MS² acquisition for identified TP candidates

For all identified TP peaks, additional MS² measurements were conducted later with a high-resolution quadrupole Orbitrap mass spectrometer (Q Exactive, Thermo Scientific or Q Exactive Plus, Thermo Scientific). Each TP was measured in an individual run, where the single-spiked reactor containing the highest amount of the TP was used preferentially. However, if the TP was significantly more abundant in the mixed spiked reactor, the mixed spiked reactor with maximum amounts of the TP was taken instead. During acquisition, six targeted-MS² experiments were conducted after each full-scan in positive ionization-mode. The acquisition was similar to the original measurement except for the following: The full-scan was acquired with a maximum injection time of 100 ms and the targeted-MS² experiments were acquired on the respective [M+H]⁺ mass for six normalized collision energies, namely 15, 30, 45, 60, 75, and 90 (dimensionless) with an AGC target value of 5×10^5 . MassBank records were created from the best MS² measurement for each compound using RMassBank.^{108,128}

B.1.4 Transformation product identification

Transformation products (TPs) were identified using commercial software to apply the underlying principles described in Helbling et al (2010)⁵⁸. For the suspect and non-target screening approach, Compound Discoverer 1.0 (Thermo Scientific) was used; Sieve 2.2 (Thermo Scientific) was also used for non-target screening. Details are described below. In principle, the suspect screening approach was used for TPs that were generated by plausible reactions, while all peaks that were present were screened in the non-target approach. The same general conditions had to be met for both screening approaches to select a peak as possible candidate TP peak:

1. the peak had to be present in both treated reactors and either absent or at significantly lower levels in the control reactor;
2. the time series pattern of the peak had to be TP-like, *i.e.* peak intensity had to continuously increase, or increase and decrease over the time of the experiment;
3. a reasonable chemical formula had to match the exact mass and the isotopic pattern.

Since the overall goal of this study was to explore and interpret the initial transformation reactions of amine-containing compounds and not to delineate complete biotransformation pathways, the focus was on the identification of first generation products. Therefore, TPs were omitted if they were clearly a higher generation product according to their time series patterns and/or if the structural evidence indicated a structure that was formed by multiple sequential reactions, for which a first generation TP had already been identified for the respective parent amine. However, TPs that were formed by multiple steps but were the only TPs of the respective parent that could be attributed to a certain primary reaction were kept.

B.1.4.1 Suspect and non-target screening using compound discoverer 1.0

For the TP identification with Compound Discoverer 1.0, each parent compound was processed individually. Samples from single-spiked and mixed spiked reactors containing the respective parent compounds were used, as well as samples of one mixed reactor that did not contain the respective compound, which were used as controls. The sampling times were used as *study factors* and assigned to each sample in order to correlate two (or four at time zero, due to the triplicate measurement of the mixed reactor) sample files and one control file at each time point. The workflow is illustrated in Figure B.1. The settings for the different nodes in the workflow are given in Figure ???. The workflow was a combined suspect and non-target screening approach. The suspect screening approach (*Expected Finder node*), screened for suspect TPs that were generated by a list of possible reactions (*Compound Generator node*) that were applied to the respective parent compound structure. The reactions applied are given in Table B.6, Table B.7, and Table B.5. Available MS²-measurements of a suspect TP peak were automatically annotated considering the fragmentation prediction for the parent compound and the atomic modification from the chemical formula of the parent compound to the respective suspect TP (*FISh Scoring node*). In the non-target-screening approach (*Unknown Detector node*), peak detection was performed on the individual raw files. The results of both approaches were consolidated. The number of consolidated peaks was reduced using the following three filter criteria:

1. maximum area greater than or equal to 25'000;
2. peaks had to be found in the single spiked sample and in the mixed spiked sample

for at least one time point;

- the peak was absent or at least 5 times lower in the control than in the sample.

The remaining consolidated peaks were then investigated manually for the following features:

- the peaks had to have a reasonable peak shape and be present in the samples of both reactors for a reasonable amount of times according to the size of the peaks;
- the areas of the peaks had to follow a TP pattern, meaning they had to continuously increase, or increase and decrease with sampling time;
- if a chemical formula was proposed, the observed isotopic pattern had to match the theoretical isotopic pattern according to the size of the peaks;
- if a MS^2 spectrum was available, the fragmentation prediction as well as matches to the observed fragments of the parent compound were further taken into account.

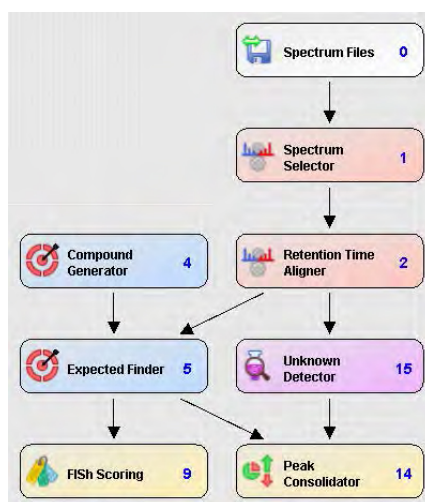


Figure B.1: A screenshot of the Compound Discoverer 1.0 workflow. The nodes show the different process steps and the arrows indicate their connections.

Table B.4: Settings for Compound Discoverer 1.0 nodes

Spectrum Files	Spectrum Selector	Retention Time Aligner	Expected Finder
Input Data: - File Name(s) (Hidden): <i>11 raw-files from the respective mix-reactor</i> <i>9 raw-files from the respective single-spiked reactor</i> <i>9 raw-files from a single-spiked reactor of the other mix-group</i>	1. General Settings: - Precursor Selection: Use MS(n - 1) Precursor - Use New Precursor Reevaluation: True - Use Isotope Pattern in Precursor Reevaluation: True 2. Spectrum Properties Filter: - Lower RT Limit: 3 - Upper RT Limit: 0 - First Scan: 0 - Last Scan: 0 - Lowest Charge State: 0 - Highest Charge State: 0 - Min. Precursor Mass: 100 Da - Max. Precursor Mass: 5000 Da - Total Intensity Threshold: 10000 - Minimum Peak Count: 1 3. Scan Event Filters: - Mass Analyzer: (not specified) - MS Order: Any - Activation Type: (not specified) - Min. Collision Energy: 0 - Max. Collision Energy: 1000 - Scan Type: Any - Polarity Mode: Is + 4. Peak Filters: - S/N Threshold (FT-only): 0 5. Replacements for Unrecognized Properties: - Unrecognized Charge Replacements: 1 - Unrecognized Mass Analyzer Replacements: ITMS - Unrecognized MS Order Replacements: MS2 - Unrecognized Activation Type Replacements: CID - Unrecognized Polarity Replacements: + - Unrecognized MS Resolution@200 Replacements: 60000 - Unrecognized MSn Resolution@200 Replacements: 30000	1. General Settings: - Alignment Model: Adaptive curve - Maximum Shift [min]: 0.5 - Mass Tolerance: 5 ppm Unknown Detector 1. General Settings: - Mass Tolerance [ppm]: 10 ppm - Intensity Tolerance [%]: 30 - S/N Threshold: 3 - Min. Peak Intensity: 10000 - Ions: <Abstractionlons Version="1"> <Abstraction ID="6" ComponentsString="2M+H" /> <Abstraction ID="12" ComponentsString="2M+Na" /> <Abstraction ID="1" ComponentsString="M+H" /> <Abstraction ID="4" ComponentsString="M+K" /> <Abstraction ID="2" ComponentsString="M+Na" /> </Abstractionlons> - Min. Element Counts: C H - Max. Element Counts: C90 H190 N10 O15 P2 S5 <i>Cl was/were added, if the respective parent compound possessed Cl-atom(s)</i> 2. Peak Detection: - Filter Peaks: True - Max. Peak Width [min]: 0.3	1. General Settings: - Mass Tolerance: 10 ppm - Intensity Tolerance [%]: 30 - Min. # Isotopes: 1 - Min. Peak Intensity: 10000 - Average Peak Width [min]: 0 Compound Generator 1. Compound Selection: - Compound: <i>respective parent compound as imported into the editor of compounds</i> 2. Dealkylation: - Apply Dealkylation: True - Apply Dearylation: True - Max. # Steps: 3 - Min. Mass [Da]: 200 3. Transformations: - Phase I: <Transformations Version="1"> <i>As defined in Table S3</i> - Phase II: <Transformations Version="1"> <i>As defined in Table S4</i> - Others: <Transformations Version="1"> <i>As defined in Table S5</i> </Transformations> - Max. # Phase II: 1 - Max. # All Steps: 3 4. Ionization: - Ions: <Abstractionlons Version="1"> <Abstraction ID="1" ComponentsString="M+H" /> <Abstraction ID="2" ComponentsString="M+Na" /> </Abstractionlons>
FISh Scoring			
1. General Settings: - Annotate Full Tree: True - Match Transformations: True - S/N Threshold: 3 - High Acc. Mass Tolerance: 2.5 mmu - Low Acc. Mass Tolerance: 0.5 Da 2. Fragment Prediction Settings: - Use Libraries: True - Use Libraries for Full Tree: False			
Peak Consolidator			
1. Peak Consolidation: - Mass Tolerance: 5 ppm - RT Tolerance [min]: 0.5 2. Compare with Control: - Compare with Control: True - Max. Sample/Control Fold: 0 - Max. Control/Sample Fold: 0			

Manually adjusted settings are marked in blue and italic.

Table B.5: Atomic modifications applied under Category Others

Name	Leaving group	Arriving group	Structural requirement in parent compound to apply reaction
Dioxidation		O ₂	
Deamination	NH ₃	O ₂	
Oxidation to carbonyl	H ₂	O	
Oxidation to acid	H ₂	O ₂	
Decarboxylation	CO ₂		Presence of 2 O-atoms
Denitro	NO ₂	H	Presence of 2 O-atoms
Deamination 2	NH ₂	OH	
Trioxidation		O ₃	
Reduction	O ₂	H ₂	Presence of 2 O-atoms
Deamination3	NH		
Demethylation	CH ₂		If group is connected to the amine N-atom
Deethylation	C ₂ H ₄		If group is connected to the amine N-atom
Desisopropylation	C ₃ H ₆		If group is connected to the amine N-atom
Depropargylation	C ₃ H ₃	H	If group is connected to the amine N-atom
Specific dealkylation 1	C ₈ H ₉ O	H	If group is connected to the amine N-atom
Specific dealkylation 2	C ₂ H ₂		If group is connected to the amine N-atom
Specific dealkylation 3	C ₅ H ₁₀		If group is connected to the amine N-atom
Specific dealkylation 4	C ₂ H ₄		If group is connected to the amine N-atom
Specific dealkylation 5	C ₃ H ₆		If group is connected to the amine N-atom
Specific dealkylation 6	C ₂ H ₄	H	If group is connected to the amine N-atom
Specific deamination 1	C ₄ H ₁₀ N	H	If group is connected to the amine N-atom
Specific deamination 2	C ₅ H ₄ N	H	If group is connected to the amine N-atom
Specific deamination 3	C ₉ H ₁₄ N ₃	H	If group is connected to the amine N-atom
Specific deamination 4	C ₄ H ₆ N	H	If group is connected to the amine N-atom
Specific deamination 5	C ₅ H ₁₂ N	H	If group is connected to the amine N-atom
Specific deamination 6	C ₂ H ₄ N		If group is connected to the amine N-atom
Specific deamination 7	C ₂ H ₆ N	O	If group is connected to the amine N-atom
Specific deamination 8	C ₄ H ₇ N		If group is connected to the amine N-atom

Table B.4: continued

Name	Leaving group	Arriving group	Structural requirement in parent compound to apply reaction
Specific deamination 9	C ₄ H ₁₀ N	O	If group is connected to the amine N-atom
Specific deamination 10	C ₅ H ₁₃ N	O	If group is connected to the amine N-atom
Specific deamination 11	C ₅ H ₁₃ N	O ₂	If group is connected to the amine N-atom
Specific deamination 12	C ₂ H ₅ N		If group is connected to the amine N-atom
Specific deamination 13	C ₃ H ₇ N		If group is connected to the amine N-atom
Specific deamination 14	C ₄ H ₈ N	H	If group is connected to the amine N-atom
Specific deamination 15	C ₂ H ₄ N	H	If group is connected to the amine N-atom

Table B.6: Atomic modifications applied under Category Phase 1

Name	Leaving group	Arriving group	Structural requirement in parent compound to apply reaction
Oxidation		O	
Reduction		H ₂	
Hydration		H ₂ O	
Desaturation	H ₂		
Dehydration	H ₂ O		Presence of O-atom
Nitro reduction	O ₂	H ₂	
Reductive defluorination	F	H	Presence of F-atom
Reductive dechlorination	Cl	H	Presence of Cl-atom
Oxidative defluorination	F	OH	Presence of F-atom
Oxidative dechlorination	Cl	OH	Presence of Cl-atom
Oxidative deamination to ketone	NH ₃	O	
Oxidative deamination to alcohol	NH ₂	OH	
Formylation		CO	

Table B.7: Atomic modifications applied under Category Phase 2

Name	Leaving group	Arriving group	Structural requirement in parent compound to apply reaction
Acetylation	H	C ₂ H ₃ O	
Methylation	H	CH ₃	
Sulfatation	H	SO ₃ H	
Glucuronide conjugation	H	C ₆ H ₉ O ₆	
Glucoside conjugation	H	C ₆ H ₁₁ O ₅	
GSH conjugation 1		C ₁₀ H ₁₅ N ₃ O ₅	
GSH conjugation 2		C ₁₀ H ₁₇ N ₃ O ₆ S	
GSH conjugation (on fluorine)	F	C ₁₀ H ₁₆ N ₃ O ₆ S	Presence of F-atom
GSH conjugation (on chlorine)	Cl	C ₁₀ H ₁₆ N ₃ O ₆ S	Presence of Cl-atom
Glycine conjugation	OH	C ₂ H ₄ NO ₂	
Glutamine conjugation	OH	C ₅ H ₉ N ₂ O ₃	
Ornithine conjugation	OH	C ₅ H ₁₁ N ₂ O ₂	
Arginine conjugation	OH	C ₆ H ₁₃ N ₄ O ₂	
Taurine conjugation	OH	C ₂ H ₆ NO ₃ S	
Palmitoyl conjugation	H	C ₁₆ H ₃₁ O	
Stearyl conjugation	H	C ₁₈ H ₃₅ O	
Acylation		C ₃ H ₄ O	
Succinylation		C ₄ H ₄ O ₃	
Fumarylation		C ₄ H ₂ O ₃	
Malonylation		C ₃ H ₂ O ₃	

B.1.4.2 Non-target screening using sieve 2.2

For the TP identification with Sieve 2.2, each mixed spiked reactor was processed individually. In each run, all raw files of the respective mixed spiked reactors were used as treated group and all raw files of one single spiked reactor that was spiked with a parent compound of another mixture were used as control group. Details of the settings are given in Table B.8. The processed data were filtered with an automatic filter as given in Table B.9, based on the following features:

1. the ratio between all control samples and at least on treated sample is greater than 10;
2. the intensity of the respective peak is greater than 1'000'000 in at least one treated sample;
3. respective peaks are present in at least two adjacent treated samples;
4. the intensity of the respective peak of at least one treated sample between sampling point 2h and 3d is greater than or equal to ten times the intensity of the respective in the treated sample at 0h or 4d.

The remaining frames were selected manually based on the plausibility of their chromatographic peak shape and their time series pattern showing a TP-like shape. Afterwards, the corresponding parent compound of the selected TPs was identified by manually checking with the Xcalibur 2.2 software for the presence of the respective peaks in the single-spiked reactors.

One TP can generate several components, *i.e.*, isotopologues, adducts, satellites, and in-source fragments, which are detected as individual peaks in the full-scan. These peaks can also be identified as possible TPs in the non-target screening approach since they also possess a TP-like behavior, *i.e.*, are formed over the time of the experiment, are not present in control reactors, etc. Therefore, the identified TP peaks were investigated manually to group them together into components (componentization). This was done based on retention time and peak shape similarity, time series patterns and matching mass differences.

Table B.8: Sieve 2.2 parameter settings.

Parameter Category	Parameter Name	Parameter Setting
Designate Experiment Type	Domain	Small Molecule
	Signal Detection Algorithm	Chromatographic Alignment and Framing
	Experiment Type	Control Compare Trend
Raw File Selection		<i>All raw file of the respective mixed spiked reactor and of one control reactor</i>
Raw File Chracterization	Groups	<i>For the raw files of the treated reactor the corresponding sampling point and for all raw files of the control reactor control</i>
	Ration group	control
Frame Parameter Adjustment	m/z Min	50.00
	m/z Max	750.00
	Retention Time Start (min)	0.5
	Retention Time Stop (min)	21
	Frame Time Width (min)	2.50
	M/Z Width (ppm)	10.00
Frame Selection	Maximum Number of Frames	20000
	Peak Intensity Threshold	100000
Scan filter selection		<i>positive mode full-scan</i>
Identification Parameters	Frames to Identify	0
SIEVE Parameters	AlignmentBypass	TRUE

Individually adjusted parameters are marked in blue and italic.

Table B.9: Filter for data processing with Sieve 2.2

Filter of mixture reactor B
$ \begin{aligned} &(\text{Ratio_2h} > 10 \text{ or Ratio_4h} > 10 \text{ or Ratio_8h} > 10 \text{ or Ratio_1d} > 10 \text{ or Ratio_15d} > 10 \\ &\text{or Ratio_2d} > 10 \text{ or Ratio_3d} > 10 \text{ or Ratio_4d} > 10) \text{ and } (\text{II_140711_38} > 1000000 \text{ or} \\ &\text{II_140711_37} > 1000000 \text{ or II_140711_36} > 1000000 \text{ or II_140711_35} > 1000000 \text{ or} \\ &\text{II_140711_34} > 1000000 \text{ or II_140711_33} > 1000000 \text{ or II_140711_32} > 1000000 \text{ or} \\ &\text{II_140711_31} > 1000000) \text{ and } (\text{II_140711_38} * \text{II_140711_37} > 0 \text{ or} \\ &\text{II_140711_37} * \text{II_140711_36} > 0 \text{ or II_140711_36} * \text{II_140711_35} > 0 \text{ or} \\ &\text{II_140711_35} * \text{II_140711_34} > 0 \text{ or II_140711_34} * \text{II_140711_33} > 0 \text{ or} \\ &\text{II_140711_33} * \text{II_140711_32} > 0 \text{ or II_140711_32} * \text{II_140711_31} > 0) \text{ and} \\ &(((\text{II_140711_32} > 10 * \text{II_140711_31}) \text{ or } (\text{II_140711_32} > 10 * \text{II_140711_40})) \text{ or} \\ &((\text{II_140711_33} > 10 * \text{II_140711_31}) \text{ or } (\text{II_140711_33} > 10 * \text{II_140711_40})) \text{ or} \\ &((\text{II_140711_34} > 10 * \text{II_140711_31}) \text{ or } (\text{II_140711_34} > 10 * \text{II_140711_40})) \text{ or} \\ &((\text{II_140711_35} > 10 * \text{II_140711_31}) \text{ or } (\text{II_140711_35} > 10 * \text{II_140711_40})) \text{ or} \\ &((\text{II_140711_36} > 10 * \text{II_140711_31}) \text{ or } (\text{II_140711_36} > 10 * \text{II_140711_40})) \text{ or} \\ &((\text{II_140711_37} > 10 * \text{II_140711_31}) \text{ or } (\text{II_140711_37} > 10 * \text{II_140711_40})) \text{ or} \\ &((\text{II_140711_38} > 10 * \text{II_140711_31}) \text{ or } (\text{II_140711_38} > 10 * \text{II_140711_40}))) \end{aligned} $

B.1.5 Generation of time series pattern and check of control reactors

In order to generate the time series patterns of the identified TPs, the respective peaks of all identified TPs, which were mostly the $[M+H]^+$ peaks, were manually integrated in the samples of the corresponding treated reactors, using Xcalibur 2.2. The resulting areas were plotted against the sampling time points, yielding the time series pattern. Additionally, to validate that the identified TPs were formed predominantly through biotic transformations, all samples of two AE and two SE control reactors as well as three high standard samples of the matrix-matched BE calibration row were manually inspected and if peaks were present at the respective exact mass and retention time, they were integrated. If the area of the maximum peak in these control samples was smaller than 10 % of the area of the maximum peak in the treated reactors, the respective TP was considered as predominantly formed by biotic processes. The remaining TPs were flagged and are mentioned explicitly in the structure elucidation pages in Chapter B.4 and in the pathway maps in Chapter B.6.

B.1.6 Structure elucidation

Structure elucidation was performed assuming that the $[M+H]^+$ ion (positive mode) was the most abundant species in the component, but the presence of other species was considered during componentization as described above.

Structure elucidation was performed using Compound Discoverer 1.0 and manual interpretation. First, the molecular formula was determined. For the suspect screening approach, the observed exact mass and isotope pattern in the full scan was compared with the calculated data from the suspect formula. For the non-target screening approach, molecular formulas were predicted for the exact mass within a mass deviation of 10 ppm using Xcalibur 2.2 Qualbrowser. The match between the predicted formula and the observed data was then investigated, along with the ability to form a plausible transformation product from the parent compound. Once the most reasonable chemical formula was proposed, MS^2 spectra were interpreted. The data-dependent MS^2 spectra of the original measurements were available within Compound Discoverer 1.0, while the reacquired targeted MS^2 spectra were interpreted manually with Xcalibur 2.2 Qualbrowser. The latter spectra were acquired at different collision energies over the

total chromatographic run, which enabled both the observation of MS² fragments at different collision energies and whether the fragments truly originate from the precursor ion using chromatographic peak shape match. The MS² fragments were assigned with chemical formulas assuming these were subformulas of the precursor ion. Interpretation of the MS² spectra considered matching fragments and neutral losses in the parent MS² spectra, fragments that matched when accounting for part or all of the atomic modification between parent and TP, additional meaningful fragments or neutral losses in the TP spectrum as well as the absence of fragments observed for the parent compound. Where one or more chemical structures could be assigned to the spectrum, the plausibility of each candidate was tested by comparing the observed MS² spectra to predicted fragments calculated using MassFrontier 7.0 (HighChem/Thermo Scientific), which was either used manually or automatically within Compound Discoverer 1.0 with default settings. If the assigned structure contained an acidic hydrogen atom (e.g. present in carboxylic acids), the presence of a signal in negative mode was checked and verified, where appropriate, using the exact mass, peak shape and MS² fragments. Where reference standards were purchased or synthesized, confirmation (or rejection) was performed via matching of retention time and MS² fragments. In general, the outcome of the structural interpretation varied between confirmed structures through to proposed molecular formulas. To transparently communicate the confidence of the structural interpretation, confidence levels were assigned as proposed and clarified in Schymanski *et al.* (2014)⁵⁹, ranging from Level 5 – *exact mass* through to Level 4 – *unequivocal molecular formula*, Level 3 – *tentative candidates*, Level 2 – *probable structure*, to Level 1 – *confirmed structure*.

B.1.7 Assignment of biotransformation reactions

In order to interpret the biotransformation reactions of amine-containing compounds, it is necessary to attribute reactions to observed parent-TP pairs. However, the certainty with which a biotransformation reaction can be attributed to an observed parent-TP pair depends on the confidence of the assigned TP structure and whether or not the formation of the respective TP from the corresponding parent compound can unambiguously be attributed to a plausible reaction. We therefore classified the reactions that were attributed to each parent-TP pair into *certain*, *likely*, *possible*, and *unknown*

as illustrated in Table B.10. In detail, attributed reactions were classified as *certain* if the TP structure had Level 1 or Level 2 and only one reaction seemed plausible. Attributed reactions were classified as *likely* if the TP structure had Level 3 with a probable structure and only one reaction seemed plausible. Attributed reactions were always classified as *possible* if more than one reaction seemed plausible. And reactions remained *unknown*, if the structure of the TP could not be sufficiently elucidated to propose a plausible reaction.

Table B.10: Assignment of reaction certainties

TP structure confidence as proposed by Schymanski <i>et al.</i>	Number of plausible reactions that can be assigned to a parent-TP pair	Reaction assignment
Level 1 and 2	1	Certain
Level 3	1	Likely
Level 1 to 3	>1	Possible
Level 4	0	Unknown

To assess the importance of different reactions in terms of how much of the parent compounds was biotransformed via a specific reaction, we considered the frequency with which a given reaction was observed and the amount of the respective TPs formed. This analysis was carried out separately for tertiary, secondary and primary amines. To assess the relative frequency of a reaction, we counted all first-generation TPs that were *certain* or *likely* to be formed through that specific reaction and related them to the number of TPs that could potentially have been formed via the same reaction. To assess the amounts of TPs formed, we determined the detected maximal peak area of each TP and related it to the amount of biotransformed parent compound at that same time point to yield a so-called *maximal relative amount*. While this procedure is fairly uncertain due to the fact that TPs and parent compounds might have different ionization efficiencies, it was considered sufficient to yield a rough estimate of the relative amount of TPs formed. To evaluate the overall importance of a given type of reaction, we summed the *maximal relative amounts* of all first-generation TPs that were *certain* or *likely* to be formed through the reaction of interest and divided it by the number of TPs that could have been formed through this reaction, resulting in a

so-called *mean maximal relative amount*. It should be noted that the actual maximal relative amount of a TP can be much higher than the observed TP areas suggest since the TP might itself be further transformed to some extent. Therefore, we additionally characterized the time series patterns as rising (r), rising and steady (rs), or rising and falling (rf) to qualitatively assess the stability of the TPs.

B.2 Identified higher generation transformation products

The chemical structure of the TPs given in Table B.11 were not elucidated since they seemed to be higher generation products either due to their time series pattern and/or if the structural evidence indicated a structure that was formed by multiple reactions, for which already direct, first generation TPs were identified for the respective parent amines.

Table B.11: Higher generation TPs, for which the structures were not elucidated

Name consisting of parent, observed <i>m/z</i> , and RT [min]	Time series pattern	proposed elemental formula	Atomic modification	MassBank ID
CLC_387.1473_16.9	1d -> 4d	C ₂₁ H ₂₃ ClN ₂ O ₃	+ C ₃ H ₂ O ₃	NA
CLC_250.1439_8.6	1d -> 4d			NA
CPP_385.1315_18.5	1.5d -> 4d	C ₂₁ H ₂₁ ClN ₂ O ₃	+ C ₄ H ₂ O ₃	ET030301-06
CPP_341.0901_10.4	1d -> 4d	C ₁₅ H ₁₇ ClN ₂ O ₅	-C ₂ H ₂ + O ₅	ET030401-06
CPP_255.0896_9.2	2d -> 4d			ET030501-06
DCA_128.0261_10.8	0h -> 2h <- 4d	C ₆ H ₆ NCI	-C ₂ H ₄	ET040101-06
DCA_156.0210_15.3	0h <- 4h	C ₇ H ₆ CINO	-CH ₄ + O	NA
DCA_173.9951_10.2	2h -> 8h <- 3d	C ₆ H ₄ CINO ₃	-C ₂ H ₆ + O ₃	ET040601-06
DEP_190.1226_15.8	2h -> 8h <- 4d	C ₁₂ H ₁₅ NO	-CH ₂ + O	NA
FLU_376.1005_15.9	2d -> 4d			NA
MEX_252.1230_15.2	0h -> 4d	C ₁₃ H ₁₇ NO ₄	+ C ₂ O ₃	ET090301-06
MEX_238.1437_13.6	4h -> 4d	C ₁₃ H ₁₉ NO ₃	+ C ₂ H ₂ O ₂	ET091001-06
NFL_442.2946_14.7	1d-> 4d			NA
NFL_222.1488_8.6	1.5d -> 4d			NA
NFL_240.9154_3.2	1d-> 4d			NA
NFL_414.9867_3.2	2d -> 4d			NA
NPE_293.1132_8.7	1d -> 4d	C ₁₄ H ₁₆ N ₂ O ₅	-CH ₂ + O ₅	ET110301-06
NPE_227.1178_10.2	2d -> 4d	C ₁₄ H ₁₄ N ₂ O	-CH ₄ + O	ET111101-06
NVE_264.0815_12.7	up and down			NA
OCP_271.0845_15.2	8h -> 4d	C ₁₂ H ₁₅ ClN ₂ O ₃	+ C ₂ H ₂ O ₃	ET130501-06
OCP_257.0689_14.6	8h -> 1.5d <- 4d	C ₁₁ H ₁₃ ClN ₂ O ₃	+ CO ₃	ET131601-06
OCP_313.0951_15.9	8h -> 4d	C ₁₄ H ₁₇ ClN ₂ O ₄	+ C ₄ H ₄ O ₄	ET131101-06
OCP_225.0425_11.5	1d -> 4d	C ₁₀ H ₉ ClN ₂ O ₂	+ O ₂ -H ₄	ET131401-06
OCP_313.0952_14.1	2h -> 2d <- 4d	C ₁₄ H ₁₇ ClN ₂ O ₄	+ C ₄ H ₄ O ₄	ET131501-06
OCP_158.0368_12.7	8h -> 3d <- 4d	C ₇ H ₈ CINO	+ O-C ₃ H ₅ N	ET131701-06
PHE_255.1855_9.6	1d -> 4d	C ₁₇ H ₂₂ N ₂	+ CH ₂	NA
PRI_176.1069_14.8	0h -> 4d	C ₁₁ H ₁₃ NO	-C ₄ H ₈ N ₂ O	NA
PRI_223.0714_10.0	4h -> 2d <- 4d	C ₁₀ H ₁₀ N ₂ O ₄	-C ₅ H ₁₁ N + O ₃	NA
PRI_109.0318_6.2	0h -> 2d <- 4d			NA

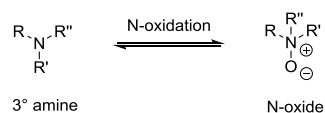
Table B.10: continued

Name consisting of parent, observed m/z , and RT [min]	Time series pattern	proposed elemental formula	Atomic modification	MassBank ID
PYR_288.1709_8.8	2h -> 4d	$C_{16}H_{21}N_3O_2$	$-CH_2 + O$	ET170501-06
PYR_153.0659_5.0	0h -> 4d	$C_7H_8N_2O_2$	$-C_{10}H_{15}N + O$	ET170601-06
PYR_258.1603_7.9	2h -> 2d <- 4d	$C_{15}H_{19}N_3O$	$-C_2H_4$	NA
PYR_352.1328_8.5	8h -> 4d	$C_{16}H_{21}N_3O_4S$	$-CH_2 + SO_3$	ET170801-06
SPI_344.2433_12.7	0h -> 4d	$C_{18}H_{33}NO_5$	$-H_2 + O_3$	ET180301-06
SPI_344.2434_9.8	2h -> 4d	$C_{18}H_{33}NO_5$	$-H_2 + O_3$	ET180401-06
SPI_286.2014_11.1	2h -> 4d	$C_{15}H_{27}NO_4$	$-C_3H_8 + O_2$	ET180501-06
SPI_344.2434_9.2	2h -> 4d	$C_{18}H_{33}NO_5$	$-H_2 + O_3$	ET180701-06
SPI_300.2172_11.7	2h -> 2d <- 4d	$C_{16}H_{29}NO_4$	$-C_2H_6 + O_2$	NA
SPI_314.2327_11.0	8h -> 4d	$C_{17}H_{31}NO_4$	$-CH_4 + O_2$	ET181201-06
SPI_330.2640_12.8	8h -> 4d	$C_{18}H_{35}NO_4$	$+ O_2$	ET181301-06
SPI_272.1857_8.8	8h -> 4d	$C_{14}H_{25}NO_4$	$-C_4H_{10} + O_2$	ET181401-06
SPI_272.2221_10.7	1d -> 4d	$C_{15}H_{29}NO_3$	$-C_3H_6 + O$	ET181701-06
SPI_345.2466_12.8	8h -> 4d			NA

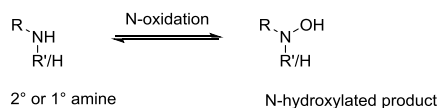
B.3 Schematic illustration of reactions of the amine functional group

N-oxidation

N-oxidation of 3° amines

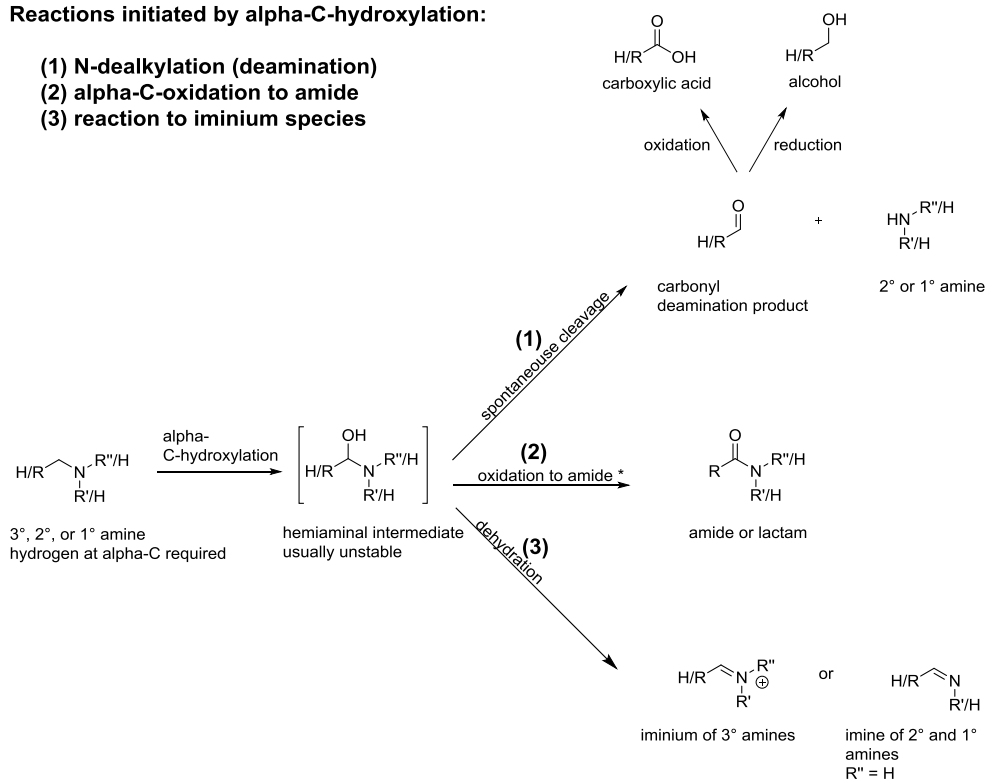


N-hydroxylation of 2° and 1° amines

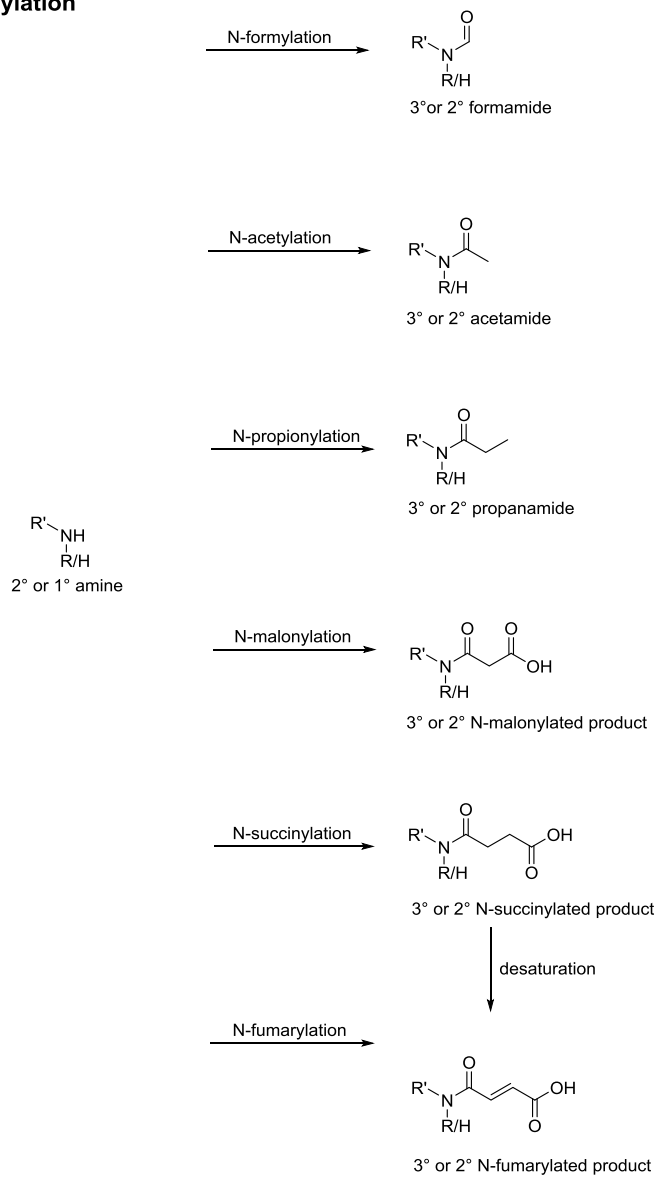


Reactions initiated by alpha-C-hydroxylation:

- (1) N-dealkylation (deamination)
- (2) alpha-C-oxidation to amide
- (3) reaction to iminium species



* requires certain stability of heminal or a ring-chain tautomerism of cyclic amines. Additionally, a second hydrogen is required at the alpha-C

N-acylation

B.4 Structure elucidation on the basis of LC-HR-MS/MS data

B.4.1 Explanation of the illustration of the structural evidence

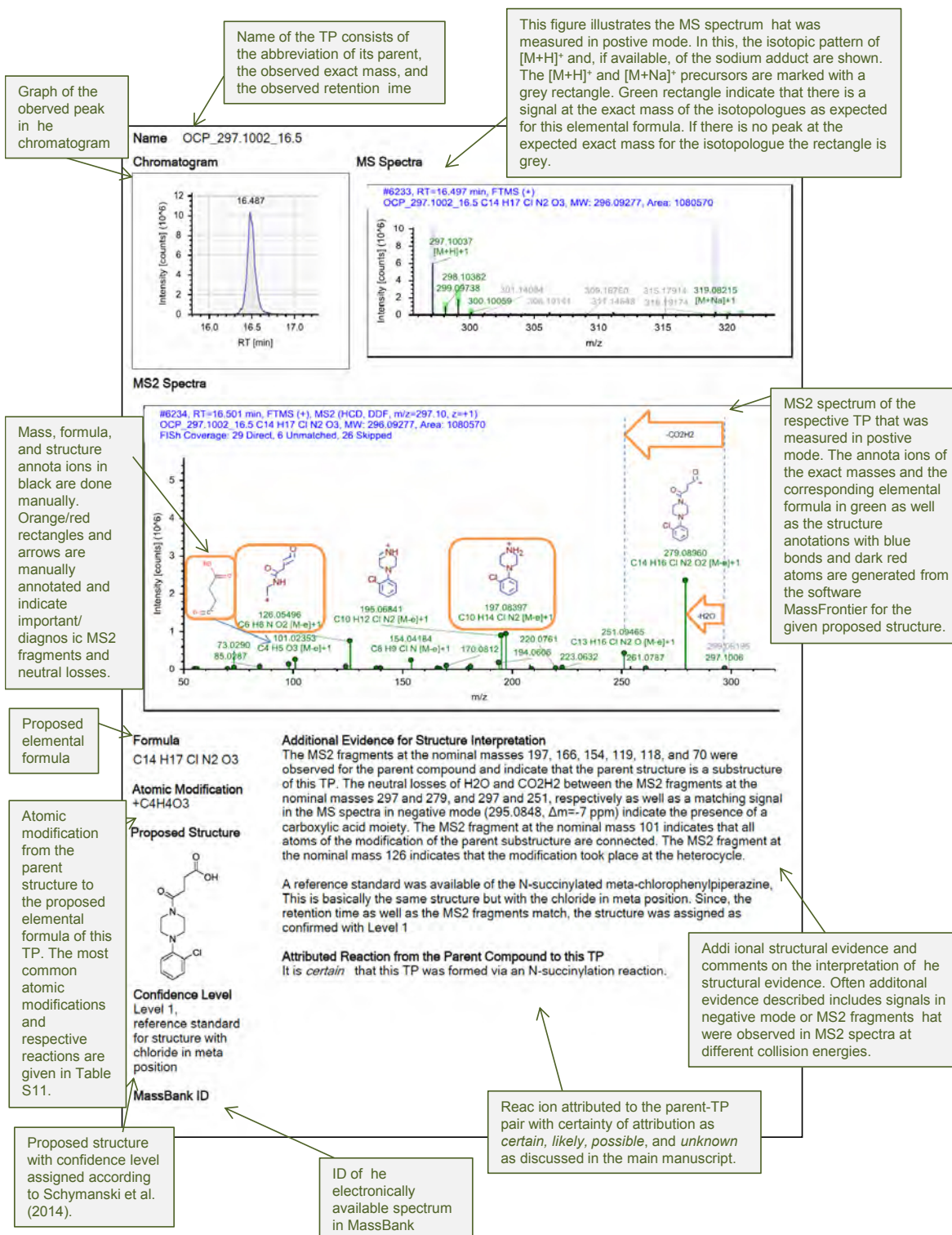
The following two pages explain how to read and interpret the structure elucidation pages. Each page shows the structural evidence for one TP. The first is an example of a regular structure elucidation page as it is reported from the software Compound Discoverer 1.0 with some minor manual additions and the second is an example for a structure elucidation page where the evidence was extracted manually rather than compiled from the Compound Discoverer 1.0 report.

Table B.12 illustrates typical observed atomic modifications and possible corresponding reactions of the amine functional group for an enhanced understanding of the following structural evidence.

Table B.12: Atomic modifications and possible corresponding amine reactions

Loss	Gain	Possible reaction
$-\text{CH}_2$		N-demethylation, O-demethylation
$-\text{C}_2\text{H}_4$		N-deethylation or two times N-demethylation
$-\text{C}_3\text{H}_6$		N-depropylation or combination of N-demethylation and N-deethylation
$-\text{C}_3\text{H}_2$		N-depropargylation
$-\text{NH}_3$	$+\text{O}_2$	deamination of primary amine and successive oxidation to carboxylic acid
$-\text{C}_2\text{H}_7\text{N}$	$+\text{O}_2$	deamination of dimethylamino group and successive oxidation to carboxylic acid
	$+\text{O}$	N-oxidation, N-hydroxylation, C-hydroxylation
$-\text{H}_2$	$+\text{O}$	oxidation of an aliphatic carbon to a carbonyl or hydroxylation ($+\text{O}$) and desaturation ($-\text{H}_2$) or N-demethylation / N-deethylation of methylamine / ethylamine and N-formylation / N-acetylation or N-hydroxylation and successive reaction to a nitron
$-\text{H}_2$	$+\text{O}_2$	hydroxylation followed by an oxidation to a carboxylic acid, two hydroxylations and the successive oxidation of one hydroxyl moiety to a carbonyl or a desaturation
$-\text{H}_2$		desaturation, transformation to an imine
	$+\text{C}_2\text{H}_2\text{O}$	N-acetylation
	$+\text{C}_4\text{H}_4\text{O}_3$	N-succinylation
	$+\text{C}_4\text{H}_2\text{O}_3$	N-fumarylation or desaturation of an N-succinylated TP
	$+\text{C}_3\text{H}_2\text{O}_3$	N-malonylation

Appendix B

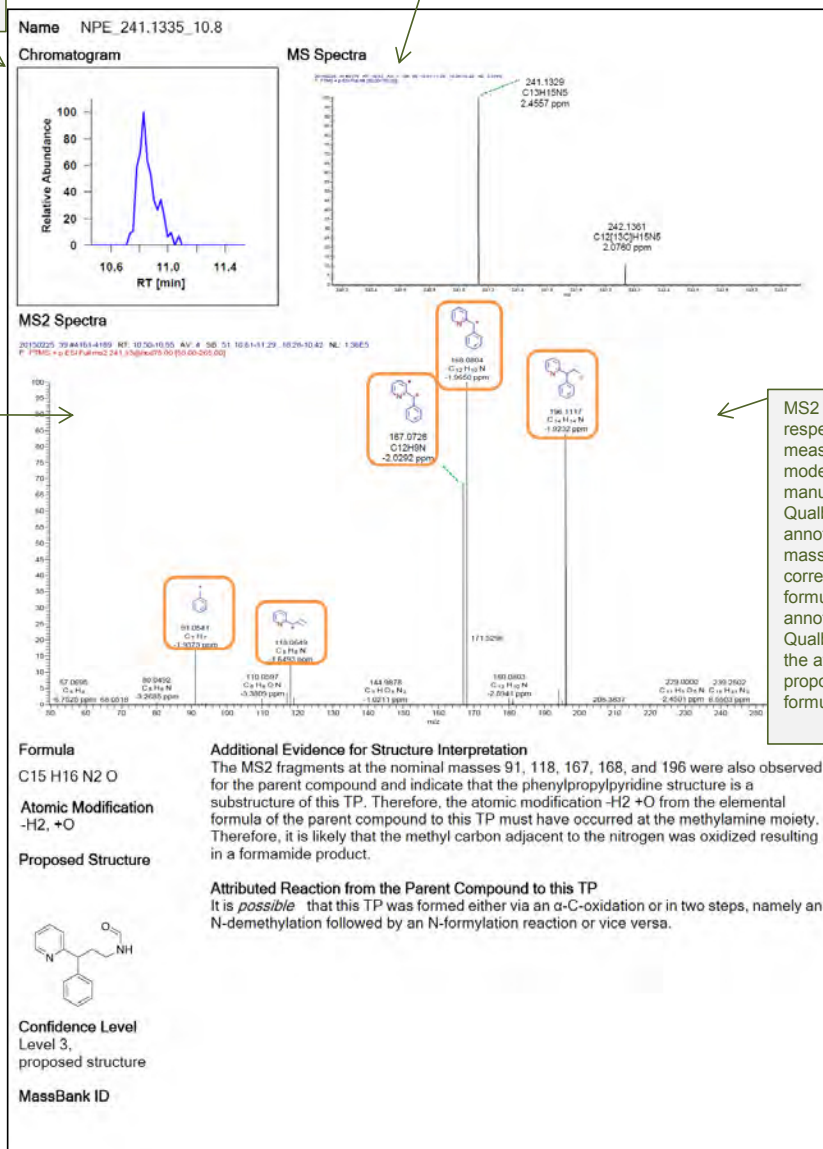


The chromatogram for the corresponding exact mass was extracted manually from Xcalibur Qualbrowser and drawn with R

The MS spectrum that was measured in positive mode was manually extracted with Xcalibur Qualbrowser and the peaks were manually annotated as given in Xcalibur Qualbrowser.

The illustrated structures for the MS2 fragments are either annotated manually (in black) or originate from the prediction of Mass Frontier for the proposed structure (in purple or in blue with dark red atoms).

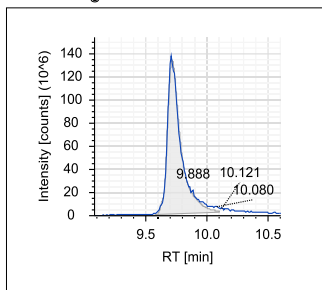
MS2 spectrum of the respective TP that was measured in positive mode was extracted manually from Xcalibur Qualbrowser. The annotations of the exact masses in black and the corresponding elemental formula originate from the annotation in Xcalibur Qualbrowser, limited to the atoms of the proposed elemental formula.



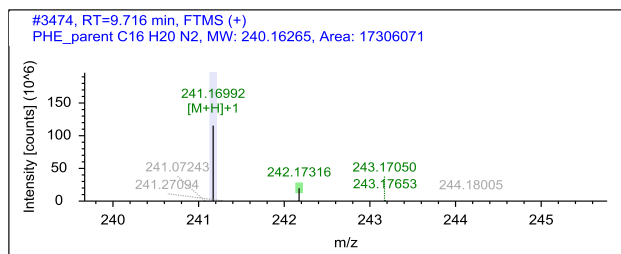
B.4.2 Structural evidence for pheniramine and its TPs

Name PHE_241.1699_9.7, parent

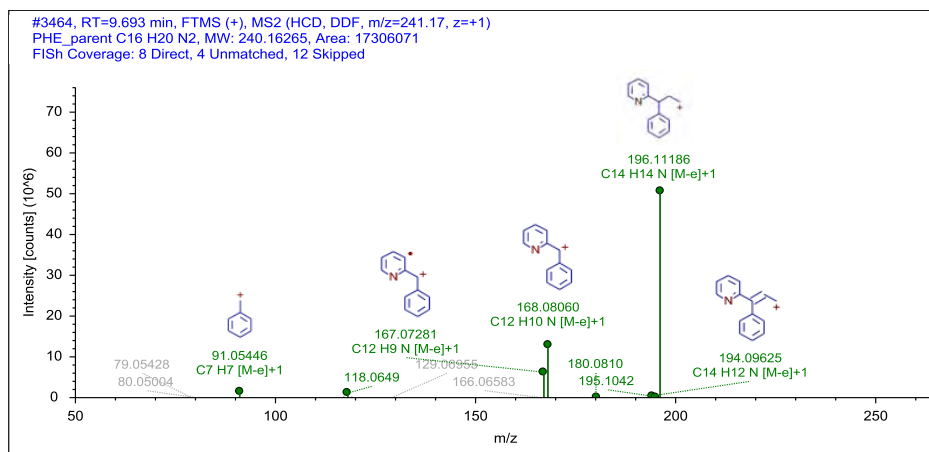
Chromatogram



MS Spectra



MS2 Spectra



Formula

C16 H20 N2

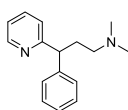
Additional Evidence for Structure Interpretation

This is the structural evidence that was observed for the parent compound PHE.

Atomic Modification

none

Proposed Structure



Confidence Level

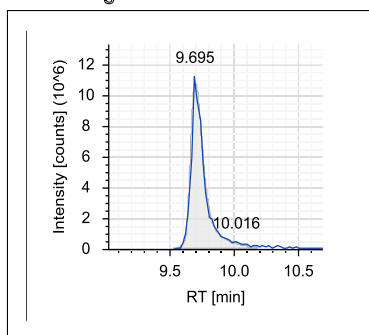
Level 1,
reference standard

MassBank ID

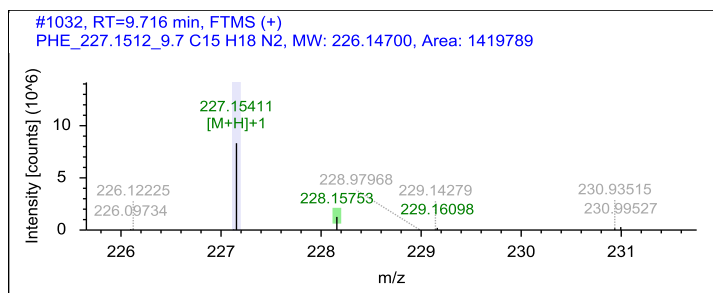
ET150001-ET150005

Name PHE_227.1542_9.7 = NPE_227.1543_9.6

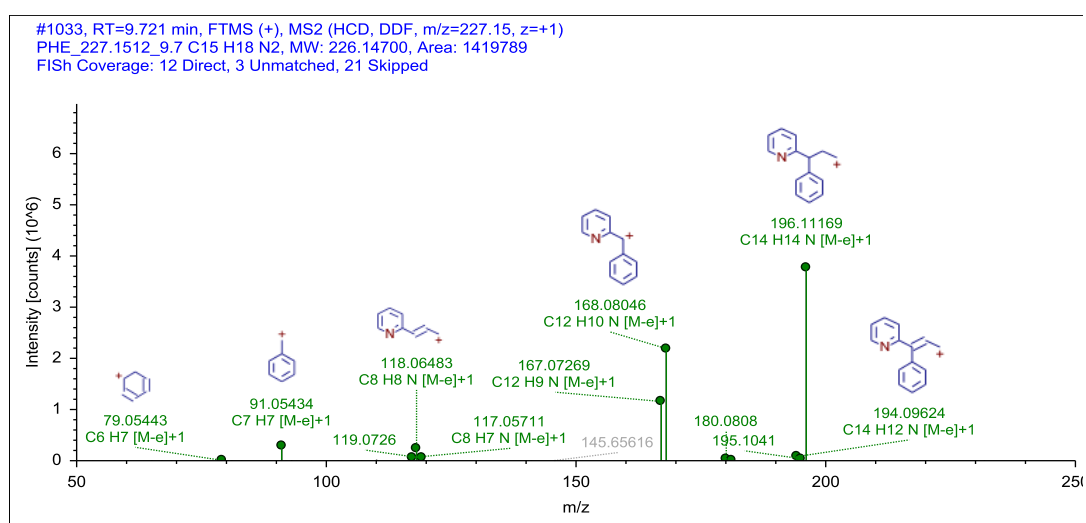
Chromatogram



MS Spectra



MS2 Spectra



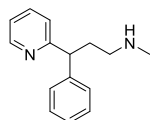
Formula

C15 H18 N2

Atomic Modification

-CH2

Proposed Structure



Confidence Level

Level 1,
reference standard

MassBank ID

ET110001-ET110005

Additional Evidence for Structure Interpretation

The structure of this TP was confirmed by a reference standard. It is a TP of PHE, but it is also the parent NPE.

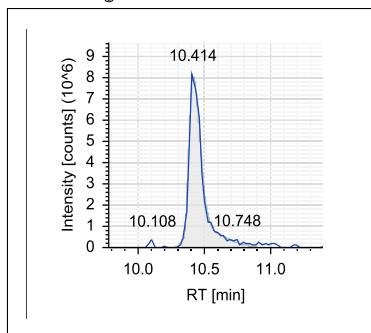
Attributed Reaction from the Parent Compound to this TP

It is *certain* that this TP was formed via an N-demethylation reaction.

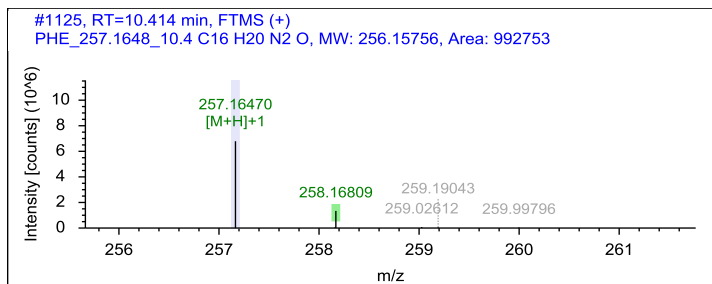
Appendix B

Name PHE_257.1648_10.4

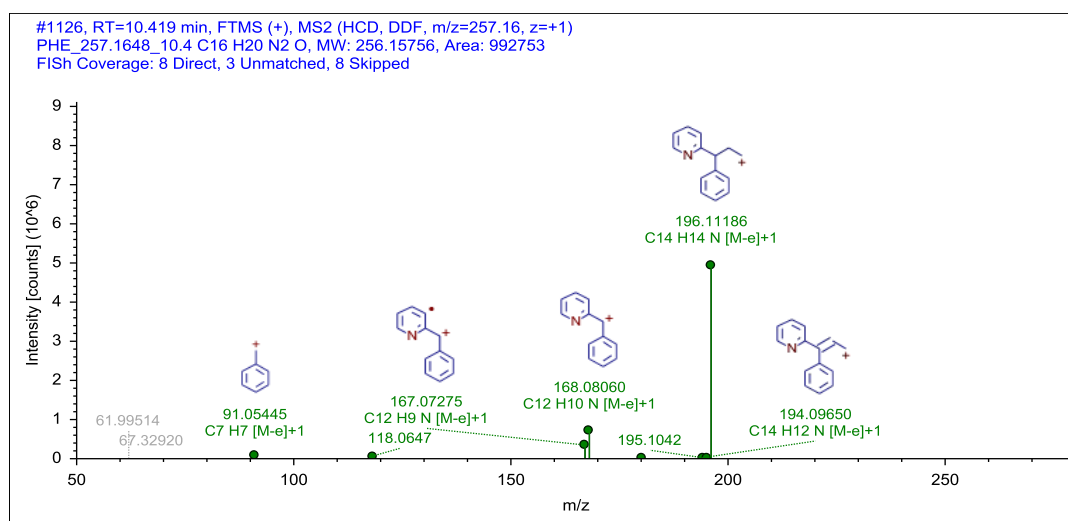
Chromatogram



MS Spectra



MS2 Spectra



Formula

C₁₆ H₂₀ N₂ O

Atomic Modification

+O

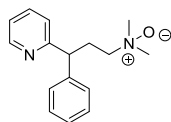
Additional Evidence for Structure Interpretation

The structure of this TP was confirmed by a reference standard.

Attributed Reaction from the Parent Compound to this TP

It is *certain* that this TP was formed via an N-oxidation reaction.

Proposed Structure



Confidence Level

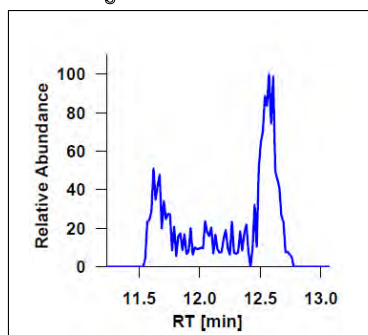
Level 1,
reference standard

MassBank ID

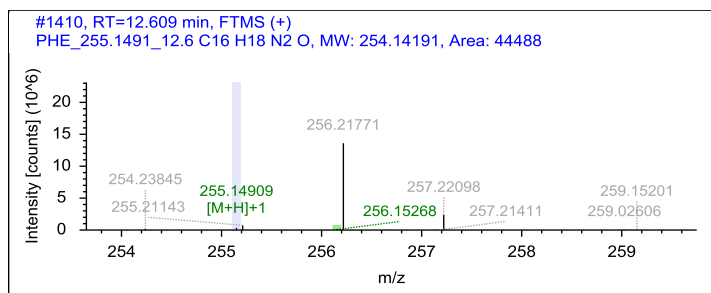
ET150201-ET150205

Name PHE_255.1491_11.6 = NPE_255.1491_11.6

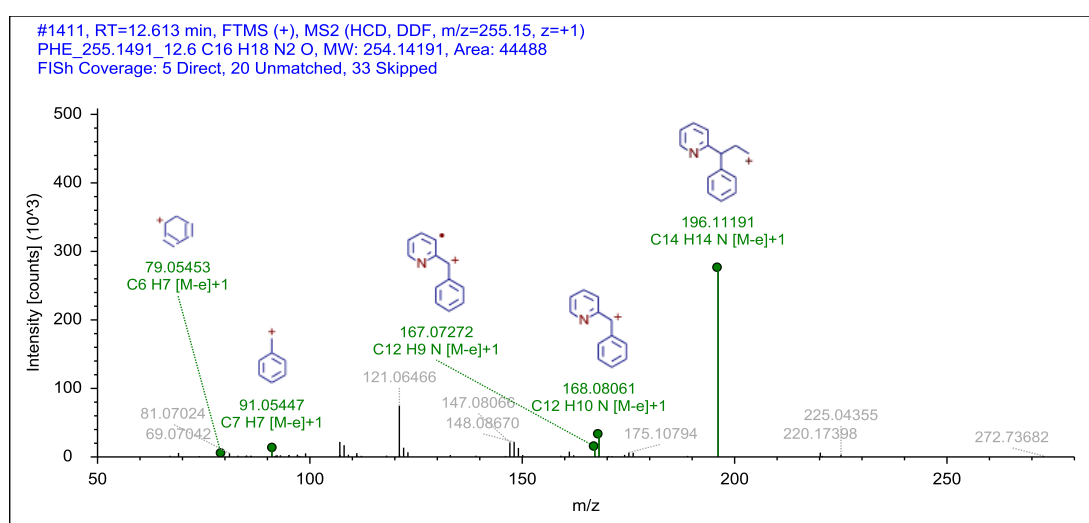
Chromatogram



MS Spectra



MS2 Spectra



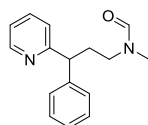
Formula

C16 H18 N2 O

Atomic Modification

-H2, +O

Proposed Structure



Confidence Level

Level 1,
synthesized standard

MassBank ID

ET110601-ET110606

Additional Evidence for Structure Interpretation

The formamide structure of this TP was confirmed by a synthesized standard. Details on the synthesis and confirmatory data from NMR measurement can be found in Chapter S5 in the SI. The chromatogram showed two maxima at 11.6 minutes and 12.6 minutes. This peak shape results from the cis-trans isomerism of the C-N bond that has some double bond character. This is in analogy with the TP PYR_300.1709_10.6 for which the resonance structures are drawn.

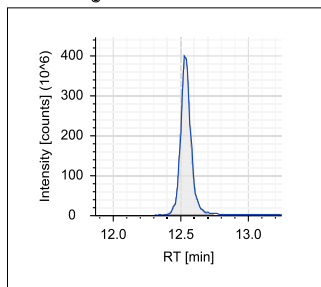
Attributed Reaction from the Parent Compound to this TP

It is *possible* that this TP was formed via an α -C-oxidation to a formamide or an N-demethylation reaction followed by an N-formylation reaction.

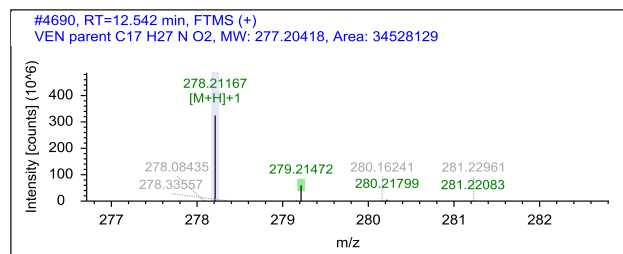
B.4.3 Structural evidence for venlafaxine and its TPs

Name VEN_278.2114_12.5, parent

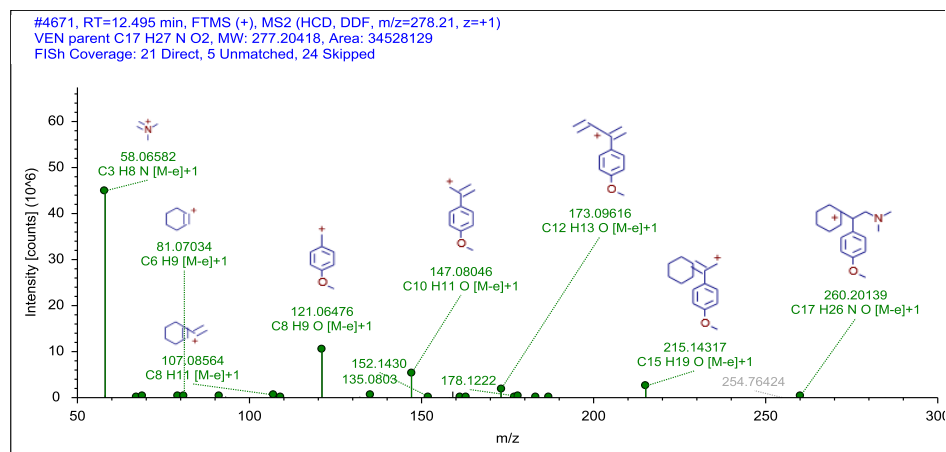
Chromatogram



MS Spectra



MS2 Spectra



Formula

C17 H27 N O2

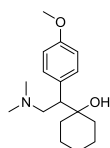
Additional Evidence for Structure Interpretation

This is the structural evidence that was observed for the parent compound VEN.

Atomic Modification

none

Proposed Structure



Confidence Level

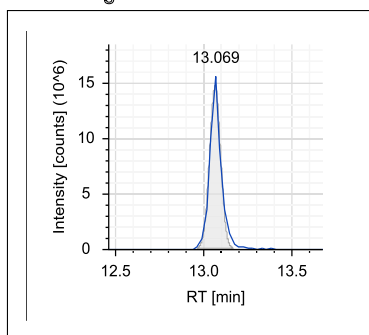
Level 1,
reference standard

MassBank ID

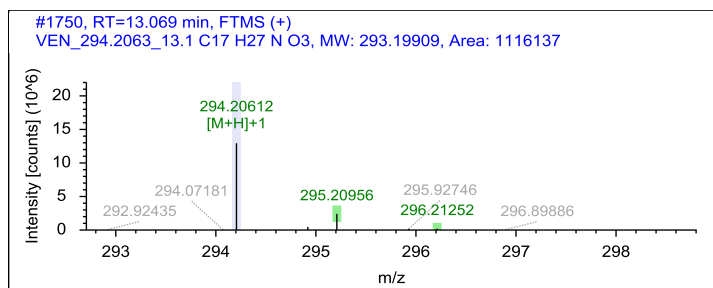
ET190001-ET190005

Name VEN_294.2063_13.1

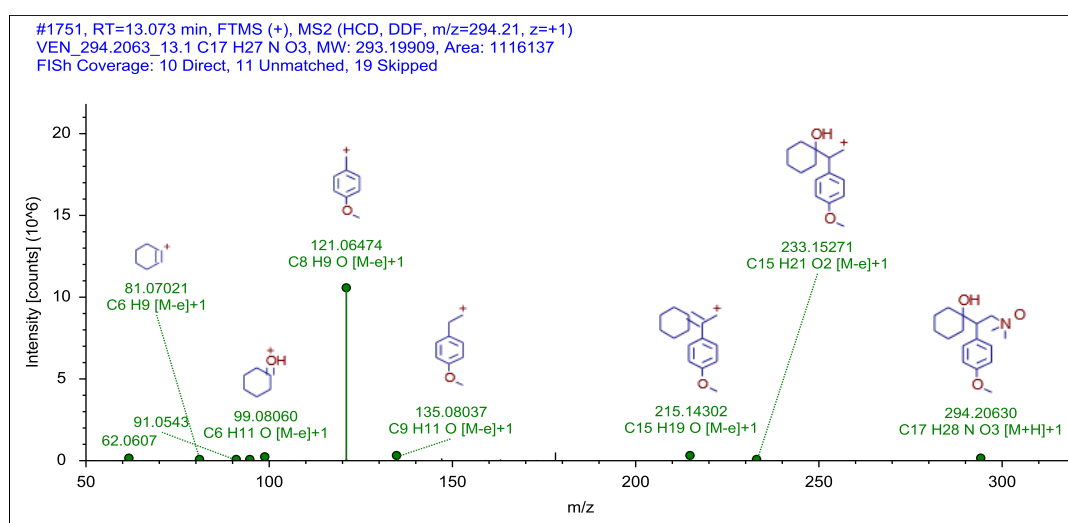
Chromatogram



MS Spectra



MS2 Spectra



Formula

C17 H27 N O3

Atomic Modification

+O

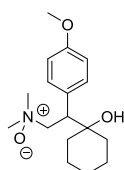
Additional Evidence for Structure Interpretation

The structure of this TP was confirmed by a reference standard.

Attributed Reaction from the Parent Compound to this TP

It is *certain* that this TP was formed via an N-oxidation reaction.

Proposed Structure



Confidence Level

Level 1,
reference standard

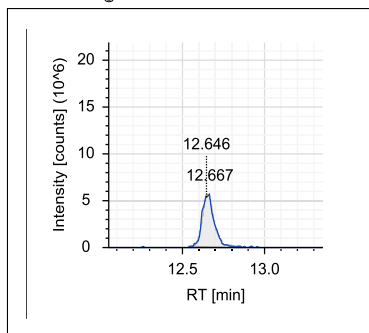
MassBank ID

ET190201-ET190205

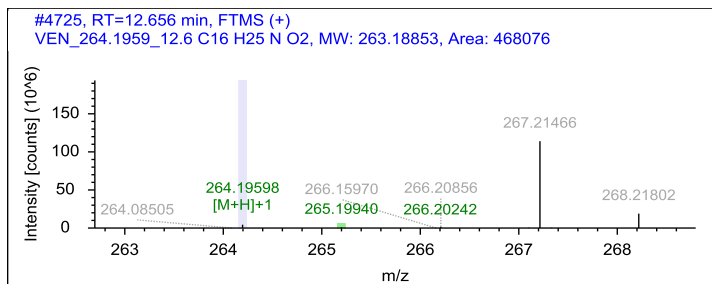
Appendix B

Name VEN_264.1959_12.6 = NVE_264.1959_12.6

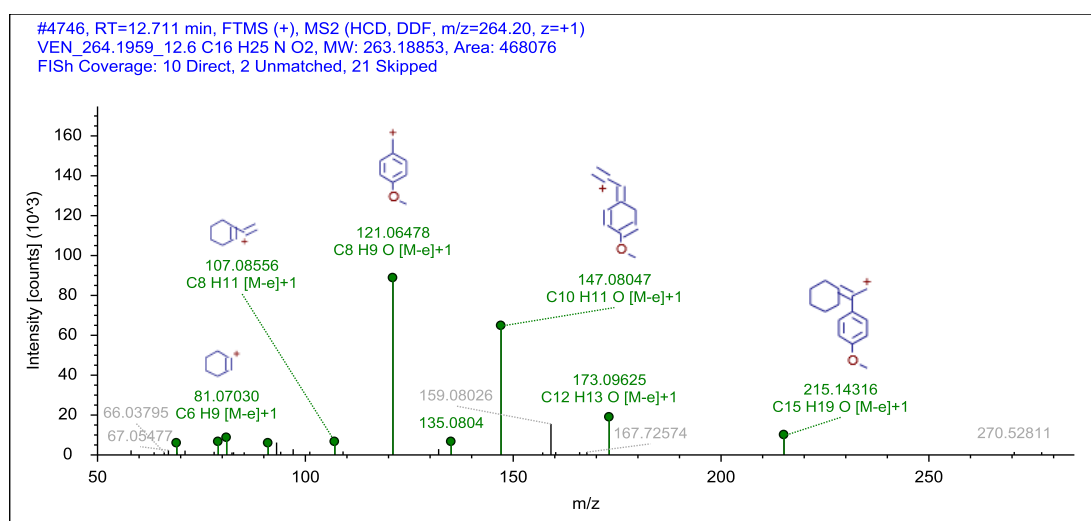
Chromatogram



MS Spectra



MS2 Spectra



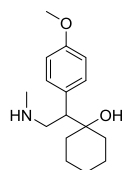
Formula

C16 H25 N O2

Atomic Modification

-CH2

Proposed Structure



Confidence Level

Level 1,
reference standard

MassBank ID

ET120001-ET120005

Additional Evidence for Structure Interpretation

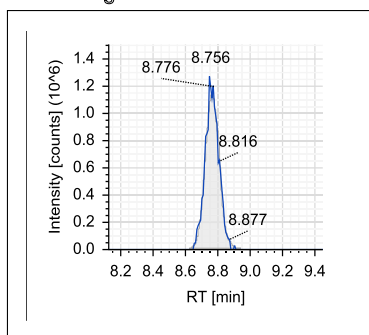
The structure of this TP was confirmed by a reference standard. It is a TP of VEN, but it is also the parent NVE.

Attributed Reaction from the Parent Compound to this TP

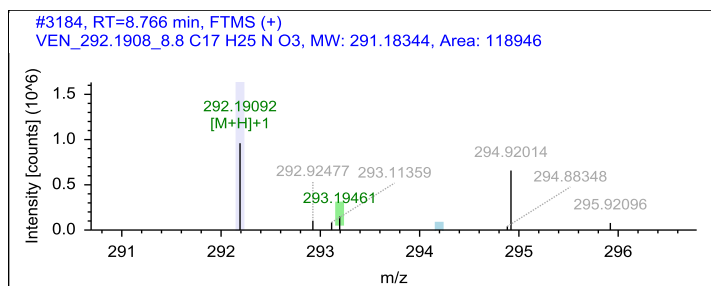
It is *certain* that this TP was formed via an N-demethylation reaction.

Name VEN_292.1908_8.8

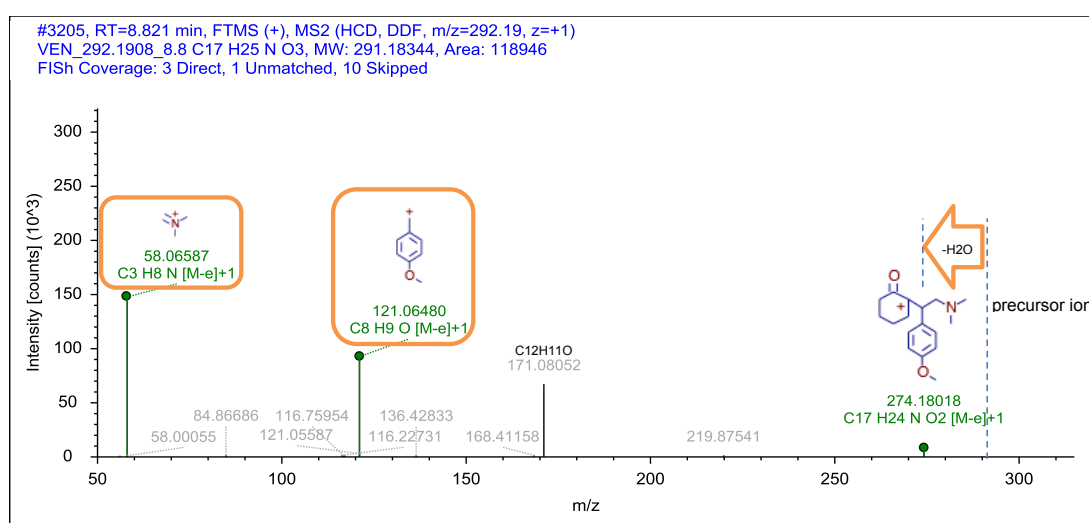
Chromatogram



MS Spectra



MS2 Spectra



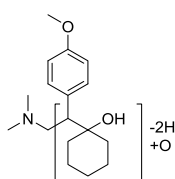
Formula

C17 H25 N O3

Atomic Modification

-H2, +O

Proposed Structure



Additional Evidence for Structure Interpretation

The MS2 fragments at the nominal masses 58 and 121 were also observed for the parent compound and indicate that the methoxybenzyl moiety and the trimethylamine moiety are substructures of this TP. Therefore, it is likely that the atomic modification of -H2 +O from the elemental formula of the parent compound to this TP took place at the ethylcyclohexyl part of the molecule. The exact type and position of the modification remain unknown. The structures of the MS2 fragments at the nominal mass 274 is drawn exemplarily. There is an analogous TP VEN_292.1908_9.6 with the same modification, but a different retention time.

Attributed Reaction from the Parent Compound to this TP

Several reaction paths are *possible* that could have formed this TP. After a hydroxylation reaction as first step, a successive oxidation to a carbonyl or an independent desaturation could have occurred.

Confidence Level

Level 3,
TP class

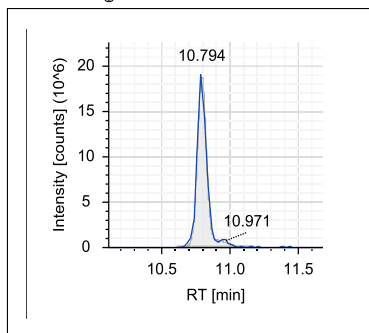
MassBank ID

ET190401-ET190406

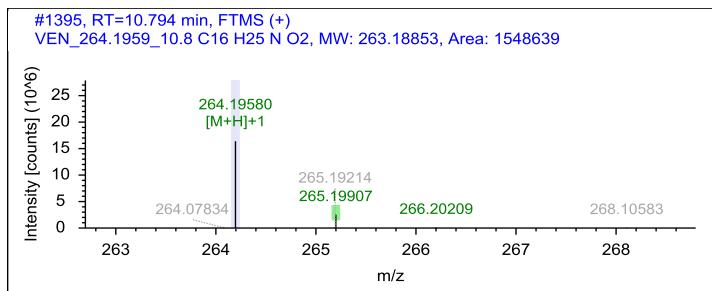
Appendix B

Name VEN_264.1959_10.8

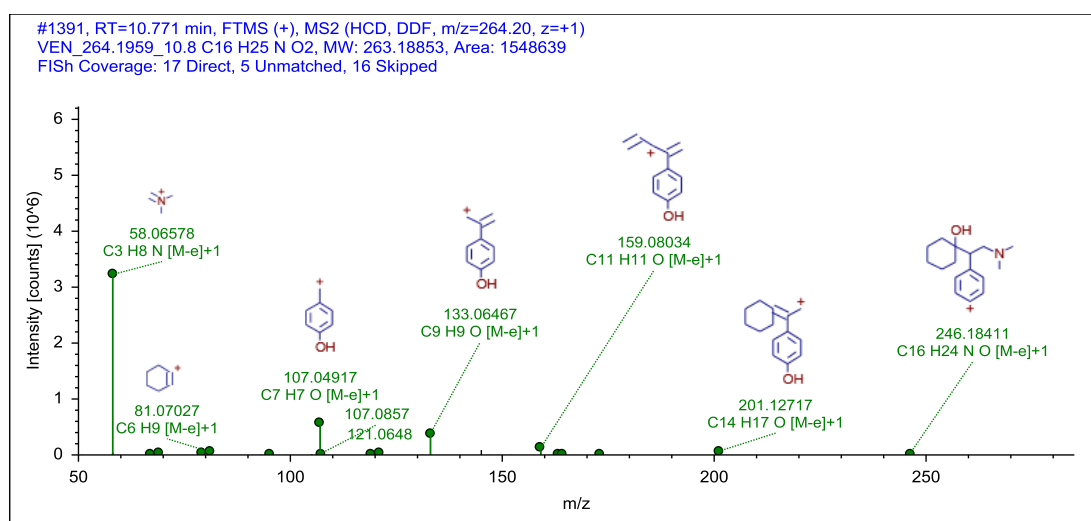
Chromatogram



MS Spectra



MS2 Spectra



Formula

C₁₆H₂₅N O₂

Additional Evidence for Structure Interpretation

The structure of this TP was confirmed by a reference standard.

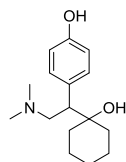
Atomic Modification

-CH₂

Attributed Reaction from the Parent Compound to this TP

It is *certain* that this TP was formed via an O-demethylation reaction.

Proposed Structure



Confidence Level

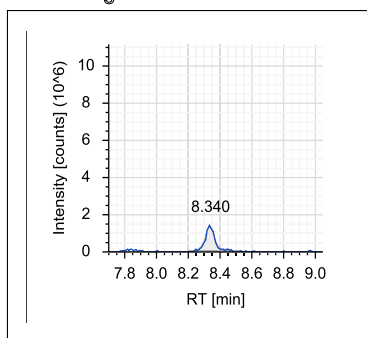
Level 1,
reference standard

MassBank ID

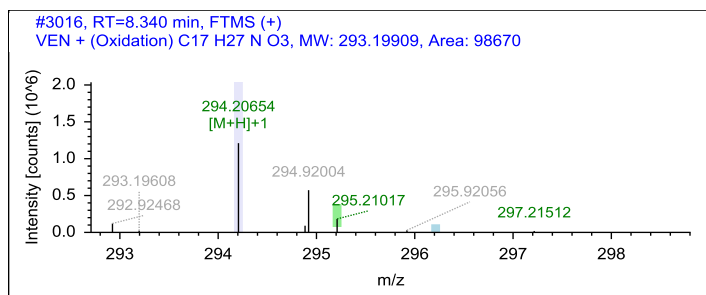
ET190101-ET190105

Name VEN_294.2065_8.3

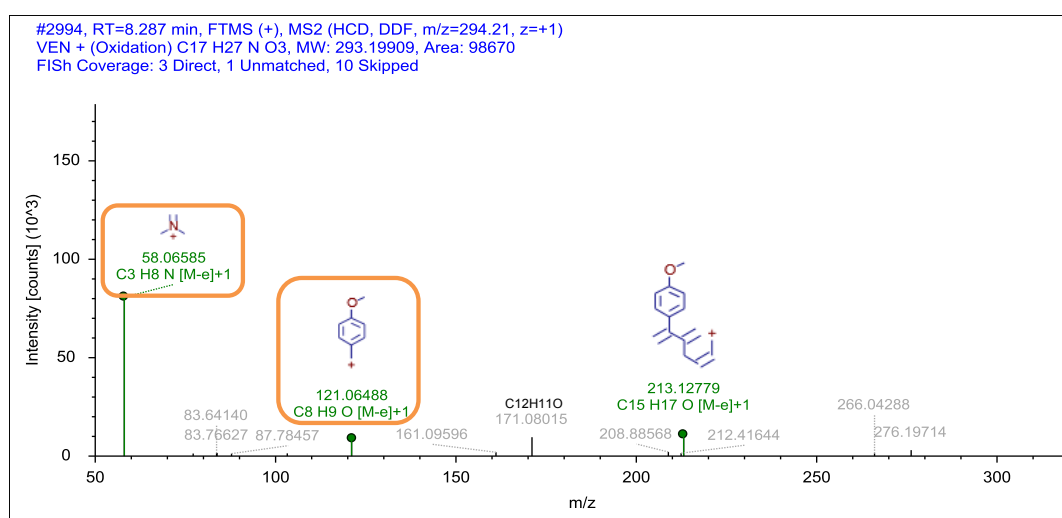
Chromatogram



MS Spectra



MS2 Spectra



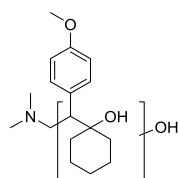
Formula

C₁₇ H₂₇ N O₃

Atomic Modification

+O

Proposed Structure



Confidence Level

Level 3,
TP class

MassBank ID

ET190501-ET190506

Additional Evidence for Structure Interpretation

The MS2 fragments at the nominal masses 58 and 121 were also observed for the parent compound and indicate that the methoxybenzyl moiety and the trimethylamine moiety are substructures of this TP. Therefore, it is likely that the modification took place at the ethylcyclohexyl part of the molecule. The atomic modification from the elemental formula of the parent compound to this TP is +O. The exact position of the modification remains unknown.

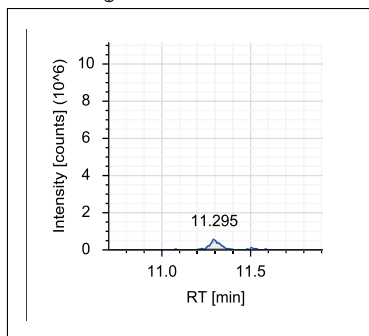
Attributed Reaction from the Parent Compound to this TP

It is *likely* that this TP was formed via a hydroxylation reaction.

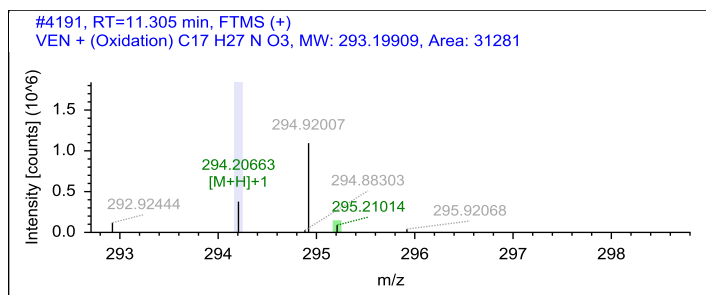
Appendix B

Name VEN_294.2065_11.3

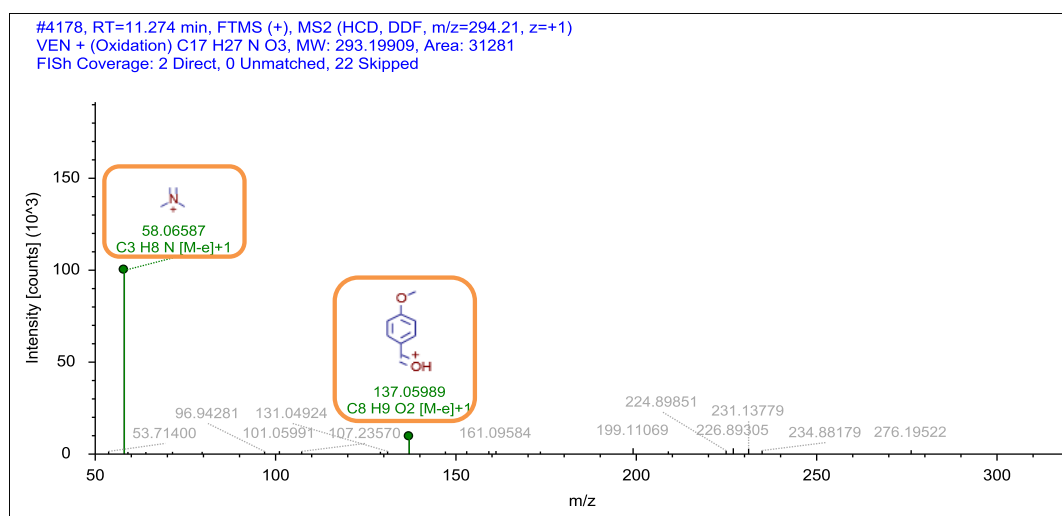
Chromatogram



MS Spectra



MS2 Spectra



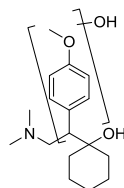
Formula

C₁₇ H₂₇ N O₃

Atomic Modification

+O

Proposed Structure



Additional Evidence for Structure Interpretation

The MS2 fragment at the nominal mass 58 was also observed for the parent compound and indicates that the trimethylamine moiety is a substructure of this TP. The atomic modification from the elemental formula of the parent compound to this TP is +O. The MS2 fragment at the nominal mass 137 indicates that the modification took place at the methoxybenzyl moiety. The exact position of the modification remains unknown. The structure of the MS2 fragment at the nominal mass 137 is drawn exemplarily.

Attributed Reaction from the Parent Compound to this TP

It is *likely* that this TP was formed via a hydroxylation reaction.

Confidence Level

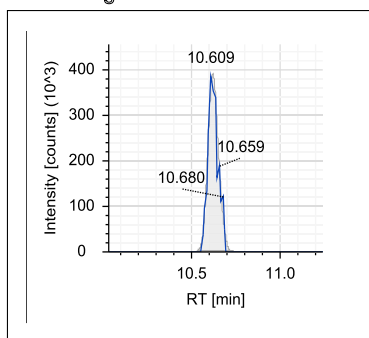
Level 3,
TP class

MassBank ID

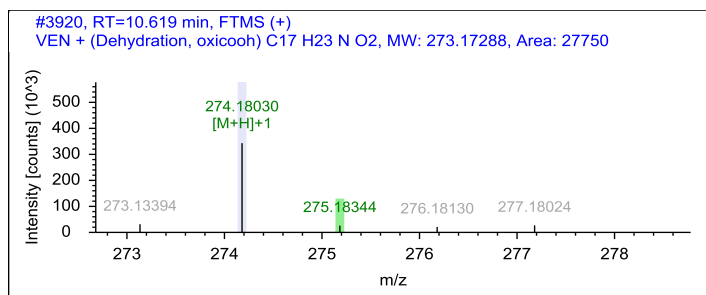
ET190601-ET190606

Name VEN_274.1801_10.6

Chromatogram

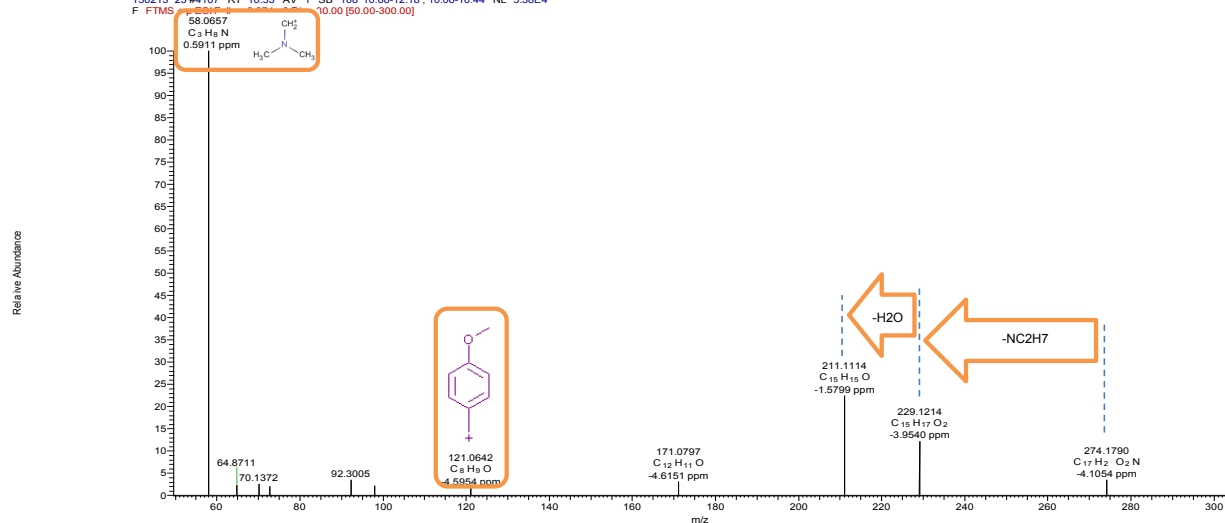


MS Spectra



MS2 Spectra

150213 23 #1107 RT 10.53 AV 1 SB 108 10.68-12.18, 10.06-10.44 NL 5.38E4
 F FTMS 58.0657 10.00 [50.00-300.00]



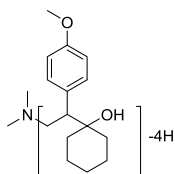
Formula

C17 H23 N O2

Atomic Modification

-H4

Proposed Structure



Additional Evidence for Structure Interpretation

The MS2 fragments at the nominal masses 58 and 121 were also observed for the parent compound. They indicate, together with the neutral loss of NC2H7, that the methoxybenzyl moiety and the trimethylamine moiety are substructures of this TP. The atomic modification from the elemental formula of the parent compound to this TP is -H4. Therefore, it is likely that the modification took place at the ethylcyclohexyl part of the molecule. The exact type and the position of the modification remain unknown.

Attributed Reaction from the Parent Compound to this TP

Several reaction paths are *possible* that could have formed this TP, namely two desaturation reactions or a combination of a dehydration to an alkene and an hydroxylation followed by a successive oxidation to a carbonyl moiety.

Confidence Level

Level 3,
 TP class

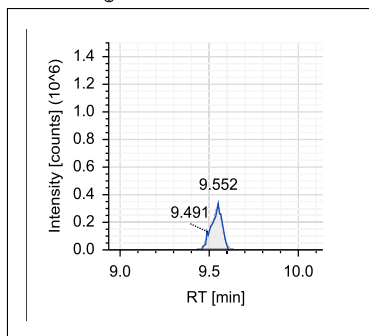
MassBank ID

ET190701-ET190706

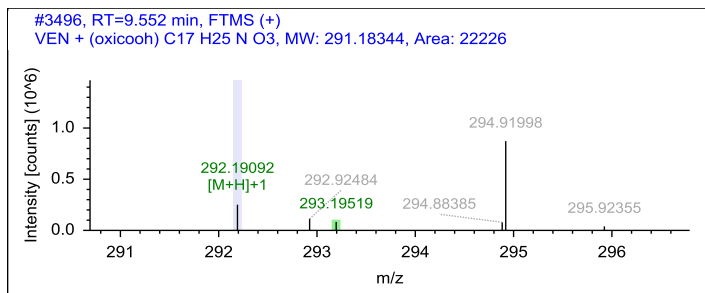
Appendix B

Name VEN_292.1908_9.6

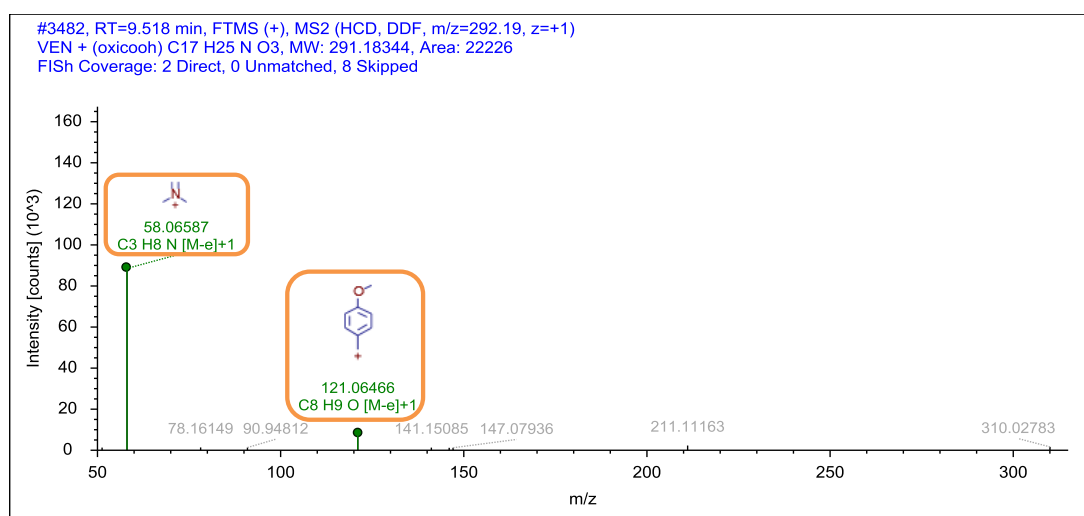
Chromatogram



MS Spectra



MS2 Spectra



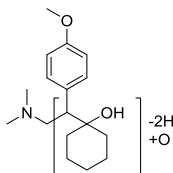
Formula

C₁₇ H₂₅ N O₃

Atomic Modification

-H₂, +O

Proposed Structure



Additional Evidence for Structure Interpretation

The MS2 fragments at the nominal masses 58 and 121 were also observed for the parent compound and indicate that the methoxybenzyl moiety and the trimethylamine moiety are substructures of this TP. Therefore, it is likely that the atomic modification of -H₂ +O from the elemental formula of the parent compound to this TP took place at the ethylcyclohexyl part of the molecule. The exact type and position of the modification remain unknown.

There is an analogous TP VEN_292.1908_8.8 with the same modification, but a different retention time.

Attributed Reaction from the Parent Compound to this TP

Several reaction paths are *possible* that could have formed this TP. After a hydroxylation reaction as first step a successive oxidation to a carbonyl or an independent desaturation could have occurred.

Confidence Level

Level 3,
TP class

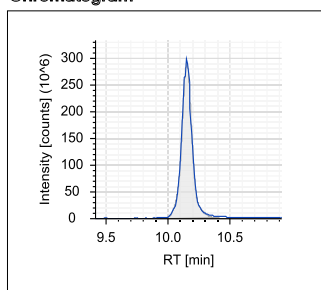
MassBank ID

ET190801-ET190806

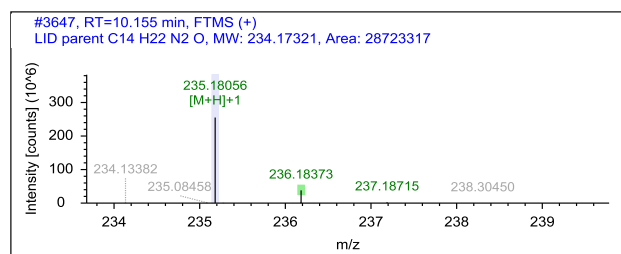
B.4.4 Structural evidence for lidocaine and its TPs

Name LID_235.1805_10.1, parent

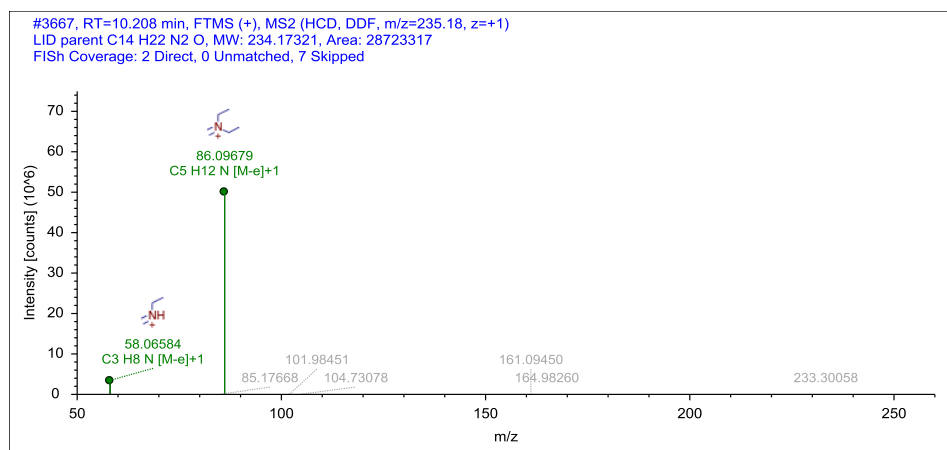
Chromatogram



MS Spectra



MS2 Spectra



Formula

C14 H22 N2 O

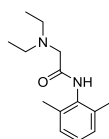
Additional Evidence for Structure Interpretation

This is the structural evidence that was observed for the parent compound LID.

Atomic Modification

none

Proposed Structure



Confidence Level

Level 1,
reference standard

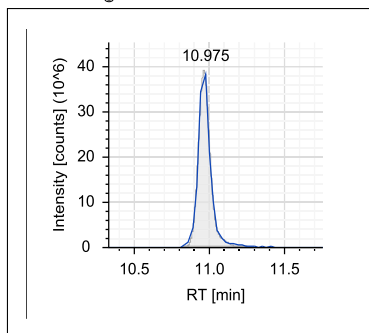
MassBank ID

ET080001-ET080005

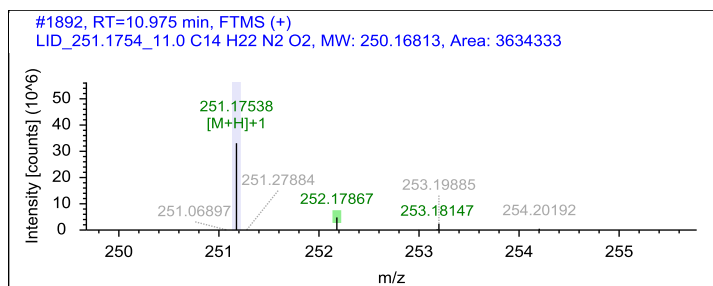
Appendix B

Name LID_251.1754_11.0

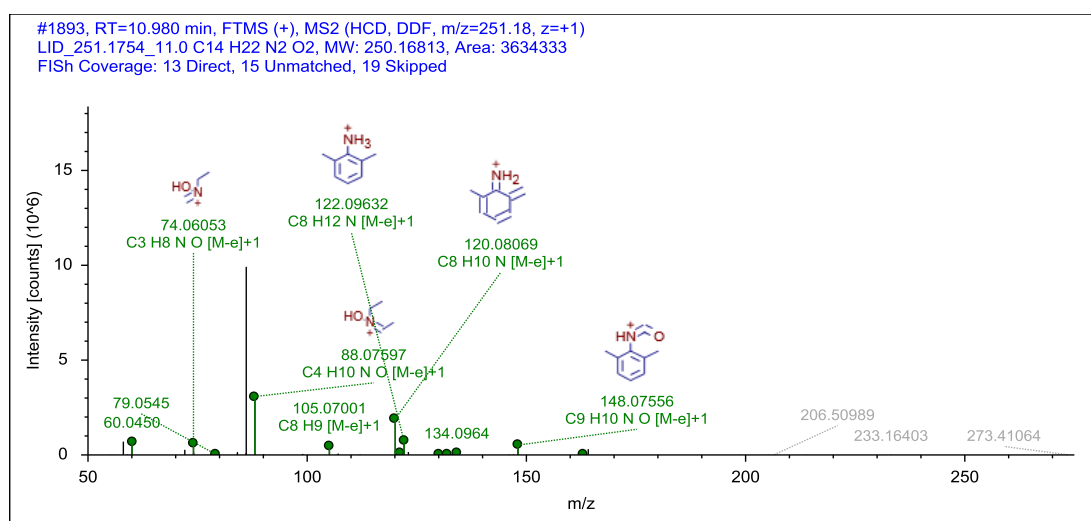
Chromatogram



MS Spectra



MS2 Spectra



Formula

C₁₄H₂₂N₂O₂

Additional Evidence for Structure Interpretation

The structure of this TP was confirmed by a reference standard.

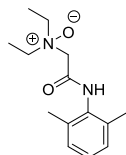
Atomic Modification

+O

Attributed Reaction from the Parent Compound to this TP

It is *certain* that this TP was formed via an N-oxidation reaction.

Proposed Structure



Confidence Level

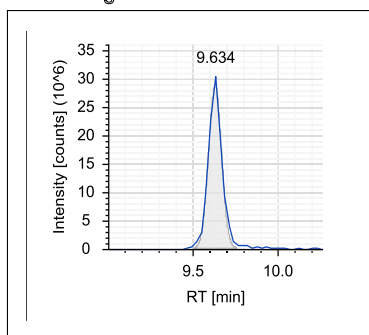
Level 1,
reference standard

MassBank ID

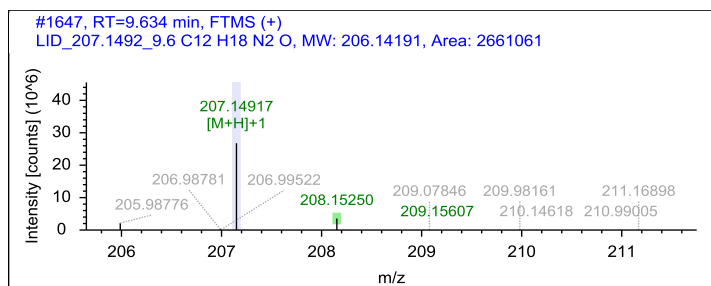
ET080101-ET080105

Name LID_207.1492_9.6

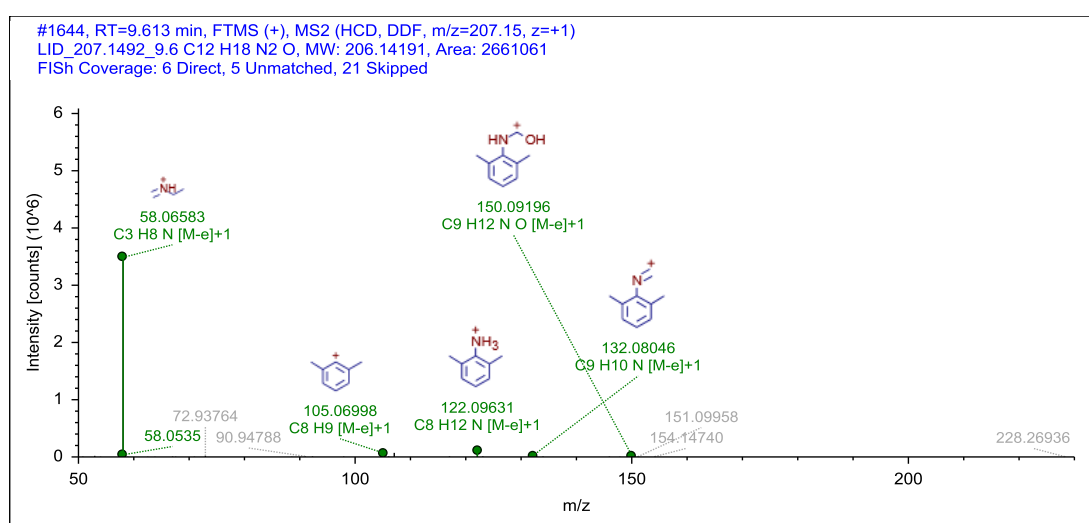
Chromatogram



MS Spectra



MS2 Spectra



Formula

C₁₂H₁₈N₂O

Additional Evidence for Structure Interpretation

The structure of this TP was confirmed by a reference standard.

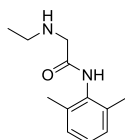
Atomic Modification

-C₂H₄

Attributed Reaction from the Parent Compound to this TP

It is *certain* that this TP was formed via an N-deethylation reaction.

Proposed Structure



Confidence Level

Level 1,
reference standard

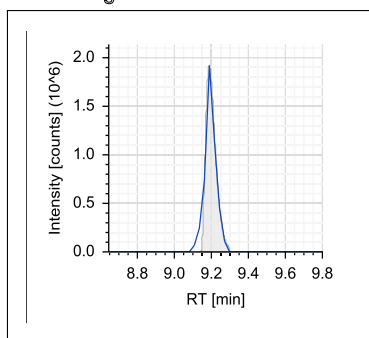
MassBank ID

ET080201-ET080205

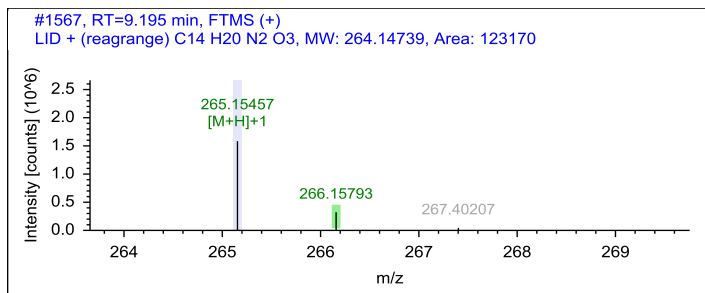
Appendix B

Name LID_265.1546_9.2

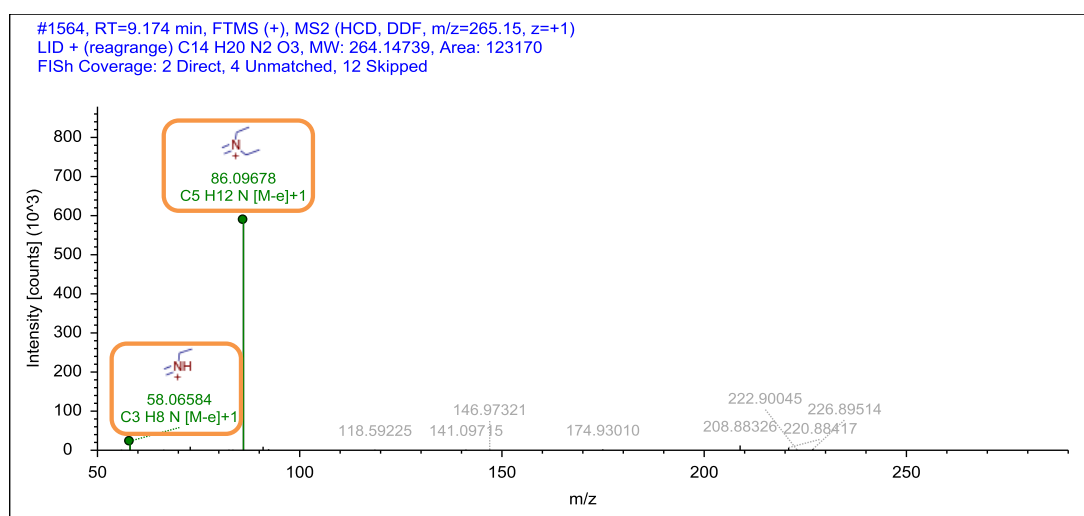
Chromatogram



MS Spectra



MS2 Spectra



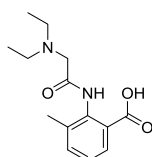
Formula

C₁₄H₂₀N₂O₃

Atomic Modification

-H₂, +O₂

Proposed Structure



Additional Evidence for Structure Interpretation

The MS2 fragments at the nominal masses 58 and 86 were also observed for the parent compound and indicate that the diethylmethylamine moiety is a substructure of this TP. Therefore, it is likely that the modification took place at the aromatic amide part of the molecule. A matching signal in the MS spectrum in negative mode was observed at the exact mass of 263.1396 (C₁₄H₁₉O₃N₂, Δm = -2.0079 ppm). This indicates that the atomic modification -H₂ + O₂ from the elemental formula of the parent compound to this TP was realized through an oxidation of a carbon atom to a carboxylic acid moiety. It is likely that the carboxylic acid moiety is located benzylic methyl groups.

Attributed Reaction from the Parent Compound to this TP

It is *likely* that this TP was formed via a hydroxylation followed by an oxidation to a carboxylic acid.

Confidence Level

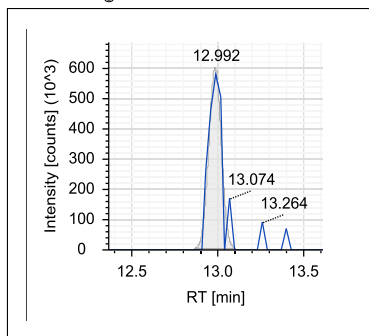
Level 3,
Proposed structure

MassBank ID

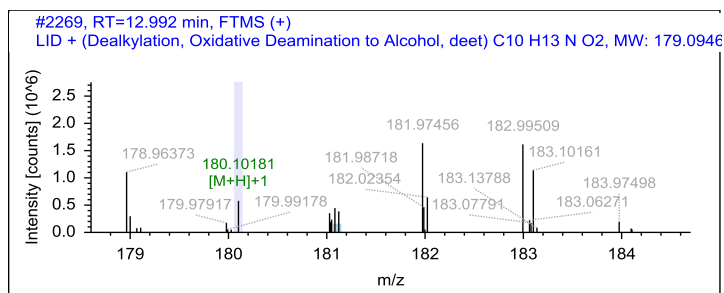
ET080301-ET080306

Name LID_180.1018_12.9

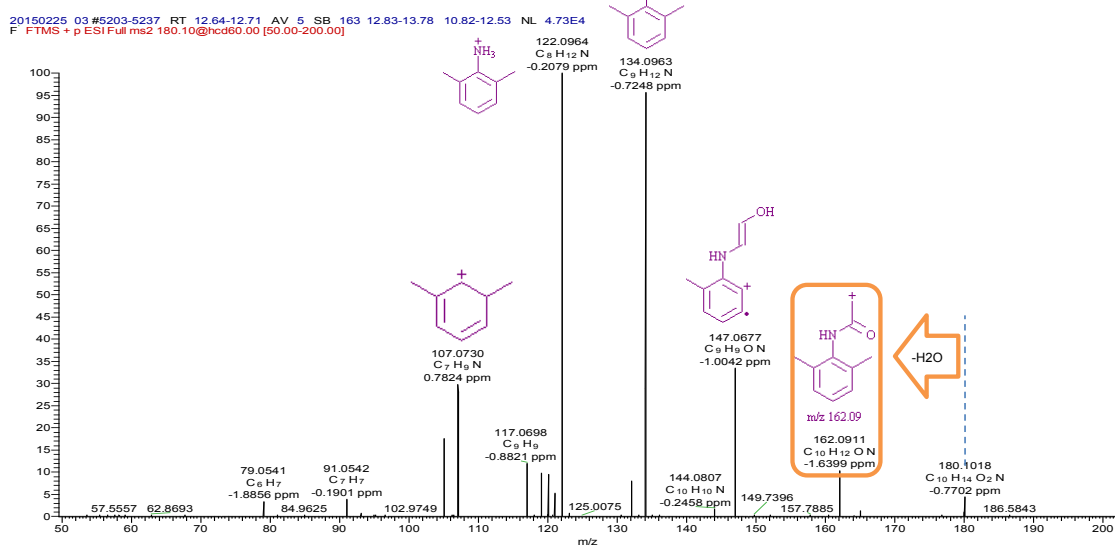
Chromatogram



MS Spectra



MS2 Spectra



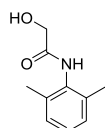
Formula

C10H13NO2

Atomic Modification

-C4H9N, +O

Proposed Structure



Additional Evidence for Structure Interpretation

The atomic modification from the elemental formula of the parent compound to this TP is -C4H9N +O. This indicates the loss of the diethylamine moiety and a gain of an oxygen atom. It is likely that a deamination followed by a successive reduction to an alcohol occurred. The neutral loss of H2O indicates the presence of a hydroxyl moiety. The MS2 fragments at the nominal masses 107, 122, 134, 147, and 162 indicate that the aromatic amide part of the molecule is unaltered. These fragments were also predicted by MassFrontier for the proposed structure and are therefore reasonable.

Attributed Reaction from the Parent Compound to this TP

It is *likely* that this TP was formed via a deamination reaction followed by a reduction to an alcohol.

Confidence Level

Level 3,
proposed structure

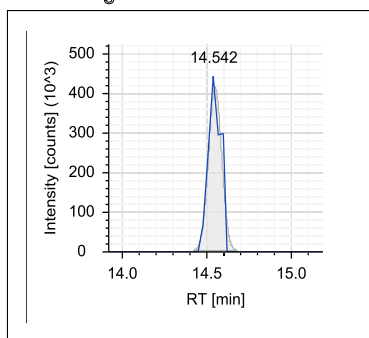
MassBank ID

ET080501-ET080506

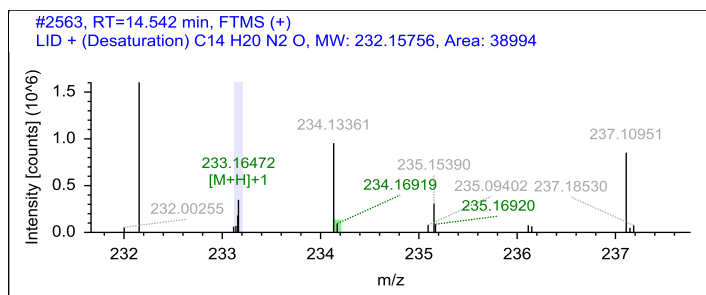
Appendix B

Name LID_233.1648_14.5

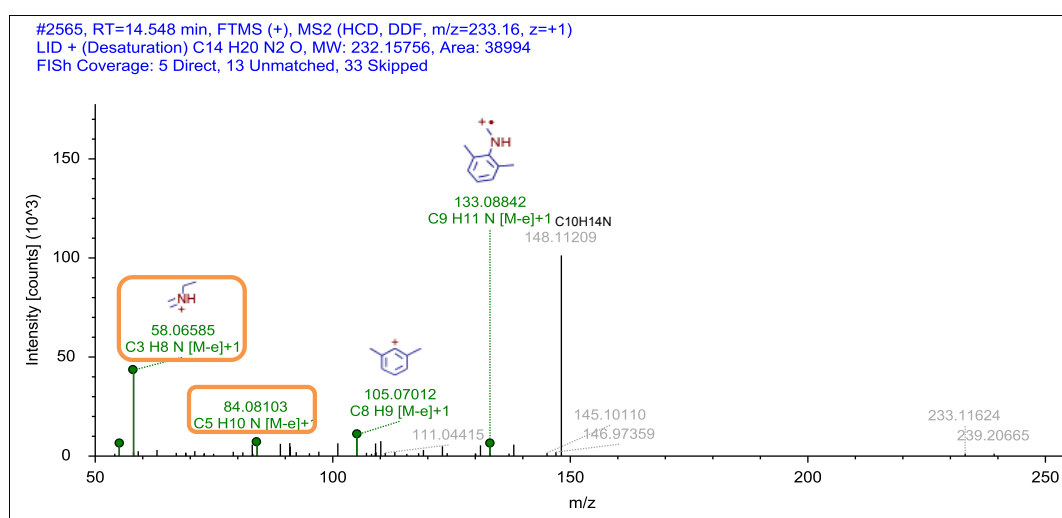
Chromatogram



MS Spectra



MS2 Spectra



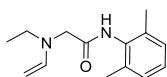
Formula

C₁₄ H₂₀ N₂ O

Atomic Modification

-H₂

Proposed Structure



Additional Evidence for Structure Interpretation

The MS2 fragment at the nominal mass 58 was also observed for the parent compound and indicates that the ethylmethanamine moiety is a substructure of this TP. The atomic modification from the elemental formula of the parent compound to this TP is -H₂. The MS2 fragment at the nominal mass 84 has a difference of -H₂ to the MS2 fragment at the nominal mass 86 that was observed for the parent compound. This indicates that the modification occurred at the ethylamine part. Since a iminium-species would lead to a atomic modification of -H this evidence is diagnostic for an alkene moiety.

Attributed Reaction from the Parent Compound to this TP

It is *certainly* that this TP was formed via a desaturation.

This TP was also observed in the sorption control reactors, in the calibration samples, and in the abiotic control reactors in a similar or higher amounts than in the biotransformation reactors. In the abiotic control reactors it was decreasing with time.

Confidence Level

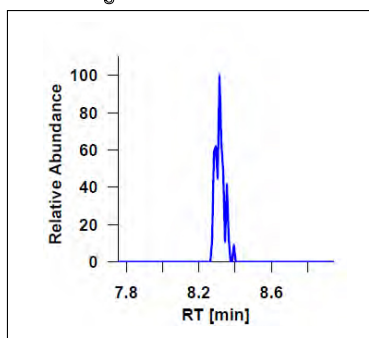
Level 2b,
diagnostic evidence

MassBank ID

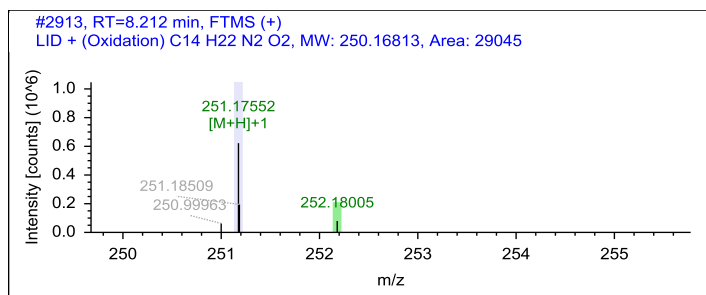
ET080403

Name LID_251.1754_8.2

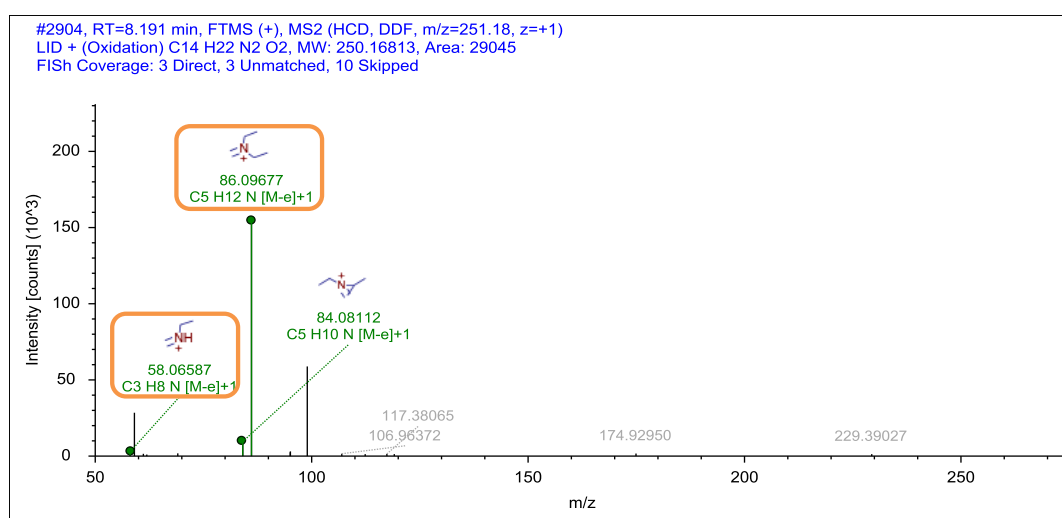
Chromatogram



MS Spectra



MS2 Spectra



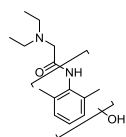
Formula

C₁₄ H₂₂ N₂ O₂

Atomic Modification

+O

Proposed Structure



Additional Evidence for Structure Interpretation

The MS2 fragments at the nominal masses 58 and 86 were also observed for the parent compound and indicate that the diethylamine moiety is substructure of this TP. The atomic modification of the elemental formula of the parent compound to this TP is +O. In an MS2 spectrum at the collision energy of 15, an additional MS2 fragment was observed at the exact mass of 233.1654 (C₁₄H₂₁ON₂, Δm=2.4905 ppm). The neutral loss between the precursor ion and this MS2 fragment is H₂O and indicates the presence of a hydroxyl moiety. Therefore, it is likely that a hydroxylation occurred at the aromatic part of the molecule.

Attributed Reaction from the Parent Compound to this TP

It is *likely* that this TP was formed via a hydroxylation reaction.

Confidence Level

Level 3,
TP class

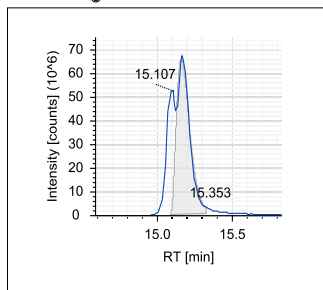
MassBank ID

ET080601-ET080606

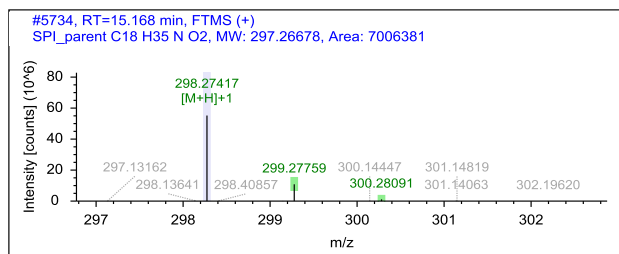
B.4.5 Structural evidence for spiroxamine and its TPs

Name SPI_298.2741_15.1, parent

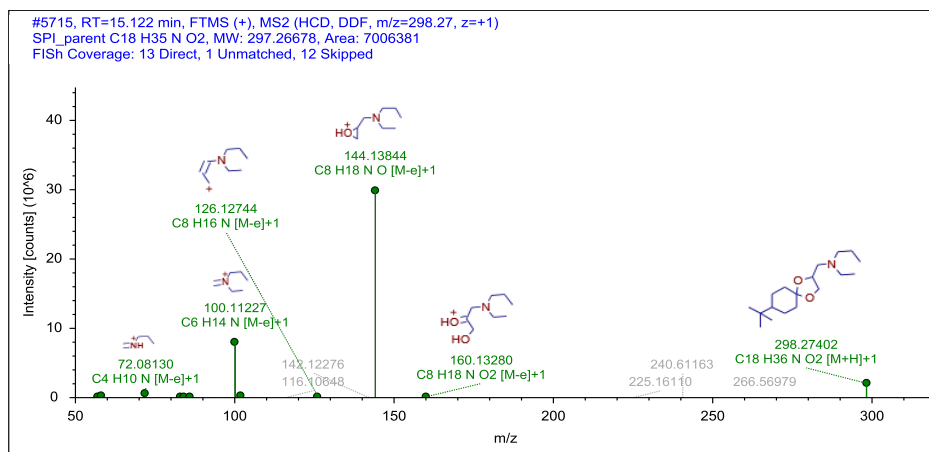
Chromatogram



MS Spectra



MS2 Spectra



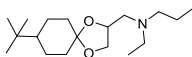
Formula

C18 H35 N O2

Atomic Modification

none

Proposed Structure



Confidence Level

Level 1,
reference standard

MassBank ID

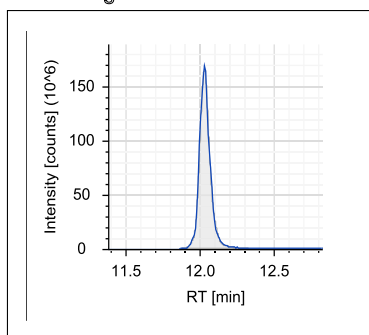
ET180001-ET180005

Additional Evidence for Structure Interpretation

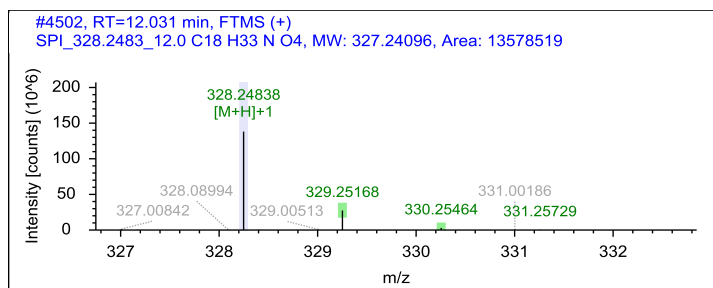
This is the structural evidence that was observed for the parent compound SPI. The peak shape with two close maxima is characteristic for this compound with the method used.

Name SPI_328.2483_12.0

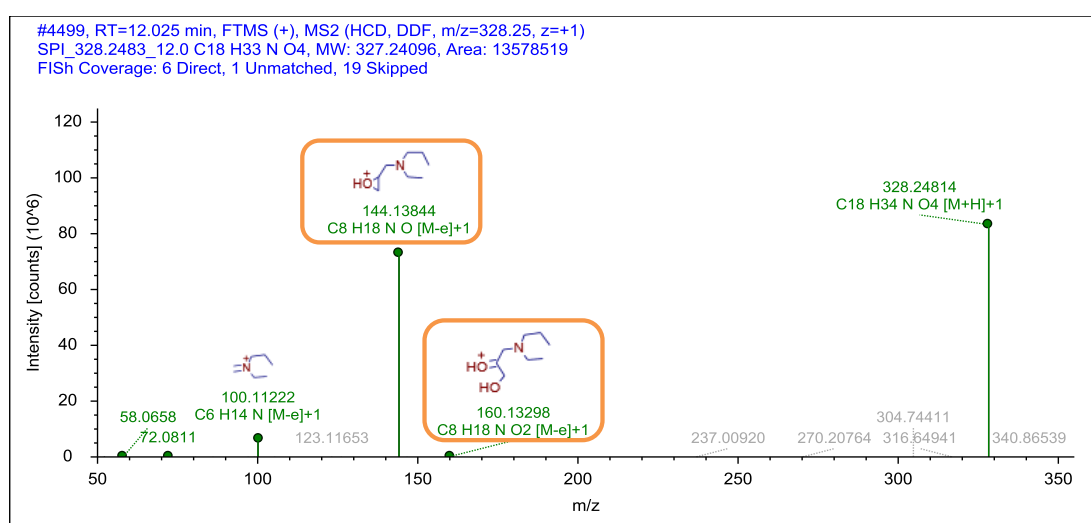
Chromatogram



MS Spectra



MS2 Spectra



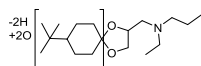
Formula

C18 H33 N O4

Atomic Modification

-H2, +O2

Proposed Structure



Additional Evidence for Structure Interpretation

The MS2 fragments at the nominal masses 58, 72, 100, 144, and 160 were also observed for the parent compound and indicate that the dioxolane amine substructure is unaltered. The atomic modification from the elemental formula of the parent compound to this TP is -H2 +O2. No matching signal was observed in the MS2 spectrum in negative mode. This indicates that no carboxylic acid is present. Therefore, it is likely that the modification took place at the tert-butyl cyclohexyl part of the molecule.

Attributed Reaction from the Parent Compound to this TP

It is *possible* that this TP was formed via a combination of several reactions, namely two hydroxylation reactions and the successive oxidation of one hydroxyl moiety to a carbonyl or a desaturation reaction.

Confidence Level

Level 3,
TP class

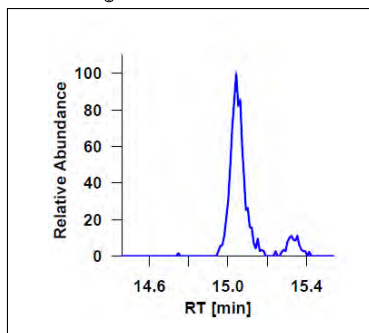
MassBank ID

ET180101-ET180106

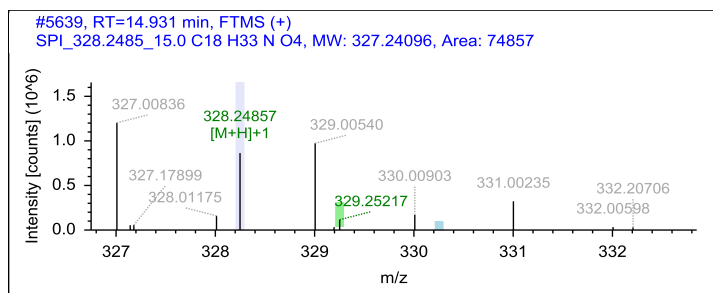
Appendix B

Name SPI_328.2485_15.0

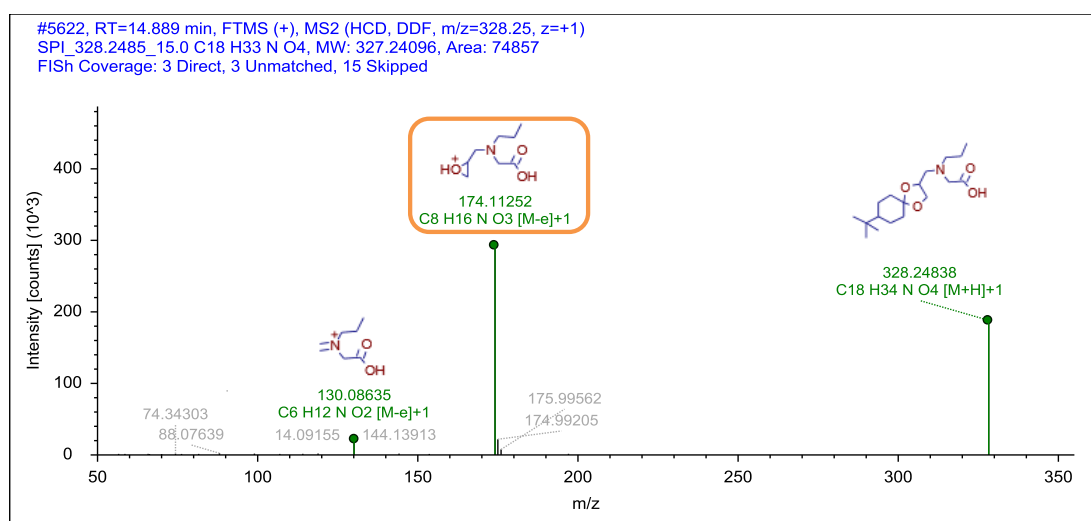
Chromatogram



MS Spectra



MS2 Spectra



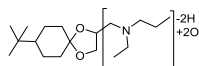
Formula

C18 H33 N O4

Atomic Modification

-H2, +O2

Proposed Structure



Additional Evidence for Structure Interpretation

The atomic modification from the elemental formula of the parent compound to this TP is -H2 +O2. The MS2 fragments at the nominal masses 130 and 174 correspond to the MS2 fragments of the parent compound at the nominal masses 100 and 144 by taking into account the modification (-H2 +O2). This indicates that the modification took place at the methylethylpropyl amine moiety. No corresponding signal was observed in the MS spectrum in negative mode. Given the low intensity of the peak and the lower sensitivity of the negative mode measurement, this does not exclude the probability of a carboxylic acid moiety. However, the exact type of transformation remains unknown. The structures of the MS2 fragments are drawn exemplarily.

Attributed Reaction from the Parent Compound to this TP

The reactions that formed this TP remains *unknown*.

Confidence Level

Level 3,

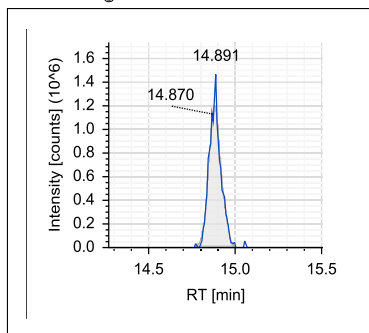
TP class

MassBank ID

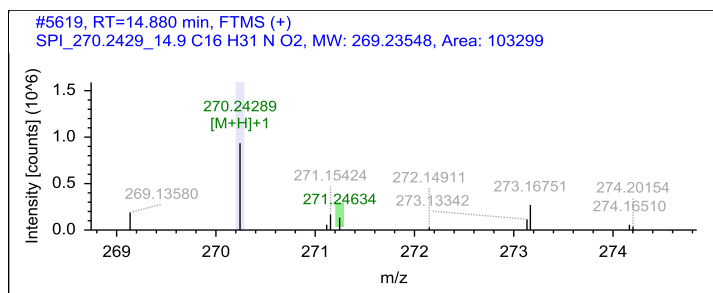
ET180601-ET180606

Name SPI_270.2429_14.9

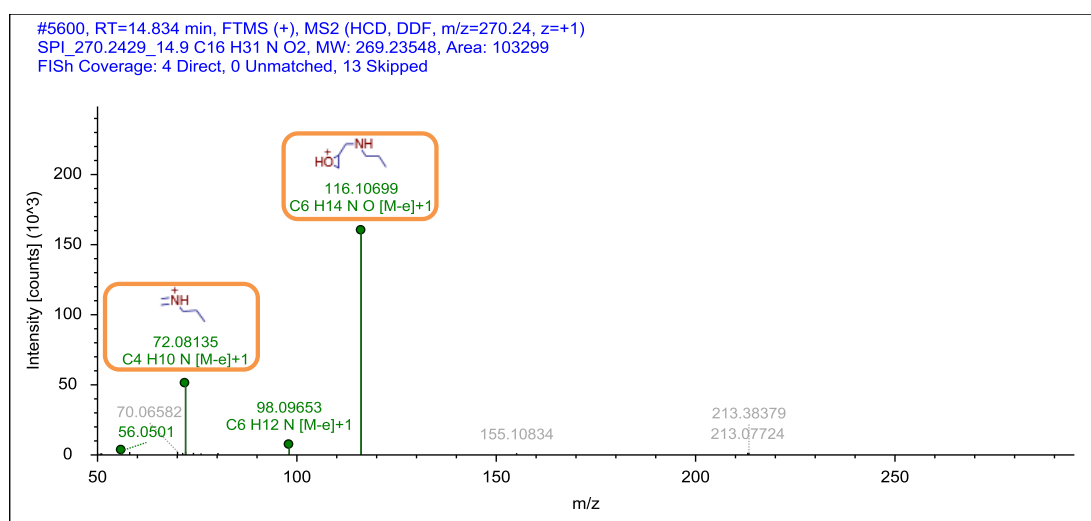
Chromatogram



MS Spectra



MS2 Spectra



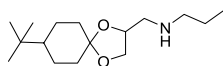
Formula

C16 H31 N O2

Atomic Modification

-C2H4

Proposed Structure



Additional Evidence for Structure Interpretation

The MS2 fragment at the nominal mass 72 was also observed for the parent compound and indicates that the propylmethyl amine moiety is a substructure of this TP. The atomic modification from the elemental formula of the parent compound to this TP is -C2H4. This modification could have occurred through a loss of the ethyl moiety. This is strengthened by the MS2 fragments at the nominal masses 98 and 116 that correspond to the MS2 fragments of the parent compound at the nominal masses 126 and 144 by taking into account the modification (-C2H4). The structural evidence is diagnostic.

Attributed Reaction from the Parent Compound to this TP

It is *certain* that this TP was formed via N-deethylation.

Confidence Level

Level 2b,
diagnostic evidence

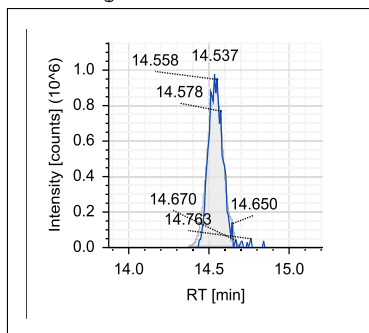
MassBank ID

ET181001-ET181006

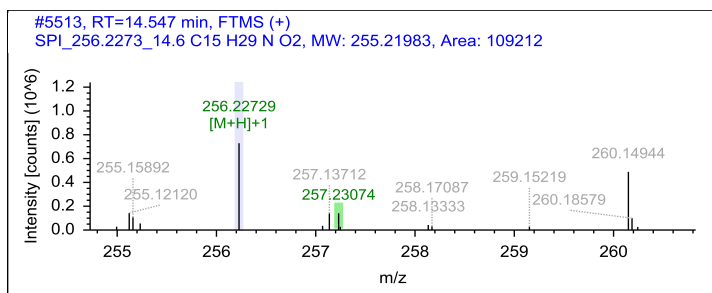
Appendix B

Name SPI_256.2273_14.6

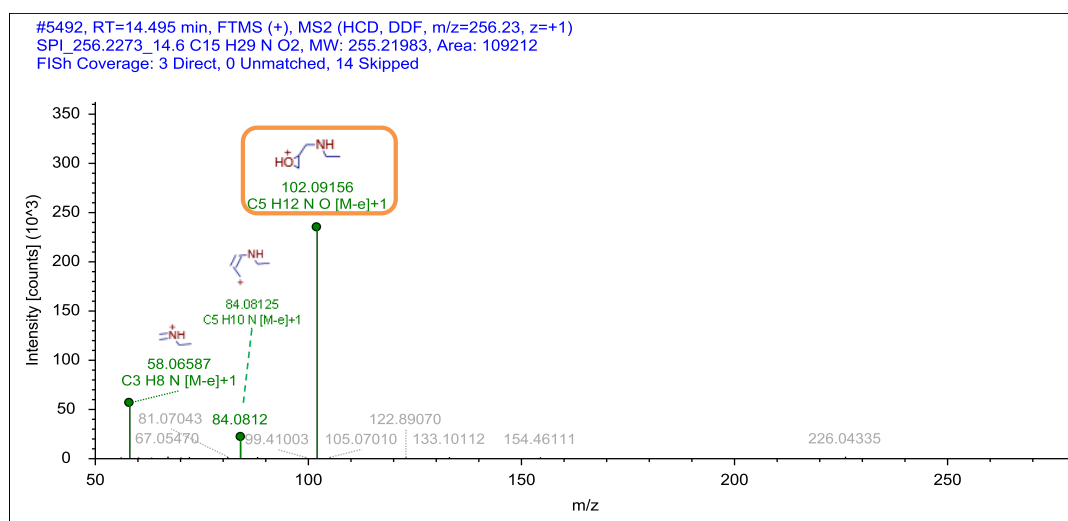
Chromatogram



MS Spectra



MS2 Spectra



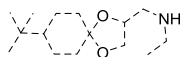
Formula

C15 H29 N O2

Atomic Modification

-C3H6

Proposed Structure



Additional Evidence for Structure Interpretation

The atomic modification from the elemental formula of the parent compound to this TP is -C3H6. This modification could have occurred through the loss of the propyl moiety. The MS2 fragments at the nominal masses 58, 84, and 102 correspond to the MS2 fragments of the parent compound at the nominal masses 72, 126, and 144 by taking into account the modification (-C3H6). The evidence for the structural proposal is diagnostic.

Attributed Reaction from the Parent Compound to this TP

It is *certain* that this TP was formed via N-depropylation.

This TP was also formed in the three abiotic control reactors, it was present in the sorption reactors, and it was present and increasing in the calibration samples in a higher amount than in the biotransformation reactors. Therefore, it is likely that this TP is formed abiotically. It could not be determined whether it is also formed biotically.

Confidence Level

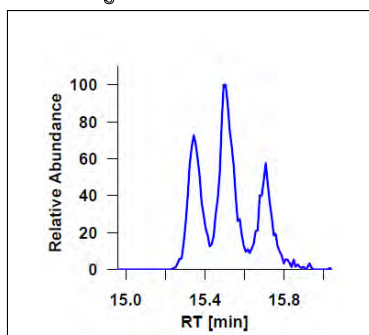
Level 2b,
diagnostic evidence

MassBank ID

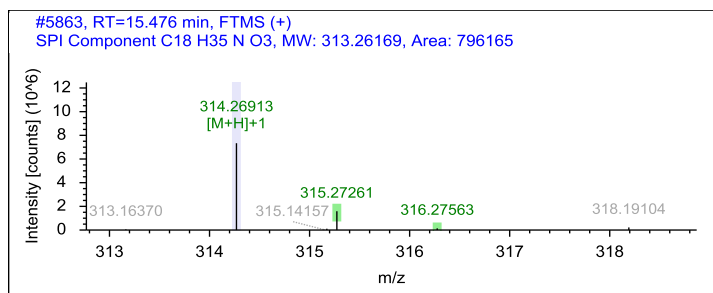
ET181101-ET181106

Name SPI_314.2691_15.4

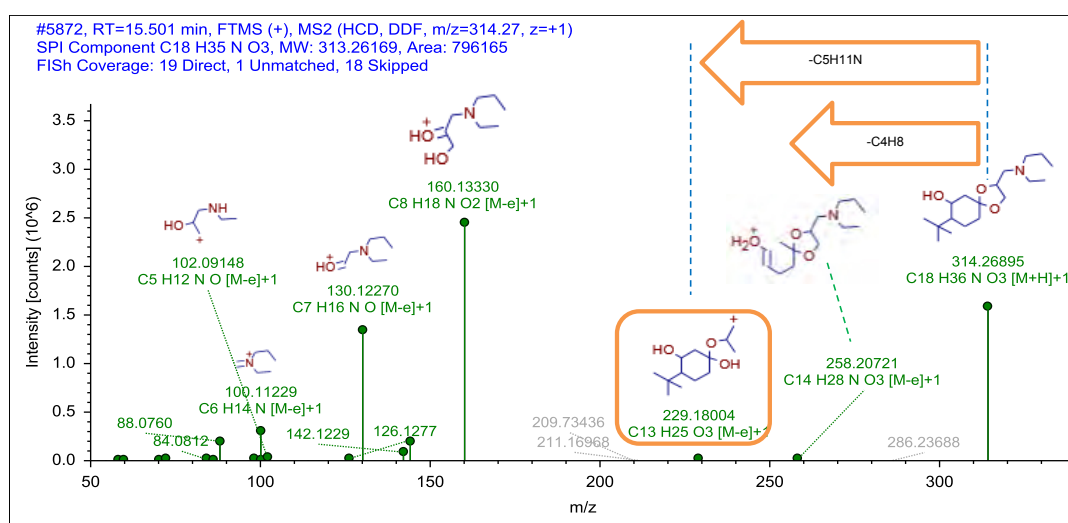
Chromatogram



MS Spectra



MS2 Spectra



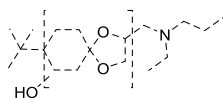
Formula

C18 H35 N O3

Atomic Modification

+O

Proposed Structure



Additional Evidence for Structure Interpretation

The observed neutral loss of -C4H8 corresponds to the loss of the tert-butyl group. The observed neutral loss of C5H11N corresponds to the loss of the ethylpropylamine moiety. These neutral losses indicate that the atomic modification +O from the elemental formula of the parent compound to this TP occurred at the cyclohexylcyclopentyl part of the molecule. The peak shape with three maxima is characteristic for this substance. The MS2 spectrum of all maxima is similar. Therefore, it is likely that a hydroxylation occurred at similar positions at the cyclohexylcyclopentyl part of the molecule. The exact positions of the modification remain unknown. The structures of the MS2 fragments are drawn exemplarily.

Attributed Reaction from the Parent Compound to this TP

It is *likely* that this TP was formed via a hydroxylation reaction.

Confidence Level

Level 3,
substituent

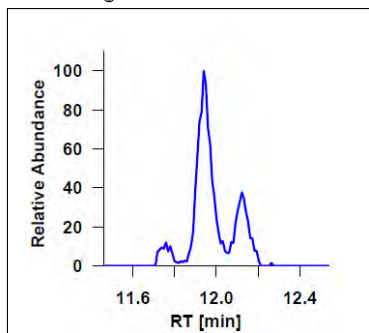
MassBank ID

ET180201-ET180206

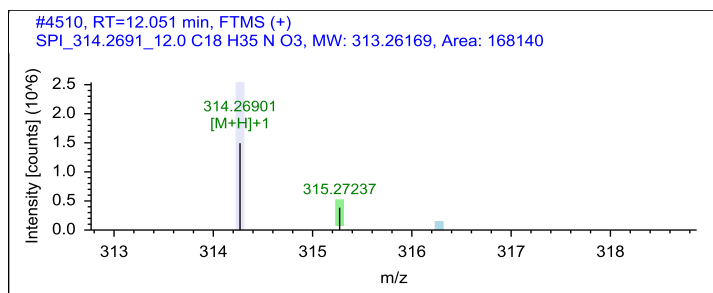
Appendix B

Name SPI_314.2691_12.0

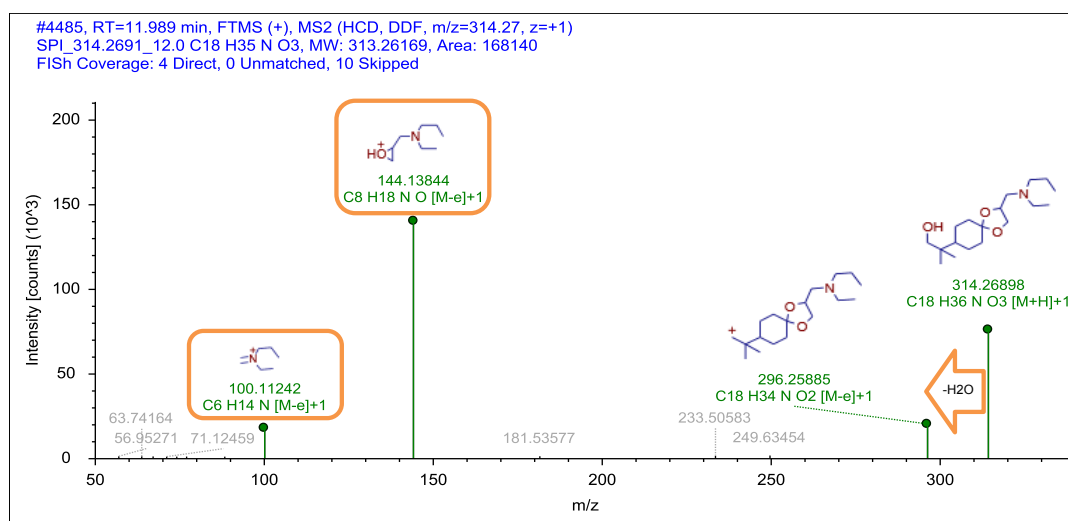
Chromatogram



MS Spectra



MS2 Spectra



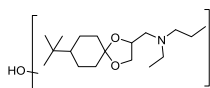
Formula

C₁₈ H₃₅ N O₃

Atomic Modification

+O

Proposed Structure



Additional Evidence for Structure Interpretation

The atomic modification of +O from the parent compound to this TP could be explained by the formation of a hydroxylated product as well as an N-oxide. The neutral loss of H₂O is possible for both moieties [Ma et al.(2005)]. However, the MS2 fragments at the nominal masses 100 and 144 were also observed for the parent compound and indicate that the methylethylpropyl amine moiety is unaltered. Additionally, the peak shape with three maxima is characteristic for this substance. The MS2 spectrum of all maxima is similar. Therefore, it is likely that a hydroxylation occurred at similar positions. The exact position of the modification remains unknown. The structures of the MS2 fragments are drawn exemplarily.

Attributed Reaction from the Parent Compound to this TP

It is *likely* that this TP was formed via a hydroxylation reaction.

Confidence Level

Level 3,

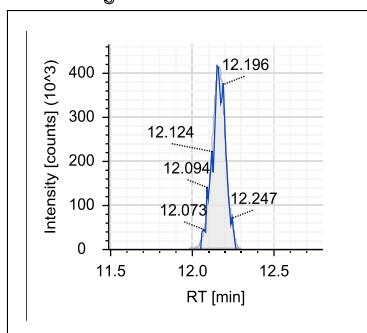
TP class

MassBank ID

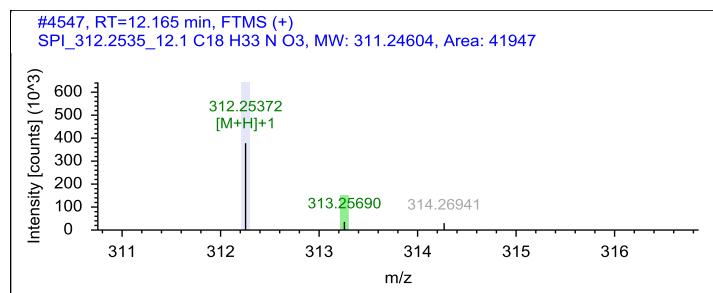
ET180801-ET180806

Name SPI_312.2535_12.1

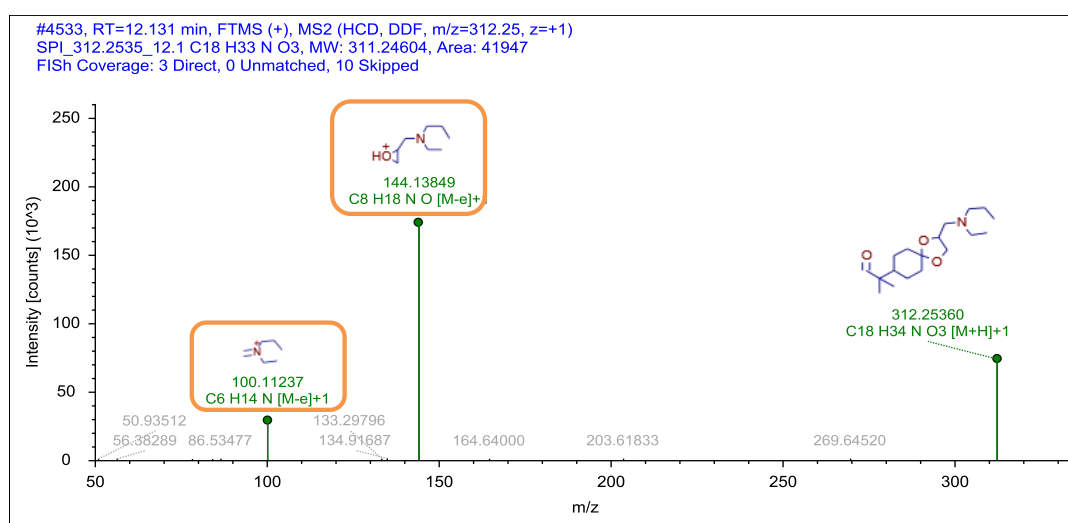
Chromatogram



MS Spectra



MS2 Spectra



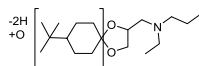
Formula

C18 H33 N O3

Atomic Modification

-H2, +O

Proposed Structure



Additional Evidence for Structure Interpretation

The MS2 fragments at the nominal masses 100 and 144 were also observed for the parent compound and indicate that the cyclopentyl amine substructure is unaltered. The atomic modification from the elemental formula of the parent compound to this TP is -H2 +O. The exact type and position of the modification remains unknown. The structure of the MS2 fragments are drawn exemplarily.

Attributed Reaction from the Parent Compound to this TP

Several reaction paths are *possible* that could have formed this TP, namely a hydroxylation followed by an oxidation to a carbonyl or a hydroxylation and a desaturation reaction.

Confidence Level

Level 3,
TP class

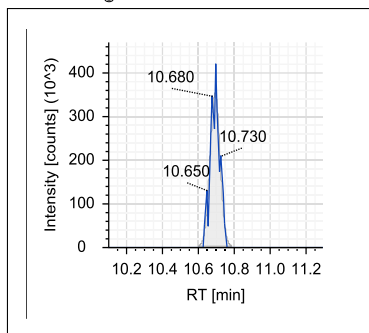
MassBank ID

ET181501-ET181506

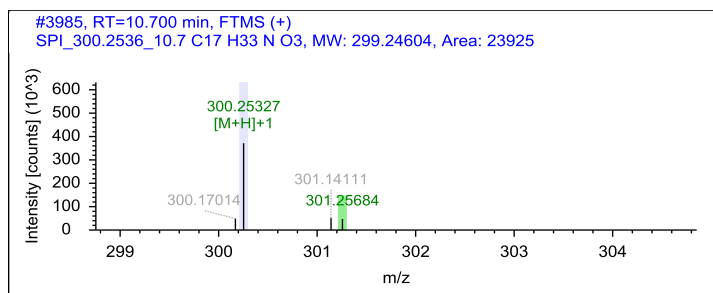
Appendix B

Name SPI_300.2536_10.7

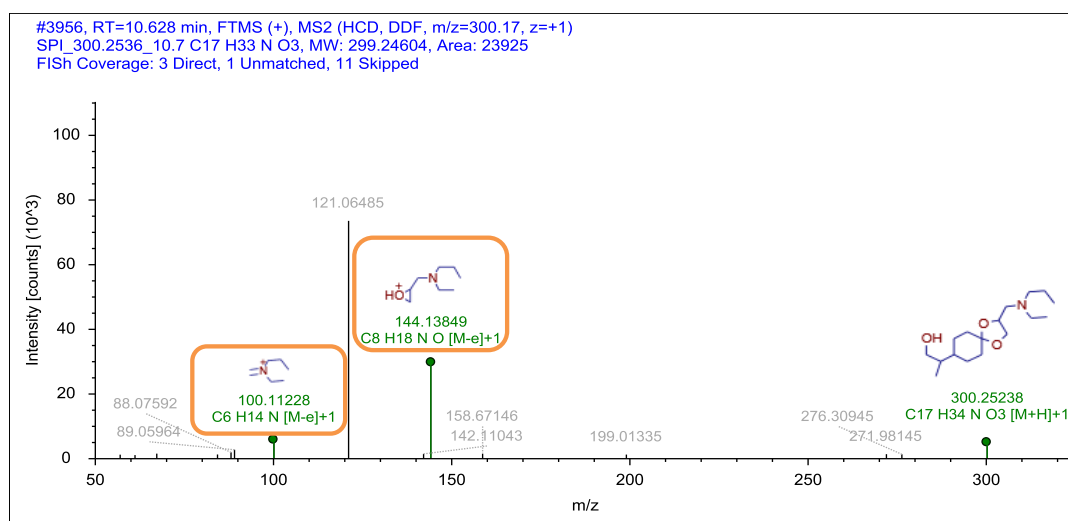
Chromatogram



MS Spectra



MS2 Spectra



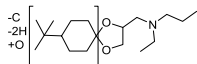
Formula

C17 H33 N O3

Atomic Modification

-CH2, +O

Proposed Structure



Additional Evidence for Structure Interpretation

The MS2 fragments at the nominal masses 100 and 144 were also observed for the parent compound and indicate that the cyclopentyl amine substructure is unaltered. The atomic modification from the elemental formula of the parent compound to this TP is -CH2 +O. The type of modification as well as the exact position remain unknown. The structure of the MS2 fragments are drawn exemplarily.

Attributed Reaction from the Parent Compound to this TP

It is *possible* that this TP was formed via a hydroxylation of a methyl of the tert-butyl moiety, followed by an oxidation to a carboxylic acid, followed by a decarboxylation and an additional hydroxylation at a different position.

Confidence Level

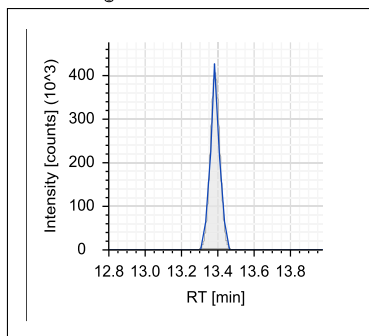
Level 3,
TP class

MassBank ID

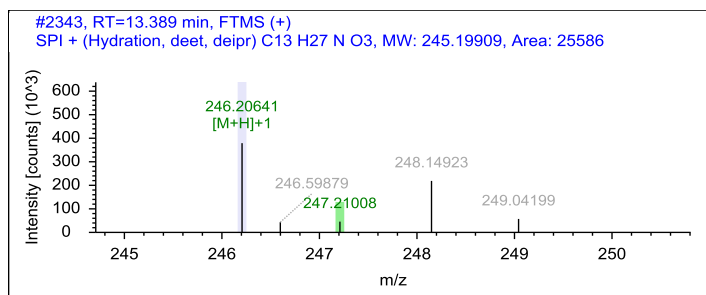
ET181601

Name SPI_246.2065_13.4

Chromatogram



MS Spectra



MS2 Spectra

There is no MS2 spectrum available, since it was not triggered during the original measurement and the peak was no longer present at the time of the remeasurement.

Formula

C13 H27 N O3

Atomic Modification

-C5H8, +O

Proposed Structure

Additional Evidence for Structure Interpretation

Due to the lack of an MS2 spectrum it is not possible to propose a structure.

Attributed Reaction from the Parent Compound to this TP

The reaction that formed this TP remains *unknown*.

Confidence Level

Level 4,
molecular formula

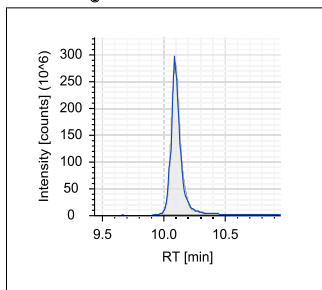
MassBank ID

NA

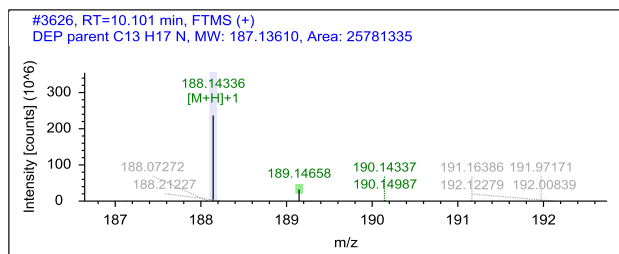
B.4.6 Structural evidence for deprenyl and its TPs

Name DEP_188.1433_10.1, parent

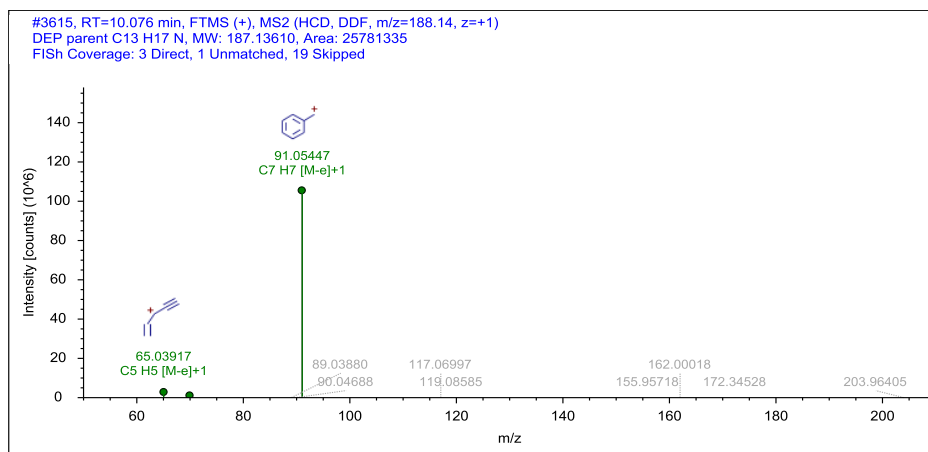
Chromatogram



MS Spectra



MS2 Spectra



Formula

C13 H17 N

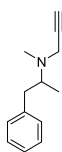
Additional Evidence for Structure Interpretation

This is the structural evidence that was observed for the parent compound DEP.

Atomic Modification

none

Proposed Structure



Confidence Level

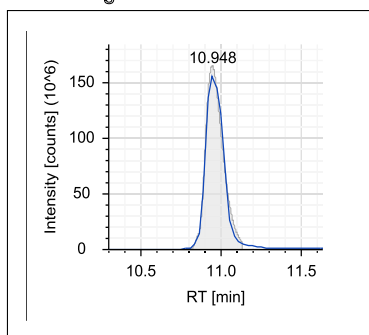
Level 1,
reference standard

MassBank ID

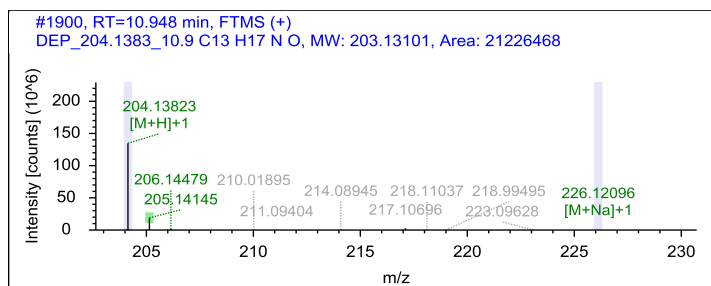
ET050001-ET050005

Name DEP_204.1383_10.9

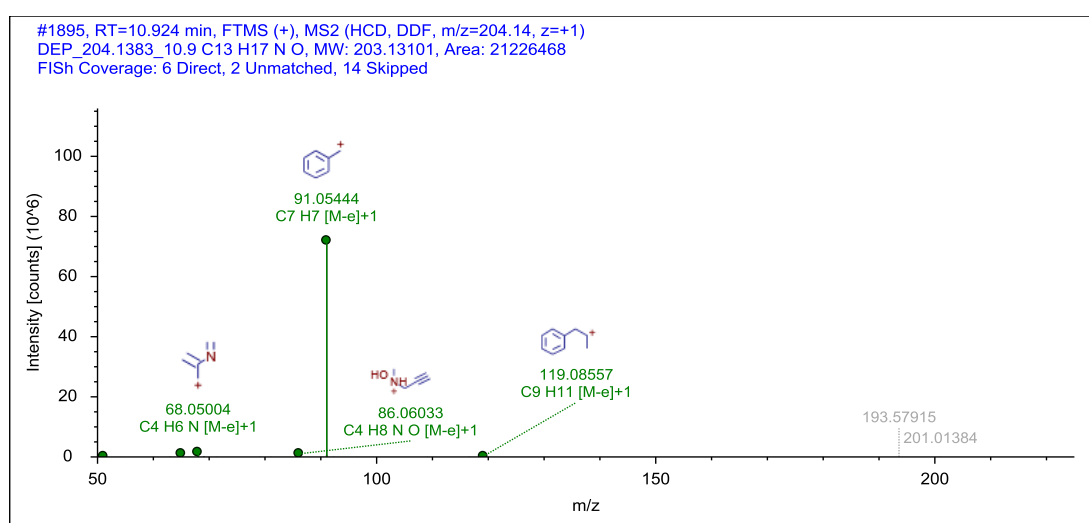
Chromatogram



MS Spectra



MS2 Spectra



Formula

C13 H17 N O

Additional Evidence for Structure Interpretation

The structure of this TP was confirmed by a reference standard.

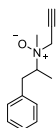
Atomic Modification

+O

Attributed Reaction from the Parent Compound to this TP

It is *certain* that this TP was formed via an N-oxidation reaction.

Proposed Structure



Confidence Level

Level 1,
reference standard

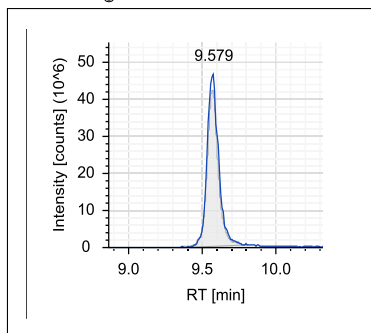
MassBank ID

ET050101-ET050105

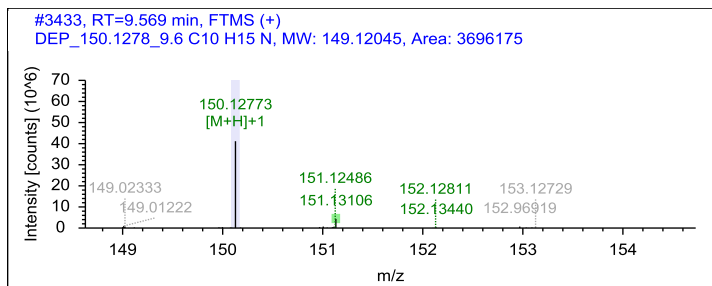
Appendix B

Name DEP_150.1278_9.6

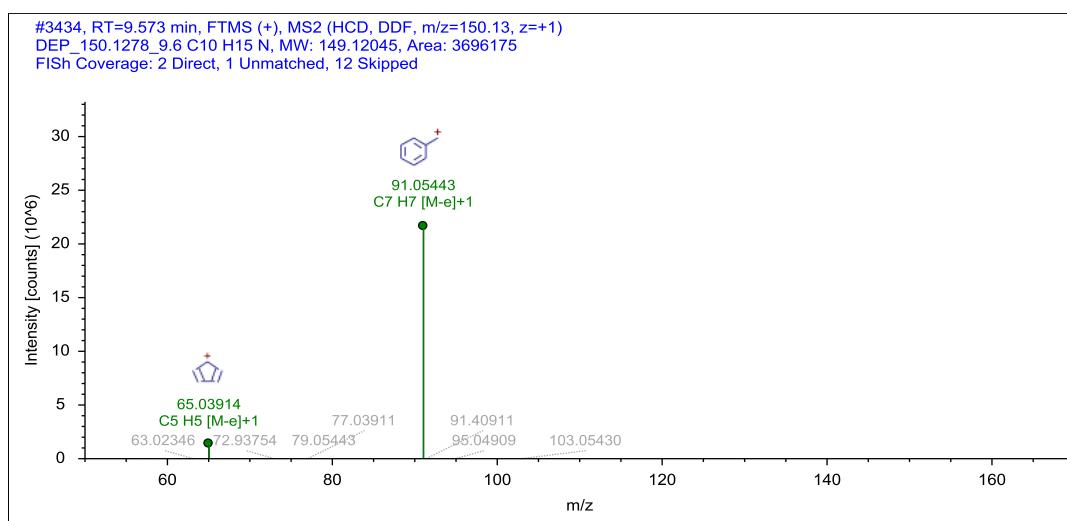
Chromatogram



MS Spectra



MS2 Spectra



Formula

C₁₀H₁₅N

Additional Evidence for Structure Interpretation

The structure of this TP was confirmed by a reference standard

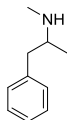
Atomic Modification

-C3H2

Attributed Reaction from the Parent Compound to this TP

It is *certain* that this TP was formed via an N-depropargylation reaction.

Proposed Structure



Confidence Level

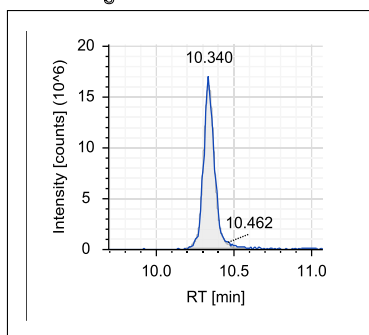
Level 1,
reference standard

MassBank ID

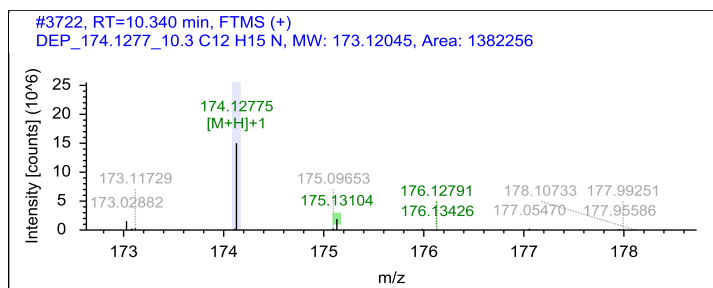
ET050201-ET050206

Name DEP_174.1277_10.3

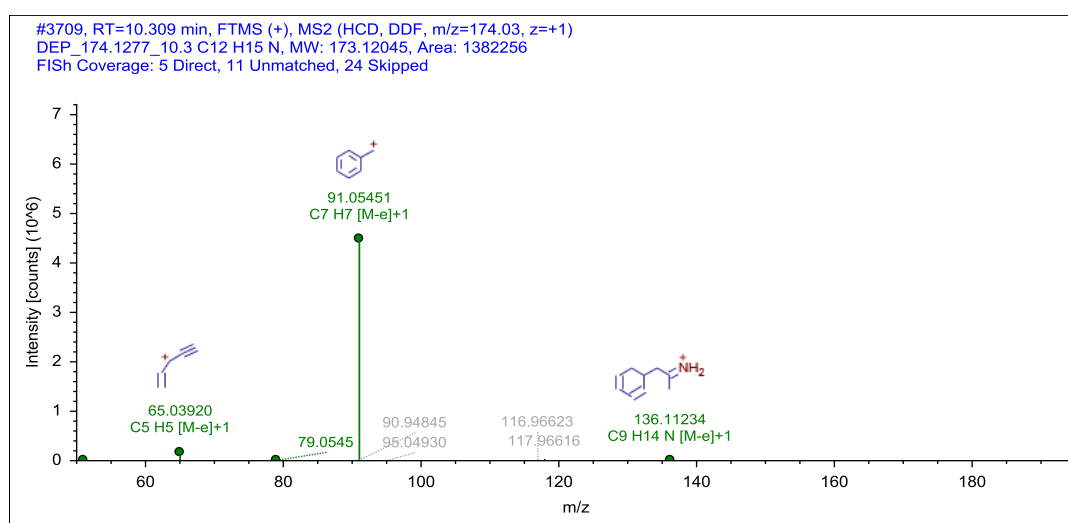
Chromatogram



MS Spectra



MS2 Spectra



Formula

C₁₂ H₁₅ N

Additional Evidence for Structure Interpretation

The structure of this TP was confirmed by a reference standard.

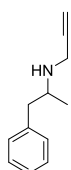
Atomic Modification

-CH₂

Attributed Reaction from the Parent Compound to this TP

It is *certain* that this TP was formed via an N-demethylation reaction.

Proposed Structure



Confidence Level

Level 1,
reference standard

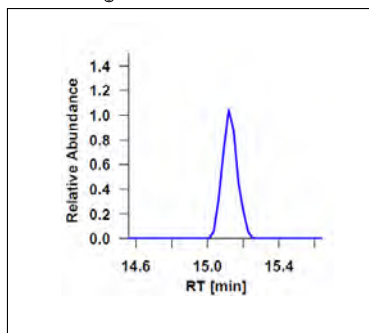
MassBank ID

ET050301-ET050305

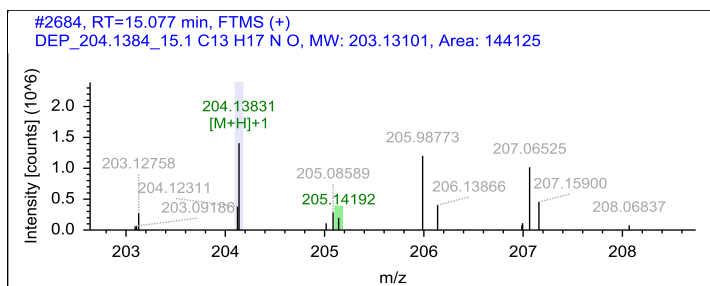
Appendix B

Name DEP_204.1384_15.1

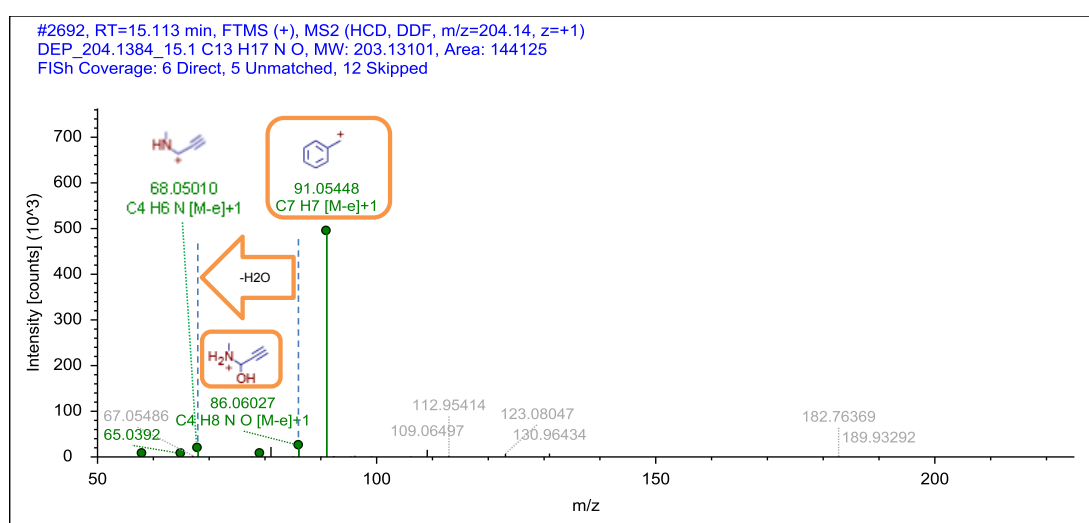
Chromatogram



MS Spectra



MS2 Spectra



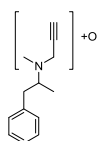
Formula

C13 H17 N O

Atomic Modification

+O

Proposed Structure



Additional Evidence for Structure Interpretation

The MS2 fragments at the nominal masses 91 and 65 were also observed for the parent compound and indicate that the aromatic part of the parent structure is a substructure of this TP. The neutral loss of H₂O between the MS2 fragments at the nominal masses 86 and 68 indicates a hydroxyl moiety. The MS2 fragment at the nominal mass 86 indicates that the hydroxyl moiety is connected to the methylpropargylamine part.

From the presented evidence, the exact position of the hydroxyl moiety remains unknown. A hydroxylation of an α -carbon would lead to a hemiaminal. Hemiaminals are in general unstable, but are known to possess a certain stability if the nitrogen is less basic, such as in aniline derivatives or amides. This is because the spontaneous cleavage of hemiaminals proceeds over the protonated form. However, the pK_a-value of DEP is with 7.5 [Shalaeva et al.(2008)] lower than for regular aliphatic amines. Therefore, it might be possible that the hemiaminals of DEP are stable. Alternatively, it possible that this TP is hydroxylated at the terminal carbon of the alkyne moiety. However, it has not been observed for mammalian systems that the oxidation of alkynes would lead to hydroxylated products.

Attributed Reaction from the Parent Compound to this TP

It is *possible* that this TP was formed via an α -C-hydroxylation to a hemiaminal, or a reaction at the terminal alkyne.

Confidence Level

Level 3,

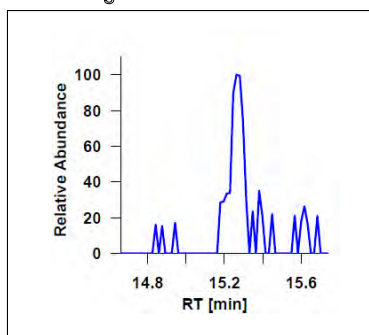
TP class

MassBank ID

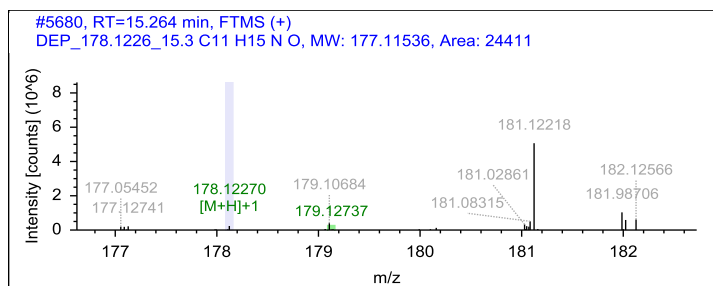
ET050401-ET050406

Name DEP_178.1226_15.3

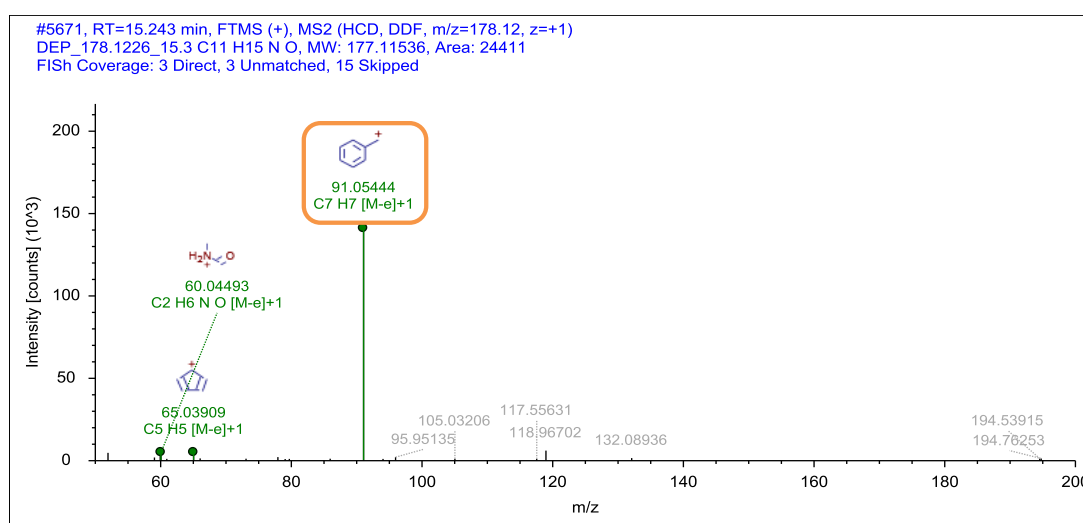
Chromatogram



MS Spectra



MS2 Spectra



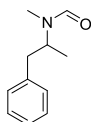
Formula

C11 H15 N O

Atomic Modification

-C2H2, +O

Proposed Structure



Additional Evidence for Structure Interpretation

The MS2 fragments at the nominal masses 91 and 65 were observed for the parent compound and indicate that the aromatic part of the parent structure is a substructure of this TP. In an MS2 spectrum measured with a collision energy of 30, an additional MS2 fragment was observed at the exact mass of 119.0854 (C₉H₁₁, $\Delta m = -1.0048$ ppm). This MS2 fragment was also observed for the parent in an MS2 spectrum measured with a collision energy of 30. This indicates that the n-propylbenzyl moiety is a substructure of this TP. The atomic modification of -C₂H₂ + O from the elemental formula of the parent compound to this TP can occur through the substitution of the propargyl moiety by a formyl group. The MS2 fragment at the nominal mass 60 indicates that the formyl group was added to the methylamine moiety.

Attributed Reaction from the Parent Compound to this TP

It is *likely* that this TP was formed in two steps, namely by an N-depropargylation followed by an N-formylation reaction.

This TP was also formed in the three abiotic control reactors in a similar amount than in the biotransformation reactors. It was not observed in the sorption control reactors or in the calibration samples.

Confidence Level

Level 3

proposed structure

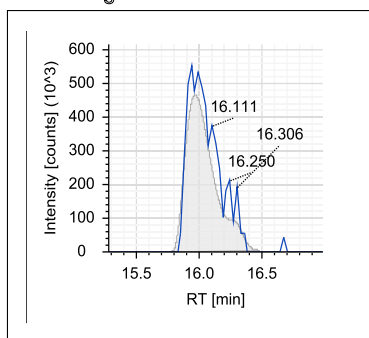
MassBank ID

ET050801-ET050806

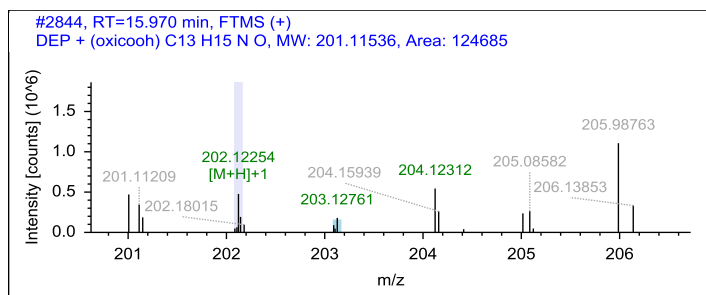
Appendix B

Name DEP_202.1225_16.0

Chromatogram

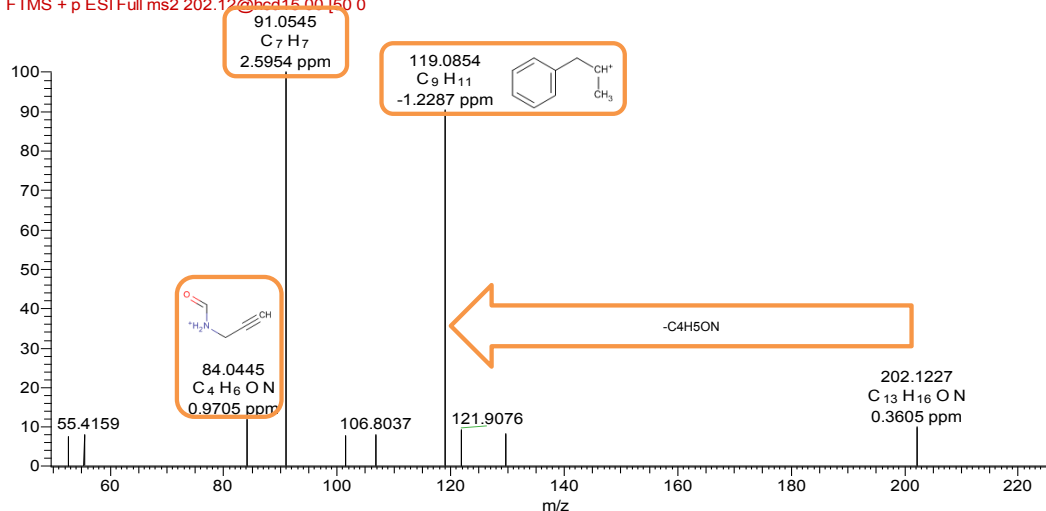


MS Spectra



MS2 Spectra

150213 07 #6421 RT: 16.01 AV: 1 SB: 434 16 37-19 06 11 03-15.66 NL: 1 27E4
F: FTMS + p ESI Full ms2 202.122500 [50 0



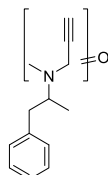
Formula

C₁₃ H₁₅ N O

Atomic Modification

-H₂, +O

Proposed Structure



Additional Evidence for Structure Interpretation

The MS2 fragment at the nominal mass 91 was observed for the parent compound and indicates that the aromatic part of the parent structure is a substructure of this TP. The MS2 fragment at the nominal mass 119 was also observed for the parent in an MS2 spectrum measured with a collision energy of 30. This indicates that the n-propylbenzyl moiety is a substructure of this TP. The MS2 fragment at the nominal mass 84 as well as the neutral loss of C₄H₅ON indicate that the atomic modification of -H₂ +O from the parent compound to this TP occurred at the methylpropargylamine moiety. The only possibility of this atomic modification at the methylpropargylamine moiety was the formation of a carbonyl, which could have occurred at the methyl group or at the secondary carbon of the propargyl group. The exact position of the carbonyl moiety remains unknown. The structure corresponding to the MS2 fragment at the nominal mass 84 was drawn exemplarily.

Attributed Reaction from the Parent Compound to this TP

It is *possible* that this TP was formed either via an α-C-oxidation reaction or in two steps, namely by an N-demethylation reaction followed by an N-formylation reaction.

Confidence Level

Level 3

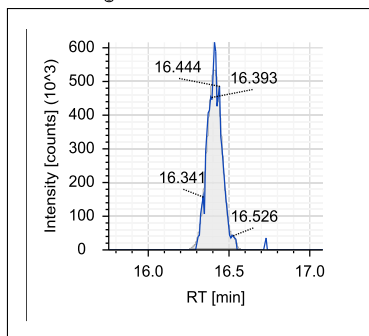
TP class

MassBank ID

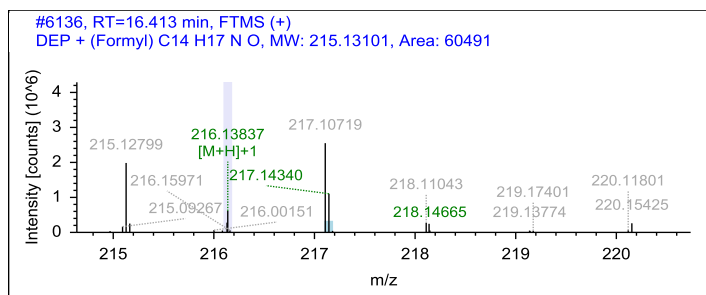
ET050501-ET050506

Name DEP_216.1383_16.4

Chromatogram



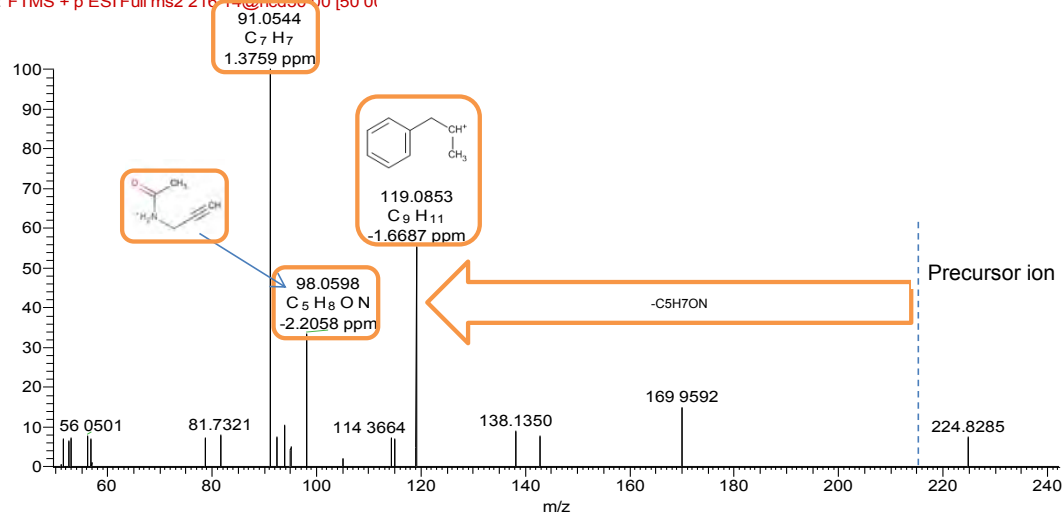
MS Spectra



MS2 Spectra

150213 08 #6555 RT: 16.32 AV: 1 SB: 5 16.02-16.10 NL: 1 50E4

F: FTMS + p ESI Full ms2 216.14@nd0000 [50.0]



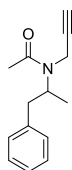
Formula

C14 H17 N O

Atomic Modification

+CO

Proposed Structure



Additional Evidence for Structure Interpretation

The MS2 fragment at the nominal mass 91 was observed for the parent compound and indicates that the aromatic part of the parent structure is a substructure of this TP. The MS2 spectrum at the nominal mass 119 was also observed for the parent in an MS2 spectrum measured with a collision energy of 30. This indicates that the n-propylbenzyl moiety is a substructure of this TP. The MS2 fragment at the nominal mass 98 as well as the neutral loss of C5H7ON indicate that the atomic modification of +CO from the parent compound to this TP occurred at the methylpropargylamine moiety. This modification can be realized by the substitution of the methyl group by an acetyl moiety.

Attributed Reaction from the Parent Compound to this TP

It is *likely* that this TP was formed in two steps, namely by an N-demethylation followed by an N-acetylation reaction. The N-demethylated TP DEP_174.1277_10.3 was observed.

Confidence Level

Level 3

proposed structure

MassBank ID

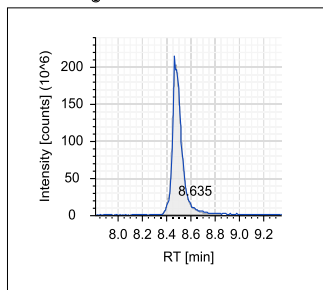
ET050601-ET050606

Appendix B

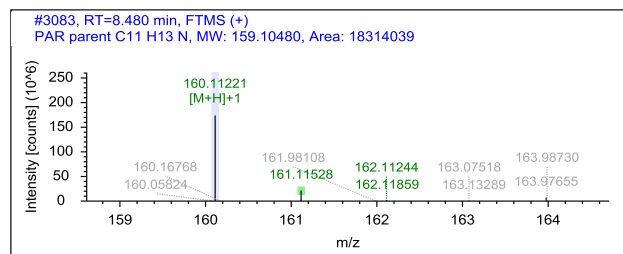
B.4.7 Structural evidence for pargyline and its TPs

Name PAR_160.1122_8.5, parent

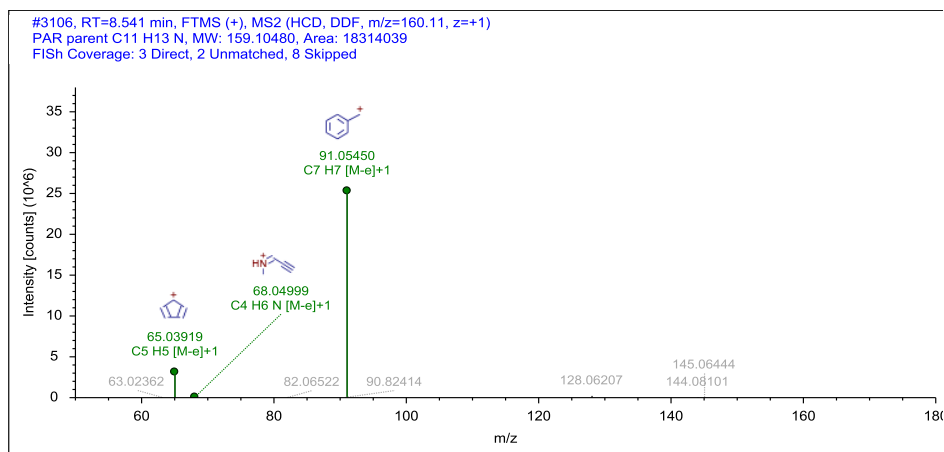
Chromatogram



MS Spectra



MS2 Spectra



Formula

C11 H13 N

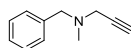
Additional Evidence for Structure Interpretation

This is the structural evidence that was observed for the parent compound PAR.

Atomic Modification

none

Proposed Structure



Confidence Level

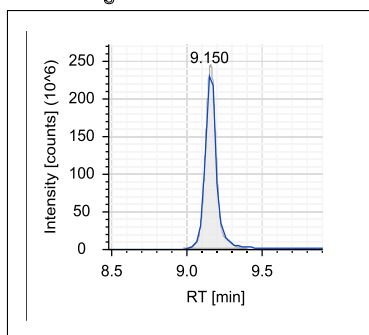
Level 1,
reference standard

MassBank ID

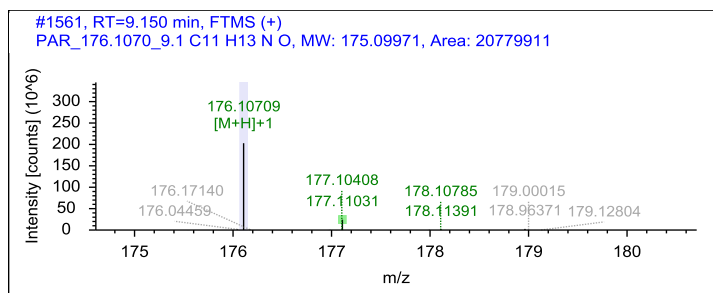
ET140001-ET140005

Name PAR_176.1070_9.1

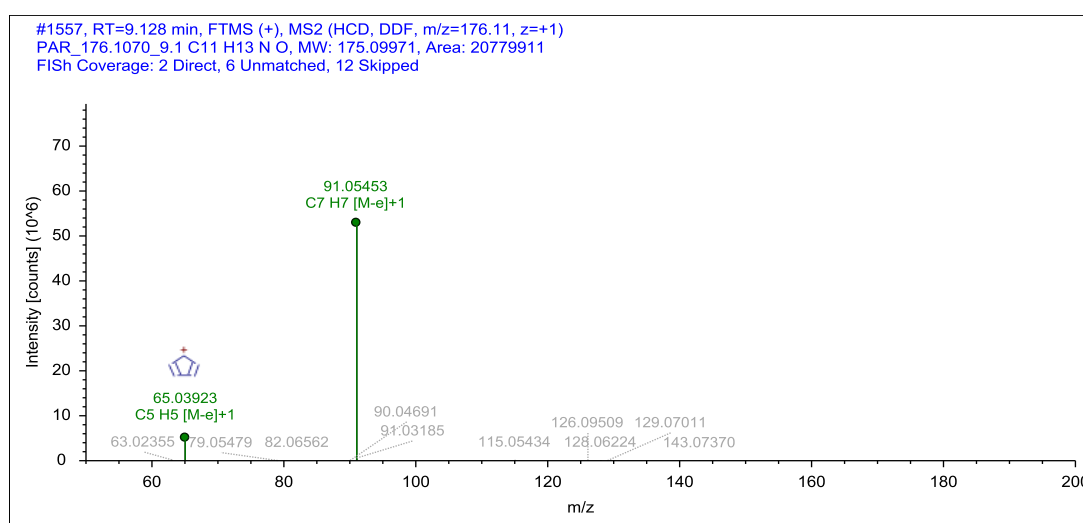
Chromatogram



MS Spectra



MS2 Spectra



Formula

C₁₁ H₁₃ N O

Additional Evidence for Structure Interpretation

The structure of this TP was confirmed by a reference standard.

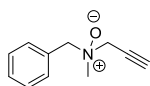
Atomic Modification

+O

Attributed Reaction from the Parent Compound to this TP

It is *certain* that this TP was formed via an N-oxidation reaction.

Proposed Structure



Confidence Level

Level 1,
reference standard

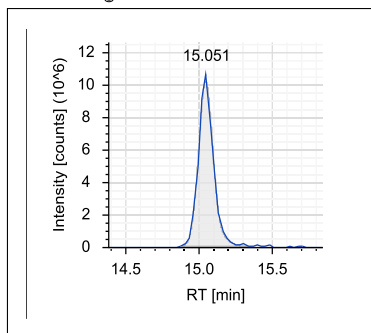
MassBank ID

ET140101-ET140105

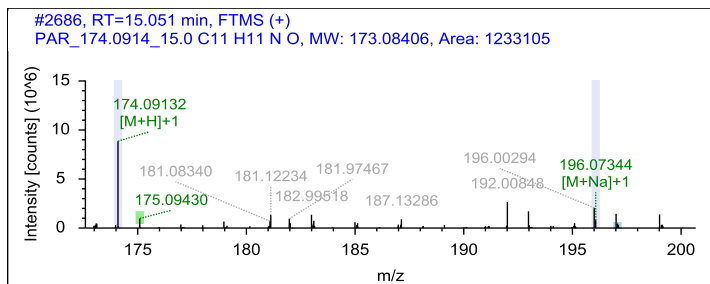
Appendix B

Name PAR_174.0914_15.0

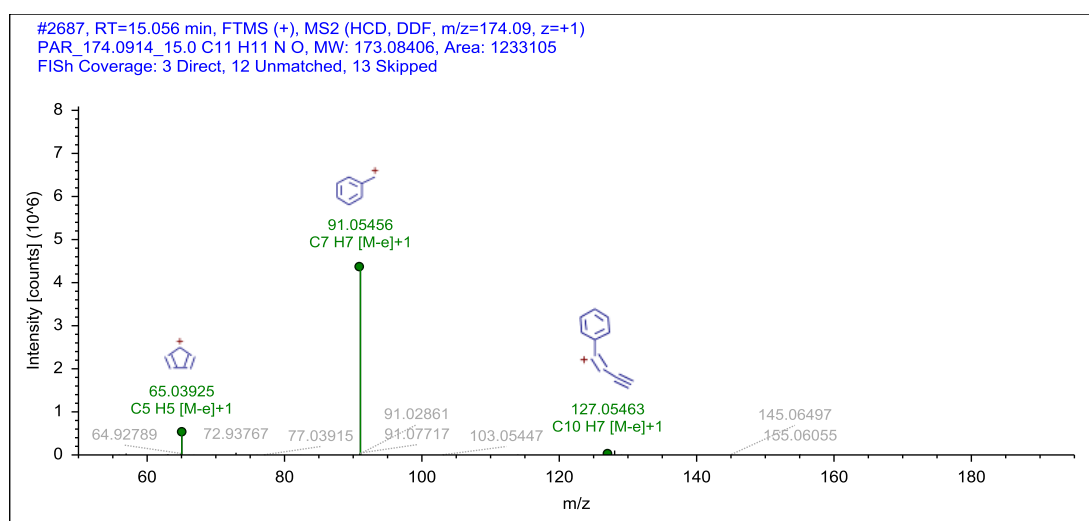
Chromatogram



MS Spectra



MS2 Spectra



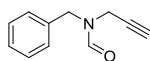
Formula

C11 H11 N O

Atomic Modification

-H2, +O

Proposed Structure



Additional Evidence for Structure Interpretation

The formamide structure of this TP was confirmed by a synthesized standard. Details on the synthesis and the NMR measurement can be found in Chapter S5 in the SI.

Attributed Reaction from the Parent Compound to this TP

It is *possible* that this TP was formed via an α -C-oxidation to a formamide or an N-demethylation followed by an N-formylation reaction.

Confidence Level

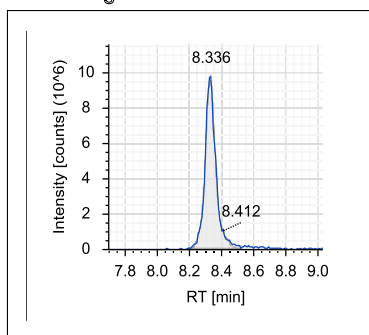
Level 1,
synthesized standard

MassBank ID

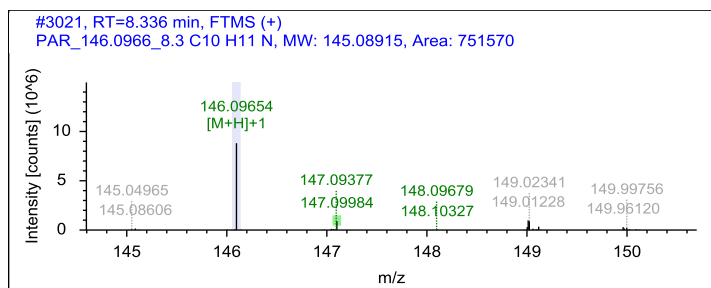
ET140201-ET140206

Name PAR_146.0966_8.3

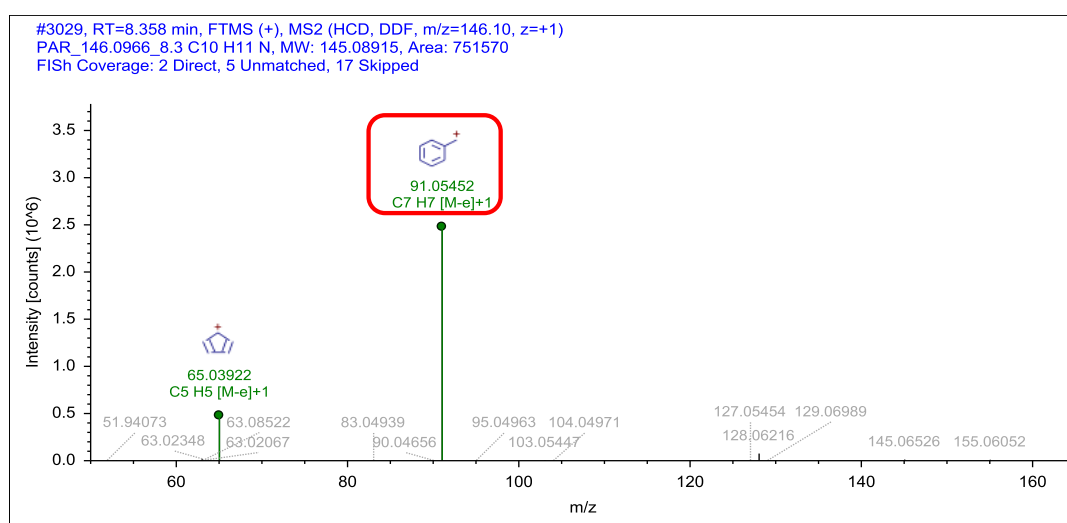
Chromatogram



MS Spectra



MS2 Spectra



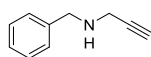
Formula

C10 H11 N

Atomic Modification

-CH2

Proposed Structure



Additional Evidence for Structure Interpretation

The MS2 fragments at the nominal masses 65 and 91 were also observed for the parent compound and indicate that the benzyl structure is a substructure of this TP. The atomic modification -CH2 from the elemental formula of the parent compound to this TP can only have occurred through the loss of the methyl moiety. Since this is the only possible structure, the structural evidence is diagnostic.

Attributed Reaction from the Parent Compound to this TP

It is *certain* that this TP was formed via an N-demethylation reaction.

Confidence Level

Level 2b,
diagnostic evidence

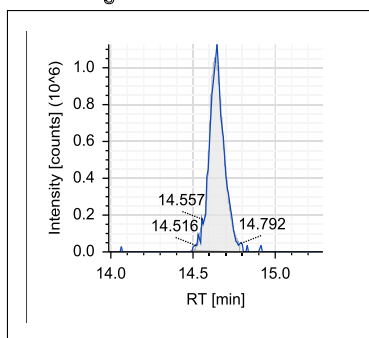
MassBank ID

ET140301-ET140306

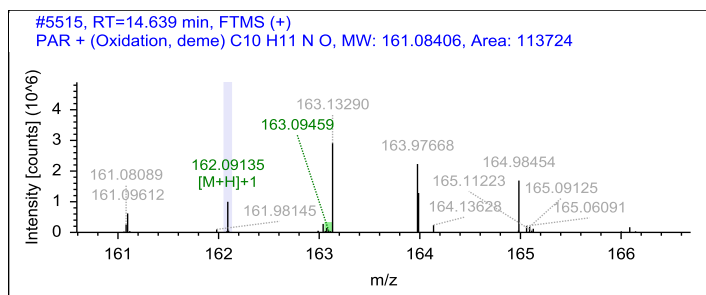
Appendix B

Name PAR_162.0915_14.7

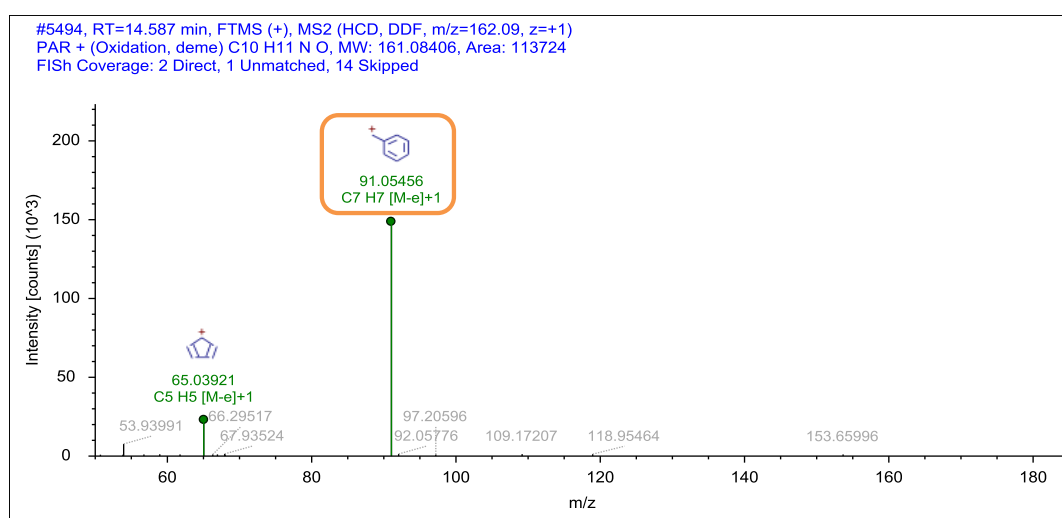
Chromatogram



MS Spectra



MS2 Spectra



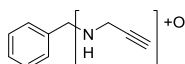
Formula

C10 H11 N O

Atomic Modification

-CH2, +O

Proposed Structure



Confidence Level

Level 3,
TP class

MassBank ID

ET140401-ET140406

Additional Evidence for Structure Interpretation

The MS2 fragments at the nominal masses 65 and 91 were also observed for the parent compound and indicate that the benzyl structure is a substructure of this TP. Therefore, it is likely that the atomic modification -CH2 +O from the elemental formula of the parent compound to this TP occurred through the loss of the methyl moiety and the addition of an oxygen to the propargyl amine moiety. From the presented structural evidence the exact position of the oxygen cannot be determined. However, the hydroxylation of the α -carbon would result in a hemiaminal. Hemiaminals are generally known to be unstable. However, hemiaminals adjacent to non-basic nitrogen, such as amides or aniline derivatives possess a certain stability. (This is because the spontaneous cleavage of hemiaminals proceed over the protonated form). PAR has a pKa of 6.9 [Albert et al. (1984)], which is lower than the pKa of regular aliphatic amines. Therefore, it might be possible that the hemiaminals of PAR are stable. Alternatively, the terminal alkyne carbon could have been hydroxylated. However, it has not been observed for mammalian systems that the oxidation of alkynes would lead to hydroxylated products. (Similar observations were made for DEP_204.1384_15.) A third possibility would be the N-hydroxylation of the secondary amine.

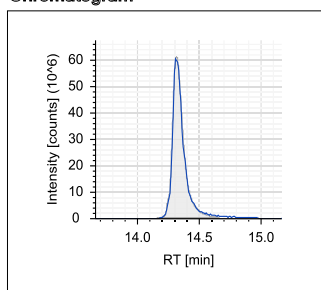
Attributed Reaction from the Parent Compound to this TP

Several reaction combinations are *possible* that could have formed this TP. As a first step an N-demethylation reaction is likely, followed by either an N-hydroxylation, an α -C-hydroxylation to a hemiaminal, or a reaction at the terminal alkyne carbon.

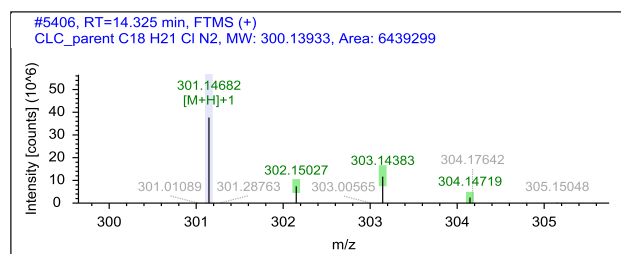
B.4.8 Structural evidence for chlorcyclizine and its TPs

Name CLC_301.1468_14.3, parent

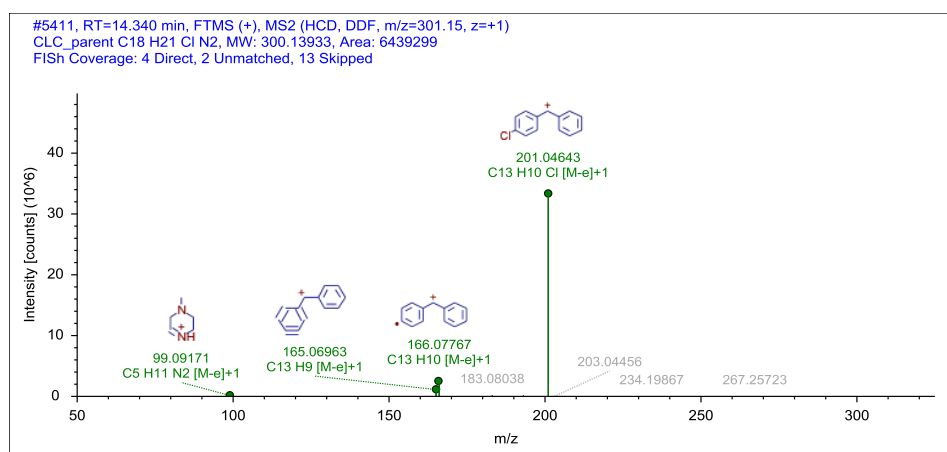
Chromatogram



MS Spectra



MS2 Spectra



Formula

C18 H21 Cl N2

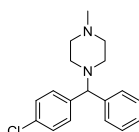
Additional Evidence for Structure Interpretation

This is the structural evidence that was observed for the parent compound CLC.

Atomic Modification

None

Proposed Structure



Confidence Level

Level 1,
reference standard

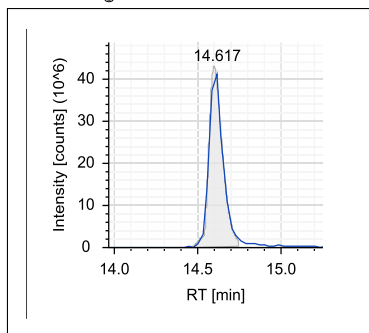
MassBank ID

ET010001-ET010005

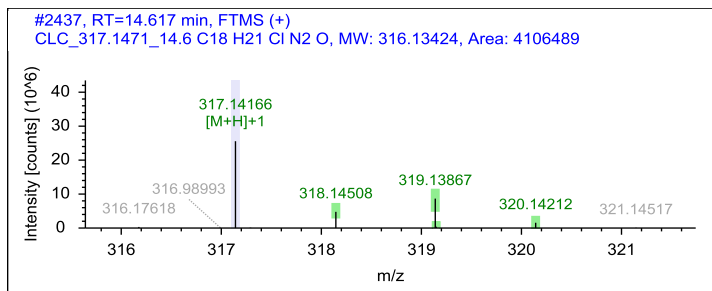
Appendix B

Name CLC_317.1471_14.6

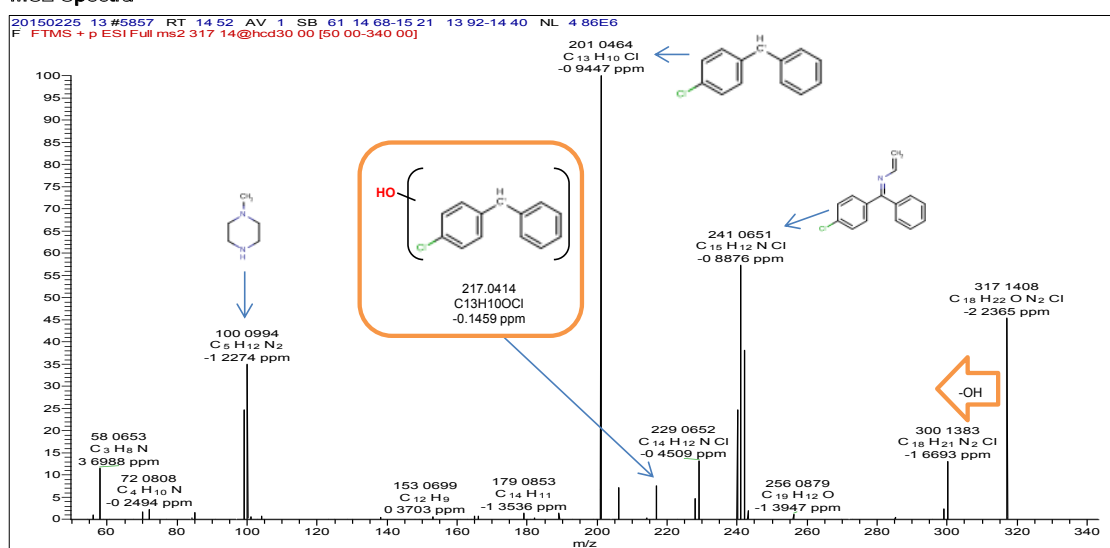
Chromatogram



MS Spectra



MS2 Spectra



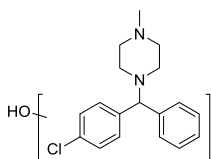
Formula

C₁₈ H₂₁ Cl N₂ O

Atomic Modification

+O

Proposed Structure



Confidence Level

Level 3,
substituent

MassBank ID

ET010106

Additional Evidence for Structure Interpretation

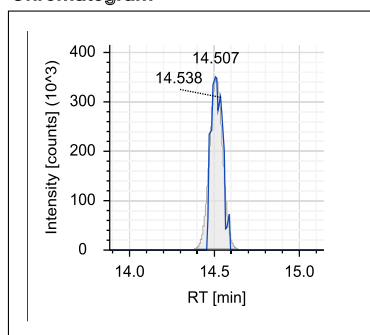
The atomic modification of +O from the parent compound to this TP could be due to the formation of a hydroxylated product or an N-oxide. The neutral loss of OH is possible for both moieties [Ma et al.(2005)] However, the MS2 fragment at the nominal mass 217 indicates that the modification occurred at the aromatic moiety.

Attributed Reaction from the Parent Compound to this TP

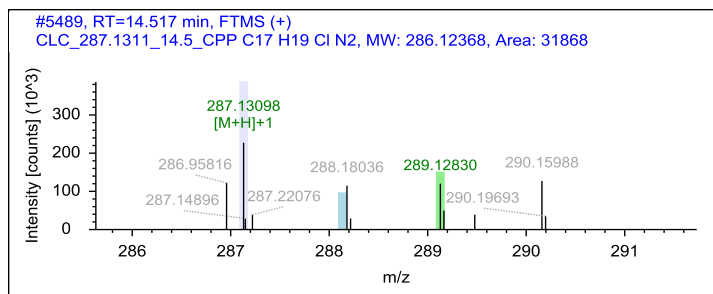
It is *likely* that this TP was formed via hydroxylation

Name CLC_287.1311_14.5 = CPP_287.1310_14.5

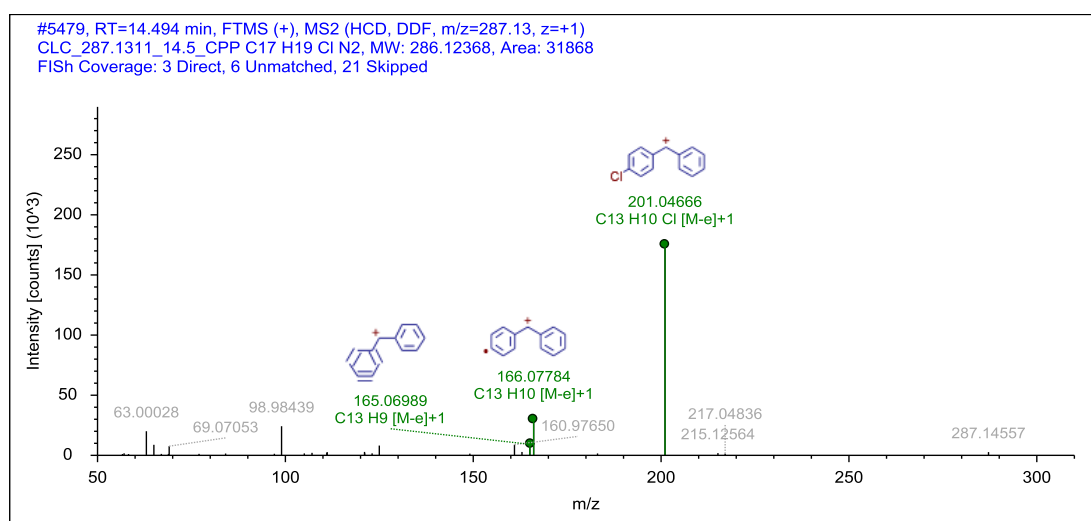
Chromatogram



MS Spectra



MS2 Spectra



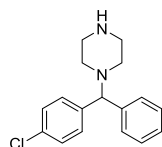
Formula

C17 H19 Cl N2

Atomic Modification

-CH2

Proposed Structure



Confidence Level

Level 1,
reference standard

MassBank ID

ET030001-ET030005

Additional Evidence for Structure Interpretation

The structure of this TP was confirmed by a reference standard. It is a TP of CLC, but also the parent CPP.

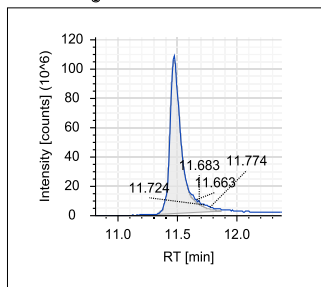
Attributed Reaction from the Parent Compound to this TP

It is *certain* that this TP was formed via an N-demethylation reaction.

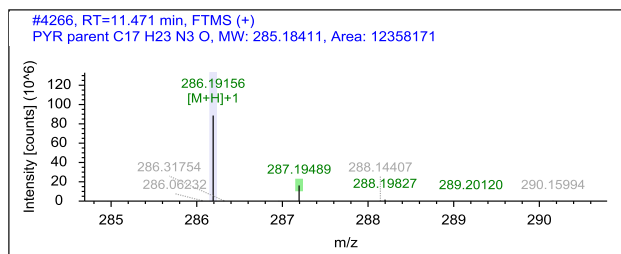
B.4.9 Structural evidence for pyrilamine and its TPs

Name PYR_286.1915_11.5, parent

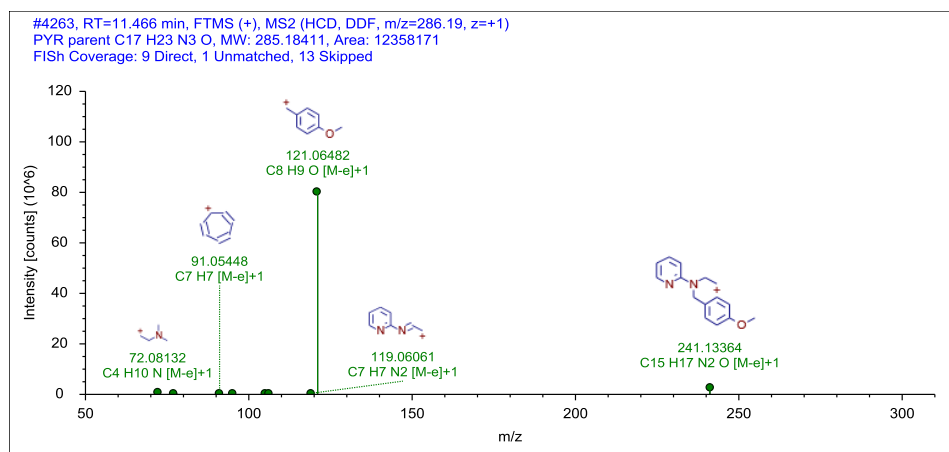
Chromatogram



MS Spectra



MS2 Spectra



Formula

C17 H23 N3 O

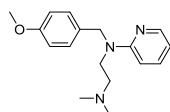
Additional Evidence for Structure Interpretation

This is the structural evidence that was observed for the parent compound PYR.

Atomic Modification

none

Proposed Structure



Confidence Level

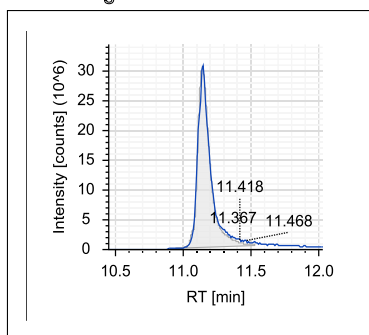
Level 1,
reference standard

MassBank ID

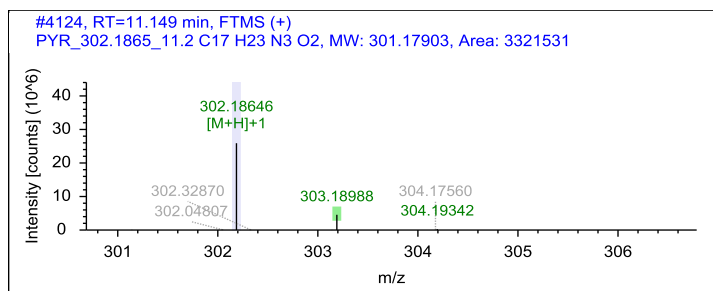
ET170001-ET170005

Name PYR_302.1865_11.2

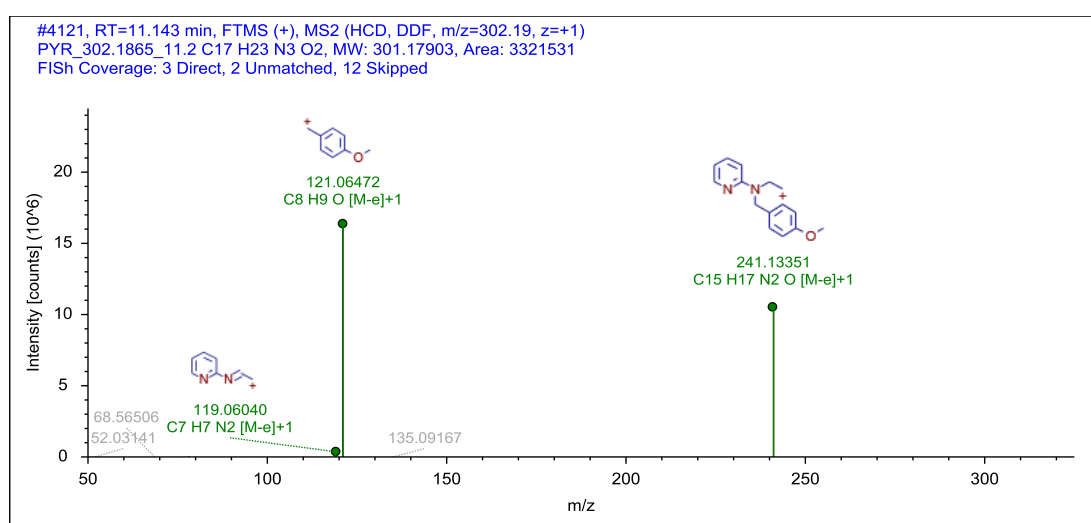
Chromatogram



MS Spectra



MS2 Spectra



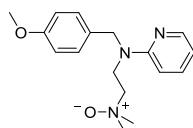
Formula

C17 H23 N3 O2

Atomic Modification

+O

Proposed Structure



Confidence Level

Level 3,
proposed structure

MassBank ID

ET170101-ET170106

Additional Evidence for Structure Interpretation

The MS2 fragment at the nominal mass 241 was observed for the parent compound and indicates that the oxygen addition took place at the dimethylamine moiety. Given that N-oxide TPs were observed and confirmed for five investigated tertiary amines (VEN, DEP, PAR, PHE, LID) it is likely that this TP is also an N-oxide.

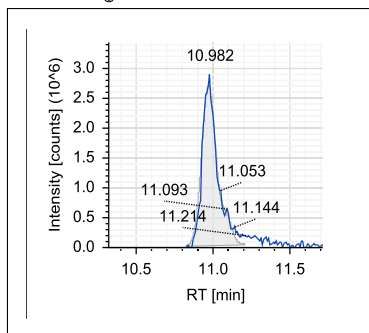
Attributed Reaction from the Parent Compound to this TP

It is *likely* that this TP was formed via an N-oxidation reaction.

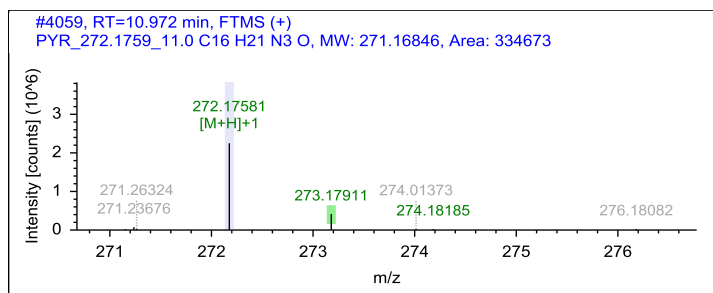
Appendix B

Name PYR_272.1759_11.0

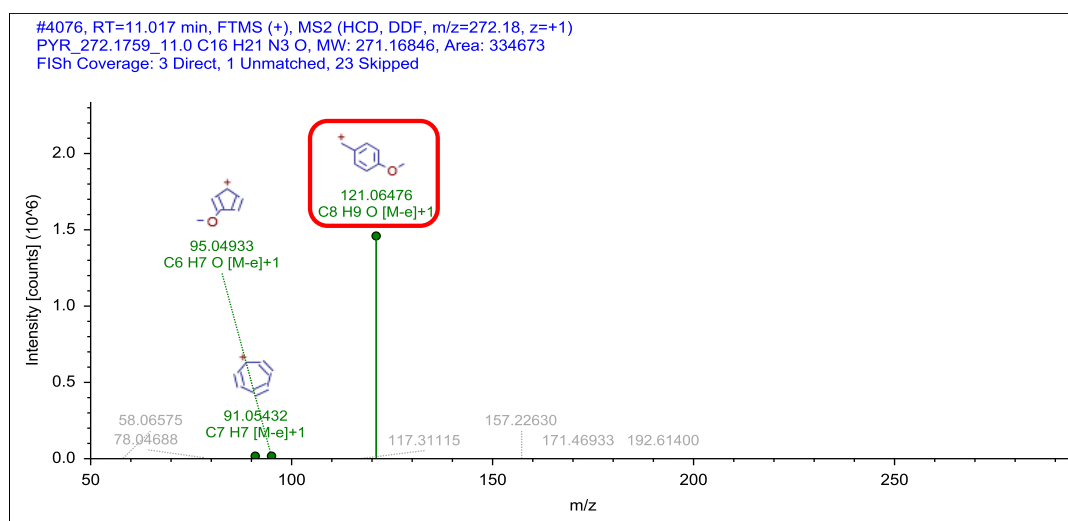
Chromatogram



MS Spectra



MS2 Spectra



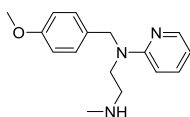
Formula

C16 H21 N3 O

Atomic Modification

-CH2

Proposed Structure



Confidence Level

Level 2b,
diagnostic evidence

MassBank ID

ET170201-ET170206

Additional Evidence for Structure Interpretation

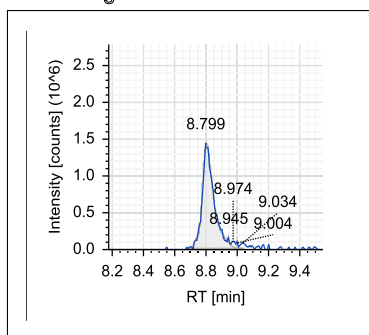
The atomic modification of -CH2 indicates the loss of a methyl moiety. There are two methyl moieties that can be lost easily, one is an amine substituent the other an ether substituent. The MS2 fragment at the nominal mass 121 was observed for the parent compound and indicates that the methylaryl ether moiety is still unaltered. Therefore, this fragment is considered diagnostic evidence that the demethylation occurred at the amine moiety. The loss of the methoxy methyl was actually observed for TP PYR_272.1759_8.8.

Attributed Reaction from the Parent Compound to this TP

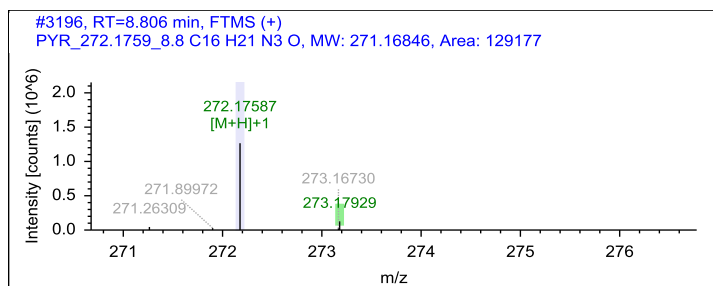
It is *certain* that this TP was formed via an N-demethylation reaction.

Name PYR_272.1759_8.8

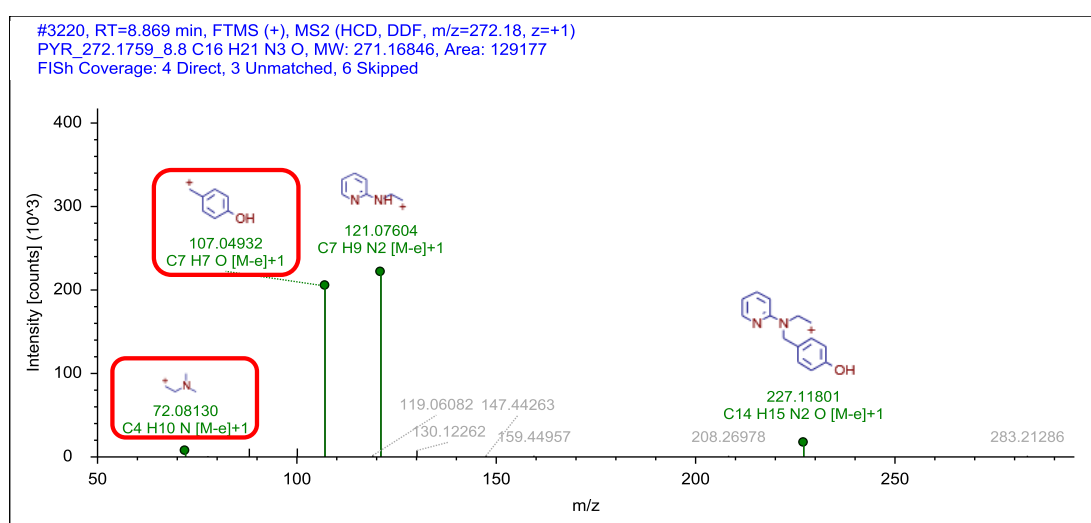
Chromatogram



MS Spectra



MS2 Spectra



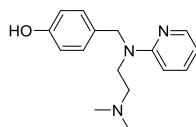
Formula

C16 H21 N3 O

Atomic Modification

-CH2

Proposed Structure



Confidence Level

Level 2b,
diagnostic evidence

MassBank ID

ET170301-ET170306

Additional Evidence for Structure Interpretation

The atomic modification of -CH2 indicates the loss of a methyl moiety. There are two methyl moieties that can be lost easily, one is an amine substituent, the other an ether substituent. The MS2 fragment at the nominal mass 72 was observed for the parent compound and indicates that the dimethyl amino group remains unaltered. The MS2 fragments at the nominal masses 72 and 107 are diagnostic evidence that the demethylation occurred at the ether moiety. The loss of an amino methyl was observed for TP PYR_272.1759_11.0.

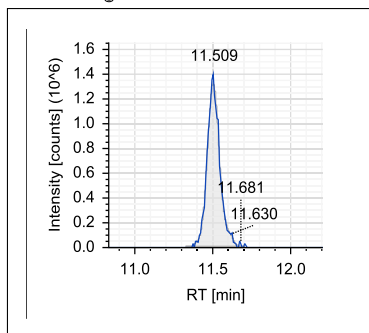
Attributed Reaction from the Parent Compound to this TP

It is *certain* that this TP was formed via an O-demethylation reaction.

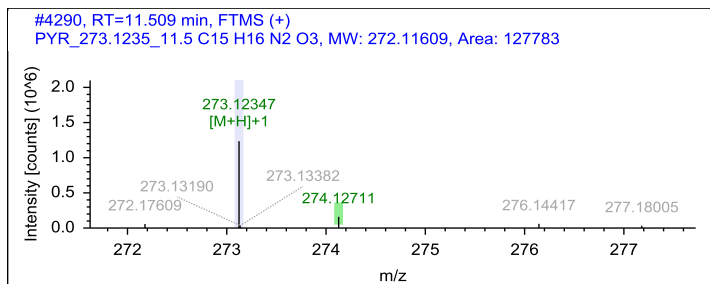
Appendix B

Name PYR_273.1235_11.5

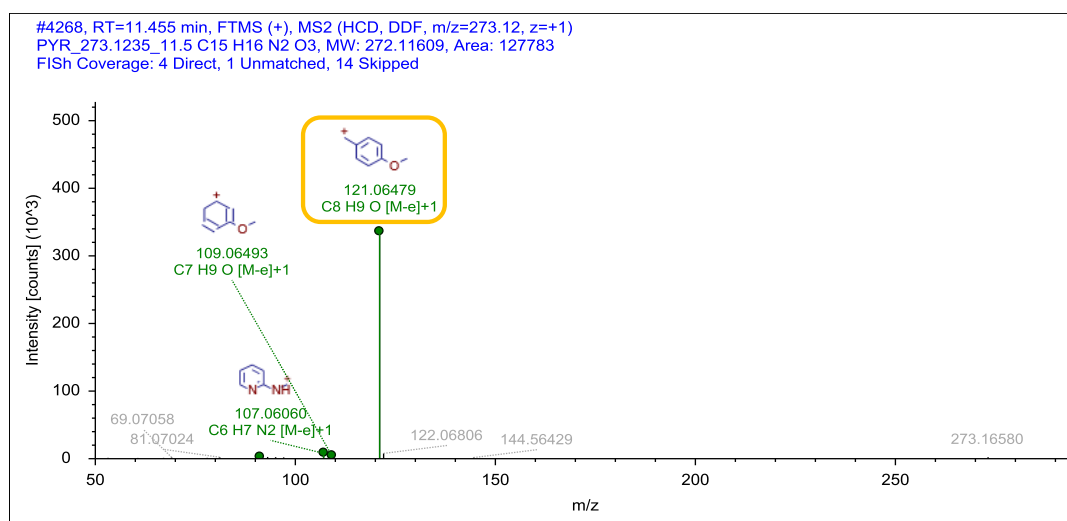
Chromatogram



MS Spectra



MS2 Spectra



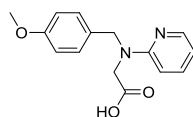
Formula

C15 H16 N2 O3

Atomic Modification

-C2H7N +O2

Proposed Structure



Additional Evidence for Structure Interpretation

The MS2 fragment at the nominal mass 121 was observed for the parent compound and indicates that the methylaryl ether moiety remains unaltered. The MS2 fragment at the nominal mass 107 indicates that the aniline aryl amine moiety of the parent structure is also present in the structure of this TP. The atomic modification of -C2H7N +O2 indicates the loss of the dimethyl amino moiety and the oxidation of the remaining terminal carbon to a carboxylic acid. A matching signal in the MS spectrum in negative mode (271.1086, $\Delta m = 3.0695$) supports the presence of a carboxylic acid moiety in the structure.

Attributed Reaction from the Parent Compound to this TP

It is *likely* that this TP was formed via an deamination followed by an oxidation to a carboxylic acid.

Confidence Level

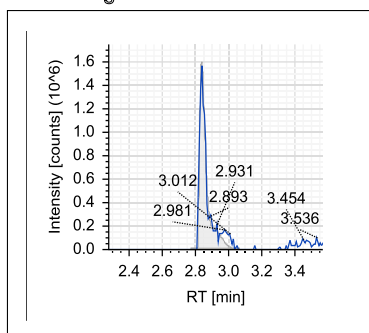
Level 3,
proposed structure

MassBank ID

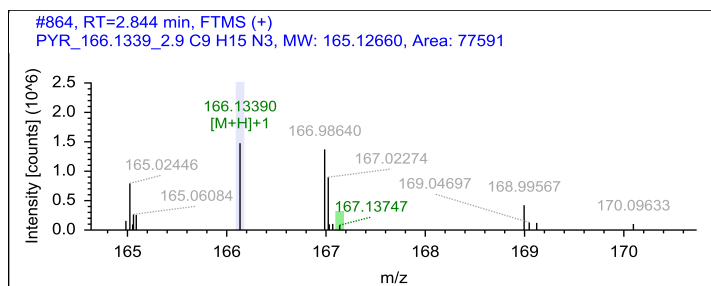
ET170401-ET170406

Name PYR_166.1340_2.9

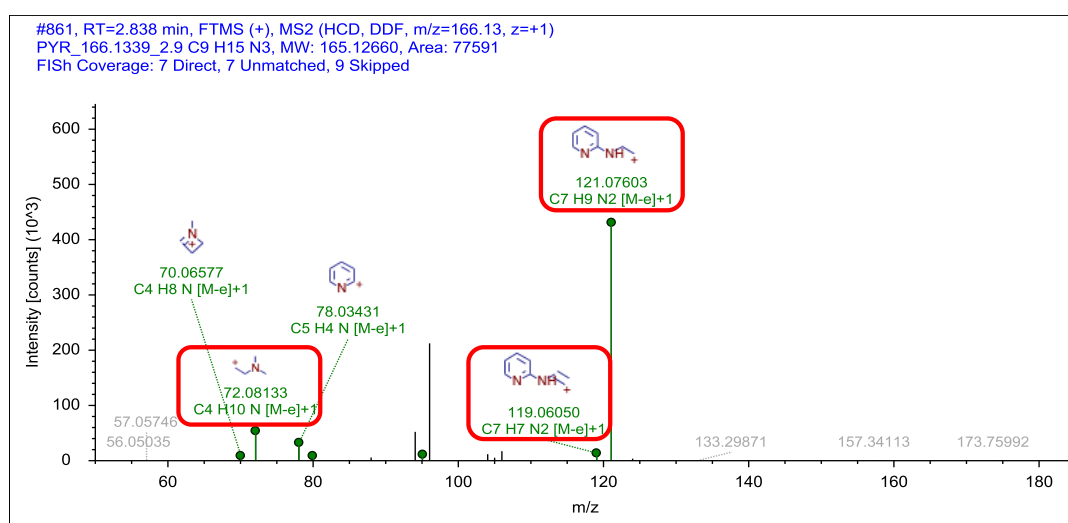
Chromatogram



MS Spectra



MS2 Spectra



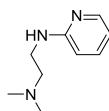
Formula

C9 H15 N3

Atomic Modification

-C8H8O

Proposed Structure



Additional Evidence for Structure Interpretation

The atomic modification of -C8H8O indicates the loss of the methoxybenzyl moiety. This assumption is strengthened by the observation of the MS2 fragments at the nominal masses 72, 119, and 121, which indicate that the dimethylethyl amine moiety as well as the ethylaryl amine moiety remain unaltered in the structure of this TP. Therefore, the MS2 fragments at the nominal masses 72, 119, and 121 are diagnostic evidence that the methoxybenzyl N-substituent was lost in this structure.

Attributed Reaction from the Parent Compound to this TP

It is *certain* that this TP was formed via an N-debenzylation reaction

Confidence Level

Level 2b,
diagnostic evidence

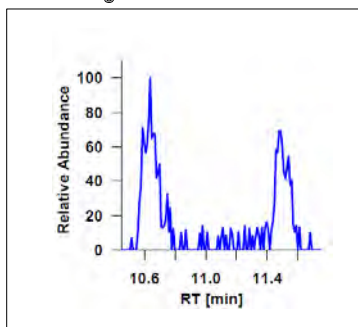
MassBank ID

ET171103

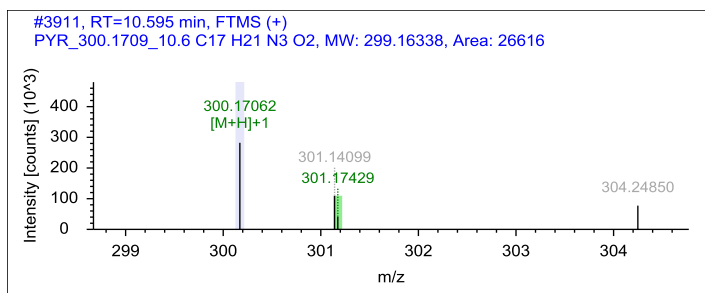
Appendix B

Name PYR_300.1709_10.6

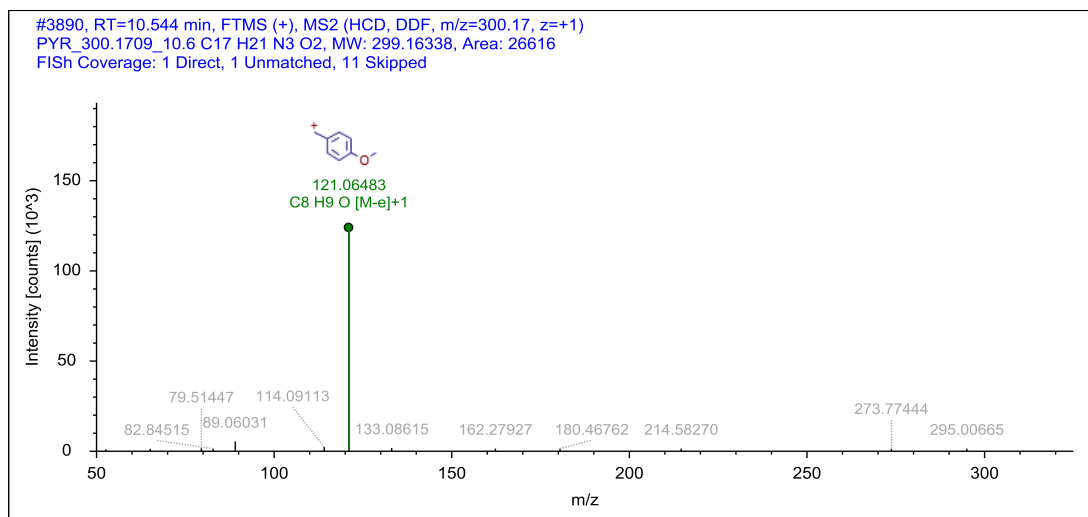
Chromatogram



MS Spectra



MS2 Spectra



Formula

C17 H21 N3 O2

Atomic Modification

-H2 +O

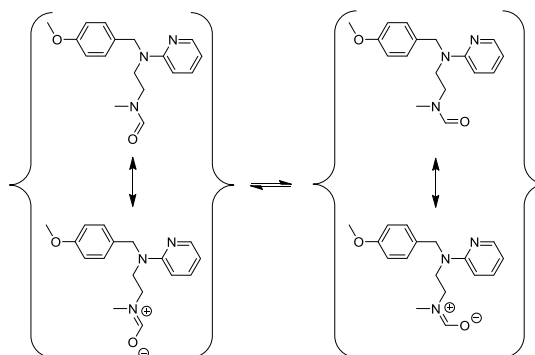
Additional Evidence for Structure Interpretation

The formamide structure of this TP was confirmed by a synthesized standard. Details on the synthesis and the NMR measurement can be found in Chapter S5. The chromatogram showed two maxima at 10.5 minutes and 11.5 minutes. This peak shape results from the cis-trans isomerism of the C-N bond that has some double bond character as can be seen from the resonance structures.

Attributed Reaction from the Parent Compound to this TP

It is *possible* that this TP was formed via an α -C-oxidation to a formamide or an N-demethylation followed by an N-formylation reaction.

Proposed Structure



Confidence Level

Level 1,
synthesized standard

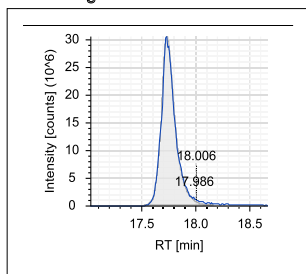
MassBank ID

ET171001-ET171006

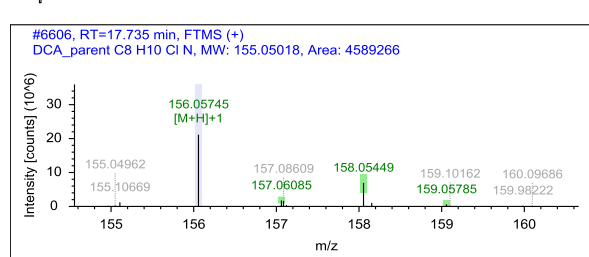
B.4.10 Structural evidence for N,N-dimethyl-p-chloroaniline and its TPs

Name DCA_156.0575_17.7, parent

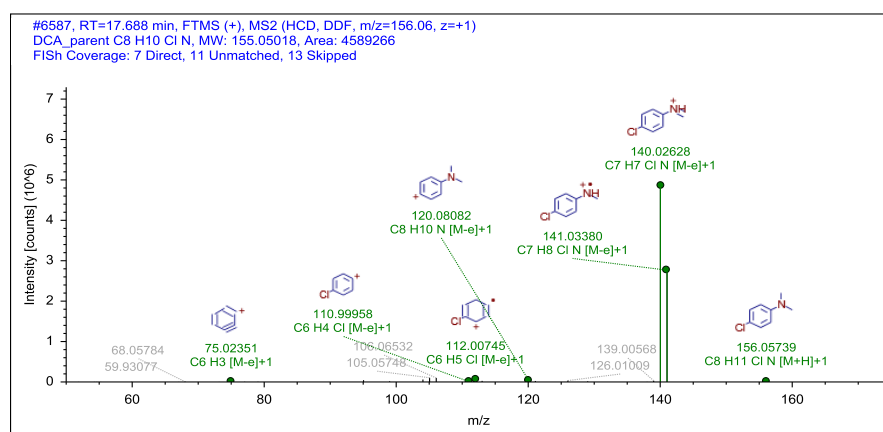
Chromatogram



MS Spectra



MS2 Spectra



Formula

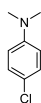
C8 H10 Cl N

Additional Evidence for Structure Interpretation

This is the structural evidence that was observed for the parent compound DCA.

Atomic Modification
none

Proposed Structure



Confidence Level

Level 1,
reference standard

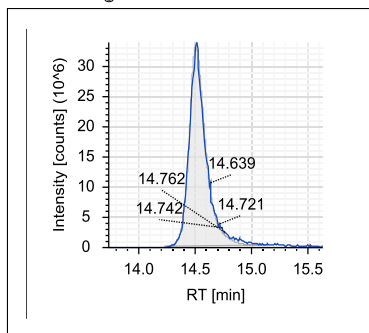
MassBank ID

ET040001-ET040005

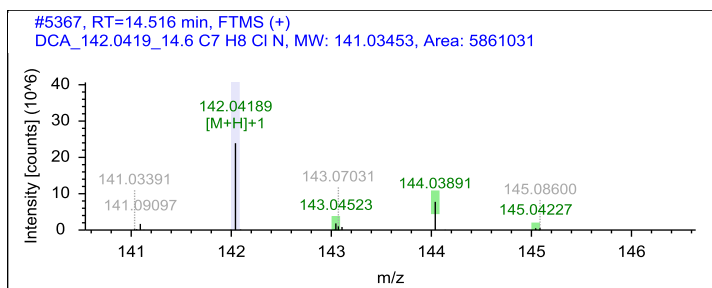
Appendix B

Name DCA_142.0419_14.6

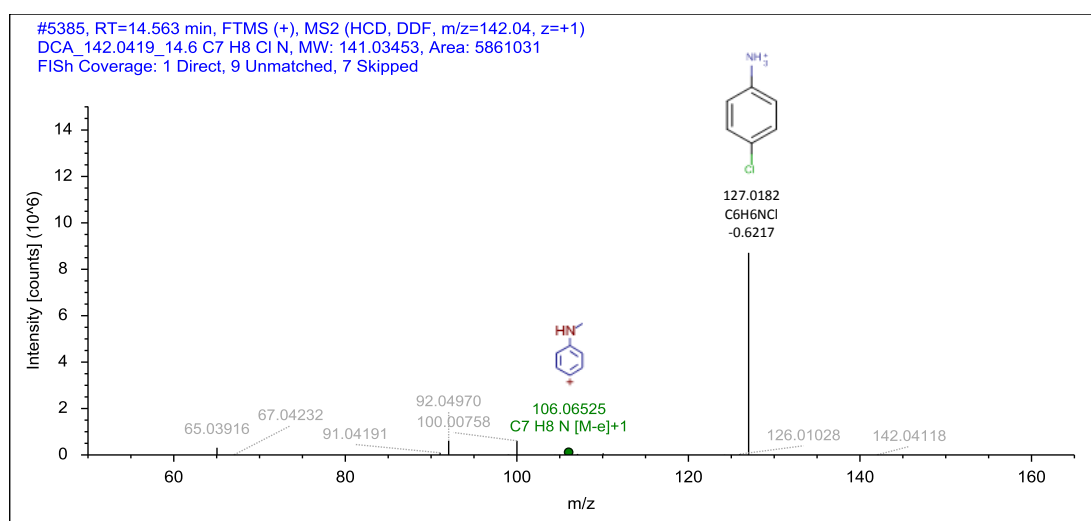
Chromatogram



MS Spectra



MS2 Spectra



Formula

C7 H8 Cl N

Additional Evidence for Structure Interpretation

The structure of this TP was confirmed by a reference standard.

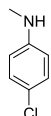
Atomic Modification

-CH2

Attributed Reaction from the Parent Compound to this TP

It is *certain* that this TP was formed via an N-demethylation reaction.

Proposed Structure



This TP was also formed in the three sorption control reactors in a similar amount as in the biotransformation reactors. It was also formed in the abiotic control reactors to a minor amount (<10% compared to the in the biotransformation reactors).

Confidence Level

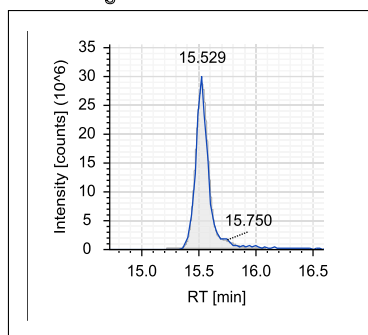
Level 1,
reference standard

MassBank ID

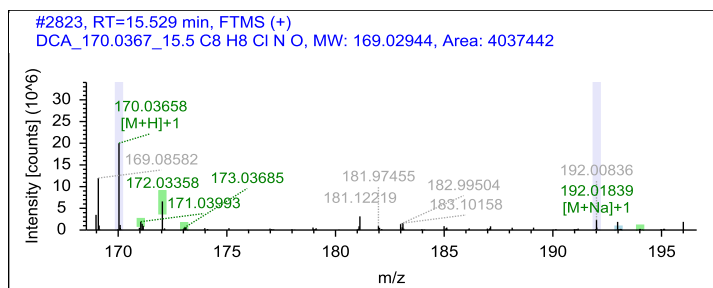
ET040201

Name DCA_170.0367_15.5

Chromatogram

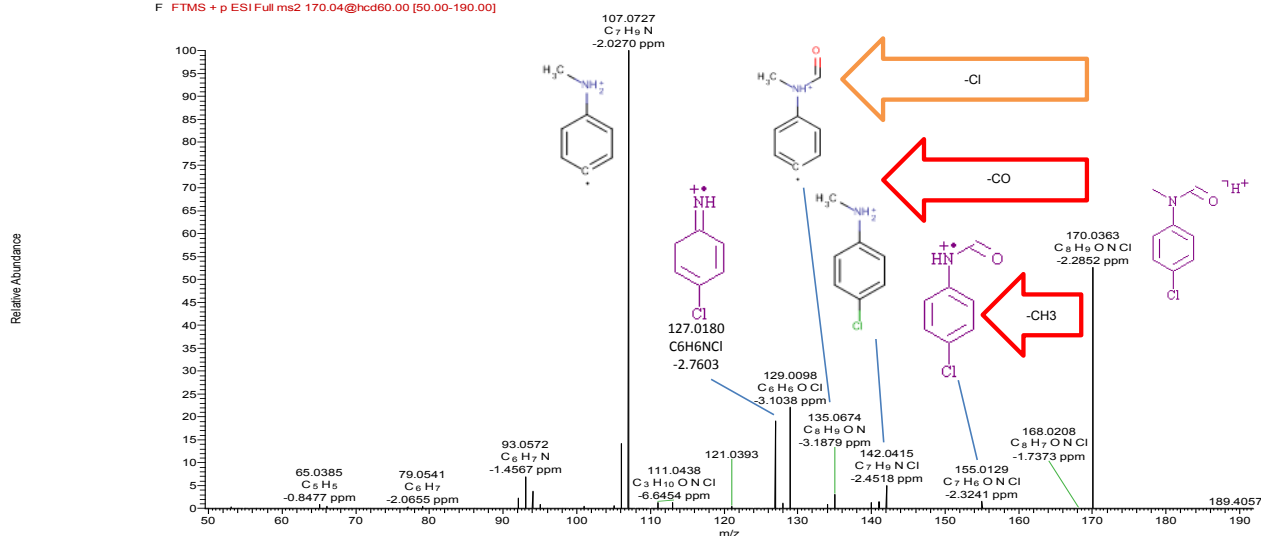


MS Spectra



MS2 Spectra

20150225 34 #8156-6190 RT 15.13-15.19 AV 5 NL 1.90E6
F FTMS + p ESI Full ms2 170.04@hcd80.00 [50.00-190.00]



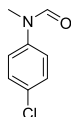
Formula

C₈H₈ClN₂O

Atomic Modification

-H₂, +O

Proposed Structure



Additional Evidence for Structure Interpretation

The atomic modification from the elemental formula of the parent compound to this TP is -H₂ + O. This modification could only have been realized through the oxidation of a carbon atom to a carbonyl moiety. The neutral loss of CO indicates a carbonyl moiety. The neutral loss of CH₃ indicates the presence of an unaltered methyl moiety. The structural evidence for the proposed structure is diagnostic.

Attributed Reaction from the Parent Compound to this TP

It is *possible* that this TP was formed via an α -C-oxidation to a formamide or an N-demethylation followed by an N-formylation reaction.

Confidence Level

Level 2b

diagnostic evidence

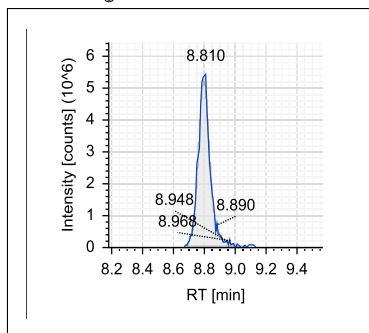
MassBank ID

ET040301-ET040306

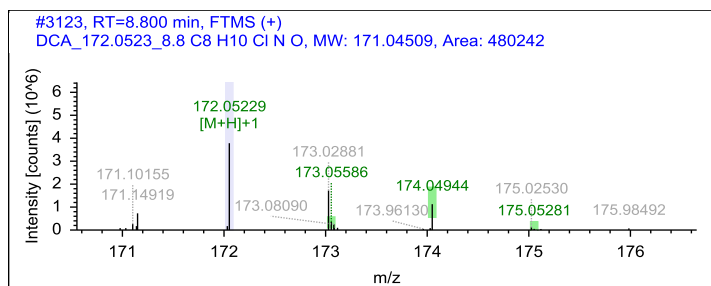
Appendix B

Name DCA_172.0523_8.8

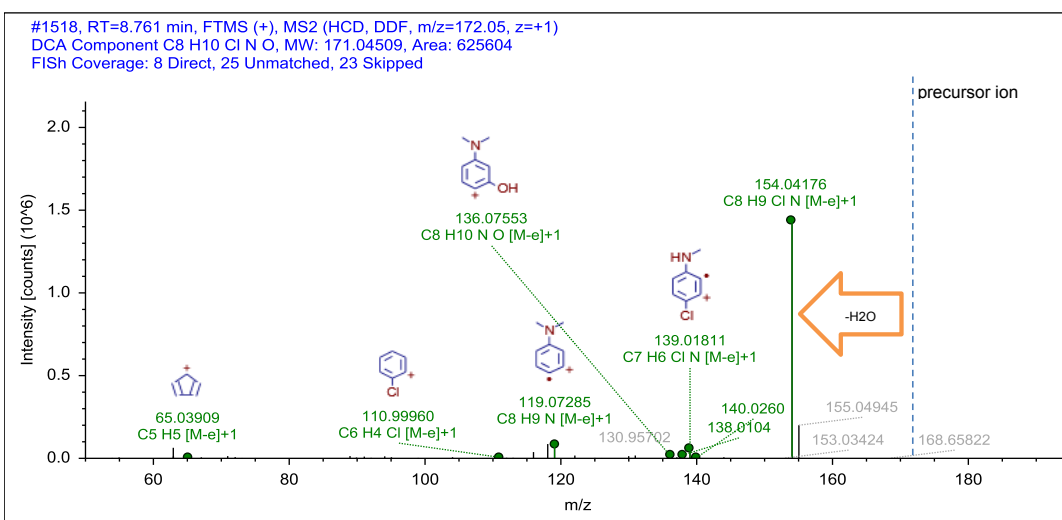
Chromatogram



MS Spectra



MS2 Spectra



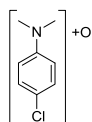
Formula

C8 H10 Cl N O

Atomic Modification

+O

Proposed Structure



Additional Evidence for Structure Interpretation

The atomic modification of +O from the parent compound to this TP could be explained by the formation of a hydroxylated product as well as an N-oxide. The neutral loss of H2O is possible for both moieties [Ma et al. (2005)]. There is no MS2 fragments that indicates the position of the modification.

Attributed Reaction from the Parent Compound to this TP

It is *possible* that this TP was formed via an N-oxidation, an α -C-hydroxylation to a hemiaminal, or a hydroxylation reaction.

Confidence Level

Level 3,
TP class

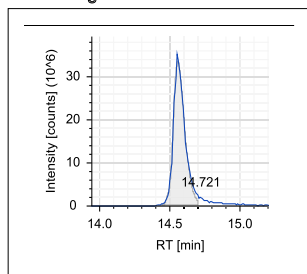
MassBank ID

ET040401-ET040406

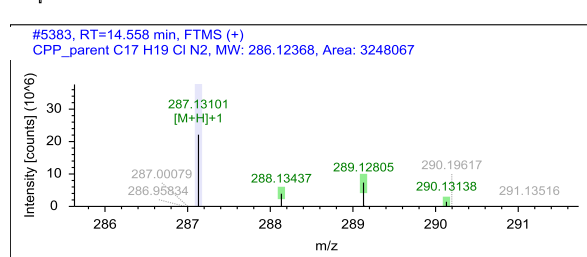
B.4.11 Structural evidence for 1[(4-chlorophenyl)-phenylmethyl]piperazine and its TPs

Name CPP_287.1310_14.5, parent = CLC_287.1310_14.5

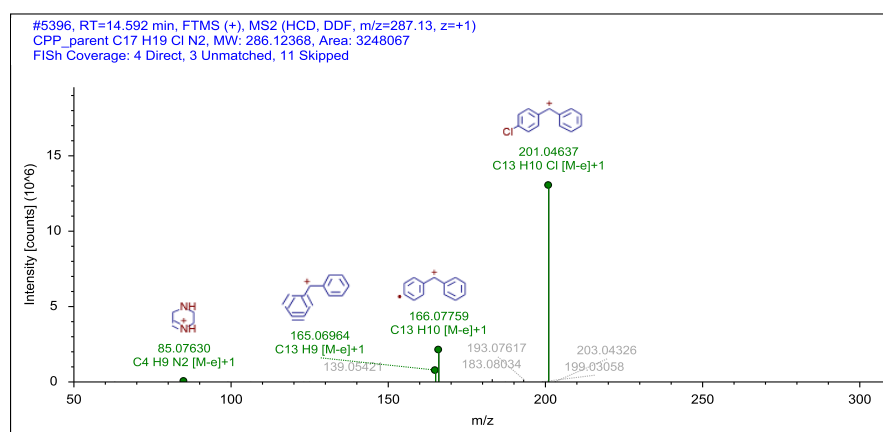
Chromatogram



MS Spectra



MS2 Spectra



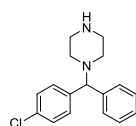
Formula
C17 H19 Cl N2

Additional Evidence for Structure Interpretation

This is the structural evidence that was observed for the parent compound CPP.

Atomic Modification
none

Proposed Structure



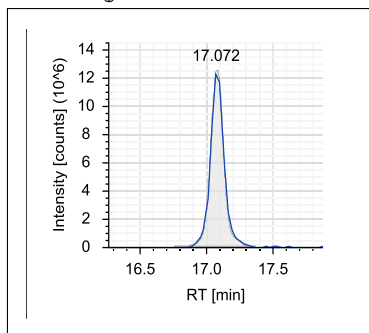
Confidence Level
Level 1,
reference standard

MassBank ID
ET030001-ET030005

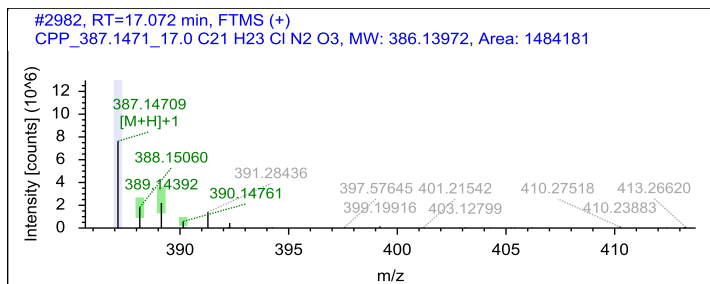
Appendix B

Name CPP_387.1471_17.0

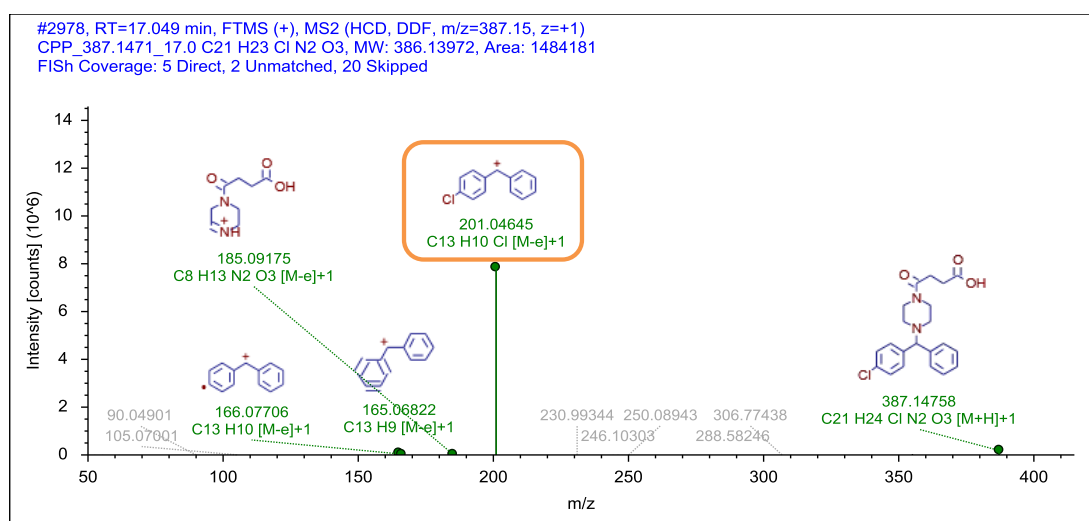
Chromatogram



MS Spectra



MS2 Spectra

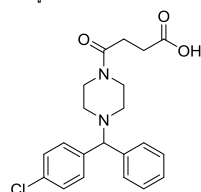


Formula

C21 H23 Cl N2 O3

Atomic Modification
+C4H4O3

Proposed Structure



Confidence Level

Level 3,
proposed structure

MassBank ID

ET030101-ET030106

Additional Evidence for Structure Interpretation

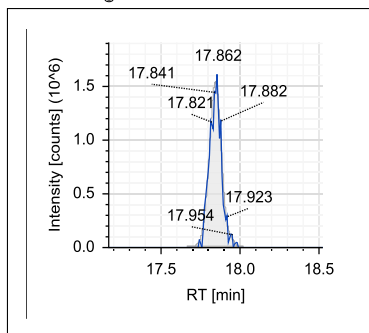
The MS2 fragments at the nominal masses 201, 166, and 165 were observed for the parent compound and indicate that the aromatic part of the parent structure is a substructure of this TP. A matching signal in the MS spectrum in negative mode (385.1323, $\Delta m = -1$ ppm) indicates the presence of a carboxylic acid moiety. The MS2 fragment (99.086, C4H3O3, $\Delta m = -1.69$ ppm) that was observed in the MS2 spectrum in negative mode, was also observed for the analogous TP OCP_297.1002_16.5. The structure of the TP of OCP was confirmed by reference standard to be an N-succinylated product.

Attributed Reaction from the Parent Compound to this TP

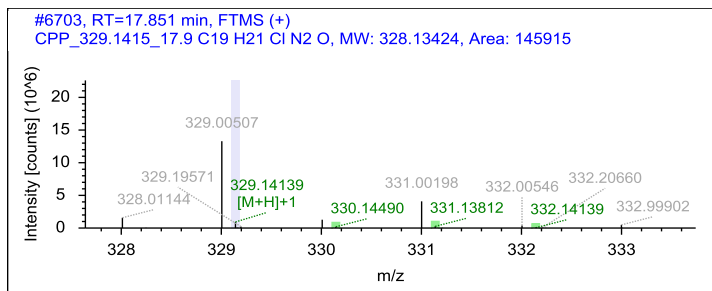
It is *likely* that this TP was formed via an N-succinylation reaction.

Name CPP_329.1415_17.9

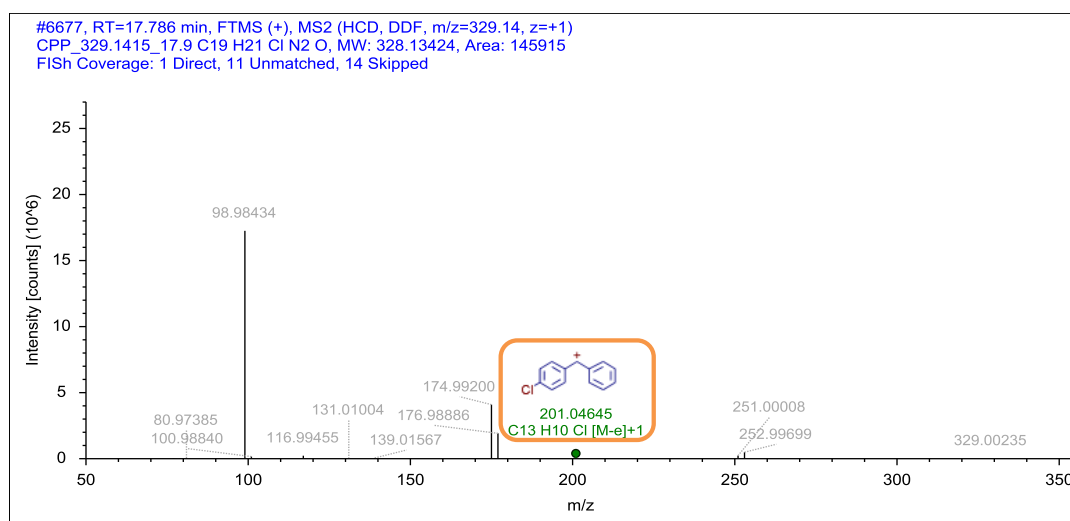
Chromatogram



MS Spectra



MS2 Spectra



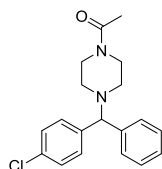
Formula

C₁₉H₂₁ClN₂O

Atomic Modification

+C₂H₂O

Proposed Structure



Confidence Level

Level 3,
proposed structure

MassBank ID

ET030201-ET030206

Additional Evidence for Structure Interpretation

The MS2 fragments at the nominal masses 176, 174, and 98 originate from a interfering precursor ion with the exact mass 329.0046. The MS2 fragment at the nominal mass 201 was observed for the parent compound and indicates that the aromatic part of the parent structure is a substructure of this TP. Due to the atomic modification, it is likely that an acetyl moiety was added to the parent structure.

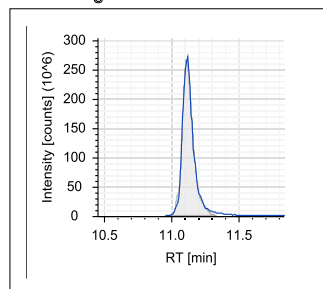
Attributed Reaction from the Parent Compound to this TP

It is *likely* that this TP was formed via an N-acetylation reaction.

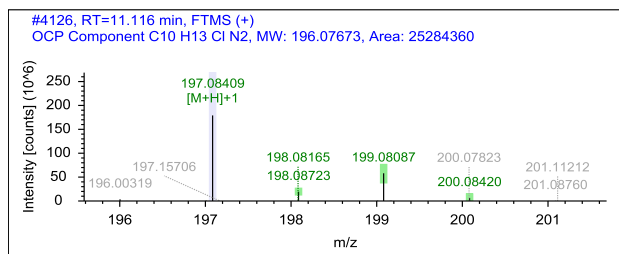
B.4.12 Structural evidence for ortho-chlorophenylpiperazine and its TPs

Name OCP_197.0840_11.1, parent

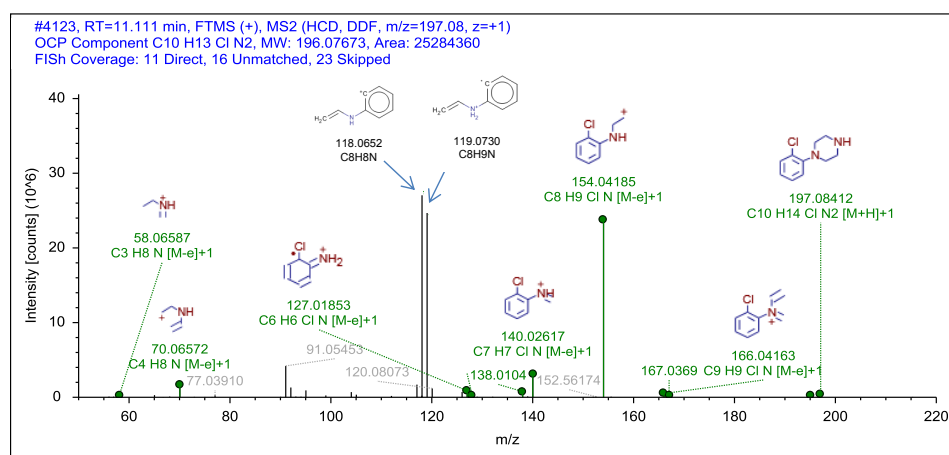
Chromatogram



MS Spectra



MS2 Spectra



Formula

C10 H13 Cl N2

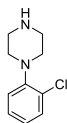
Additional Evidence for Structure Interpretation

This is the structural evidence that was observed for the parent compound OCP.

Atomic Modification

none

Proposed Structure



Confidence Level

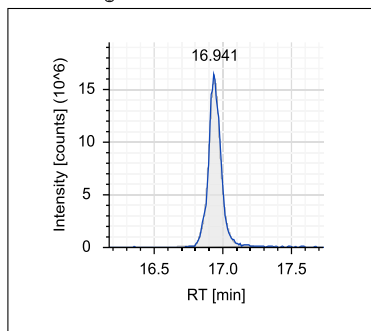
Level 1,
reference standard

MassBank ID

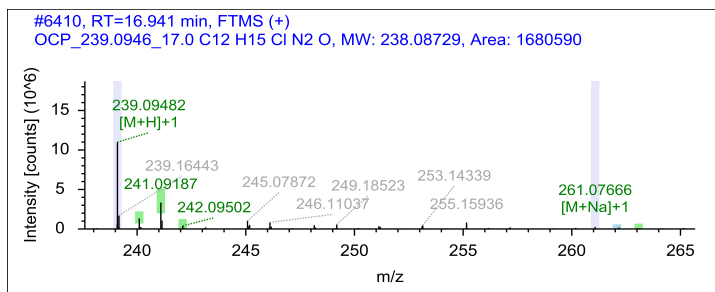
ET130001-ET130005

Name OCP_239.0946_17.0

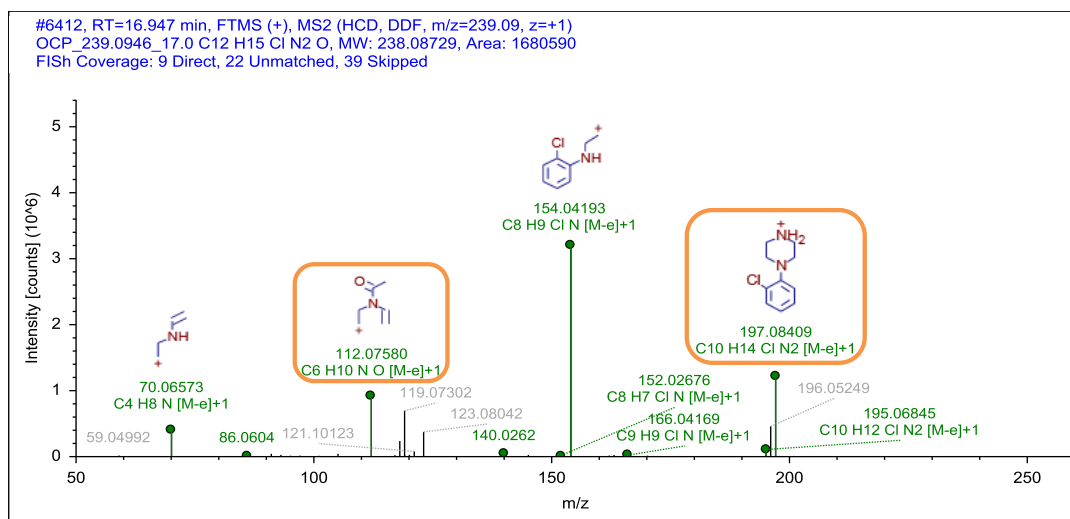
Chromatogram



MS Spectra



MS2 Spectra



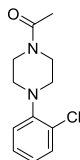
Formula

C12 H15 Cl N2 O

Atomic Modification

+C2H2O

Proposed Structure



Confidence Level

Level 3,
proposed structure

MassBank ID

ET130101-ET130106

Additional Evidence for Structure Interpretation

The MS2 fragments at the nominal masses 197, 166, 154, 119, 118, and 70 were observed for the parent compound and indicate that the parent structure is a substructure of this TP. The atomic modification from the parent structure to this TP was +C2H2O, which indicates the substitution of a hydrogen by an acetyl moiety. The MS2 fragment at the nominal mass 112 indicates that the modification took place at the heterocycle.

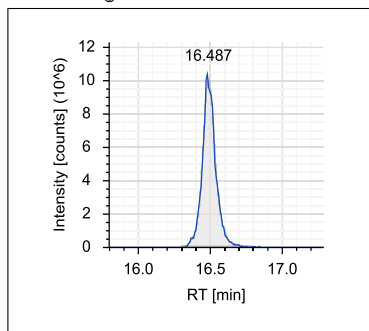
Attributed Reaction from the Parent Compound to this TP

It is *likely* that this TP was formed via an N-acetylation.

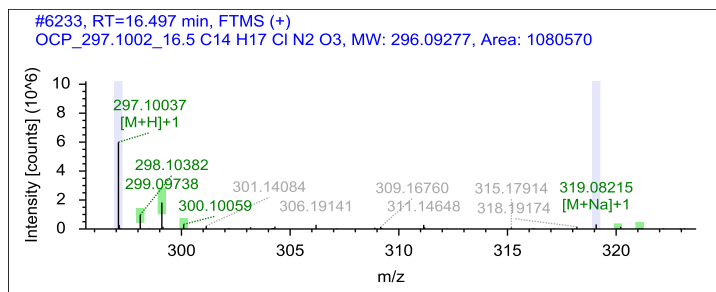
Appendix B

Name OCP_297.1002_16.5

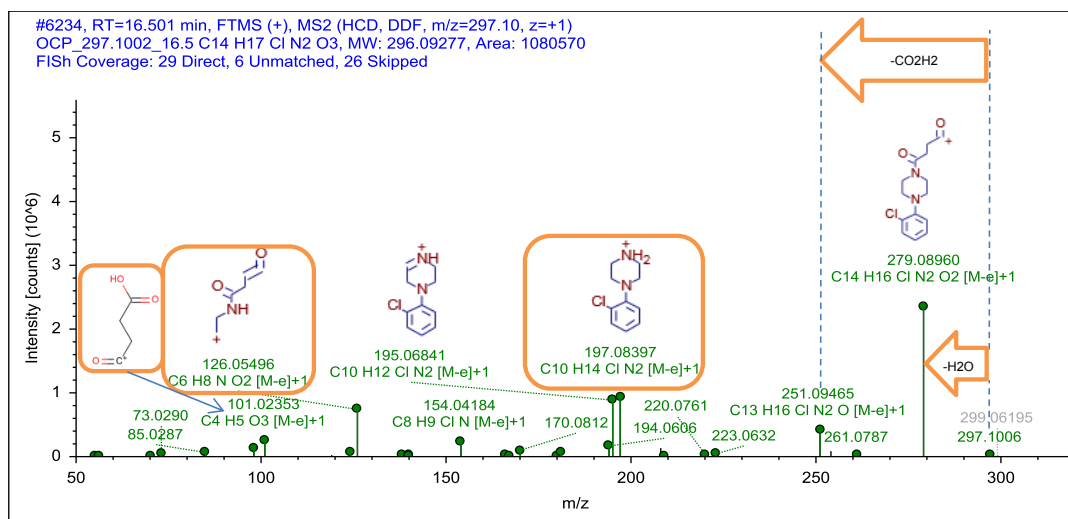
Chromatogram



MS Spectra



MS2 Spectra



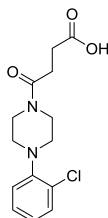
Formula

C14 H17 Cl N2 O3

Atomic Modification

+C4H4O3

Proposed Structure



Confidence Level

Level 1,
reference standard for
structure with chloride in
meta position

MassBank ID

ET130201-ET130206

Additional Evidence for Structure Interpretation

The MS2 fragments at the nominal masses 197, 166, 154, 119, 118, and 70 were observed for the parent compound and indicate that the parent structure is a substructure of this TP. The neutral losses of H₂O and CO₂H₂ between the MS2 fragments at the nominal masses 297 and 279, and 297 and 251, respectively, as well as a matching signal in the MS spectrum in negative mode (295.0848, $\Delta m = -7$ ppm) indicate the presence of a carboxylic acid moiety. The MS2 fragment at the nominal mass 101 indicates that all atoms of the modification of the parent substructure are connected. The MS2 fragment at the nominal mass 126 indicates that the modification took place at the heterocycle.

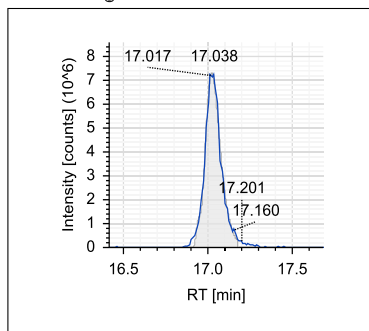
A reference standard was available of the N-succinylated meta-chlorophenylpiperazine. This is basically the same structure but with the chloride in meta position. Since, the retention time as well as the MS2 fragments match, the structure was assigned as confirmed with Level 1

Attributed Reaction from the Parent Compound to this TP

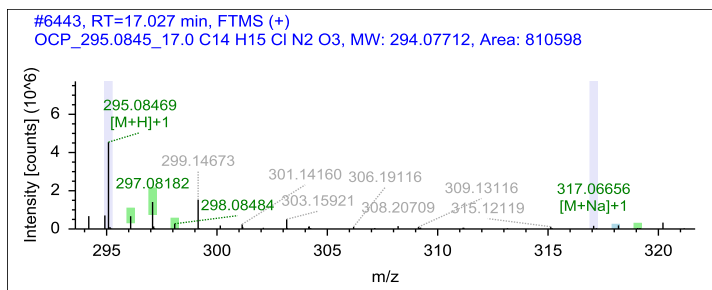
It is *certain* that this TP was formed via an N-succinylation reaction.

Name OCP_295.0845_17.0

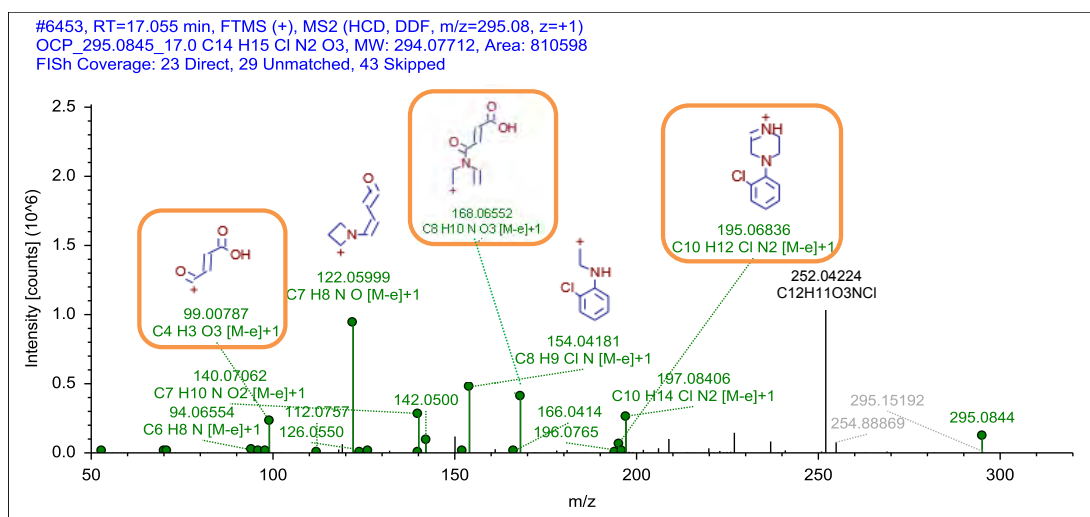
Chromatogram



MS Spectra



MS2 Spectra



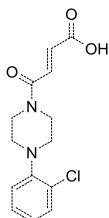
Formula

C14 H15 Cl N2 O3

Atomic Modification

+C4H2O3

Proposed Structure



Confidence Level

Level 3,
proposed structure

MassBank ID

ET130301-ET130306

Additional Evidence for Structure Interpretation

The MS2 fragments at the nominal masses 197, 195, 166, 154, 119, 118, and 70 were observed for the parent compound and indicate that the parent structure is a substructure of this TP. A matching signal in the MS spectrum in negative mode (293.0695, $\Delta m = -3$ ppm) indicates a carboxylic acid moiety. The atomic modification from the parent structure to this TP was +C4H2O3. The MS2 fragment at the nominal mass 99 indicates that all atoms of this modification are connected. The MS2 fragment at the nominal mass 168 indicates that the modification took place at the heterocycle.

A reference standard was available for the maleic structure (cis configuration of alkene moiety) with the chloride in meta position. The retention time (16.4 min) and the MS2 fragments (for example 277.0741 and 124.0394) did not match. Since the N-succinylated TP matched the reference standard with the chloride in meta position, it is unlikely that the meta position is causing the different structural features. It is more likely that the TP is a N-fumarylated TP (trans configuration of alkene moiety). An analogous N-fumarylated TP was observed for MEX_278.1387_17.3, which was confirmed by a synthesized reference standard.

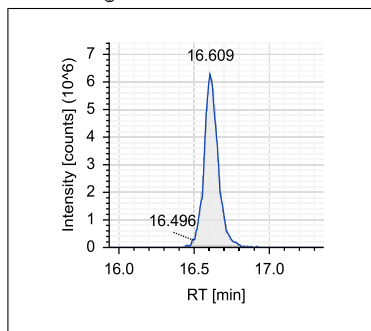
Attributed Reaction from the Parent Compound to this TP

It is *possible* that this TP was formed via an N-fumarylation reaction or a desaturation reaction following an N-succinylation reaction.

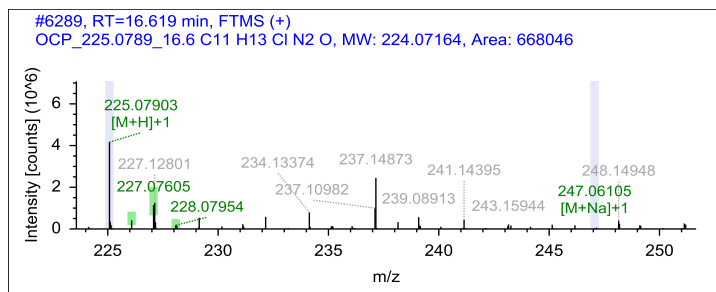
Appendix B

Name OCP_225.0789_16.6

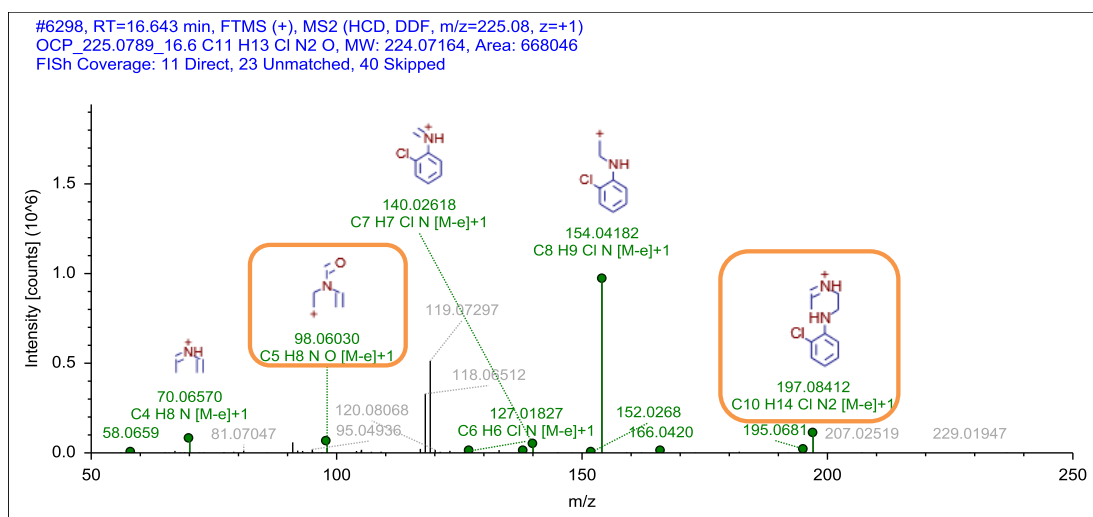
Chromatogram



MS Spectra



MS2 Spectra

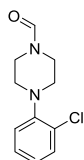


Formula

C11 H13 Cl N2 O

Atomic Modification
+CO

Proposed Structure



Additional Evidence for Structure Interpretation

The MS2 fragments at the nominal masses 197, 195, 166, 154, 119, 118, and 70 were observed for the parent compound and indicate that the parent structure is a substructure of this TP. The MS2 fragment at the nominal mass 98 indicates that the modification of +CO took place at the heterocycle.

Attributed Reaction from the Parent Compound to this TP

It is *likely* that this TP was formed via an N-formylation reaction.

Confidence Level

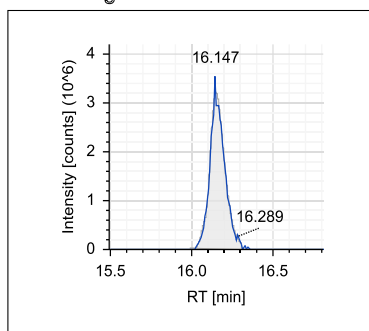
Level 3,
proposed structure

MassBank ID

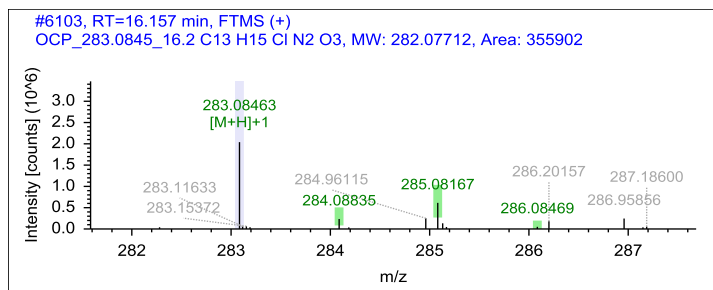
ET130401-ET130406

Name OCP_283.0845_16.2

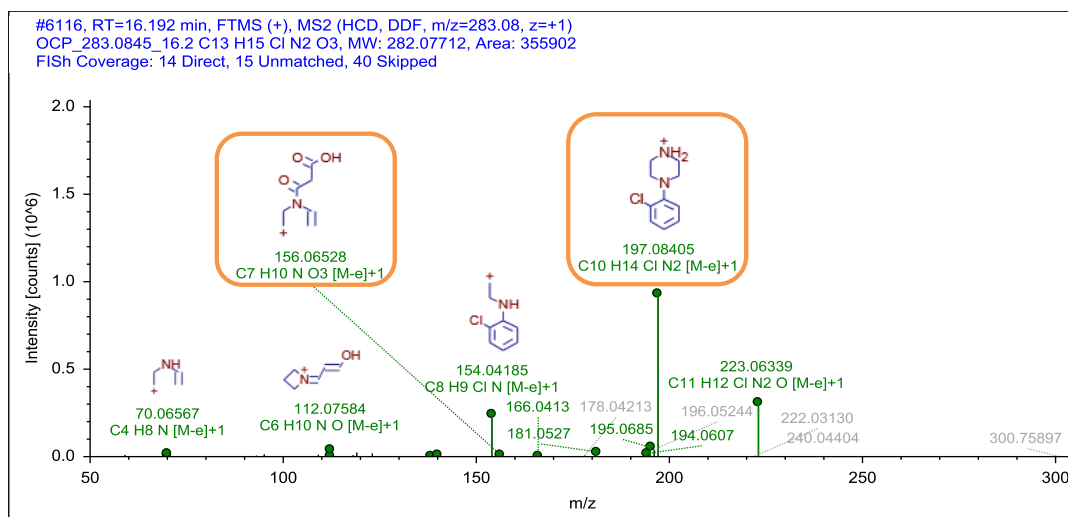
Chromatogram



MS Spectra



MS2 Spectra



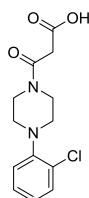
Formula

C13 H15 Cl N2 O3

Atomic Modification

+C3H2O3

Proposed Structure



Confidence Level

Level 3,
proposed structure

MassBank ID

ET130601-ET130606

Additional Evidence for Structure Interpretation

The MS2 fragments at the nominal masses 197, 166, 154, and 70 were observed for the parent compound and indicate that the parent structure is a substructure of this TP. In an MS2 spectrum measured with a collision energy of 15, additional MS2 fragments were observed at the exact masses of 283.0840 (C13H16O3N2Cl, $\Delta m = -1.6$ ppm) and 239.0942 (C12H16ON2Cl, $\Delta m = -1.7$ ppm). The neutral loss of CO₂ between these MS2 fragments as well as a matching signal in the MS spectra in negative mode (281.0691, $\Delta m = -7$ ppm) indicate a carboxylic acid moiety. The MS2 fragment at the nominal mass 156 indicates that the modification of +C3H2O3 took place at the heterocycle.

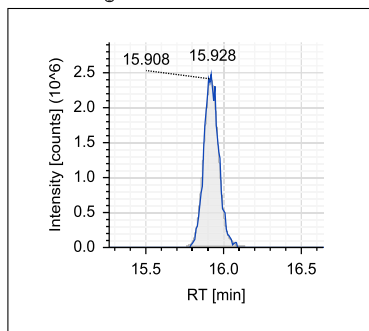
Attributed Reaction from the Parent Compound to this TP

It is *likely* that this TP was formed via an N-malonylation reaction.

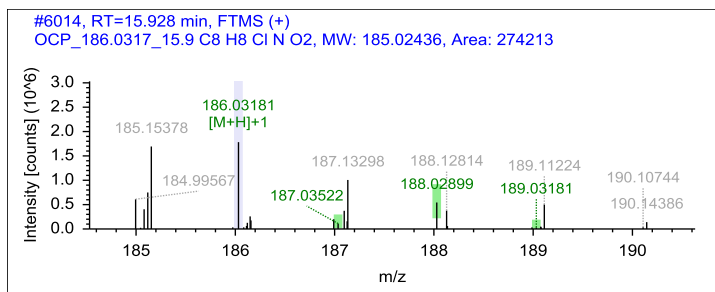
Appendix B

Name OCP_186.0317_15.9

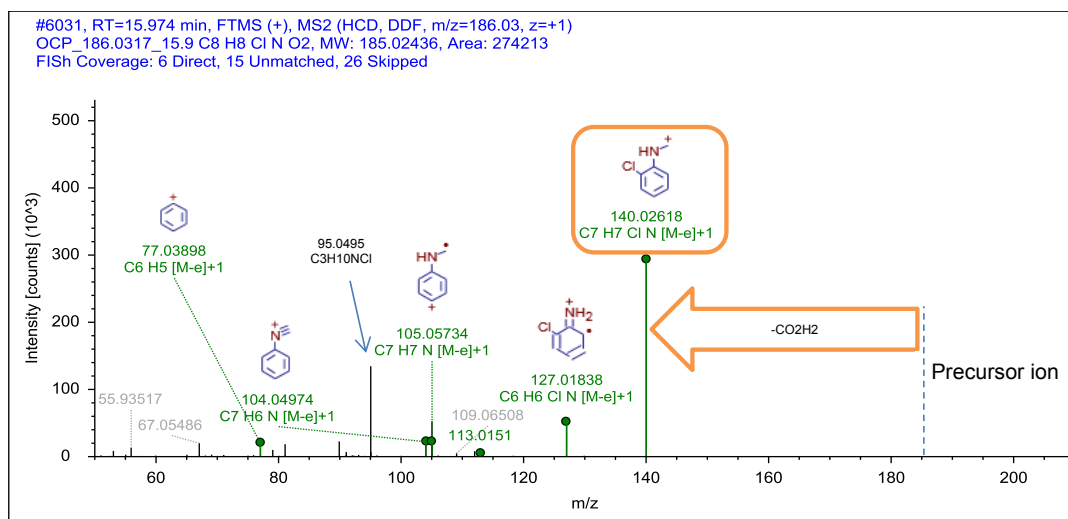
Chromatogram



MS Spectra



MS2 Spectra

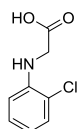


Formula

C8 H8 Cl N O2

Atomic Modification
-C2H5N +O2

Proposed Structure



Confidence Level

Level 3,
proposed structure

MassBank ID

ET130701-ET130706

Additional Evidence for Structure Interpretation

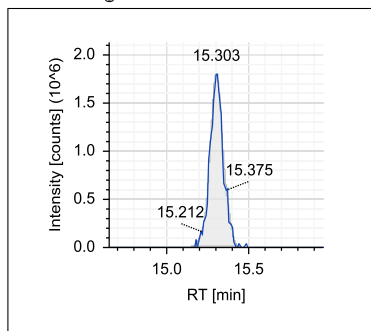
The MS2 fragments at the nominal masses 140 and 127 were observed for the parent compound and indicate that the 2-chloro-N-methylaniline substructure of the parent structure is a substructure of this TP. The neutral losses of CO2H2 as well as a matching signal in the MS spectra in negative mode (184.0168, $\Delta m = -3$ ppm) indicate a carboxylic acid moiety.

Attributed Reaction from the Parent Compound to this TP

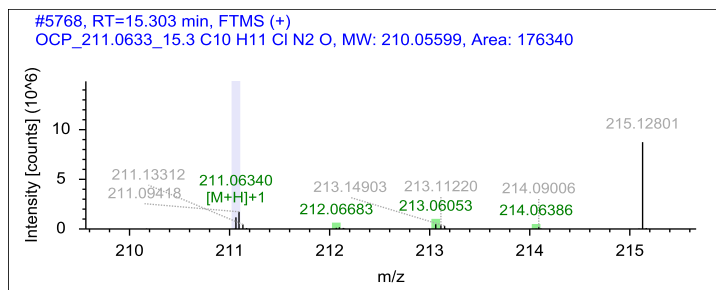
It is *likely* that this TP was formed via an N-dealkylation of the tertiary nitrogen and a deamination with a subsequent oxidation to a carboxylic acid moiety of the secondary amine moiety.

Name OCP_211.0633_15.3

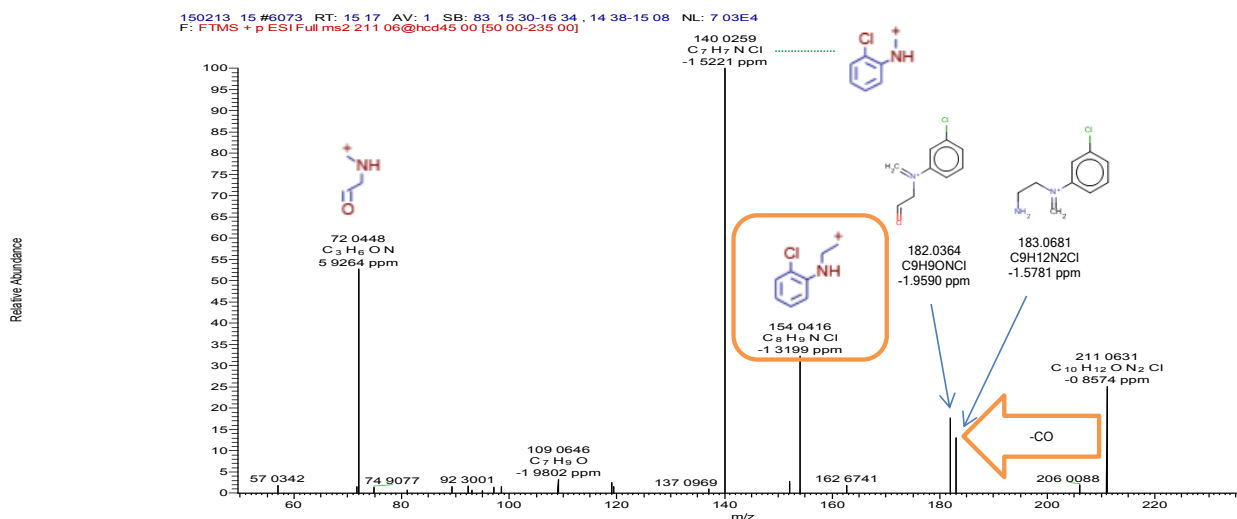
Chromatogram



MS Spectra



MS2 Spectra



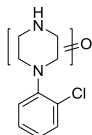
Formula

C10H11ClN2O

Atomic Modification

-H2 + O

Proposed Structure



Confidence Level

Level 3,
TP class

MassBank ID

ET130801-ET130806

Additional Evidence for Structure Interpretation

The MS2 fragments at the nominal masses 154 and 140 were observed for the parent compound and indicate that the 2-chloro-N-ethylaniline substructure of the parent structure is a substructure of this TP. This indicates that the atomic modification of -H2 + O occurred at the piperazine moiety. This modification could have been realized by an α -C-oxidation to a lactam or by an N-hydroxylation followed by a further reaction to a nitron. (The combination of C-hydroxylation and independent desaturation is unlikely, since hydroxylation of carbons adjacent to nitrogens lead to hemiaminals, which are not stable.) The MS2 fragments at the nominal masses 182 and 183 indicate that the oxygen and the nitrogen are not connected. Therefore, it is likely that this TP structure is a lactam. The neutral loss of CO strengthens this assumption. It remains unknown if the lactam of the tertiary or secondary amine was formed. The structures that belong to the MS2 fragments at the nominal masses 182 and 183 are exemplarily drawn. An analogous TP, namely OCP_211.0633_14.3, with the same atomic modification but a different retention time was observed. For this TP, the exact type and position of the modification remains unknown.

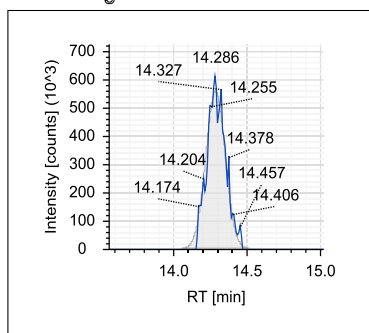
Attributed Reaction from the Parent Compound to this TP

It is *likely* that this TP was formed via an α -C-oxidation reaction to an lactam. However, it remains unknown if the lactam of the tertiary or secondary amine was formed.

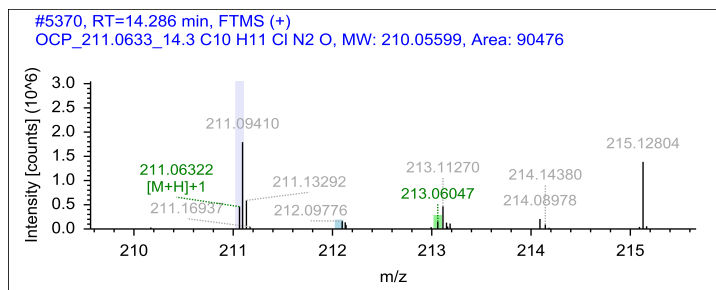
Appendix B

Name OCP_211.0633_14.3

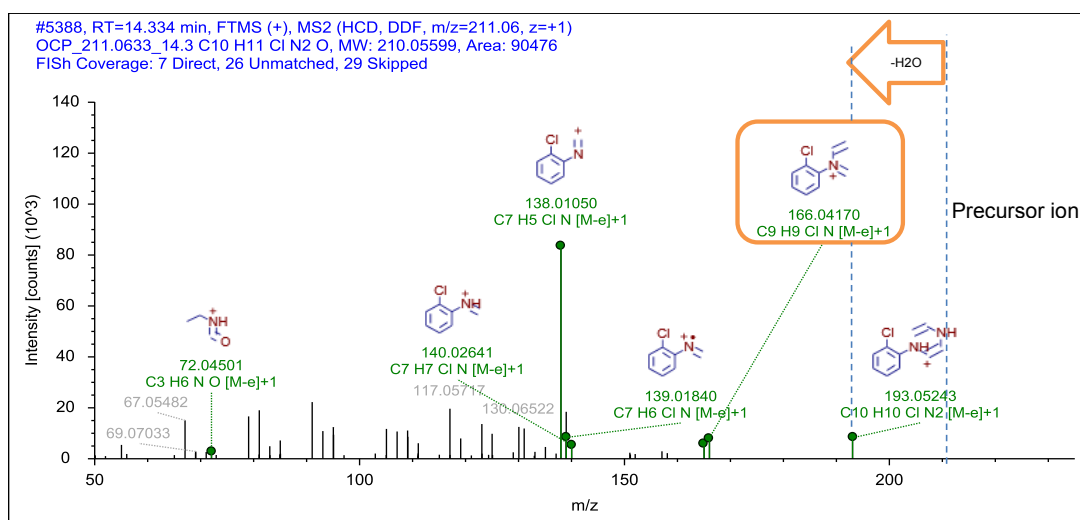
Chromatogram



MS Spectra



MS2 Spectra



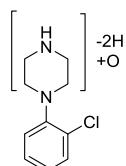
Formula

C10 H11 Cl N2 O

Atomic Modification

-H2 +O

Proposed Structure



Confidence Level

Level 3,
TP class

MassBank ID

ET131201-ET131206

Additional Evidence for Structure Interpretation

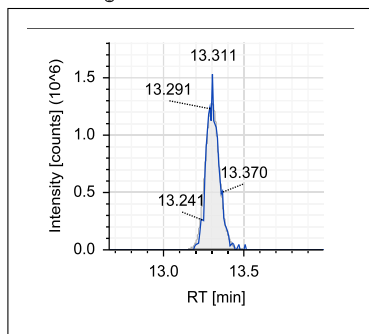
The MS2 fragments at the nominal masses 166, 140, and 138 were observed for the parent compound and indicate that the 2-chloro-N,N-methylethylaniline substructure of the parent structure is a substructure of this TP. This indicates that the atomic modification of -H2 +O occurred at the piperazine moiety. This modification could have been realized by an α -C-oxidation to a lactam or by an N-hydroxylation followed by a further reaction to a nitron. (The combination of C-hydroxylation and independent desaturation is unlikely, since hydroxylation of carbons adjacent to nitrogens lead to hemiaminals, which are not stable.) The neutral loss of H2O is predicted for both structures by MassFrontier. Therefore, the exact type and position of the atomic modification remains unknown. An analogous TP, namely OCP_211.0633_15.3, with the same atomic modification, but a different retention time was observed. For this TP a lactam structure was proposed.

Attributed Reaction from the Parent Compound to this TP

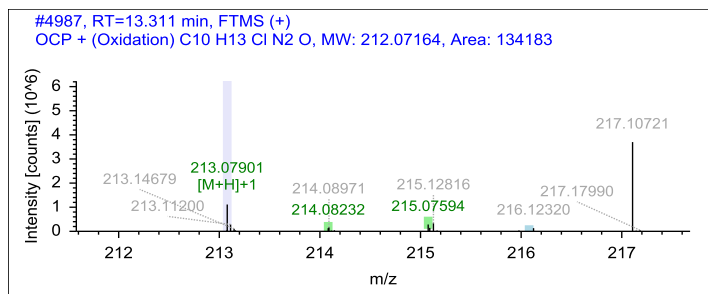
It is *possible* that this TP was formed via an α -C-oxidation reaction to a lactam or in two steps, namely an N-hydroxylation followed by an successive reaction to a nitron.

Name OCP_213.0790_13.3

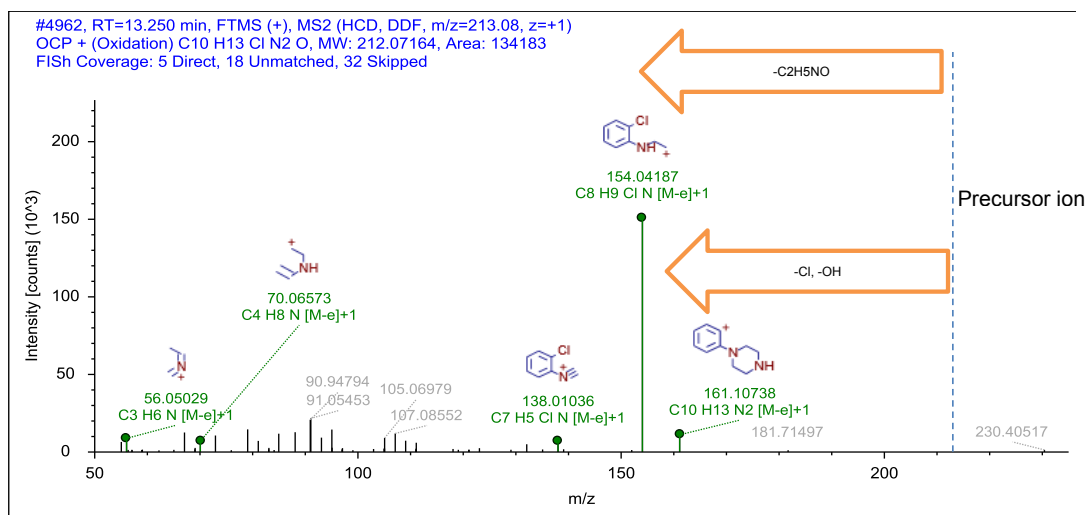
Chromatogram



MS Spectra



MS2 Spectra



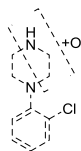
Formula

C10 H13 Cl N2 O

Atomic Modification

+O

Proposed Structure



Confidence Level

Level 3,
TP class

MassBank ID

ET131002

Additional Evidence for Structure Interpretation

The MS2 fragments at the nominal masses 70 and 154 were observed for the parent compound and indicate that the 2-chloro-N-ethylaniline substructure of the parent structure is a substructure of this TP. The neutral loss of OH indicates a hydroxyl moiety. The neutral loss of C₂H₅NO indicates that a hydroxylation occurred at the ethylamine part of the molecule. From the presented evidence it remains unknown if the hydroxylation took place at a carbon atom or the secondary nitrogen atom of the ethylamine part. However, a C-hydroxylation would lead to a hemiaminal, which are generally known to be unstable. However, hemiaminals adjacent to non-basic nitrogen, such as amides or aniline derivatives, possess a certain stability. (This is because the spontaneous cleavage of hemiaminals proceeds over the protonated form). It might be possible that also cyclic hemiaminals possess a certain stability, since they are known to form lactams. The reaction mechanism is reported to proceed over a hemiaminal, which must possess a certain stability to be able to further react. Therefore, it remains unknown, if this TP could be a stable hemiaminal of OCP. It is also possible that this TP is an N-hydroxylated product.

Three additional peaks were observed in the MS spectrum with the same exact mass (213.0790) and retention times of 7.8 minutes, 8.6 minutes, and 10.0 minutes. Their corresponding peak area was below the threshold for TP elucidation. However, they indicate that N-oxidation at the tertiary amine and / or hydroxylation of the benzene ring might also have occurred.

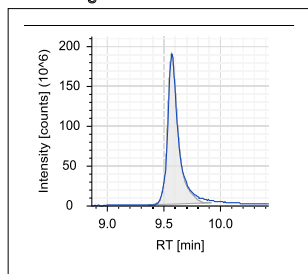
Attributed Reaction from the Parent Compound to this TP

It is *possible* that this TP was formed via an N-hydroxylation reaction or a C-hydroxylation reaction forming an hemiaminal.

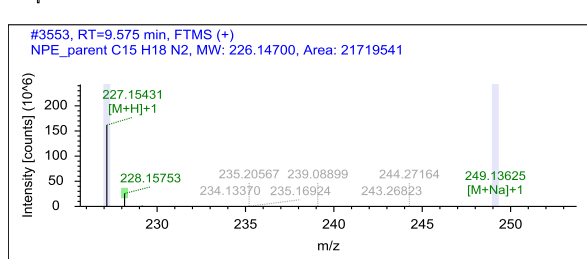
B.4.13 Structural evidence for N-demethylpheniramine and its TPs

Name NPE_227.1543_9.6, parent, PHE_227.1542_9.7

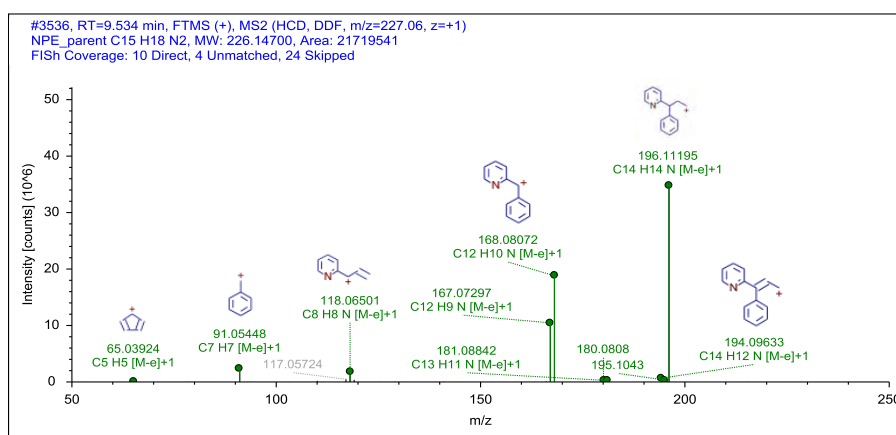
Chromatogram



MS Spectra



MS2 Spectra



Formula

C15 H18 N2

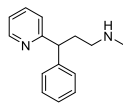
Additional Evidence for Structure Interpretation

This is the structural evidence that was observed for the parent compound NPE.

Atomic Modification

none

Proposed Structure



Confidence Level

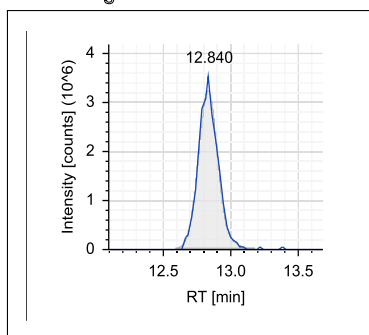
Level 1,
reference standard

MassBank ID

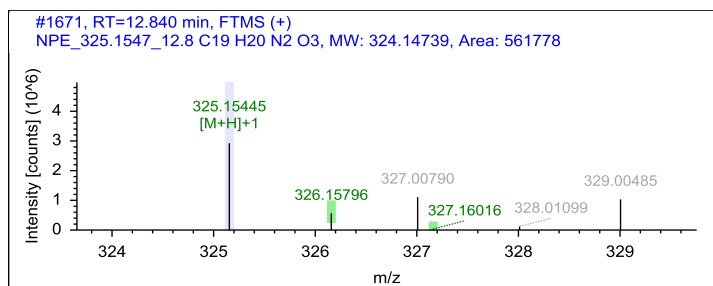
ET110001-ET110005

Name NPE_325.1547_12.8

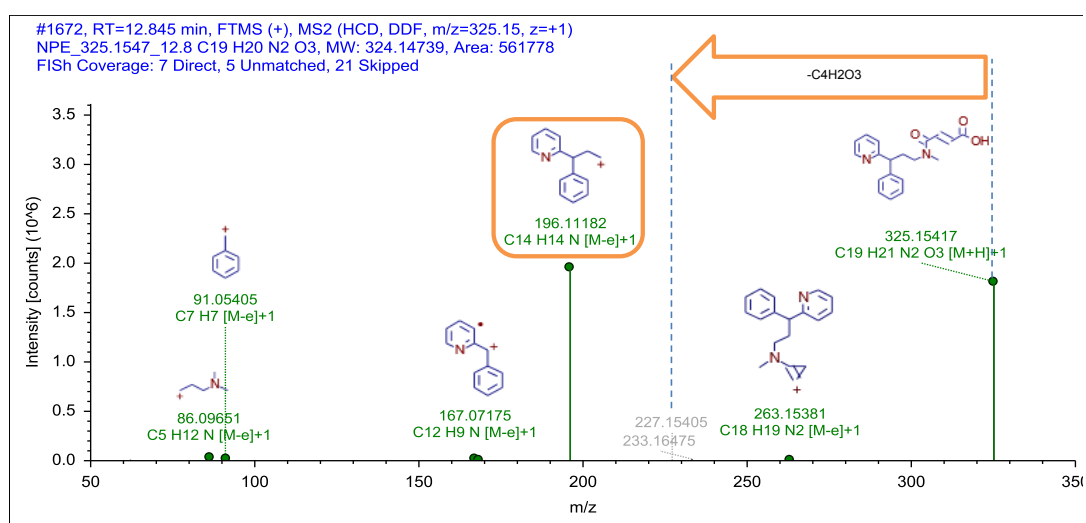
Chromatogram



MS Spectra



MS2 Spectra



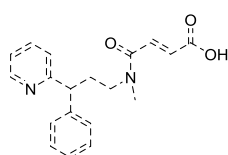
Formula

C19 H20 N2 O3

Atomic Modification

+C4H2O3

Proposed Structure



Confidence Level

Level 3,
proposed structure

MassBank ID

ET110101-ET110106

Additional Evidence for Structure Interpretation

The MS2 fragments at the nominal masses 91, 167, 196, and 227 were also observed for the parent compound either in the shown MS2 spectrum or in one measured with a collision energy of 15. These fragments indicate that the parent structure is a substructure of this TP. In an MS2 spectrum measured with a collision energy of 75, an additional MS2 fragment was observed at the exact mass of 99.0075 (C4H3O3 $\Delta m = -1.3191$ ppm). This fragment and the neutral loss between the MS2 fragments at the nominal masses 325 and 227 indicate that all atoms of the modification +C4H2O3 are connected. In an MS2 spectrum measured with a collision energy of 30, an additional MS2 fragment was observed at the exact mass of 307.1429 (C19H19O2N2 $\Delta m = -3.9392$ ppm). The neutral loss between the MS2 fragment at the nominal mass of 325 and this fragment corresponds to H2O. The neutral loss of H2O and a matching signal in the MS spectra in negative mode (323.1394, C19H19N2O3, $\Delta m = 1.0732$ ppm) indicate a carboxylic acid moiety. An analogous N-fumarylated TP was observed for MEX_278.1387_17.3, which was confirmed by a synthesized reference standard.

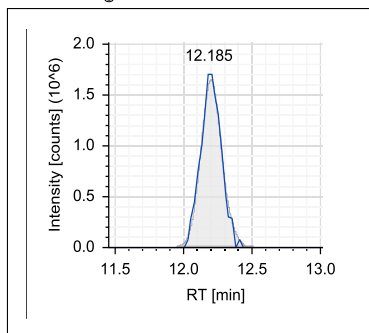
Attributed Reaction from the Parent Compound to this TP

It is *possible* that this TP was formed via an N-fumarylation reaction or a successive desaturation reaction after an N-succinylation reaction.

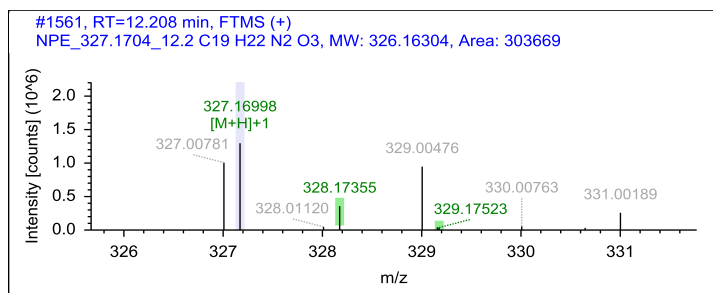
Appendix B

Name NPE_327.1704_12.2

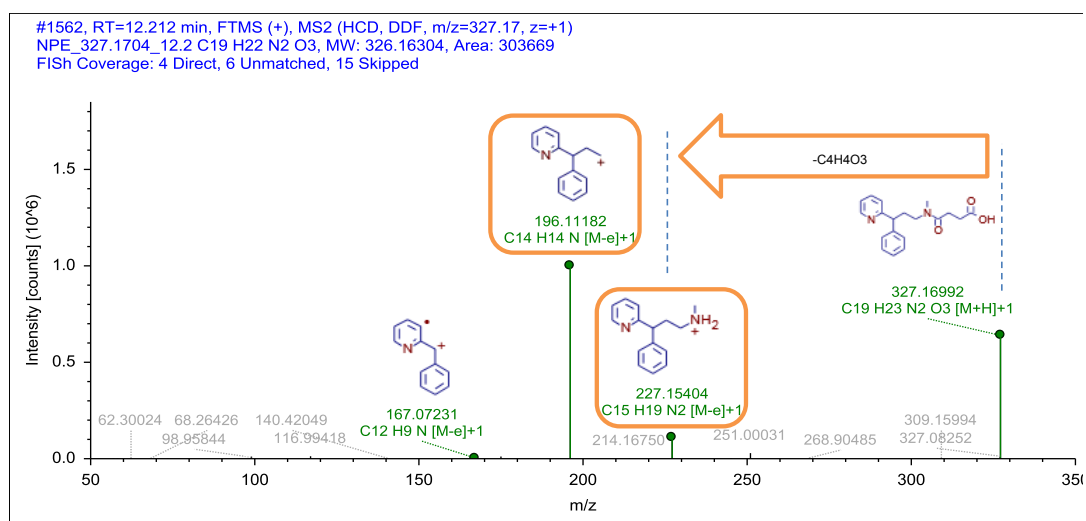
Chromatogram



MS Spectra



MS2 Spectra



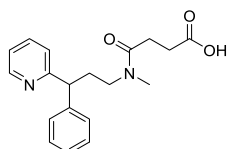
Formula

C₁₉H₂₂N₂O₃

Atomic Modification

+C₄H₄O₃

Proposed Structure



Additional Evidence for Structure Interpretation

The MS2 fragments at the nominal masses 167, 196, and 227 were also observed for the parent compound either in the shown MS2 spectrum or in one measured with a collision energy of 15. These fragments indicate that the parent structure is a substructure of this TP. In an MS2 spectrum measured with a collision energy of 60, an additional MS2 fragment was observed at the exact mass of 101.0230 (C₄H₅O₃ Δm=-3.3736 ppm). This fragment and the neutral loss between the MS2 fragments at the nominal masses 327 and 227 indicate that all atoms of the modification of +C₄H₄O₃ are connected. A matching signal in the MS spectra in negative mode (325.1553, C₁₉H₂₁N₂O₃, Δm=1.8351 ppm) indicates a carboxylic acid moiety. An analogous N-succinylated TP was observed for OCP_297.1002_16.5, which was confirmed by a synthesized reference standard.

Attributed Reaction from the Parent Compound to this TP

It is *likely* that this TP was formed via an N-succinylation reaction.

Confidence Level

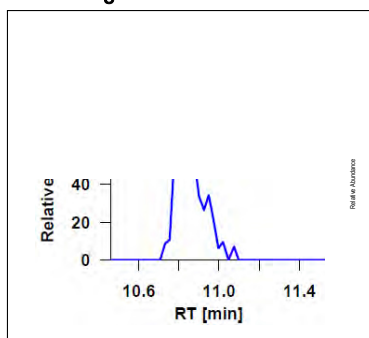
Level 3,
proposed structure

MassBank ID

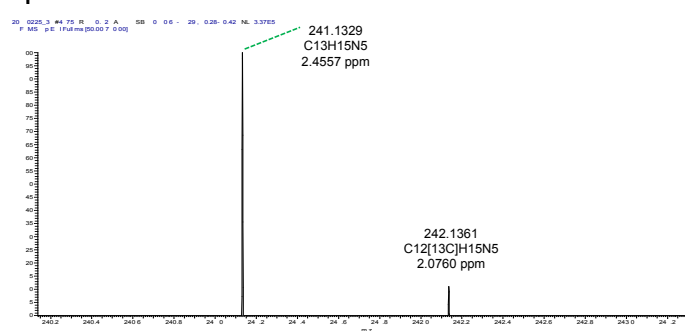
ET110201-ET110206

Name NPE_241.1335_10.8

Chromatogram

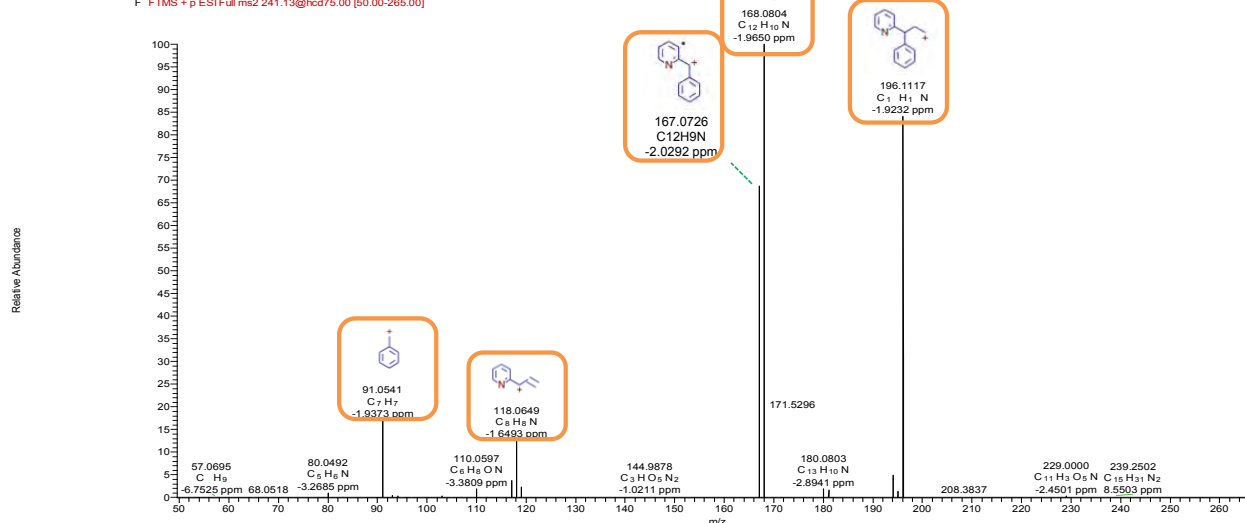


MS Spectra



MS2 Spectra

20150225 39 #4161-4189 RT 10.50-10.55 AV 4 SB 51 10.61-11.29, 10.28-10.42 NL 1.36E5
F FTMS + p ESI Full ms2 241.13@hcd75.00 [50.00-265.00]



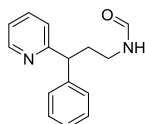
Formula

C15 H16 N2 O

Atomic Modification

-H2, +O

Proposed Structure



Confidence Level

Level 3,
proposed structure

MassBank ID

ET111301-ET111306

Additional Evidence for Structure Interpretation

The MS2 fragments at the nominal masses 91, 118, 167, 168, and 196 were also observed for the parent compound and indicate that the phenylpropylpyridine structure is a substructure of this TP. Therefore, the atomic modification -H2 +O from the elemental formula of the parent compound to this TP must have occurred at the methylamine moiety. Therefore, it is likely that the methyl carbon adjacent to the nitrogen was oxidized to a formamide product.

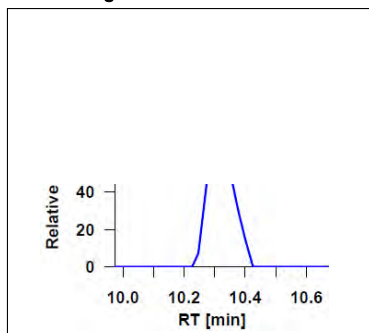
Attributed Reaction from the Parent Compound to this TP

It is *possible* that this TP was formed either via an α -C-oxidation to a formamide or in two steps, namely an N-demethylation followed by an N-formylation reaction or vice versa.

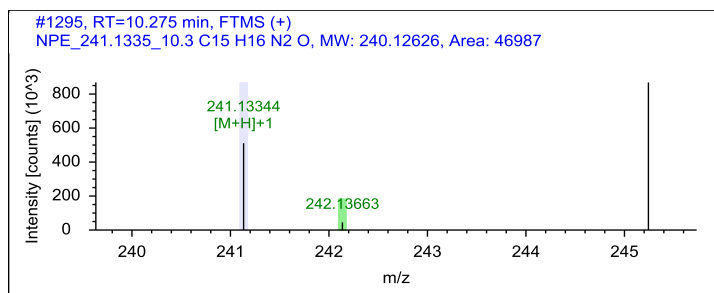
Appendix B

Name NPE_241.1335_10.3

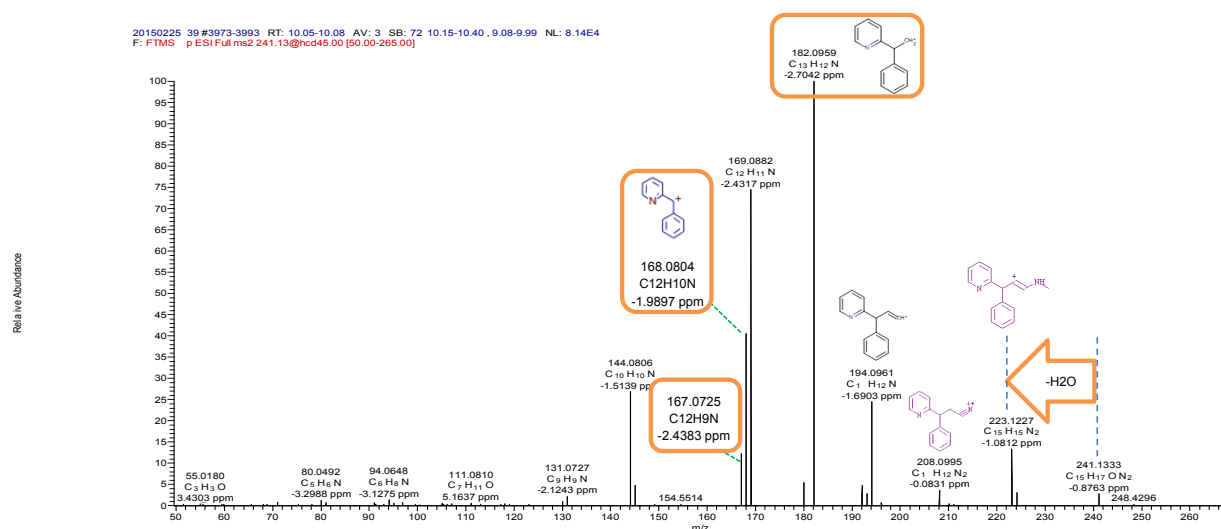
Chromatogram



MS Spectra



MS2 Spectra



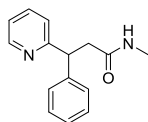
Formula

C₁₅H₁₆N₂O

Atomic Modification

-H₂ +O

Proposed Structure



Additional Evidence for Structure Interpretation

The MS2 fragments at the nominal masses 167 and 168 were also observed for the parent compound. These fragments as well as the MS2 fragment at the nominal mass 182 indicate that the phenylethylpyridine structure is a substructure of this TP. All TPs of NPE that were modified at the methylamine moiety have an MS2 spectrum similar to the MS2 spectrum of the parent. However, the MS2 spectrum of this TP is different, which can be seen from the unique MS2 fragments at the nominal masses 144, 169, 208, and 223. Therefore, it is likely that the atomic modification -H₂ +O from the elemental formula of the parent compound to this TP occurred at the ethyl chain carbon atom that is adjacent to the nitrogen. The neutral loss of H₂O points towards an amide moiety.

Attributed Reaction from the Parent Compound to this TP

It is *likely* that this TP was formed via an α -C-oxidation reaction

Confidence Level

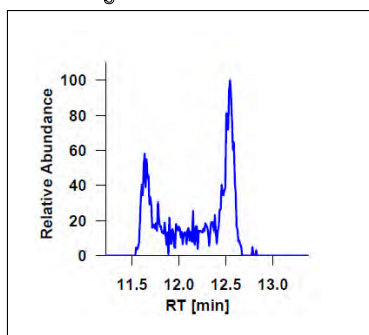
Level 3,
proposed structure

MassBank ID

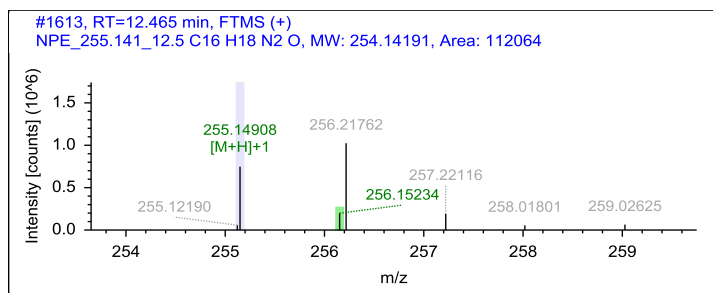
ET110801-ET110806

Name NPE_255.1491_11.6 = PHE_255.1497_11.6

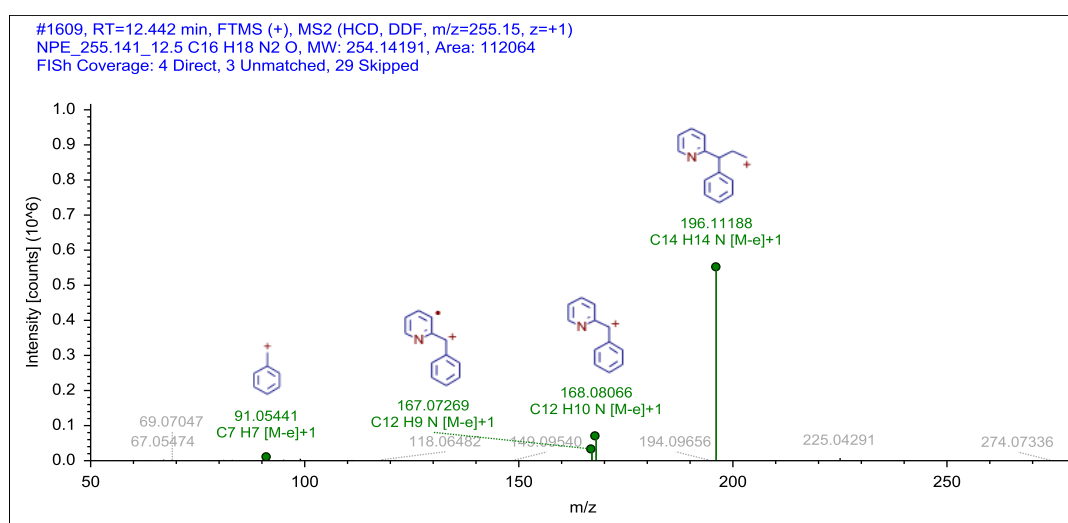
Chromatogram



MS Spectra



MS2 Spectra



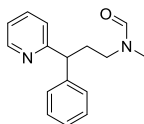
Formula

C₁₆ H₁₈ N₂ O

Atomic Modification

+CO

Proposed Structure



Confidence Level

Level 1,
synthesized standard

MassBank ID

ET110601-ET110606

Additional Evidence for Structure Interpretation

The formamide structure of this TP was confirmed by a synthesized standard. Details on the synthesis and the NMR measurement can be found in Chapter S5. The chromatogram showed two maxima at 11.6 minutes and 12.6 minutes. This peak shape results from the cis-trans isomerism of the C-N bond that has some double bond character. This is in analogy with the TP PYR_300.1709_10.6 for which the resonance structures were drawn.

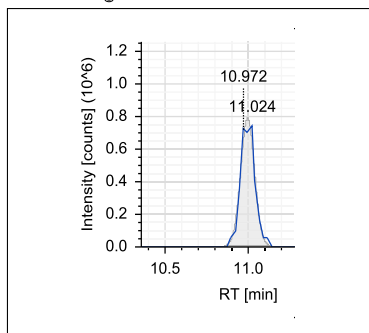
Attributed Reaction from the Parent Compound to this TP

It is *certain* that this TP was formed via an N-formylation reaction.

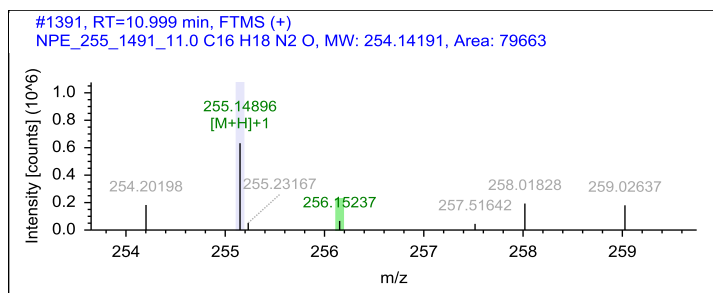
Appendix B

Name NPE_255.1491_11.0

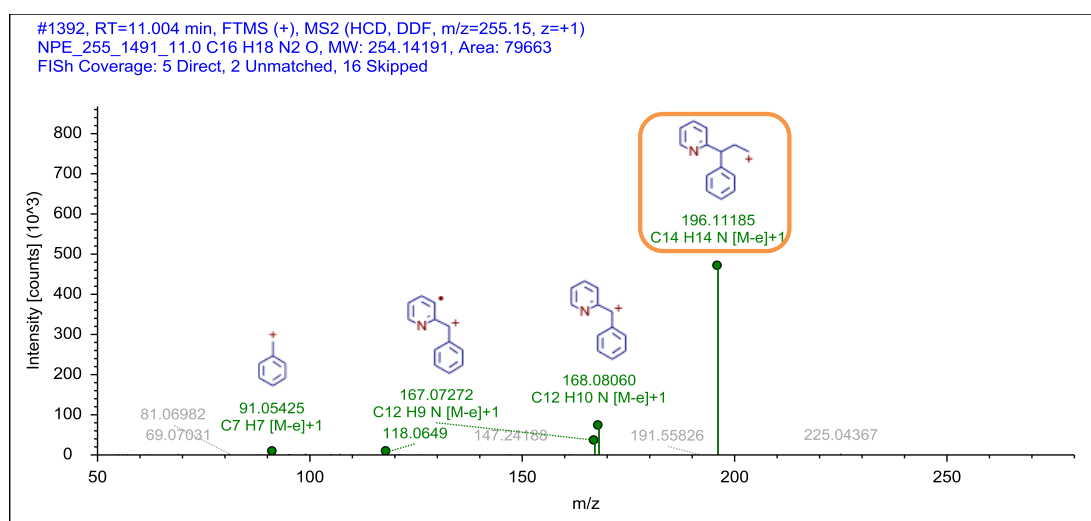
Chromatogram



MS Spectra



MS2 Spectra



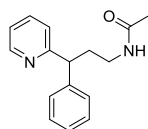
Formula

C16 H18 N2 O

Atomic Modification

+CO

Proposed Structure



Confidence Level
Level 3,
proposed structure

MassBank ID
ET110701-ET110706

Additional Evidence for Structure Interpretation

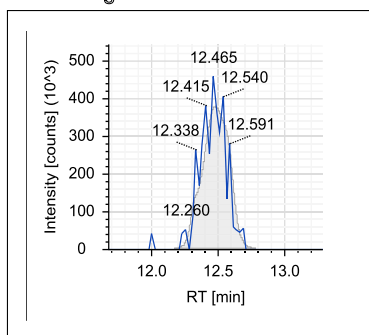
The MS2 fragments at the nominal masses 91, 118, 167, 168, and 196 were also observed for the parent compound and indicate that the phenylpropylpyridine structure is a substructure of this TP. Therefore, the atomic modification +CO from the elemental formula of the parent compound to this TP must have occurred at the methylamine moiety. A reference standard was available to confirm the structure of the TP NPE_255.1491_11.6, which had the same exact mass and exhibits a methylformylamine moiety. The MS2 spectrum of the TP NPE_255.1491_11.6 showed the same MS2 fragments as this one, since they exclusively correspond to the phenylpropylpyridine moiety. However, the retention time of the reference standard matched the one of the TP NPE_255.1491_11.6. No peak was observed at the retention time of 11.0 for the reference standard indicating that remaining atoms NC2H4O are connected differently.

Attributed Reaction from the Parent Compound to this TP

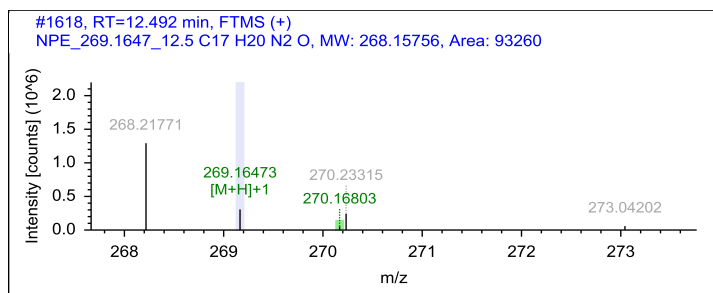
It is *possible* that this TP was formed in two steps either via an N-demethylation of the secondary amine followed by an N-acetylation or via an N-acetylation of the secondary amine followed by an N-demethylation of the tertiary amide.

Name NPE_269.1647_12.5

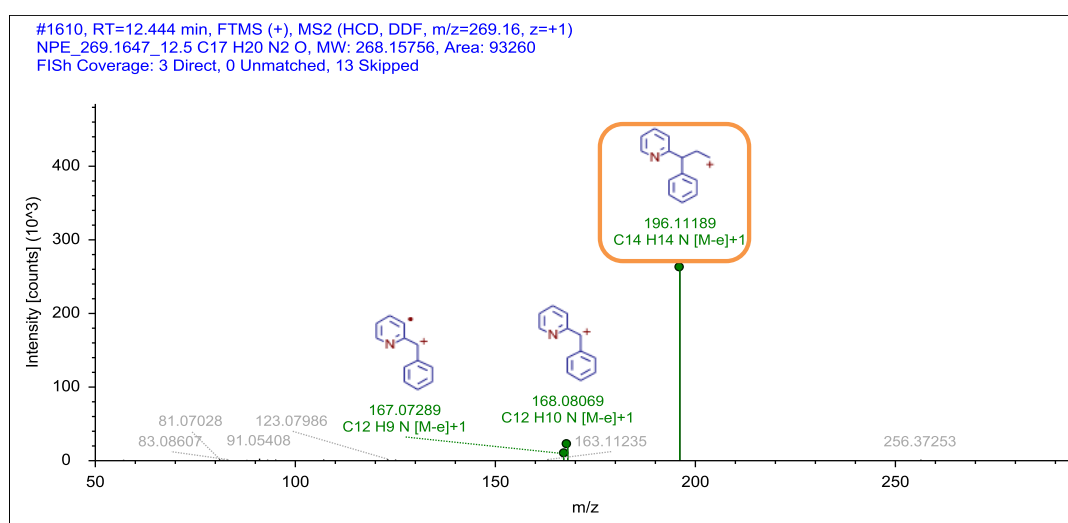
Chromatogram



MS Spectra



MS2 Spectra



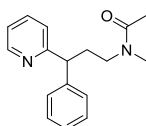
Formula

C17 H20 N2 O

Atomic Modification

+C2H2O

Proposed Structure



Additional Evidence for Structure Interpretation

The MS2 fragments at the nominal masses 167, 168, and 196 were also observed for the parent compound and indicate that the phenylpropylpyridine structure is a substructure of this TP. Therefore, the atomic modification +C2H2O from the elemental formula of the parent compound to this TP must have occurred at the methylamine moiety

Attributed Reaction from the Parent Compound to this TP

It is *likely* that this TP was formed via an N-acetylation reaction.

Confidence Level

Level 3,
proposed structure

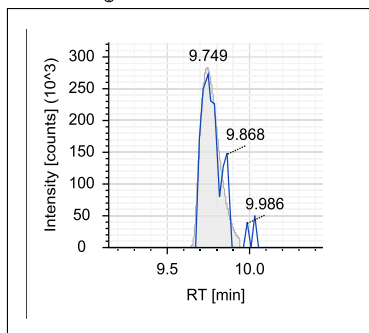
MassBank ID

ET110501-ET110506

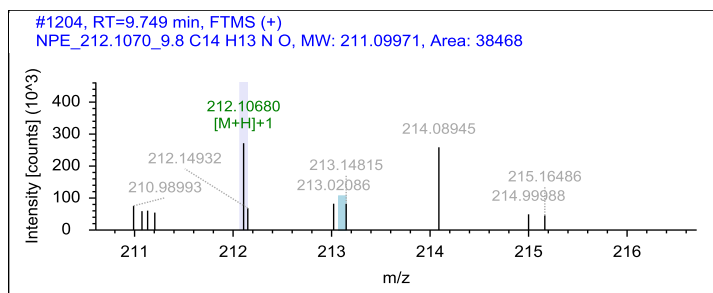
Appendix B

Name NPE_212.1070_9.8

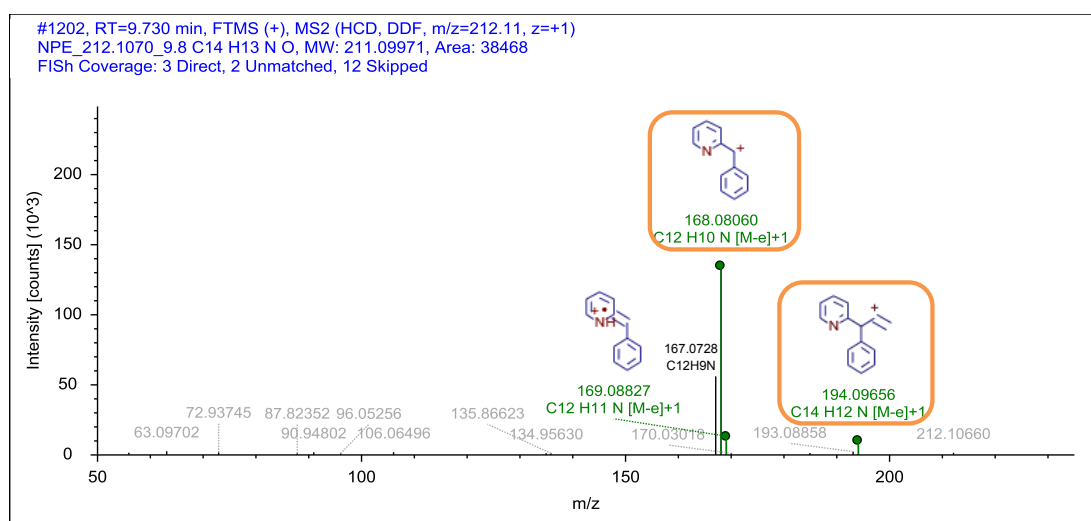
Chromatogram



MS Spectra



MS2 Spectra



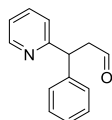
Formula

C₁₄ H₁₃ N O

Atomic Modification

-CH₅N, +O

Proposed Structure



Confidence Level

Level 3,
proposed structure

MassBank ID

ET110903

Additional Evidence for Structure Interpretation

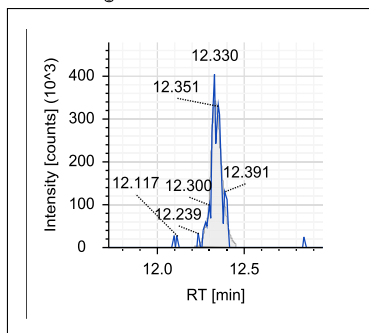
The MS2 fragments at the nominal masses 167, 168, and 194 were also observed for the parent compound and indicate that the phenylpropylpyridine structure is a substructure of this TP. The atomic modification from the elemental formula of the parent compound to this TP is -CH₅N +O.

Attributed Reaction from the Parent Compound to this TP

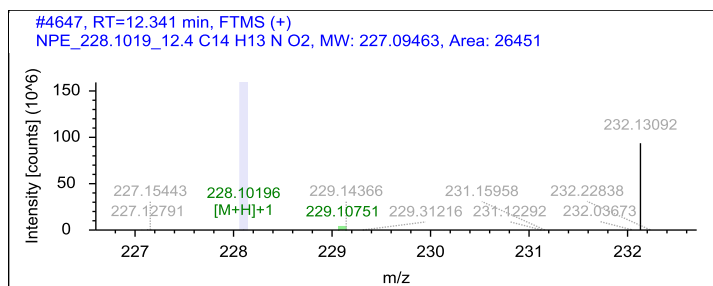
It is *likely* that this TP was formed via a deamination reaction.

Name NPE_228.1019_12.4

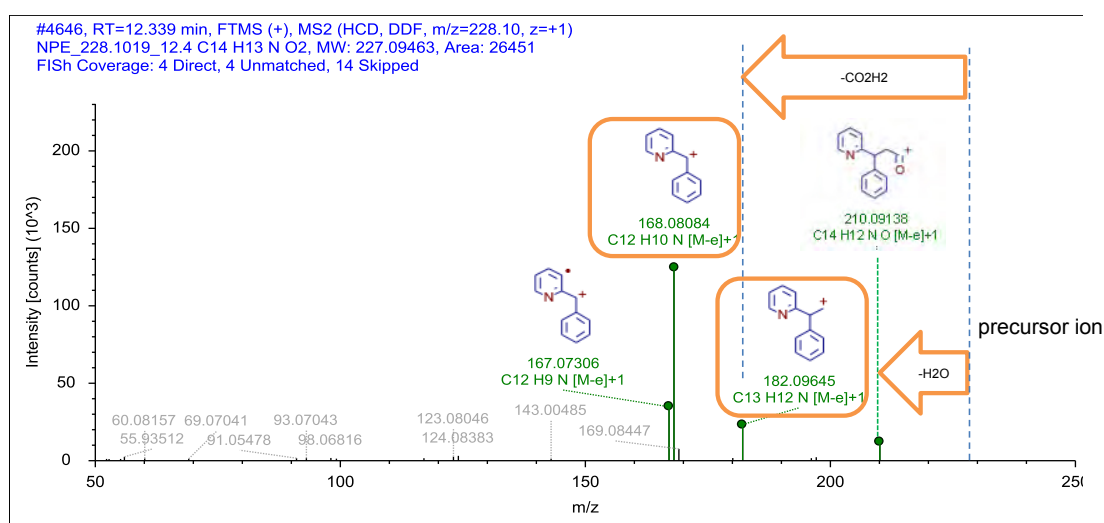
Chromatogram



MS Spectra



MS2 Spectra



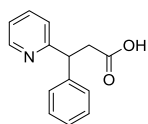
Formula

C14 H13 N O2

Atomic Modification

-CH5N, +O2

Proposed Structure



Additional Evidence for Structure Interpretation

The MS2 fragments at the nominal masses 167 and 168 were also observed for the parent compound. These fragment and the MS2 fragment at the nominal mass 182 indicate that the phenylethylpyridine structure is a substructure of this TP. The atomic modification from the elemental formula of the parent compound to this TP is -CH5N +O2. The neutral losses of H2O and CO2H2 indicate a carboxylic acid moiety. (No matching signal was observed in the MS spectrum in negative mode. However, the intensity of the peak is rather low and the sensitivity in negative mode is lower.)

Attributed Reaction from the Parent Compound to this TP

It is *likely* that this TP was formed via a deamination reaction followed by an oxidation to a carboxylic acid.

Confidence Level

Level 3,
proposed structure

MassBank ID

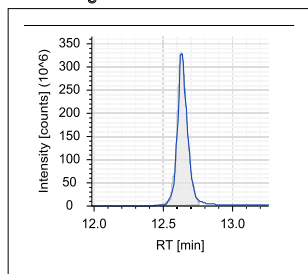
ET111201-ET111206

Appendix B

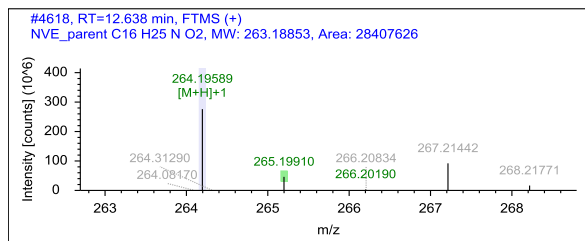
B.4.14 Structural evidence for N-demethylvenlafaxine and its TPs

Name NVE_264.1959_12.6, parent = VEN_264.1959_12.6

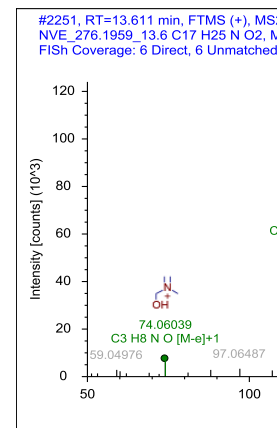
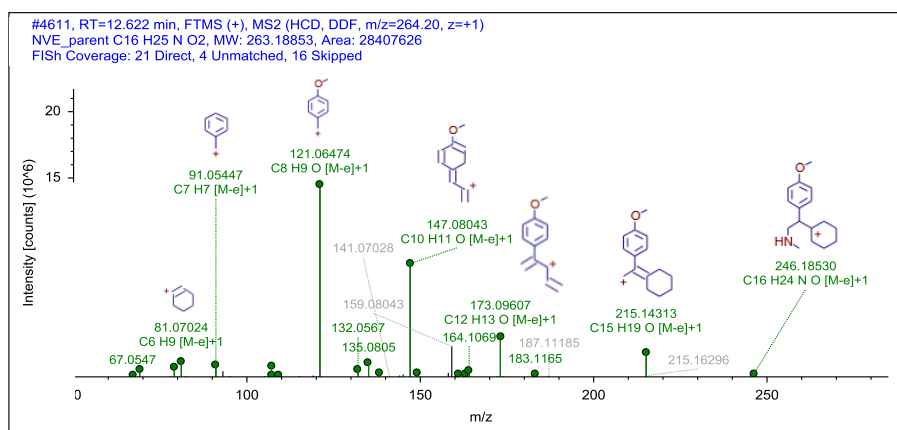
Chromatogram



MS Spectra



MS2 Spectra



Formula

C16 H25 N O2

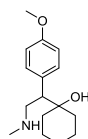
Additional Evidence for Structure Interpretation

This is the structural evidence that was observed for the parent compound NVE.

Atomic Modification

none

Proposed Structure



Confidence Level

Level 1

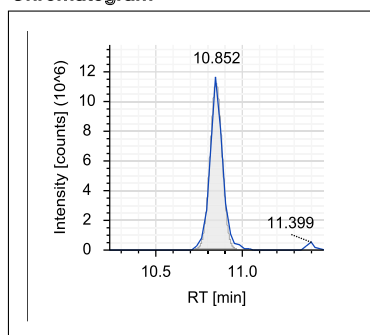
reference standard

MassBank ID

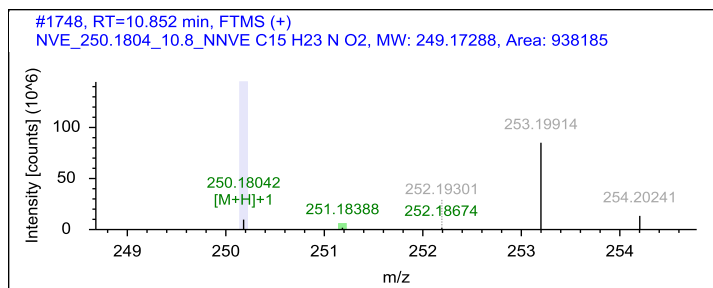
ET120001-ET120005

Name NVE_250.1804_10.8

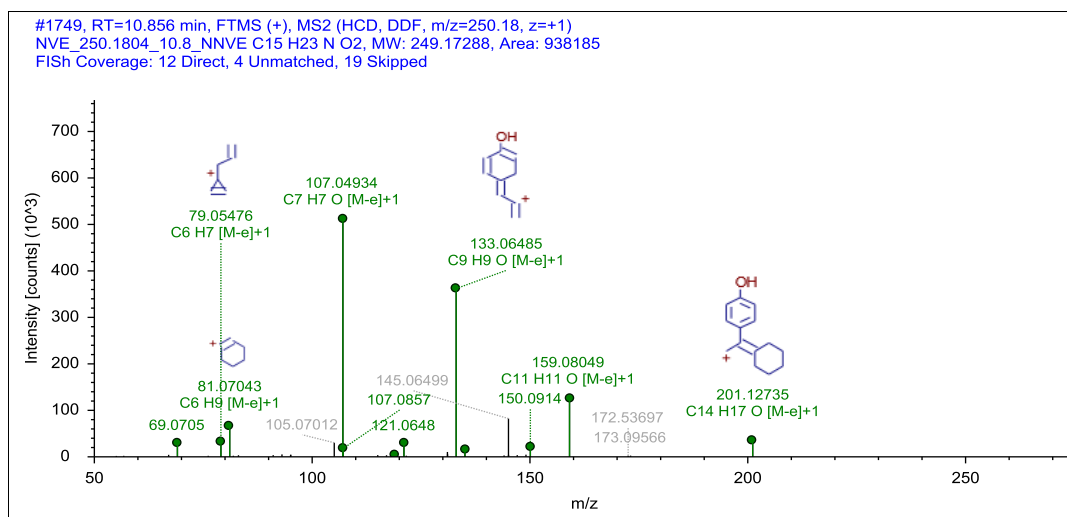
Chromatogram



MS Spectra



MS2 Spectra



Formula

C15 H23 N O2

Additional Evidence for Structure Interpretation

The structure of this TP was confirmed by a reference standard.

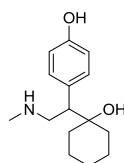
Atomic Modification

-CH2

Attributed Reaction from the Parent Compound to this TP

It is *certain* that this TP was formed via an O-demethylation reaction.

Proposed Structure



Confidence Level

Level 1,
reference standard

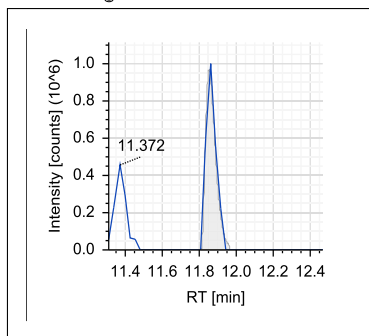
MassBank ID

ET120101-ET120105

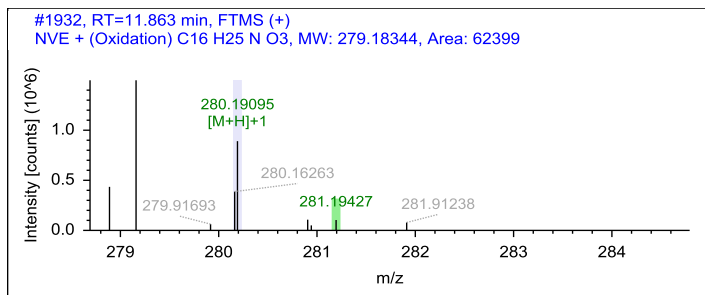
Appendix B

Name NVE_280.1909_11.8

Chromatogram

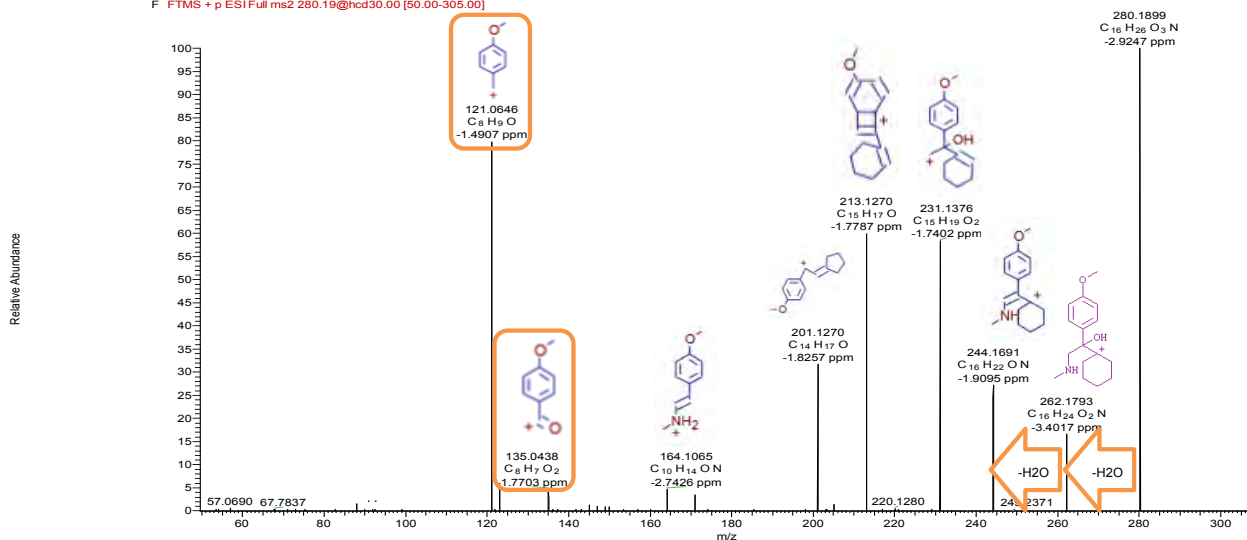


MS Spectra



MS2 Spectra

20150225 08:4677-4700 RT 11.77-11.81 AV 3 SB 119 11.92-12.91 10.57-11.55 NL 8.64E4
F FTMS + p ESI Full ms2 280.19@hcd30.00 [50.00-305.00]



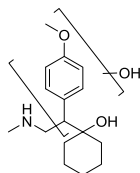
Formula

C₁₆H₂₅N O₃

Atomic Modification

+O

Proposed Structure



Additional Evidence for Structure Interpretation

The MS2 fragment at the nominal mass 121 was also observed for the parent compound and indicates that the methoxybenzyl moiety is a substructure of this TP. The atomic modification from the elemental formula of the parent compound to this TP is +O. Two neutral losses of H₂O were observed that indicate the presence of two hydroxyl moieties, whereby one was already present in the parent structure. The MS2 fragment at the nominal masses 135 indicates that the modification took place at the methoxybenzyl moiety.

Attributed Reaction from the Parent Compound to this TP

It is *likely* that this TP was formed via a hydroxylation reaction.

Confidence Level

Level 3

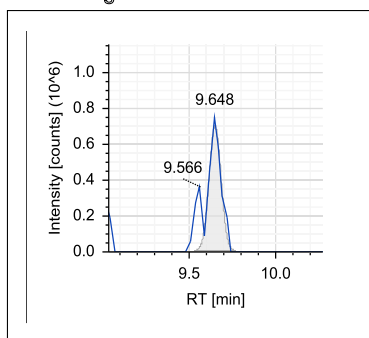
TP class

MassBank ID

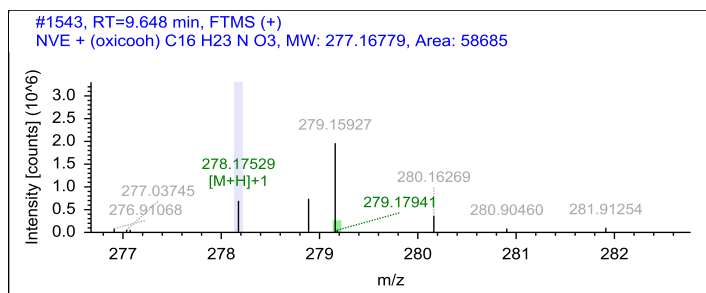
ET120401-ET120406

Name NVE_278.1753_9.6

Chromatogram

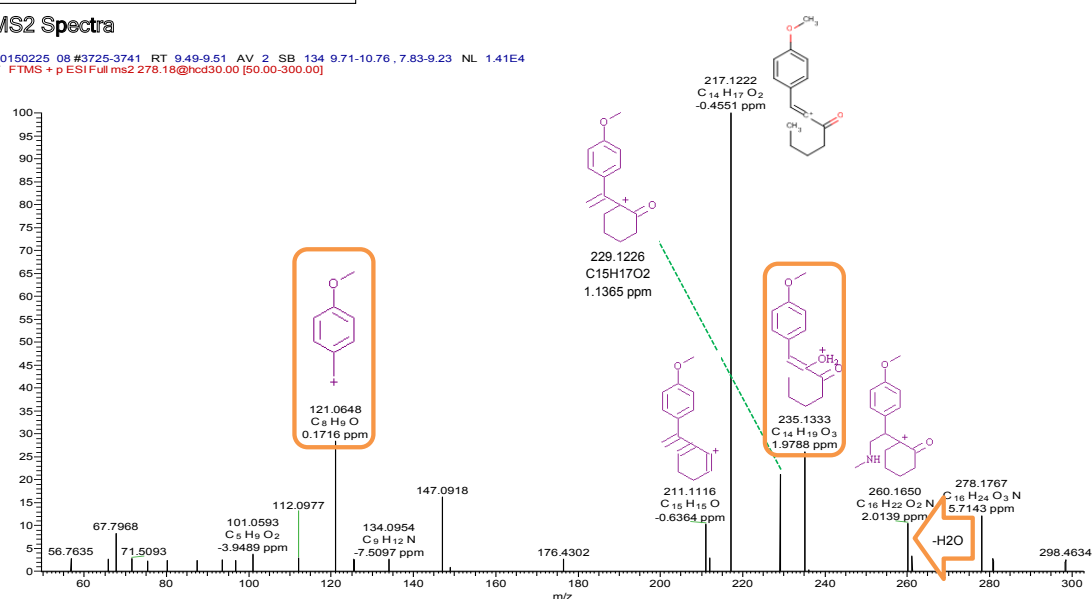


MS Spectra



MS2 Spectra

20150225 08 #3725-3741 RT 9.49-9.51 AV 2 SB 134 9.71-10.76, 7.83-9.23 NL 1.41E4
F FTMS + p ESI Full ms2 278.18@hcd30.00 [50.00-300.00]



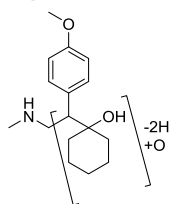
Formula

C16 H23 N O3

Atomic Modification

-H2, +O

Proposed Structure



Additional Evidence for Structure Interpretation

The MS2 fragment at the nominal mass 121 was also observed for the parent compound and indicates that the methoxybenzyl moiety is a substructure of this TP. The atomic modification from the elemental formula of the parent compound to this TP is -H2 +O. The MS2 fragments at the nominal masses 121 and 235 indicate that the modification took place at the hydroxycyclohexyl moiety. The exact type and position of the modification remain unknown. The structures of the MS2 fragments are indicative.

Attributed Reaction from the Parent Compound to this TP

Several reaction paths are *possible* that could have formed this TP. After initial hydroxylation a successive oxidation to a carbonyl or an independent desaturation could have occurred.

Confidence Level

Level 3,
TP class

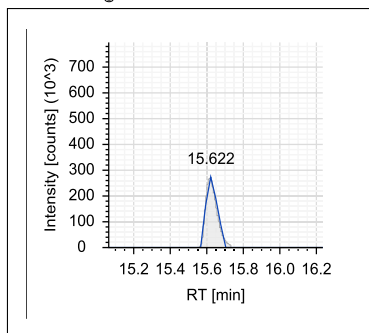
MassBank ID

ET120501-ET120506

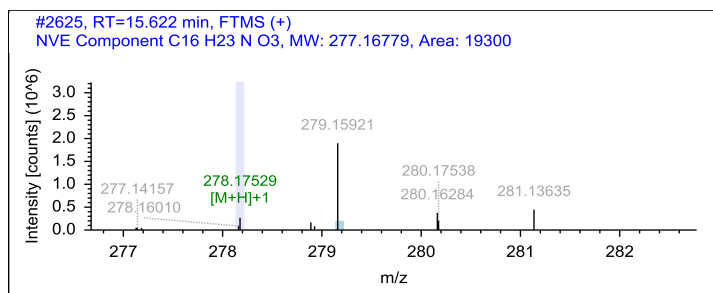
Appendix B

Name NVE_278.1753_15.6

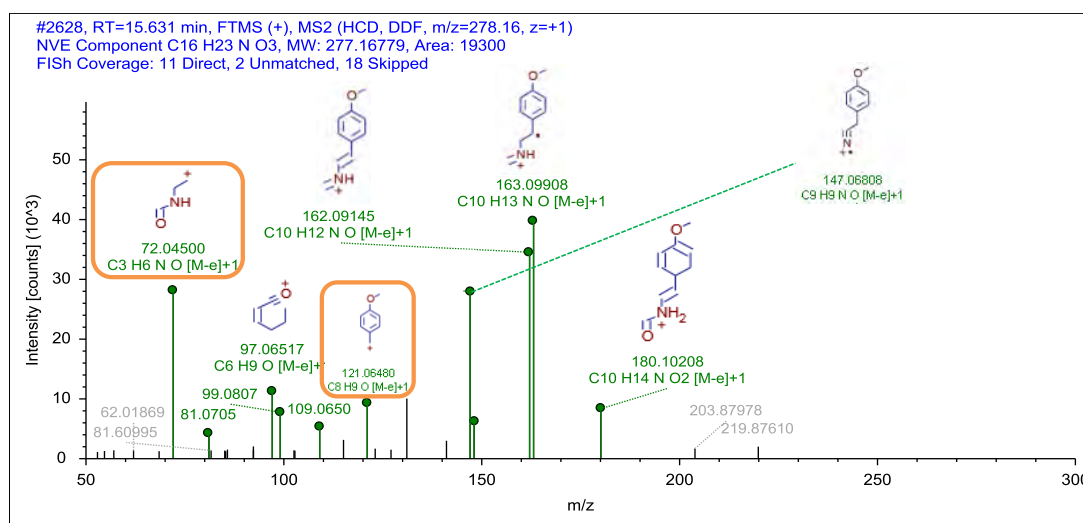
Chromatogram



MS Spectra



MS2 Spectra



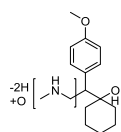
Formula

C16 H23 N O3

Atomic Modification

-H2, +O

Proposed Structure



Additional Evidence for Structure Interpretation

The MS2 fragment at the nominal mass 121 was also observed for the parent compound and indicates that the methoxybenzyl moiety is a substructure of this TP. The atomic modification from the elemental formula of the parent compound to this TP is -H2 +O. The MS2 fragment at the nominal masses 72 indicates that the modification took place at the methylmethylamine moiety. The exact type and position of the modification remain unknown. The structures of the MS2 fragments are drawn exemplarily.

Attributed Reaction from the Parent Compound to this TP

Several reaction paths are *possible* that could have formed this TP, such as an α-C-oxidation to an amide, an N-demethylation followed by an N-formylation or vice versa, and an N-hydroxylation followed by an successive reaction to a nitron.

Confidence Level

Level 3,

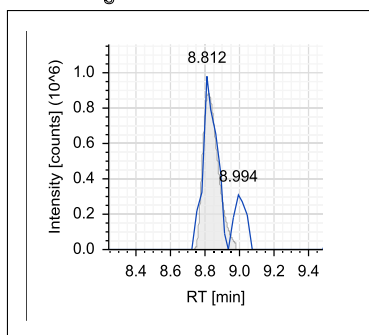
TP class

MassBank ID

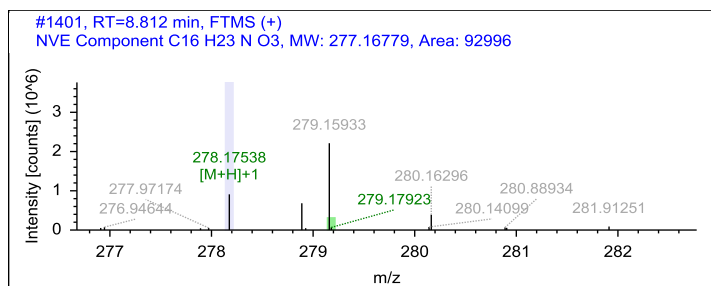
ET121103

Name NVE_278.1754_8.8

Chromatogram

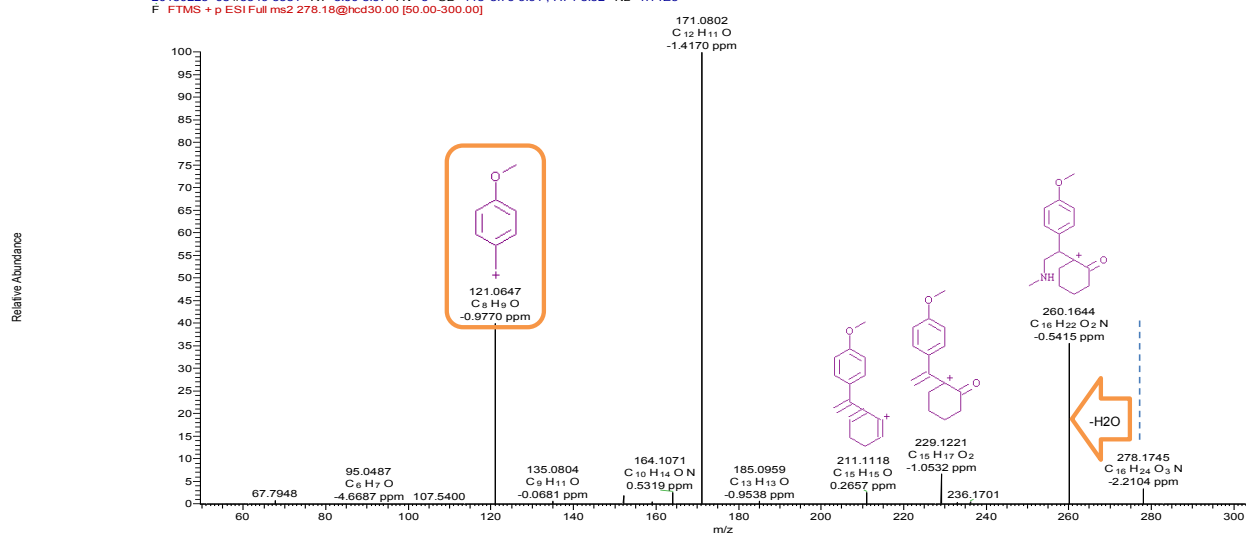


MS Spectra



MS2 Spectra

20150225 08 #3349-3381 RT 8.60-8.67 AV 5 SB 118 8.76-9.91, 7.74-8.52 NL 1.14E5
F FTMS + p ESI Full ms2 278.18@hcd30.00 [50.00-300.00]



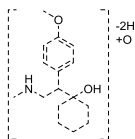
Formula

C₁₆ H₂₃ N O₃

Atomic Modification

-H₂ +O

Proposed Structure



Additional Evidence for Structure Interpretation

The MS2 fragment at the nominal mass 121 was also observed for the parent compound and indicates that the methoxybenzyl moiety is a substructure of this TP. The atomic modification from the elemental formula of the parent compound to this TP is -H₂ +O. The exact type and position of the modification remain unknown. The structures of the MS2 fragments are drawn exemplarily.

Attributed Reaction from the Parent Compound to this TP

Several reaction paths are *possible* that could have formed this TP, such as a C-hydroxylation followed by an oxidation to a carbonyl, C-hydroxylation in combination with desaturation, an α-C-oxidation to an amide or formamide, an N-demethylation followed by an N-formylation or vice versa, and an N-hydroxylation followed by a successive reaction to a nitrone.

Confidence Level

Level 3,
TP class

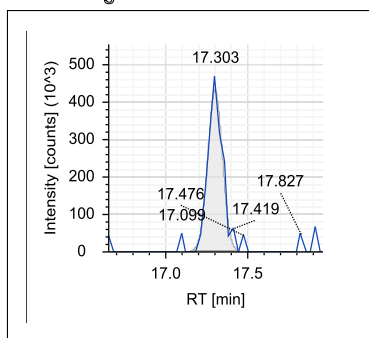
MassBank ID

ET121001-ET121006

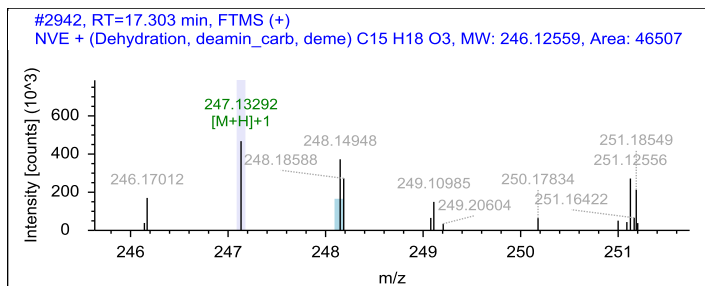
Appendix B

Name NVE_247.1330_17.3

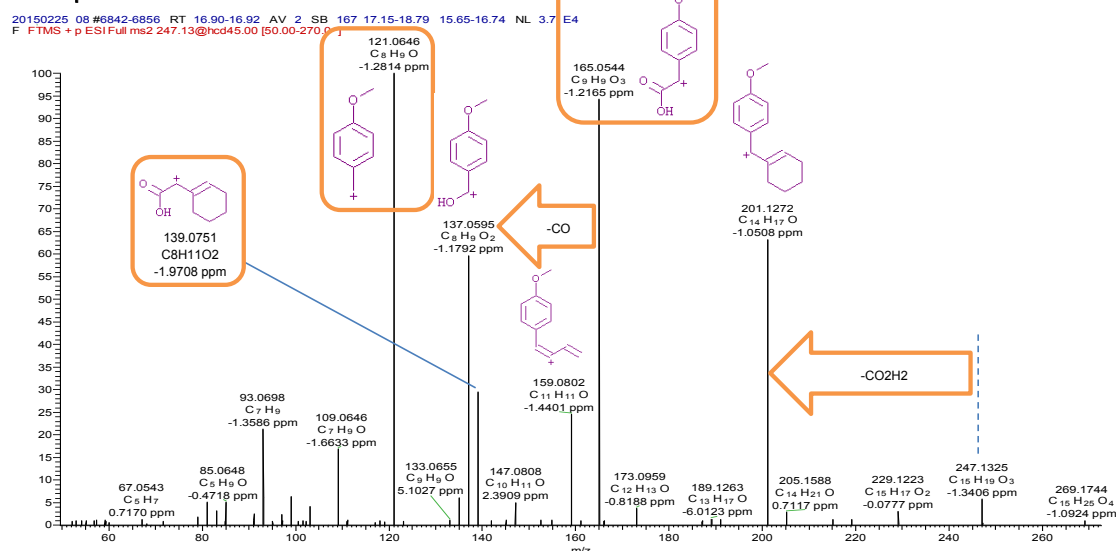
Chromatogram



MS Spectra



MS2 Spectra



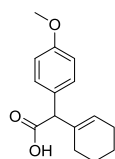
Formula

C15 H18 O3

Atomic Modification

-CH7, +O

Proposed Structure



Confidence Level

Level 3,
proposed structure

MassBank ID

ET120601-ET120606

Additional Evidence for Structure Interpretation

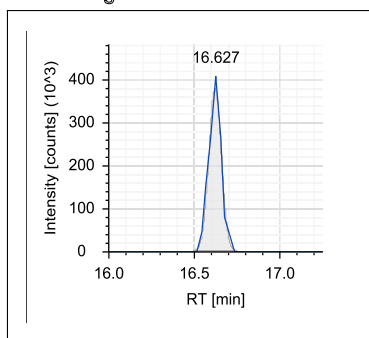
The MS2 fragment at the nominal mass 121 was also observed for the parent compound and indicates that the methoxybenzyl moiety is a substructure of this TP. The atomic modification from the elemental formula of the parent compound to this TP is $-\text{CH}_7\text{N} + \text{O}$. It is possible that this is a combination of a deamination ($-\text{CH}_5\text{N} + \text{O}_2$) and successive oxidation of the carbonyl moiety to a carboxylic acid and an elimination of the hydroxyl group to an alkene moiety ($-\text{H}_2\text{O}$). The observed neutral losses of CO_2H_2 and CO strengthens the evidence for a carboxylic acid moiety. No matching signal was observed in the MS measured in negative mode. However, this cannot be expected due to the low intensity of the peak and the lower sensitivity of the negative mode. The MS2 fragments at the nominal masses 137, 139, 159, 165, and 165 are predicted for this structure by Massfrontier and are therefore reasonable.

Attributed Reaction from the Parent Compound to this TP

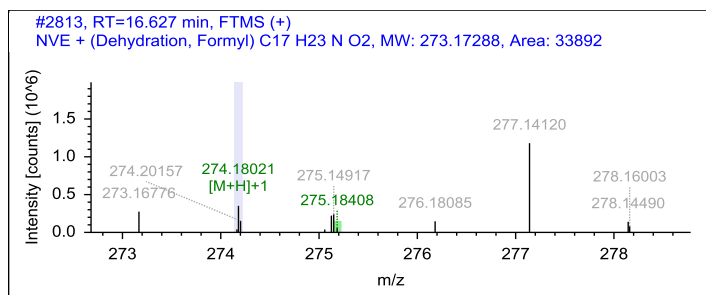
It is *likely* that this TP was formed by a combination of several reactions, namely a deamination followed by an oxidation of the carbonyl moiety to a carboxylic acid and a dehydration to an alkene moiety.

Name NVE_274.1802_16.6

Chromatogram

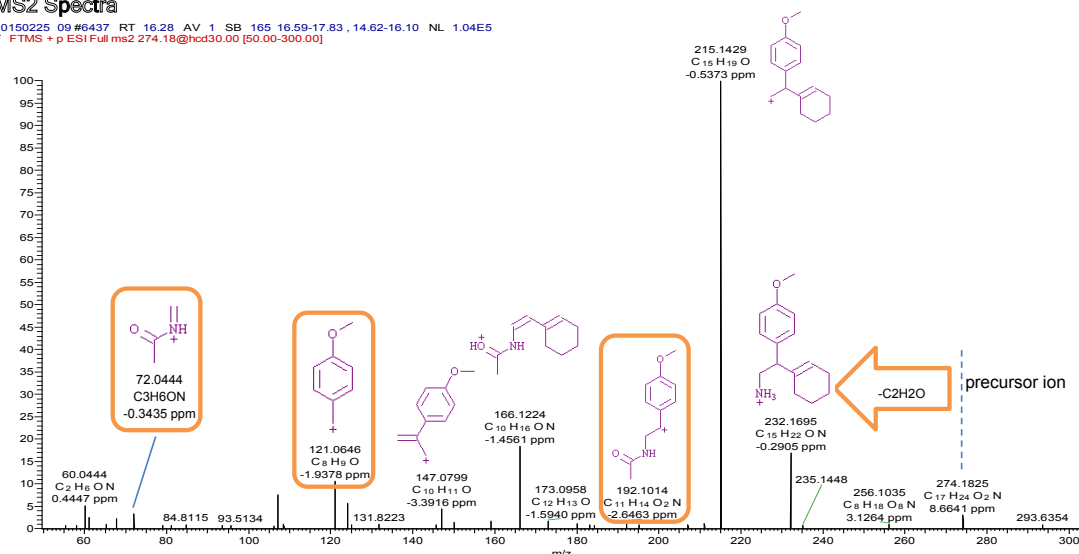


MS Spectra



MS2 Spectra

20150225 09 #5437 RT 16.28 AV 1 SB 165 16.59-17.83, 14.62-16.10 NL 1.04E5
F FTMS + p ESI Full ms2 274.18@hcd30.00 [50.00-300.00]



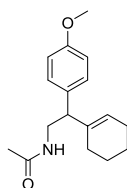
Formula

C17 H23 N O2

Atomic Modification

-H2, +O

Proposed Structure



Confidence Level

Level 3,
proposed structure

MassBank ID

ET120701-ET120706

Additional Evidence for Structure Interpretation

The MS2 fragments at the nominal masses 121 and 215 were also observed for the parent compound and indicate that the methoxybenzylcyclohexyl moiety is a substructure of this TP. The atomic modification from the elemental formula of the parent compound to this TP is -H2 +C. It is possible that this is a combination of a carbonyl addition (+CO) and an elimination of the hydroxyl group to an alkene moiety (-H2O). The addition of a carbonyl could occur via an N-formylation or by an N-demethylation and a successive N-acetylation. The observed neutral loss of C2H2O indicates that the respective atoms are connected and therefore point towards the N-acetylation product. The MS2 fragments at the nominal masses 72, 121, 147, 166, 192, 215, and 232 are predicted for this structure by Massfrontier and are therefore reasonable.

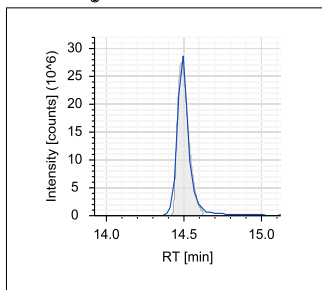
Attributed Reaction from the Parent Compound to this TP

It is *likely* that this TP was formed via a combination of several reactions, namely an N-demethylation followed by an N-acetylation or vice versa and a dehydration to an alkene moiety.

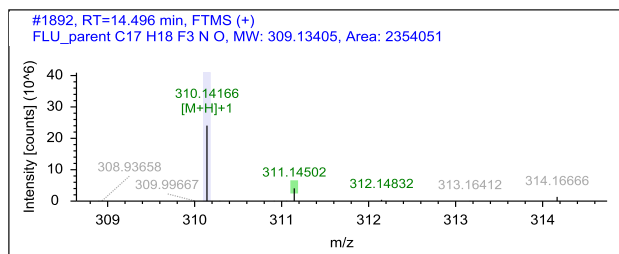
B.4.15 Structural evidence for fluoxetine and its TPs

Name FLU_310.1415_14.5, parent

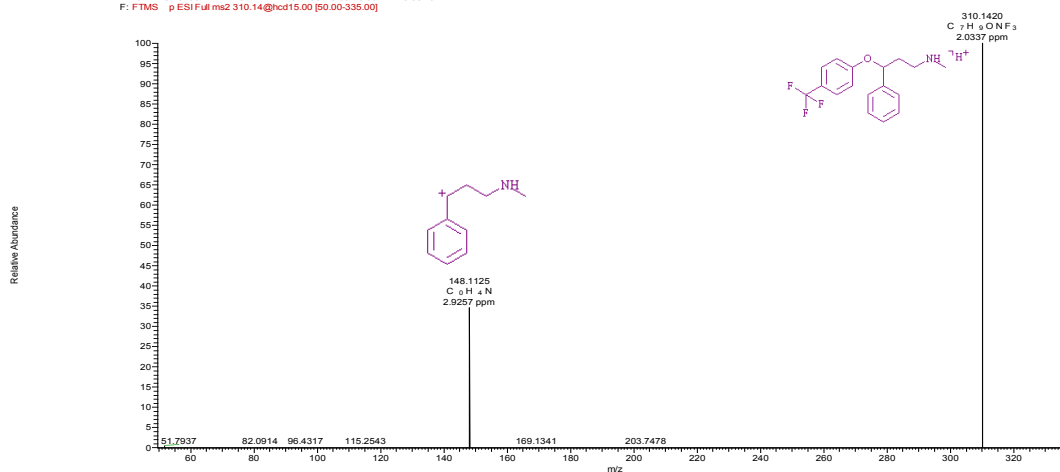
Chromatogram



MS Spectra



MS2 Spectra

141021 28 #5783 RT: 14.81 AV: 1 SB: 53 18.05-18.99 NL: 5.58E6
F: FTMS p ESI Full ms2 310.14@ncd15.00 [50.00-335.00]

Formula

C₁₇H₁₈F₃N O

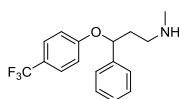
Additional Evidence for Structure Interpretation

This is the structural evidence that was observed for the parent compound FLU.

Atomic Modification

none

Proposed Structure



Confidence Level

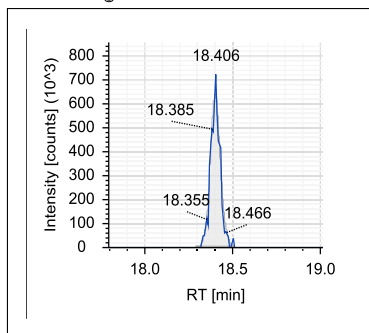
Level 1,
reference standard

MassBank ID

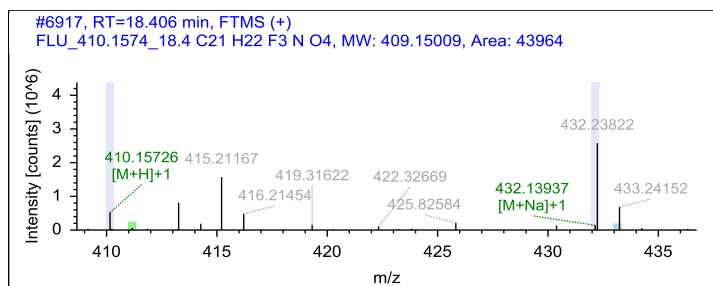
ET070001-ET070005

Name FLU_410.1574_18.4

Chromatogram

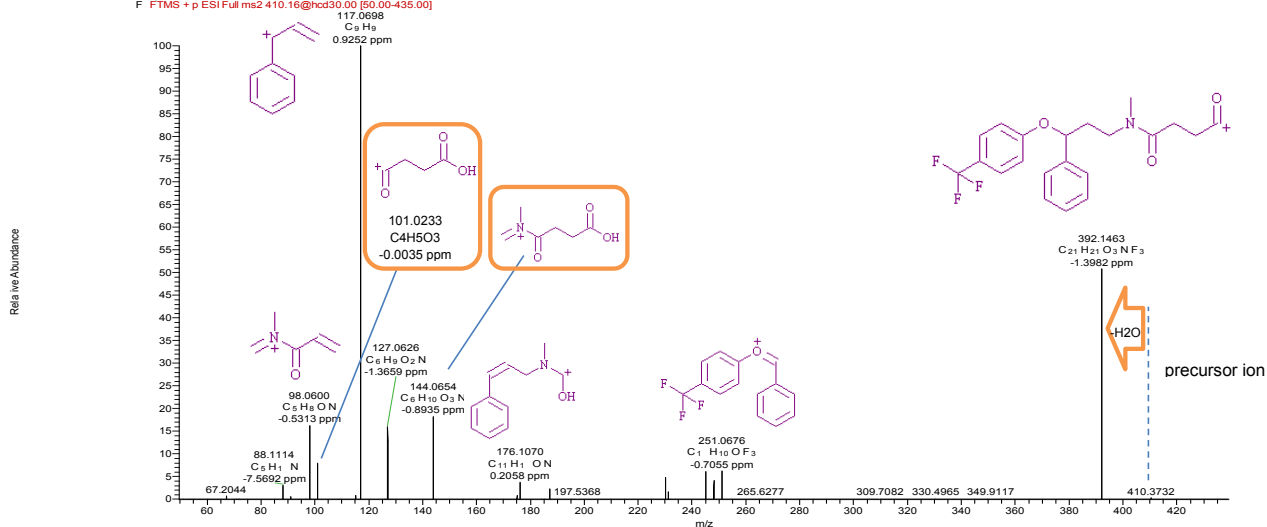


MS Spectra



MS2 Spectra

20150225 05 #7370-7398 RT 17.96-18.01 AV 4 SB 110 18.16-19.06 16.88-17.80 NL 122E5
F FTMS + p ESI Full ms2 410.16@hcd30.00 [50.00-435.00]



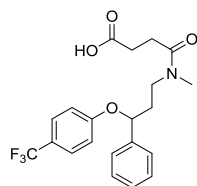
Formula

C21 H22 F3 N O4

Atomic Modification

+C4H4O3

Proposed Structure



Confidence Level

Level 3,
proposed structure

MassBank ID

ET070201-ET070206

Additional Evidence for Structure Interpretation

The atomic modification from the elemental formula of the parent compound to this TP is +C4H4O3. The MS2 fragment at the nominal mass 101 indicates that all atoms of the modification are connected. The MS2 fragment at the nominal mass 144 indicates that the modification occurred at the dimethylamine moiety. The neutral loss of H2O as well as a matching signal in the MS spectrum in negative mode (408.1426, C21H21O4NF3, $\Delta m = -0.4799$ ppm) indicate a carboxylic acid moiety. An analogous N-succinylated TP was observed for OCP_297.1002_16.5, which was confirmed by a synthesized reference standard.

(The following observations are relevant for the understanding of the structural evidence of further TPs of FLU and NFL. The in-source fragment (C14H18NO3, 248.1283, $\Delta m = -3.5346$ ppm), which lost the trifluoromethylphenolic moiety (C7H5OF3), is observed in the MS spectrum in positive mode with a higher signal (170% of the area) than the [M+H]⁺ ion.)

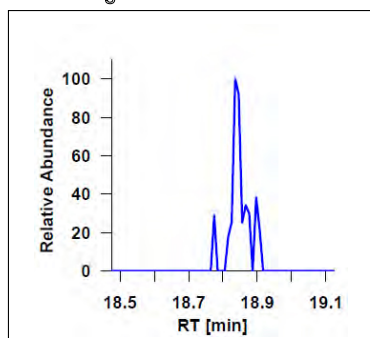
Attributed Reaction from the Parent Compound to this TP

It is *likely* that this TP was formed via an N-succinylation reaction.

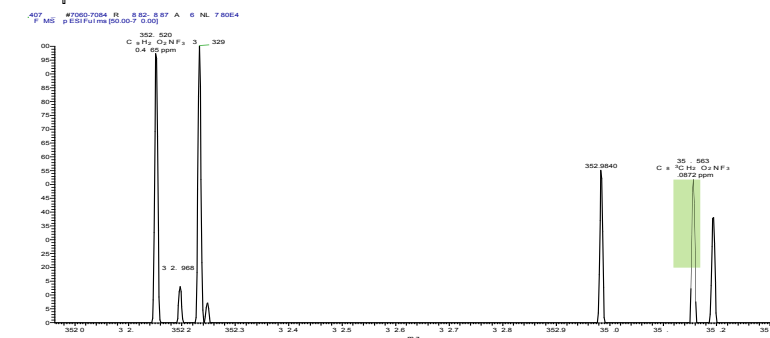
Appendix B

Name FLU_352.1520_18.8 (FLU_190.1228_18.8 in-source fragment)

Chromatogram

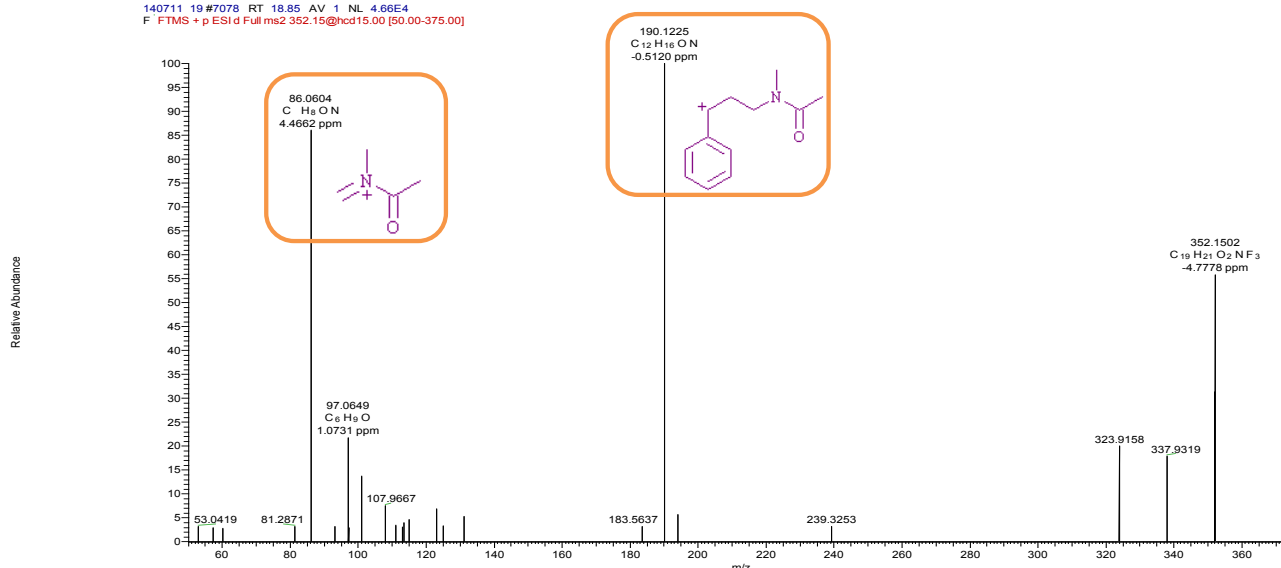


MS Spectra



MS2 Spectra

140711 19 #7078 RT 18.85 AV 1 NL 4.66E4
F FTMS + p ESI d Full ms2 352.15@hcd15.00 [50.00-375.00]



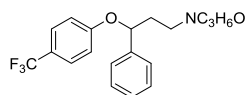
Formula

C19H20NO2F3

Atomic Modification

+C2H2O

Proposed Structure



Additional Evidence for Structure Interpretation

The atomic modification from the elemental formula of the parent compound to this TP is +C2H2O. The MS2 fragment at the nominal mass 86 indicates that the modification occurred at the dimethylamine moiety. This modification could be realized by an N,N-methylacetyl moiety or by an N-propionyl moiety. The MS2 fragment at the nominal mass 190 was also observed in the MS spectrum in positive mode as in-source fragment (C12H16ON, 190.1227, $\Delta m = 0.2103$ ppm) with a higher signal (300% of the area) than the [M+H]⁺ ion. A similar TP was also observed for NFL, namely the NFL_190.1228_18.8. There, only the in-source fragment was detected. Since the retention time of this TP (FLU_352.1520_18.8) and that of NFL (NFL_190.1228_18.8) is the same, it is likely that it is the same TP. For the TP of NFL the formation of an N-propionylated product is more likely since the parent NFL is already the N-demethylated form of FLU. However, it is also possible that the TP of FLU and NFL have different structures, namely an N,N-methylacetyl substructure and an N-propionyl substructure. All in all, it is not possible to propose a more refined structure for this TP. The structures shown for the MS2 fragments are exemplarily for the N-methylacetyl option.

Confidence Level

Level 3,
TP class

MassBank ID

ET070403

For the visualization of the time series pattern both peaks, FLU_352.150_18.8 and FLU_190.1228_18.8, are integrated.

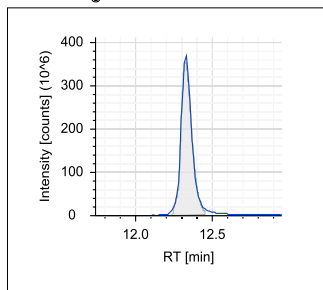
Attributed Reaction from the Parent Compound to this TP

Several reaction paths are *possible* that could have formed this TP, namely an N-acetylation or the combination of N-demethylation and N-propionylation.

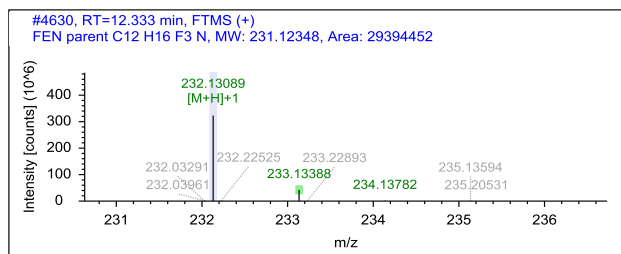
B.4.16 Structural evidence for feniramine and its TPs

Name FEN_232.1308_12.4, parent

Chromatogram

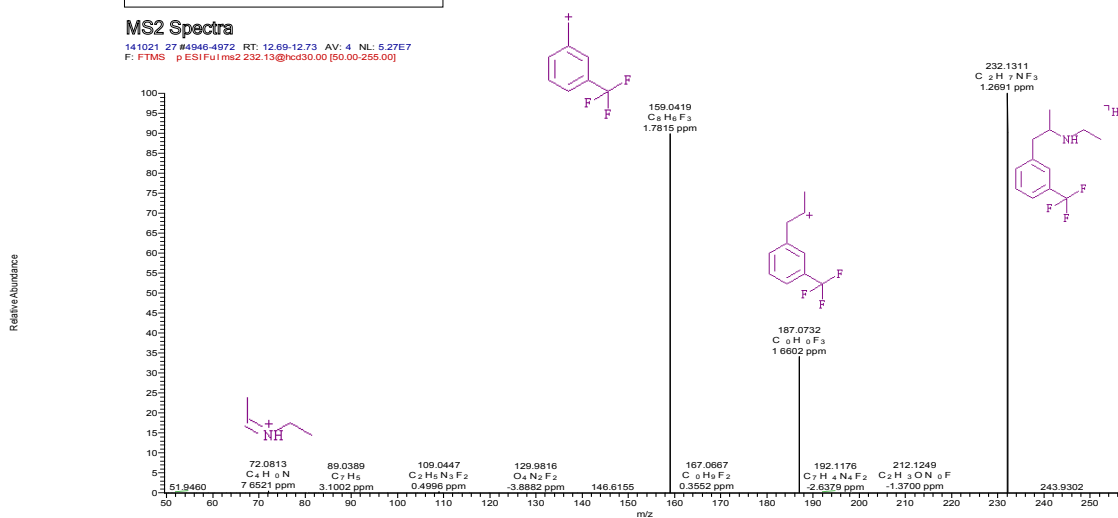


MS Spectra



MS2 Spectra

141021 27 #4946-4972 RT: 12.69-12.73 AV: 4 NL: 5.27E7
F: FTMS p ESI+Fu1me2 232.13@hcd30.00 [50.00-255.00]



Formula

C12 H16 F3 N

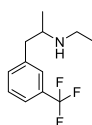
Additional Evidence for Structure Interpretation

This is the structural evidence that was observed for the parent compound FEN.

Atomic Modification

none

Proposed Structure



Confidence Level

Level 1,
reference standard

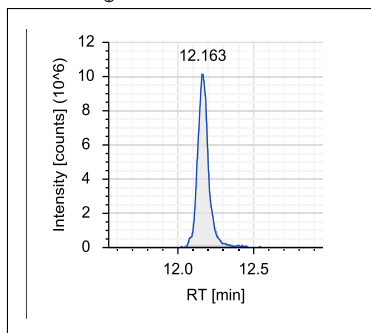
MassBank ID

ET060001-ET060005

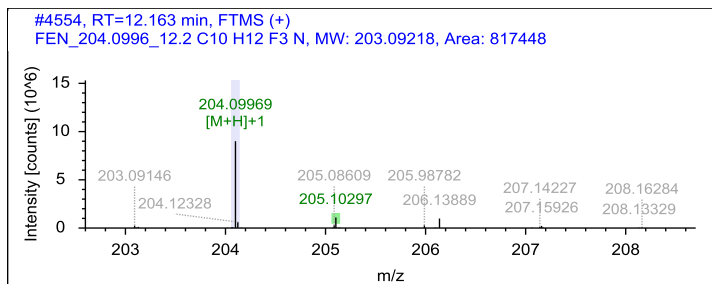
Appendix B

Name FEN_204.0996_12.2

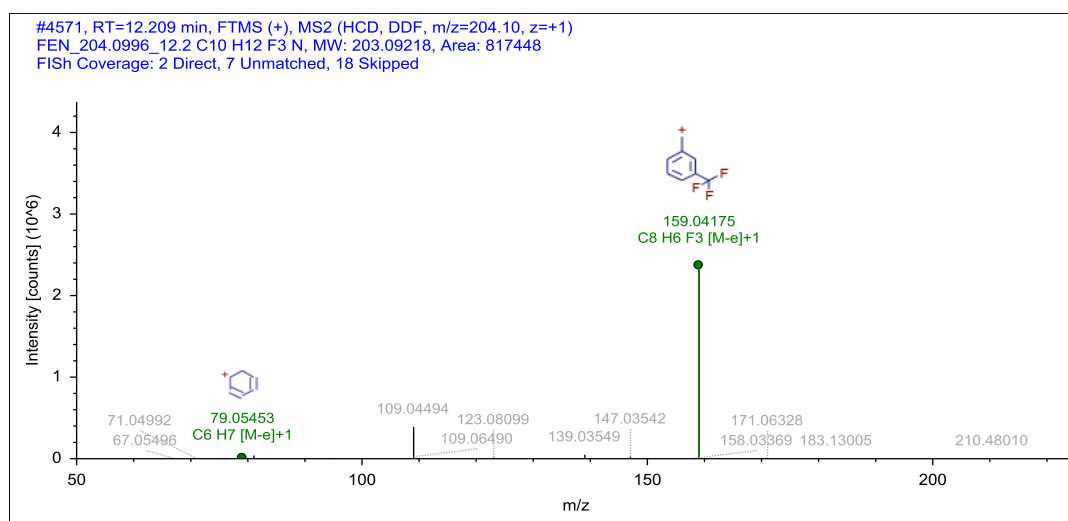
Chromatogram



MS Spectra



MS2 Spectra



Formula

C₁₀H₁₂F₃N

Additional Evidence for Structure Interpretation

The structure of this TP was confirmed by a reference standard

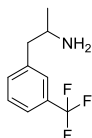
Atomic Modification

-C₂H₄

Attributed Reaction from the Parent Compound to this TP

It is *certain* that this TP was formed via an N-deethylation reaction.

Proposed Structure



Confidence Level

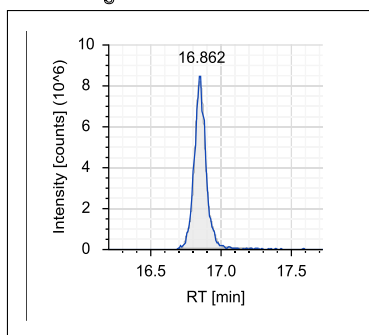
Level 1,
reference standard

MassBank ID

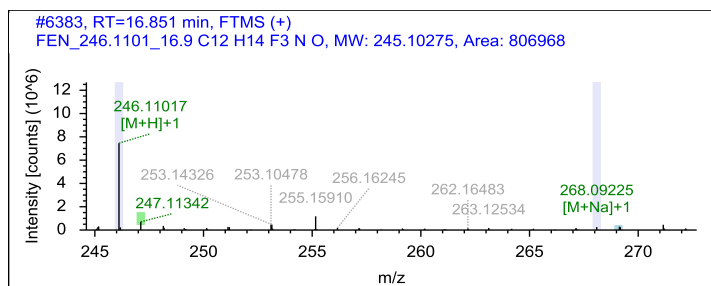
ET060101-ET060105

Name FEN_246.1101_16.9

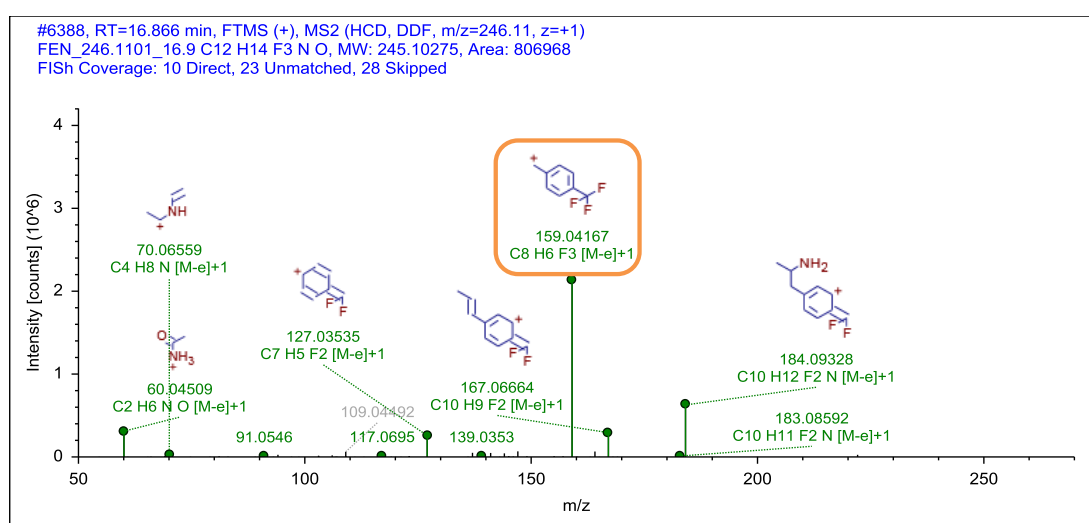
Chromatogram



MS Spectra



MS2 Spectra



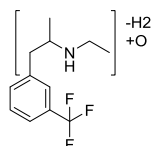
Formula

C12 H14 F3 N O

Atomic Modification

-H2, +O

Proposed Structure



Confidence Level

Level 3,

TP class

MassBank ID

ET060201-ET060206

Additional Evidence for Structure Interpretation

The MS2 fragment at the nominal mass 159 as well as an MS2 fragment at the exact mass of 187.0727 (C10H10F3, $\Delta m = -1.0056$ ppm) that was measured at a collision energy of 30, were also observed for the parent compound. An additional MS2 fragment was observed at the exact mass 204.1009 (C10H13NF3, $\Delta m = 7.1584$ ppm) in an MS2 spectrum measured at a collision energy of 30. They indicate that the norfenfluramine structure is a substructure of this TP. The atomic modification of the elemental formula of the parent compound to this TP is -H2 +O. The MS2 fragment at the nominal mass 60 indicates that this modification took place at the ethylamine moiety. There is a corresponding TP with the same mass but a different retention time, namely FEN_246.1101_16.1 for which the secondary acetamide substructure was proposed. Therefore, it is more likely that this TP was modified a different position

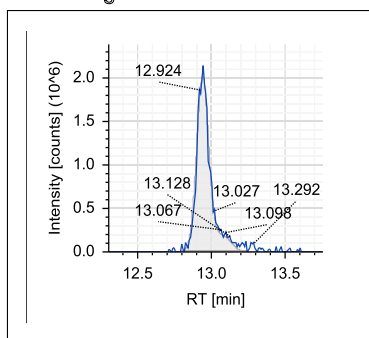
Attributed Reaction from the Parent Compound to this TP

Several reaction paths are *possible* that could have formed this TP, namely a hydroxylation followed by an oxidation to a carbonyl, a hydroxylation and a desaturation reaction, an N-hydroxylation followed by a reaction to a nitron, an α -C-oxidation to an amide, or a N-deethylation followed by an N-acetylation. However, for the related TP FEN_246.1101_16.1 the latter two reaction paths are more likely.

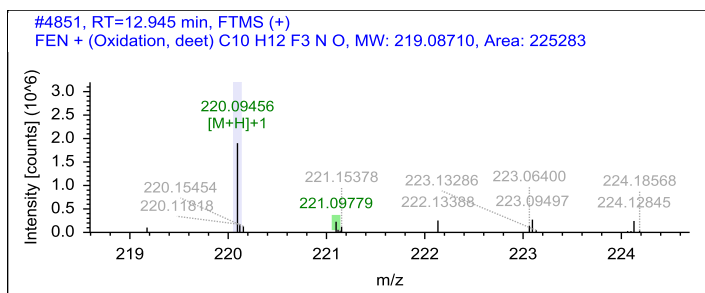
Appendix B

Name FEN_220.0944_12.9

Chromatogram

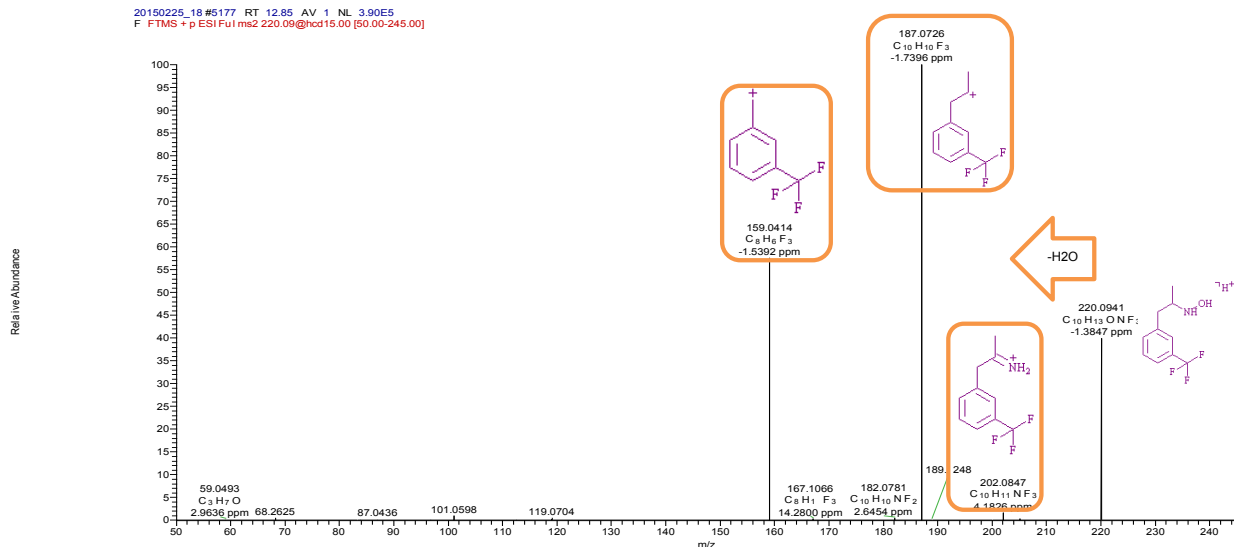


MS Spectra



MS2 Spectra

20150225_18 #5177 RT 12.85 AV 1 NL 3.90E5
F FTMS + p ESI/Ful ms2 220.09@hcd15.00 [50.00-245.00]



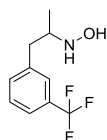
Formula

C₁₀H₁₂F₃N O

Atomic Modification

-C₂H₄, +O

Proposed Structure



Additional Evidence for Structure Interpretation

The MS2 fragments at the nominal masses 159 and 187 were also observed for the parent compound and indicate that the trifluoropropyl structure is a substructure of this TP. The atomic modification from elemental formula of the parent compound to this TP is -C₂H₄ +O. Therefore, it is likely that the ethyl moiety that was connected to the nitrogen was lost. Additionally, an oxygen was added. The neutral loss of H₂O indicates a hydroxyl moiety. The exact position of the hydroxyl group remains unknown. However, since the fragments at the nominal mass of 159 and 187 are unaltered as for the parent compound, it is likely that the hydroxyl group was added to the nitrogen.

Attributed Reaction from the Parent Compound to this TP

It is *likely* that this TP was formed in two steps via an N-deethylation followed by an N-hydroxylation reaction or vice versa.

Confidence Level

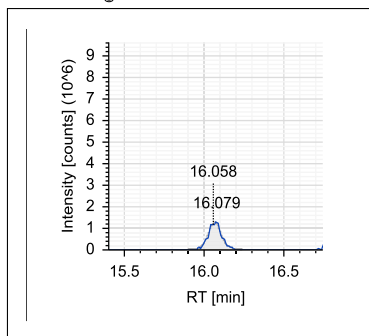
Level 3,
proposed structure

MassBank ID

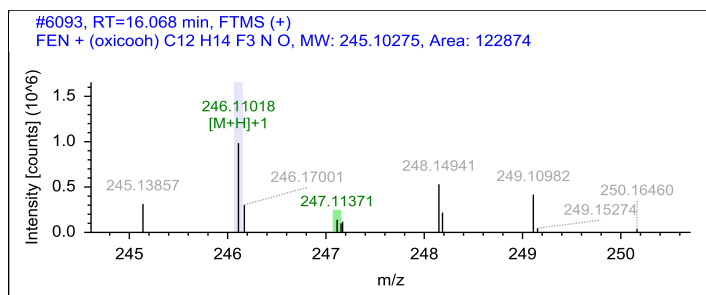
ET060301-ET060306

Name FEN_246.1101_16.1

Chromatogram

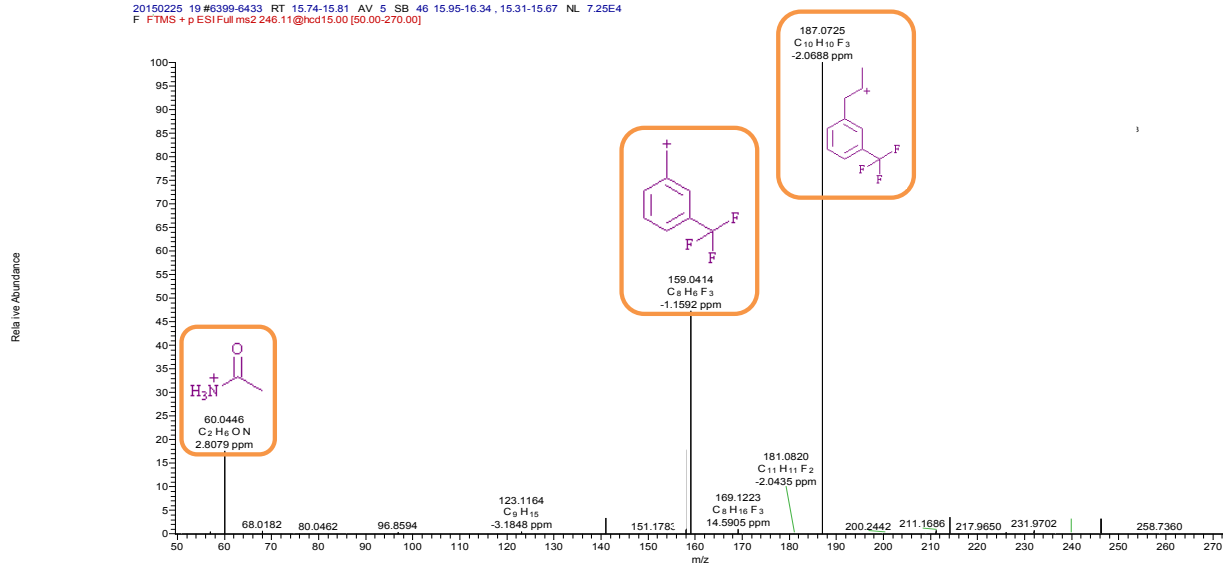


MS Spectra



MS2 Spectra

20150225 19 86398-6433 RT 15.74-15.81 AV 5 SB 48 15.95-16.34, 15.31-15.67 NL 7.25E4
F FTMS + p ESI Full ms2 246.11@hcd15.00 [50.00-270.00]



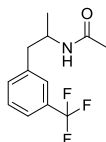
Formula

C₁₂ H₁₄ F₃ N O

Atomic Modification

-H₂, +O

Proposed Structure



Additional Evidence for Structure Interpretation

The MS2 fragments at the nominal masses 159 and 187 were also observed for the parent compound and indicate that the trifluoropropyl structure is a substructure of this TP. The atomic modification from elemental formula of the parent compound to this TP is -H₂ +O. The MS2 fragment at the nominal mass 60 indicates that this modification took place at the ethylamine moiety.

There is a corresponding TP with the same mass but a different retention time, namely FEN_246.1101_16.9. It shows the same MS2 fragments as this TP, but possesses also some additional ones with different intensity distribution. Due to the similarity of this MS2 spectrum to the one of the parent, it is more likely that this TP was modified at the N-substituent rather than at the trifluorophenylpropyl part of the molecule.

Attributed Reaction from the Parent Compound to this TP

It is *possible* that this TP was formed via an α -C-oxidation to an acetamide or an N-deethylation followed by an N-acetylation reaction or vice versa.

Confidence Level

Level 3,
proposed structure

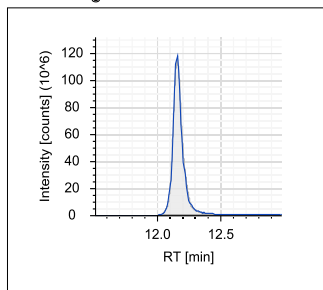
MassBank ID

ET060401-ET060406

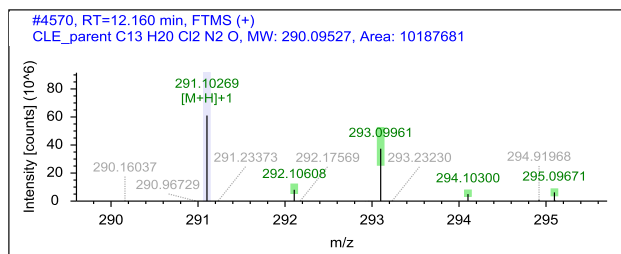
B.4.17 Structural evidence for clenisopenterol and its TPs

Name CLE_291.1026_12.2, parent

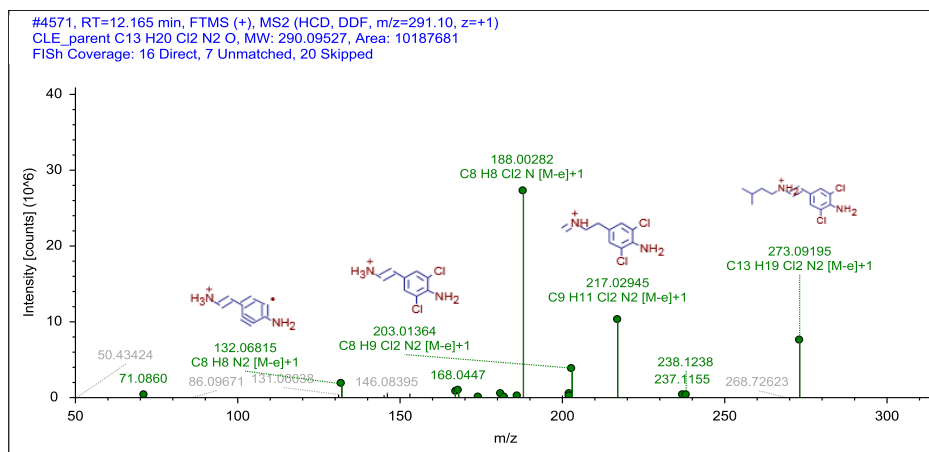
Chromatogram



MS Spectra



MS2 Spectra



Formula

C13 H20 Cl2 N2 O

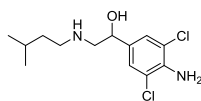
Additional Evidence for Structure Interpretation

This is the structural evidence that was observed for the parent compound CLE.

Atomic Modification

none

Proposed Structure



Confidence Level

Level 1

reference standard

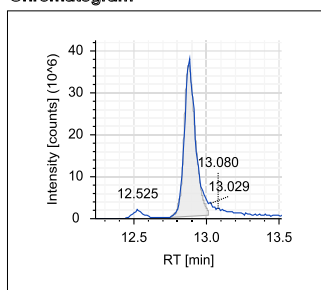
MassBank ID

ET020001-ET020005

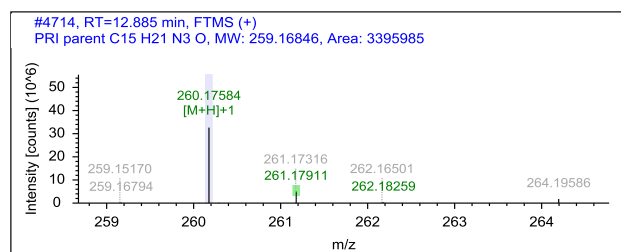
B.4.18 Structural evidence for primaquine and its TPs

Name PRI_260.1759_12.9, parent

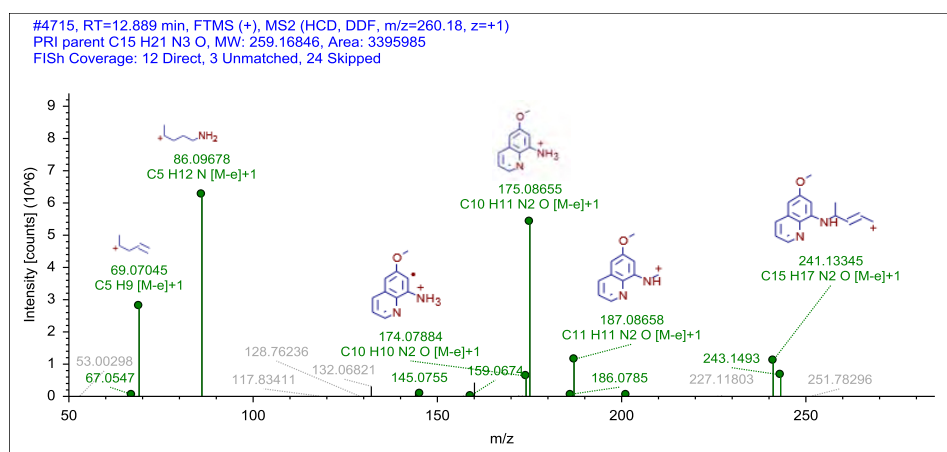
Chromatogram



MS Spectra



MS2 Spectra



Formula

C₁₅H₂₁N₃O

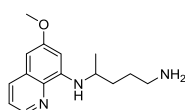
Additional Evidence for Structure Interpretation

This is the structural evidence that was observed for the parent compound PRI.

Atomic Modification

none

Proposed Structure



Confidence Level

Level 1,

reference standard

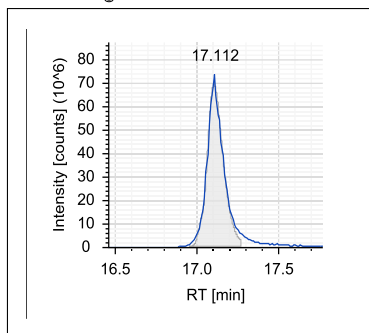
MassBank ID

ET160001-ET160005

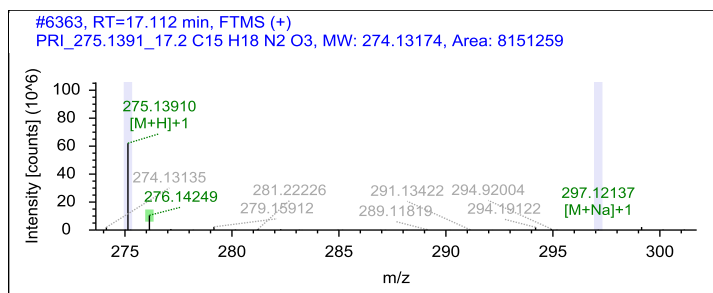
Appendix B

Name PRI_275.1391_17.2

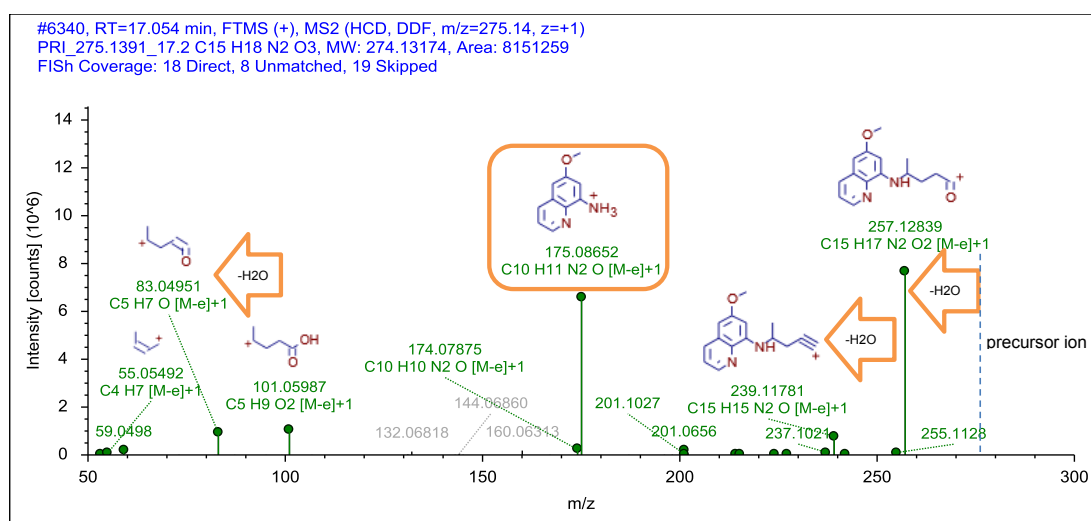
Chromatogram



MS Spectra



MS2 Spectra



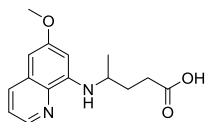
Formula

C₁₅H₁₈N₂O₃

Atomic Modification

-NH₃, +O₂

Proposed Structure



Confidence Level

Level 3,
proposed structure

MassBank ID

ET160101-ET160106

Additional Evidence for Structure Interpretation

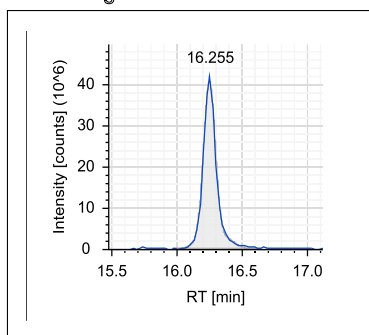
The MS2 fragment at the nominal mass 175 was also observed for the parent compound and indicates that the corresponding aromatic structure is a substructure of this TP. The neutral loss of H₂O as well as a matching signal in the MS in negative mode (273.1243, C₁₅H₁₇O₃N₂, Δm=3.5920 ppm) indicate a carboxylic acid moiety.

Attributed Reaction from the Parent Compound to this TP

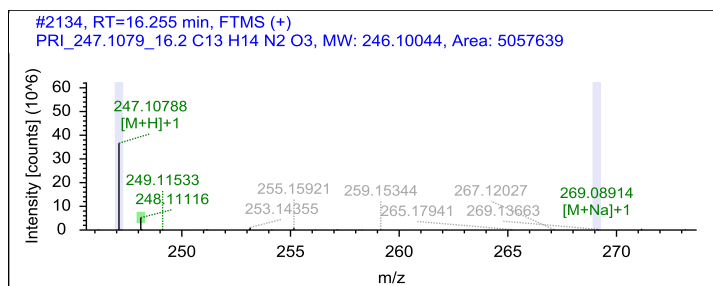
It is *likely* that this TP was formed via a deamination followed by a oxidation to a carboxylic acid.

Name PRI_247.1079_16.2

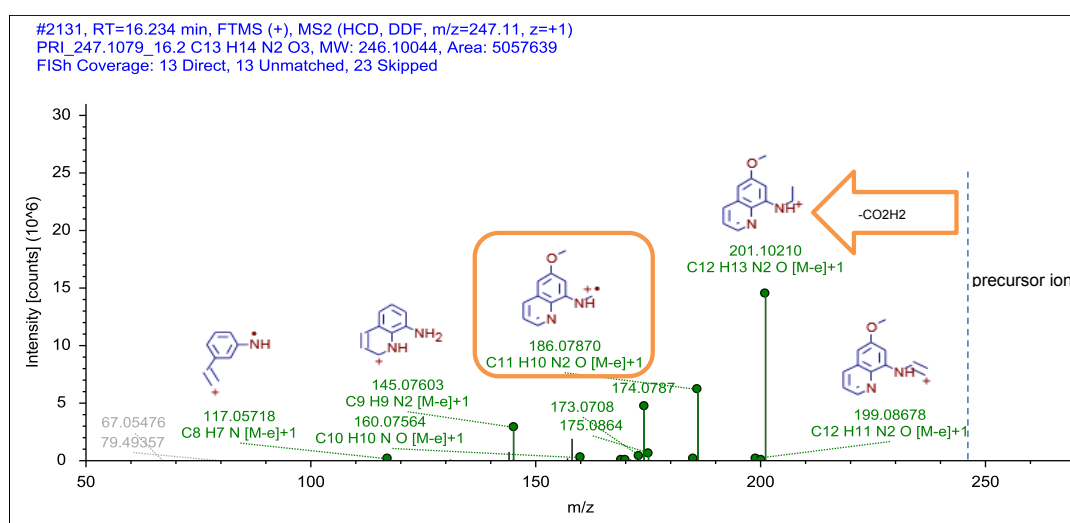
Chromatogram



MS Spectra



MS2 Spectra



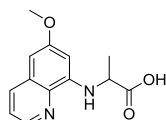
Formula

C13 H14 N2 O3

Atomic Modification

-C2H7N, +O2

Proposed Structure



Additional Evidence for Structure Interpretation

The MS2 fragment at the nominal mass 186 was also observed for the parent compound and indicates that the corresponding aromatic structure is a substructure of this TP. The neutral loss of CO₂H₂ as well as a matching signal in the MS in negative mode (245.0929, C₁₃H₁₃O₃N₂ Δm=3.3323 ppm) indicate a carboxylic acid moiety.

Attributed Reaction from the Parent Compound to this TP

It is *likely* that this TP was formed via a combination of deamination reaction, a successive oxidation to a carboxylic acid, and a β-oxidation.

Confidence Level

Level 3,
proposed structure

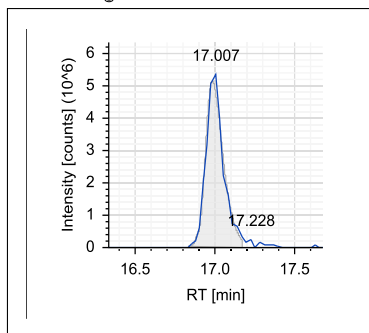
MassBank ID

ET160201-ET160206

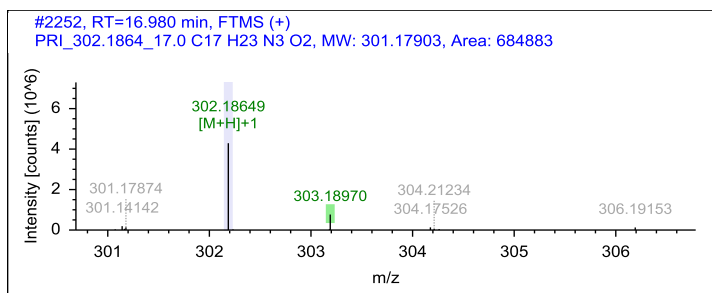
Appendix B

Name PRI_302.1864_17.0

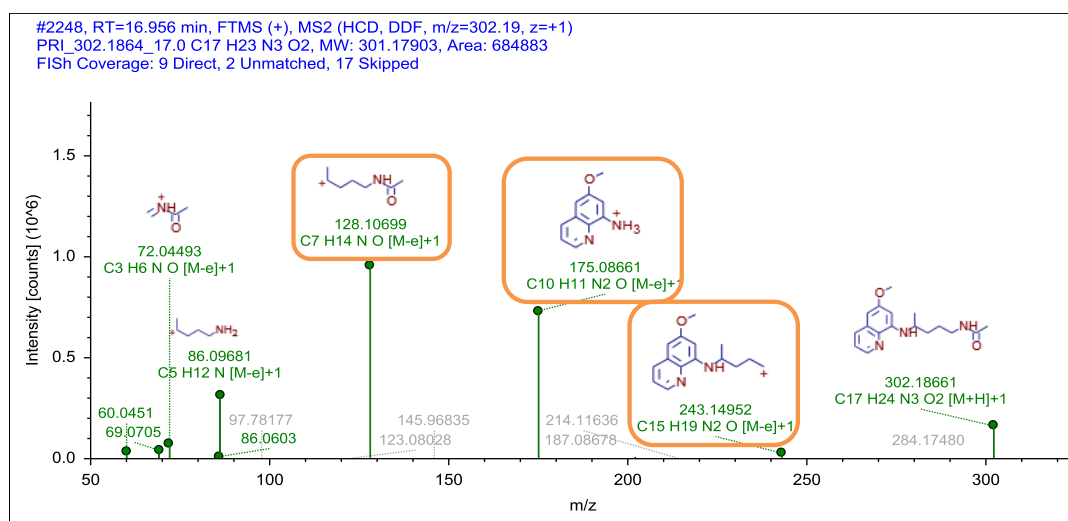
Chromatogram



MS Spectra



MS2 Spectra



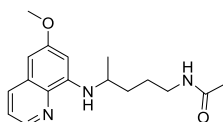
Formula

C17 H23 N3 O2

Atomic Modification

+C2H2O

Proposed Structure



Confidence Level

Level 3,
proposed structure

MassBank ID

ET160401

Additional Evidence for Structure Interpretation

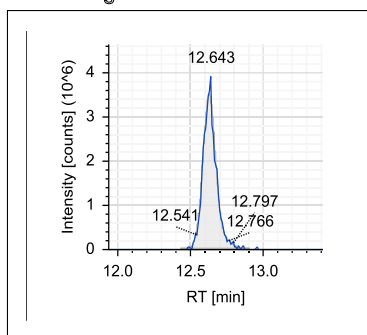
The MS2 fragments at the nominal masses 175 and 243 were also observed for the parent compound and indicate that the corresponding structure is a substructure of this TP. The atomic modification from the elemental formula of the parent compound to this TP is +C2H2O. The MS2 fragment at the nominal mass 128 indicates that the modification occurred at the pentyl amine moiety.

Attributed Reaction from the Parent Compound to this TP

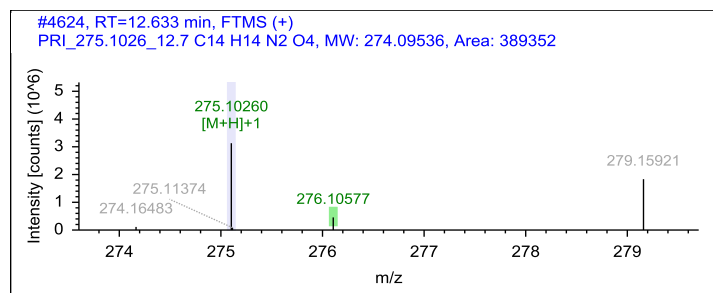
It is *likely* that this TP was formed via N-acetylation.

Name PRI_275.1026_12.7

Chromatogram

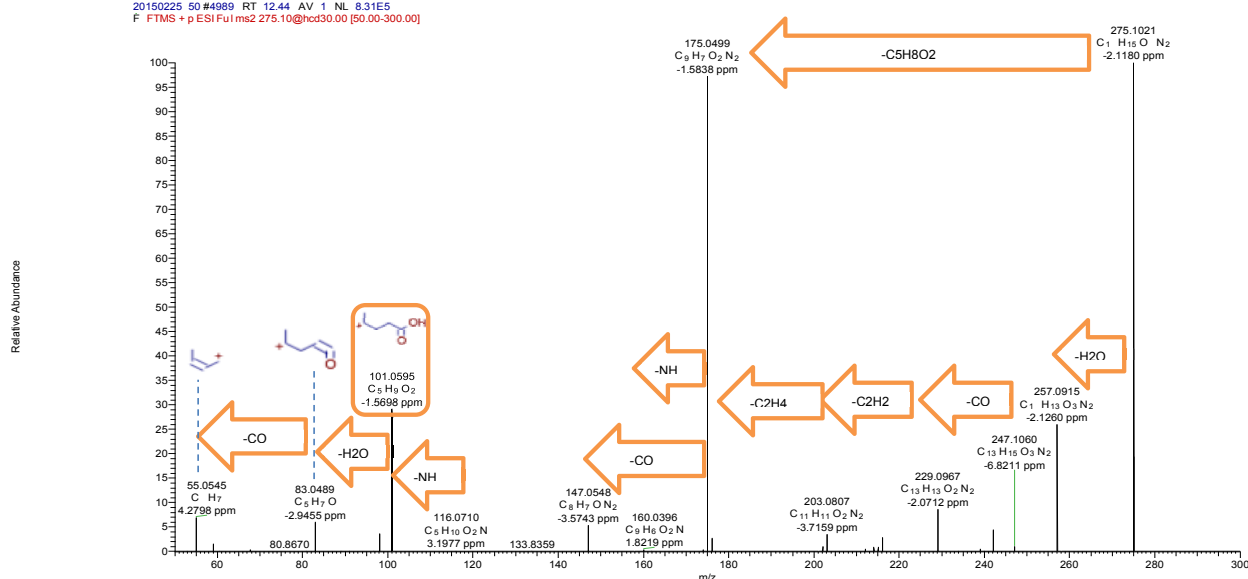


MS Spectra



MS2 Spectra

20150225 50 #4989 RT 12.44 AV 1 NL 8.31E5
F: FTMS + p ESI Full ms2 275.10@hcd30.00 [50.00-300.00]



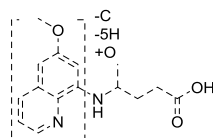
Formula

C14 H14 N2 O4

Atomic Modification

-CH7N, +O3

Proposed Structure



Additional Evidence for Structure Interpretation

The MS2 fragments at the nominal masses 55, 83, and 101 were also observed for the TP PRI_275.1391_17.2. There they represent a pentanoic acid moiety that is attached to the aromatic amine moiety. This indicates the presence of a pentanoic acid for this TP, which also corresponds to the neutral loss of C5H8O2. The neutral loss of H2O and CO2H2 as well as a matching signal in the MS in negative mode (273.0880, C14H13O4N2, $\Delta m = 3.6515$ ppm) give additional evidence for a carboxylic acid. However, for the rest of the molecular structure which corresponds to the MS2 fragment at the nominal mass 175 and therefore consists of C9H7O2N2, no structure can be assigned.

Attributed Reaction from the Parent Compound to this TP

The reaction that formed this TP remains *unknown*.

Confidence Level

Level 3,

TP class

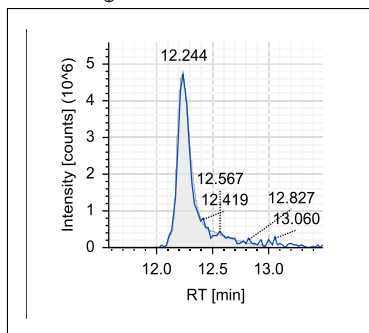
MassBank ID

ET160601-ET160606

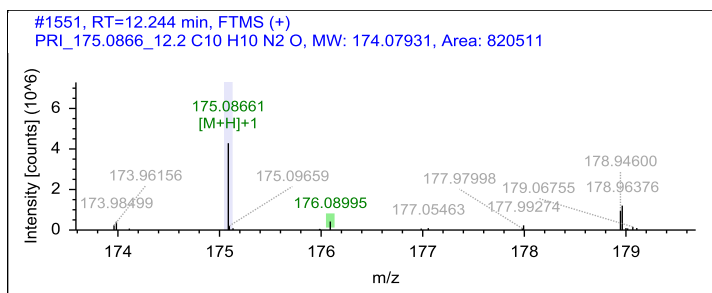
Appendix B

Name PRI_175.0866_12.2

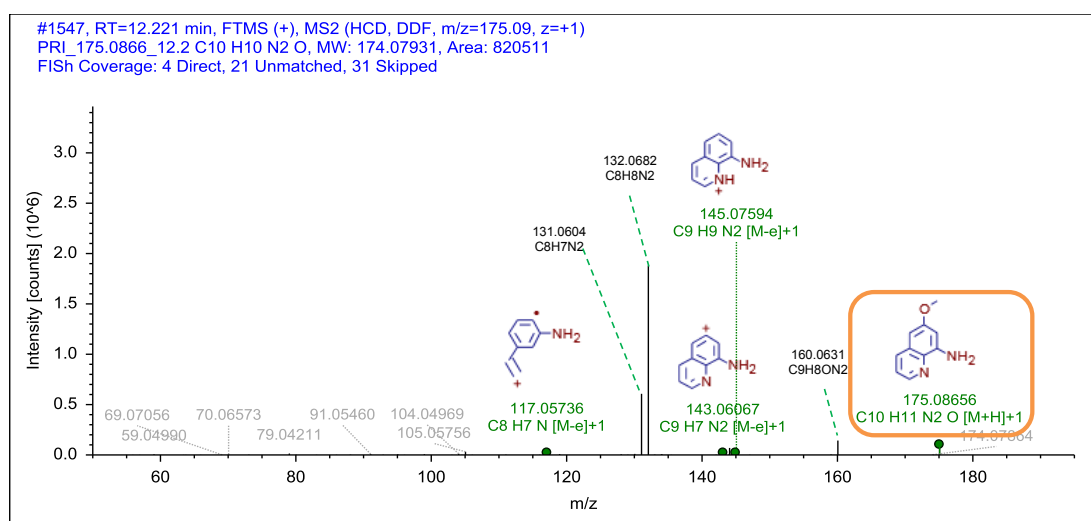
Chromatogram



MS Spectra



MS2 Spectra



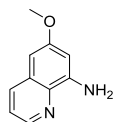
Formula

C₁₀ H₁₀ N₂ O

Atomic Modification

-C₅H₁₁N

Proposed Structure



Additional Evidence for Structure Interpretation

The MS2 fragments at the nominal masses 131, 132, 145, 160, and 175 were also observed for the parent compound and indicate that the structure of this TP is a substructure of the parent compound. The structural evidence for this TP structure is diagnostic.

Attributed Reaction from the Parent Compound to this TP

It is *certain* that this TP was formed via an N-dealkylation of the α -branched ω -amino alkyl chain.

Confidence Level

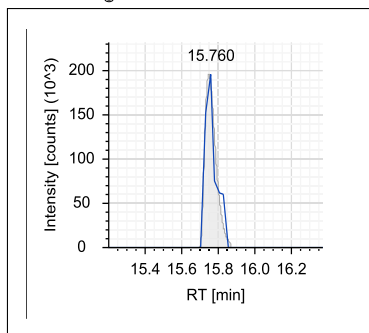
Level 2b,
diagnostic evidence

MassBank ID

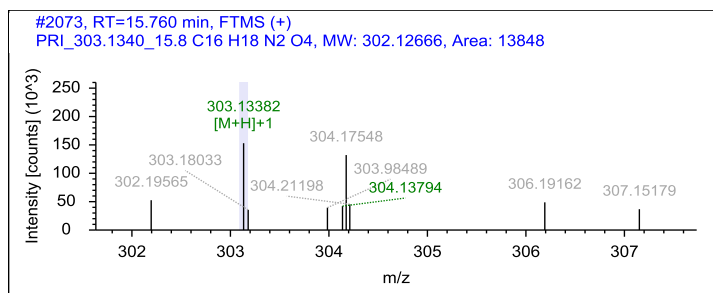
ET160301

Name PRI_303.1340_15.8

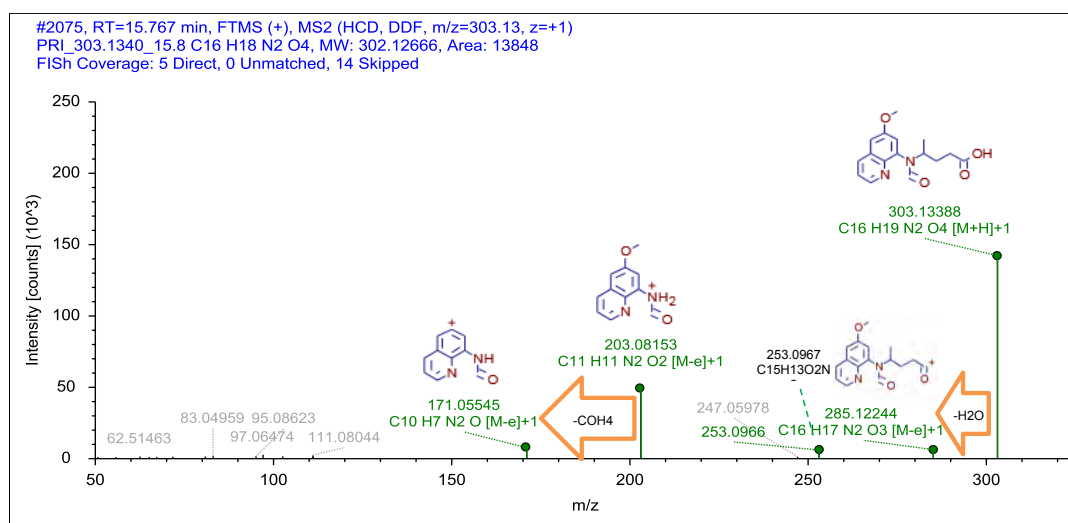
Chromatogram



MS Spectra



MS2 Spectra



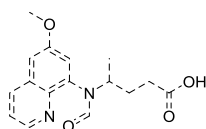
Formula

C16 H18 N2 O4

Atomic Modification

-NH3, +CO3

Proposed Structure



Confidence Level

Level 3,
proposed structure

MassBank ID

ET161201-ET161206

Additional Evidence for Structure Interpretation

An additional MS2 fragment with the exact mass of 101.0595 (C5H9O2, $\Delta m = -2.0228$ ppm) was observed in an MS2 spectrum that was measured with a collision energy of 45. It was also observed for the TP PRI_275.1391_17.2 and indicates a pentanoic acid moiety. (No matching signal was observed in the MS spectrum in negative mode. However, due to the low intensity of the peak and the lower sensitivity in negative mode, this does not exclude the possibility of a carboxylic acid moiety.) In addition to this modification, the elemental formula suggests a modification of +CO.

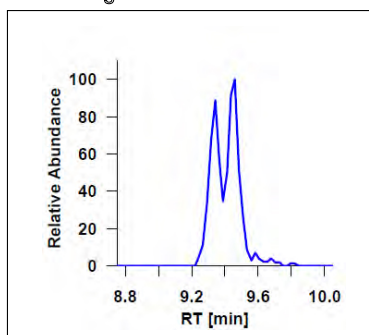
Attributed Reaction from the Parent Compound to this TP

It is *likely* that this TP was formed via a deamination of the primary amine followed by an oxidation to a carboxylic acid and an N-formylation of the secondary amine or vice versa.

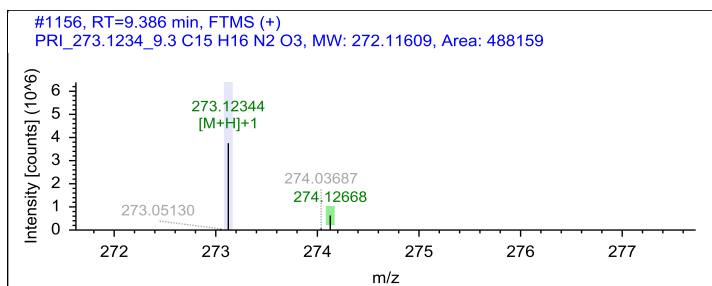
Appendix B

Name PRI_273.1234_9.3

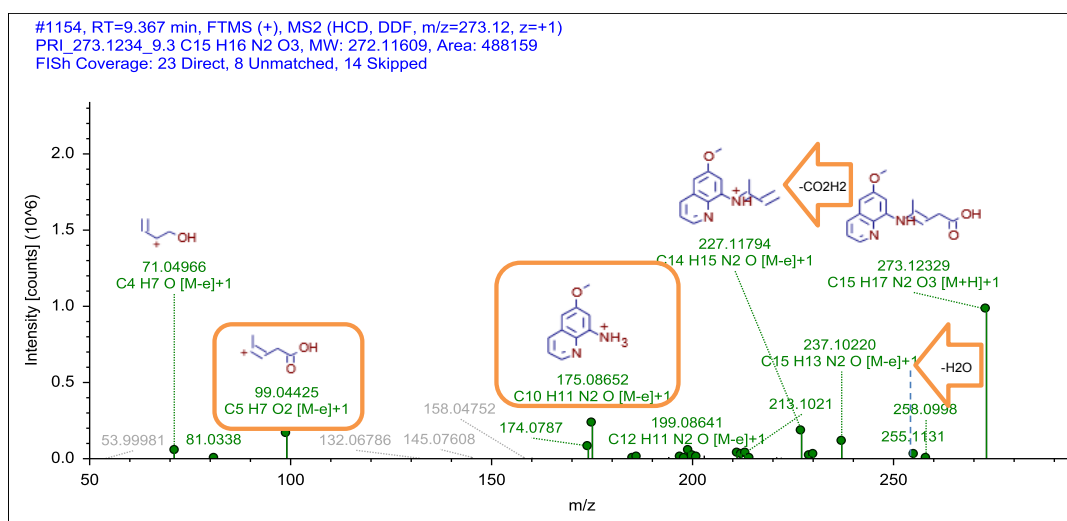
Chromatogram



MS Spectra



MS2 Spectra



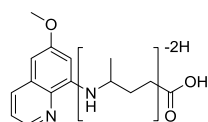
Formula

C15 H16 N2 O3

Atomic Modification

-NH5, +O2

Proposed Structure



Additional Evidence for Structure Interpretation

The atomic modification from elemental formula of the parent compound to this TP is -NH5 +O2. This is the same modification as to the TP PRI_275.1391_17.2 with an additional -H2. For PRI_275.1391_17.2, it is likely that a deamination of the primary amine and a successive oxidation to an carboxylic acid occurred. The MS2 fragment at the nominal mass 175 was observed for PRI_275.1391_17.2 as well as for the parent compound and indicates that the basic aromatic structure is a substructure of this TP. For PRI_275.1391_17.2 an MS2 fragment at the nominal mass 101 (C5H9O2) was observed that corresponds to the MS2 fragment of this TP at the nominal mass 99, which has two hydrogen atoms less. This indicates a desaturated pentanoic acid moiety. Additional evidence for this structural hypothesis is a matching signal in the MS in negative mode at the exact mass 271.1091 (C15H15N2O6, $\Delta m = 1.1627$ ppm) and the neutral losses of H2O and CO2H2. It is possible that the double peak shape originates from a cis-trans isomerism. The exact position of the desaturation remains unknown. The structures of the MS2 fragments are drawn exemplarily.

Attributed Reaction from the Parent Compound to this TP

It is *possible* that this TP was formed via a deamination of the primary amine followed by an oxidation to a carboxylic acid and a desaturation reaction or a oxidation of the secondary amine to an imine. A desaturation that resulted in a double bond between the carbon atoms in α - and β -position to the carboxylic acid is likely since it is an intermediate of a β -oxidation reaction, which was also observed (PRI_247.1079_16.2).

Confidence Level

Level 3,

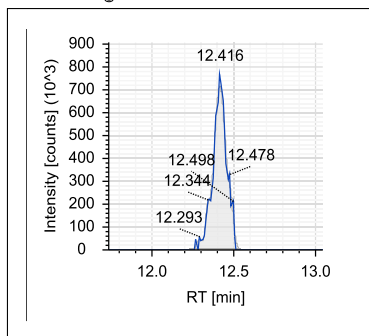
TP class

MassBank ID

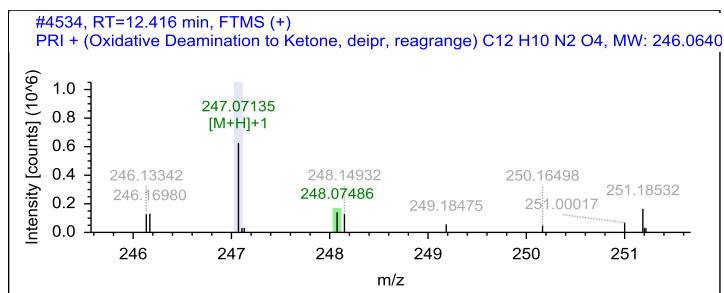
ET160501-ET160506

Name PRI_247.0714_12.4

Chromatogram



MS Spectra



MS2 Spectra

There is no MS2 spectrum available, since it was not triggered during the original measurement and the peak was no longer present at the time of the remeasurement.

Formula

C₁₂H₁₀N₂O₄

Atomic Modification

-C₃H₁₁N, +O₃

Proposed Structure

Additional Evidence for Structure Interpretation

A matching signal in the MS spectrum in negative mode at the exact mass 245.0566 (C₁₂H₉N₂O₄, 3.5953 ppm) indicates a carboxylic acid moiety. However, due to the missing MS2 spectrum it is not possible to propose a structure.

Attributed Reaction from the Parent Compound to this TP

The reaction that formed this TP remains *unknown*.

Confidence Level

Level 4,
molecular formula

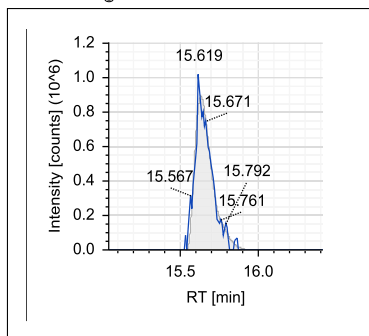
MassBank ID

NA

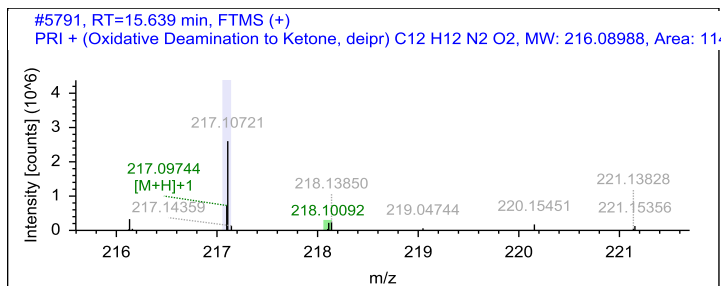
Appendix B

Name PRI_217.0974_15.7

Chromatogram



MS Spectra



MS2 Spectra

There is no MS2 spectrum available, since it was not triggered during the original measurement and the peak was no longer present at the time of the remeasurement.

Formula

C₁₂H₁₂N₂O₂

Atomic Modification

-C₃H₉N, +O

Additional Evidence for Structure Interpretation

Due to the lack of an MS2 spectrum it is not possible to propose a structure.

Attributed Reaction from the Parent Compound to this TP

The reaction that formed this TP remains *unknown*.

Proposed Structure

Confidence Level

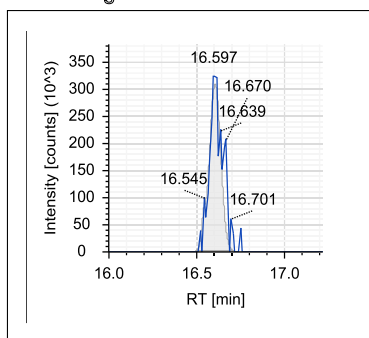
Level 4,
molecular formula

MassBank ID

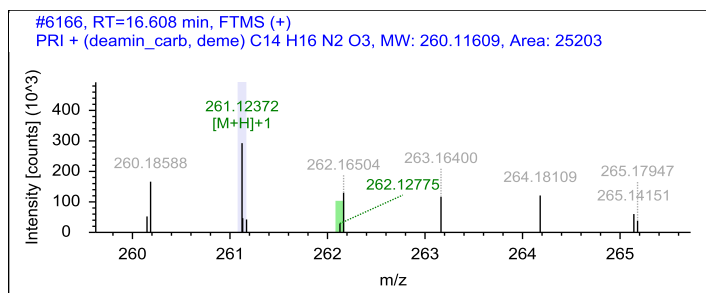
NA

Name PRI_261.1236_16.6

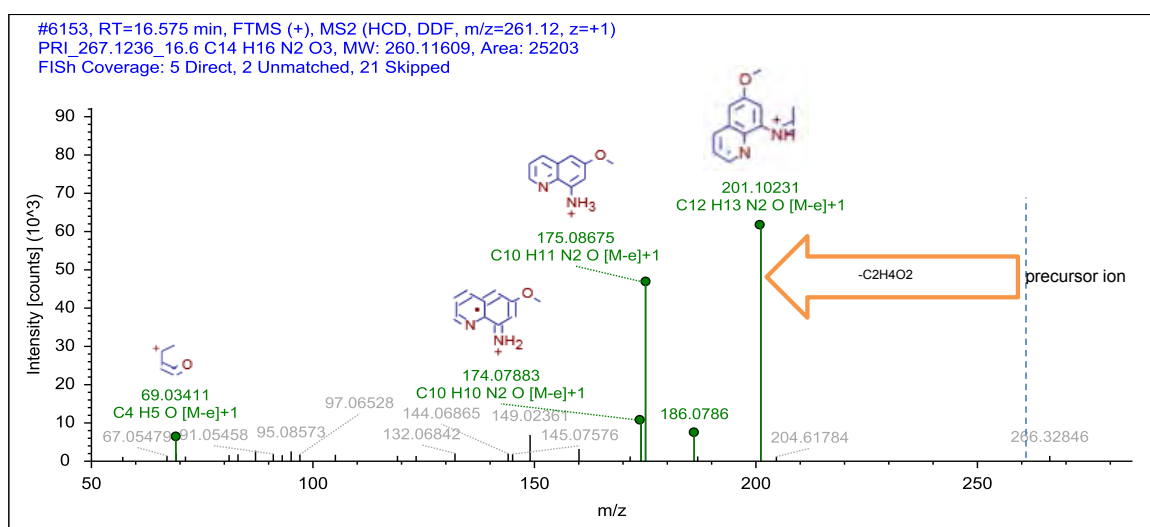
Chromatogram



MS Spectra



MS2 Spectra



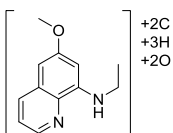
Formula

C₁₄ H₁₆ N₂ O₃

Atomic Modification

-CH₅N, +O₂

Proposed Structure



Additional Evidence for Structure Interpretation

The MS2 fragments at the nominal masses 175, 186, and 201 were also observed for the parent compound in an MS2 spectrum that was measured with a collision energy of 60. They indicate that the structure that is shown for the MS2 fragment at the nominal mass 201 is a substructure of this TP. No matching signal was observed in the MS spectrum in negative mode. However, due to the low intensity of the peak and the lower sensitivity of the negative mode, this does not exclude the presence of a carboxylic acid moiety. The neutral loss between the M+H ion and the MS2 fragment at the nominal mass 201 is C₂H₄O₂. This neutral loss could have been caused by an acetic acid. However, there is no additional evidence for that.

Attributed Reaction from the Parent Compound to this TP

The reaction that formed this TP remains *unknown*.

Confidence Level

Level 3,
TP class

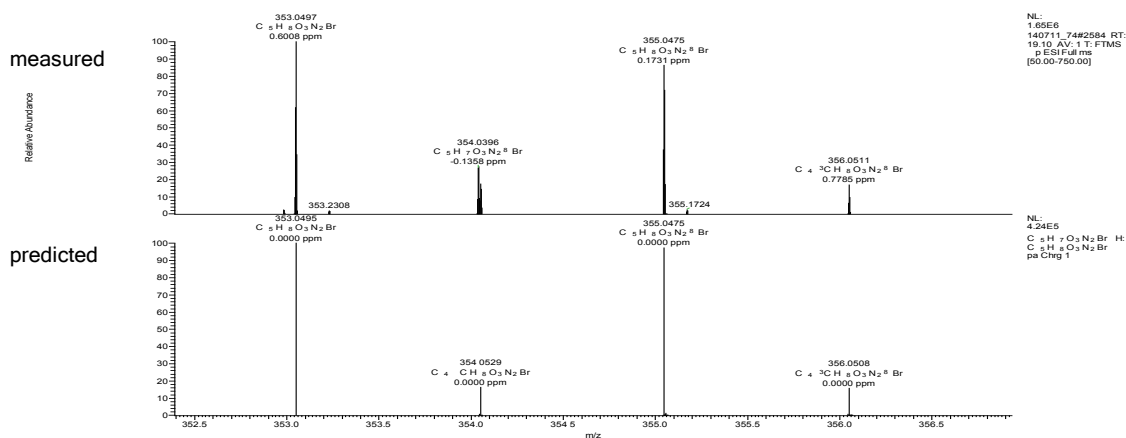
MassBank ID

ET161503

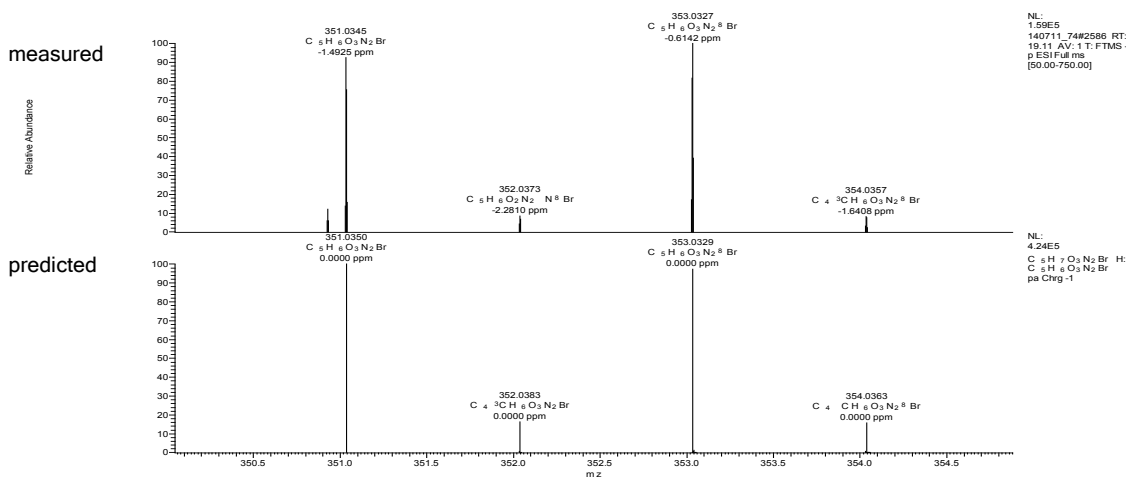
Appendix B

Name PRI_353.0497_19.1

MS Spectrum in positive mode



MS Spectrum in negative mode



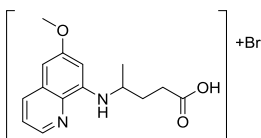
Formula

C₁₅H₁₇N₂O₃Br

Atomic Modification

-NH₄, +O₂Br

Proposed Structure



MS2 Spectra

There is no MS2 spectrum available, since it was not triggered during the original measurement and the peak was no longer present at the time of the remeasurement.

Additional Evidence for Structure Interpretation

The isotopic pattern clearly indicates the presence of a bromine in the elemental formula of this TP. The matching signal in the MS spectrum in negative mode indicates a carboxylic acid moiety.

Attributed Reaction from the Parent Compound to this TP

The reaction that formed this TP remains *unknown*.

Confidence Level

Level 3,
TP class

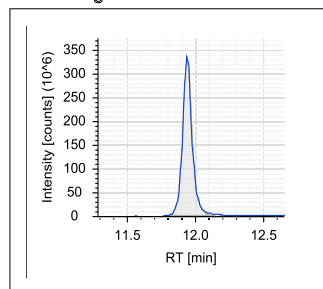
MassBank ID

NA

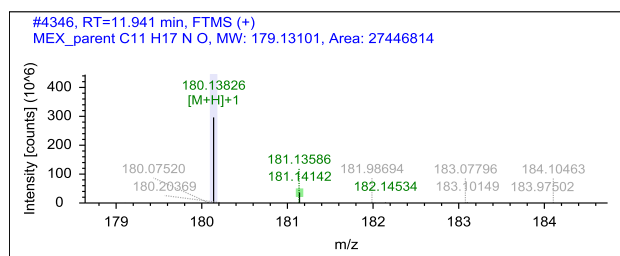
B.4.19 Structural evidence for mexiletine and its TPs

Name MEX_180.1383_11.9, parent

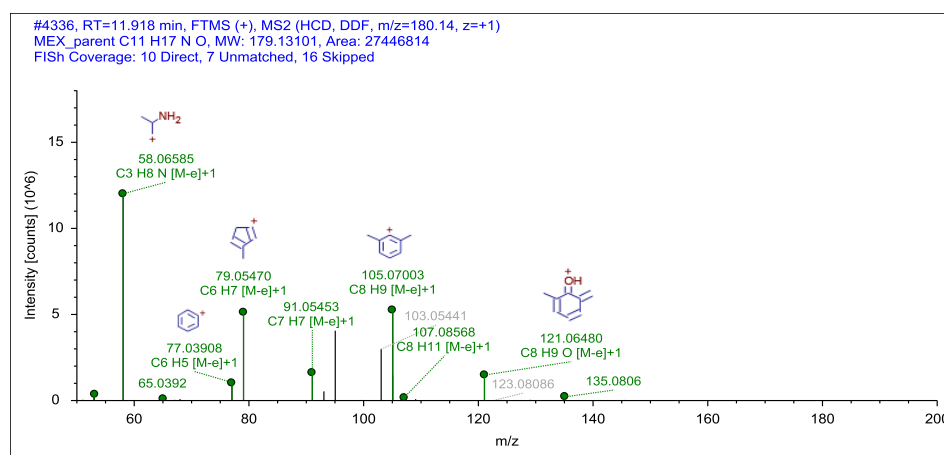
Chromatogram



MS Spectra



MS2 Spectra



Formula

C11 H17 N O

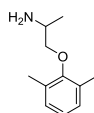
Additional Evidence for Structure Interpretation

This is the structural evidence that was observed for the parent compound MEX.

Atomic Modification

none

Proposed Structure



Confidence Level

Level 1,
reference standard

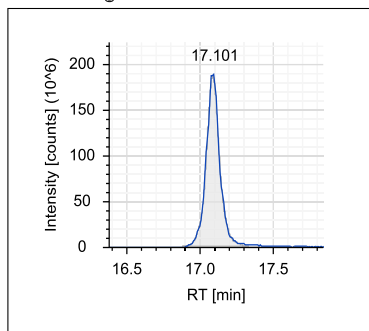
MassBank ID

ET090001-ET090005

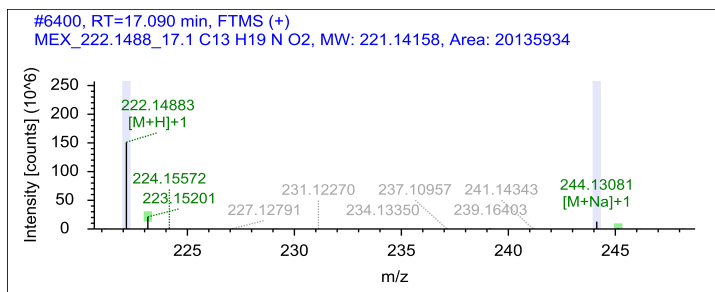
Appendix B

Name MEX_222.1488_17.1

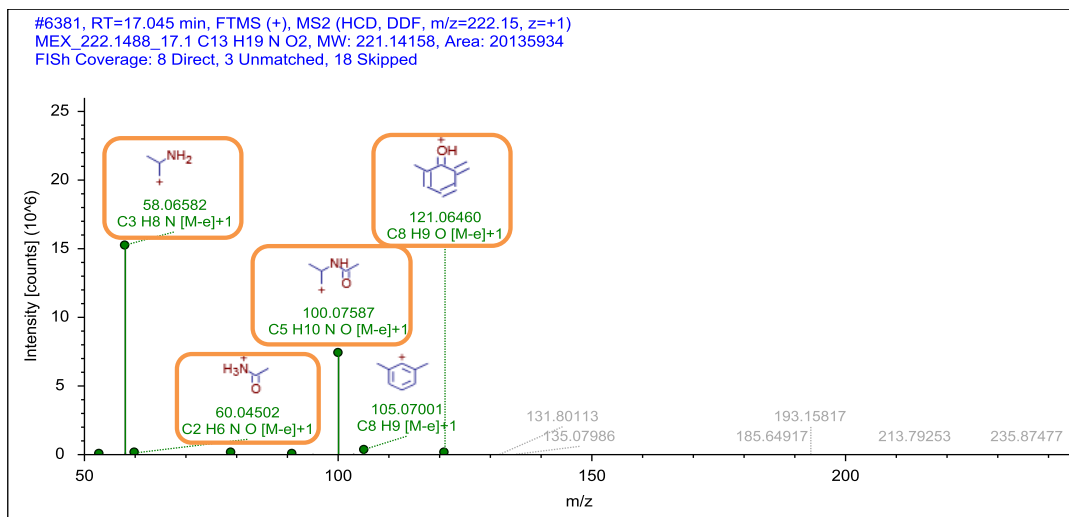
Chromatogram



MS Spectra



MS2 Spectra

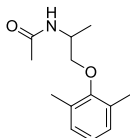


Formula

C13 H19 N O2

Atomic Modification
+C2H2O

Proposed Structure



Additional Evidence for Structure Interpretation

The MS2 fragments at the nominal masses 58, 105, and 121 were also observed for the parent compound. In an MS2 spectrum measured with a collision energy of 15, an additional MS2 fragment was observed at the exact mass of 180.1378 (C11H18NO, $\Delta m = -2.4583$ ppm) that was also observed in an MS2 spectrum for the parent compound measured at the same collision energy. This fragment represents the $[M+H]^+$ ion of the parent compound and indicates, together with the previously mentioned fragments, that the parent structure is a substructure of this TP. The modification of the elemental formula of the parent compound to this TP is +C2H2O. The MS2 fragments at the nominal masses 60 and 100 indicate that the modification took place at the nitrogen atom.

Attributed Reaction from the Parent Compound to this TP

It is *likely* that this TP was formed via an N-acetylation reaction.

Confidence Level

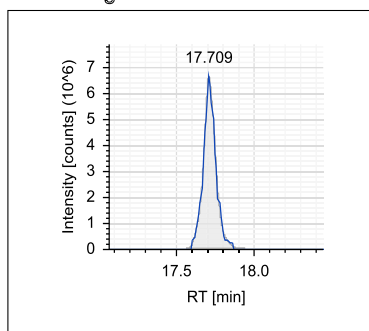
Level 3
proposed structure

MassBank ID

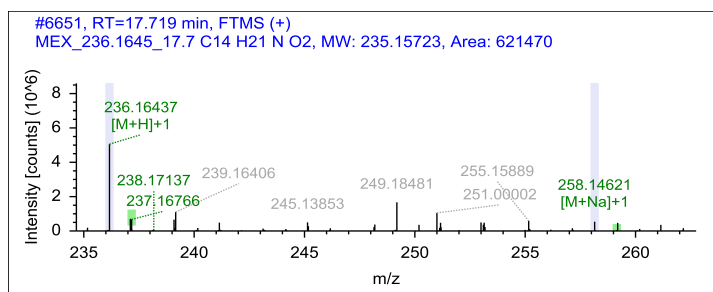
ET090101-ET090106

Name MEX_236.1645_17.7

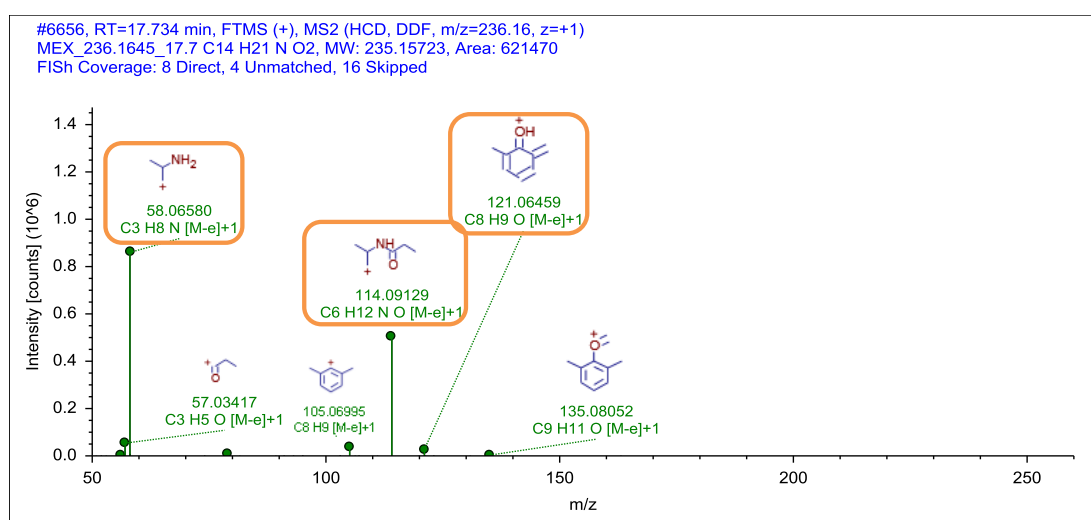
Chromatogram



MS Spectra



MS2 Spectra



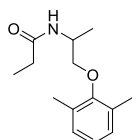
Formula

C14 H21 N O2

Atomic Modification

+C3H4O

Proposed Structure



Additional Evidence for Structure Interpretation

The MS2 fragments at the nominal masses 58, 105, 121 and 135 were also observed for the parent compound. In an MS2 spectrum measured with a collision energy of 15, an additional MS2 fragment was observed at the exact mass of 180.1378 (C11H18NO, $\Delta m = -2.5430$ ppm) that was also observed in an MS2 spectrum for the parent compound measured at the same collision energy. This fragment represents the [M+H]⁺ ion of the parent compound and indicates, together with the previously mentioned fragments, that the parent structure is a substructure of this TP. The modification of the elemental formula of the parent compound to this TP is +C3H4O. The MS2 fragment at the nominal mass 114 and an MS2 fragment observed at a collision energy of 60 with the exact mass of 74.0600 (C3H8ON, $\Delta m = 0.0391$ ppm) indicate that the modification took place at the nitrogen atom.

Attributed Reaction from the Parent Compound to this TP

It is *likely* that this TP was formed via an N-propionylation reaction.

Confidence Level

Level 3,
proposed structure

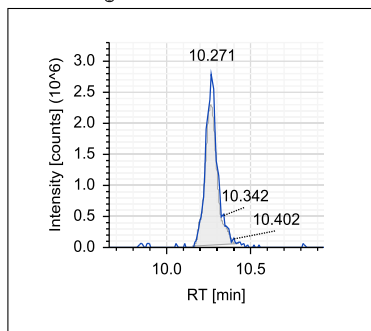
MassBank ID

ET090201-ET090206

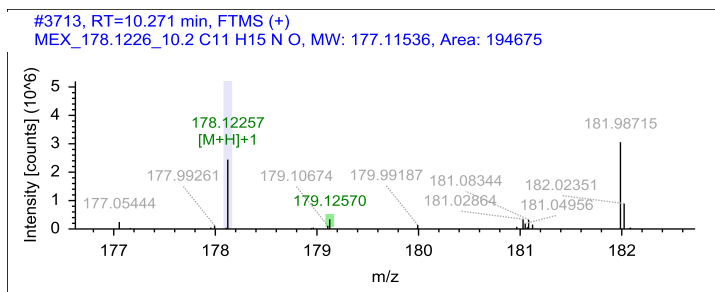
Appendix B

Name MEX_178.1226_10.2

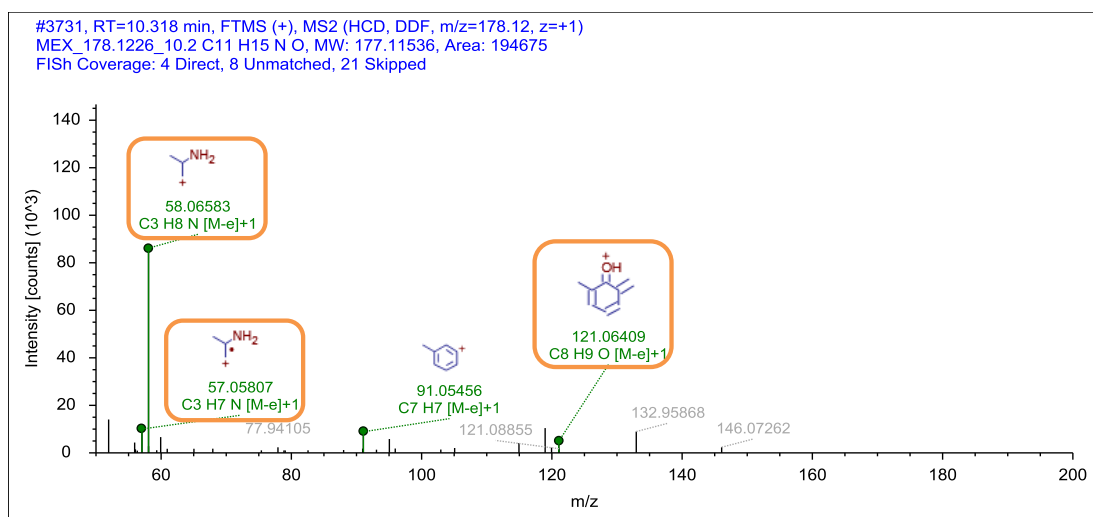
Chromatogram



MS Spectra



MS2 Spectra



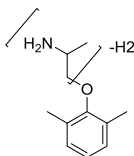
Formula

C11 H15 N O

Atomic Modification

-H2

Proposed Structure



Confidence Level

Level 3
TP class

MassBank ID

ET090601-ET090606

Additional Evidence for Structure Interpretation

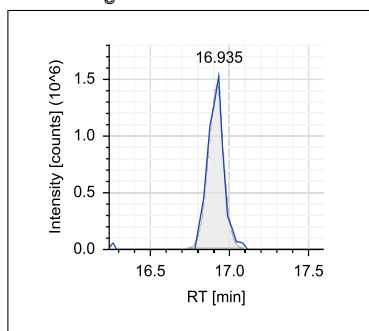
The MS2 fragment at the nominal mass 58 was also observed for the parent compound and indicates that the isopropylamine moiety is a substructure of this TP. The MS2 fragments at the nominal masses 91 and 121 were also observed for the parent compound and indicate that the 2,6-dimethylphenol moiety is a substructure of this TP. The modification of the elemental formula of the parent compound to this TP is -H2, indicating a desaturation. The MS2 fragment at the nominal mass 57 was not observed for the parent compound and indicates that the modification took place at the isopropylamine moiety.

Attributed Reaction from the Parent Compound to this TP

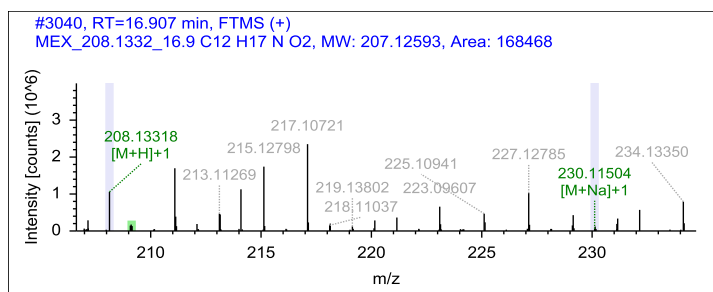
It is *possible* that this TP was formed via an desaturation reaction or a oxidation to an imine.

Name MEX_208.1332_16.9

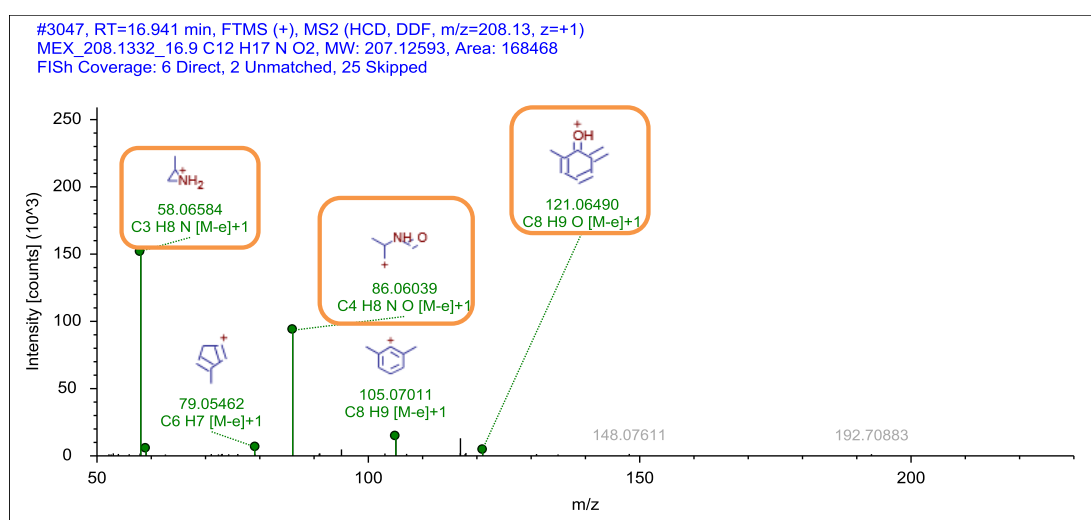
Chromatogram



MS Spectra



MS2 Spectra

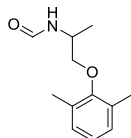


Formula

C12 H17 N O2

Atomic Modification
+CO

Proposed Structure



Confidence Level

Level 3

proposed structure

MassBank ID

ET090701-ET090706

Additional Evidence for Structure Interpretation

The MS2 fragments at the nominal masses 58, 105, and 121 were also observed for the parent compound. In an MS2 spectrum measured with a collision energy of 15, an additional MS2 fragment was observed at the exact mass of 180.1377 (C11H18NO, $\Delta m = -3.0513$ ppm) that was also observed in an MS2 spectrum for the parent compound measured at the same collision energy. This fragment represents the $[M+H]^+$ ion of the parent compound and indicates, together with the previously mentioned fragments, that the parent structure is a substructure of this TP. The modification of the elemental formula of the parent compound to this TP is +CO. The MS2 fragment at the nominal mass 86 indicates that the modification took place at the nitrogen atom.

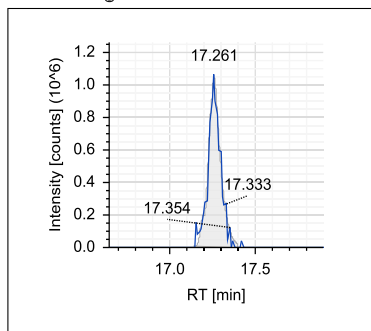
Attributed Reaction from the Parent Compound to this TP

It is *likely* that this TP was formed via an N-formylation reaction.

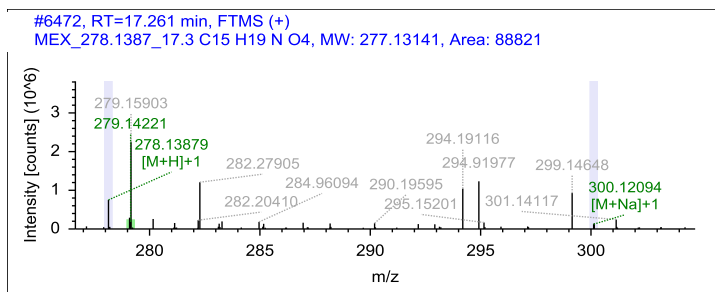
Appendix B

Name MEX_278.1387_17.3

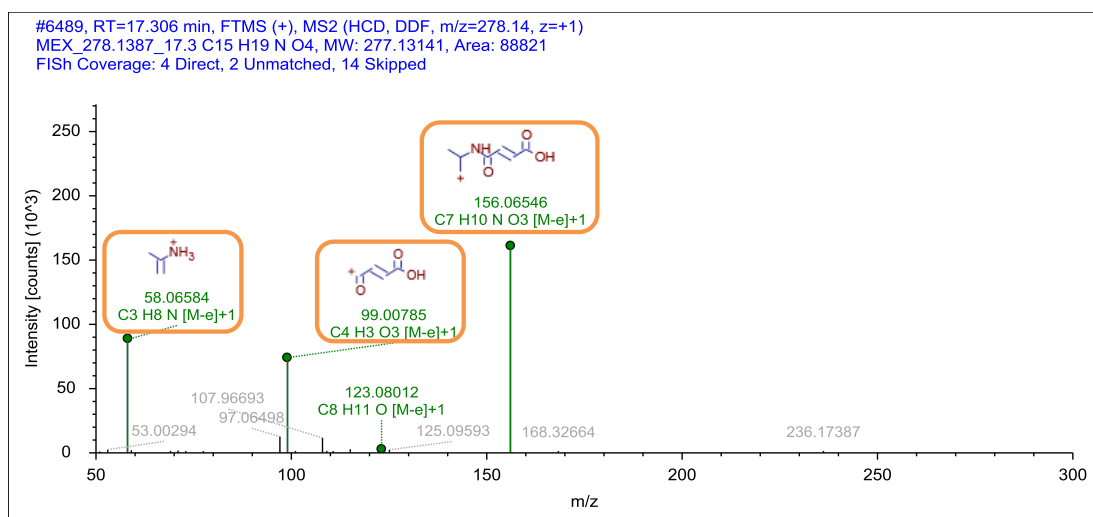
Chromatogram



MS Spectra



MS2 Spectra



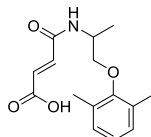
Formula

C15 H19 N O4

Atomic Modification

+C4H2O3

Proposed Structure



Additional Evidence for Structure Interpretation

The structure of this TP was confirmed by a synthesized reference standard. Details on the synthesis and the NMR measurement can be found in Chapter S5.

Attributed Reaction from the Parent Compound to this TP

It is *possible* that this TP was formed either via an N-fumarylation reaction or in two steps, namely an N-succinylation reaction followed by a desaturation reaction.

Confidence Level

Level 1

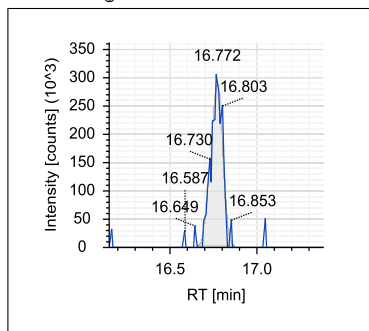
synthesized standard

MassBank ID

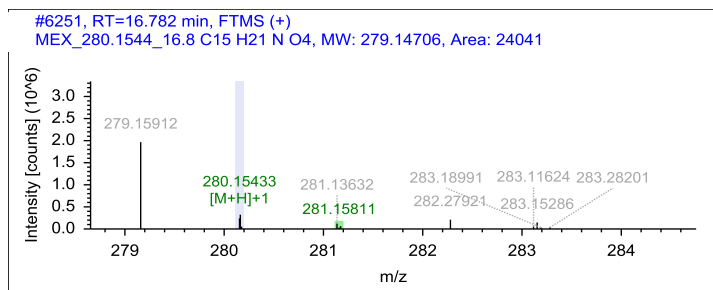
ET090801-ET090806

Name MEX_280.1544_16.8

Chromatogram

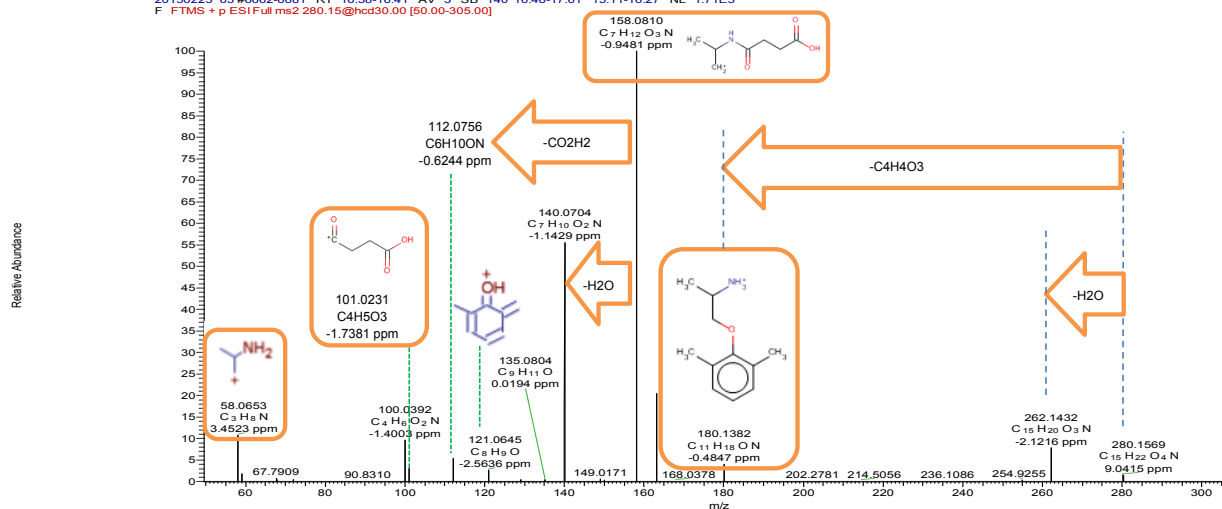


MS Spectra



MS2 Spectra

20150225 63 #6662-6681 RT 16.38-16.41 AV 3 SB 140 16.48-17.61 15.11-16.27 NL 1.71E5
F FTMS + p ESI Full ms2 280.15@hcd30.00 [50.00-305.00]

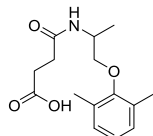


Formula

C15 H21 N O4

Atomic Modification
+C4H4O3

Proposed Structure



Additional Evidence for Structure Interpretation

The MS2 fragments at the nominal masses 58, 121, and 180 were also observed for the parent compound either in the shown MS2 spectrum or in one measured with a collision energy of 15. These fragments indicate that the parent structure is a substructure of this TP. The MS2 fragment at the nominal mass 101 and the neutral loss between the MS2 fragments at the nominal masses 280 and 180 indicate that all atoms of the modification of +C4H4O3 are connected. A matching signal in the MS spectra in negative mode (278.1398, C15H20O4N, $\Delta m = -0.2586$ ppm) as well as the neutral losses of -H2O and -CO2H2 indicate a carboxylic acid moiety. The MS2 fragment at the nominal mass 158 indicates that the modification took place at the isopropylamine moiety. An analogous N-succinylated TP was observed for OCP_297.1002_16.5, which was confirmed by a synthesized reference standard.

Attributed Reaction from the Parent Compound to this TP

It is *likely* that this TP was formed via an N-succinylation reaction.

Confidence Level

Level 3
proposed structure

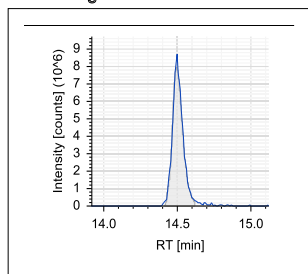
MassBank ID

ET090901-ET090906

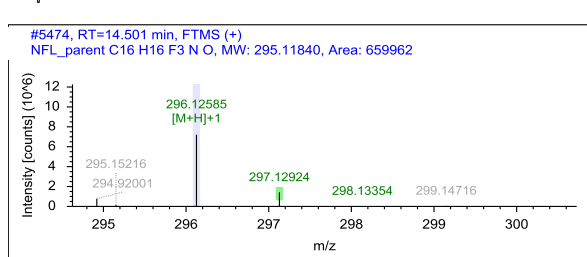
B.4.20 Structural evidence for N-demethylfluoxetine and its TPs

Name NFL_296.1257_14.5, parent

Chromatogram

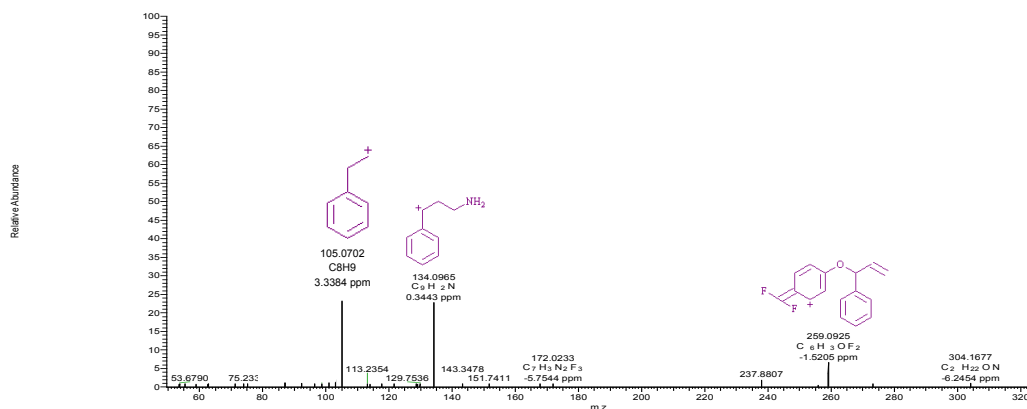


MS Spectra



MS2 Spectra

141021 22 #5781-5804 RT: 14.83-14.86 AV: 3 SB: 88 15.02-16.21, 14.01-14.39 NL: 4.71E4
F: FTMS p ESI Full ms2 296.13@ms300.00 [50.00-300.00]



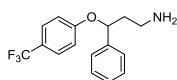
Formula

C₁₆H₁₆F₃N O

Atomic Modification

none

Proposed Structure



Additional Evidence for Structure Interpretation

This is the structural evidence that was observed for the parent compound NFL. Additionally, the MS2 fragment at the nominal mass 134 was also observed as in-source fragment in the MS spectrum with 22% of the area of the [M+H]⁺ ion. This indicates that the trifluoromethylphenol (loss of C₇H₅F₃O m=162.0295) moiety is readily cleaved in the ESI source.

Confidence Level

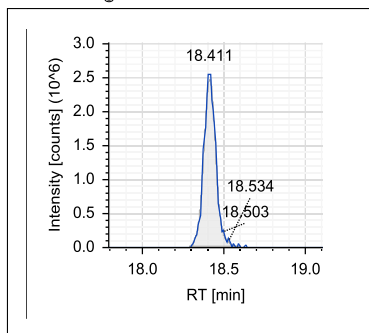
Level 1,
reference standard

MassBank ID

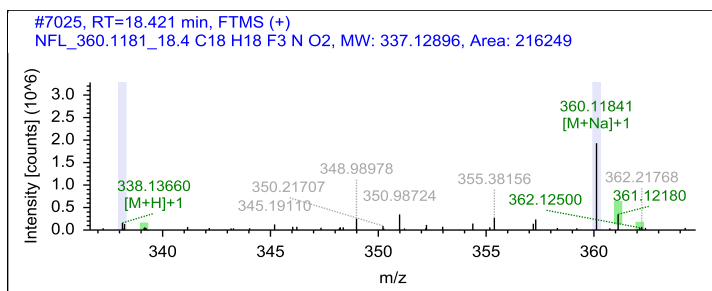
ET100001-ET100005

Name NFL_360.1181_18.4 sodium adduct (NFL_176.1069_18.4 in-source fragment)

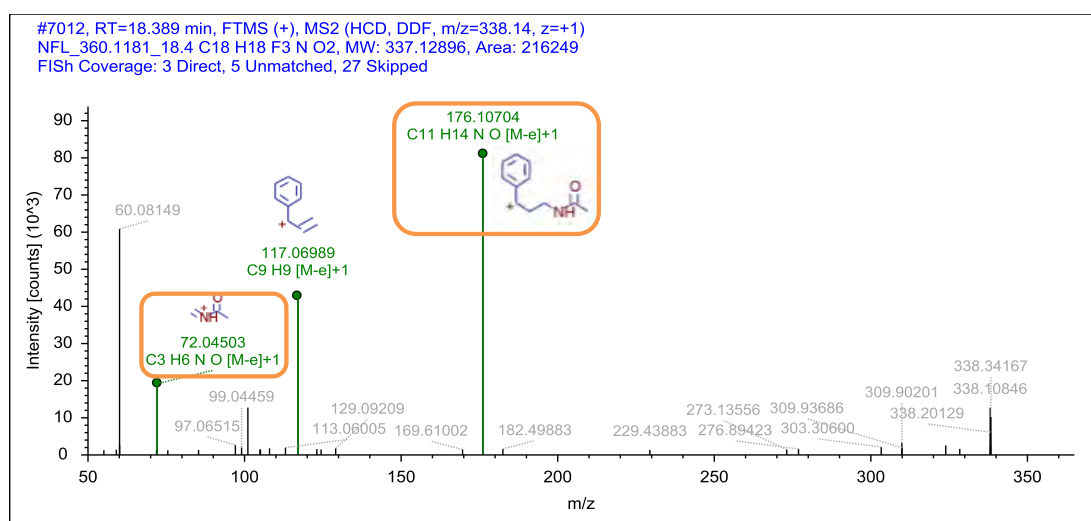
Chromatogram



MS Spectra



MS2 Spectra



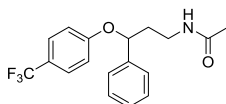
Formula

C18H18F3NO2

Atomic Modification

+C2H2O

Proposed Structure



Confidence Level

Level 3,
proposed structure

MassBank ID

NA

Additional Evidence for Structure Interpretation

Several peaks were found in the MS spectrum at the retention time of 18.4 min with the exact masses 360.1181 (C18H18F3NO2Na), 338.1366 (C18H19F3NO2), and 176.1069 (C11H14NO), which seem to belong to the same compound. The different peaks correspond to the sodium adduct, the hydrogen adduct, and an ion-source fragment. For the in-source fragment of this TP the same part of the molecule, namely the trifluoromethylphenol moiety (loss of C7H5F3O, $m=162.0290$), was cleaved as observed for the parent compound and further TPs of NFL and FLU. Since the sodium adduct FLU_360.1181_18.4 and the in-source fragment FLU_176.1069_18.4 have a higher response signal, these peaks were integrated for the visualization of the time series pattern.

For the structure elucidation, the MS2 spectrum of the hydrogen adduct is used. However, MS2 spectra of the sodium adduct and the in-source fragment are consistent with this one.

The atomic modification of the parent compound to this TP is +C2H2O, which could be realized through an N-acetylation. The MS2 fragment at the nominal mass 72 gives evidence for the attachment of the acetyl group to the nitrogen. The MS2 fragment at the nominal mass 176 corresponds to the MS2 fragment of the parent compound at the nominal mass 134 taking into account the modification of +C2H2O.

Attributed Reaction from the Parent Compound to this TP

It is *likely* that this TP was formed via an N-acetylation reaction.

Appendix B

Name NFL_234.1126_18.2 in-source fragment

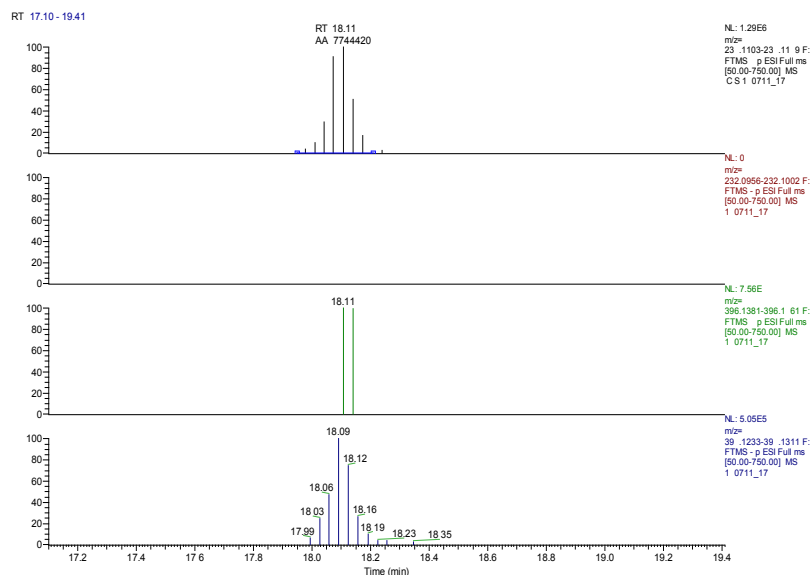
Chromatogram

MS spectrum in positive mode
for the exact mass 234.1126,
C₁₃H₁₆O₃N

MS spectrum in negative mode
for the exact mass 232.0979,
C₁₃H₁₆O₃N

MS spectrum in positive mode
for the exact mass 396.1421,
C₂₀H₂₁O₄NF₃

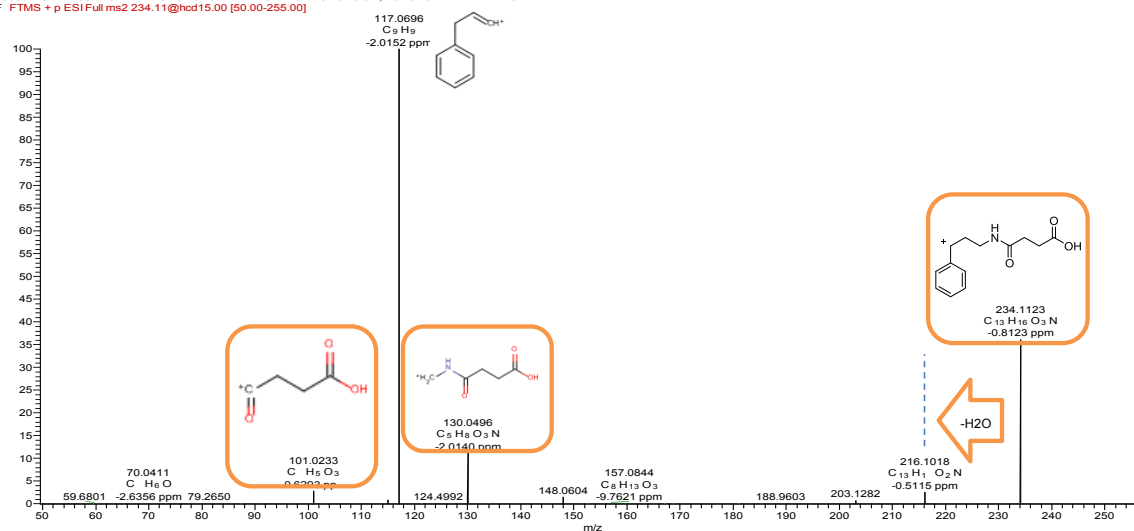
MS spectrum in negative mode
for the exact mass 394.1272,
C₂₀H₂₁O₄NF₃



MS2 Spectra

150602 02 #7236-7262 RT 18.18-18.23 AV 4 SB 131 18.40-19.32, 16.73-18.07 NL 6.93E5
F FTMS + p ESI Full ms2 234.11@hcd15.00 [50.00-255.00]

Relative Abundance



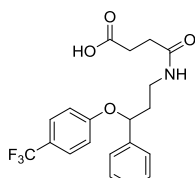
Formula

C₂₀H₂₁O₄NF₃

Atomic Modification

+C₄H₄O₃

Proposed Structure



Confidence Level

Level 3,
proposed structure

MassBank ID

NA

Additional Evidence for Structure Interpretation

The peak found at the retention time of 18.2 min in the MS spectrum at the exact mass of 234.1126 (C₁₃H₁₆O₃N) is most likely the in-source fragment of the [M+H]⁺ ion at the exact mass of 396.1421 (C₂₀H₂₁O₄NF₃). For the in-source fragmentation, the same part of the molecule, namely the trifluoromethylphenol moiety (loss of C₇H₅F₃O m=162.0290), was cleaved as observed for the parent compound and further TPs of NFL and FLU. As can be seen in the chromatograms that show the peaks measured in positive mode, the response of the in-source fragment is higher than the one of the [M+H]⁺ ion. However, the measurements in negative mode show the opposite. This is reasonable since the proposed structure contains a carboxylic acid moiety and therefore ionizes in negative mode. The in-source fragment, in contrast, is already positively charged and can only be detected in positive mode. For the visualization of the time series pattern the peaks of the in-source fragment in positive mode NFL_234.1126_18.2 are integrated.

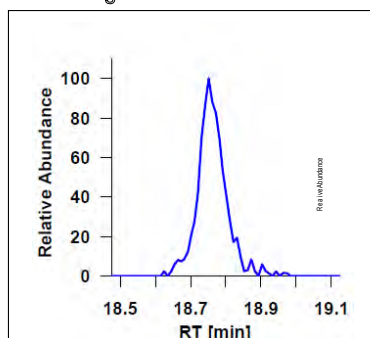
The MS2 spectrum for the in-source fragment is used for structure elucidation. The atomic modification from the elemental formula of the parent compound to this TP is +C₄H₄O₃. The MS2 fragment at the nominal mass 101 indicates that all atoms of the modification are connected. The MS2 fragment at the nominal mass 130 indicates that the modification took place at the methylamine moiety. The neutral loss of H₂O and the matching signal in negative mode indicate a carboxylic acid. An analogous N-succinylated TP was observed for OCP_297.1002_16.5, which was confirmed by a synthesized reference standard.

Attributed Reaction from the Parent Compound to this TP

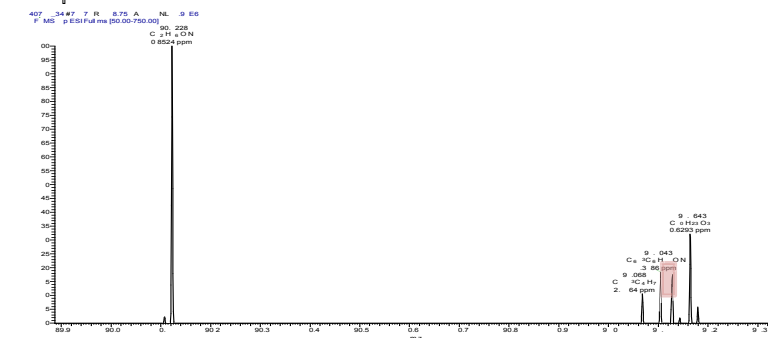
It is *likely* that this TP was formed via an N-succinylation reaction.

Name NFL_190.1228_18.8 in-source fragment

Chromatogram

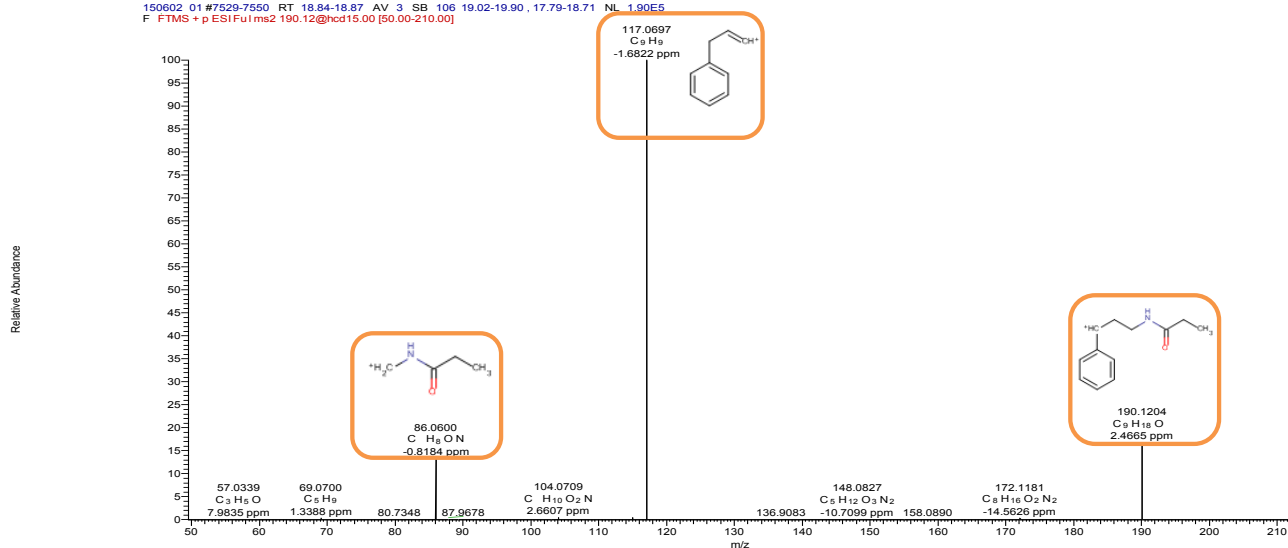


MS Spectra



MS2 Spectra

150602 01 #7529-7550 RT 18.84-18.87 AV 3 SB 106 19.02-19.90, 17.79-18.71 NL 1.90E5
 F TMS + p ESI Full ms2 190.12@hcd15.00 [50.00-210.00]



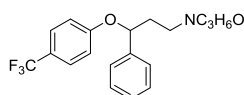
Formula

C₁₉H₂₀NO₂F₃

Atomic Modification

+C₃H₄O

Proposed Structure



Confidence Level

Level 3,
TP class

MassBank ID

NA

Additional Evidence for Structure Interpretation

The elemental formula of C₁₉H₁₆NO could be assigned to the exact mass of 190.1228 ($\Delta m = 0.8524$ ppm) that was observed in the MS spectrum at the retention time of 18.8. Due to the experience for the parent compound as well as for the other TPs of NFL and FLU, it is likely that this peak is an in-source fragment, which lost the trifluoromethylphenolic moiety (C₇H₅O₂F₃, $m = 162.0287$). The corresponding $[M+H]^+$ ion would then consist of C₁₉H₂₁NO₂F₃ (352.1519). However, no signal was observed at this mass. Since the signal of the in-source fragment was significantly higher than for the $[M+H]^+$ ion of other NFL TPs, it is possible that the same is true for this TP and the signal for the $[M+H]^+$ is too low to be detected. Therefore, we suspect that the original TP had the elemental formula of C₁₉H₂₀NO₂F₃. However, for the visualization of the time series pattern the peaks of the in-source fragment in positive mode NFL_190.1228_18.8 are integrated.

The MS2 spectrum for the in-source fragment was used for structure elucidation. The atomic modification from the elemental formula of the parent compound to this TP is +C₃H₄O. The MS2 fragment at the nominal mass 117 indicates that the propylphenyl moiety is a substructure of this TP. The MS2 fragment at the nominal mass 86 indicates that the modification took place at the methylamine moiety. There are several structures that would fit the structural evidence, like an N-propionyl moiety or an N,N-methylacetyl moiety.

Attributed Reaction from the Parent Compound to this TP

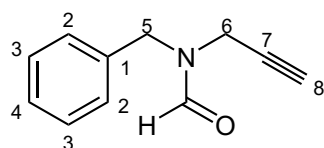
It is *possible* that this TP was formed via an N-propionylation.

B.5 Protocol of synthesis and NMR data of reference standards

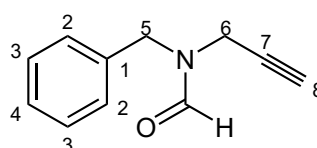
B.5.1 Reference standard for PAR_174.0914_15.0

N-benzyl-N-(prop-2-ynyl)formamide (Norpargyline Formamide, **1**)

1A



1B



Benzylamine (10.9 mL, 0.1 mol) was gently added to ethyl formate (80.8 mL, 1 mol), resulting in a slightly exothermic reaction and the precipitation of a white solid, which dissolved after the mixture was heated at reflux. Heating under reflux was continued for 24 hours. Excess ethyl formate was removed under reduced pressure, producing N-benzylformamide (13.6 g, quantitative yield) as white solid, which was used in the next step without further purification.

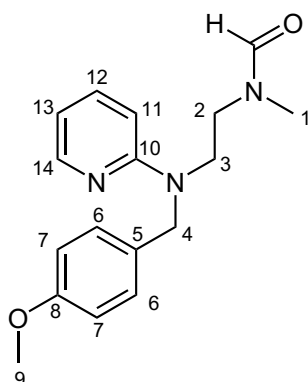
To a cooled (0 °C) solution of sodium hydride (60%, 1.60 g, 40 mmol) in anhydrous tetrahydrofuran (100 mL), a solution of N-benzylformamide (5.4 g, 40 mmol) in tetrahydrofuran (10 mL) was added and the mixture was stirred for 1 hour at 0 °C. Propargyl bromide (80% in toluene, 9 mL, 80 mmol) was added dropwise and the stirred mixture was allowed to warm slowly to room temperature. Stirring was continued at room temperature for 24 hours. The mixture was quenched with water (200 mL) and extracted with ethyl acetate (3 x 100 mL). The organic layer was dried (MgSO₄) and the solvent removed under reduced pressure. The crude product was purified by flash chromatography on silica gel (300 g, elution with hexane/ethyl acetate 2:1 to 1:1), to form the formamide **1** (0.69 g, 10%) as a pale yellow oil, and recover the starting N-benzylformamide (4.05 g, 75%).

B.5.2 Reference standard for PYR_300.1709_10.6

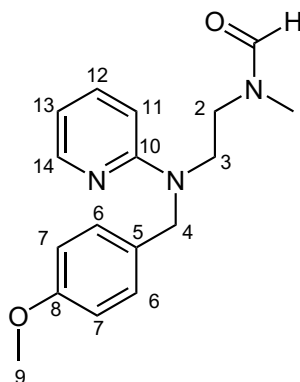
N-(2-((4-methoxybenzyl)(pyridin-2-yl)amino)ethyl)-N-methylformamide (Norpyrilamine Formamide, 2)

De-methylation according to¹³⁰, Formamide formation according to:¹³¹.

2A



2B

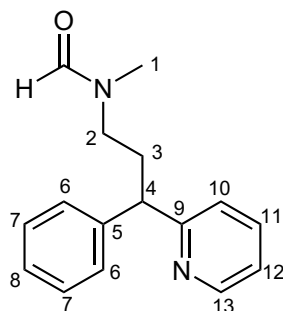
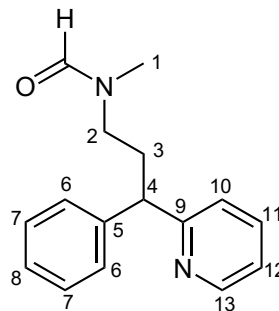


Pyrilamine (7.11 g, 25 mmol) was dissolved in 1,2-dichloroethane (150 mL) and sodium carbonate (500 mg) was then added. The mixture was cooled to 0 °C and 1-chloroethyl chloroformate (5.5 mL, 50 mmol) was added dropwise. After stirring for 10 minutes at 0 °C, the mixture was heated to 50 °C for 2 hours. The solid was filtered off and the filtrate reduced *in vacuo*. Then methanol (200 mL) was added to the pale green-brown oily residue and the resulting solution heated under reflux for 2 hours. The solvent was removed under reduced pressure. Aqueous sodium hydroxide solution (2 mol/L, 100 mL) was added to the residual brown oil and the mixture extracted with ethyl acetate (3 x 100 mL). The combined organic phases were dried (MgSO₄) and the solvent was removed under reduced pressure. The residue was purified by flash chromatography on silica gel (300 g, ethyl acetate/methanolic ammonia 4.5 mol/L 10:1) to produce norpyrilamine as a pale yellow oil (0.37 g, 5.5%).

Formamide (2 mL, 50 mmol) was added to the obtained norpyrilamine (350 mg, 1.3 mmol). The flask was flushed with argon, sealed and stirred for 24 hours at 80 °C. Thin layer chromatography (ethyl acetate/methanolic ammonia 4.5 mol/L 20:1) showed the expense of starting amine. The reaction mixture was reduced *in vacuo* to obtain the required formamide **2** as yellow oil (385 mg, quantitative yield).

B.5.3 Reference standard for PHE_255.1491_11.6 and NPE_255.1491_11.6

N-methyl-N-(3-phenyl-3-(pyridin-2-yl)propyl)formamide (Norpheniramine Formamide, **3**)

3A**3B**

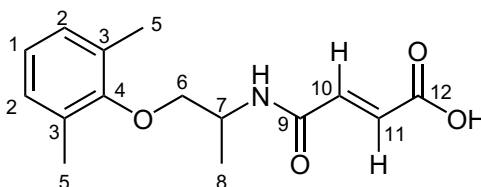
Pheniramine (5.98 g, 25 mmol) was dissolved in 1,2-dichloroethane (150 mL) and sodium carbonate (500 mg) was then added. The mixture was cooled to 0 °C and 1-chloroethyl chloroformate (5.5 mL, 50 mmol) was added dropwise. After stirring for 10 minutes at 0 °C, the mixture was heated to 50 °C for 2 hours. The solid was filtered off and the filtrate was reduced *in vacuo*. Then methanol (200 mL) was added to the brownish oily residue and the resulting solution heated under reflux for 2 hours. The solvent was removed under reduced pressure. Aqueous sodium hydroxide solution (2 mol/L, 100 mL) was added to the residual brown oil and the mixture extracted with ethyl acetate (3 x 100 mL). The combined organic phases were dried (MgSO₄) and the solvent removed under reduced pressure. The residue was purified by flash chromatography on silica gel (300 g, ethyl acetate/methanolic ammonia 4.5 mol/L 10:1) to produce norpyrilamine as a pale yellow oil (0.17 g, 3.0%).

Formamide (2 mL, 50 mmol) was added to the obtained norpyrilamine (157 mg, 0.7 mmol). The flask was flushed with argon, sealed and stirred for 22 hours at 80 °C. Thin layer chromatography (ethyl acetate/methanolic ammonia 4.5 mol/L 20:1) showed the expense of starting amine. The reaction mixture was reduced *in vacuo* to obtain the required formamide **3** as yellow oil (177 mg, quantitative yield).

B.5.4 Reference standard for MEX_278.1387_17.3

(E)-4-(1-(2,6-dimethylphenoxy)propan-2-ylamino)-4-oxobut-2-enoic acid
(Mexiletine-fumaramide acid, **4**¹³²)

4



Mexiletine · HCl (2.15 g, 10 mmol) was suspended in Et₂O (100 mL) and treated with an aqueous solution of NaOH (1 mol/L, 100 mL). After vigorous stirring, the phases were separated and the aqueous phase was extracted with Et₂O (2 × 100 mL). The combined organic layers were dried over sodium sulfate and concentrated *in vacuo*. The remaining colourless oil (mexiletine free base) was taken up in CH₂Cl₂ (150 mL) and fumaric acid monoethylester (1.50 g, 10 mmol) and 4-DMAP (1.32 g, 11 mmol) were added. The solution was stirred and cooled on an ice bath before EDCI · HCl (2.08 g, 11 mmol) was added. The solution was allowed to warm to room temperature overnight and after 16 h the solution was consecutively washed with HCl aq. (2 mol/L, 3 × 50 mL), NaHCO₃ (5% aq., 50 mL) and brine (50 mL) and the organic layer dried over anhydrous sodium sulfate and concentrated *in vacuo* to produce the crude mexiletine fumaramide ethyl ester as a very pale yellow oil (2.83 g, 97%). The crude product was used in the next step without further purification.

To a stirred solution of crude mexiletine fumaramide ethyl ester (2.81 g, 9.5 mmol) in EtOH (50 mL) an aqueous solution of NaOH (1 mol/L, 11 mL, 11 mmol) was added dropwise. The initially colourless reaction mixture slowly turned pink and a precipitate was formed. After 6 h thin layer chromatography analysis showed the expense of starting ester. The mixture was reduced *in vacuo*, taken up in H₂O (100 mL) and washed with Et₂O (100 mL). The layers were separated and the aqueous phase was acidified by the addition of HCl aq. (1 mol/L, 20 mL). The required fumaramide **4** immediately precipitated as a white solid, which was filtered off, washed thoroughly with H₂O (5 × 20 mL) and dried to constant weight (**4**, 2.14 g, 82%).

B.5.5 NMR data of synthesized reference standards

The ^1H and ^{13}C NMR spectra were recorded at 400.2 and 100.6 MHz on a Bruker Avance III 400 NMR spectrometer (Bruker Biospin AG, Fällanden, Switzerland). The 1D ^1H and ^{13}C NMR spectra, as well as the ^1H - ^{13}C HSQC, ^1H - ^{13}C HMBC, ^1H - ^1H DQF-COSY, and ^1H - ^1H NOESY 2D correlation NMR experiments were performed at 298 K using the Bruker standard pulse programs and parameter sets on a 5 mm CryoProbe™ Prodigy probe equipped with z-gradient applying 90° pulse lengths of 11.4 μs (^1H) and 10.0 μs (^{13}C). Chemical shifts (δ) in ppm are calibrated to residual solvent peaks (CDCl_3 : $\delta = 7.26$ and 77.0 ppm; DMSO-d_6 : $\delta = 2.49$ and 39.5 ppm).

Table B.13: ¹H- and ¹³C-NMR data of synthesized reference standards 1

compound	solvent	position	¹ H-NMR			¹³ C-NMR	HMBC, DQF-COSY, and NOE* data
			δ	cp	J [Hz]	no.H	
1A (59%)	CDCl ₃	CHO	8.26	s		1	HMBC: H-2 → C-(2, 4, 5); H-3 → C-(1, 3); H-4 → C-(2); H-5 → C-(1, 2, 6, CHO); H-6 → C-(5, 7, 8, CHO); H-8 → C-(6); CHO → C-(5w, 6) DQF-COSY: H-2 → H-(5); H-5 → H-(2, 6, CHO); H-6 → H-(5, 8, CHO); H-8 → H-(6); CHO → H-(5, 6) NOE: H-5 → CHO
		1				161.9	
		2	7.25	m		134.9	
		3				127.8	
		4	7.36	m		128.9	
		5	7.33	m		128.2	
		6	4.52	s		50.1	
		7	4.02	d	2.6	30.5	
1B (41%)	CDCl ₃	CHO	8.22	s		1	HMBC: H-2 → C-(5); H-3 → C-(1); H-5 → C-(1, 2, 6, CHO); H-6 → C-(5, 7, 8, CHO); H-8 → C-(6); CHO → C-(5, 6w) DQF-COSY: H-2 → H-(5); H-5 → H-(2, 6, CHO); H-6 → H-(5, 8, CHO); H-8 → H-(6); CHO → H-(5, 6) NOE: No interaction of H-5 → CHO
		1				162.0	
		2	7.27	m		135.4	
		3				128.5	
		4	7.31	m		128.7	
		5	7.28	m		127.8	
		6	4.64	s		44.9	
		7	3.85	d	2.5	36.1	
		8	2.35	t	2.5	1	NOE: No interaction of H-5 → CHO
						77.2	
						73.8	

For ¹H NMR data coupling patterns (cp) are described as s = singlet, d = doublet, t = triplet, q = quartet, m = multiplet. The number of hydrogens is abbreviated by no.H. For ¹³C NMR data multiplicities of carbons (mult.) are mentioned as s = quaternary, d = CH, t = CH₂, and q = CH₃. *Only the NOEs that were important for structure elucidation are shown.

Table B.14: ¹H- and ¹³C-NMR data of synthesized reference standards 2A

compound	solvent	position	¹ H-NMR				¹³ C-NMR		HMBC, DQF-COSY, and NOE* data
			δ	cp	J [Hz]	no.H	δ	mult.	
2A CDCl ₃ (62%)		CHO	7.88	s		1	162.9	d	HMBC: CHO → C-(1, 2w); H-1 → C-(CHO, 2); H-2 → C-(CHO, 1, 3); H-3 → C-(2, 4, 10); H-4 → C-(3, 5, 6, 10); H-6 → C-(4, 6, 7w, 8); H-7 → C-(5, 7, 8); H-9 → C-(8); H-11 → C-(10, 13); H-12 → C-(10, 14); H-13 → C-(11, 12w, 14); H-14 → C-(10, 11w, 12, 13) DQF-COSY: CHO → H-(1w); H-1 → H-(CHOW); H-2 → H-(3); H-3 → H-(2); H-4 → H-(6w); H-6 → H-(4w, 7); H-7 → H-(6); H-11 → H-(12); H-12 → H-(11, 13); H-13 → H-(12, 14); H-14 → H-(13) NOE: CHO → H-(2)
		1	2.90	s		3	30.1	q	
		2	3.48	t	6.2	2	47.6	t	
		3	3.75	m		2	46.8	t	
		4	4.55	m		2	52.4	t	
		5					129.5	s	
		6	7.09	"d"	8.7	2	127.7	d	
		7	6.84	"d"	8.7	2	114.1	d	
		8					158.8	s	
		9	3.77	s		3	55.21	q	
		10					157.7	s	
		11	6.44	ddd	8.5/0.8/0.8	1	106.1	d	
		12	7.38	m		1	137.4	d	
		13	6.58	ddd	7.1/5.0/0.8	1	112.5	d	
		14	8.16	m		1	147.9	d	

For ¹H NMR data coupling patterns (cp) are described as s = singlet, d = doublet, t = triplet, q = quartet, m = multiplet. The number of hydrogens is abbreviated by no.H. For ¹³C NMR data multiplicities of carbons (mult.) are mentioned as s = quaternary, d = CH, t = CH₂, and q = CH₃. *Only the NOEs that were important for structure elucidation are shown.

Table B.15: ^1H - and ^{13}C -NMR data of synthesized reference standards 2B

compound	solvent	position	^1H -NMR			^{13}C -NMR	HMBC, DQF-COSY, and NOE* data
			δ	cp	J [Hz]	no.H	
2B (38%)	CDCl_3	CHO	7.96	s		1	HMBC: CHO \rightarrow C-(1w, 2); H-1 \rightarrow C-(CHO, 2); H-2 \rightarrow C-(CHO, 1, 3); H-3 \rightarrow C-(2, 4); H-4 \rightarrow C-(3, 5, 6, 10); H-6 \rightarrow C-(4, 6, 7w, 8); H-7 \rightarrow C-(5, 7, 8); H-9 \rightarrow C-(8); H-11 \rightarrow C-(10, 13); H-12 \rightarrow C-(10, 14); H-13 \rightarrow C-(11, 12w, 14); H-14 \rightarrow C-(10, 11w, 12, 13) DQF-COSY: CHO \rightarrow H-(1w); H-1 \rightarrow H-(CHOw); H-2 \rightarrow H-(3); H-3 \rightarrow H-(2); H-4 \rightarrow H-(6w); H-6 \rightarrow H-(4w, 7); H-7 \rightarrow H-(6); H-11 \rightarrow H-(12); H-12 \rightarrow H-(11, 13); H-13 \rightarrow H-(12, 14); H-14 \rightarrow H-(13) NOE: CHO \rightarrow H-(1)
		1	2.95	s		3	
		2	3.52	t	7.1	2	
		3	3.76	m		2	
		4	4.67	m		2	
		5					
		6	7.14	"d"	8.7	2	
		7	6.82	"d"	8.7	2	
		8					
		9	3.76	s		3	
		10					
		11	6.54	m		1	
		12	7.38	m		1	
		13	6.54	m		1	
		14	8.14	m		1	

For ^1H NMR data coupling patterns (cp) are described as s = singlet, d = doublet, t = triplet, q = quartet, m = multiplet. The number of hydrogens is abbreviated by no.H. For ^{13}C NMR data multiplicities of carbons (mult.) are mentioned as s = quaternary, d = CH, t = CH_2 , and q = CH_3 . *Only the NOEs that were important for structure elucidation are shown.

Table B.16: ¹H- and ¹³C-NMR data of synthesized reference standards 3A

compound	solvent	Position	¹ H-NMR				¹³ C-NMR		HMBC, DQF-COSY, and NOE* data
			δ	cp	J [Hz]	no.H	δ	mult.	
3A (70%) CDCl ₃	CHO	7.79	s			1	162.7	d	HMBC: CHO → C-(1, 2w); H-1 → C-(CHO, 2); H-2 → C-(CHO, 1, 3, 4); H-3 → C-(1, 4, 5, 9); H-4 → C-(2, 3, 5, 6, 9, 10); H-6 → C-(4, 6, 8); H-7 → C-(5, 7); H-8 → C-(6); H-10 → C-(4, 9, 12); H-11 → C-(9, 13); H-12 → C-(10, 13); H-13 → C-(9, 10, 11, 12) DQF-COSY: CHO → H-(1w); H-1 → H-(CHOW); H-2 → H-(3, 4w); H-3 → H-(2, 4); H-4 → H-(2w, 3); H-10 → H-(11); H-11 → H-(10, 13w); H-12 → H-(13); H-13 → H-(11w, 12) NOE: CHO → H-(2)
	1	2.85	s			3	29.3	q	
	2	3.19	t	6.9		2	47.7	t	
	3	2.61+2.29	m			2	32.6	t	
	4	3.98	t	7.7		1	50.0	d	
	5						142.4	s	
	6	7.31	m			2	127.80	d	
	7	7.29	m			2	128.7	d	
	8	7.20	m			1	126.8	d	
	9						162.1	s	
	10	7.08	m			1	123.2	d	
	11	7.53	m			1	136.6	d	
	12	7.09	m			1	121.6	d	
	13	8.57	m			1	149.3	d	

For ¹H NMR data coupling patterns (cp) are described as s = singlet, d = doublet, t = triplet, q = quartet, m = multiplet. The number of hydrogens is abbreviated by no.H. For ¹³C NMR data multiplicities of carbons (mult.) are mentioned as s = quaternary, d = CH, t = CH₂, and q = CH₃. *Only the NOEs that were important for structure elucidation are shown.

Table B.17: ¹H- and ¹³C-NMR data of synthesized reference standards 3B

compound	solvent	Position	¹ H-NMR				¹³ C-NMR		HMBC, DQF-COSY, and NOE* data
			δ	cp	J [Hz]	no.H	δ	mult.	
3B (30%)	CDCl ₃	CHO	7.93	s		1	162.4	d	HMBC: CHO → C-(1w, 2); H-1 → C-(CHO, 2); H-2 → C-(CHO, 1, 3, 4); H-3 → C-(1, 4, 5, 9); H-4 → C-(2, 3, 5, 6, 9, 10); H-6 → C-(4, 6, 8); H-7 → C-(5, 7); H-8 → C-(6); H-10 → C-(4, 9, 12); H-11 → C-(9, 13); H-12 → C-(10, 13); H-13 → C-(9, 10, 11, 12) DQF-COSY: CHO → H-(1w); H-1 → H-(CHOw); H-2 → H-(3, 4w); H-3 → H-(2, 4); H-4 → H-(2w, 3); H-10 → H-(11); H-11 → H-(10, 12, 13w); H-12 → H-(13); H-13 → H-(11w, 12) NOE: CHO → H-(1)
		1	2.85	s		3	34.5	q	
		2	3.28	m		2	43.1	t	
		3	2.56+2.27	m		2	31.6	t	
		4	4.06	t	7.6	1	51.1	d	
		5					143.0	s	
		6	7.31	m		2	127.77	d	
		7	7.26	m		2	128.5	d	
		8	7.17	m		1	126.6	d	
		9					162.6	s	
		10	7.14	m		1	123.1	d	
		11	7.53	m		1	136.5	d	
		12	7.08	m		1	121.4	d	
		13	8.54	m		1	149.0	d	

For ¹H NMR data coupling patterns (cp) are described as s = singlet, d = doublet, t = triplet, q = quartet, m = multiplet. The number of hydrogens is abbreviated by no.H. For ¹³C NMR data multiplicities of carbons (mult.) are mentioned as s = quaternary, d = CH, t = CH₂, and q = CH₃. *Only the NOEs that were important for structure elucidation are shown.

Table B.18: ¹H- and ¹³C-NMR data of synthesized reference standards 4

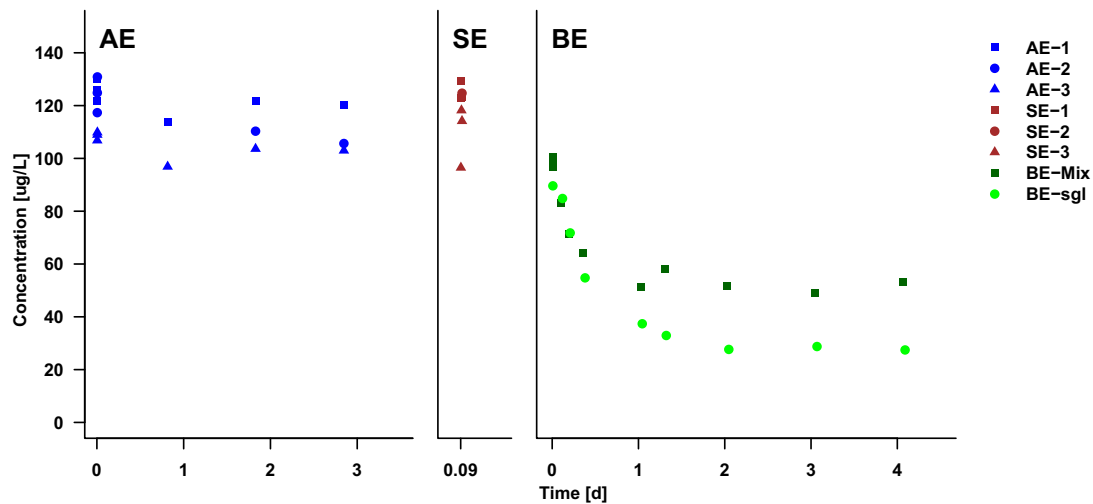
compound		¹ H-NMR			¹³ C-NMR		HMBC, DQF-COSY, and NOE* data	
solvent	Position	δ	cp	J [Hz]	no.H	δ		mult.
DMSO	1	6.88	m		1	123.8	d	HMBC: H-1 → C-(3); H-2 → C-(2, 4, 5); H-5 → C-(2, 3, 4); H-6 → C-(4, 7, 8); H-7 → C-(6, 8, 9); H-8 → C-(6, 7); H-10 → C-(9, 11, 12); H-11 → C-(9, 10, 12); NH → C-(7, 8, 9, 10) DQF-COSY: H-1 → H-(2); H-2 → H-(1); H-6 → H-(7); H-7 → H-(NH, 6, 8); H-8 → H-(7); H-10 → H-(11); H-11 → H-(10); NH → H-(7) NOE NH → H-(10)
	2	6.98	m		2	128.8	d	
	3					130.3	s	
	4					154.9	s	
	5	2.18	s		6	15.8	q	
	6	3.67	d	4.9	2	73.6	t	
	7	4.22	m		1	45.2	d	
	8	1.27	d	6.8	3	17.0	q	
	9					162.7	s	
	10	6.99	d	15.5	1	137.2	d	
	11	6.54	d	15.5	1	129.7	d	
	12					166.5	s	
NH	8.62	d	7.9	1				

For ¹H NMR data coupling patterns (cp) are described as s = singlet, d = doublet, t = triplet, q = quartet, m = multiplet. The number of hydrogens is abbreviated by no. H. For ¹³C NMR data multiplicities of carbons (mult.) are mentioned as s = quaternary, d = CH, t = CH₂, and q = CH₃. *Only the NOEs that were important for structure elucidation are shown.

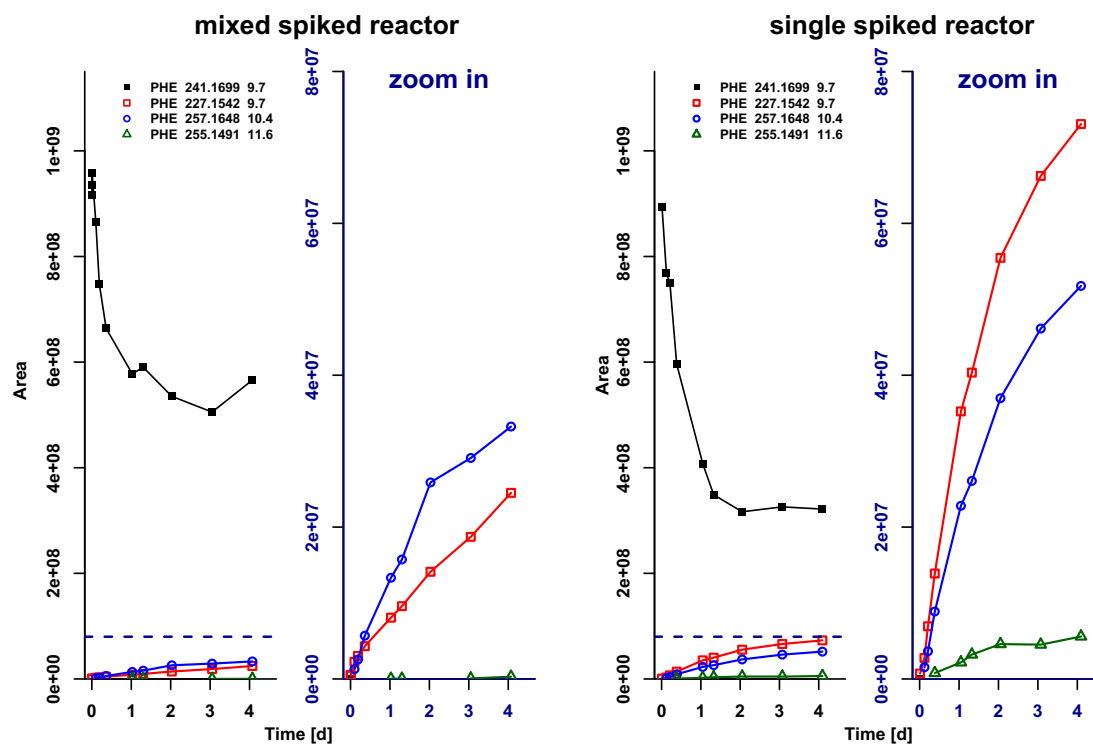
**B.6 Biotransformation pathways, concentration
time series of parents, time series pattern of
transformation products**

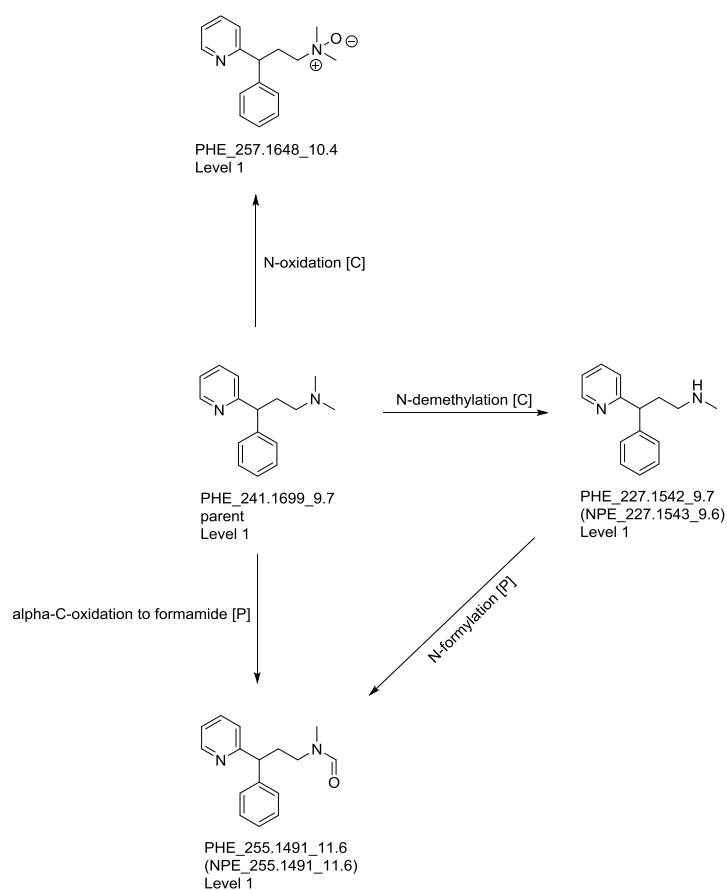
Pheniramine

Concentration time series of parent compound



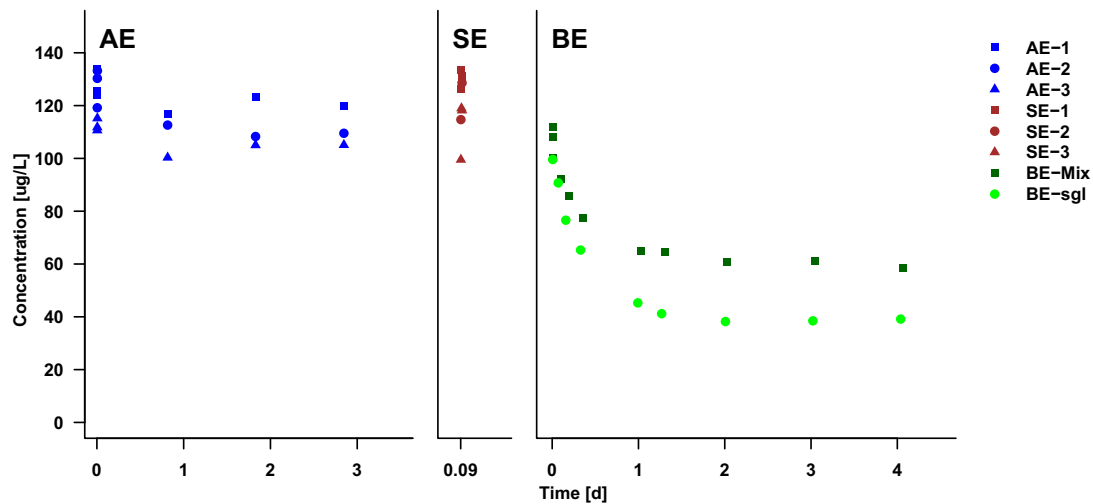
Time series pattern of parent and transformation products in area units



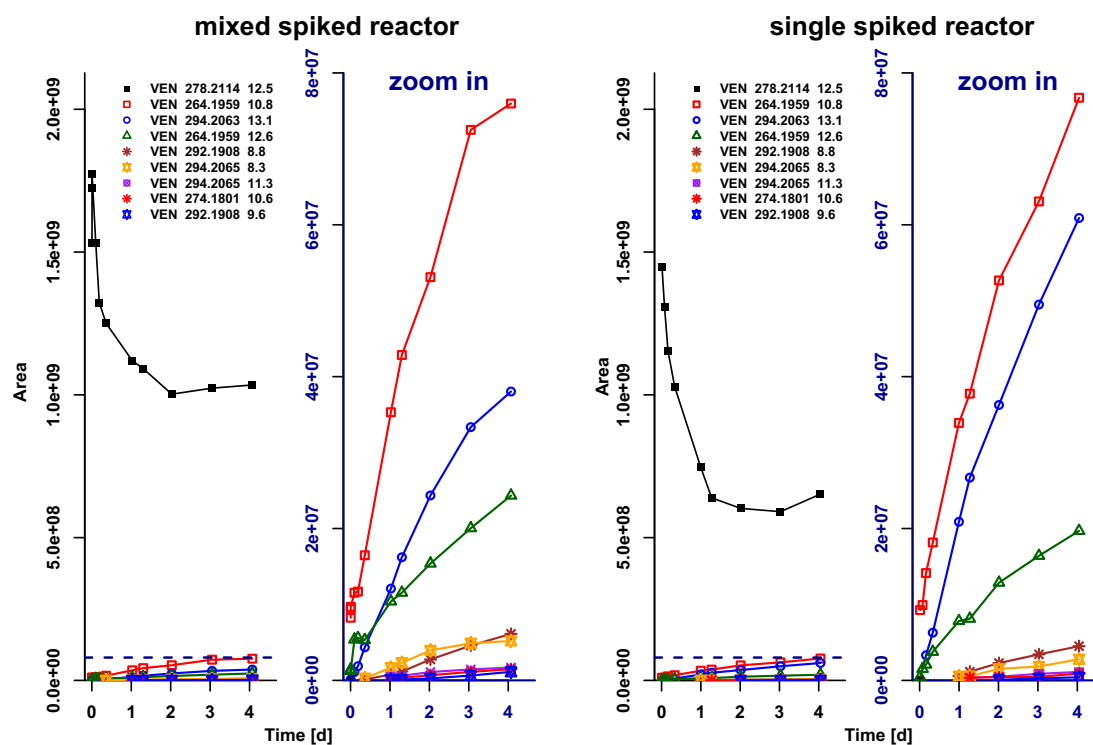


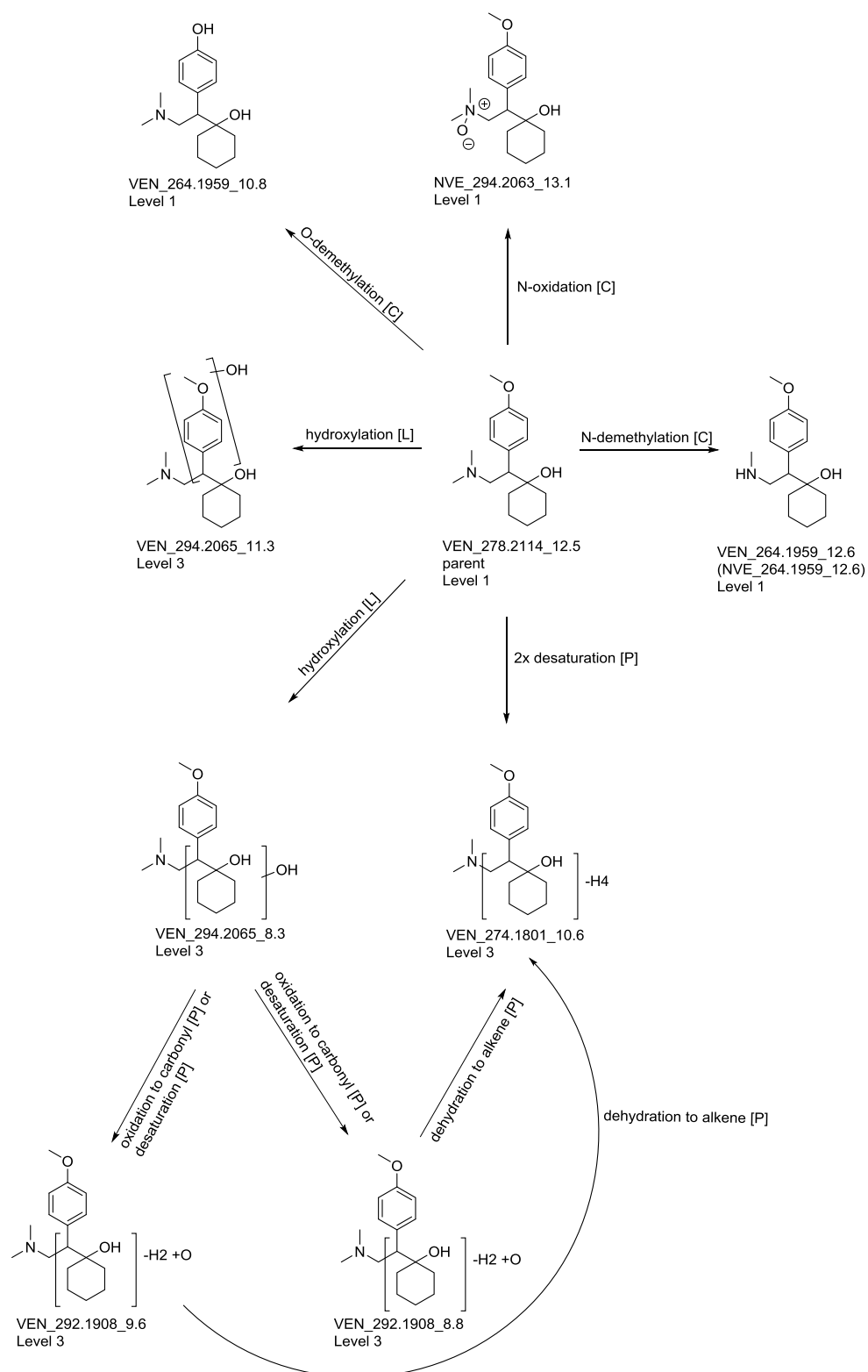
Venlafaxine

Concentration time series of parent compound



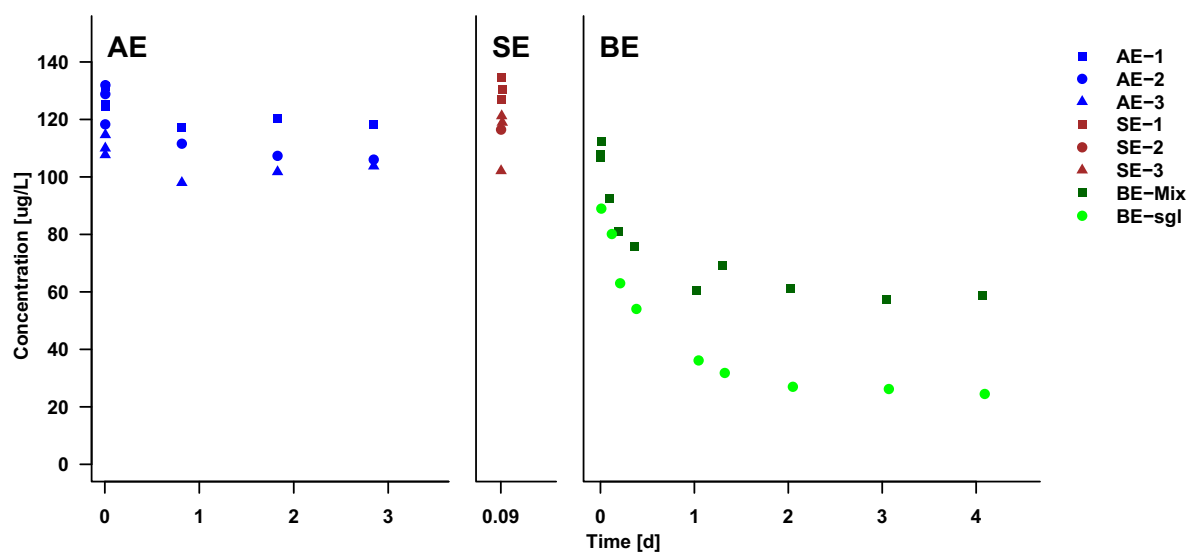
Time series pattern of parent and transformation products in area units



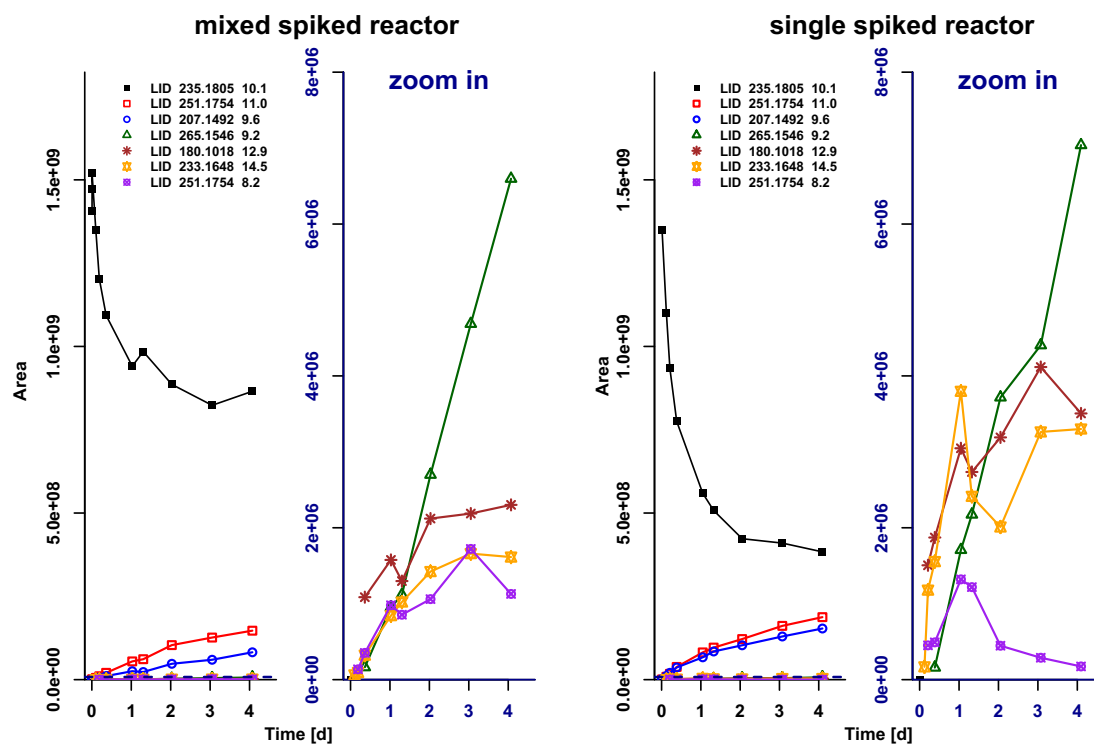


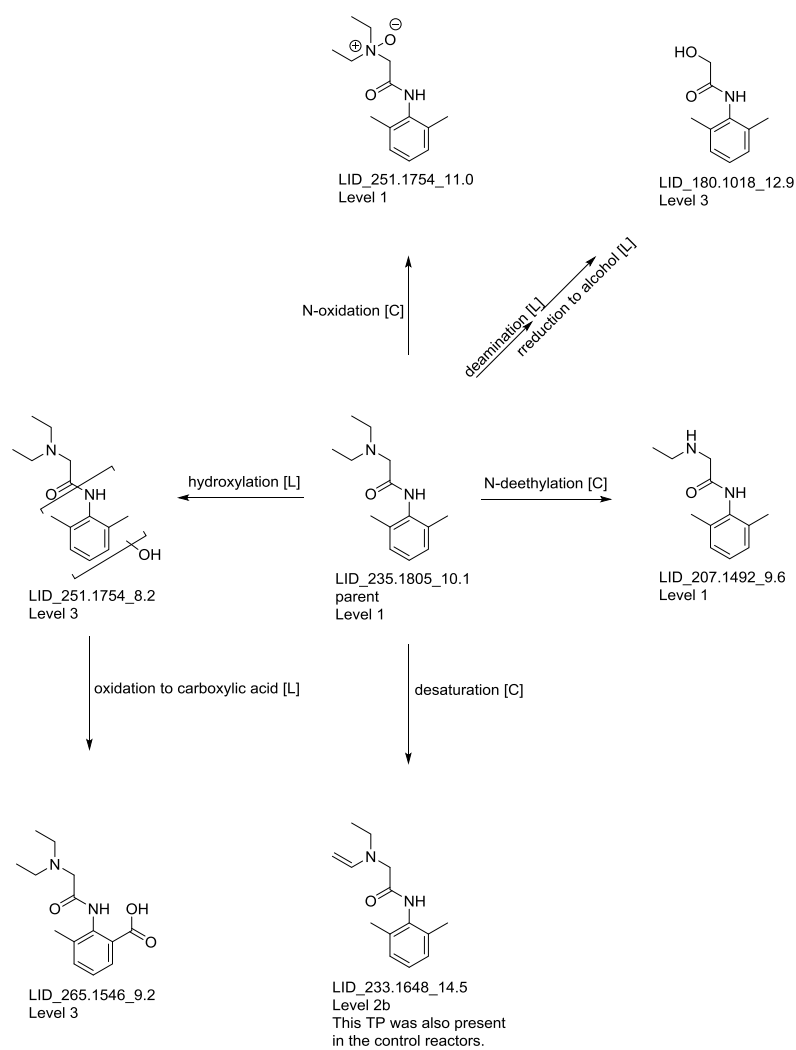
Lidocaine

Concentration time series of parent compound



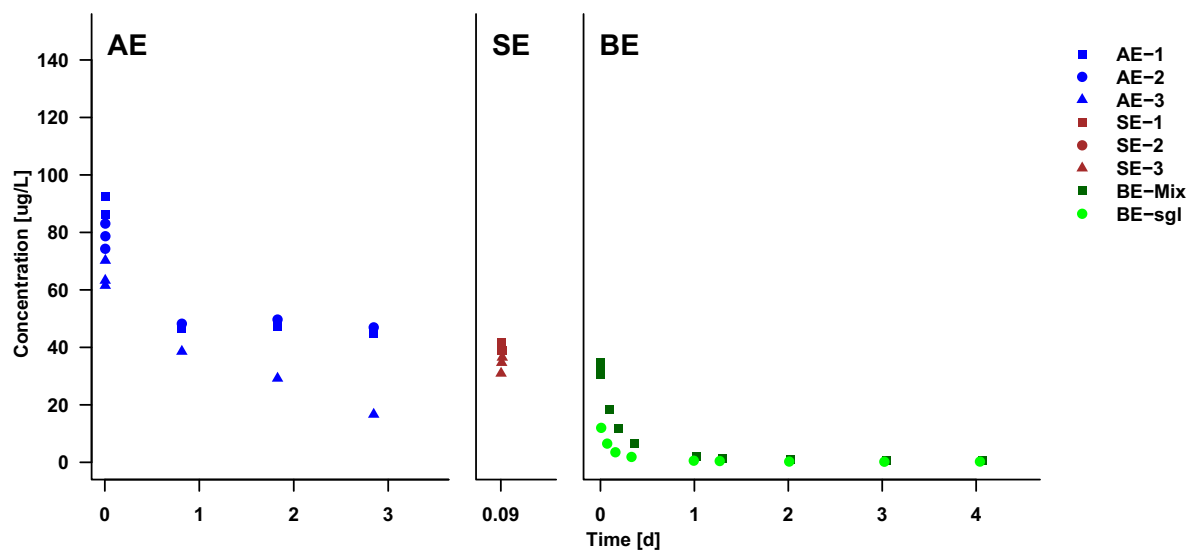
Time series pattern of parent and transformation products in area units





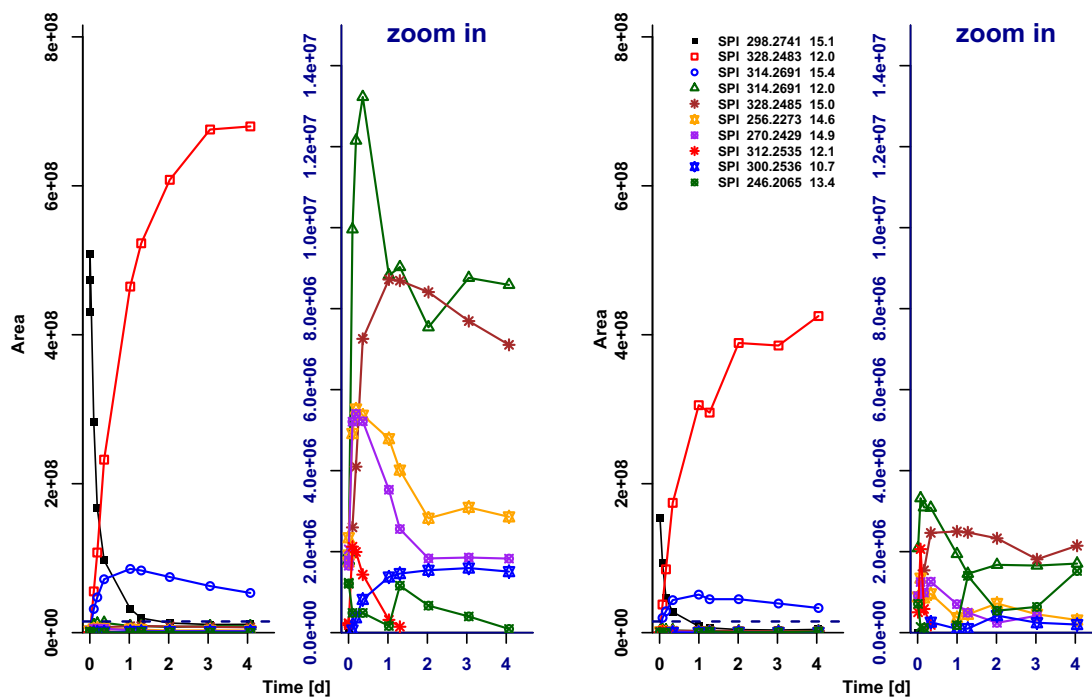
Spiroxamine

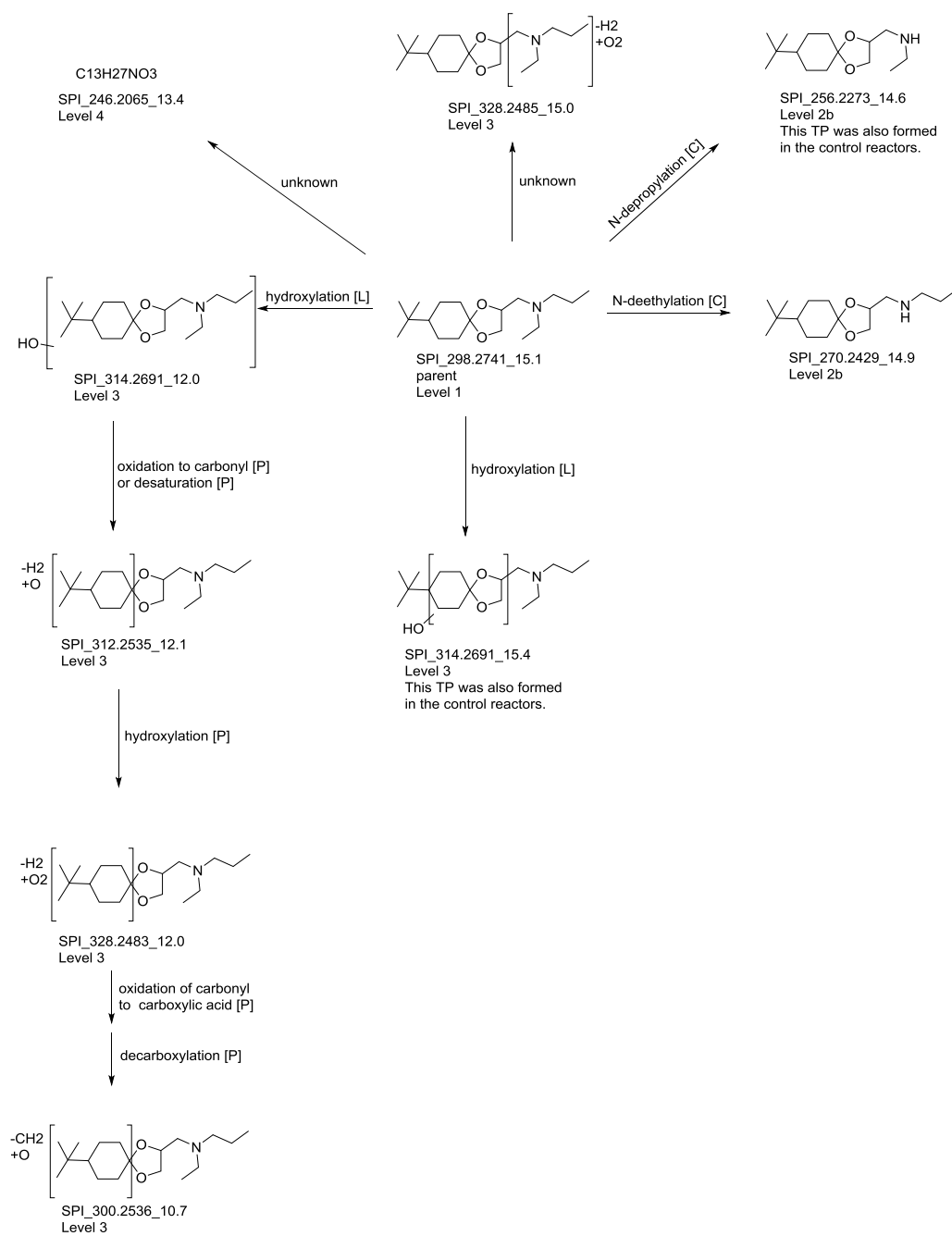
Concentration time series of parent compound



Time series pattern of parent and transformation products in area units

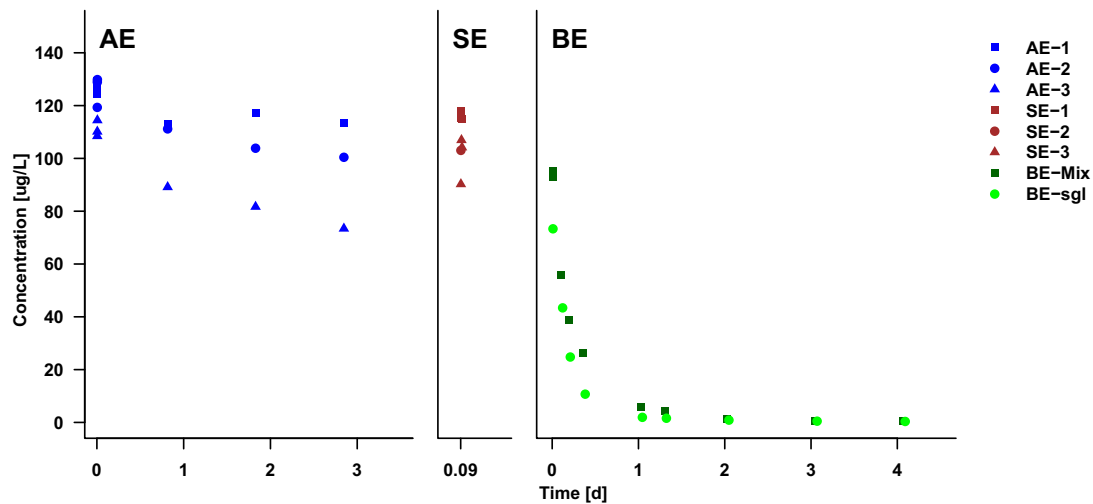
mixed spiked reactor single spiked reactor



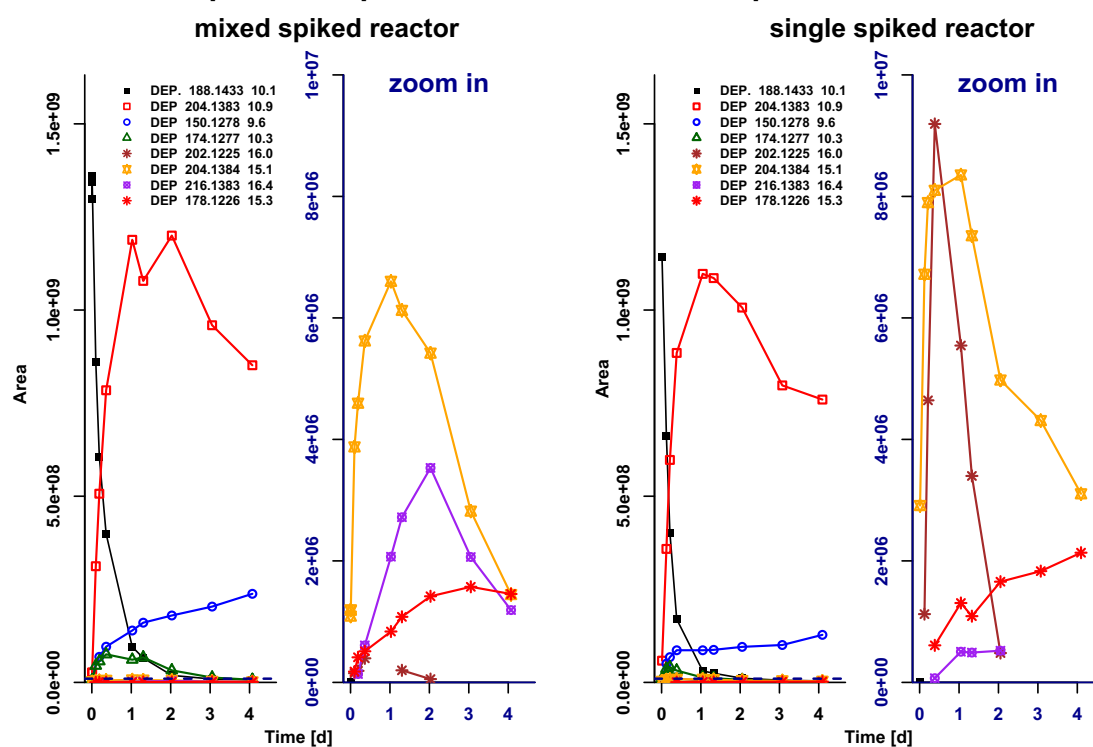


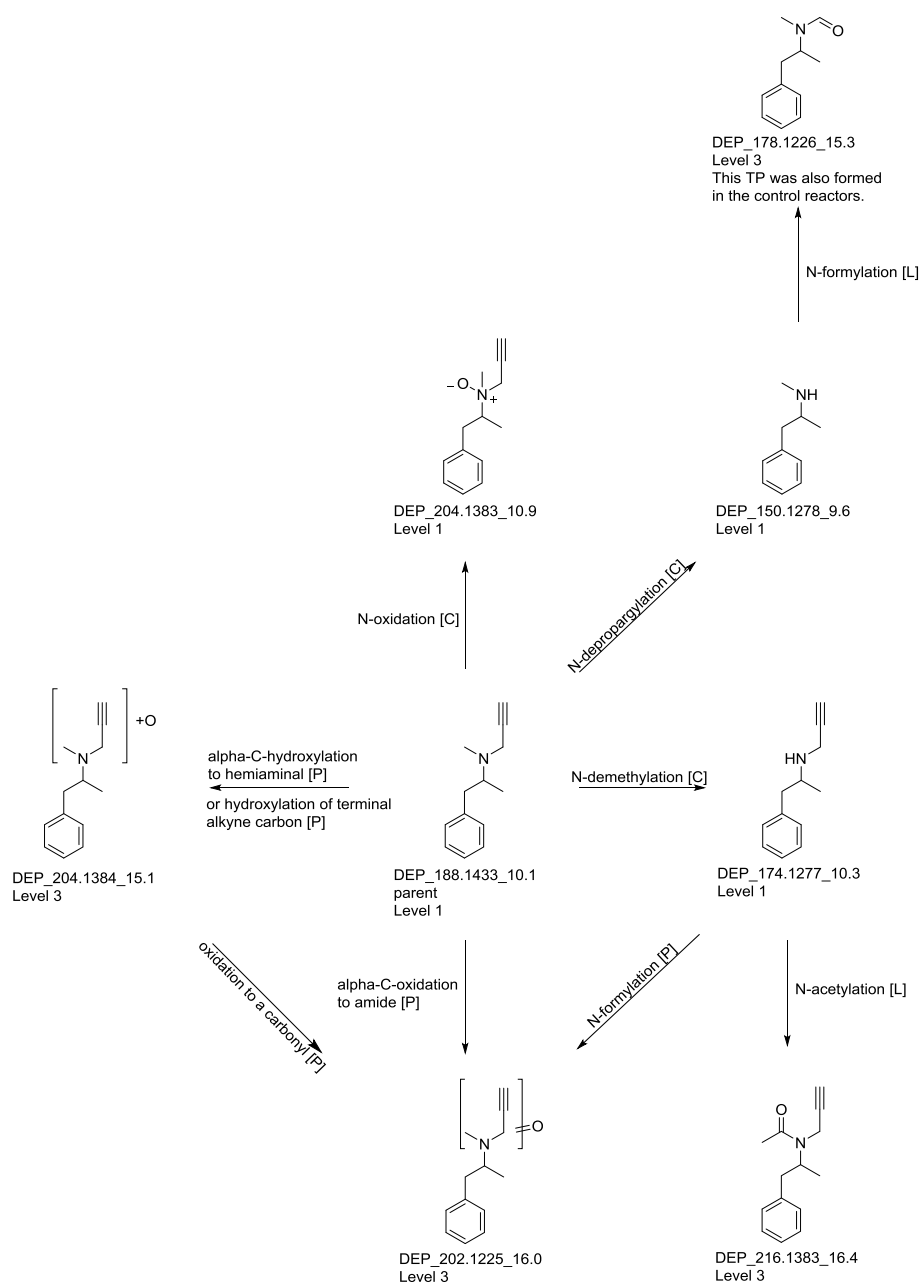
Deprenyl

Concentration time series of parent compound



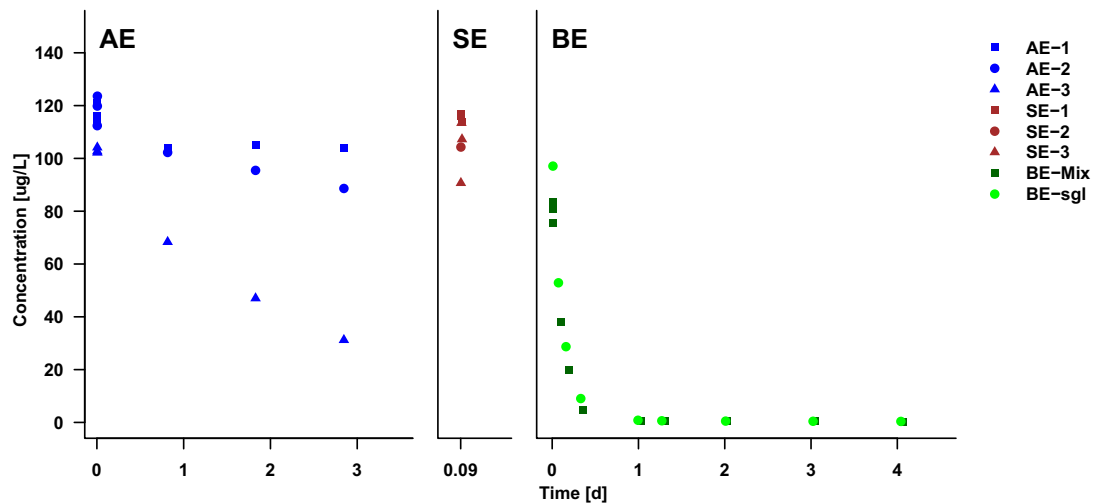
Time series pattern of parent and transformation products in area units



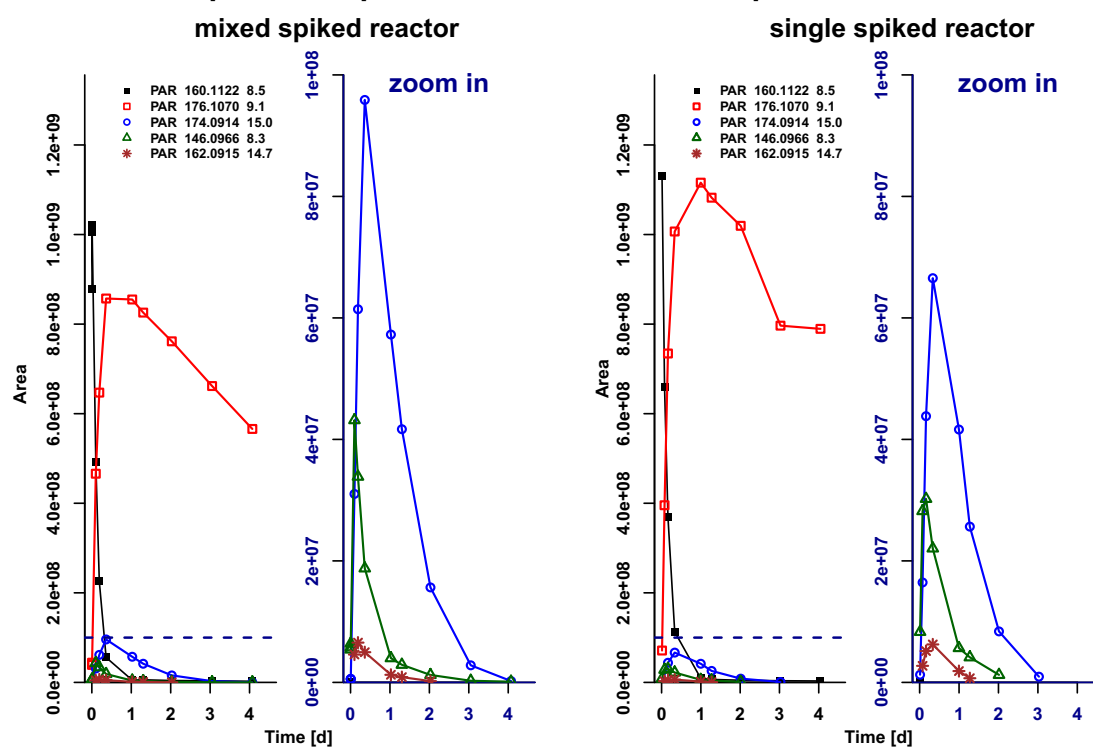


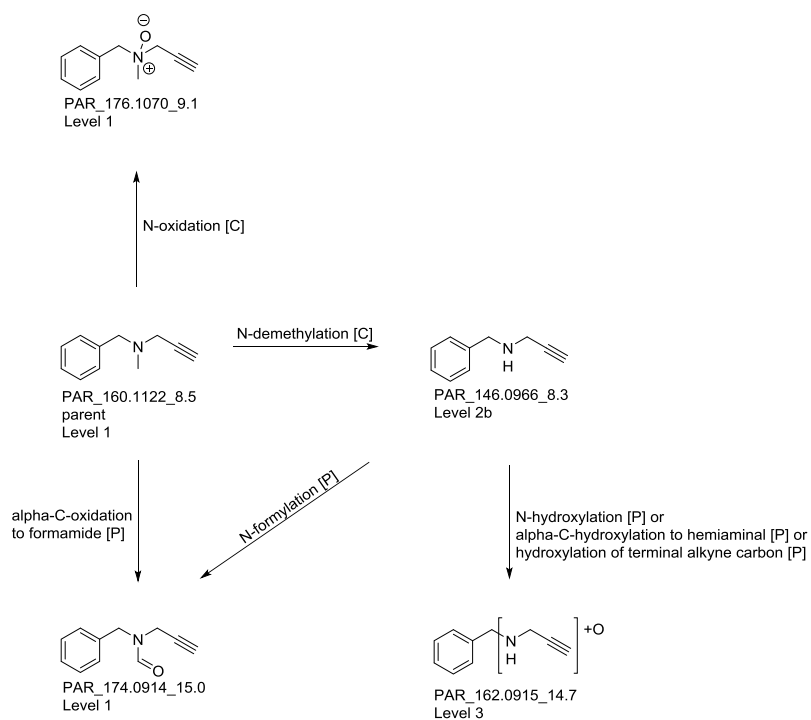
Pargyline

Concentration time series of parent compound



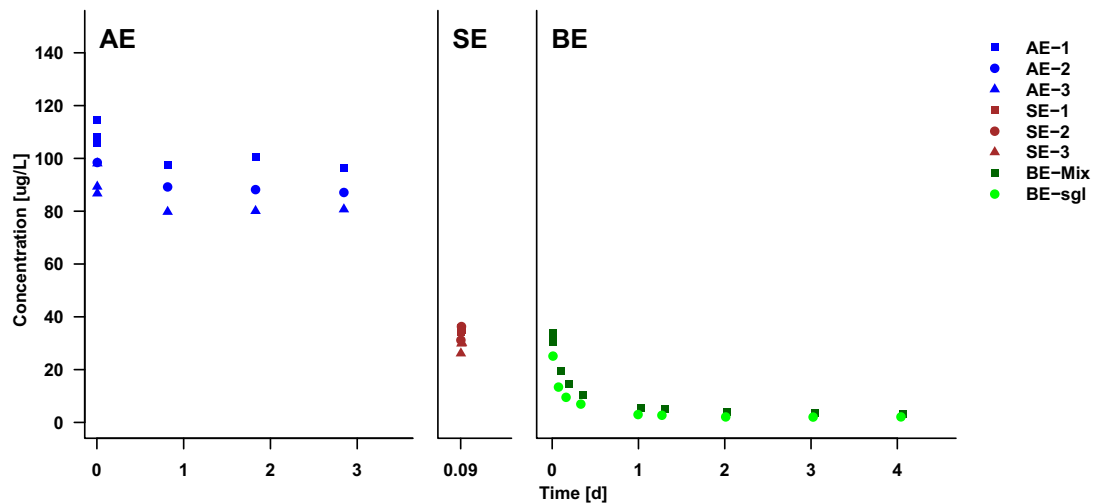
Time series pattern of parent and transformation products in area units



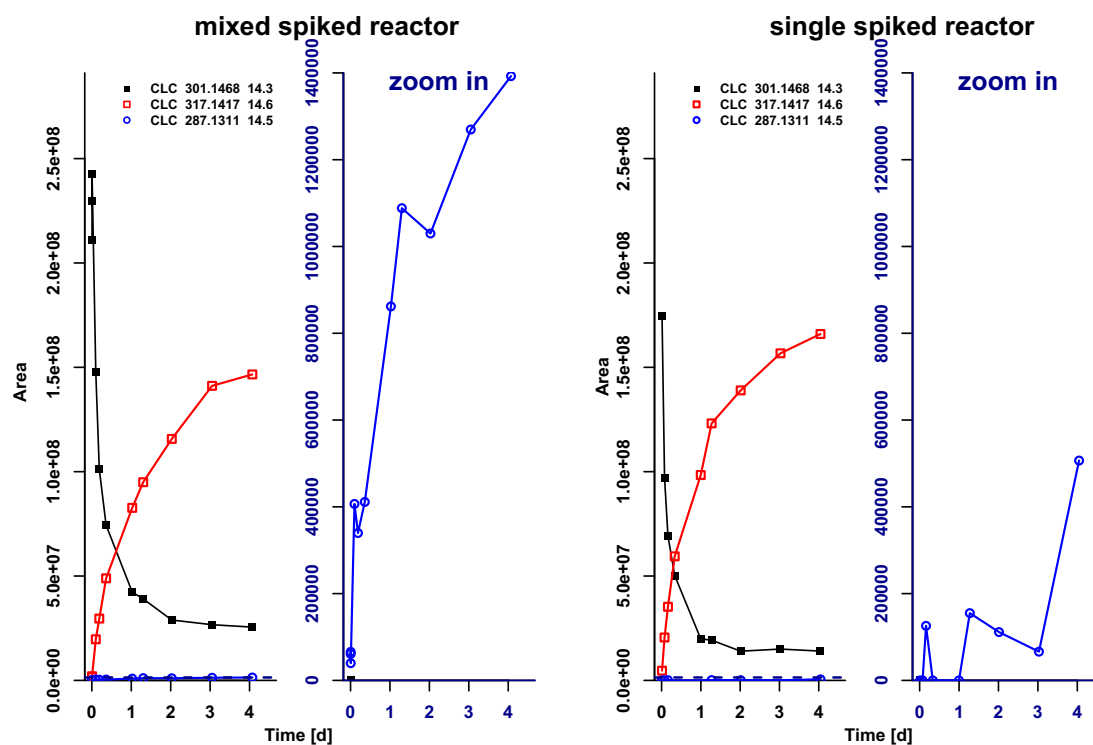


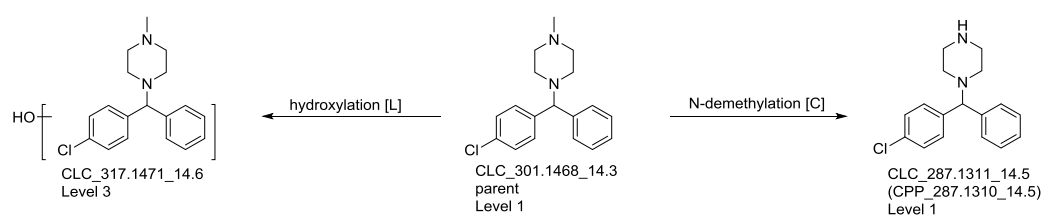
Chlorcyclizine

Concentration time series of parent compound



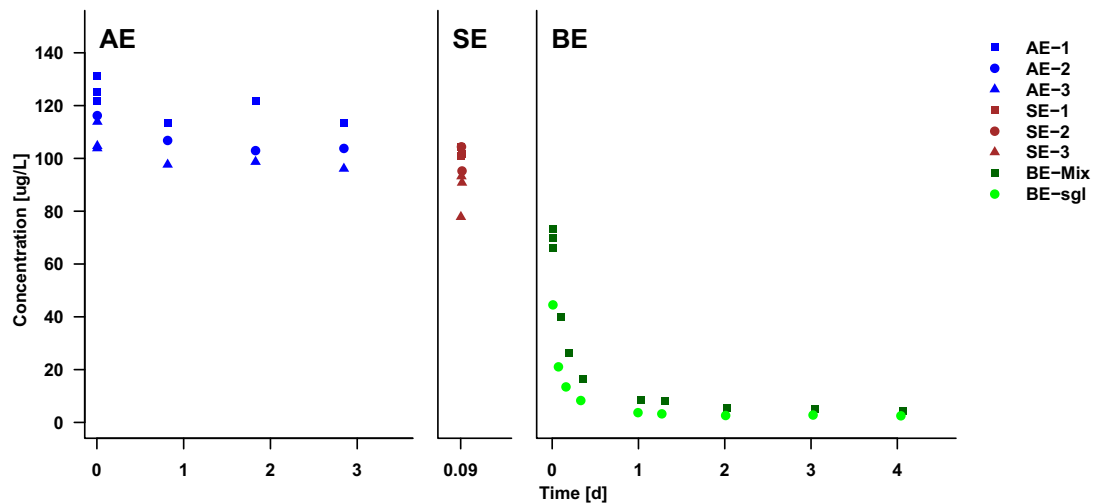
Time series pattern of parent and transformation products in area units



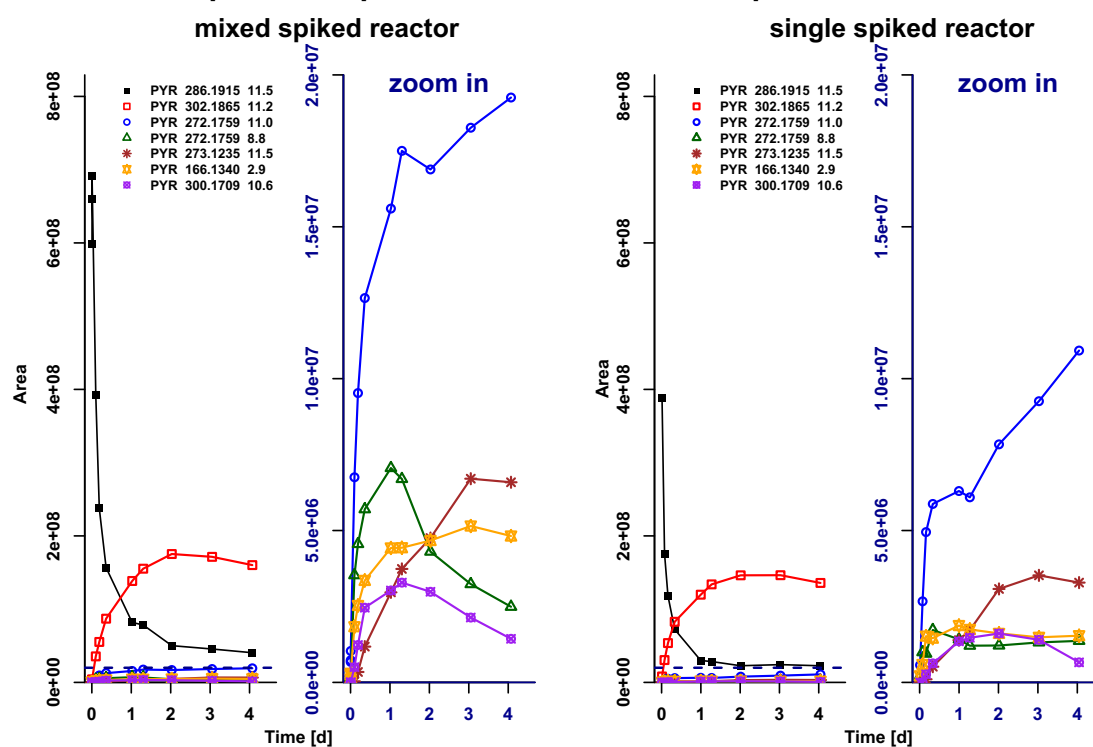


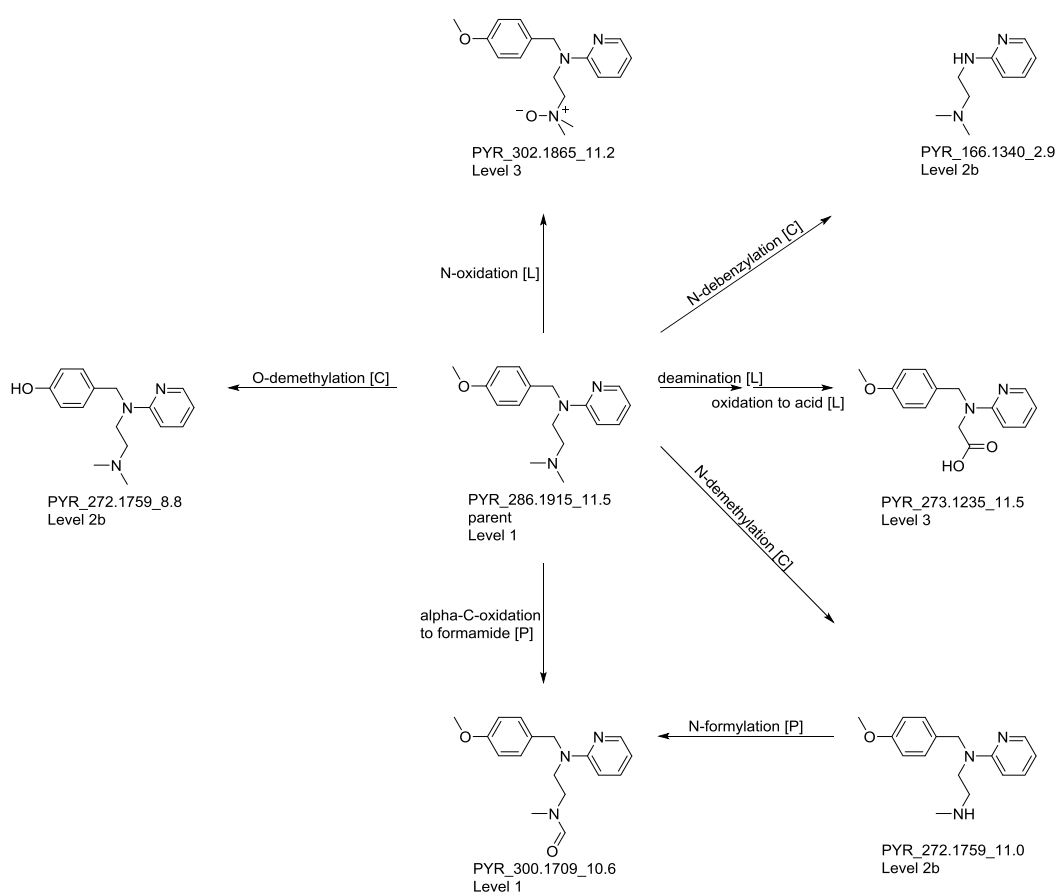
Pyrilamine

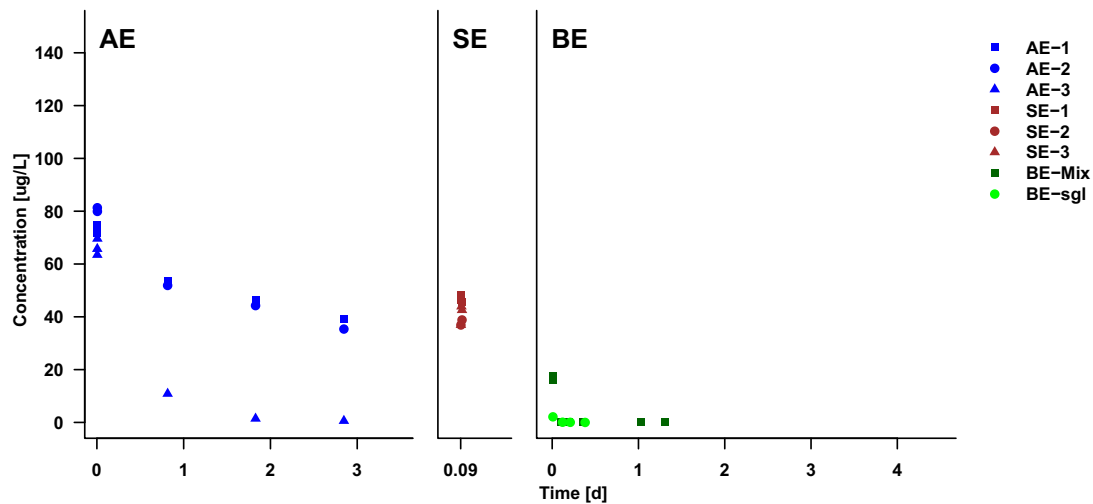
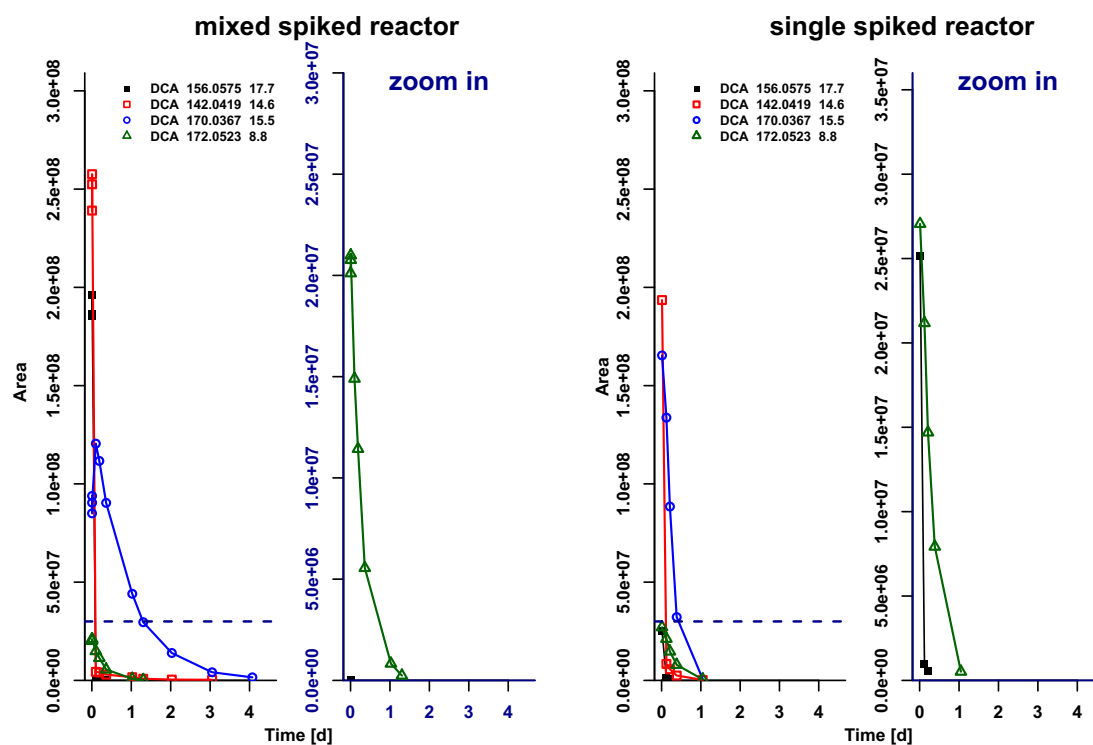
Concentration time series of parent compound

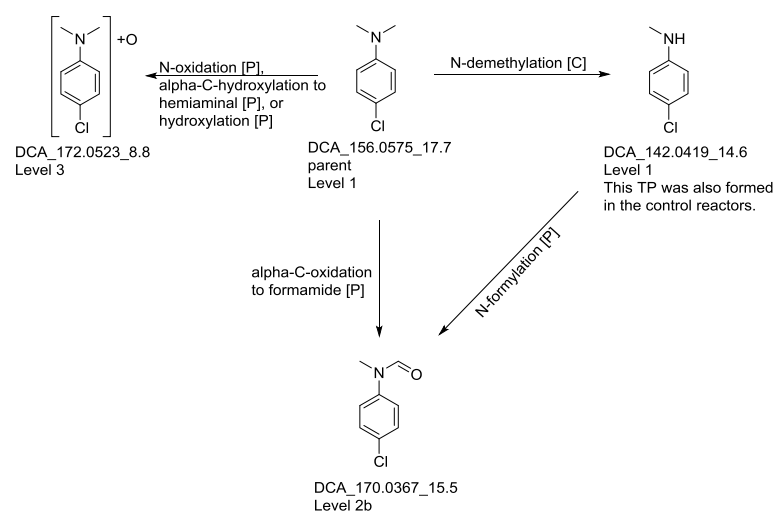


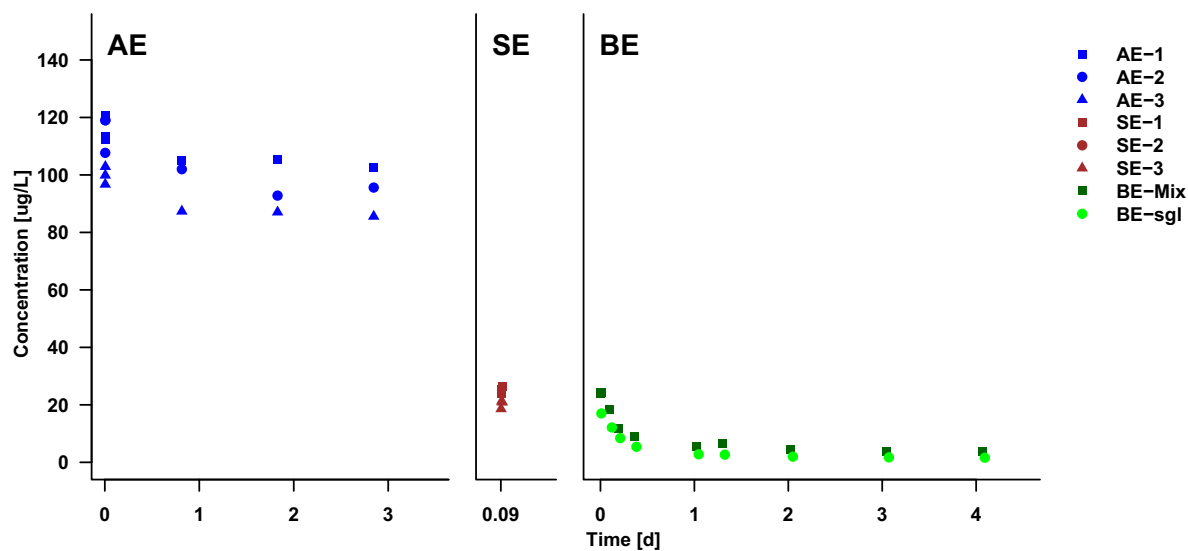
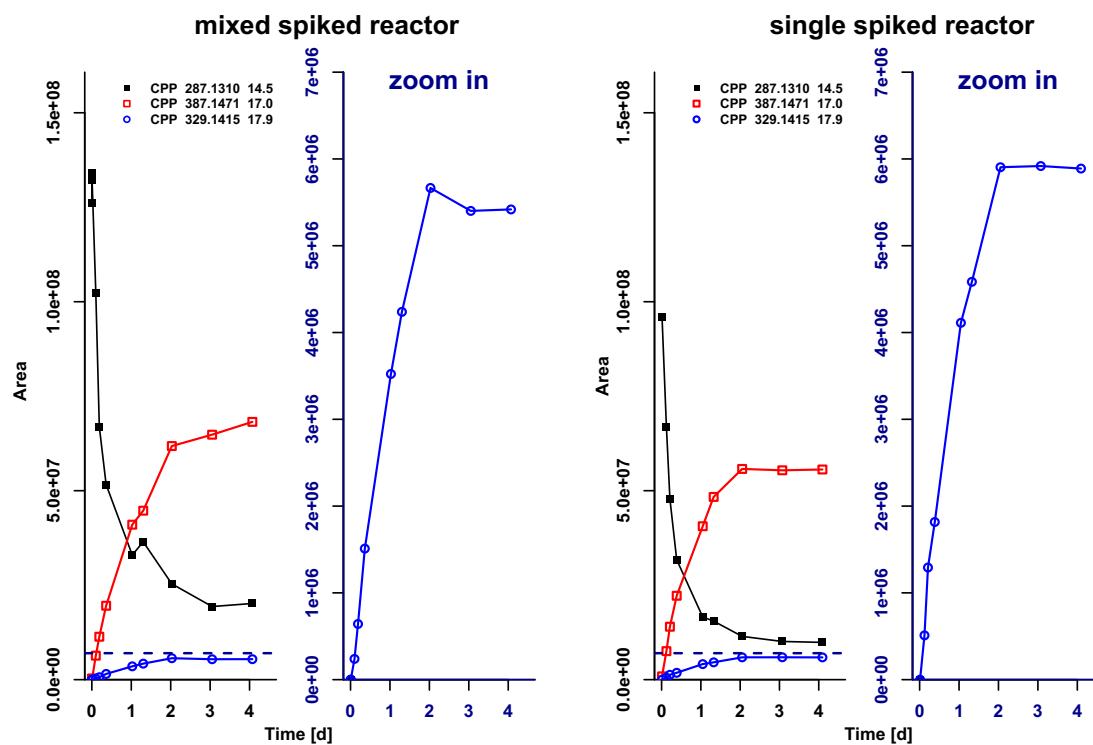
Time series pattern of parent and transformation products in area units

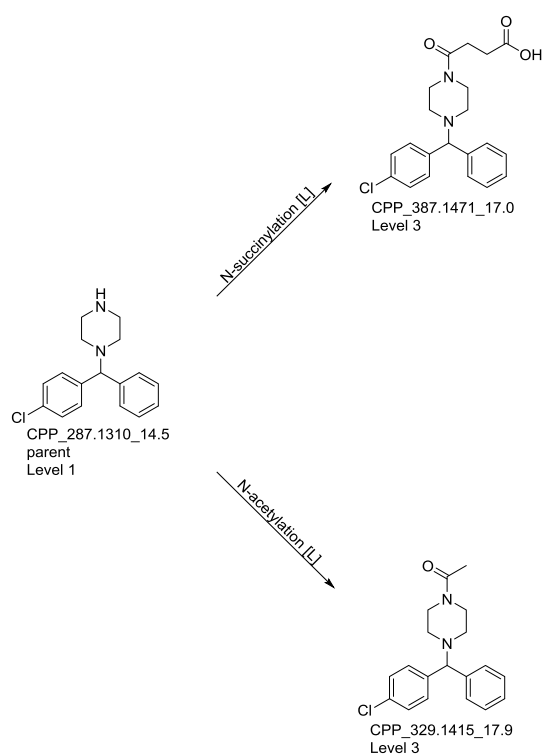




N,N-dimethyl-p-chloroaniline**Concentration time series of parent compound****Time series pattern of parent and transformation products in area units**

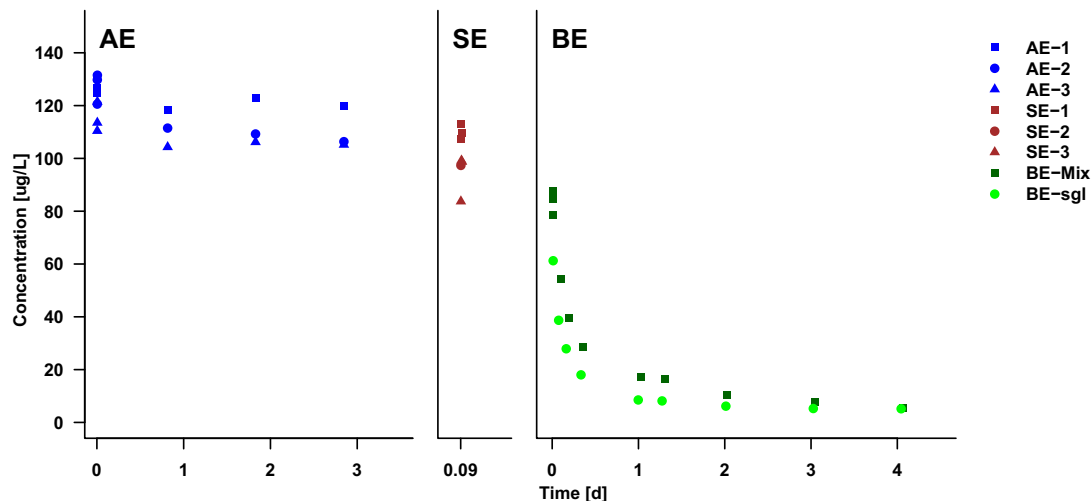


1[(4-chlorophenyl)phenylmethyl]piperazine**Concentration time series of parent compound****Time series pattern of parent and transformation products in area units**

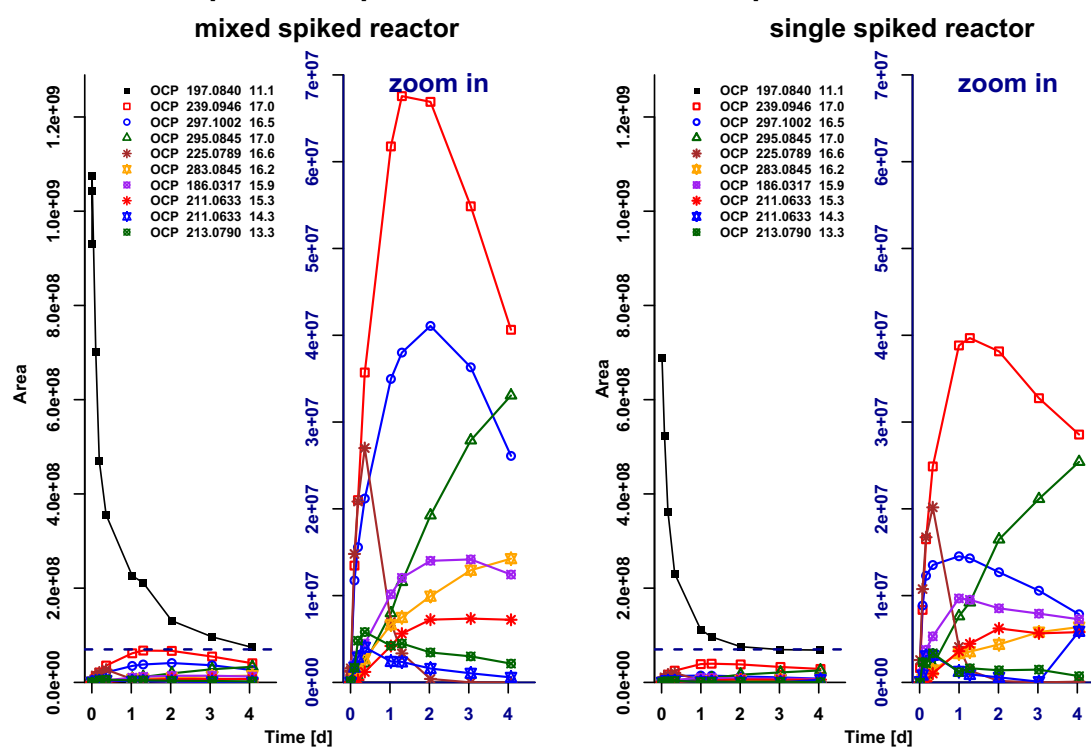


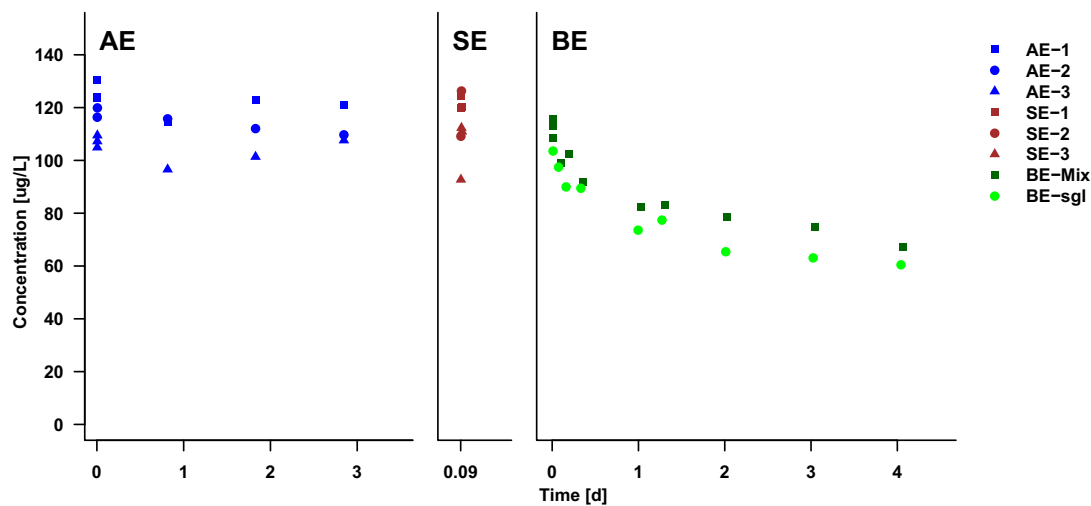
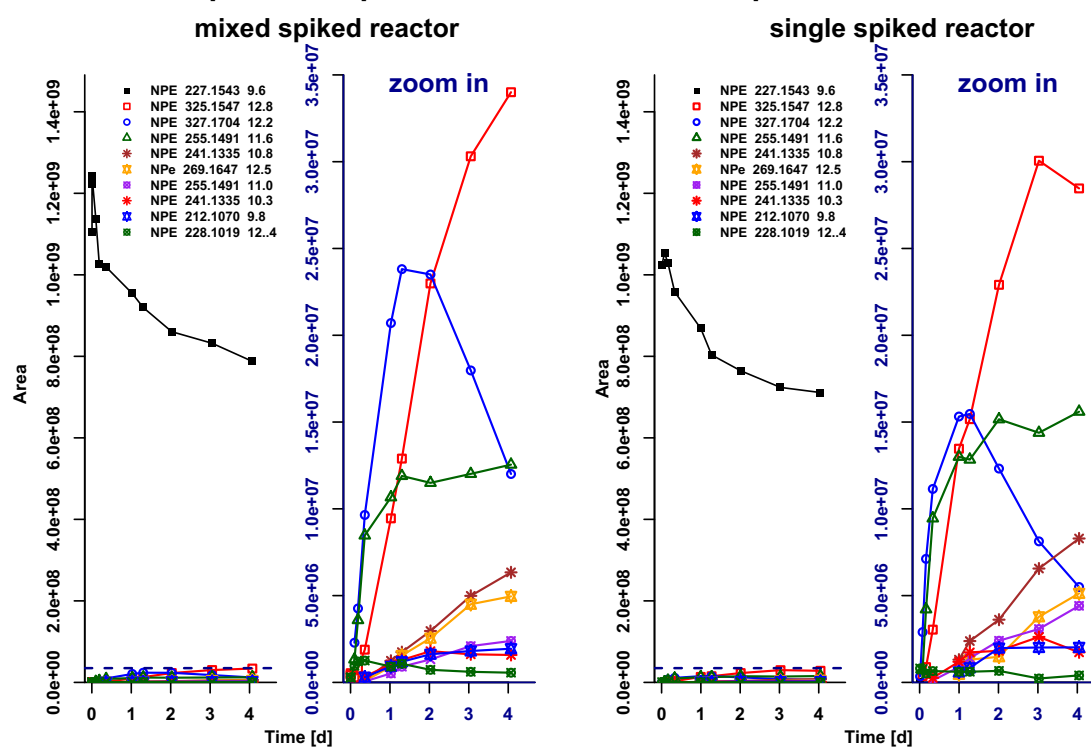
Ortho-chlorophenylpiperazine

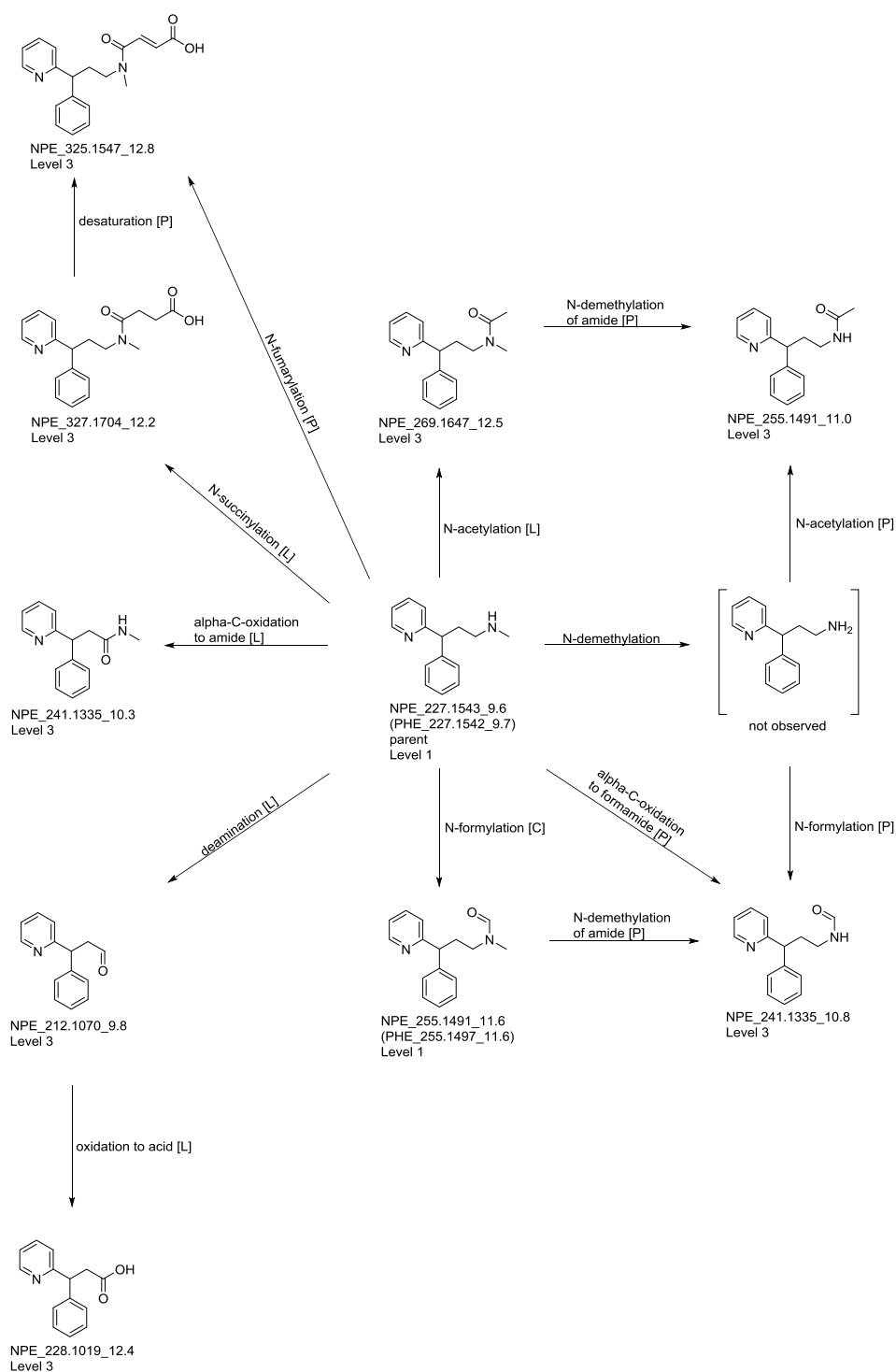
Concentration time series of parent compound

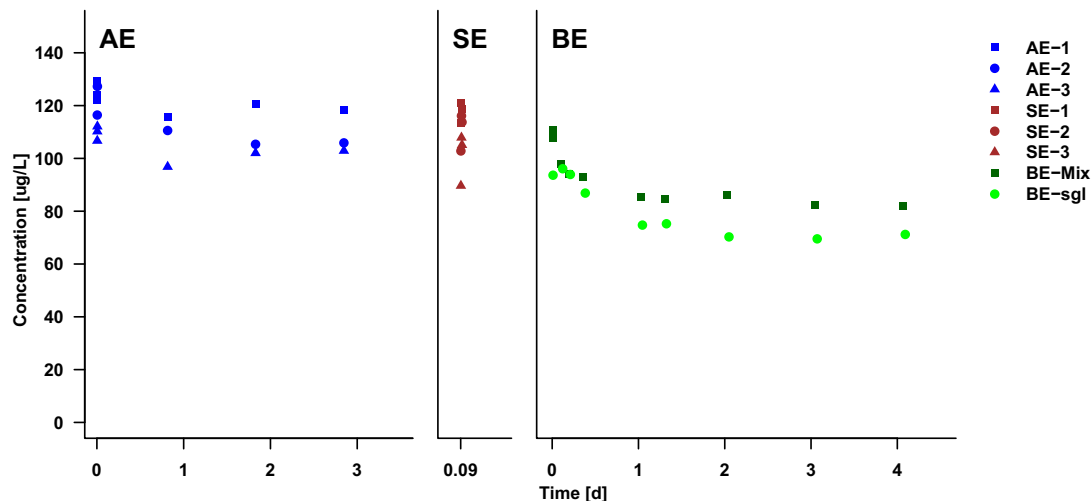
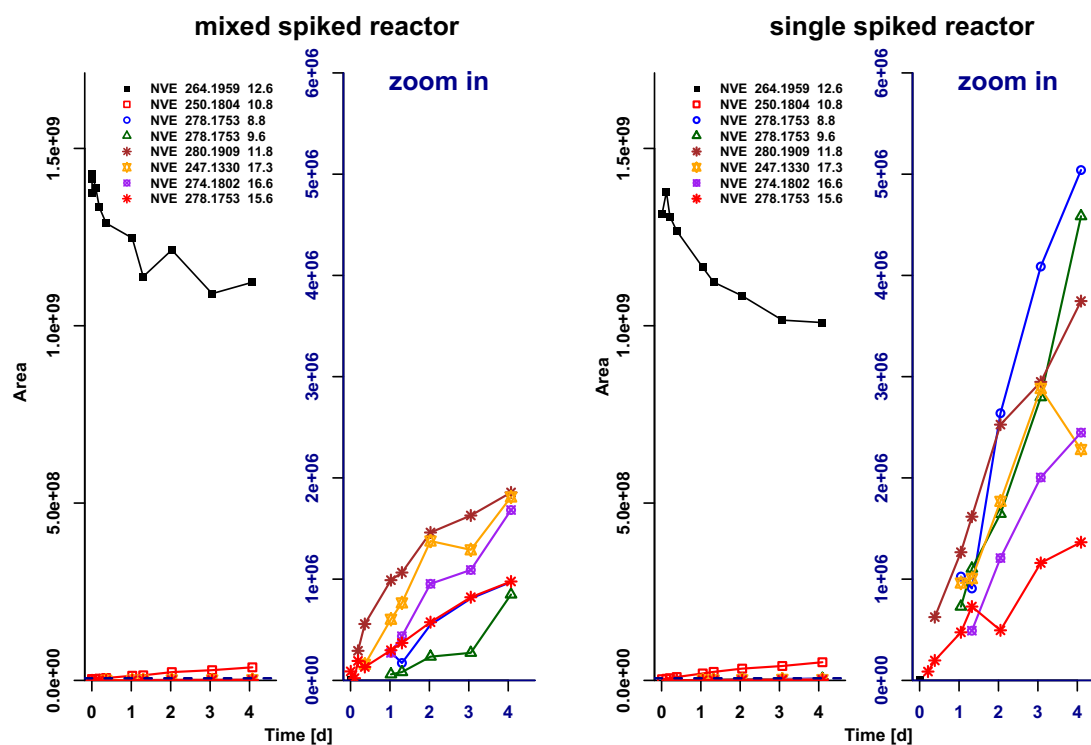


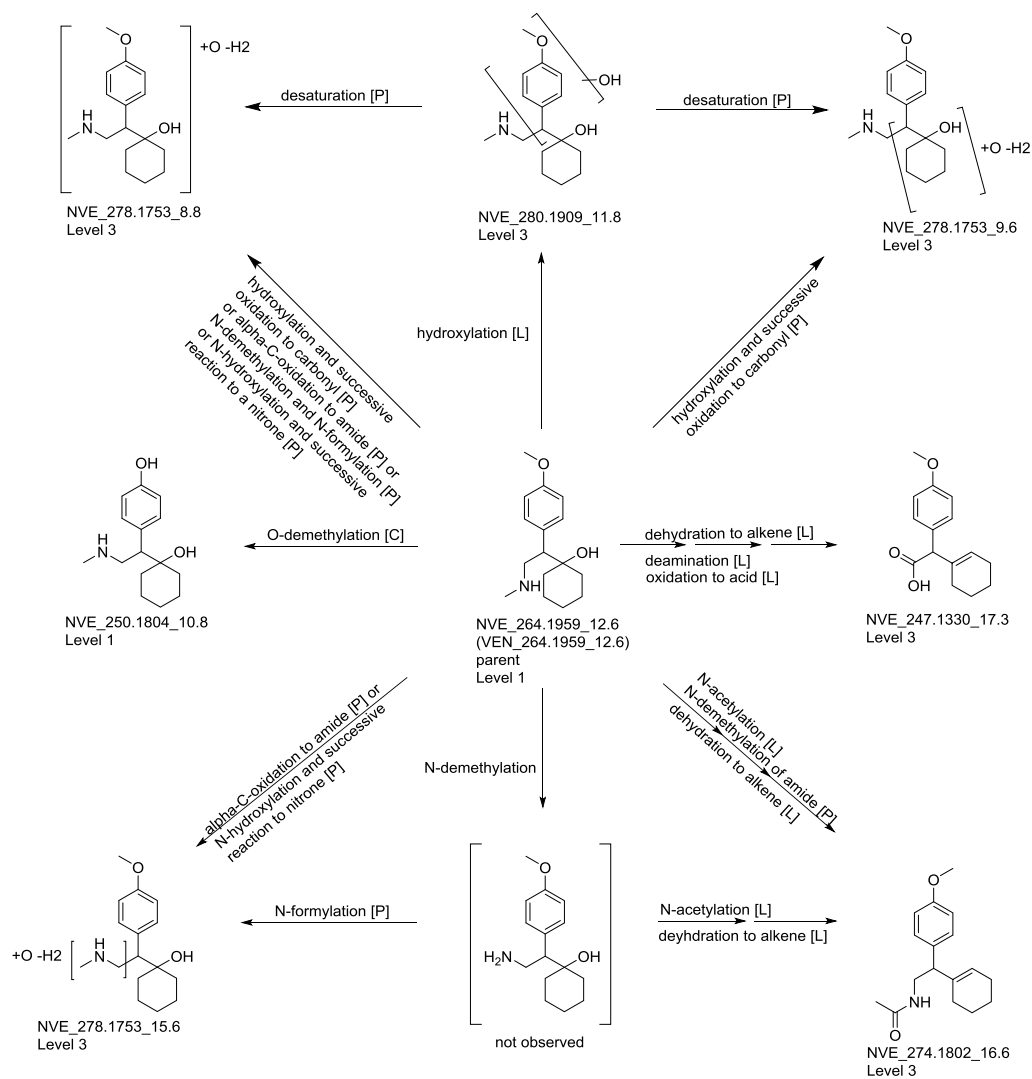
Time series pattern of parent and transformation products in area units



N-demethylpheniramine**Concentration time series of parent compound****Time series pattern of parent and transformation products in area units**

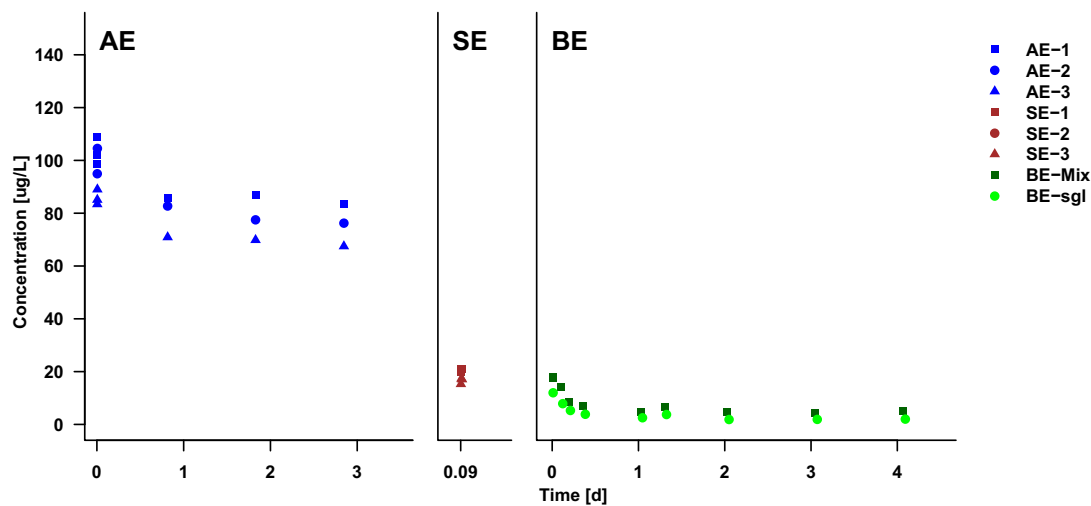


N-demethylvenlafaxine**Concentration time series of parent compound****Time series pattern of parent and transformation products in area units**

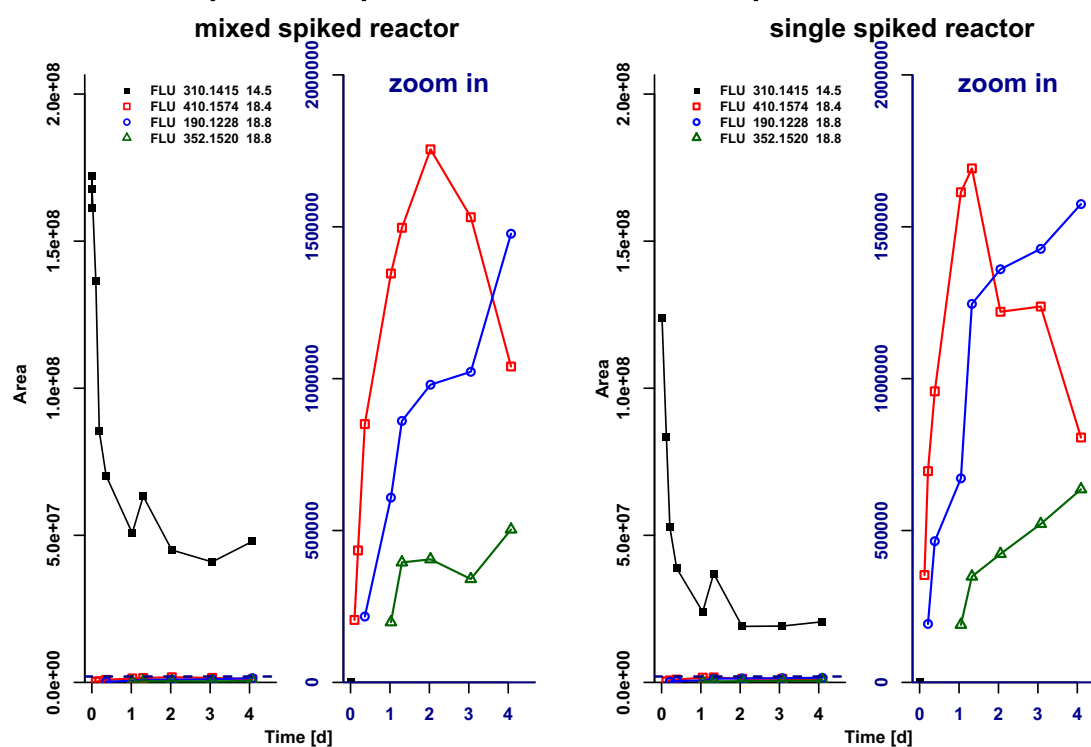


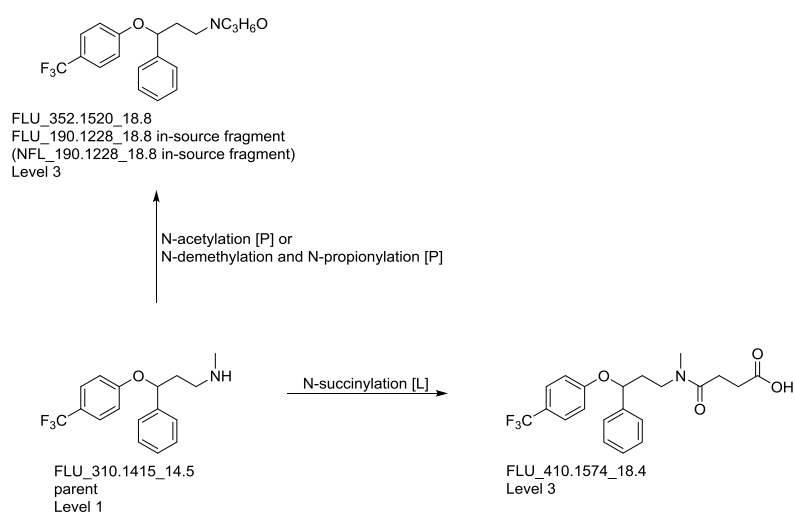
Fluoxetine

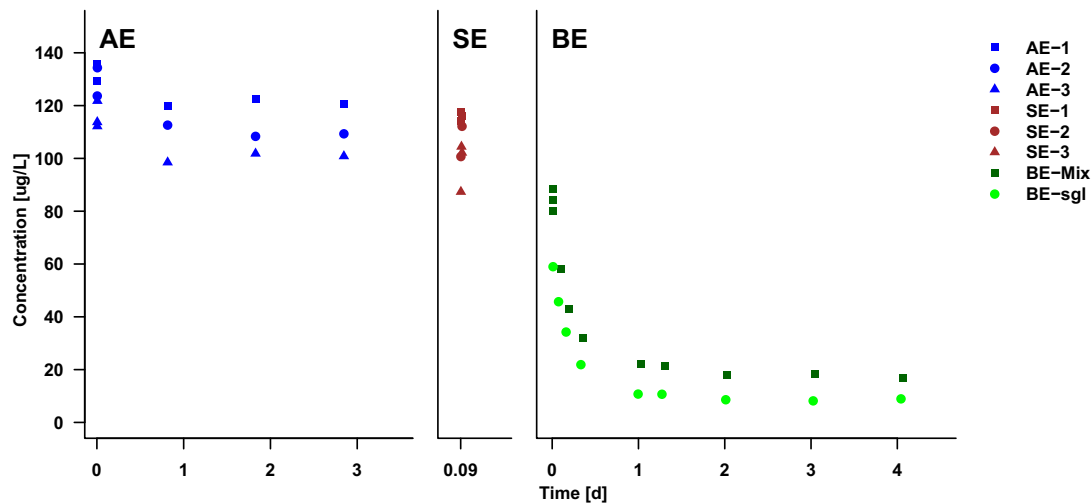
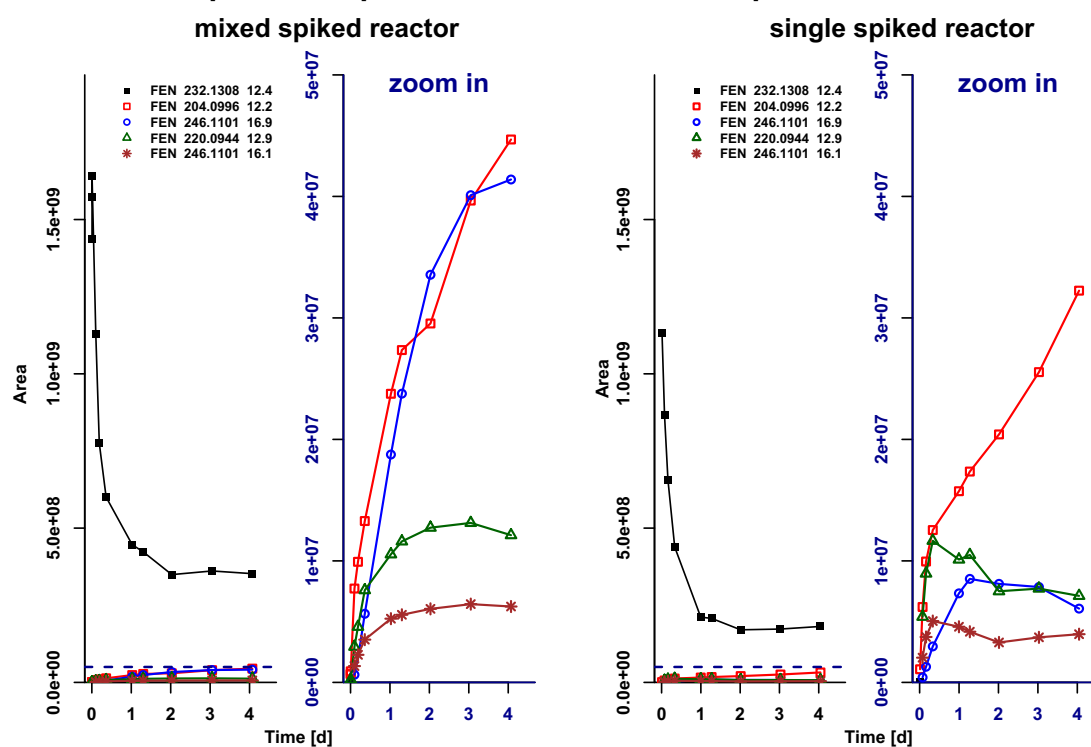
Concentration time series of parent compound

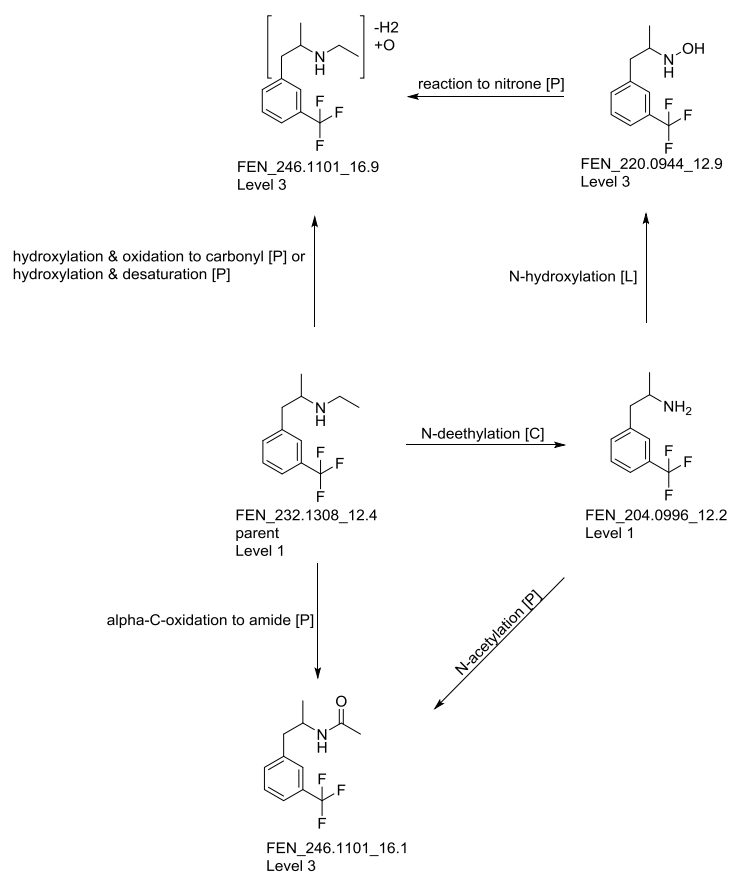


Time series pattern of parent and transformation products in area units



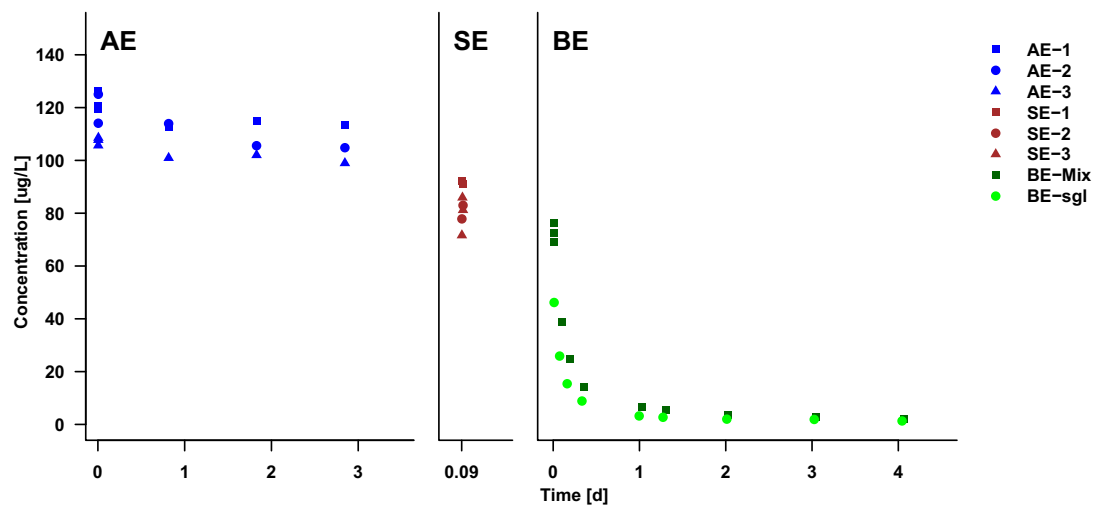


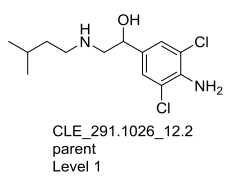
Feniramine**Concentration time series of parent compound****Time series pattern of parent and transformation products in area units**



Clenisopenterole

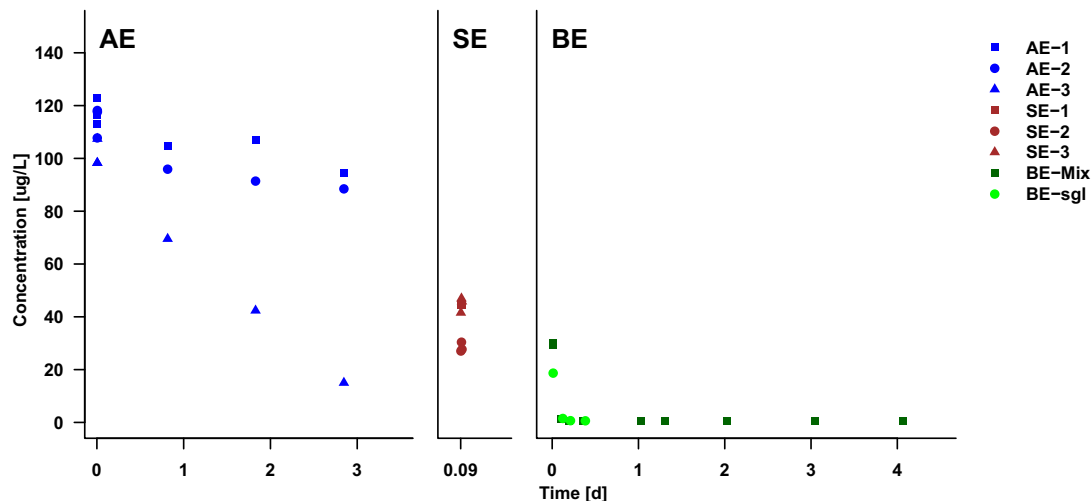
Concentration time series of parent compound





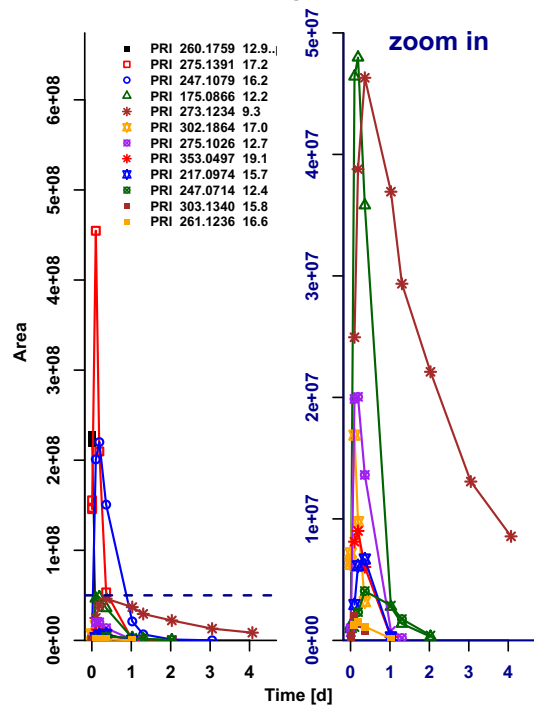
Primaquine

Concentration time series of parent compound

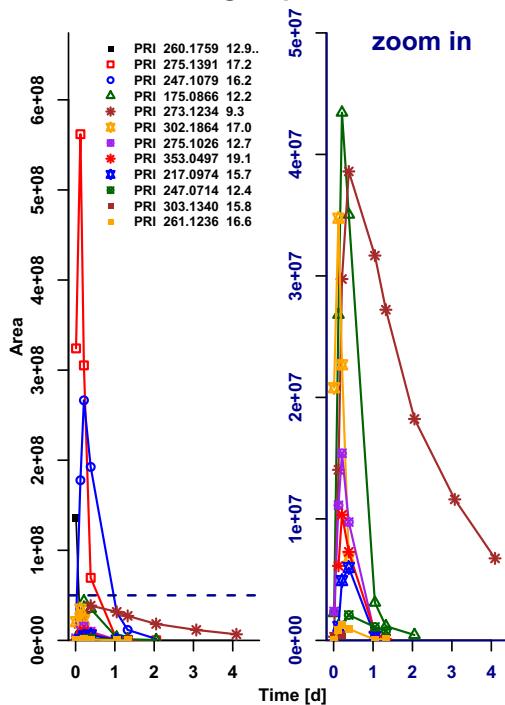


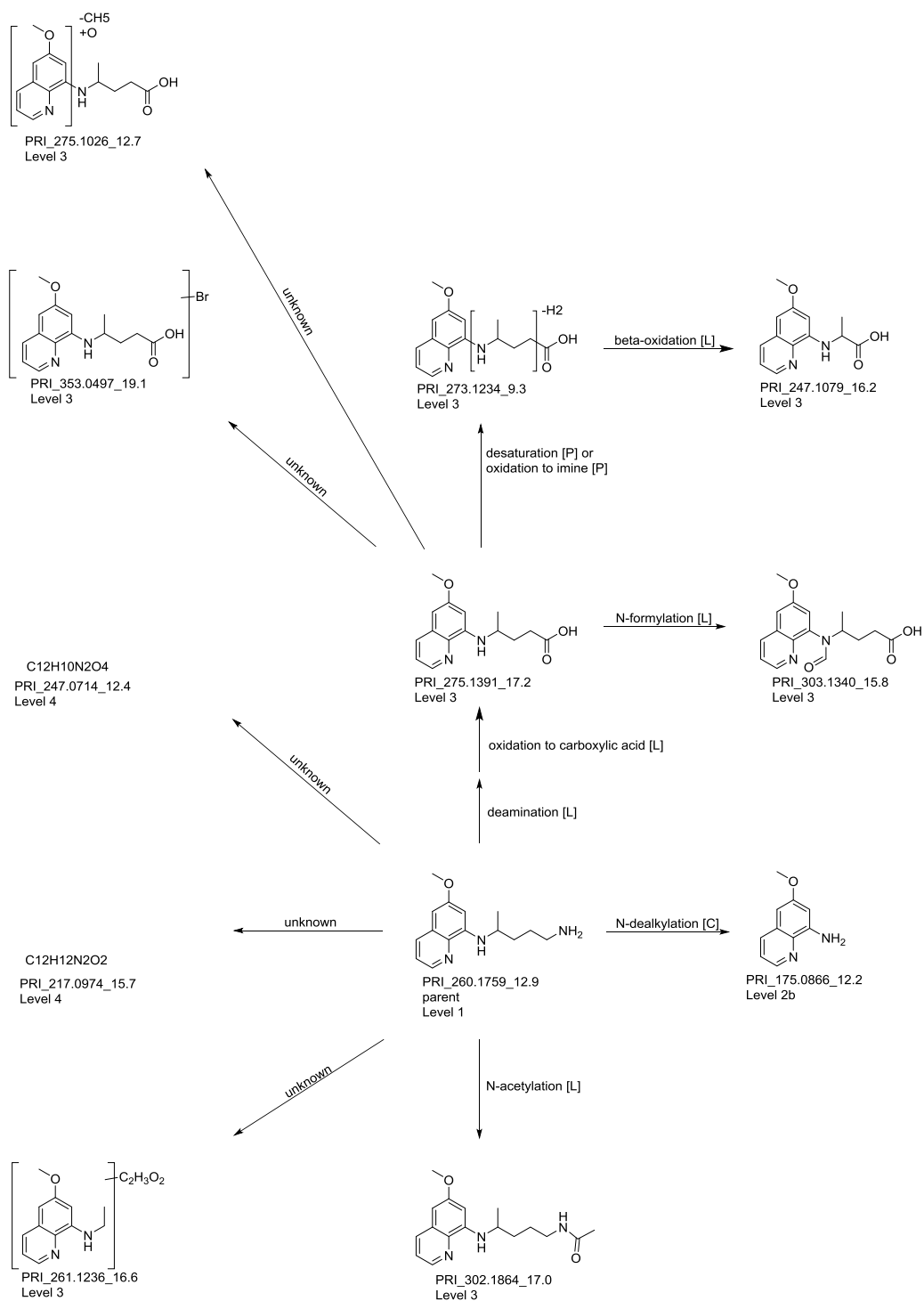
Time series pattern of parent and transformation products in area units

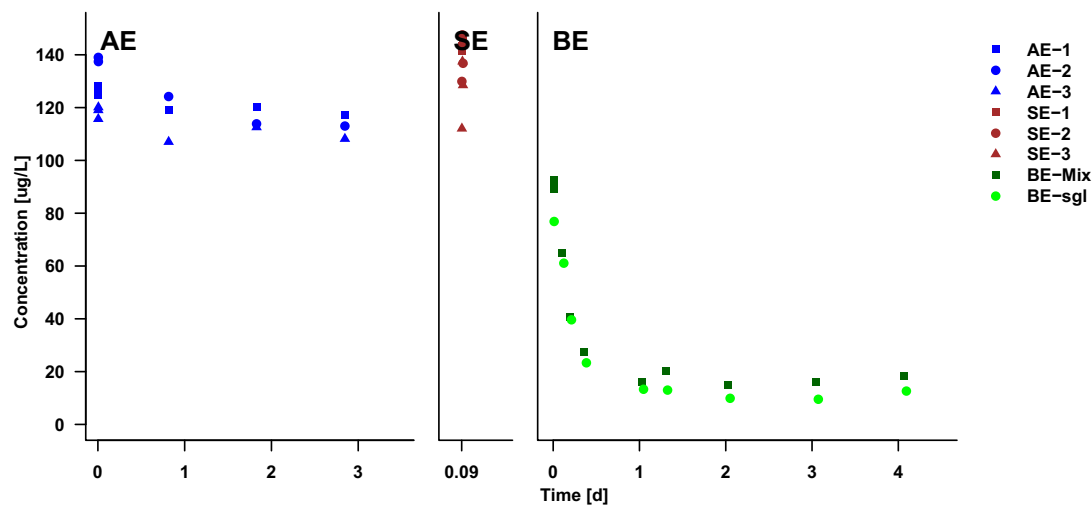
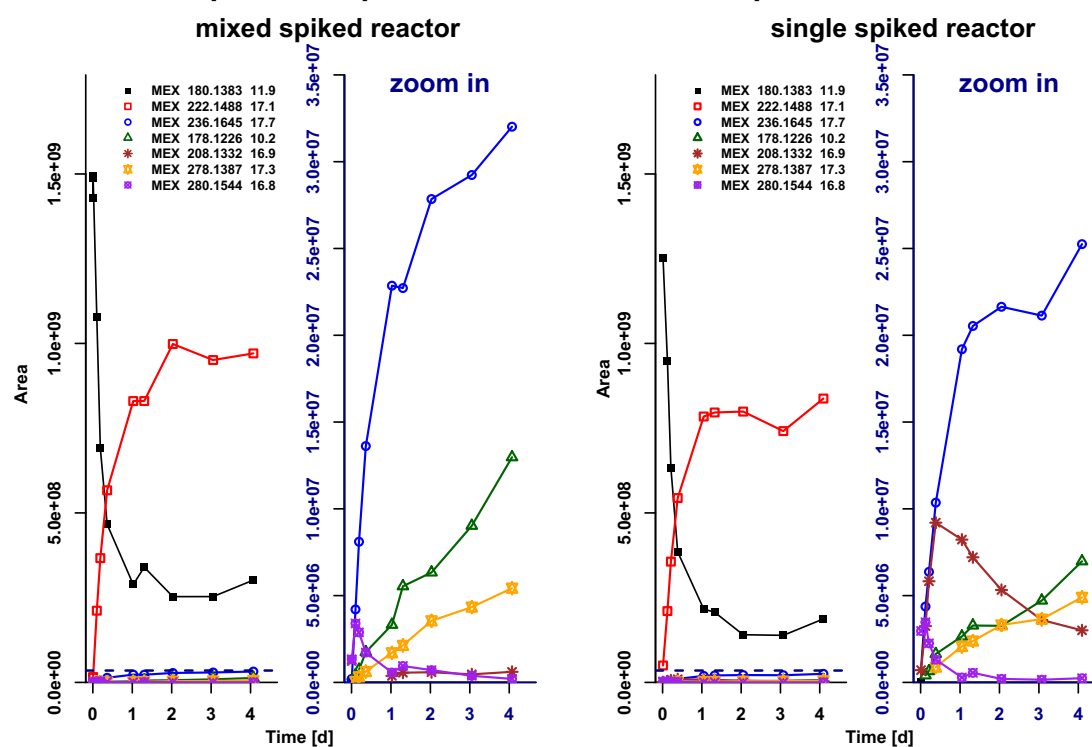
mixed spiked reactor

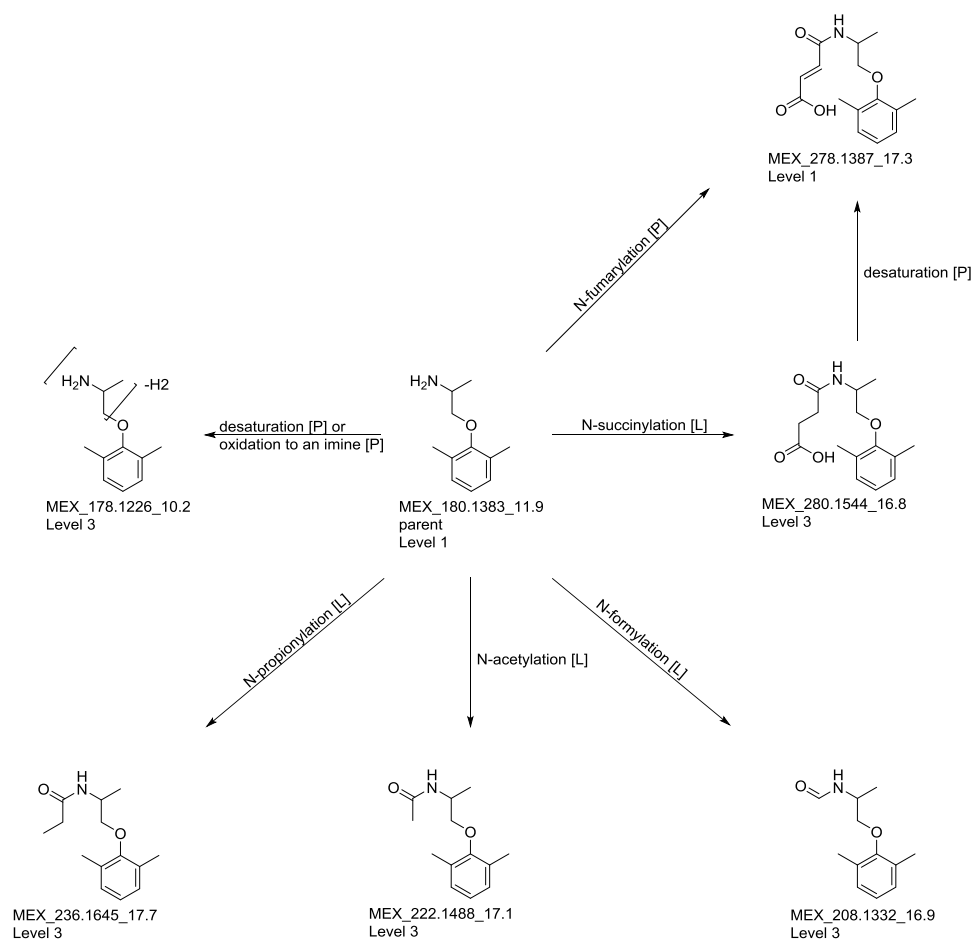


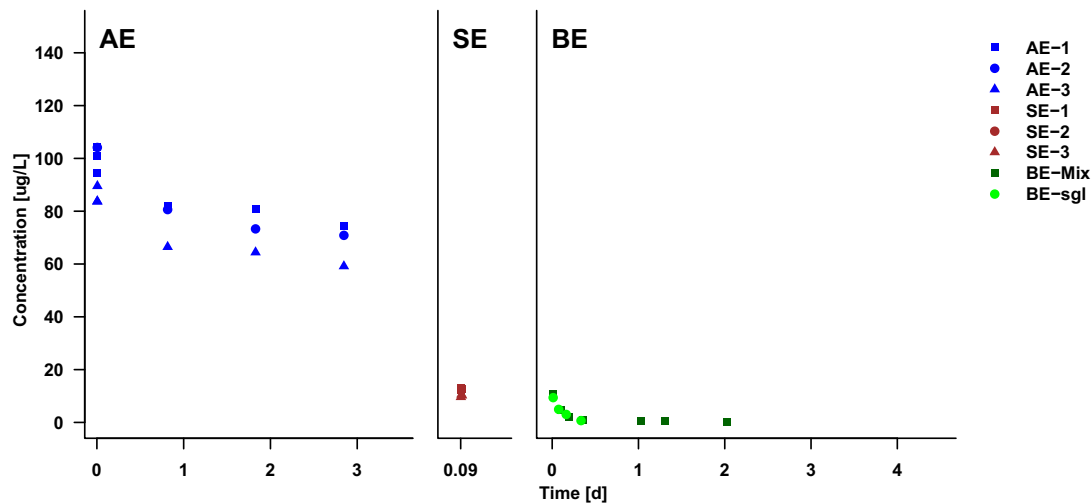
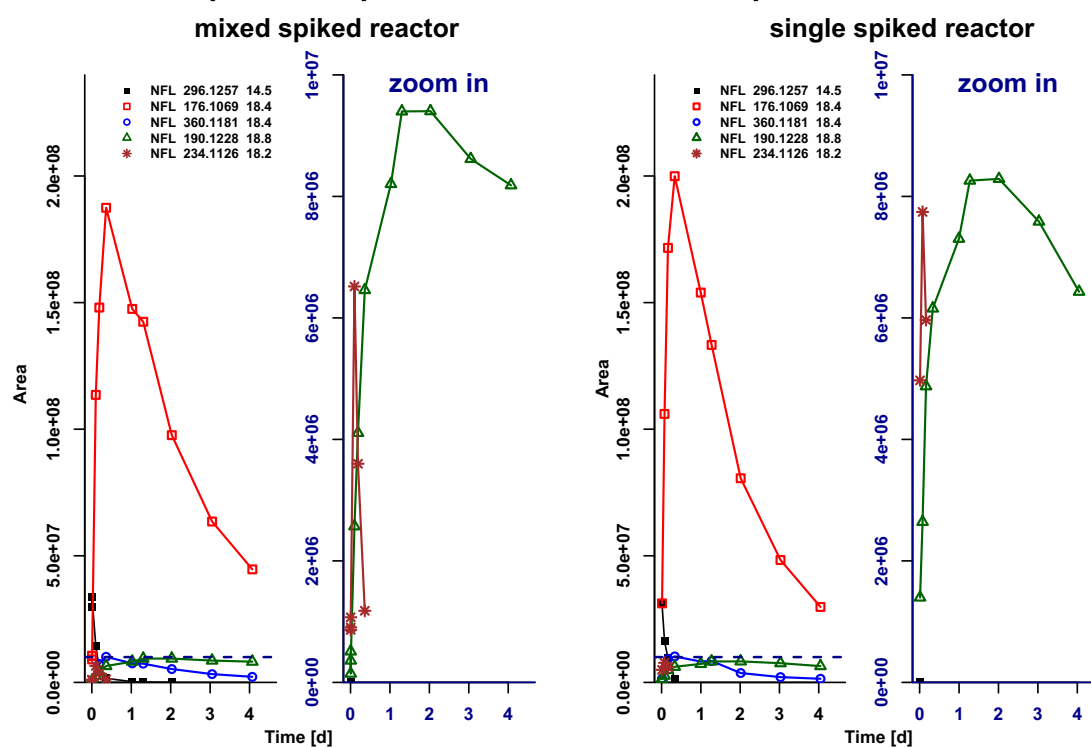
single spiked reactor

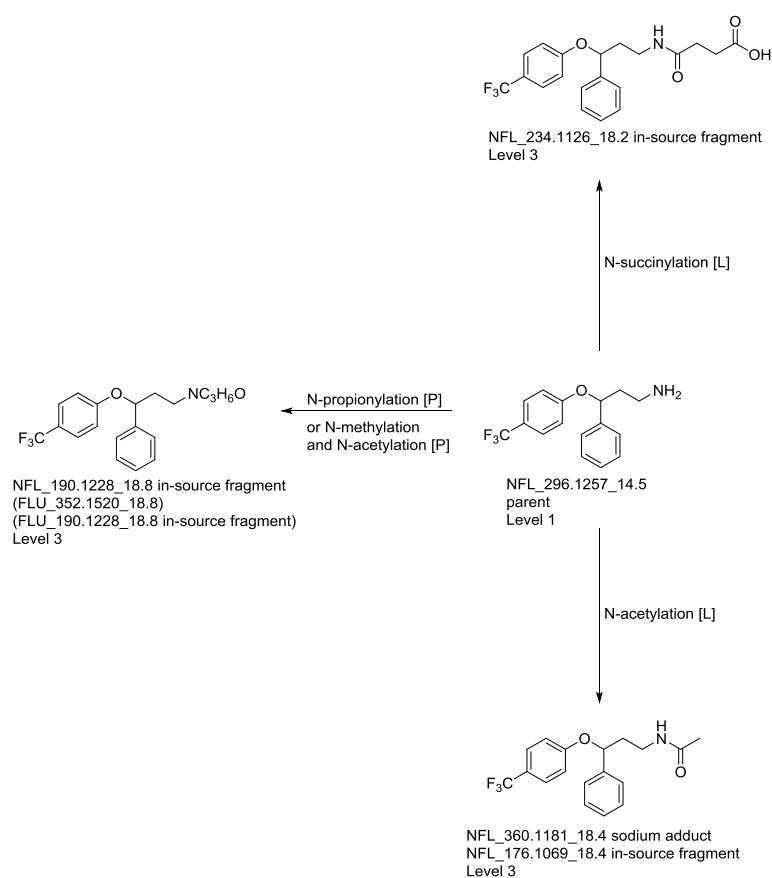




Mexiletine**Concentration time series of parent compound****Time series pattern of parent and transformation products in area units**

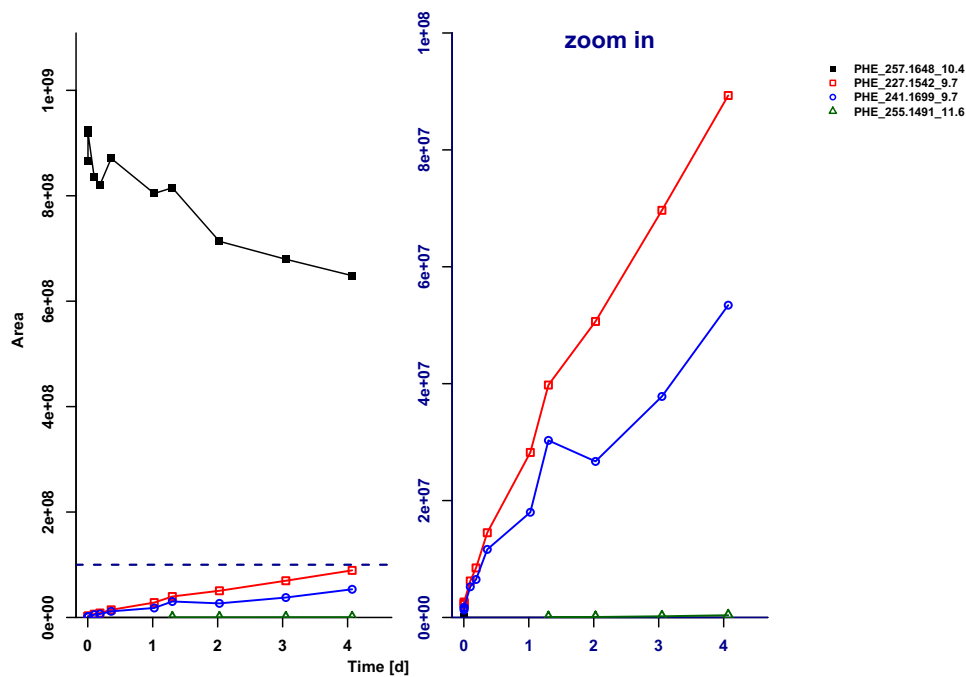


N-demethylfluoxetine**Concentration time series of parent compound****Time series pattern of parent and transformation products in area units**

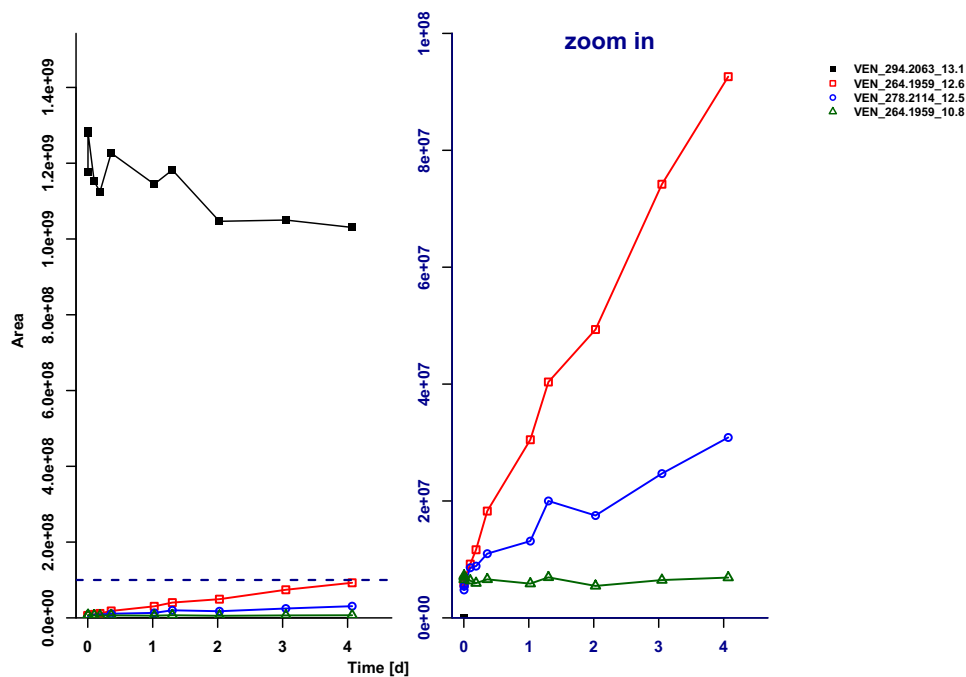


B.7 Time series pattern of reactor spiked with N-oxide mixture

Pheniramine N-oxide

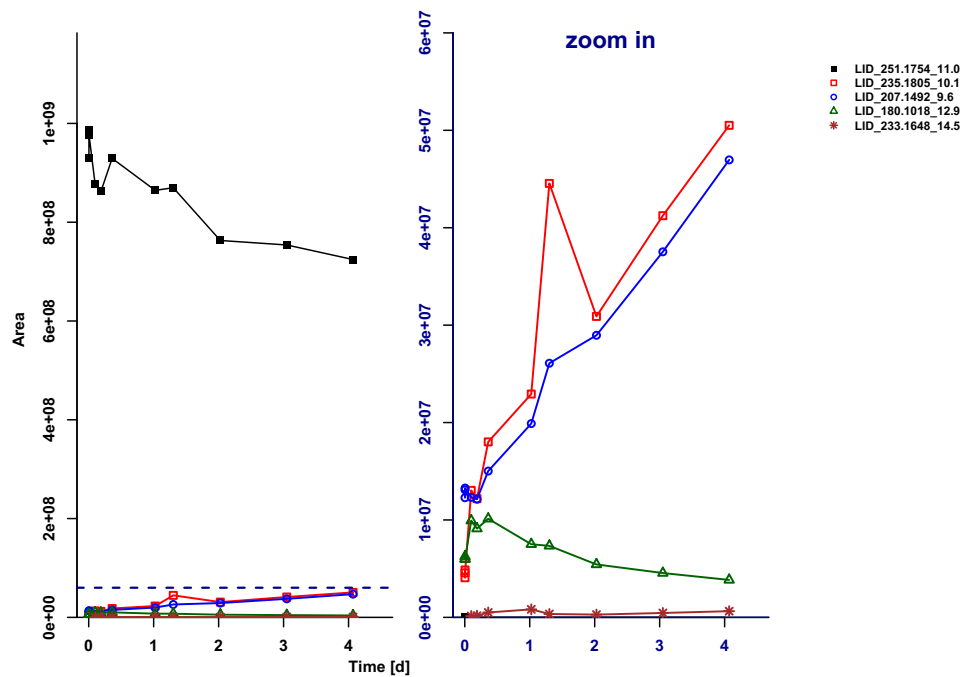


Venlafaxine N-oxide

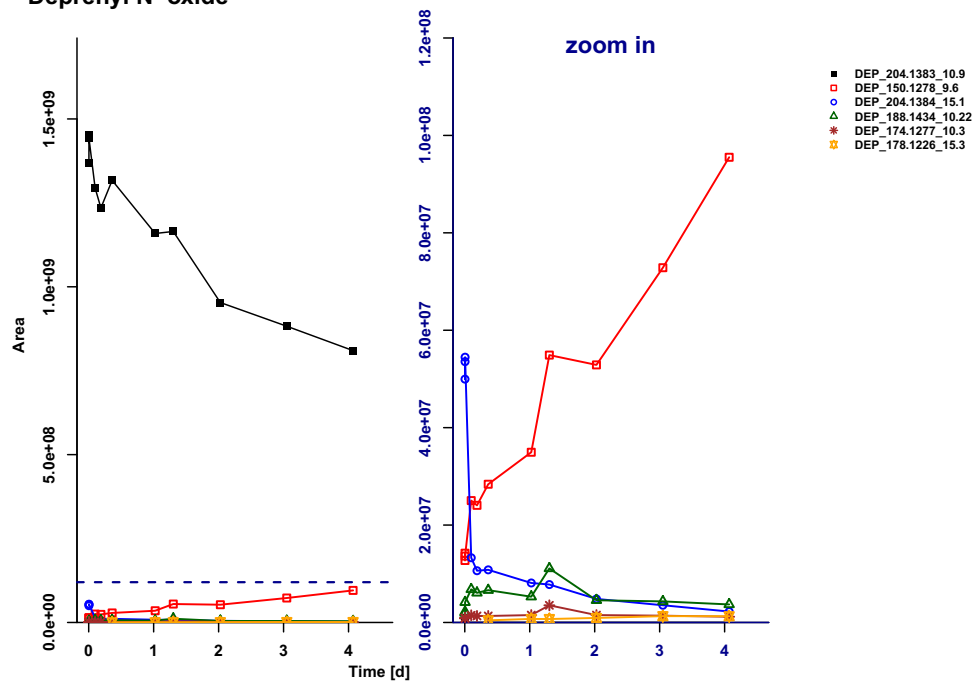


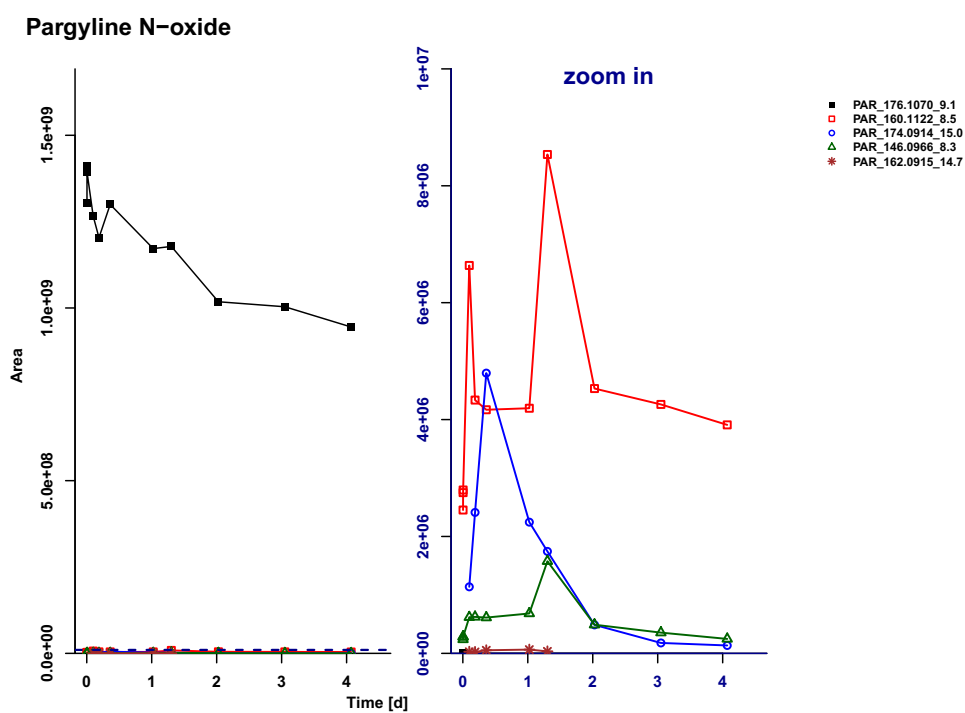
Appendix B

Lidocaine N-oxide



Deprenyl N-oxide





B.8 Products and reactions not involving the amine functional group

Structure	Reaction	A*	B*	C*	Structure	Reaction	A*	B*	C*
	Venlafaxine (VEN)					Chlorocyclizine (CLC)			
	O-demethylation	C ^P	9.5	r		hydroxylation	L	20.6	r
	hydroxylation	L	0.6	r		Pyrilamine (PYR)			
	hydroxylation	L	0.2	r		O-demethylation	C	0.7	rf
	hydroxylation followed by either oxidation to carbonyl or desaturation	P	0.8	r		N-demethylvenlafaxine (NVE)			
	hydroxylation reaction followed by either oxidation to carbonyl or desaturation	P	0.1	r		O-demethylation	C ^P	10.6	r
	either two desaturation reactions or combination of dehydration to alkene and hydroxylation followed by oxidation to carbonyl	P	0.2	r		hydroxylation	L	0.8	r
	Lidocaine (LID)					hydroxylation followed by either desaturation or oxidation to carbonyl	P	0.9	r
	desaturation	C	0.4	rs		Primaquine (PRI)			
	hydroxylation	L	0.2	rf		N-dealkylation (deamination) of 1° amine followed by oxidation to carboxylic acid followed by beta-oxida ion	L	30.5	rf
	hydroxylation followed by oxidation to carboxylic acid	L	0.9	r		unknown	U	0.2	rf
	Spiroxamine (SPI)					unknown	U	2.3	rf
	hydroxylation	L	0.8	rf		unknown		1.2	rf
	unknown	U	0.5	rf		unknown	U	0.5	rf
	hydroxylation	L	4.9	rf		unknown	U	0.8	rf
	hydroxylation followed by either desaturation or oxidation to carbonyl	P	0.1	rf					
	two hydroxylation and desaturation or oxidation of one hydroxyl group to carbonyl	P	38.7	r					
	combination of hydroxylation, oxidation to carboxylic acid, and decarboxylation and a further hydroxylation	P	0.1	rs					
	unknown	U	0.1	u					

* A: certainty of assigned reaction as *certain* (C), *likely* (L), *possible* (P), and *unknown* (U). ^P and ^S indicate TP structures that were confirmed by purchased respectively synthesized reference standards; No subscript for TPs with certainty C indicates *propable* TP structures with Level 2; B: maximal relative amount in %; and C: characterization of time series pattern as rising (r), rising and steady (rs), and rising and falling (rf)

B.9 Comparison of EAWAG-PPS predictions with experimental results

Table B.19: Comparison of predicted and experimentally identified transformation products

	number of predicted TPs	number of predicted higher generation TPs*	number of predicted first generation TPs	number of predicted first generation TPs that were not identified (false positives)	number of predicted first generation TPs that were identified (true positives)	number of identified TPs	number of identified TPs that were not predicted (false negatives)	percentage of predicted first generation TPs that were identified (selectivity) [%]	percentage of identified TPs that were not predicted (100-sensitivity) [%]
PHE	16	11	5	4	1	3	2	20	67
VEN	22	15	7	2	5	8	3	71	38
LID	50	40	10	8	2	6	4	20	67
SPI	69	55	14	9	5	9	4	36	44
DEP	38	27	11	9	2	7	5	18	71
PAR	61	51	10	9	1	4	3	10	75
CLC	89	72	17	14	2	2	0	12	0
PYR	57	47	10	6	4	6	2	40	33
DCA	19	17	2	1	1	3	2	50	67
CPP	76	65	11	11	0	2	2	0	100
OCP	39	32	7	7	0	9	9	0	100
NPE	15	8	7	4	3	9	6	43	67
NVE	21	13	8	5	3	7	4	38	57
FLU	19	13	6	6	0	2	2	0	100
FEN	22	13	9	7	2	4	2	22	50
CLE	48	34	14	14	0	0	0	0	0
PRI	39	29	10	8	2	11	9	20	82
MEX	36	29	7	7	0	6	6	0	100
NFL	14	9	5	5	0	3	3	0	100
total	750	580	170	136	33	101	68	19	67

* including TPs that are too small ($m/z < 50$) to be measured.

B.10 Comparison of ionization efficiencies of transformation products and parent compounds

The comparison of the amounts of parent compounds and the respective TPs is uncertain when only areas are considered since the ionization efficiency between parent compound and TP can vary. However, it can be hypothesized that a specific transformation influences the change of the ionization efficiency from the parent to the TP in a consistent way. To explore this, we looked at all parent-TP pairs for which a calibration row was available. The respective compounds are listed in Table B.20. The ratio of the response of the TP and its parent was calculated by calculating the ratio for each of the 20 calibration points (ranging from 0.5 µg/L to 125 µg/L) and then taking the average and standard deviation of these.

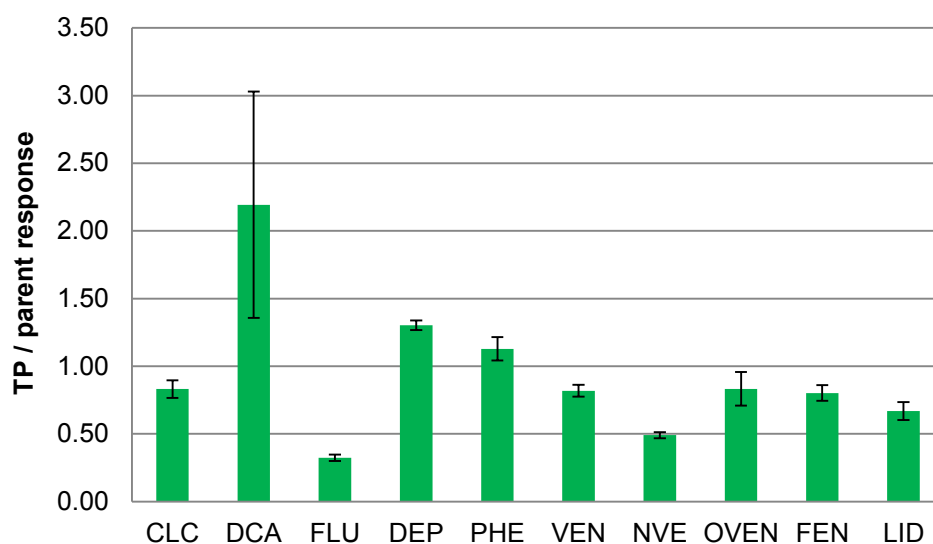
The results can be seen in Table B.20 and Figure B.2. As can be seen, the results falsify the above hypothesis that the ionization efficiency is changed in a consistent way by a specific transformation. For both investigated transformation reactions, namely N-dealkylation and N-oxidation, the observed ionization efficiency was increasing for some and decreasing for other parent-TP pairs. However, we also found that the differences between parent and corresponding TPs are always below a factor of 3.1, and around 1.5 in average.

Table B.20: Comparison of ionization efficiencies of transformation products and parent compounds

Transformation	Parent compound	TP / parent response	factor
N-demethylation	Chlorocyclizine	0.83 ± 0.07	1.20
N-demethylation	N,N-dimethyl-p-chloroaniline	2.2 ± 0.8	2.2
N-demethylation	Fluoxetine	0.32 ± 0.02	3.1
N-demethylation	Deprenyl	1.30 ± 0.04	1.3
N-demethylation	Pheniramine	1.13 ± 0.09	1.1
N-demethylation	Venlafaxine	0.82 ± 0.04	1.2
N-demethylation	N-demethylvenlafaxine	0.49 ± 0.02	2.0
N-demethylation	O-demethylvenlafaxine	0.8 ± 0.1	1.2
N-deethylation	Feniramine	0.80 ± 0.06	1.3
N-deethylation	Lidocaine	0.67 ± 0.07	1.5
N-oxidation	Deprenyl	1.06 ± 0.03	1.1
N-oxidation	Lidocaine	0.58 ± 0.03	1.7
N-oxidation	Pheniramine	1.2 ± 0.1	1.2
N-oxidation	Venlafaxine	0.89 ± 0.06	1.1
N-oxidation	Pargyline	1.26 ± 0.09	1.3

a)

Comparison of ionization efficiencies of parent and TP

N-dealkylation

b)

Comparison of ionization efficiency of parent and TP

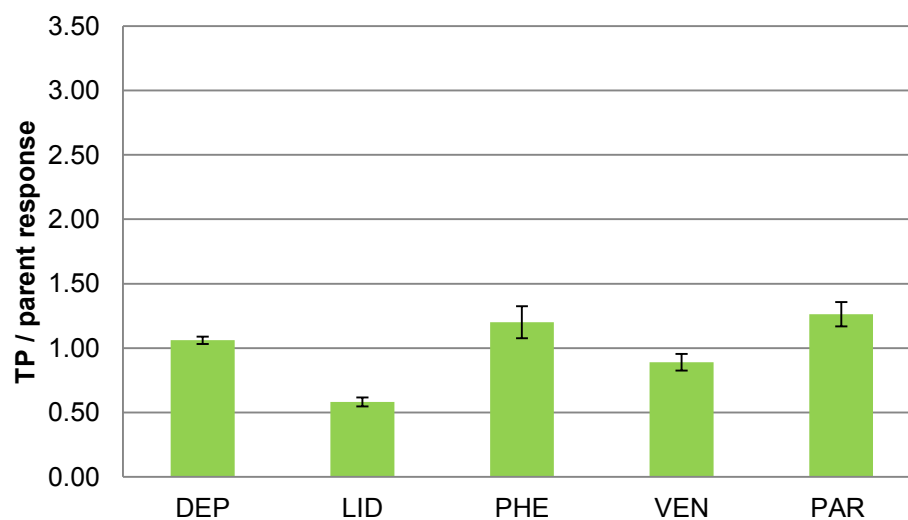
N-oxidation

Figure B.2: Ratio of the response of TP and parent that are formed through a) N-dealkylation and b) N-oxidation

Appendix C:

List of abbreviations

Appendix C

AE	Abiotic control experiment
ARA	Abwasserreinigungsanlage
BE	Biotransformation experiment
CAS	Conventional activated sludge
DMSO	Dimethylsulfoxid
ESI	Electrospray ionization
Eawag-PPS	Eawag pathway prediction system
f_{aq}	Disolved compound fraction
f_{n}	Neutral fraction
g_{ss}	Gram suspended solids
k_{a}	Abiotic transformation rate constant
k_{bio}	Biotransformation rate constant
K_{d}	Sorption coefficient
K_{H}	Henry's law constant
LC-HR-MS/MS	Liquid-chromatography high-resolution tandem mass spectrometry
$[\text{M}+\text{H}]^{+}$	Ion to be analyzed in positive mode (exact mass plus one proton, positively charged)
$[\text{M}-\text{H}]^{-}$	Ion to be analyzed in negative mode (exact mass minus one proton, negatively charged)
MP	Micropollutant
MS	Mass spectrum
MS/MS or MS^2	Tandem mass spectrum
m/z	Mass to charge ratio
NMR	Nuclear magnetic resonance
$\text{p}K_{\text{a}}$	Acidic dissociation constant
QSBR	Quantitative structure biodegradability relationship
rpm	Rotation per minute
SE	Sorption control experiment

TP	Transformation product
TSS	Total suspended solids concentration
UM-PPS	University of Minnesota Pathway Prediction System
WWTP	Wastewater treatment plant

C.1 Abbreviations of micropollutants

ATE	Atenolol
AZO	Azoxystrobin
CHLO	1-(3-chlorophenyl)piperazine
CLC	Chlorocyclizine
CLE	Clenisopenterol
CPP	1[(4-chlorophenyl)phenylmethyl]piperazine
DCA	N,N-dimethyl-p-chloroaniline
DENO	Deprenyl N-oxide
DEP	Deprenyl
FEN	Feniramine
FLU	Fluoxetine
ISO	Isoproturon
LID	Lidocaine
LINO	Lidocaine N-oxide
MIA	Mianserine
MEX	Mexiletine
NFL	N-demethylfluoxetine
NIC	Nicotine
NPE	N-demethylpheniramine
NVE	N-demethylvenlafaxine
OCP	Ortho-chlorophenylpiperazine
ORP	Orphenadrine

Appendix C

PANO	Pargyline N-oxide
PAR	Pargyline
PENO	Pheniramine N-oxide
PHE	Pheniramine
PRA	Pramoxine
PRI	Primaquine
PRO	Propranolol
PYR	Pyrilamine
SPI	Spiroxamine
TRI	Trinexapacethyl
VEN	Venlafaxine
VENO	Venlafaxine N-oxide

Literature

- [1] Luo, Y., Guo, W., Ngo, H. H., Nghiem, L. D., Hai, F. I., Zhang, J., Liang, S., Wang, X. C., A review on the occurrence of micropollutants in the aquatic environment and their fate and removal during wastewater treatment, *Sci. Total Environ.*, **2014**, 473-474, 619 – 641.
- [2] Pico, Y., Barcelo, D., Transformation products of emerging contaminants in the environment and high-resolution mass spectrometry: a new horizon, *Anal. Bioanal. Chem.*, **2015**, 407, 6257–6273.
- [3] Evgenidou, E. N., Konstantinou, I. K., Lambropoulou, D. A., Occurrence and removal of transformation products of PPCPs and illicit drugs in wastewaters: A review, *Sci. Total Environ.*, **2015**, 505, 905 – 926.
- [4] Vajda, A. M., Barber, L. B., Gray, J. L., Lopez, E. M., Woodling, J. D., Norris, D. O., Reproductive disruption in fish downstream from an estrogenic wastewater effluent, *Environ. Sci. Technol.*, **2008**, 42, 3407–3414.
- [5] Liney, K. E., Hagger, J. A., Tyler, C. R., Depledge, M. H., Galloway, T. S., Jobling, S., Health effects in fish of long-term exposure to effluents from wastewater treatment works, *Environ. Health Perspect.*, **2006**, 114, 81–89.
- [6] Stalter, D., Magdeburg, A., Quednow, K., Botzat, A., Oehlmann, J., Do contaminants originating from state-of-the-art treated wastewater impact the ecological quality of surface waters?, *PloS one*, **2013**, 8, e60616.
- [7] Malaj, E., von der Ohe, P. C., Grote, M., Kühne, R., Mondy, C. P., Usseglio-Polatera, P., Brack, W., Schäfer, R. B., Organic chemicals jeopardize the health of freshwater ecosystems on the continental scale, *Proc. Natl. Acad. Sci. U. S. A.*, **2014**, 111, 9549–9554.
- [8] Hollender, J., Zimmermann, S. G., Koepke, S., Krauss, M., McArdell, C. S., Ort, C., Singer, H. P., von Gunten, U., Siegrist, H., Elimination of organic

- micropollutants in a municipal wastewater treatment plant upgraded with a full-scale post-ozonation followed by sand filtration, *Environ. Sci. Technol.*, **2009**, 43, 7862–7869.
- [9] Escher, B. I., Fenner, K., Recent advances in environmental risk assessment of transformation products, *Environ. Sci. Technol.*, **2011**, 45, 3835–3847.
- [10] Ternes, T. A., Joss, A., Siegrist, H., Scrutinizing pharmaceuticals and personal care products in wastewater treatment, *Environ. Sci. Technol.*, **2004**, 38, 392A–399A.
- [11] Prasse, C., Stalter, D., Schulte-Oehlmann, U., Oehlmann, J., Ternes, T. A., Spoilt for choice: A critical review on the chemical and biological assessment of current wastewater treatment technologies, *Water Res.*, **2015**, 87, 237–270.
- [12] Oulton, R. L., Kohn, T., Cwiertny, D. M., Pharmaceuticals and personal care products in effluent matrices: A survey of transformation and removal during wastewater treatment and implications for wastewater management, *J. Environ. Monit.*, **2010**, 12, 1956–1978.
- [13] Lapertot, M. E., Pulgarin, C., Biodegradability assessment of several priority hazardous substances: Choice, application and relevance regarding toxicity and bacterial activity, *Chemosphere*, **2006**, 65, 682 – 690.
- [14] Helbling, D. E., Johnson, D. R., Honti, M., Fenner, K., Micropollutant biotransformation kinetics associate with wwtp process parameters and microbial community characteristics, *Environ. Sci. Technol.*, **2012**, 46, 10579–10588.
- [15] Joss, A., Keller, E., Alder, A. C., Göbel, A., McArdell, C. S., Ternes, T. A., Siegrist, H., Removal of pharmaceuticals and fragrances in biological wastewater treatment, *Water Res.*, **2005**, 39, 3139–3152.
- [16] Ternes, T. A., Herrmann, N., Bonerz, M., Knacker, T., Siegrist, H., Joss, A., A rapid method to measure the solid-water distribution coefficient (K_d) for pharmaceuticals and musk fragrances in sewage sludge, *Water Res.*, **2004**, 38, 4075 – 4084.
- [17] Tadkaew, N., Hai, F. I., McDonald, J. A., Khan, S. J., Nghiem, L. D., Removal of trace organics by mbr treatment: The role of molecular properties, *Water Res.*, **2011**, 45, 2439 – 2451.
- [18] Rogers, H. R., Sources, behaviour and fate of organic contaminants during sewage treatment and in sewage sludges, *Sci. Total Environ.*, **1996**, 185, 3 – 26.

-
- [19] Götz, C. W., Stamm, C., Fenner, K., Singer, H., Schärer, M., Hollender, J., Targeting aquatic microcontaminants for monitoring: Exposure categorization and application to the swiss situation, *Environ. Sci. Pollut. Res.*, **2010**, 17, 341–354.
- [20] Helbling, D. E., Hollender, J., Kohler, H. P. E., Fenner, K., Structure-based interpretation of biotransformation pathways of amide-containing compounds in sludge-seeded bioreactors, *Environ. Sci. Technol.*, **2010**, 44, 6628–6635.
- [21] Howard, P. H., Stiteler, W. M., Meylan, W. M., Hueber, A. E., Beauman, J. A., Larosche, M. E., Boethling, R. S., Predictive model for aerobic biodegradability developed from a file of evaluated biodegradation data, *Environ. Toxicol. Chem.*, **1992**, 11, 593–603.
- [22] Boethling, R. S., Howard, P. H., Meylan, W., Stiteler, W., Beauman, J., Tirado, N., Group contribution method for predicting probability and rate of aerobic biodegradation, *Environ. Sci. Technol.*, **1994**, 28, 459–465.
- [23] Tunkel, J., Howard, P. H., Boethling, R. S., Stiteler, W., Loonen, H., Predicting ready biodegradability in the japanese ministry of international trade and industry test, *Environ. Toxicol. Chem.*, **2000**, 19, 2478–2485.
- [24] Yu, J. T., J., B. E., Coelhan, M., Occurrence and biodegradability studies of selected pharmaceuticals and personal care products in sewage effluent, *Agricultural Water Management*, **2006**, 86, 72 – 80.
- [25] Fernandez-Fontaina, E., Omil, F., Lema, J. M., Carballa, M., Influence of nitrifying conditions on the biodegradation and sorption of emerging micropollutants, *Water Res.*, **2012**, 46, 5434–5444.
- [26] Suarez, S., Lema, J. M., Omil, F., Removal of pharmaceutical and personal care products (ppcps) under nitrifying and denitrifying conditions, *Water Res.*, **2010**, 44, 3214–3224.
- [27] Clara, M., Kreuzinger, N., Strenn, B., Gans, O., Kroiss, H., The solids retention time - suitable design parameter to evaluate the capacity of wastewater treatment plants to remove micropollutants, *Water Res.*, **2005**, 39, 97 – 106.
- [28] Wick, A., Fink, G., Joss, A., Siegrist, H., Ternes, T. A., Fate of beta blockers and psycho-active drugs in conventional wastewater treatment, *Water Res.*, **2009**, 43, 1060 – 1074.
- [29] Stasinakis, A. S., Kordoutis, C. I., Tsiouma, V. C., Gatidou, G., Thomaidis, N. S., Removal of selected endocrine disrupters in activated sludge systems:

- Effect of sludge retention time on their sorption and biodegradation, *Bioresour. Technol.*, **2010**, 101, 2090–2095.
- [30] Qiang, Z., Dong, H., Zhu, B., Qu, J., Nie, Y., A comparison of various rural wastewater treatment processes for the removal of endocrine-disrupting chemicals (edcs), *Chemosphere*, **2013**, 92, 986–992.
- [31] Zwiener, C., Frimmel, F. H., Short-term tests with a pilot sewage plant and biofilm reactors for the biological degradation of the pharmaceutical compounds clofibric acid, ibuprofen, and diclofenac, *Sci. Total Environ.*, **2003**, 309, 201–211.
- [32] Goel, A., Müller, M. B., Sharma, M., Frimmel, F. H., Biodegradation of nonylphenol ethoxylate surfactants in biofilm reactors, *Acta hydrochim. hydrobiol.*, **2003**, 31, 108–119.
- [33] Huang, M., Li, Y., Gu, G., The effects of hydraulic retention time and sludge retention time on the fate of di-(2-ethylhexyl) phthalate in a laboratory-scale anaerobic–anoxic–aerobic activated sludge system, *Bioresour. Technol.*, **2008**, 99, 8107–8111.
- [34] Drewes, J. E., Fox, P., Jekel, M., Occurrence of iodinated x-ray contrast media in domestic effluents and their fate during indirect potable reuse, *J. Environ. Sci. Health., Part A*, **2001**, 36, 1633–1645.
- [35] Alvarino, T., Suarez, S., Lema, J. M., Omil, F., Understanding the removal mechanisms of ppcps and the influence of main technological parameters in anaerobic uasb and aerobic cas reactors, *J. Hazard. Mater.*, **2014**, 278, 506–513.
- [36] Boxall, A. B. A., Sinclair, C. J., Fenner, K., Kolpin, D., Maund, S. J., When synthetic chemicals degrade in the environment, *Environ. Sci. Technol.*, **2004**, 38, 368A–375A.
- [37] Bletsou, A. A., Jeon, J., Hollender, J., Archontaki, E., Thomaidis, N. S., Targeted and non-targeted liquid chromatography-mass spectrometric workflows for identification of transformation products of emerging pollutants in the aquatic environment, *TrAC-Trend. Anal. Chem.*, **2015**, 66, 32 – 44.
- [38] Stadler, L. B., Ernstoff, A. S., Aga, D. S., Love, N. G., Micropollutant fate in wastewater treatment: redefining removal, *Environ. Sci. Technol.*, **2012**, 46, 10485–10486.

- [39] Haddad, T., Baginska, E., Kuemmerer, K., Transformation products of antibiotic and cytostatic drugs in the aquatic cycle that result from effluent treatment and abiotic/biotic reactions in the environment: An increasing challenge calling for higher emphasis on measures at the beginning of the pipe, *Water Res.*, **2015**, 72, 75 – 126.
- [40] Schymanski, E. L., Singer, H. P., Longrée, P., Loos, M., Ruff, M., Stravs, M. A., Ripollés Vidal, C., Hollender, J., Strategies to characterize polar organic contamination in wastewater: Exploring the capability of high resolution mass spectrometry, *Environ. Sci. Technol.*, **2014**, 48, 1811–1818.
- [41] Manallack, D. T., The acid-base profile of a contemporary set of drugs: implications for drug discovery, *SAR QSAR Environ. Res.*, **2009**, 20, 611–655.
- [42] Verlicchi, P., Al Aukidy, M., Zambello, E., Occurrence of pharmaceutical compounds in urban wastewater: Removal, mass load and environmental risk after a secondary treatment - a review, *Sci. Total Environ.*, **2012**, 429, 123 – 155.
- [43] Erickson, R. J., McKim, J. M., Lien, G. J., Hoffman, A. D., Batterman, S. L., Uptake and elimination of ionizable organic chemicals at fish gills: I. model formulation, parameterization, and behavior, *Environ. Toxicol. Chem.*, **2006**, 25, 1512–1521.
- [44] Erickson, R. J., McKim, J. M., Lien, G. J., Hoffman, A. D., Batterman, S. L., Uptake and elimination of ionizable organic chemicals at fish gills: II. observed and predicted effects of pH, alkalinity, and chemical properties, *Environ. Toxicol. Chem.*, **2006**, 25, 1522–1532.
- [45] Rendal, C., Kusk, K. O., Trapp, S., Optimal choice of pH for toxicity and bioaccumulation studies of ionizing organic chemicals, *Environ. Toxicol. Chem.*, **2011**, 30, 2395–2406.
- [46] Neuwoehner, J., Escher, B. I., The pH-dependent toxicity of basic pharmaceuticals in the green algae *Scenedesmus vacuolatus* can be explained with a toxicokinetic ion-trapping model, *Aquat. Toxicol.*, **2011**, 101, 266–275.
- [47] Testa, B., *Biochemistry of Redox Reactions*, Academic Press, **1995**.
- [48] Testa, B., Krämer, S. D., The biochemistry of drug metabolism - an introduction: Part 1. principles and overview, *Chem. Biodiversity*, **2006**, 3, 1053–1101.
- [49] Testa, B., Krämer, S. D., The biochemistry of drug metabolism - an introduction: Part 2. redox reactions and their enzymes, *Chem. Biodiversity*, **2007**, 4, 257–405.

- [50] Testa, B., Krämer, S. D., The biochemistry of drug metabolism - an introduction: Part 3. reactions of hydrolysis and their enzymes, *Chem. Biodiversity*, **2007**, 4, 2031–2122.
- [51] Testa, B., Krämer, S. D., The biochemistry of drug metabolism - an introduction: Part 4. reactions of conjugation and their enzymes, *Chem. Biodiversity*, **2008**, 5, 2171–2336.
- [52] Rose, J., Castagnoli, N. I., The metabolism of tertiary amines, *Med. Res. Rev.*, **1983**, 3, 73–88.
- [53] Azerad, R., Microbial models for drug metabolism., *Adv. Biochem. Eng. Biotechnol.*, **1999**, 63, 169–218.
- [54] Celiz, M. D., Tso, J., Aga, D. S., Pharmaceutical metabolites in the environment: Analytical challenges and ecological risks, *Environ. Toxicol. Chem.*, **2009**, 28, 2473–2484.
- [55] Hollender, J., Bourgin, M., Fenner, K. B., Longrée, P., Mcardell, C. S., Moschet, C., Ruff, M., Schymanski, E. L., Singer, H. P., Exploring the behaviour of emerging contaminants in the water cycle using the capabilities of high resolution mass spectrometry, *Chimia*, **2014**, 68, 793–798.
- [56] Schymanski, E. L., et al., Non-target screening with high-resolution mass spectrometry: critical review using a collaborative trial on water analysis, *Anal. Bioanal. Chem.*, **2015**, 407, 6237–6255.
- [57] Schollée, J., Schymanski, E. L., Avak, S., Loos, M., Hollender, J., Prioritizing unknown transformation products from biologically-treated wastewater using high-resolution mass spectrometry, multivariate statistics, and metabolic logic, *Anal. Chem.*, submitted.
- [58] Helbling, D. E., Hollender, J., Kohler, H. P. E., Singer, H., Fenner, K., High-throughput identification of microbial transformation products of organic micropollutants, *Environ. Sci. Technol.*, **2010**, 44, 6621–6627.
- [59] Schymanski, E. L., Jeon, J., Gulde, R., Fenner, K., Ruff, M., Singer, H. P., Hollender, J., Identifying small molecules via high resolution mass spectrometry: Communicating confidence, *Environ. Sci. Technol.*, **2014**, 48, 2097–2098.
- [60] Blair, B. D., Crago, J. P., Hedman, C. H., Treguer, R. J. F., Magruder, C., Royer, L. S., Klaper, R. D., Evaluation of a model for the removal of pharmaceuticals, personal care products, and hormones from wastewater, *Sci. total Environ.*, **2013**, 444, 515 – 521.

- [61] Tran, N. H., Urase, T., Ngo, H. H., Hu, J., Ong, S. L., Insight into metabolic and cometabolic activities of autotrophic and heterotrophic microorganisms in the biodegradation of emerging trace organic contaminants, *Bioresour. Technol.*, **2013**, 146, 721–731.
- [62] Eggen, R. L., Hollender, J., Joss, A., Schärer, M., Stamm, C., Reducing the discharge of micropollutants in the aquatic environment: The benefits of upgrading wastewater treatment plants, *Environ. Sci. Technol.*, **2014**, 48, 7683–7689.
- [63] Urase, T., Kikuta, T., Separate estimation of adsorption and degradation of pharmaceutical substances and estrogens in the activated sludge process, *Water Res.*, **2005**, 39, 1289–1300.
- [64] Tadkaew, N., Sivakumar, M., Khan, S. J., McDonald, J. A., Nghiem, L. D., Effect of mixed liquor pH on the removal of trace organic contaminants in a membrane bioreactor, *Bioresour. Technol.*, **2010**, 101, 1494–1500.
- [65] Kimura, K., Hara, H., Watanabe, Y., Elimination of selected pharmaceuticals by biosolids from municipal wastewater treatment plants: Importance of modest pH change and degree of mineralization, *Water Sci. Technol.*, **2010**, 62, 1084–1089.
- [66] Wang, J., Huang, C. P., Allen, H. E., Surface physical-chemical characteristics of sludge particulates, *Water Environ. Res.*, **2000**, 72, 545–553.
- [67] Droge, S., Goss, K.-U., Effect of sodium and calcium cations on the ion-exchange affinity of organic cations for soil organic matter, *Environ. Sci. Technol.*, **2012**, 46, 5894–5901.
- [68] Droge, S., Goss, K.-U., Ion-exchange affinity of organic cations to natural organic matter: Influence of amine type and nonionic interactions at two different pHs, *Environ. Sci. Technol.*, **2013**, 47, 798–806.
- [69] Hörsing, M., Ledin, A., Grabic, R., Fick, J., Tysklind, M., la Cour Jansen, J., Andersen, H. R., Determination of sorption of seventy-five pharmaceuticals in sewage sludge, *Water Res.*, **2011**, 45, 4470 – 4482.
- [70] Hyland, K. C., Dickenson, E. R. V., Drewes, J. E. D., Higgins, C. P., Sorption of ionized and neutral emerging trace organic compounds onto activated sludge from different wastewater treatment configurations, *Water Res.*, **2012**, 46, 1958 – 1968.
- [71] Karthikeyan, K. G., Chorover, J., Humic acid complexation of basic and neutral polycyclic aromatic compounds, *Chemosphere*, **2002**, 48, 955 – 964.

- [72] Stevens-Garmon, J., Drewes, J. E., Khan, S. J., McDonald, J. M., Dickenson, E. R. V., Sorption of emerging trace organic compounds onto wastewater sludge solids, *Water Res.*, **2011**, 45, 3417 – 3426.
- [73] Suzuki, I., Dular, U., Kwok, S. C., Ammonia or ammonium ion as substrate for oxidation by nitrosomonas europaea cells and extracts, *J. Bacteriol.*, **1974**, 120, 556–558.
- [74] Udert, K. M., Wächter, M., Complete nutrient recovery from source-separated urine by nitrification and distillation, *Water Res.*, **2012**, 46, 453–464.
- [75] Eyer, K., Paech, F., Schuler, F., Kuhn, P., Kissner, R., Belli, S., Dittrich, P. S., Krämer, S. D., A liposomal fluorescence assay to study permeation kinetics of drug-like weak bases across the lipid bilayer, *J. Controlled Release*, **2014**, 173, 102–109.
- [76] Albert, A., Serjeant, E. P., eds., *The Determination of Ionization Constants: A Laboratory Manual*, 3rd ed., New York: Lchapman and Hall, **1984**.
- [77] Jchem for excel v5.10.1.710 from chemaxon.
- [78] Shalaeva, M., Kenseth, J., Lombardo, F., Bastin, A., Measurement of dissociation constants (pka values) of organic compounds by multiplexed capillary electrophoresis using aqueous and cosolvent buffers, *J. Pharm. Sci.*, **2008**, 97, 2581–2606.
- [79] Mokrosz, J. L., Pietrasiewicz, M., Duszyńska, B., Cegla, M. T., Structure-activity relationship studies of central nervous system (cns) agents. 5. effect of the hydrocarbon chain on the affinity of 4-substituted 1-(3-chlorophenyl)piperazines for 5-HT_{1A} receptor sites, *J. Med. Chem.*, **1992**, 35, 2369–2374.
- [80] Lemke, T. L., Williams, D. A., Roche, F. R., Zito, S. W., eds., *Foye's Principles of Medicinal Chemistry*, 7th ed., Baltimore: Lippincott Williams & Wilkins, **2012**.
- [81] Avdeef, A., ed., *Absorption and drug development: solubility, permeability and charge state*, New Jersey: John Wiley and Sons, Inc., **2003**.
- [82] University of hertfordshire (2013) the pesticide properties database (ppdb) developed by the agriculture & environment research unit (aeru).
- [83] Kern, S., Baumgartner, R., Helbling, D. E., Hollender, J., Singer, H., Loos, M. J., Schwarzenbach, R. P., Fenner, K., A tiered procedure for assessing the

- formation of biotransformation products of pharmaceuticals and biocides during activated sludge treatment, *J. Environ. Monit.*, **2010**, 12, 2100–2111.
- [84] Kern, S., Fenner, K., Singer, H. P., Schwarzenbach, R. P., Hollender, J., Identification of transformation products of organic contaminants in natural waters by computer-aided prediction and high-resolution mass spectrometry, *Environ. Sci. Technol.*, **2009**, 43, 7039–7046.
- [85] Hornik, K., Friedrich, L., Zeileis, A., eds., *JAGS: A Program for Analysis of Bayesian Graphical Models Using Gibbs Sampling*, TU Wien, Vienna, Austria, **2003**.
- [86] Garardi, M. H., ed., *Nitrification and Denitrification in the Activated Sludge Process*, 1st ed., New York: John Wiley and Sons, Inc., **2002**.
- [87] Joss, A., Zabczynski, S., Goebel, A., Hoffmann, B., Loeffler, D., McArdell, C. S., Ternes, T. A., Thomsen, A., Siegrist, A., Biological degradation of pharmaceuticals in municipal wastewater treatment: Proposing a classification scheme, *Water Res.*, **2006**, 40, 1686 – 1696.
- [88] Saarikoski, J., Lindström, R., Tyynelä, M., Viluksela, M., Factors affecting the absorption of phenolics and carboxylic acids in the guppy (*poecilia reticulata*), *Ecotox. Environ. Safe.*, **1986**, 11, 158 – 173.
- [89] Slonczewski, J. L., Fujisawa, M., Dopson, M., Krulwich, T. A., Cytoplasmic pH measurement and homeostasis in bacteria and archaea, *Adv. Microb. Physiol.*, **2009**, 55, 1–79,317.
- [90] Luft, A., Wagner, M., Ternes, T. A., Transformation of biocides irgarol and terbutryn in the biological wastewater treatment, *Environ. Sci. Technol.*, **2014**, 48, 244–254.
- [91] Rubirola, A., Llorca, M., Rodriguez-Mozaz, S., Casas, N., Rodriguez-Roda, I., Barcelo, D., Buttiglieri, G., Characterization of metoprolol biodegradation and its transformation products generated in activated sludge batch experiments and in full scale wwtps, *Water Res.*, **2014**, 63, 21 – 32.
- [92] Berkner, S., Claudia, T., Biodegradability and transformation of human pharmaceutical active ingredients in environmentally relevant test systems, *Environ. Sci. Pollut. R.*, **2014**, 21, 9461–9467.
- [93] Toolaram, A. P., Kuemmerer, K., Schneider, M., Environmental risk assessment of anti-cancer drugs and their transformation products: A focus on their genotoxicity characterization-state of knowledge and short comings, *Mutat. Res.-Rev. Mutat.*, **2014**, 760, 18 – 35.

- [94] Moschet, C., Piazzoli, A., Singer, H., Hollender, J., Alleviating the reference standard dilemma using a systematic exact mass suspect screening approach with liquid chromatography-high resolution mass spectrometry, *Anal. Chem.*, **2013**, 85, 10312–10320.
- [95] Chiaia-Hernandez, A. C., Schymanski, E., Praveen, K., Singer, H., Hollender, J., Suspect and nontarget screening approaches to identify organic contaminant records in lake sediments, *Anal. Bioanal. Chem.*, **2014**, 406, 7323–7335.
- [96] Hug, C., Ulrich, N., Schulze, T., Brack, W., Krauss, M., Identification of novel micropollutants in wastewater by a combination of suspect and nontarget screening, *Environ. Pollut.*, **2014**, 184, 25 – 32.
- [97] Moriya, Y., Shigemizu, D., Hattori, M., Tokimatsu, T., Kotera, M., Goto, S., Kanehisa, M., Pathpred: an enzyme-catalyzed metabolic pathway prediction server, *Nucleic Acids Res.*, **2010**, 38, W138–W143.
- [98] The CRAFT website; <http://www.molecular-networks.com/products/craft>.
- [99] The OECD QSAR Toolbox website; <http://www.oecd.org/chemicalsafety/risk-assessment/theoecdqsartoolbox.htm>.
- [100] Gao, J., Ellis, L. B. M., Wackett, L. P., The university of minnesota pathway prediction system: multi-level prediction and visualization, *Nucleic Acids Res.*, **2011**, 39, W406–W411.
- [101] Ellis, L., Wackett, L., Use of the university of minnesota biocatalysis/biodegradation database for study of microbial degradation, *Microb. Inform. Exp.*, **2012**, 2, 1.
- [102] EAWAG-BBD Pathway Prediction System website; <http://eawag-bbd.ethz.ch/predict/>.
- [103] Fenner, K., Gao, J., Kramer, S., Ellis, L., Wackett, L., Data-driven extraction of relative reasoning rules to limit combinatorial explosion in biodegradation pathway prediction, *Bioinformatics*, **2008**, 24, 2079–2085.
- [104] Fischer, K., Majewsky, M., Cometabolic degradation of organic wastewater micropollutants by activated sludge and sludge-inherent microorganisms, *Appl. Microbiol. Biotechnol.*, **2014**, 98, 6583–6597.
- [105] Smith, R. V., Rosazza, J. P., Microbial models of mammalian metabolism, *J. Pharm. Sci.*, **1975**, 64, 1737–1759.

- [106] Gulde, R., Helbling, D. E., Scheidegger, A., Fenner, K., pH-dependent biotransformation of ionizable organic micropollutants in activated sludge, *Environ. Sci. Technol.*, **2014**, 48, 13760–13768.
- [107] MetaPrint2D website; <http://www-metaprint2d.ch.cam.ac.uk/metaprint2d-react>.
- [108] The MassBank website; www.massbank.eu.
- [109] Castle, L. A., et al., Discovery and directed evolution of a glyphosate tolerance gene, *Science*, **2004**, 304, 1151–1154.
- [110] Clark, A. M., Evans, S. L., Hufford, C. D., McChesney, J. D., Microbial n-acetylation of primaquine by two streptomyces species: Time course studies and hplc analyses, *J. Nat. Prod.*, **1982**, 45, 574–581.
- [111] Asha, S., Vidyavathi, M., Cunninghamella - a microbial model for drug metabolism studies - a review, *Biotechnol. Adv.*, **2009**, 27, 16–29.
- [112] Choudhary, C., Weinert, B. T., Nishida, Y., Verdin, E., Mann, M., The growing landscape of lysine acetylation links metabolism and cell signalling, *Nat. Rev. Mol. Cell Biol.*, **2014**, 15, 536–550.
- [113] Kosono, S., Tamura, M., Suzuki, S., Kawamura, Y., Yoshida, A., Nishiyama, M., Yoshida, M., Changes in the acetylome and succinylome of bacillus subtilis in response to carbon source, *PLoS ONE*, **2015**, 10.
- [114] Terzic, S., Senta, I., Matosic, M., Ahel, M., Identification of biotransformation products of macrolide and fluoroquinolone antimicrobials in membrane bioreactor treatment by ultrahigh-performance liquid chromatography/quadrupole time-of-flight mass spectrometry, *Anal. Bioanal. Chem.*, **2011**, 401, 353–363.
- [115] Ellis, L. B. M., Gao, J., Fenner, K., Wackett, L. P., The university of minnesota pathway prediction system: predicting metabolic logic, *Nucleic Acids Res.*, **2008**, 36, W427–W432.
- [116] Wicker, J., Lorschach, T., Gütlein, M., Schmid, E., Latino, D., Kramer, S., Fenner, K., envipath - the environmental contaminant biotransformation pathway resource, *Nucleic Acids Res.*, **2015**, gkv1229.
- [117] Lange, F., Cornelissen, S., Kubac, D., Sein, M. M., von Sonntag, J., Hannich, C. B., Golloch, A., Heipieper, H. J., Möder, M., von Sonntag, C., Degradation of macrolide antibiotics by ozone: A mechanistic case study with clarithromycin, *Chemosphere*, **2006**, 65, 17 – 23.

- [118] Rusch, M., Kauschat, A., Spielmeyer, A., Römpf, A., Hausmann, H., Zorn, H., Hamscher, G., Biotransformation of the antibiotic danofloxacin by *xylaria longipes* leads to an efficient reduction of its antibacterial activity, *J. Agric. Food Chem.*, **2015**, 63, 6897–6904.
- [119] Qu, S., et al., Product-to-parent reversion of trenbolone: Unrecognized risks for endocrine disruption, *Science*, **2013**, 342, 347–351.
- [120] Bonvin, F., Omlin, J., Rutler, R., Schweizer, W. B., J., A. P., Strathmann, T. J., McNeill, K., Kohn, T., Direct photolysis of human metabolites of the antibiotic sulfamethoxazole: Evidence for abiotic back-transformation, *Environ. Sci. Technol.*, **2013**, 47, 6746–6755.
- [121] Meier, U., *N-oxide Formation in the Activated Sludge Treatment Step of Wastewater Treatment Plants*, Master's thesis, ETH Zürich, **2015**.
- [122] Göbel, A., McArdell, C. S., Joss, A., Siegrist, H., Giger, W., Fate of sulfonamides, macrolides, and trimethoprim in different wastewater treatment technologies, *Sci. Total Environ.*, **2007**, 372, 361 – 371.
- [123] Blair, B., Nikolaus, A., Hedman, C., Klaper, R., Grundl, T., Evaluating the degradation, sorption, and negative mass balances of pharmaceuticals and personal care products during wastewater treatment, *Chemosphere*, **2015**, 134, 395 – 401.
- [124] Sawyer, C., McCarty, P., Parkin, G., eds., *Chemistry for Environmental Engineering and Science*, The McGraw-Hill series in civil and environmental engineering, McGraw-Hill Education, **2003**.
- [125] Clesceri, L. S., Greenber, A. E., Eaton, A. D., eds., *Standard methods for the examination of water and wastewater*, 20th ed., American Public Health Association, **1998**.
- [126] Boyer, S., Zamora, I., New methods in predictive metabolism, *Journal of Computer-Aided Molecular Design*, **2002**, 16, 403–413.
- [127] Boyer, S., Catrin Arnby, C. H., Carlsson, L., Smith, J., Stein, V., , Glen, R. C., Reaction site mapping of xenobiotic biotransformations, *Journal of Chemical Information and Modeling*, **2007**, 47, 583–590.
- [128] Stravs, M. A., Schymanski, E. L., Singer, H. P., Hollender, J., Automatic recalibration and processing of tandem mass spectra using formula annotation, *J. Mass Spectrom.*, **2013**, 48, 89–99.

- [129] Ma, S., Chowdhury, S. K., , Alton, K. B., Thermally induced n-to-o rearrangement of tert-n-oxides in atmospheric pressure chemical ionization and atmospheric pressure photoionization mass spectrometry: Differentiation of n-oxidation from hydroxylation and potential determination of n-oxidation site, *Anal. Chem.*, **2005**, 77, 3676–3682.
- [130] Wagner, E., Wittmann, H.-J., Elz, S., Strasser, A., Mepyramine-jnj7777120-hybrid compounds show high affinity to hh1r, but low affinity to hh4r, *Bioorg. Med. Chem. Lett.*, **2011**, 21, 6274 – 6280.
- [131] Lebleu, T., Kotsuki, H., Maddaluno, J., Legros, J., Formylation of amines through catalyst- and solvent-free transamidation reaction, *Tetrahedron Lett.*, **2014**, 55, 362 – 364.
- [132] Altieri, A., Bottari, F., G. and Dehez, Leigh, D. A., Wong, J. K. Y., Zerbetto, F., Remarkable positional discrimination in bistable light- and heat-switchable hydrogen-bonded molecular shuttles, *Angew. Chem. Int. Ed.*, **2003**, 42, 2296–2300.

Curriculum vitae

Name	Rebekka Gulde
Email	rebekka.gulde@gmail.com
Nationality	German
Date of birth	August 18, 1984

2011 - 2015	PhD thesis, Department Environmental Chemistry, Eawag Dübendorf / ETH Zürich, Switzerland
2007 - 2011	Diploma in Chemistry, Karlsruhe Institute of Technology (KIT), Germany
2010 - 2011	Diploma thesis, Department of Theoretical Chemistry, Karlsruhe Institute of Technology (KIT), Germany
2009	Semester abroad, Queensland University of Technology (QUT), Brisbane, Australia
2005 - 2007	Prediploma in Chemistry, Albert-Ludwigs-University Freiburg, Germany
1995 - 2004	Abitur, Bildungszentrum Markdorf, Germany